Development, Evaluation and Improvement of Correlations for Interphase Friction in Gas-Liquid Vertical Upflow

Randy Raymond Clark, Jr.

Thesis submitted to the faculty of the Virginia Polytechnic Institute and State University in partial fulfillment of the requirements for the degree of

Doctor of Philosophy

in

Mechanical Engineering

Alan A. Kornhauser, Chair
John H. Jones
Yang Liu
Mark A. Pierson
Danesh K. Tafti

August 28, 2015
Blacksburg, Virginia

Keywords: Two-Phase Flow, Interphase Friction, RELAP

Development, Evaluation and Improvement of Correlations for Interphase Friction in Gas-Liquid Vertical Upflow

Randy Raymond Clark, Jr.

ABSTRACT

In this study, liquid-vapor vertical upflow has been research with the intent of finding an improved method of modelling the interphase friction in two-phase vertical flow in nuclear thermal-hydraulic codes. An improved method of modelling interphase friction should allow for better prediction of pressure gradient, void fraction and the phasic velocities.

Data has been acquired from several available published resources and analyzed to determine the interphase friction using a force balance between the liquid and vapor phases. Using the Buckingham Pi Theorem, a dimensionless interphase friction force was tested and refined before being compared against seven other dimensionless parameters. Three correlations have been developed that establish a dimensionless interphase friction force as a function of the Weber number, the Froude number and the mixture Froude number. Statistical analysis of the three correlations shows that the mixture Froude number correlation should be the most accurate correlation. The correlations have a weakness that makes them ineffective mostly for bubbly flow and some slug flow scenarios, while they should perform significantly better for annular flow cases.

Comparisons have been made against the interphase friction calculations published in the manuals of RELAP5/MOD2, RELAP5/MOD3.3, RELAP5-3D and TRACE. The findings have generally shown that the equations in the manuals provide very inaccurate approximations of the interphase friction compared to the interphase friction that was found via force balance. When analyzing the source code of RELAP5/MOD3.3, several differences were noticed between the source code and manual, which have been discussed. Calculations with the source code

equations reveal that the source code provides a modestly improved prediction of the interphase friction force, but still has significant errors.

Despite the fact that the manual and source code equations indicate that RELAP5/MOD3.3 should perform poorly in modelling interphase friction, actual RELAP5/MOD3.3 model runs perform very well in predicting pressure gradient, void fraction, the liquid and vapor velocities and the interphase friction force. This is largely due to RELAP5/MOD3.3 being able to adjust parameters to converge to a solution that fits within the boundary conditions established in the input file.

Modifications to the RELAP5/MOD3.3 code were first made with the three correlations developed using dimensionless parameters, and were tested with data points that the RELAP5/MOD3.3 flow regime map had predicted would be annular flow. While the mixture Froude number correlation has been analyzed to be the most statistically accurate of the three correlations, it was found that the Weber number correlation performed best when implemented into RELAP5/MOD3.3. In a parametric study of the Weber number correlation, it performed optimally at 150% of the original correlation, improving upon the original RELAP model in almost every metric examined.

Additional investigations were performed with individual annular flow correlations that model specific physical parameters. Results with the annular flow physical models were inconclusive as no particular model provided a significant improvement over the original RELAP5/MOD3.3 model, and there was no clear indication that combining the models would provide significant improvement.

Acknowledgements

The author of this dissertation would like to acknowledge the assistance of several individuals whose advice, support and encouragement have made completing this project possible.

First, I would like to thank the Nuclear Regulatory Commission for providing the funding that has allowed me to pursue my dream of earning a doctoral degree, and without which this would not be a possibility.

Second, I would like to acknowledge the help and assistance that was provided by Mr. Mark Baird of the Radiation Safety Information Computational Center at Oak Ridge National Laboratory, who had worked with me over the course of several months in attempting to compile RELAP5/MOD3.3 first in a Windows environment and later in a Linux environment. Although our efforts were ultimately unsuccessful, it helped us both learn more about RELAP5/MOD3.3, Cygwin, Linux and the related computer programs that are necessary to compile the RELAP5/MOD3.3 source code.

Third, I would like to thank Mr. William Woodruff of Floyd, Virginia for gracious donating the Toshiba™ Satellite laptop computer, and installing Red Hat Linux 9.0 so that I may be able to compile and modify the source code for RLEAP5/MOD3.3. Without the laptop with Red Hat Linux 9.0, there would have been no way to modify the RELAP5/MOD3.3 source code to test the various correlations that have been studied for this dissertation.

Lastly, I would like to thank my wife, Shana, for her support throughout the last five years, as I have pursued both my Masters and Doctorate of Philosophy degrees. The last year as been especially trying with the arrival of our son, AJ, who motivated me every day to strive to finish this project, even as new obstacles came in the way of completing my research.

Table of Contents

List of Figures

List of Tables

Nomenclature

Variables

a	Interfacial Area per Unit Volume
A	Cross-Sectional Area, Coefficient
B	Body Force, Coefficient
C	Coefficient
D	Diameter, Coefficient
$DISS$	Energy Dissipation Function
E	Entrainment
f	Friction Factor
F	Force per Unit Volume
FIF	Interphase Drag Coefficient on the Liquid
FIG	Interphase Drag Coefficient on the Vapor
Fr	Froude Number
FWF	Wall Friction Drag Coefficient on the Liquid
FWG	Wall Friction Drag Coefficient on the Vapor
g	Acceleration Due to Gravity
G	Mass Flux
h	Specific Enthalpy
j	Superficial Velocity, Volumetric Flux
K	Coefficient Used in EPRI Drift Velocity Model, Kinetic Energy Coefficient
L	Function of Vapor Void Fraction and Pressure, or Length
m	Lockhart-Martinelli Exponent for Vapor Phase Wall Friction
n	Lockhart-Martinelli Exponent for Liquid Phase Wall Friction
p	Perimeter
P	Pressure
Q	Volume Flow Rate or Heat Transfer
R	Ratio
Re	Reynolds Number
t	Time
u	Specific Internal Energy
v	Velocity
V	Specific Volume
W	Mass Flow Rate
We	Weber Number
x	Quality
X	Lockhart-Martinelli Parameter
z	Height
α	Void Fraction
δ	Film Thickness
ε	Ratio
Γ	Vapor Generation
λ	Virtual Mass Parameter
Λ	Property Group
μ	Dynamic Viscosity

v	Kinematic Viscosity
ρ	Density
σ	Standard Deviation, Surface Tension
τ	Shear Stress
Φ	Dimensionless Wall Friction

Subscripts

ann	Annular
avg	Average over a Given Interval
b	Bubble
c	Continuous, Constant
crit	Critical Value
d	Drift Difference
D	Drag
f	Liquid Phase
fI	Liquid Interface
fp	Liquid for the Entire Pipe
fw	Liquid at Wall
fzz	Liquid along the Vertical Plane
g	Vapor Phase
gf	Vapor to Liquid
gI	Vapor Interface
gj	Vapor to Total Superficial
gp	Vapor for the Entire Pipe
gw	Vapor at Wall
gzz	Vapor along the Vertical Plane
H	Hydraulic
if	Interface to Liquid
ig	Interface to Vapor
int	Non-Dimensionalized Interphase
INT	Interphase
int,n	Non-Dimensionalized Interphase and Normalized
k	k-th Phase, Kurtosis
K	Kozloff Calculation
L	Loss
m	Mixture
mK	Mixture using Kozloff's Calculations
p	Particle
r	Relative
ref	Reference
s	Skewness
sb	Small Bubble
st	Static
T	Taylor Bubble
V	Volumetric

VM	Virtual Mass
w	Wall
wf	Wall to Liquid
wg	Wall to Vapor
zz	Along the Vertical Plane

Superscripts

s	Saturation
T	Turbulent

Acronyms

IATE	Interfacial Area Transport Equation
INEL	Idaho National Engineering Laboratory
ORNL	Oak Ridge National Laboratory
RELAP	Reactor Excursion and Leak Analysis Program
RMS	Root Mean Square
RSICC	Radiation Safety Information Computational Center
TRAC	Transient Reactor Analysis Code
TRACE	TRAC/RELAP Advanced Computational Engine

I. Introduction

1.1: Overview

When designing a nuclear power plant, the most important considerations are the ability for the plant to operate safely and to generate electrical power efficiently. As all nuclear power plants in current use and being developed in the near future employ steam and water, an understanding of nuclear thermal hydraulics is necessary to design nuclear power plants and their components. In order to predict how the thermal hydraulics of a particular design react to various conditions encountered by a power plant, a number of different computer models have been developed that simulate the thermal hydraulic behavior of a nuclear power plant.

The thermal hydraulic codes that have been developed operate primarily as one-dimensional two-fluid models, although there are a few that include three-dimensional components. These codes allow an engineer to simulate steady-state and transient behaviors within a nuclear power plant, and determine how the thermal hydraulics operates under those scenarios. As most nuclear power plants use water as the primary coolant of the reactor core, and use steam to generate power in turbines, the two-fluid models used in the nuclear power industry have been designed to model steam/water and air-water two-phase flows. Due to a lack of computing power, most models were originally developed as one-dimensional models, following the axis of components through which water flowed, with limited use of three-dimensional components becoming only a recent addition to the models.

As there are many scenarios where an engineer would need to model steam/water or air-water flowing together within a nuclear power plant, it is necessary for these thermal hydraulic computer models to produce accurate predictions of how the two phases interact when flowing

through the various components of a nuclear power plant. Among the most important interactions is the interphase friction that occurs between the liquid phase and the vapor phase.

The motivation to undertake this project originates with the work of Clark and Kornhauser. [16] Steam-water downflow in the downcomer of a once-through steam generator (OTSG) was studied and modeled in RELAP5/MOD2. It was discovered that RELAP5/MOD2 was not able to accurately model the liquid-vapor distribution within the downcomer and that the interphase friction needed to be increased in order to achieve a vapor distribution that was reflective of the data. Clark and Kornhauser proposed modifying an existing correlation within the version of RELAP5/MOD2 that had been provided to them by Areva, Inc., such that the correlation provided an optimal amount of interphase friction to produce a result that matched the reported data. It was found that the TRAC-RELAP Advanced Computing Engine (TRACE) had similar deficiencies with steam-water downflow, but TRACE did not allow for the user to modify the interphase friction. Based on these results, the need for an improved interphase friction correlation for all one-dimensional two-fluid nuclear safety codes became apparent. Thus, it has been the goal of this project to examine experimental data in an effort to produce a new correlation for interphase friction can be easily implemented into RELAP or TRACE.

In this study, data has been collected from several published sources with the intent to determine the interphase friction that occurs with each trial run. Most of the data available was provided in English units, and for the sake of consistency, all units in this paper have been converted to English units. The interphase friction has been calculated by performing a force balance on a control volume, and the interphase friction has been correlated against known quantities from the published data. Known and unknown variables will be selected in such a way that they are compatible with the solution technique of widely used one-dimensional two-

fluid models. To assist in the analysis, all values have been non-dimensionalized, which is not a unique approach in fluid dynamics, but appears to be an underutilized technique with respect to interphase friction. This is in part due to a lack of agreement as to which dimensionless variables are appropriate for two-phase flow analysis. Additionally, comparisons of the annular flow data points have been made against individual correlations that have been developed for components of annular flow.

The correlations have been compared to those provided in the manuals of RELAP5/MOD2, RELAP5-3D and TRACE, and in the source code for RELAP5/MOD3.3, which has been obtained from the Radiation Safety Information Computational Center (RSICC) at Oak Ridge National Laboratory (ORNL).

II. Background

2.1: Two-Phase Liquid-Vapor Co-Current Vertical Flow

Multiphase flow is defined as the simultaneous flow of more than one phase (solid, liquid or gas) at a given place and time. The simplest version of multiphase flow to understand and model is two-phase flow. These may be liquid-solid flow, liquid-gas flow or solid-gas flow. It may also be liquid-liquid flow when the two liquids are immiscible, such as oil and water. Two-phase flow may be single component, where the phases are of the same substance (e.g. steam/water), or two-component, where the phases are different substances (e.g. air-water). [84]

While any imaginable scenario with two-phase flow within a nuclear power plant takes place under considerably higher pressures and temperatures than the average person would ever experience, the amount of heat transfer to the surroundings is often negligible, and heat transfer between the phases is usually very rapid. Since there is usually little heat transfer between phases within two-phase flow, it would imply that there is also minimal mass transfer. As such, the heat and mass transfer have been neglected in this study, with focus placed on the momentum transfer, which is dominated by the interphase friction. All studies that have been used to develop the interphase friction correlations are documented as adiabatic, with observations confirming negligible heat and mass transfer between phases in each case.

Within any type of piping system, there may exist pipes that are horizontal, vertical or at any given angle in between. While there has been some research on two-phase flow occurring at varying angles, most notably the work of Crawford [19], designing an apparatus that can adjust angles presents numerous challenges for the research. Therefore, most research on liquid-vapor flow has concentrated on either horizontal or vertical flow. Furthermore, there appears to be a

greater variety and availability of data in vertical flow, and as the original inspiration for this project was a vertical flow scenario, only vertical flow was examined for this study.

2.1.1: Analysis Models

There have been numerous different approaches to analyzing one-dimensional two-phase liquid-vapor co-current vertical flow and can be divided into three broad categories, the homogeneous flow method, the separated flow method and the drift-flux method. [84] Each method is governed by its own set of conservation equations. As the focus of this study is on in the interphase friction force, special attention will be paid to the conservation of momentum equations. The continuity equations will also be examined as they are also needed to calculate the interphase friction force. Since the scenarios that are being discussed are assumed to be adiabatic, the energy balance equations will be neglected.

2.1.1.1: Homogeneous Equilibrium Flow Model

The one-dimensional homogeneous equilibrium model is the simplest approach to modeling and evaluating two-phase flow. Both phases are assumed to occupy a given point with a concentration level equal to that of the entire pipe cross-section, to be in thermal equilibrium and have the same velocity. The homogeneous equilibrium model density at any given point is defined as:

$$\rho_m = \alpha\rho_g + (1-\alpha)\rho_f \qquad 1$$

where α is the vapor volume fraction, ρ_m is the mean density of two-phase flow, ρ_f is the density of the liquid phase and ρ_g is the density of the vapor phase. [84]

The homogeneous equilibrium flow velocity, v, is:

$$v = v_g = v_f = j = \frac{Q_g + Q_f}{A} \qquad 2$$

where v_g is the velocity of the vapor phase, v_f is the velocity of the liquid phase, j is the volumetric flux through a given pipe, Q_g is the volumetric flow rate of the vapor, Q_f is the volumetric flow rate of the liquid and A is the cross sectional area of the pipe. [84]

These assumptions that are required for the homogeneous equilibrium model result in a system described by three conservation equations, one each for the mixture's mass, momentum and energy. For the homogeneous model, the continuity equation for one-dimensional two-phase vertical flow is given in Equation 3. [84]

$$\frac{\partial \rho_m}{\partial t} = -\frac{\partial (\rho_m v)}{\partial z} \qquad 3$$

The term on the left represents the time rate of change in the average density of the fluid, and the term on the right side of the equation represents the change in mass flux with respect to height. [84]

The conservation of momentum equation for the homogeneous equilibrium model for vertical flow is shown in Equation 4.

$$\frac{\partial (\rho_m v)}{\partial t} + \frac{\partial (\rho_m v^2)}{\partial z} = -\frac{\partial P}{\partial z} - \rho_m g - \frac{p}{A}\tau_w \qquad 4$$

where p is the perimeter of the pipe, A is the cross-sectional area of the pipe and τ_w is the shear stress induced on the homogeneous mixture by the wall. [84]

On the left side Equation 4 is the one-dimensional total derivative of the homogeneous mixture's momentum. The three terms on the right side of Equation 4 are the overall pressure gradient, the pressure gradient due to gravity and the pressure gradient due to wall friction, respectively. Solving for the overall pressure gradient, Equation 4 can be rewritten as:

$$\frac{\partial P}{\partial z} = -\left[\frac{\partial (\rho_m v)}{\partial t} + \frac{\partial (\rho_m v^2)}{\partial z}\right] - \rho_m g - \frac{p}{A}\tau_w \qquad 5$$

where the total derivative of the homogeneous mixture's momentum can be considered the pressure gradient due to acceleration. Therefore, the total pressure gradient can be thought of as the sum of the accelerational, hydrostatic and frictional pressure gradients. [84]

Note that the conservation of momentum equation for a homogeneous flow does not include a term for interphase friction. Since the velocities for each phase are equal to each other, then there is no slip between the phases. In order for there to be an interphase friction force, also known as a drag force, between the liquid and vapor phases, there needs to be a velocity difference between the two phases. Thus, the homogeneous equilibrium model is not suitable for calculating the interphase friction force.

2.1.1.2: Separated Flow Model

The separated flow model calls for each phase to be separated into two distinct regions that are proportional in size to each phase's concentration level. Thus, in a typical analysis of a two-phase flow system with the separated flow model, a minimum of six conservation equations are used; two for continuity, two for conservation of momentum and two for conservation of energy. Additionally, there are coupling equations that are used to calculate e interphase transfer terms of mass, momentum and energy.

Ishii and Mishima [46] identified two different approaches to the separated flow model. First, they described the control volume approach where each phase flowed separately and in parallel through a hypothesized control volume. Within this control volume, each phase would be subject to the conservation of mass, momentum and energy, with the transfer of each occurring through an interface that separated the phases. While this method could prove to be accurate for cases where two-phase flow was separated, such as annular flow, Ishii and Mishima were concerned that this approach would miss effects such as phase distribution, velocity and

temperature which could vary radially within a given pipe. Also, this approach would not be appropriate for transient conditions, such as a loss of coolant accident (LOCA) or reflood.

For the control volume method, the continuity equation for the liquid phase is given in Equation 6.

$$\frac{\partial\left[(1-\alpha)\rho_f\right]}{\partial t}+\frac{\partial\left[(1-\alpha)\rho_f v_f\right]}{\partial z}=\Gamma_f \tag{6}$$

where Γ_f is the mass transfer rate of vapor to liquid in the flow. [84]

The continuity equation for the vapor phase is shown in Equation 7.

$$\frac{\partial\left(\alpha\rho_g\right)}{\partial t}+\frac{\partial\left(\alpha\rho_g v_g\right)}{\partial z}=\Gamma_g \tag{7}$$

where Γ_g is the mass transfer rate of liquid to vapor in the flow. [84]

Assuming that there are no sinks or sources within a given section of pipe, then it is assumed that Γ_f and Γ_g are the result of phase change. In that case:

$$\Gamma_f=-\Gamma_g \tag{8}$$

The conservation of liquid momentum equation is:

$$\frac{\partial\left(\rho_f v_f\right)}{\partial t}+\frac{\partial\left(\rho_f {v_f}^2\right)}{\partial z}=\rho_f g+F_f-\frac{\partial P}{\partial z} \tag{9}$$

where F_f represents the external forces that are acting upon the liquid phase. [84]

The conservation of vapor momentum equation is:

$$\frac{\partial\left(\rho_g v_g\right)}{\partial t}+\frac{\partial\left(\rho_g {v_g}^2\right)}{\partial z}=\rho_g g+F_g-\frac{\partial P}{\partial z} \tag{10}$$

where F_g represents the external forces that are acting on the vapor phase. [84]

The terms F_f and F_g constitute forces and stresses that are exerted on the liquid and vapor phases, respectively, including the wall friction forces and the interphase friction forces on each

phase. While Equations 9 and 10 represent very basic interpretations of separated two-phase flow, they can serve as the basis of a more comprehensive analysis. [84]

The preferred method of analysis of Ishii and Mishima [46] was the averaging method, with which the measured properties are averaged with respect to time or area, so as to minimize the effect of anomalies or fluctuations in such properties with respect to time and space. The main purpose of area-averaging values is to simulate two-dimensional and three-dimensional systems as one-dimensional. In many ways, the conservation equations are the same as that for the control volume method, only with special emphasis placed on the properties of the two-phase flow, and how the values are applied to the conservation equations. For example, the area average value of a property, *B*, is defined as:

$$\langle B \rangle = \frac{1}{A} \int B \, dA \tag{11}$$

In some cases, the property needs to be weighed against the concentration of the phase that it represents, which is known as the void fraction weighted mean value. For example, the void fraction weighted mean value of the property B_g of the vapor phase would be: [46]

$$\langle\langle B_g \rangle\rangle = \frac{\langle \alpha B_g \rangle}{\langle \alpha \rangle} = \frac{\int \alpha B_g \, dA}{\int \alpha \, dA} \tag{12}$$

Quantities that need to be area-averaged include the void fraction, phasic mass change rates and the interphase friction. The velocities of each phase are void fraction weighted averaged. The continuity equation for the vapor phase using the area-averaged approach for separated flow is given in Equation 13. [46]

$$\frac{\partial\left(\langle \alpha \rangle \rho_g\right)}{\partial t} + \frac{\partial\left(\langle \alpha \rangle \rho_g \, \langle\langle v_g \rangle\rangle\right)}{\partial z} = \langle \Gamma_g \rangle \tag{13}$$

For the liquid phase, the area-averaged continuity equation is: [46]

$$\frac{\partial\left(\langle 1-\alpha\rangle\rho_f\right)}{\partial t}+\frac{\partial\left(\langle 1-\alpha\rangle\rho_f\,\langle\langle v_f\rangle\rangle\right)}{\partial z}=\langle\Gamma_f\rangle \tag{14}$$

The area-averaged conservation of momentum equation for the vapor phase is:

$$\begin{aligned}&\frac{\partial\left(\langle\alpha\rangle\rho_g\,\langle\langle v_g\rangle\rangle\right)}{\partial t}+\frac{\partial\left(C_{vg}\langle\alpha\rangle\rho_g\,\langle\langle v_g\rangle\rangle^2\right)}{\partial z}\\&\quad=-\langle\alpha\rangle\frac{\partial P}{\partial z}+\frac{\partial\left(\langle\alpha\rangle\,\langle\langle\tau_{gzz}+{\tau_{gzz}}^{T}\rangle\rangle\right)}{\partial z}-\frac{4\alpha_{gw}\tau_{gw}}{D}-\langle\alpha\rangle\rho_g g\\&\quad+\langle\Gamma_g\rangle\,\langle\langle v_{gI}\rangle\rangle+\langle {M_g}^{d}\rangle\end{aligned} \tag{15}$$

where C_{vg} is the distribution parameter of the convective momentum flux on the vapor phase that accounts for the difference between the product of the averaged void fraction and square of vapor velocity and the average of the product of the void fraction and square of the vapor velocity, τ_{gzz} is the viscous stress of the vapor phase, ${\tau_{gzz}}^{T}$ is the turbulent stress on the vapor phase, α_{gw} is the vapor volume fraction at the wall, τ_{gw} is the shear stress that the vapor phase has with the wall, and ${M_g}^{d}$ is the total interfacial stress, including the interphase friction force. [46]

The liquid phase area-averaged conservation of momentum equation is:

$$\begin{aligned}&\frac{\partial\left(\langle 1-\alpha\rangle\rho_f\,\langle\langle v_f\rangle\rangle\right)}{\partial t}+\frac{\partial\left(C_{vf}\langle 1-\alpha\rangle\rho_f\,\langle\langle v_f\rangle\rangle^2\right)}{\partial z}\\&\quad=-\langle 1-\alpha\rangle\frac{\partial P}{\partial z}+\frac{\partial\left(\langle 1-\alpha\rangle\,\langle\langle\tau_{fzz}+{\tau_{fzz}}^{T}\rangle\rangle\right)}{\partial z}-\frac{4\alpha_{fw}\tau_{fw}}{D}\\&\quad-\langle 1-\alpha\rangle\rho_f g+\langle\Gamma_f\rangle\,\langle\langle v_{fI}\rangle\rangle+\langle {M_f}^{d}\rangle\end{aligned} \tag{16}$$

where C_{vf} is the distribution parameter of the convective momentum flux on the liquid phase that accounts for the difference between the average of the product of the liquid volume fraction and the square of the liquid velocity and the product of the average liquid volume fraction and the square of the average liquid velocity, τ_{fzz} is the viscous stress of the liquid phase, ${\tau_{fzz}}^{T}$ is the turbulent stress on the liquid phase, α_{fw} is the liquid volume fraction at the wall, τ_{fw} is the shear

stress that the liquid phase has with the wall, and M_f^d is the total interfacial stress acting on the liquid phase. [46]

2.1.1.3: Drift-Flux Model

The drift-flux model for analyzing two-phase flow is an intermediate model between the simplistic homogeneous equilibrium model and the more complicated separated flow model. Like the homogeneous equilibrium model, the drift-flux model is based primarily on the flow of the mixture, but also accounts for the dispersed phase moving at a different velocity than the continuous phase. Focus is placed on the total volumetric flux, *j*, and the difference between the total volumetric flux and the velocity of the dispersed phase. The difference is known as the drift velocity, v_{dj}, and customarily the dispersed phase is the vapor phase, making it the vapor drift velocity, v_{gj}, and is defined by Equation 17. [41]

$$v_{gj} = v_g - j = v_g - \left[(1-\alpha)v_f + \alpha v_g\right] = (1-\alpha)\left(v_g - v_f\right) \qquad 17$$

A total of four equations are used to formulate the drift-flux model, one for the conservation of mass of the mixture, along with a second continuity equation for the dispersed phase, along with conservation of momentum and energy equations for the mixture. For a one-dimensional two-phase liquid-vapor vertical flow, the mixture continuity equation is: [41]

$$\frac{\partial \rho_m}{\partial t} + v\frac{\partial \rho_m}{\partial z} + \rho_m \frac{\partial v}{\partial z} = 0 \qquad 18$$

The continuity equation for the dispersed phase, which for this purpose of this report will be the vapor phase, is:

$$\frac{\partial\left(\alpha\rho_g\right)}{\partial t} + \frac{\partial\left(\alpha\rho_g v\right)}{\partial z} = \Gamma_g - \frac{\partial\left(\frac{\alpha\rho_f\rho_g}{\rho_m}v_{gj}\right)}{\partial z} \qquad 19$$

where Γ_g is the rate of vapor generation from phase change. [41]

The drift-flux model mixture momentum equation for a liquid-vapor vertical flow is:

$$\frac{\partial(\rho_m v)}{\partial t} + \frac{\partial(\rho_m v^2)}{\partial z} = -\frac{\partial P}{\partial z} - \frac{\partial}{\partial z}\left(\tau_{zz} + {\tau_{zz}}^T - \frac{\alpha}{1-\alpha}\frac{\rho_f \rho_g}{\rho_m}{v_{gj}}^2\right) \quad (20)$$

where τ_{zz} is the viscous stress on the mixture and ${\tau_{zz}}^T$ is the turbulent stress on the mixture. [41]

2.1.1.4: The Lockhart-Martinelli Correlation

While all of the forces that have been discussed in the conservation of momentum equations are important, one that has been extensively studied is the wall friction that occurs with two-phase flow. While there have been several studies that have yielded correlations that can be used to calculate the wall friction force that acts on a two-phase flow through a pipe, the original correlation to which all others appear to be measured against, hence making it the standard wall friction correlation, is the Lockhart-Martinelli correlation. [15]

Lockhart and Martinelli [51] developed their correlation by evaluating the pressure drop in a horizontal pipe, which ranged in diameter between 0.0586 in. to 1.017 in., for two-phase flows involving air and several different liquids, including water, kerosene, benzene and oil. For their analysis, Lockhart and Martinelli non-dimensionalized the pressure drop against the theoretical pressure drop of each phase on its own to develop the non-dimensional parameters, Φ_f and Φ_g, which are then correlated to a non-dimensionalized parameter, X, which has come to be known as the Lockhart-Martinelli parameter.

The Lockhart-Martinelli [51] correlation divides the two-phase flow into four categories, based on whether each phase's flow can be categorized as viscous (also known as laminar) or turbulent, which is determined by the phase's Reynolds number for the whole pipe. Equations 21 are 22 used to calculate the Reynolds number for the liquid and vapor phases, respectively:

$$Re_{fp} = \frac{4W_f}{\pi D \mu_f} \quad (21)$$

$$Re_{gp} = \frac{4W_g}{\pi D \mu_g} \quad (22)$$

where W_f is the mass flow rate of the liquid and W_g is the mass flow rate of the vapor phase. [51]

Lockhart and Martinelli [51] divided the two-phase flow within a pipe into two separate cylinders, such that the cross-sectional area of each cylinder was equal to the product of the phase's volume fraction and the pipe's cross-sectional area. In other words, for the liquid and vapor phases:

$$A_f = (1-\alpha)\frac{\pi D^2}{4} = \alpha_{LM}\frac{\pi {D_f}^2}{4} \quad (23)$$

$$A_g = \alpha\frac{\pi D^2}{4} = \beta_{LM}\frac{\pi {D_g}^2}{4} \quad (24)$$

where A_f is the cross-sectional area of the liquid phase flow, α_{LM} is a ratio of the liquid flow area to the actual flow area, D_f is the hydraulic diameter of the liquid flow, A_g is the cross-sectional area of the vapor phase flow, β_{LM} is a ratio of the vapor flow area to the actual flow area, and D_g is the hydraulic diameter of the vapor flow.

It was shown by Lockhart and Martinelli [51] that the wall friction within a pipe could be found by applying the Fanning equation to each phase:

$$F_W = 2f_f\frac{\rho_f {v_f}^2}{D_f g_c} = 2f_g\frac{\rho_g {v_g}^2}{D_g g_c} \quad (25)$$

where F_W is the wall friction force per unit volume, f_f and f_g are friction factors on the liquid and vapor phases, respectively, and g_c is the gravitational correction constant (32.174 lb_m-ft/lb_f-s^2).

The friction factors for each phase are determined using Equations 26 and 27: [51]

$$f_f = \frac{C_f}{\left(\frac{4W_f}{\pi\alpha D_f \mu_f}\right)^n} \quad (26)$$

$$f_g = \frac{C_g}{\left(\frac{4W_g}{\pi\beta D_g \mu_g}\right)^m} \quad (27)$$

The coefficients C_f and C_g and the exponents n and m are determined based on whether the flow for it respective phase is viscous to turbulent. Values that are given for each constant are provided in Table 1. [51]

Table 1: Coefficients and Exponents Used to Calculated Lockhart-Martinelli Wall Friction [51]

Liquid-Vapor	Turbulent-Turbulent	Viscous-Turbulent	Turbulent-Viscous	Viscous-Viscous
n	0.2	1	0.2	1
m	0.2	0.2	1	1
C_f	0.046	16	0.046	16
C_g	0.046	0.046	16	16

For each phase, Lockhart and Martinelli [51] defined the wall friction on the liquid and vapor phases, respectively, as:

$$F_{Wf} = 2\frac{C_f}{\left(\frac{4W_f}{\pi D \mu_f}\right)^n}\frac{16{W_f}^2}{\pi^2 D^5 \rho_f g_c} \quad (28)$$

$$F_{Wg} = 2\frac{C_g}{\left(\frac{4W_g}{\pi D \mu_g}\right)^n}\frac{16{W_g}^2}{\pi^2 D^5 \rho_g g_c} \quad (29)$$

where F_{Wf} and F_{Wg} are the wall friction forces per unit volume acting on the liquid and vapor phases respectively.

Using the wall friction force Lockhart and Martinelli [51] defined the three non-dimensionalized parameters, Φ_f, Φ_g and X as:

$$\Phi_f = \sqrt{\frac{F_W}{F_{Wf}}} = {\alpha_{LM}}^{\frac{n-2}{2}}\left(\frac{D}{D_f}\right)^{\frac{5-n}{2}} \quad (30)$$

$$\Phi_g = \sqrt{\frac{F_W}{F_{Wg}}} = \beta_{LM}{}^{\frac{m-2}{2}} \left(\frac{D}{D_g}\right)^{\frac{5-m}{2}} \quad 31$$

$$X = \sqrt{\frac{F_{Wf}}{F_{Wg}}} = \frac{\Phi_g}{\Phi_f} \quad 32$$

Table 2: Lockhart-Martinelli Parameter Wall Friction Coordinates [51]

Liquid-Vapor	Turbulent-Turbulent		Viscous-Turbulent		Turbulent-Viscous		Viscous-Viscous	
X	Φ_f	Φ_g	Φ_f	Φ_g	Φ_f	Φ_g	Φ_f	Φ_g
0.01	128.00	1.28	120.00	1.20	112.00	1.12	105.00	1.05
0.02	68.40	1.37	64.00	1.28	58.00	1.16	53.50	1.07
0.04	38.50	1.54	34.00	1.36	31.00	1.24	28.00	1.12
0.07	24.40	1.71	20.70	1.45	19.30	1.35	17.00	1.19
0.10	18.50	1.85	15.20	1.52	14.50	1.45	12.40	1.24
0.20	11.20	2.23	8.90	1.78	8.70	1.74	7.00	1.40
0.40	7.05	2.83	5.62	2.25	5.50	2.20	4.25	1.70
0.70	5.04	3.53	4.07	2.85	4.07	2.85	3.08	2.16
1.00	4.20	4.20	3.48	3.48	3.48	3.48	2.61	2.61
2.00	3.10	6.20	2.62	5.25	2.62	5.25	2.06	4.12
4.00	2.38	9.50	2.05	8.20	2.15	8.60	1.76	7.00
7.00	1.96	13.70	1.73	12.10	1.83	12.80	1.60	112.00
10.00	1.75	17.50	1.59	15.90	1.66	16.60	1.50	15.00
20.00	1.48	29.50	1.40	28.00	1.44	28.80	1.36	27.30
40.00	1.29	51.50	1.25	50.00	1.25	50.00	1.25	50.00
70.00	1.17	82.00	1.17	82.00	1.17	82.00	1.17	82.00
100.00	1.11	111.00	1.11	111.00	1.11	111.00	1.11	111.00

Lockhart and Martinelli [51] plotted the non-dimensionalized parameters Φ_f and Φ_g against what has come to be known as the Lockhart-Martinelli parameter, X, and developed a set of curves for each case whether the liquid and vapor phase flows were viscous or turbulent. Instead of providing an equation that could be used to model the curves, Lockhart and Martinelli provided a table of coordinates along which their curve fit for each case of two-phase flow, and is provided here in Table 2.

2.1.1.5: Virtual Mass Force and the Basset Force

The conservation of momentum equations account for the many different forces that act on the two-phase flow as it moves through a pipe. However, there are some forces that are unique to two-phase flow, that do not exist in single-phase flow. Two of the more documented forces are the virtual mass force and the Basset force. [84]

The virtual mass force begins with the simple concept of a vapor bubble in a liquid column. As the vapor bubble is less dense than the surrounding liquid, it will rise with respect to the liquid and will have to push it aside. The force that pushes the liquid is known as the virtual mass force. For a single spherical bubble, the virtual mass force is given in Equation 33.

$$F_{VM} = -\frac{2}{3}\pi {r_b}^3 \rho_f \frac{dv_b}{dt} \tag{33}$$

where F_{VM} is the virtual mass force, r_b is the radius of a bubble, and v_b is the velocity of the bubble, relative to that of the liquid. [20]

In applying the virtual mass force to a general two-phase flow with many bubbles of various shapes, there have been several attempts to quantify the virtual mass force. Zuber [88] showed that for spherical bubbly flow, the virtual mass force could be calculated as:

$$F_{VM} = \frac{2}{3}\rho_f \frac{1+2\alpha}{1-\alpha}\pi {r_b}^3 \left(\frac{dv_g}{dt} - \frac{dv_f}{dt}\right) \tag{34}$$

Ishii and Chawla [42] proposed that the virtual mass force could be calculated using Equation 35:

$$F_{VM} = -\rho_f {B_d}^* \left[\frac{D_g v_g}{Dt} - \frac{D_f v_f}{Dt} + (1+\lambda)\overrightarrow{v_r}\cdot\nabla\overrightarrow{v_r}\right] \tag{35}$$

The Basset force is another force that can act on bubbles that are accelerating with respect to the liquid that are not resolved through a control volume force balance. It describes

the force that can act on an accelerating bubble resulting from the transient effects of its surrounding boundary layer. [84]

2.1.2: Flow Regimes

In an attempt to better understand the physics that occur with two-phase flow, there has been a convention to categorize two-phase flow situations into different flow patterns or regimes. Many different schemes, or flow regime maps, have been derived to help engineers predict the flow regime for a given set of conditions, which in turn helps engineers make further calculations regarding the system. In thermal-hydraulic modelling programs like RELAP5/MOD3.3, the flow regime helps determine how the interphase friction is calculated between the phases, among other parameters.

2.1.2.1: Description of Flow Regimes

Although there is no standard list of two-phase flow patterns, the general agreement amongst most sources is that there are four primary two-phase flow patterns: bubbly, slug, churn-turbulent and annular flow. However, there is disagreement between sources regarding the existence of transitional flow regimes. [15,50,59,67,79,83,84]

The bubbly flow regime is generally described as having small bubbles that flow within a continuous liquid. Bubbles are usually fairly evenly distributed throughout the flow, with a small concentration towards the center of the pipe. Bubbly flow is usually associated with small void fractions and small vapor volumetric fluxes relative to the liquid component. [15,50,59,67,79,83,84]

As the amount of vapor flow in a pipe with respect to the liquid flow is increased, the bubbles of vapor will collide and merge into larger bubbles. As the diameter of the bubble approaches that of the pipe, the general flow within the pipe will distort the bubble into a bullet

shape. These bullet-shaped bubbles, also known as Taylor bubbles, are separated from the pipe wall by a thin liquid film and from each other by liquid slugs. Hence, this flow regime is known as slug flow. [15,79,83,84] Kozloff [50] refers to this type of flow as plug flow. Oshinowo and Charles [59] divided the slug flow regime into two different regimes; quiet slug and dispersed slug. Quiet slug featured very few bubbles within the liquid slugs or the liquid film, while dispersed slug showed an increased concentration of small bubbles in the liquid portion of the flow.

The churn-turbulent flow regime is a transitional flow regime that occurs between slug flow and annular flow. As the amount of vapor flow increases, the Taylor bubbles become increasingly unstable. In an upflow scenario, smaller bubbles will break off of the tail of a leading Taylor bubbles and create a wake that can cause the liquid slug behind the leading Taylor bubble to collapse into a second Taylor bubble. [15,79] Churn-turbulent flow has also been known as froth or frothy flow, while Kozloff [50] broke the churn-turbulent flow regime up into two different regimes that he called dispersed-plug flow and emulsion flow. [59,79] Oshinowo and Charles [59] also identified a transitional flow regime between the dispersed slug and froth flow regimes that they called frothy-slug flow.

Annular flow develops as the vapor flow increases with respect to the liquid flow and is named for the liquid film that forms along the walls of the pipe, while the vapor phase becomes continuous within the center of the pipe. Liquid droplets are also entrained in the vapor core, while small bubbles may still exist in the liquid film. [15,50,59,67,79,84] Should the liquid film along the wall disappear, then the flow pattern is known simply as mist or droplet flow. [50,67,84]

To help predict the flow regime that a two-phase flow will experience, flow regime maps have been developed. Generally, they are developed to correspond with the observations of a particular study, and are often subject to the researcher's visual interpretation of a given flow regime. Typically, they are developed from a series of two-phase flow experiments where several parameters are studied, and the relationship between the flow regimes is correlated against two parameters. Most flow regime maps fall into two broad categories, those that correlate the flow regime based on the flow of each phase (normally the volumetric flux of each phase), and those that correlate the flow regime based on two non-dimensionalized parameters. [79] Examples of flow regime maps that are based on the volumetric flux include those of Vince and Lahey [83] and Taitel, Bornea and Dukler. [79] Studies that developed flow regime maps using dimensionless parameters include, but are not limited to the work of Kozloff [50], Oshinowo and Charles [58,59] and Griffith and Wallis. [33]

2.1.2.2: Flow Regime Maps

The flow regime map used by RELAP5/MOD2 [65], RELAP5/MOD3.3 [40,67] and RELAP5-3D [66] is primarily based on that of Vince and Lahey [83], although it incorporates criteria specified in other studies, most notably Taitel et al [79]. Both flow regime maps are based on using the volumetric fluxes of each phase to determine the flow regime. Meanwhile, TRACE [81] does not use a flow regime map in the same sense that RELAP5 does, but rather uses weighted averages of interphase friction for all flow regimes based on the void fraction.

Vince and Lahey [83] conducted a series of experiments with air and water flowing in a Plexiglas pipe with an inner diameter of 1 in., upon which dual beam x-rays were projected into the pipe at six different chords, including the diameter. By calculating the attenuation of the x-rays, Vince and Lahey were able to develop probability density functions and power spectral

density functions that established a quantitative relationship between the void fraction and the flow regime. In their analysis they found that the variance of the void fraction power density functions with respect to space proved to be the best indicator of where the flow regime transitions occurred, and developed the flow regime map shown in Figure 1.

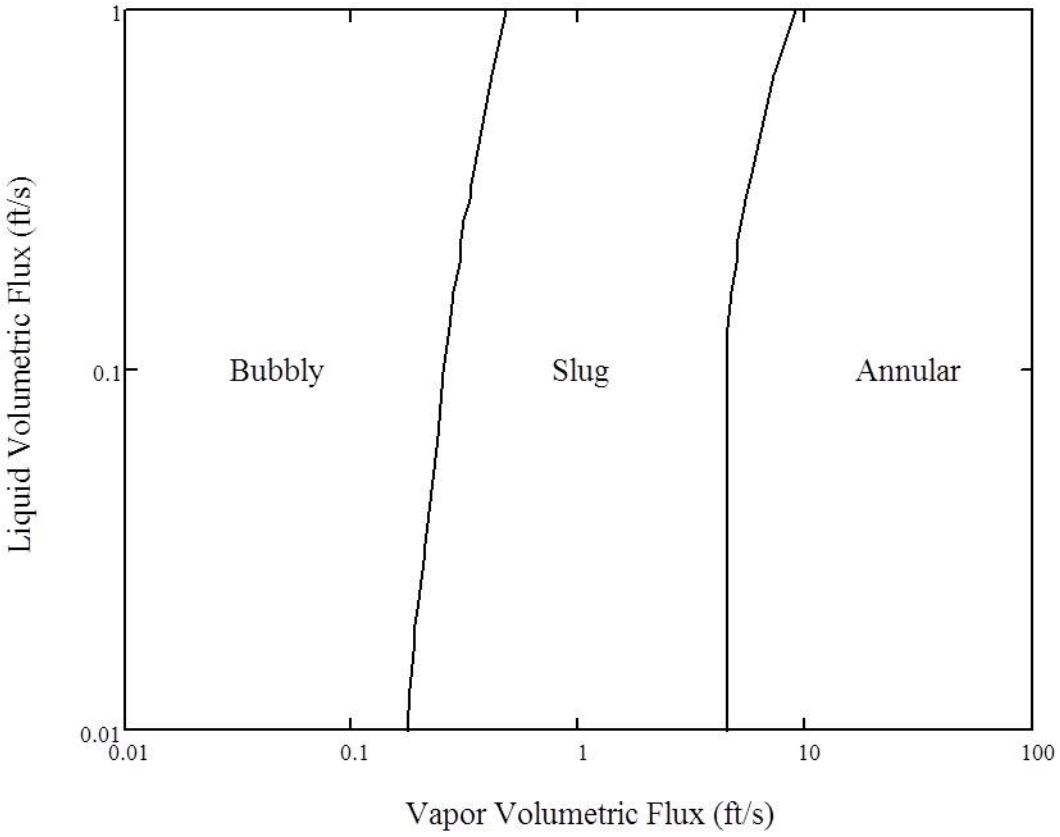

Figure 1: Vince and Lahey's [83] Flow Regime Map for Air-Water Upflow in a 1 in. Inner Diameter Pipe

Taitel et al [79] developed a flow regime map based on a series of equations that were derived from physical knowledge of each flow regime. In the case of bubbly flow, Taitel et al began by considering the velocity difference between the liquid and vapor phases in terms of their volumetric flux, arriving at Equation 36:

$$j_f = \frac{1-\alpha}{\alpha} j_g - (1-\alpha)\Delta v \qquad 36$$

where j_f and j_g are the volumetric fluxes of the liquid and vapor phases, respectively.

To find Δv, Taitel et al [79] substituted Harmathy's [34] equation for bubble rise velocity of large bubbles, which Taitel et al found suitable for small bubbles as well.

$$\Delta v = 1.53 \sqrt[4]{\frac{(\rho_f - \rho_g) g \sigma}{{\rho_f}^2}} \tag{37}$$

Taitel et al [79] considered that if spherical bubbles were arranged in a cubic structure, the maximum void fraction would be 0.52. It was assumed by Taitel et al that the bubbles would begin to collide and merge when the average distance between the bubbles was half of the average bubble radius. This occurs at a void fraction of approximately 0.25, and was corroborated by the observations of Griffith and Wallis. [33] Thus, Taitel et al combined Equations 36 and 37, and used a void fraction of 0.25 to arrive at the bubbly-slug transition line in Equation 38.

$$j_f = 3.0 j_g - 1.15 \sqrt[4]{\frac{(\rho_f - \rho_g) g \sigma}{{\rho_f}^2}} \tag{38}$$

Taitel et al [79] defined churn-turbulent flow as occurring when the liquid phase flowed in oscillations, with an unstable liquid film and liquid slugs collapsing on the Taylor bubbles. Experiments conducted by Taitel et al with 1 in. and 2 in. diameter pipes on the transition from slug flow to churn-turbulent flow showed that churn-turbulent flow was not a stable flow regime, but an entrance region phenomenon, which over a sufficiently long region of flow would become slug flow. Taitel et al started by examining the velocity of a Taylor bubble, which was found by Nicklin and Davidson [55] to be:

$$v_g = 1.2 v_f + 0.35 \sqrt{gD} \tag{39}$$

with the first term on the right side representing the liquid velocity at the center of the pipe and the second term on the right side of Equation 39 representing the velocity of a Taylor bubble in stagnant liquid, which had first been derived in the works of Davies and Taylor [20], as well as Dumitrescu. [22]

Taitel et al [79] noticed that previously documented research on slug flow by Govier and Aziz [30] and Akagawa and Sakaguchi [1] showed that the ratio of the length of the liquid slug at 8*D*. However, in their experiments, Taitel et al found that given sufficient pipe length, the liquid slug stabilized at 16*D*, concluding that previous observations showed two slugs that would merge into one given sufficient length. Taitel et al derived that the length of pipe necessary for the liquid slug to stabilize at 16*D* was:

$$l_e = 35.5 v_g \sqrt{\frac{D}{g}} \tag{40}$$

where l_e is the entrance length necessary for the liquid slugs to reach a length of $16D_H$.

When Equation 40 is combined with Equation 39, Taitel et al [79] derived that the transition between slug and churn-turbulent flow was a function of the volumetric flux, and occurred when the ratio between the pipe length and pipe diameter satisfied the criterion established in Equation 41.

$$\frac{L}{D} = 40.6\left(\frac{j_g + j_f}{\sqrt{gD}} + 0.22\right) \tag{41}$$

where *L* is the length of the pipe.

In addition to the bubbly, slug and churn-turbulent flow regimes, Taitel et al [79] also identified a separate finely-dispersed bubbly flow regime, where the turbulence within the liquid flow is enough to break apart the vapor bubbles and prevent them from merging. It was derived

by Taitel et al that the transition between bubbly flow and finely dispersed bubbly flow occurred when:

$$j_f = 4.0 \frac{D^{0.429} \left(\frac{\sigma_f}{\rho_f}\right)^{0.089}}{{\nu_f}^{0.072}} \left[\frac{g(\rho_f - \rho_g)}{\rho_g}\right]^{0.446} - j_g \quad 42$$

where ν_f is the kinematic viscosity of the liquid phase.

As discussed earlier, the maximum void fraction for bubbly flow is 0.52, which Taitel et al [79] derived to occur for finely dispersed bubbly flow when:

$$j_f = \frac{0.48 j_g}{0.52} \quad 43$$

In developing the equation used to determine the transition to annular flow, Taitel et al [79] considered a vapor core with liquid film along the wall. As droplets break off of the liquid film, the velocity of the vapor core must meet or exceed the terminal velocity of the droplets, otherwise, the droplets merge, and would ultimately form the liquid slugs characteristic of slug or churn-turbulent flow. Taitel et al calculated that the minimum superficial vapor velocity necessary to entrain liquid droplets was:

$$j_g = 3.1 \frac{\sqrt[4]{(\rho_f - \rho_g)\sigma g}}{\sqrt{\rho_g}} \quad 44$$

An example of Taitel et al's [79] flow regime map is provided in Figure 2. As the flow regime map relies on the physical properties of the vapor and liquid, along with the characteristics of the pipe and the flow of each phase, it has a distinct advantage over many other flow regime maps in that it has applicability beyond a particular vapor and liquid system over a narrow range of pipe diameters. Theoretically, it should be applicable to any two-phase vertical concurrent flow system.

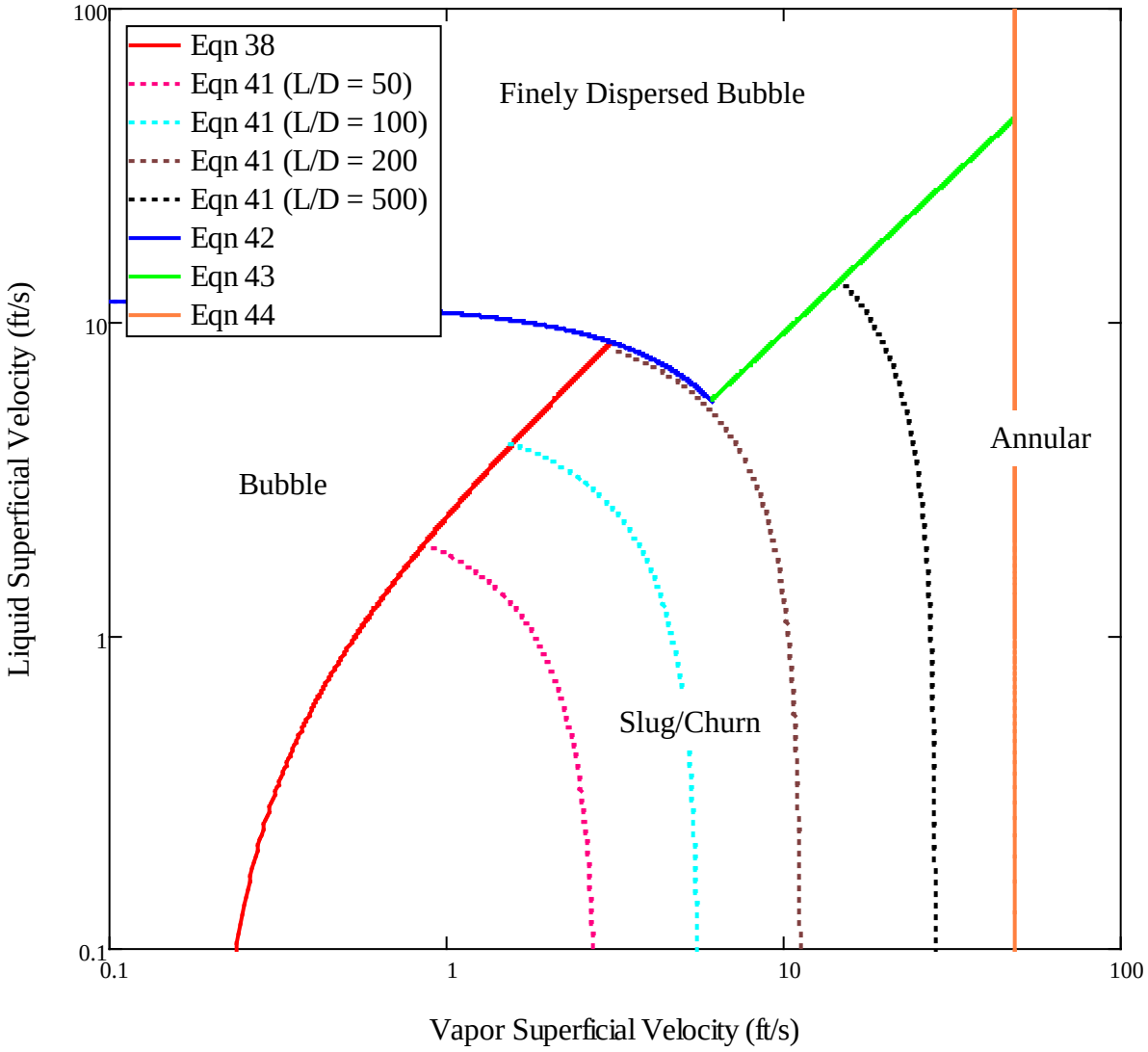

Figure 2: Taitel et al [79] Flow Regime Map for Air-Water Upflow in a 1 in. Diameter Pipe at 14.696 psia and 70°F

The first flow regime map that was developed using dimensionless parameters was by Kozloff [51], who studied air-water flow in a 1 in. diameter pipe. Kozloff found that two variables governed the transitions between flow regimes; the flow void fraction, β, and the total volumetric flux, j_K, which Kozloff non-dimensionalized into the form of the mixture Froude number, Fr_{mK}. Kozloff uses the flow void fraction rather than the static void fraction to calculate the average density of the two-phase mixture, which is then used to calculate the volumetric flux

and the mixture Froude number. To differentiate these calculations from other calculations for mixture density, total volumetric flux and mixture Froude number, an additional suffix *K* is used in Equations 46 through 48 that show how Kozloff formulated each parameter:

$$\beta = \frac{Q_g}{Q_g + Q_f} \tag{45}$$

$$j_K = \frac{4W}{\pi {D_H}^2 \rho_{mK}} \tag{46}$$

$$\rho_{mK} = \rho_f - \beta(\rho_f - \rho_g) \tag{47}$$

$$Fr_{mK} = \frac{{j_K}^2}{g D_H} \tag{48}$$

where *W* is the total mass flow rate.

Kozloff [51] observed six different flow regimes: Bubble, Plug, Dispersed Plug, Emulsion, Film-Emulsion and Drop flow. The bubble flow regime is described as being very similar to the bubbly flow that is described in most literary sources, and the plug flow regime is described similarly as slug flow. Dispersed plug flow is described as featuring pieces of the liquid breaking off from the wall film and liquid plugs, and falling through the large vapor bubbles, which is similar to the descriptions of churn-turbulent flow. Emulsion flow is described as a froth of liquid film that separates vapor bubbles that flow together within the pipe. Film emulsion flow is described to be similar to annular flow, with a vapor core flowing in the center of the pipe, while the liquid concentrates along the pipe wall forming a film, with small waves of liquid breaking off to form droplets within the vapor core. Finally, drop flow is described as being similar to mist flow, with only a small liquid film along the wall that flows with the vapor with very few and very small waves that break off.

Kozloff [51] published both a chart that depicted the boundaries between each flow regime, along with a series of equations that can be used to model the flow regime boundaries. However, the equations proposed do not appear to match the lines that are presented by Kozloff. The boundary for the bubble and plug flow regimes is:

$$\beta = 0.05 {Fr_{mK}}^{0.2} \quad 49$$

The boundary between the plug flow regime and the dispersed plug flow regime is: [51]

$$\beta = 0.12 {Fr_{mK}}^{0.15} \quad 50$$

The equation for modeling the boundary between dispersed plug flow and emulsion flow is: [51]

$$\beta = 0.5 {Fr_{mK}}^{0.1} \quad 51$$

The boundary between emulsion flow and film emulsion flow is modeled as: [50]

$$\beta = 0.65 {Fr_{mK}}^{0.05} \quad 52$$

Finally, the line that marks the boundary between film emulsion and drop flow is modeled as: [51]

$$\beta = 0.85 {Fr_{mK}}^{0.02} \quad 53$$

Kozloff's [51] flow regime map, using Equations 49 through 53, is given in Figure 3.

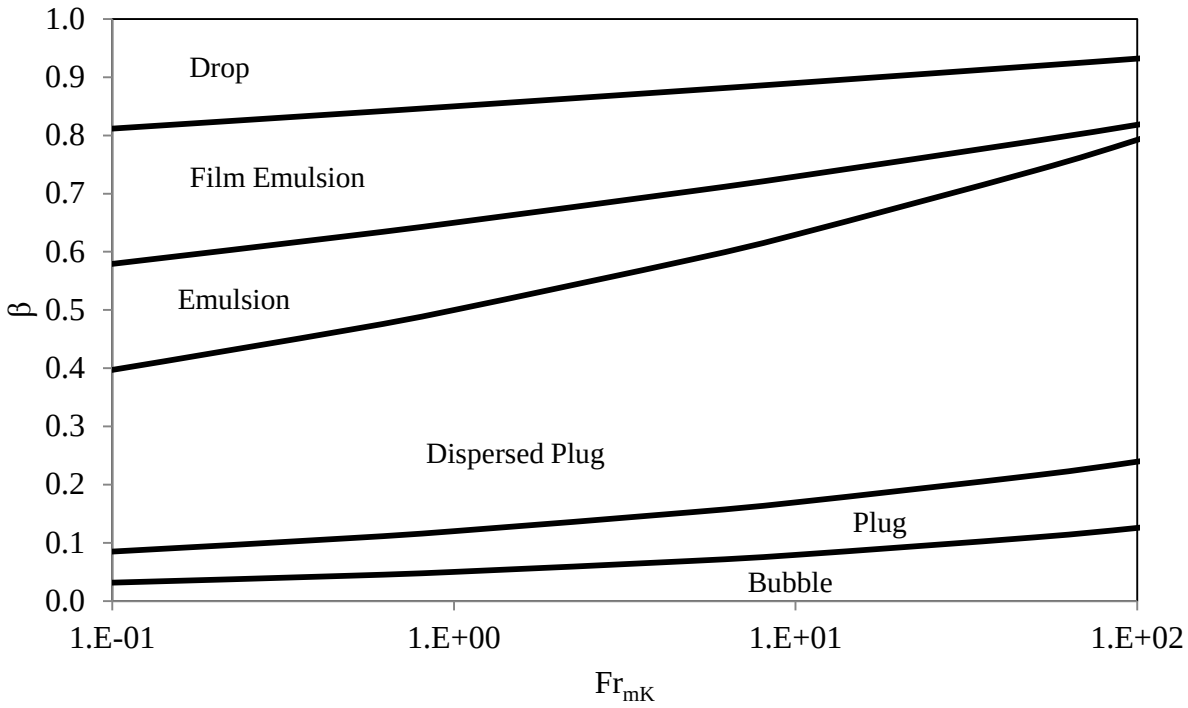

Figure 3: Kozloff's [51] Flow Regime Map Using Equations 49 through 53

Griffith and Wallis [33] proposed the flow regime map shown in Figure 4, based on their observations with air-water slug flow and its transitions with bubbly and annular flow. The mixture Froude number, Fr_m, and flow void fraction were selected as coordinates based on the work of Kozloff [51]. The mixture Froude number is calculated using Equation 54.

$$Fr_m = \frac{\left(\frac{Q_g - Q_f}{A}\right)^2}{gD_H} \tag{54}$$

where A is the cross-sectional area of the pipe.

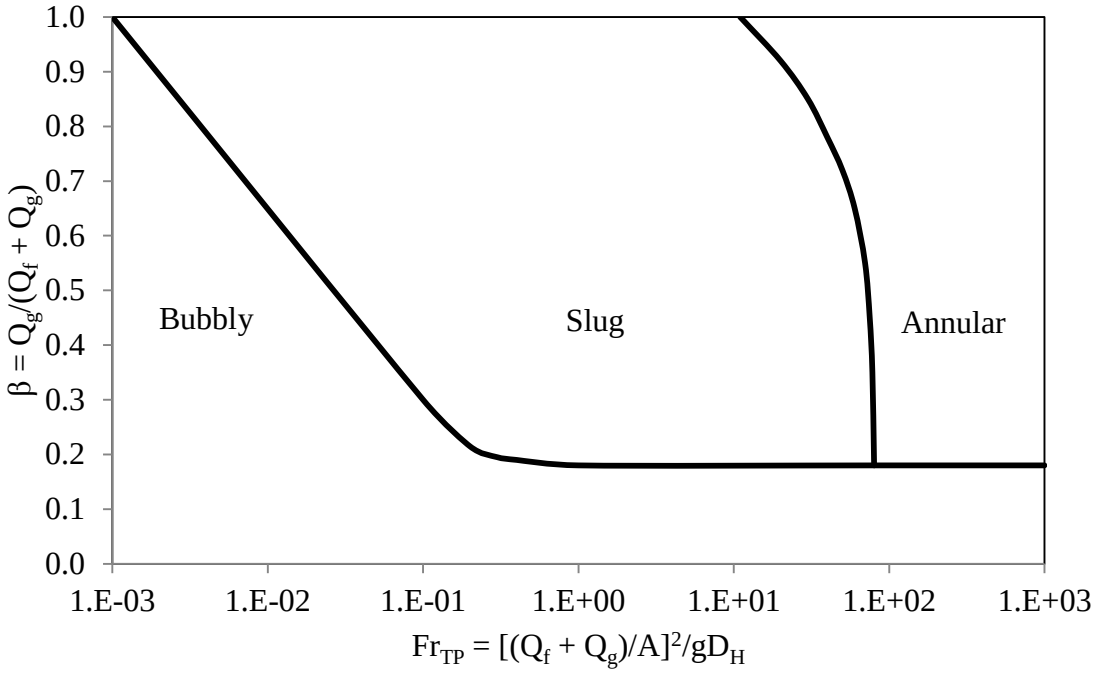

Figure 4: Flow Regime Map Proposed by Griffith and Wallis [33]

Griffith and Wallis [33] found slug flow to be the most stable flow regime, noting that when two-phase flow entered a slug flow pattern that the conditions had to change very significantly to attain a different flow regime. The bubbly-slug flow regime transition was determined based on the observation that bubbles were unlikely to coalesce into slugs for void fractions less than 0.18, although some slug data points fell within the bubbly region. The slug-annular flow transition was identified as the upper boundary of the slug data points that Griffith and Wallis identified, as there were no observations of annular flow in their study.

Oshinowo and Charles [59,60] developed the flow regime map shown in Figure 5, drawing inspiration from the work of Kozloff [51] and Griffith and Wallis [33], among others. However, in correlating their data for varying concentrations of glycerol in water, it was found that some modifications to the coordinates were necessary. Oshinowo and Charles found that as the properties of the liquid phase changed with changing concentrations of glycerol, there was a shift in the flow regime boundaries, with respect to the mixture Froude number. It was

determined that in order to account for this shift, a modifier could be applied to the mixture Froude number, which Oshinowo and Charles developed as a property constant, Λ, which is defined as:

$$\Lambda = \frac{\mu_s}{\sqrt[4]{S_L \sigma_s{}^3}} \tag{55}$$

where μ_s is the specific viscosity of the liquid, S_L is the specific gravity of the vapor and σ_s is the specific surface tension of the liquid.

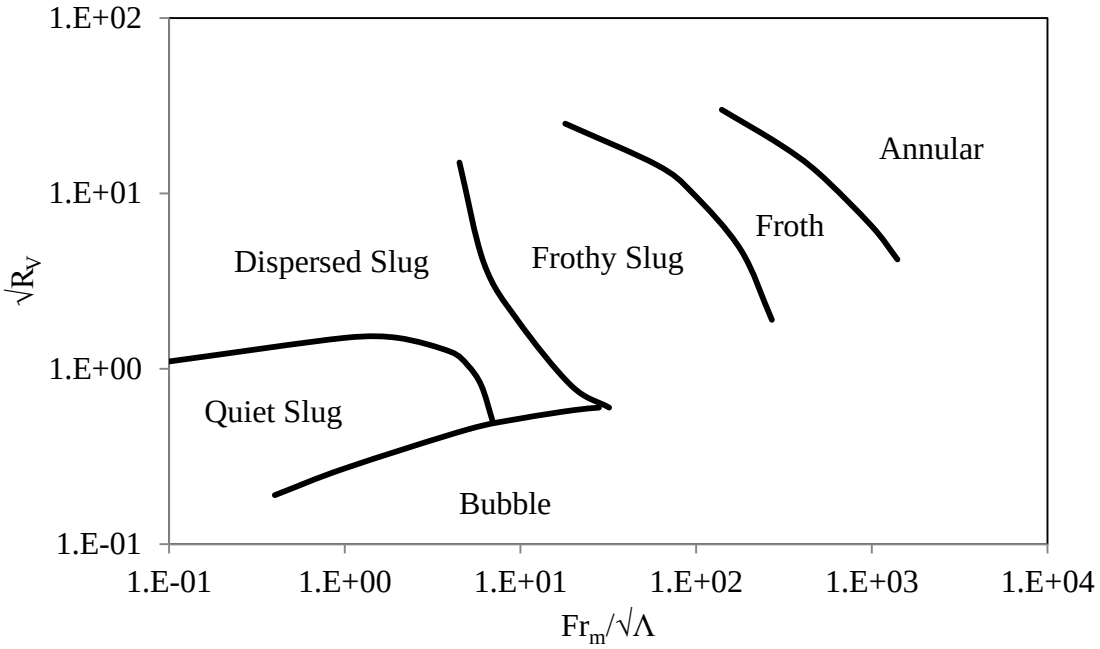

Figure 5: Oshinowo and Charles [59,60] Flow Regime Map for Two-Phase Vertical Upflow

Rather than correlating the mixture Froude number with the flow void fraction, Oshinowo and Charles [59,60] chose to correlate the flow regimes against the ratio of vapor volumetric flow to liquid volumetric flow, R_V, which is shown in Equation 56. The ratio was chosen because it allowed for greater sensitivity when the flow rate of the vapor phase was high.

$$R_V = \frac{Q_g}{Q_f} = \frac{\beta}{1-\beta} \tag{56}$$

2.1.3: Interphase Friction Models

Presently, when interphase friction is modeled in two-phase flow, there are two approaches that are used. The first approach is the drag coefficient method, where the interphase friction force between the two phases is modeled as if one phase is causing drag on the other. The second approach is the drift flux method, with which the velocity difference between the phases is described as the difference between the velocity of the dispersed phase and the volumetric flux of the mixture as a whole. [69] RELAP5/MOD2 [66] only uses the drag coefficient method for calculating interphase friction. RELAP5/MOD3.3 [40,69] and RELAP5-3D [67] use the drift flux method for calculating interphase friction for vertical bubbly and slug flow, while the drag coefficient method is used for annular and mist flow. TRACE [83] also uses a combination of the drift flux and drag coefficient methods for calculating the interphase friction.

2.1.3.1: Drag Coefficient Model

The drag coefficient model is based on the concept that the drag force that acts on a single stationary object with an infinite fluid that moves past the object at a velocity, *v*, is defined by Equation 57:

$$F_D = \frac{1}{2} C_D \rho v^2 A \qquad 57$$

where F_D is the drag force, C_D is the drag coefficient, ρ is the density of the fluid and A is the projected area of the object. [54]

Ishii and Chawla [42] applied the drag force equation to an individual spherical object moving within an infinite fluid using Equation 58:

$$F_D = \frac{1}{2} C_D \rho |v_r| v_r \pi {r_d}^2 \qquad 58$$

where ρ_c is the density of the infinite fluid, v_r is the relative velocity between the object and the infinite fluid and r_d is the radius of the spherical object.

From Equation 58, Ishii and Chawla [42] established drag coefficients for four different two-phase flow regimes; Undistorted Particles, Distorted Particles, Churn-Turbulent Bubbles and Slug Flow.

Ishii and Chawla [42] defined the undistorted particle regime as having spherical bubbles within a continuous liquid flow, such that the bubbles experienced little to no deformation either from bubble instability or from turbulence within the liquid. This would be akin to bubbly flow identified previously. The drag coefficient for undistorted particle flow is given in Equation 59, with the particle Reynolds number defined in Equation 60 and the mixture viscosity for bubbly flow defined in Equation 61.

$$C_D = \frac{24}{Re}(1 + 0.1Re^{0.75}) \tag{59}$$

$$Re = \frac{2\rho_f|\Delta v|r_d}{\mu_m} \tag{60}$$

$$\mu_m = \frac{\mu_f}{1-\alpha} \tag{61}$$

where ρ_f is the density of the liquid, Δv is the velocity difference between the liquid and the bubble, r_d is the average radius of the bubbles, μ_f is the dynamic viscosity of the liquid and α is the vapor volume fraction within the two-phase flow.

The resulting interphase drag force for undistorted bubbles in liquid is:

$$F_D = -\frac{1}{2}\left[\frac{24(1.0 + 0.1Re^{0.75})}{Re}\right]\rho_f|\Delta v|\Delta v\pi {r_d}^2 \tag{62}$$

With increasing flow, turbulent eddies can form, particularly in the wake of other bubbles. The flow regime changes to what Ishii and Chawla [42] identify as the distorted

particle regime. Drag on the bubbles increases in this flow regime, and the drag coefficient is calculated as:

$$C_D = \frac{4}{3} r_d \sqrt{\frac{(\rho_f - \rho_g)g}{\sigma}} \left[\frac{1 + 17.67(1-\alpha)^{1.3}}{18.67(1-\alpha)^{1.5}}\right]^2 \quad 63$$

where ρ_g is the density of the vapor in the bubble and σ is the surface tension of the liquid.

For the distorted particle regime, the interphase drag force is: [42]

$$F_D = -\frac{2}{3} \sqrt{\frac{(\rho_f - \rho_g)g}{\sigma}} \left[\frac{1 + 17.67(1-\alpha)^{1.3}}{18.67(1-\alpha)^{1.5}}\right]^2 \rho_f |\Delta v| \Delta v \pi {r_d}^3 \quad 64$$

As the size of the bubbles increase, the boundary layers of the bubbles and their wake increase to the extent that they overlap. This increased influence of the boundary layer and wake on other bubbles means that the bubbles flow with respect to the total volumetric flux of the two-phase flow, rather than the average liquid velocity alone. Therefore, Ishii and Chawla [42] concluded that the drag coefficient for this flow regime, named the churn-turbulent flow regime, should be based on the drift velocity, v_{gj}, rather than the velocity difference, Δv. As such, the drag coefficient in terms of the drift velocity for churn-turbulent flow is:

$$C_D = \frac{8}{3} \quad 65$$

Thus, the interphase drag force is: [42]

$$F_D = -\frac{4}{3} \rho_f |v_{gj}| v_{gj} \pi {r_d}^2 \quad 66$$

However, as Equation 15 shows: [42]

$$v_{gj} = (1-\alpha)(v_g - v_f) \quad 67$$

Thus, in terms of the velocity difference, the drag coefficient for churn-turbulent flow becomes: [42]

$$C_D = \frac{8}{3}(1-\alpha)^2 \quad (68)$$

The interphase drag force as a function of the velocity difference is: [42]

$$F_D = -\frac{4}{3}(1-\alpha)^2\rho_f|\Delta v|\Delta v\pi {r_d}^2 \quad (69)$$

As the size of the bubbles continue to grow, eventually they attain a diameter that is roughly that of the pipe and can become significantly longer than they are wide. Liquid exists only in a thin film between bubble and the pipe wall, and in liquid slugs that separate the bubbles from each other, hence the name slug flow. Ishii and Chawla found that the interphase drag coefficient for slug flow is: [42]

$$C_D = 9.8(1-\alpha)^3 \quad (70)$$

The interphase drag force for slug flow is: [42]

$$F_D = -\frac{1}{2}9.8(1-\alpha)^3\rho_f|\Delta v|\Delta v\pi {r_d}^2 \quad (71)$$

2.1.3.2: Drift-Velocity Model

The drift-velocity model for predicting interphase friction is based on the concept that the dispersed phase in two-phase flow experiences drag against the total volumetric flux, rather than the velocity of the continuous phase. Thus, the velocity difference that is used to calculate the interphase friction for the two-phase flow is not the relative velocity, v_g-v_f, but the vapor drift velocity, v_{gj}. While based on the drift flux model for two-phase flow, the drift-velocity interphase friction model has been developed for use in separated flow models, such as TRACE [83] and RELAP5/MOD3.3. [69,70]

The drift-velocity model defines the interphase friction force as: [69,70,83]

$$F_{INT} = -C_i|v_{gj}|v_{gj} \quad (72)$$

In order to determine the interphase friction coefficient, C_i, a simplified force balance is conducted on the vapor and liquid phases, given in Equations 73 and 74 respectively. [69,70,83]

$$0 = \alpha \frac{dP}{dz} - \alpha \rho_g g + F_{INT} \quad (73)$$

$$0 = (1-\alpha) \frac{dP}{dz} - (1-\alpha) \rho_f g - F_{INT} \quad (74)$$

By multiplying Equation 73 by (*1-α*) and Equation 74 by *–α*, and summing the two equations together, a relationship is obtained between the interphase friction force and the density difference and is given in Equation 75. [69,70,83]

$$F_{INT} = -\alpha(1-\alpha)\left(\rho_f - \rho_g\right) g \quad (75)$$

Thus the interphase friction coefficient, C_i, is defined as: [67,68,81]

$$C_i = \frac{\alpha(1-\alpha)\left(\rho_f - \rho_g\right) g}{\left|v_{gj}\right| v_{gj}} \quad (76)$$

Correlations are used to determine the value of the vapor drift velocity, v_{gj}, based on Equation 77 that was first proposed by Zuber and Findlay [89]:

$$v_{gb} = \frac{\langle j_g \rangle}{\langle \alpha \rangle} = C_0 \langle j \rangle + \frac{\langle \alpha v_{gj} \rangle}{\langle \alpha \rangle} \quad (77)$$

where v_{gb} is the void-fraction weighted vapor velocity, $\langle j_g \rangle$ is the area-averaged volumetric flux of the vapor phase, as defined in Equation 11 and C_0 is a distribution parameter.

The distribution parameter, C_0, is used to account for unequal distributions of vapor within the two-phase flow. When $C_0 = 1$, vapor is equally distributed between the wall and the center of the pipe. For $C_0 > 1$, there is more vapor in the core of the two-phase flow, and less vapor at the wall, while $C_0 < 1$ indicates that there is more vapor at the wall than in the center of the pipe. Zuber and Findlay [89] defined the distribution parameter as:

$$C_0 = \frac{\langle \alpha j \rangle}{\langle \alpha \rangle \langle j \rangle} \quad (78)$$

As the distribution coefficient, C_0, and the vapor drift velocity, v_{gj}, can be difficult to determine from Equation 77, several correlations have been developed to predict C_0 and v_{gj}, so that the interphase friction force can be determined using the drift-velocity method. RELAP5/MOD3.3 [40,69] uses several of these correlations under varying circumstances and these correlations are described in detail in Section 2.3.2.3.1.

2.1.4: Interfacial Area Transport

The transfer of mass, momentum or energy from one phase to another in a two-phase flow system is proportional to two different parameters; the force that drives the transfer from one phase to the other, and the interfacial area through which the transfer occurs. Interphase friction represents a transfer in momentum from one phase to the other, driven by the equal and opposite forces that occur on each phase along the interface. However, the amount of interphase friction that occurs is also a product of how much interface there is between the two phases. In all thermal hydraulic codes that have been studied, the interfacial area is determined by a set of equations that differ based on the flow regime. While the equations may be accurate for their given flow regime, they rely on several assumptions and simplifications that limit their usefulness. [44,45]

The interfacial area transport equation (IATE) represents a more recent development of modeling the interphase exchanges of mass, momentum and energy. It is designed to predict the interfacial area between the phases in bubbly, slug and churn-turbulent flow, by using a set of equations that can adjust to the transient conditions of the two-phase flow more readily than steady-state flow regime based correlations that are presently used in most thermal-hydraulic codes. [44,45]

There are two forms of the IATE; a one-group equation that is designed for bubbly flow, and the two-group equations, for which one equation is used to model the bubbles that are mostly spherical, while a second equation is used to model Taylor bubbles characteristic of slug flow, as well as churn-turbulent flow. [44]

The one-group IATE is:

$$\frac{\partial a_i}{\partial t} + \nabla \cdot (a_i \overrightarrow{v_i}) = \frac{2}{3}\frac{a_i}{\alpha}\left[\frac{\partial \alpha}{\partial t} + \nabla \cdot \left(\alpha \overrightarrow{v_g}\right)\right] + \frac{1}{3\psi}\left(\frac{\alpha}{a_i}\right)^2 \left[R_{TI} - R_{RC} - R_{WE} + R_{ph}\right] \quad (79)$$

where a_i is the interfacial area per unit volume, v_i is the velocity of the interphase, v_g is the average velocity of the vapor phase, ψ is a shape factor, R_{TI} is the interfacial area source term for bubbles created through break up in eddies, R_{RC} is a sink term for bubbles that merge when colliding in eddies, R_{WE} is a sink term for bubbles that merge by one overtaking the other in the leading bubble's wake and R_{ph} is a source term for bubbles of the same chemical nature as the liquid that form through nucleate boiling at the pipe wall. [44,45] The terms on the left side of the equation represent the total derivative of the interfacial area with respect to time and space. Meanwhile, the first term on the right, which includes the total derivative of the void fraction, represents the change in interfacial area per unit volume due to the changing of the bubble size caused by pressure changes. [44]

The weakness of the one-group IATE is that it only can model the interfacial area concentration for two-phase flow involving small bubbles, as the physics that govern larger bubbles that occur with slug and churn-turbulent differ from those of smaller spherical or

distorted bubbles. Thus, a two-group IATE was developed, that differentiates between bubbles that are smaller or larger than a critical volume, V_c, for which:

$$V_c = \frac{\pi {D_{d,max}}^3}{6} \tag{80}$$

where $D_{d,max}$ represents the maximum distorted bubble diameter. Ishii and Zuber [45] defined the maximum distorted bubble diameter as:

$$D_{d,max} = 4\sqrt{\frac{\sigma}{(\rho_f - \rho_g)g}} \tag{81}$$

In the two-group IATE, the maximum distorted bubble diameter is factored through a non-dimensionalized parameter that is the ratio of the maximum distorted bubble diameter to that of the Sauter mean diameter of the bubbles of Group 1, D_{sm1}, and is shown in Equation 82:

$${D_{c1}}^* = \frac{D_{d,max}}{D_{sm1}} \tag{82}$$

The two-group IATE is:

$$\begin{aligned} &\frac{\partial a_{i1}}{\partial t} + \nabla \cdot (a_{i1}\overrightarrow{v_{i1}}) \\ &\quad = \left(\frac{2}{3} - C{D_{c1}}^{*2}\right)\frac{a_{i1}}{\alpha_1}\left[\frac{\partial \alpha_1}{\partial t} + \nabla \cdot \left(\alpha_1 \overrightarrow{v_{g1}}\right) - \eta_{ph1}\right] + \sum_j \phi_{j,1} \\ &\quad + \phi_{ph} \end{aligned} \tag{83}$$

$$\begin{aligned} &\frac{\partial a_{i2}}{\partial t} + \nabla \cdot (a_{i2}\overrightarrow{v_{i2}}) \\ &\quad = \frac{2}{3}\frac{a_{i2}}{\alpha_2}\left[\frac{\partial \alpha_2}{\partial t} + \nabla \cdot \left(\alpha_2 \overrightarrow{v_{g2}}\right) - \eta_{ph2}\right] \\ &\quad + C{D_{c1}}^{*2}\frac{a_{i1}}{\alpha_1}\left[\frac{\partial \alpha_1}{\partial t} + \nabla \cdot \left(\alpha_1 \overrightarrow{v_{g1}}\right) - \eta_{ph1}\right] + \sum_j \phi_{j,2} + \phi_{ph2} \end{aligned} \tag{84}$$

where the subscripts 1 and 2 represent the group of bubbles that the parameter represents, C is a coefficient used to model exchanges between the groups that can be caused by changes in pressure or phase, η_{ph1} and η_{ph2} represent changes in phase that occur as a result of changes in pressure for each given group, $\phi_{j,1}$ and $\phi_{j,2}$ represent the source and sink terms that are described by R_{TE}, R_{RC} and R_{WE} in the one-group IATE, and ϕ_{ph1} and ϕ_{ph2} represent the source terms from phase change occurring as a result of nucleate boiling along the wall. The terms η_{ph2} and ϕ_{ph2} can be neglected under normal conditions, as Taylor and churn-turbulent bubbles are very unlikely to be produced through nucleate boiling, or condense before shrinking to Group 1 bubbles. [45]

2.2: Dimensionless Parameters

One of the great challenges with studying fluid flow is that there are several different properties that govern the behavior of the flow, even when considering only a single, homogeneous phase. When an experiment is conducted with single-phase flow, dimensional results are only valid for the conditions under which the experiment was conducted, and it can be difficult to compare results from different studies, even if most of the conditions are the same. However, if the results can be normalized in such a way that made the conditions as similar as possible, then comparison of the results between different studies is possible. Non-dimensionalization is the process of determining the ratio of two qualities of a particular fluid flow that are equal in dimension, resulting in a dimensionless quality that can be compared against data attained under varying conditions to develop more universal correlations. [54]

Among the more common dimensionless parameters that are used for fluid flow are the Reynolds number, the Froude number and the Weber number.

The Reynolds number, *Re*, is defined as the ratio of the inertial force to the viscous force of a given fluid flow, and is used in many applications in fluid flow. For single phase flow is determined using Equation 85:

$$Re = \frac{\rho v l}{\mu} \tag{85}$$

where ρ is the density of the fluid, v is the velocity at which the fluid is moving, l represents a characteristic length of the fluid flow, usually length along an object or diameter in a pipe, and μ is the dynamic viscosity of the given fluid. [54]

The Froude number, *Fr*, is defined as the ratio of the inertial force of a fluid flow to the gravitational force.

$$Fr = \frac{v^2}{gl} \tag{86}$$

where g is the gravitational acceleration and l is the characteristic length.

The Weber number, *We*, represents the ratio of the inertial forces to the surface tension of the fluid.

$$We = \frac{\rho v^2 l}{\sigma} \tag{87}$$

where σ represents the surface tension of the fluid.

A common approach to studying fluid flow with dimensionless parameters is the Buckingham Pi Theorem. According to Buckingham Pi Theorem, for a given equation where there are k variables that are dimensionally homogeneous, and r independent dimensions, then the equation can be reduced to being a function of k-r independent dimensionless variables, also known as pi terms. To apply the Buckingham Pi Theorem to solve for a given dependent variable, one must first identify all of the relevant variables, including the dependent variable, along with the dimensions of each variable. Once the quantity of relevant variables and

dimensions is known, the number of dimensionless variables can be established. The relevant variables are then divided into two groups, one with *k-r* variables that are used only once, and the other with *r* variables that are used repeatedly. One requirement of the repeating variables is that they should be chosen such that when raised to the power of a nonzero integer, the repeating variables cannot be multiplied together to form a dimensionless value, a condition known as being dimensionally independent. Each non-repeating variable, raised to the power of a nonzero integer, is multiplied by all of the repeating variables, each raised to the power of a nonzero integer, so that the product results in a dimensionless parameter, becoming a pi term. The net result should be a collection of pi terms, where the pi term containing the dependent variable is a function of the other pi terms. [54]

There has been very limited use of the Buckingham Pi Theorem to two-phase liquid vapor flow, which is likely due to the fact that there is little agreement as to which dimensionless variables best represent two-phase flow. Balasubramianiam et al [6] developed a generalized Buckingham Pi theorem derivation using the variables: j_f, j_g, μ_f, μ_g, ρ_f, ρ_g, σ, D, g and φ, where φ is the angle at which the flow is occurring. With ten independent variables and three dimensions (mass, length and time), a set of seven dimensionless variables was proposed by Balasubramianiam et al, acknowledging that more than one set could be derived for the given variables and dimensions.

$$Re_{fs} = \frac{\rho_f j_f D}{\mu_f} \qquad Re_{gs} = \frac{\rho_g j_g D}{\mu_g} \qquad Fr_f = \frac{\rho_f - \rho_g}{\rho_f}\frac{gD}{{j_f}^2}$$

$$We_f = \frac{\rho_f {j_f}^2 D}{\sigma} \qquad \frac{\mu_g}{\mu_f} \qquad \frac{\rho_g}{\rho_f}$$

$$\varphi$$

In addition to application of the Buckingham Pi Theorem, Balasubramianam et al [6] cited three other dimensionless parameters that are important to consider with two-phase flow; the slip ratio, *S*, the Suratman number, *Su*, and the Bond number, *Bo*, which are defined in Equations 88 through 90:

$$S = \frac{j_g}{j_f} \tag{88}$$

$$Su = \frac{{Re_{fs}}^2}{We_f} = \frac{\rho_f D \sigma}{{\mu_f}^2} \tag{89}$$

$$Bo = \frac{(\rho_f - \rho_g) g D^2}{\sigma} \tag{90}$$

Of course there are many more dimensionless parameters that have been used to describe different phenomena with two-phase flow, than those mentioned by Balasubramianiam et al [6]. With regards to interphase friction, the most meaningful work with dimensionless parameters has come in form of the drag coefficient, C_D, which is shown to be a function of the particle Reynolds number for small spherical bubbles, and the void fraction for larger Taylor bubbles in Section 2.1.3.1.

2.3: Nuclear Thermal Hydraulic Models

Several thermal hydraulic codes have been developed with the purpose of modeling the behavior of nuclear power plants during both steady-state operation and during transient events. The two most well-known and widely used thermal hydraulics codes are RELAP and TRACE, and have served as the focus of this study. In the following sections regarding each model, only the manual was available for RELAP5/MOD2 [66], RELAP5-3D [67] and TRACE [83], and so the equations and calculations that are presented for those models are based solely on the manual for those codes. However, upon obtaining the source code for RELAP5/MOD3.3 [40], it was

discovered that the descriptions of the equations in the manual [69] did not necessarily provide a completely accurate description of the equations as they are used in the source code. Thus, the equations that are presented for RELAP5/MOD3.3 are those that are in the source code, with additional description provided by the manual.

2.3.1: RELAP5/MOD2

RELAP5/MOD2 [66] was developed in the early 1980s as an improvement on RELAP5/MOD1 which had been released in 1980. RELAP5/MOD1 was the first version of RELAP to model two-phase flow with a nonhomogeneous, non-equilibrium model. RELAP5/MOD2 was the first version of RELAP for which a two-fluid nonhomogeneous, non-equilibrium model was developed, utilizing conservation equations of mass, momentum and energy for each phase.

2.3.1.1: Separated Flow Model

The continuity equation for the vapor phase in RELAP5/MOD2 [66] is:

$$\frac{\partial(\alpha\rho_g)}{\partial t}+\frac{1}{A}\frac{\partial(\alpha\rho_g v_g A)}{\partial z}=\Gamma_g \qquad 91$$

where Γ_g represents the change in mass with respect to time for a given volume, the second term is the change in vapor mass due to advection and the term on the right side of the equation is the vapor mass created from phase change.

The continuity equation for the liquid phase in RELAP5/MOD2 [66] is similar to that for the vapor continuity equation given in Equation 88, as the each term carries the same physical meaning as it vapor phase counterpart. Note that the vapor generation term is in the opposite direction for Equation 89, as it is implied that the vapor generated is being produced from evaporating liquid:

$$\frac{\partial\left((1-\alpha)\rho_f\right)}{\partial t}+\frac{1}{A}\frac{\partial\left((1-\alpha)\rho_f v_f A\right)}{\partial z}=-\Gamma_g \tag{92}$$

The conservation of momentum for the vapor phase in RELAP5/MOD2 [64] is:

$$\begin{aligned}\alpha\rho_g A\frac{\partial v_g}{\partial t}+\frac{1}{2}\alpha\rho_g A\frac{\partial {v_g}^2}{\partial z}&\\ =-\alpha A\frac{\partial P}{\partial z}&\\ +\alpha\rho_g g\sin(\theta)A-\left(\alpha\rho_g A\right)FWGv_g+\Gamma_g A\left(v_{gI}-v_g\right)&\\ -\left(\alpha\rho_g A\right)FIG\left(v_g-v_f\right)-C\alpha(1-\alpha)\rho A\frac{\partial\left(v_g-v_f\right)}{\partial t}&\end{aligned} \tag{93}$$

where the terms on the left side of Equation 93 represent the time rate of change in momentum and the change with respect to position in the pipe. On the right side of Equation 93 are terms for the pressure gradient, body force, wall friction, momentum transfer due to mass transfer, interphase friction and the virtual mass force, respectively.

As was the case with the continuity equations, the conservation of momentum for the liquid phase in RELAP5/MOD2 [66] has the same terms as the conservation of momentum for the vapor phase. Although calculating each term varies based on the properties of the liquid and can vary in direction, as is the case with the momentum transfer due to mass transfer. The conservation of momentum for the liquid phase is given in Equation 94.

$$\begin{aligned}(1-\alpha)\rho_f A\frac{\partial v_f}{\partial t}+\frac{1}{2}(1-\alpha)\rho_f A\frac{\partial {v_f}^2}{\partial z}&\\ =-(1-\alpha)A\frac{\partial P}{\partial z}+(1-\alpha)\rho_f g\sin(\theta)A&\\ -\left[(1-\alpha)\rho_f A\right]FWFv_f-\Gamma_g A\left(v_{fI}-v_f\right)&\\ -\left[(1-\alpha)\rho_f A\right]FIF\left(v_f-v_g\right)-C(1-\alpha)\alpha\rho A\frac{\partial\left(v_f-v_g\right)}{\partial t}&\end{aligned} \tag{94}$$

2.3.1.2: Flow Regime Map

The vertical flow regime map for pre-Critical Heat Flux (CHF) flow that is employed by RELAP5/MOD2 [66] is primarily based on the work of Vince and Lahey [85] and of Taitel et al [81]. Flow is divided into three flow regimes: bubbly, slug and annular, and the thresholds are a function of the mass flux and the void fraction.

In order to determine the bubbly-slug transition void fraction, α_{BS}, in RELAP5/MOD2 [66], the flow has been divided into three categories, a low mass flux category (less than 410 lb_m/ft^2-s or 2000 kg/m^2-s), a high mass flux category (greater than 614 lb_m/ft^2-s or 3000 kg/m^2-s), and an intermediate category (between 410 lb_m/ft^2-s and 614 lb_m/ft^2-s). These divisions are based on the work of Taitel et al [79], which identified two different types of bubbly flow that occur at different volumetric fluxes, bubbly flow at low volumetric fluxes and finely dispersed bubbly flow, which occurs at high volumetric fluxes. The intermediate category serves as a transitional zone from the bubbly flow to the finely dispersed bubbly flow, and the value for α_{BS} is interpolated between that for bubbly flow and for finely dispersed bubbly flow.

Taitel et al [79] generally considered that the transition from bubbly flow to slug flow occurred at a void fraction of approximately 0.25, which serves as the maximum value of α_{BS} for RELAP5/MOD2 [66] at low mass fluxes. An additional limit is placed on the bubbly-slug transition void fraction for low mass fluxes, that limits the velocity of a small bubble that is rising in a vertical pipe to be less than or equal to that of a Taylor bubble. If the velocity of a small bubble were to exceed that of a large bubble then it would merge with the Taylor bubble, and the bubbly flow would transition into slug flow. The velocities of the small bubble and the Taylor bubble are determined using Equations 95 and 96:

$$v_{sb} = 1.53 \sqrt[4]{\frac{(\rho_f - \rho_g) g \sigma}{{\rho_f}^2}} \quad (95)$$

$$v_{tb} = 0.35 \sqrt{\frac{(\rho_f - \rho_g) g D}{\rho_f}} \quad (96)$$

where v_{sb} is the velocity of a rising small bubble in a pipe and v_{tb} is the velocity of a Taylor bubble rising in a pipe.

When we combine Equations 95 and 96 into the inequality, $v_{sb} \leq v_{tb}$, and solve for the pipe diameter, D, we find that the in order for bubbly flow to occur, a minimum criterion of the dimensionless pipe diameter or Bond number, D^*, must be true and is given in Equation 97: [66]

$$D^* = D \sqrt{\frac{(\rho_f - \rho_g) g}{\sigma}} \geq 19 \quad (97)$$

The relationship given by Equations 95 through 97 imply that for similar thermodynamic conditions, Taylor bubbles will travel at slower speeds in a small diameter pipe than that with a larger diameter, while the velocity of the small bubbles would be constant in either scenario. This means that in smaller diameter pipes, small bubbles are more likely to meet or exceed the velocity of Taylor bubbles, causing small bubbles to merge into Taylor bubbles. Thus, the transitional void fraction for bubbly-slug flow at low mass fluxes is given in Equation 98. The ratio of the Bond number to its critical value of 19 is raised to the eighth power for the purpose of smoothing the transition from 1 to the ratio. [66]

$$\alpha_L = 0.25 \times \min\left(1.0, \left(\frac{D^*}{19}\right)^8\right) \quad (98)$$

Taitel et al [79] also discussed a form of bubbly flow that they called finely dispersed bubbly flow, which occurred at higher volumetric fluxes than regular bubbly flow. For these scenarios, a maximum void fraction for which finely dispersed bubbly flow could occur was

identified as 0.54, however, in RELAP5/MOD2 [66] in this was simplified to 0.5 for a mass flux greater than 614 lb_m/ft^2-s. In summary,

$$\alpha_{BS} = \begin{cases} \alpha_L \, if \; G \leq 410 \dfrac{lb_m}{ft^2 s} \\ \alpha_L + \dfrac{0.5 - \alpha_L}{204 \dfrac{lb_m}{ft^2 s}} \times \left(G - 410 \dfrac{lb_m}{ft^2 s} \right) if \; 410 \dfrac{lb_m}{ft^2 s} < G < 614 \dfrac{lb_m}{ft^2 s} \\ 0.5 \, if \; G \geq 614 \dfrac{lb_m}{ft^2 s} \end{cases} \quad 99$$

where *G* is the mass flux through the pipe defined as:

$$|G| = \left| \alpha \rho_g v_g + (1 - \alpha) \rho_f v_f \right| \quad 100$$

The slug-annular flow regime transition void fraction, α_{SA}, is based on the vapor velocity necessary in the core of annular flow for which liquid droplets can be entrained, as determined by Taitel et al [79]. However, a coefficient of 1.4 was found to produce more accurate results in RELAP5/MOD2 [66] code assessments than the derived value of 3.1. Additionally, α_{SA} has a constraint that prevents the transition from occurring at a void fraction of less than 0.75. In summary:

$$\alpha_{SA} = \max \left(0.75, \frac{1.4 \sqrt[4]{(\rho_f - \rho_g) g \sigma}}{v_g \sqrt{\rho_g}} \right) \quad 101$$

A sample RELAP5/MOD2 [64] flow regime map is shown in Figure 6. For this particular flow regime map, steam-water at 65 psia is flowing through a 1.75 in. diameter pipe.

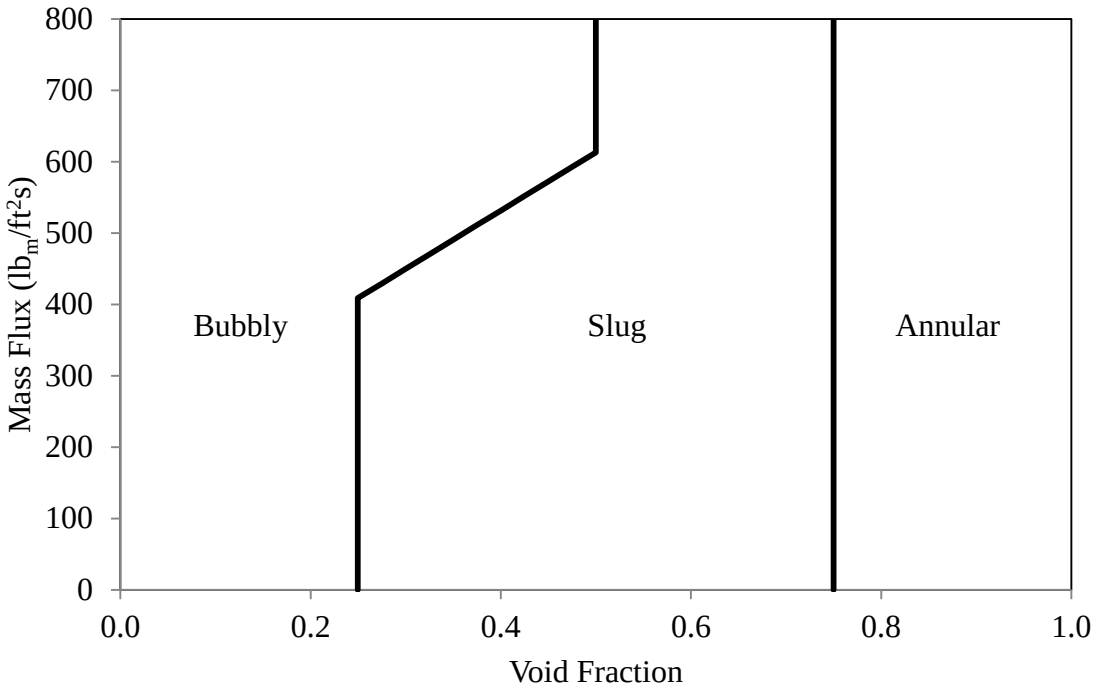

Figure 6: Sample Flow Regime Map for RELAP5/MOD2 [66]

2.3.1.3: Interphase Friction Model

In RELAP5/MOD2, [66] the drag coefficient method is used to determine the interphase friction for all three flow regimes. The general equation for determining the interphase friction is:

$$FI_{gf} = -\frac{\rho_c S_F a_{gf} C_D |v_g - v_f|(v_g - v_f)}{8} \qquad 102$$

where ρ_c is the density of the continuous phase, S_F is shape factor, and always assumed to equal 1, a_{gf} is the interfacial area per unit volume and C_D is the drag coefficient.

The calculation for interphase friction is more straightforward for bubbly flow than it is for slug and annular flow, as there is only one mechanism by which the vapor phase interacts with the liquid phase, through small bubbles. For bubbly flow, the continuous phase is liquid. [66]

In order to determine a_{gf}, the Sauter mean diameter of the bubbles must first be determined. This is found by assuming a maximum Weber number at which bubbles can exist, and assuming that the average bubble is half that size. In RELAP5/MOD2, [66] the maximum Weber number is 10 for bubbles. Therefore, the average bubble diameter is found to be:

$$d_{avg} = \frac{5\sigma}{\rho_f \left(v_g - v_f\right)^2} \tag{103}$$

The interfacial area per unit volume of the bubbles can be found as: [66]

$$a_{gf} = \frac{3.6(1-\alpha)}{d_{avg}} \tag{104}$$

RELAP5/MOD2 [66] uses the drag coefficient that Ishii and Chawla [42] proposed for viscous flow:

$$C_D = \frac{24}{Re}(1 + 0.1Re^{0.75}) \tag{105}$$

$$Re = \frac{2\rho_f |\Delta v| r_d}{\mu_m} \tag{106}$$

$$\mu_m = \frac{\mu_f}{1-\alpha} \tag{107}$$

Therefore, for bubbly flow the interphase friction force is: [66]

$$FI_{gf} = -\frac{10.8\rho_f(1-\alpha)(1+0.1Re^{0.75})\left|v_g - v_f\right|\left(v_g - v_f\right)}{d_{avg}Re} \tag{108}$$

For slug flow, the interphase friction force is divided into two parts, that which acts with the Taylor bubbles and that which acts with the smaller bubbles within the liquid film and slugs. In order to account for the differences between the Taylor bubble and the smaller bubbles, two additional void fractions have been derived. First, to account for the bubbles within the liquid film and slugs, α_{gs}, represents the average void fraction within those regions, and can be solved as: [66]

$$\alpha_{gs} = \alpha_{BS} e^{\frac{-10(\alpha-\alpha_{BS})}{\alpha_{SA}-\alpha_{BS}}} \quad (109)$$

Meanwhile, the average volume fraction of a Taylor bubble, α_b, is: [66]

$$\alpha_b = \frac{\alpha - \alpha_{gs}}{1 - \alpha_{gs}} \quad (110)$$

Thus, when the interfacial area per unit volume is determined, it is broken up into two parts, one for the Taylor bubbles, $a_{gf,tb}$, and one for the bubbles within the slugs and film, $a_{gf,sb}$, which are given as: [66]

$$\alpha_{gf,tb} = \frac{4.5 C_t}{D} \alpha_b \quad (111)$$

$$a_{gf,sb} = \frac{3.6 \alpha_{gs}}{d_{avg}} (1 - \alpha_b) \quad (112)$$

where C_t is a roughness parameter that is assumed to be 1. [66]

For the bubbles within the liquid slugs and film, the drag coefficient is the same as that for bubbly flow. The drag coefficient for the Taylor bubbles, $C_{D,tb}$ is also taken from Ishii and Chawla: [42,66]

$$C_D = 9.8(1 - \alpha_b)^3 \quad (113)$$

Thus, the interphase friction force for slug flow can be calculated as: [66]

$$FI_{gf} = -\left[\frac{5.51 \rho_f (1-\alpha_b)^3 \left|v_g - v_f\right| \left(v_g - v_f\right)}{D} + \frac{10.8 \rho_f \alpha_{gs} (1-\alpha_b)(1 + 0.1 Re^{0.75}) \left|v_g - v_f\right| \left(v_g - v_f\right)}{d_{avg} Re}\right] \quad (114)$$

Annular flow differs from bubbly and slug flow as it is the only flow regime where the continuous phase is the vapor phase, and not the liquid. However, like slug flow, annular flow interphase friction must account for two separate components, specifically the friction between the vapor core and the liquid film and the friction between the vapor core and liquid droplets. In

order to determine the interfacial area, the average liquid volume fraction in the film, α_{ff}, and the average liquid volume fraction in the core, α_{fd}, must be determined. For vertical flow, the average liquid void fraction in the film is:

$$\alpha_{ff} = (1-\alpha)C_f e^{-7.5\times10^{-5}\left(\frac{\alpha v_g}{u_c}\right)^6} \quad 115$$

$$u_c = 3.1\frac{\sqrt[4]{(\rho_f-\rho_g)g\sigma}}{\sqrt{\rho_g}} \quad 116$$

$$C_f = 10^{-4}(1-\alpha)\rho_f v_f \frac{D}{\mu_f} \quad 117$$

where u_c is minimum velocity necessary to entrain droplets. [66]

The average liquid volume fraction within the core, α_{fd}, is: [66]

$$\alpha_{fd} = \frac{1-\alpha-\alpha_{ff}}{1-\alpha_{ff}} \quad 118$$

Similar to the average bubble size for bubbly flow, the average droplet size for annular flow is calculated using a critical Weber number, which is set to 3.0 for droplets in RELAP5/MOD2. [66] Thus:

$$d_{avg,d} = \frac{1.5\sigma}{\rho_g\left(v_g - v_f\right)^2} \quad 119$$

Then the interfacial area per unit volume between the vapor core and the liquid film, $a_{gf,f}$ is:

$$a_{gf,f} = \frac{4C_{ann}}{D}\sqrt{1-\alpha_{ff}} \quad 120$$

where C_{ann} is a roughness parameter, assumed to be 1. [66]

The interfacial area between the liquid droplets and the vapor core, $a_{gf,d}$, is: [66]

$$a_{gf,d} = \frac{3.6\alpha_{fd}}{d_{avg,d}}\left(1 - \alpha_{ff}\right) \quad (121)$$

The drag coefficient for the liquid droplets in the vapor core is determined using the same equation from Ishii and Chawla [42] as is used for bubbly flow. The only difference is in how the Reynolds number is calculated:

$$Re = \frac{\rho_g \left| v_g - v_f \right| d_{avg,d}}{\mu_m} \quad (122)$$

$$\mu_m = \frac{\mu_g}{\alpha^{2.5}} \quad (123)$$

For the interphase friction between the vapor core and the liquid film, a friction factor is used instead of a drag coefficient, and is solved as:

$$f_i = 4\left[0.005 + \left(10^{-0.56+\frac{9.07}{D^*}}\right)\left(\delta\sqrt{\frac{\left(\rho_f - \rho_g\right)g}{\sigma}}\right)^{1.63+\frac{4.74}{D^*}}\right] \quad (124)$$

where f_i is the interphase friction factor between the vapor core and the liquid film and δ is the liquid film thickness. [66]

The interphase friction force for annular flow can be summarized as: [66]

$$FI_{gf} = -\left[\frac{\rho_g f_i \sqrt{1-\alpha_{ff}}}{2D} + \frac{10.8\rho_g \alpha_{fd}(1 + 0.1Re^{0.75})\left(1-\alpha_{ff}\right)}{d_{avg,d}Re}\right] \quad (125)$$

2.3.2: RELAP5/MOD3.3

RELAP5/MOD3.3 [40,69] differs from other versions of RELAP as it was developed by Information Systems Laboratory, Inc. for the Nuclear Regulatory Commission, rather than by Idaho National Laboratory. The basic equations and algorithms remain largely unchanged in RELAP5/MOD3.3 from earlier and later versions, with only minor differences to be noted between the RELAP5/MOD3.3 manual and the RELAP5/MOD3.2 [68] manual. However, in

reviewing the source code for RELAP5/MOD3.3, it was found that several differences were found between the RELAP5/MOD3.3 manual and source code. Most of these differences can be attributed to vague descriptions within the manual that become more clearly understood upon reviewing the source code. Discrepancies between the RELAP5/MOD3.3 source code and manual have been noted in this description.

2.3.2.1: Separated Flow Model

RELAP5/MOD3.3 [40,69] models two-phase flow using the separated flow model, with each phase governed by its own set of conservation equations. The continuity of the vapor mass equation is:

$$\frac{\partial(\alpha\rho_g)}{\partial t} + \frac{1}{A}\frac{\partial(\alpha\rho_g v_g A)}{\partial z} = \Gamma_g \qquad 126$$

The continuity of liquid mass equation is: [40,69]

$$\frac{\partial[(1-\alpha)\rho_f]}{\partial t} + \frac{1}{A}\frac{\partial[(1-\alpha)\rho_f v_f A]}{\partial z} = \Gamma_f \qquad 127$$

The first term on the left side of Equations 126 and 127 represent the time rate of change of the vapor and liquid phases, respectively, within a given volume. Meanwhile, the second term describes the change in mass that is entering and exiting a given volume. The terms Γ_g and Γ_f, represent the rate of vapor and liquid generation, respectively, with values greater than zero indicating that mass is being added to that particular phase. If there are no sinks or sources within a given volume, then: [40,69]

$$\Gamma_g = -\Gamma_f \qquad 128$$

The conservation of vapor momentum equation used in RELAP5/MOD3.3 [40,69] is shown in Equation 129:

$$\alpha\rho_g A\frac{\partial v_g}{\partial t}+\frac{1}{2}\alpha\rho_g A\frac{\partial {v_g}^2}{\partial z}$$
$$=-\alpha A\frac{\partial P}{\partial z}+\alpha\rho_g gA-\left(\alpha\rho_g Av_g\right)FWG+\Gamma_g A\left(v_{gI}-v_g\right)$$
$$-\left(\alpha\rho_g A\right)FIG\left(v_g-v_f\right) \quad (129)$$
$$-C\alpha(1-\alpha)\rho_m A\left[\frac{\partial\left(v_g-v_f\right)}{\partial t}+v_f\frac{\partial v_g}{\partial z}-v_g\frac{\partial v_f}{\partial z}\right]$$

where *FWG* is the wall friction coefficient for the vapor phase, v_{gI} is the velocity of the vapor at the liquid-vapor interface, *FIG* is the interphase friction coefficient for the vapor phase, and *C* is the coefficient of virtual mass.

The conservation of liquid momentum equation that is used in RELAP5/MOD3.3 [40,69] is:

$$(1-\alpha)\rho_f A\frac{\partial v_f}{\partial t}+\frac{1}{2}(1-\alpha)\rho_f A\frac{\partial {v_f}^2}{\partial z}$$
$$=-(1-\alpha)A\frac{\partial P}{\partial z}+(1-\alpha)\rho_f gA-\left[(1-\alpha)\rho_f Av_f\right]FWF$$
$$+\Gamma_f A\left(v_{fI}-v_f\right)-\left[(1-\alpha)\rho_f A\right]FIF\left(v_f-v_g\right) \quad (130)$$
$$-C\alpha(1-\alpha)\rho_m A\left[\frac{\partial\left(v_f-v_g\right)}{\partial t}+v_g\frac{\partial v_f}{\partial z}-v_f\frac{\partial v_g}{\partial z}\right]$$

where *FWF* is the wall friction coefficient for the liquid phase, v_{fI} is the velocity of the liquid phase at the interface, and *FIF* is the interphase friction coefficient for the liquid phase.

The terms on the left side of Equations 129 and 130 represent the changes in linear momentum for each phase with respect to both time and height. On the right side of Equations 129 and 130, the first term is the pressure gradient, followed by the hydrostatic force of each phase, the wall friction force on each phase, the transfer in momentum between phases that

occurs at the interface due to phase change, the interphase friction force, and lastly, the virtual mass force. The virtual mass force is discussed in further detail in Section 2.1.1.5. [40,69]

The conservation of momentum equations that are used in RELAP5/MOD3.3 [40,69] use several assumptions in order to simplify the equation. Most notable of the simplifications is the assumption that the viscous and turbulent stresses within each phase are negligible. Also, in vertical flow, the pressure at any given height is assumed to be the same whether it is the liquid phase, vapor phase or at the interface. Additional terms that are neglected include the covariance terms and any momentum storage in the interface. The forces acted upon each phase by the wall and the interface are assumed to be adequately modeled by the wall friction terms and interphase friction terms, respectively.

2.3.2.2: Flow Regime Map

The flow regime map for RELAP5/MOD3.3 [40,69] varies slightly from that for RELAP5/MOD2 [66], but both are based on the work of Vince and Lahey [85] and Taitel et al [81]. To avoid redundancy, the flow regime map for RELAP5/MOD3.3 will be discussed more in comparison to flow regime map of RELAP5/MOD2 than being discussed on its own.

For vertical co-current flow during which the critical heat flux (CHF) has not been surpassed, RELAP5/MOD3.3 [40,69] models four flow regimes; bubbly, slug, annular-mist and mist flow. Mist flow is the only flow regime that is not considered in RELAP5/MOD2 [66]. Another key difference between RELAP5/MOD2 and RELAP5/MOD3.3 is how the mass flux is calculated, for which the RELAP5/MOD3.3 calculation is provided in Equation 131:

$$G = \alpha\rho_g|v_g| + (1-\alpha)\rho_f|v_f| \qquad 131$$

As long as the two phases are traveling concurrently, there should be no difference in the total mass flux. However, should the pipe experience counter current flow, this may prove problematic.

The lower limit of α_{BS} is determined in a similar manner in RELAP5/MOD3.3 [40,69] as was the case with RELAP5/MOD2 [66]. However, there is one small difference with the normalizing of the non-dimensionalized pipe diameter in that it is divided by 22.22 rather than 19. This was done because RELAP assessments since the publication of the RELAP5/MOD2 manual showed a more accurate prediction of flow regime prediction with 22.22 than with 19. Therefore:

$$\alpha_L = 0.25 \times \min\left(1.0, \left(\frac{D^*}{22.22}\right)^8\right) \tag{132}$$

Otherwise the bubbly-slug transition void fraction is calculated the same in RELAP5/MOD3.3 [40,69] as in RELAP5/MOD2 [66].

For the transition from slug flow to annular flow, the process is a bit more detailed for RELAP5/MOD3.3 [40,69] than for RELAP5/MOD2 [66]. In RELAP5/MOD3.3, the process to determine the transition void fraction from slug to annular-mist flow, α_{DE}, begins with finding the void fractions at which the liquid film can be dragged upward by the vapor core, and the void fraction at which droplets within the core can be suspended. The void fraction at which the film does not flow backwards is:

$${\alpha_{crit}}^f = \frac{1}{v_g}\sqrt{\frac{(\rho_f - \rho_g)Dg}{\rho_g}} \tag{133}$$

The void fraction at which droplet entrainment begins is: [40,69]

$$\alpha_{crit}{}^{e} = \frac{3.2}{v_g}\sqrt[4]{\frac{(\rho_f - \rho_g)\sigma g}{\rho_g{}^2}} \quad (134)$$

In addition to the two criteria void fractions for film holdup and droplet entrainment, the slug-annular transition void fraction is bounded by a maximum value of 0.9, and a minimum value of the bubbly-slug transition void fraction. Thus, the slug-annular transition void fraction can be solved as: [40,69]

$$\alpha_{SA} = \max(\min(0.9, \alpha_{crit}{}^{e}, \alpha_{crit}{}^{f}), \alpha_{BS}) \quad (135)$$

In the RELAP5/MOD3.3 manual [69], the void fraction at which droplet entrainment begins, α_{DE}, is referenced, but is not discussed as to how it pertains to the slug-annular transition.

$$\alpha_{DE} = \max(\alpha_{SA} - 0.05, \alpha_{BS}) \quad (136)$$

The void fraction at which droplet entrainment begins is used to weight how close the slug flow is to annular flow and how the interphase friction should be calculated accordingly. This is accomplished using two exponents, *fanm* and *fslug*, which are defined in Equations 137 and 138, respectively. How they are implemented will be discussed in Section 2.3.2.3. [40]

$$fanm = \max(\min(20(\alpha - \alpha_{DE}), 1.0), 0.0) \quad (137)$$

$$fslug = \max(\min(1 - fanm, 1.0), 0.0) \quad (138)$$

The void fraction at which the flow regime transitions from annular-mist to mist flow, α_{AM}, is 0.9999, for which it is assumed that all liquid within the flow is in entrained droplet form. [40,69]

2.3.2.3: Interphase Friction Model

RELAP5/MOD3.3 [40,69] implements both the drag coefficient and drift flux methods of determining the interphase friction force, depending on the orientation of the flow and the flow regime. As the interphase friction force is calculated at each junction within a given model, the

interphase friction force is For vertical co-current flow, the drift flux method is used for bubbly and slug flows, while the drag coefficient method is used for annular-mist and mist flow.

The interphase friction force is defined as

$$F_i = C_i|v_R|v_R \tag{139}$$

where C_i is a coefficient and v_R is the relative velocity. Both the coefficient and the relative velocity are formulated based on whether the drift-flux or drag coefficient methods are used. [40,69]

2.3.2.3.1: Drift Flux Interphase Friction Models

Beginning with the drift flux approach used for bubbly and slug flow, RELAP5/MOD3.3 [40,69] uses several published correlations to derive the vapor drift velocity, v_{gj}, and the distribution parameter, C_0, depending on the mass flux and the pipe geometry. The distribution parameter, C_0, is used to find a second distribution parameter, C_1, which is defined as:

$$C_1 = \frac{1 - \alpha C_0}{1 - \alpha} \tag{140}$$

In the RELAP5/MOD3.3 source code [40], the parameters C_0 and C_1 are used to determine the relative velocity, v_R, as:

$$v_R = C_1 v_g - C_0 v_f \tag{141}$$

In the RELAP5/MOD3.3 manual [69], it is stated that the relative velocity calculated using Equation 141 should be equal to that produced by Equation 142. However, as will be shown later in this dissertation, that is not necessarily the case.

$$v_R = \frac{v_{gj}}{1 - \alpha} \tag{142}$$

where v_{gj} is the vapor drift velocity determined from the given correlation.

Meanwhile, the interphase friction coefficient, C_i, is solved for as: [40,69]

$$C_i = \frac{\alpha(1-\alpha)^3(\rho_f - \rho_g)g}{{v_{gj}}^2} \quad 143$$

The various schemes that are used by RELAP5/MOD3.3 [40,69] to predict the interphase friction using the drift-velocity model are described below and summarized in Table 3.

The EPRI model, as described by Chexal and Lellouche [12], is used for rod bundles and is also used for pipes that are less than 0.262 ft. in diameter with mass fluxes in excess of 20.5 $lb_m/(ft^2s)$. [40,69]

For pipes with a diameter of less than 0.0591 ft. and a mass flux of less than 10.24 $lb_m/(ft^2s)$ the coefficients are calculated by using the formulations proposed by Zuber and Findlay [91], while the values for C_0 and v_{gj} are interpolated between the Zuber-Findlay model and the EPRI model [12] when the mass flux is between 10.24 $lb_m/(ft^2s)$ and 20.5 $lb_m/(ft^2s)$. [40,69]

Table 3: RELAP5/MOD3.3 [40,69] Drift-Flux Interphase Friction Calculation Decision Matrix

Flow Rate (lb_m/ft^2s)	Rod Bundles	Pipes		
		D ≤ 0.0591 ft.	0.0591ft < D ≤ 0.262 ft.	D > 0.262 ft.
|G| ≥ 20.5	EPRI (Chexal-Lellouche)	EPRI (Chexal-Lellouche)	EPRI (Chexal-Lellouche)	Churn-Turbulent (if $j_g^+ \leq 0.5$) Kataoka-Ishii (if $j_g^+ \geq 1.768$) Interpolation (Otherwise)
20.5 > |G| > 10.24		Interpolation	Interpolation	
|G| ≤ 10.24		Zuber-Findlay	Churn-Turbulent (if $j_g^+ \leq 0.5$) Kataoka-Ishii (if $j_g^+ \geq 1.768$) Interpolation (Otherwise)	

When the pipe diameter is between 0.0591 ft. and 0.262 ft., and the flow is less than 10.24 $lb_m/(ft^2s)$, RELAP5/MOD3.3 [40,69] choses between the Churn-Turbulent bubbly flow

model and the Kataoka-Ishii [48] model for determining the vapor drift velocity. Both use the same equation to determine the distribution parameter, C_0. This decision is based on the value of the non-dimensionalized vapor volumetric flux, j_g^+, which is derived in Equation 144:

$$j_g^+ = \frac{j_g}{\sqrt[4]{\frac{(\rho_f - \rho_g)\sigma g}{{\rho_f}^2}}} \qquad 144$$

If j_g^+ is less than or equal to 0.5, the Churn-Turbulent model is used, while the Kataoka-Ishii model is used when j_g^+ greater than 1.768. In between those values, RELAP5/MOD3.3 interpolates between the two models. When the mass flux is between 10.24 $lb_m/(ft^2s)$ and 20.5 $lb_m/(ft^2s)$, and the pipe diameter is between 0.0591 ft. and 0.262 ft., the distribution coefficient and the vapor drift velocity are interpolated between the EPRI model [12] and the Churn-Turbulent and/or the Kataoka-Ishii models.

For pipes with a diameter greater than 0.262 ft., RELAP5/MOD3.3 [40,69] uses the Churn-Turbulent model and the Kataoka-Ishii [48] model for all mass fluxes. The choice between the two models is made using the same criterion described using Equation 144.

The EPRI model [12] determines the distribution parameter C_0 using Equation 145. Equations 146 through 154 are used to derive the parameters necessary to calculate Equation 145.

$$C_0 = \frac{L(\alpha, P)}{K_o + (1 - K_o)\alpha^r} \qquad 145$$

$$L(\alpha, P) = \frac{1 - e^{-C_1\alpha}}{1 - e^{-C_1}} \qquad 146$$

$$C_1 = \left| \frac{4{P_{crit}}^2}{P(P_{crit} - P)} \right| \qquad 147$$

$$K_o = B_1 + (1 - B_1)\sqrt[4]{\frac{\rho_g}{\rho_f}} \quad (148)$$

$$B_1 = \min(0.8, A_1) \quad (149)$$

$$A_1 = \frac{1}{1 + e^{-\left(\frac{Re}{60000}\right)}} \quad (150)$$

$$Re = \begin{cases} Re_g \; if \; Re_g > Re_f \; or \; Re_g < 0 \\ Re_f \; otherwise \end{cases} \quad (151)$$

$$Re_g = \frac{\rho_g j_g D}{\mu_g} \quad (152)$$

$$Re_f = \frac{\rho_f j_f D}{\mu_f} \quad (153)$$

$$r = \frac{1 + 1.57\frac{\rho_g}{\rho_f}}{1 - B_1} \quad (154)$$

where P_{crit} represents the critical pressure. [40,69]

The Chexal-Lellouche model [12] determines the vapor drift velocity using Equations 155 through 163:

$$v_{gj} = 1.41\sqrt[4]{\frac{(\rho_f - \rho_g)\sigma g}{{\rho_f}^2} C_2 C_3 C_4 C_9} \quad (155)$$

$$C_2 = \begin{cases} 1 \; if \; C_5 \geq 1 \\ \frac{1}{1 - e^{-C_6}} \; otherwise \end{cases} \quad (156)$$

$$C_5 = \sqrt{150\frac{\rho_g}{\rho_f}} \quad (157)$$

$$C_6 = \frac{C_5}{1 - C_5} \quad (158)$$

$$C_4 = \begin{cases} 1 \; if \; C_7 \geq 1 \\ \dfrac{1}{1 - e^{-C_8}} \; otherwise \end{cases} \tag{159}$$

$$C_7 = \left(\frac{0.300ft}{D}\right)^{0.6} \tag{160}$$

$$C_8 = \frac{C_7}{1 - C_7} \tag{161}$$

$$C_9 = \begin{cases} (1-\alpha)^{B_1} \; if \; Re_g \geq 0 \\ \min(0.7, (1-\alpha)^{0.65}) \; otherwise \end{cases} \tag{162}$$

$$C_3 = \max\left(0.5, 2e^{-\frac{\left|\frac{\rho_f j_f D}{\mu_f}\right|}{60000}}\right) \tag{163}$$

Note that Equation 162 which is used to calculate the coefficient C_9 for the Chexal-Lellouche [12] drift flux velocity appears in the RELAP5/MOD3.3 manual [40] as a typographical error in the form of Equation 164. This typographical error is mentioned within this dissertation because it is one of several differences noticed between the manual and source code. [69]

$$C_9 = \begin{cases} (1-\alpha)B_1 \; if \; Re_g \geq 0 \\ \min(0.7, (1-\alpha)^{0.65}) \; otherwise \end{cases} \tag{164}$$

For the Zuber-Findlay [91] correlation, the distribution parameter, C_0 is equal to 1.2, while the drift velocity is solved by Equation 165: [40,69]

$$v_{gj} = 0.35\sqrt{\frac{(\rho_f - \rho_g)Dg}{\rho_f}} \tag{165}$$

The distribution parameter for both the Churn-Turbulent and the Kataoka-Ishii [48] drift flux methods is determined using Equations 166 and 167: [40,69]

$$C_0 = C_\infty - (C_\infty - 1)\sqrt{\frac{\rho_g}{\rho_f}} \tag{166}$$

$$C_\infty = \min\left\{1.2, 1.393 - 0.0155\log\left[\frac{\rho_f(1-\alpha)|v_f|D_H}{\mu_f}\right]\right\} \tag{167}$$

In the RELAP5/MOD3.3 manual [69], the calculation for the variable C_∞ is given as Equation 168.

$$C_\infty = 1 + 0.2\sqrt{\frac{\rho_f\sqrt{Dg}}{|G_m| + 2\times10^{-4}\frac{lb_m}{ft^2 s}}} \tag{168}$$

The Churn-Turbulent drift velocity is calculated using Equation 169: [40,69]

$$v_{gj} = 1.41\sqrt[4]{\frac{(\rho_f - \rho_g)\sigma g}{{\rho_f}^2}} \tag{169}$$

The Kataoka-Ishii [48] drift velocity is evaluated using Equations 170 and 171. The non-dimensionalized pipe diameter is solved using Equation 97:

$$v_{gj} = \begin{cases} 0.0019{D^*}^{0.809}\left(\frac{\rho_g}{\rho_f}\right)^{-0.157}{N_{\mu f}}^{-0.562}\sqrt[4]{\frac{(\rho_f-\rho_g)\sigma g}{{\rho_f}^2}} & for\ D^* \le 30 \\ 0.030\left(\frac{\rho_g}{\rho_f}\right)^{-0.157}{N_{\mu f}}^{-0.562}\sqrt[4]{\frac{(\rho_f-\rho_g)\sigma g}{{\rho_f}^2}} & otherwise \end{cases} \tag{170}$$

$$N_{\mu f} = \frac{\mu_f}{\sqrt{\rho_f\sigma\sqrt{\frac{\sigma}{(\rho_f-\rho_g)g}}}} \tag{171}$$

where $N_{\mu f}$ is the viscosity number. [40,69]

Not mentioned in the RELAP5/MOD3.3 manual [69], is an additional limit that is imposed on the Churn-Turbulent and Kataoka-Ishii [48] drift flux correlations that applies when

the void fraction is greater than 0.8. When the void fraction is greater than 0.8, the distribution parameter and vapor drift velocities using the Churn-Turbulent and Kataoka-Ishii correlations, and not the Chexal-Lellouche [12] correlation, are modified as:

$$C_0 = 5.0\left[(\alpha - 0.8) + (1-\alpha)C_{0,old}\right] \quad 172$$

$$v_{gj} = 5.0(1-\alpha)v_{gj,old} \quad 173$$

where $C_{0,old}$ and $v_{gj,old}$ are the values for C_0 and v_{gj} that are produced by the Churn-Turbulent and Kataoka-Ishii correlations, before being modified should the void fraction exceed 0.8.

If the variable, *fslug*, is less than 1.0, then the interphase friction factor, C_i, and the drift flux distribution parameter, C_0, are modified by Equations 174 and 175, respectively.

$$C_{i,new} = C_i^{\,fslug} \quad 174$$

$$C_{0,new} = C_0^{\,fslug} \quad 175$$

where C_i is in metric units, $C_{i,new}$ is the interphase friction factor after the modification and $C_{0,new}$ is the distribution parameter after the modification. [40]

2.3.2.3.2: Drag Coefficient Interphase Friction Models

When the flow regime is either annular-mist or mist-pre-CHF, the drag coefficient method is used. For the drag coefficient interphase friction models, the interphase friction force per unit volume is calculated using Equation 176:

$$F_i = \frac{\rho_c C_D S_F a_{gf} \left|v_g - v_f\right| \left(v_g - v_f\right)}{8} \quad 176$$

where ρ_c is the density of the continuous phase, C_D is the drag coefficient, S_F is the shape factor and a_{gf} is the interfacial area per unit volume. [40,69]

When equated to Equation 137, we find that the relative velocity is simply: [40,69]

$$v_R = v_g - v_f \quad 177$$

And that the interphase friction coefficient is: [40,69]

$$C_i = \frac{\rho_c C_D S_F a_{gf}}{8} \tag{178}$$

For both the annular-mist and mist flow regimes, the continuous phase is considered to be the vapor phase. Meanwhile, the shape factor, S_F, is always assumed to equal 1. The main difference between the two flow regimes is the existence of a liquid film along the wall that occurs with annular-mist flow, which must be factored into the interphase friction force. Otherwise, the calculation for interphase friction for the mist phase is the same as that for the liquid entrained droplets of the annular-mist flow regime. [40,69]

The interfacial area per unit volume for the annular-mist flow regime is broken into two components, that for the interface between the liquid film and the vapor core, and the interfaces between the vapor core and the entrained liquid droplets. To calculate the interfacial area for the liquid droplets in the vapor core, $a_{gf,ld}$, the process is very similar to that described for RELAP5/MOD2 [66] with Equations 115 through 119 and Equation 121. However, there are a couple of differences with Equations 116 and 117, and are shown in Equations 179 and 180: [69]

$$u_c = 3.2 \sqrt[4]{\frac{(\rho_f - \rho_g)\sigma g}{{\rho_g}^2}} \tag{179}$$

$$C_f = 1.0 - 10^{-4} \sqrt[4]{\frac{(1-\alpha)\rho_f |v_f| D}{\mu_f}} \tag{180}$$

The interfacial area per unit volume of the liquid film, $a_{gf,lf}$, is determined using the same equation as RELAP5/MOD2 [66] (Equation 120), however the RELAP5/MOD3.3 source code and manual [40,69,70] provides Equation 181 to calculate the roughness parameter for the waves in the liquid film.

$$C_{ann} = \left(30\alpha_{ff}\right)^{0.125} \quad 181$$

The drag coefficient for the entrained liquid droplets in the vapor core is determined by the same process as in RELAP5/MOD2 [66], using Equation 102, 119 and 120. Meanwhile, the drag coefficient for the vapor core-liquid film interaction is replaced with an interphase friction factor, f_i, which is solved by the following equation: [40,69]

$$f_i = \begin{cases} \dfrac{64}{Re_g} \; if \; Re_g \leq 500 \\ \dfrac{1500 - Re_g}{1000}\dfrac{64}{Re_g} + \dfrac{Re_g - 500}{1000} 0.02\left[1 + 150\left(1 - \sqrt{1 - \alpha_{ff}}\right)\right] \\ \quad if \; 500 < \; Re_g < 1500 \\ 0.02\left[1 + 150\left(1 - \sqrt{1 - \alpha_{ff}}\right)\right] \; otherwise \end{cases} \quad 182$$

As discussed with slug flow, there is also an adjustment made to the interphase friction factor, C_i, for annular flow if *fanm* is less than 1.0, shown in Equation 183.

$$C_{i,new} = C_i^{\,fanm} \quad 183$$

where C_i is in metric units and $C_{i,new}$ represents the modified interphase friction factor. [40]

2.3.3: RELAP5-3D

RELAP5-3D [66] represents the latest incarnation of RELAP that is available, and sets itself apart from earlier versions of RELAP5 as being the first to include a vessel component that can be modeled in three dimensions, hence the name RELAP5-3D. All other components are modeled as one-dimensional components. For one-dimensional components, there are many similarities between RELAP5/MOD3.3 [40,68] and RELAP5-3D. The conservation of mass, momentum and energy equations for one-dimensional flow are identical, as are the flow regime maps used by both models. There are a few differences in the interphase friction correlations used by RELAP5/MOD3.3 and RELAP5-3D.

2.3.3.1: Interphase Friction Model

Like RELAP5/MOD3.3 [40,68], RELAP5-3D [66] uses drift flux correlations to calculate the interphase friction for bubbly and slug vertical flow, while the drag coefficient method is used for annular and mist vertical flow. For bubbly and slug flow, RELAP5-3D uses the same correlations that are identified in RELAP5/MOD3.3 for the same conditions that are cited in Table 3. However, there does appear to be some modifications to the Chexal-Lellouche [12,13,14] correlation for calculating the vapor drift velocity, v_{gj}, for concurrent vertical flow, following additional research by Chexal and Lellouche.

The new formulation for the vapor drift velocity is shown in Equations 184 through 192.

$$v_{gj} = 1.41\sqrt[4]{\frac{(\rho_f - \rho_g)\sigma g}{{\rho_f}^2}}\, C_1 C_2 C_3 C_4 \tag{184}$$

$$C_1 = \begin{cases} (1-\alpha)^{B_1} \; if \; Re_g \geq 0 \\ \sqrt{1-\alpha} \; if \; Re_g < 0 \end{cases} \tag{185}$$

$$C_2 = \begin{cases} 1 \; if \; \dfrac{\rho_f}{\rho_g} \geq 18 \; and \; C_5 \geq 1 \; or \; if \; \dfrac{\rho_f}{\rho_g} \geq 18, C_5 < 1 \; and \; C_6 \geq 85 \\ \dfrac{1}{1-e^{-C_6}} \; if \; \dfrac{\rho_f}{\rho_g} \geq 18, C_5 < 1 \; and \; C_6 < 85 \\ 0.4757\left[\ln\left(\dfrac{\rho_f}{\rho_g}\right)\right]^{0.7} \; otherwise \end{cases} \tag{186}$$

$$C_3 = \max\left[0.5, 2e^{-\frac{Re_f}{300000}}\right] \tag{187}$$

$$C_4 = \begin{cases} 1 \; if \; C_7 \geq 1 \\ \dfrac{1}{1-e^{-C_8}} \; otherwise \end{cases} \tag{188}$$

$$C_5 = \sqrt{150\frac{\rho_f}{\rho_g}} \tag{189}$$

$$C_6 = \frac{C_5}{1 - C_5} \tag{190}$$

$$C_7 = \left(\frac{0.300ft}{D}\right)^{0.6} \tag{191}$$

$$C_8 = \frac{C_7}{1 - C_7} \tag{192}$$

where B_1 is the same parameter identified in Equation 149 and Re_g is calculated the same as in Equation 152. [66]

RELAP5-3D [66] also contains a drift flux correlation specific to narrow rectangular pipes that is used for all mass fluxes. The distribution parameter is calculated using Equation 193, while the vapor drift velocity is calculated using Equation 194.

$$C_0 = 1.35 - 0.35\sqrt{\frac{\rho_g}{\rho_f}} \tag{193}$$

$$v_{gj} = \left(0.23 + 0.13\frac{W}{S}\right)\sqrt{\frac{(\rho_f - \rho_g)gS}{\rho_f}} \tag{194}$$

where W is the short length and S is the long length of the rectangular pipe. [66]

The interphase friction force for annular flow in RELAP5-3D [66] is calculated using identical methods as were used for calculating the interphase friction force for annular flow in RELAP5/MOD3.3. [40,69]

2.3.4: TRAC-RELAP Advanced Computing Engine (TRACE)

The TRACE-RELAP Advanced Computing Engine (TRACE) [82] is the result of a project that the Nuclear Regulatory Commission has undertaken to combine the two most commonly used nuclear thermal-hydraulic codes used in the industry into a single safety analysis model.

2.3.4.1: Separated Flow Model

Several assumptions are made in developing the separated flow model for TRACE [82], most of which are the same as those made with RELAP [40,67,69]. Unique to TRACE is the specification that the variables are time averaged and volume averaged in the derivation of the field equations. However, the greatest difference between TRACE and RELAP is that RELAP includes the virtual mass force in its momentum calculations, while TRACE neglects the virtual mass force, with the TRACE manual citing insufficient evidence that it plays a role in reactor safety.

The one-dimensional vertical flow continuity equation for the liquid phase is:

$$\frac{\partial\left[(1-\alpha)\rho_f\right]}{\partial t}+\frac{\partial\left[(1-\alpha)\rho_f v_f\right]}{\partial z}=-\Gamma_g \tag{195}$$

The continuity equation for the vapor phase is: [81]

$$\frac{\partial\left[\alpha\rho_g\right]}{\partial t}+\frac{\partial\left[\alpha\rho_g v_g\right]}{\partial z}=\Gamma_g \tag{196}$$

The conservation of linear momentum for the liquid phase in vertical flow is:

$$\begin{aligned}\frac{\partial\left[(1-\alpha)\rho_f v_f\right]}{\partial t}+\frac{\partial\left[(1-\alpha)\rho_f {v_f}^2\right]}{\partial z}+(1-\alpha)\frac{\partial P}{\partial z}\\ =f_i+f_{wf}+(1-\alpha)\rho_f g-\Gamma_g v_i\end{aligned} \tag{197}$$

where f_i is the interphase friction force, f_{wf} is the wall friction force acting on the liquid, v_i is the vertical velocity of the interface. [81]

The conservation of linear momentum for the vapor phase in vertical flow is:

$$\frac{\partial\left[\alpha\rho_g v_g\right]}{\partial t}+\frac{\partial\left[\alpha\rho_g {v_g}^2\right]}{\partial z}+\alpha\frac{\partial P}{\partial z}=-f_i+f_{wg}+\alpha\rho_g g+\Gamma_g v_i \tag{198}$$

where f_{wg} is the wall friction force acting on the vapor. [81]

2.3.4.2: Interphase Friction Model

The TRACE [83] interphase friction model takes a very different approach to modeling interphase friction than the RELAP models [40,67,69]. The most distinctive difference is that there is no strict dependence on flow regimes, rather TRACE computes the interphase friction for bubbly, slug and annular flow and weighs each value based on the likelihood that a given flow regime is occurring.

The calculation for the interphase drag force for two-phase vertical flow in TRACE begins simply with Equation 199:

$$F''' = C_i v_r |v_r| \tag{199}$$

where *F'''* is the interphase friction force per unit volume. [83]

The relative velocity, v_r, is defined as the difference between the void-weighted area-averaged vapor and liquid velocities, as shown in Equation 200. [83]

$$v_r = \overline{v_g} - \overline{v_f} = \frac{\langle \alpha v_g \rangle}{\langle \alpha \rangle} - \frac{\langle (1-\alpha) v_f \rangle}{\langle (1-\alpha) \rangle} \tag{200}$$

When considering bubbly or slug flow, TRACE [83] calculates the interphase drag coefficient, $C_{i,BS}$, as:

$$C_{i,BS} = \frac{\alpha(1-\alpha)^3(\rho_f - \rho_g)g}{\overline{v_{gJ}}^2} \cdot \frac{\left(\frac{1 - C_0\langle\alpha\rangle}{1-\langle\alpha\rangle}\overline{v_g} - C_0\overline{v_f}\right)^2}{{v_r}^2} \tag{201}$$

For bubbly flow, TRACE [83] uses Equations 202 and 203 to find the vapor drift velocity and the distribution parameter.

$$\overline{v_{gJ}} = \sqrt{2} \cdot \sqrt[4]{\frac{(\rho_f - \rho_g)\sigma g}{{\rho_f}^2}} \tag{202}$$

$$C_0 = 1.2 - 0.2\sqrt{\frac{\rho_f}{\rho_g}} \quad 203$$

Meanwhile, for slug flow, TRACE [83] uses the Kataoka-Ishii [48] method for determining the vapor drift velocity, as described using Equations 167 and 168. The distribution coefficient is found using the same equation that was used for bubbly flow.

TRACE [83] does not have a specific criterion for the flow regime changes from bubbly to slug flow, but instead allows for the interphase friction calculation to transition from bubbly to slug flow as the void fraction increases. For air-water two-phase flow, TRACE calculates the vapor drift velocity using Equation 199, for void fraction values of up to 0.2, while the Kataoka-Ishii [48] correlation is used when the void fraction is greater than 0.3. When the void fraction is between 0.2 and 0.3, the vapor drift velocity is interpolated between both methods. For steam-water, a similar process is followed, except that the void fraction boundaries are determined as:

$$\alpha_B = 0.2 \cdot \min\left(1, \frac{T_{sat} - T_f}{9}\right) \quad 204$$

$$\alpha_S = \alpha_B + 0.1 \quad 205$$

where α_B is the bubbly flow transition void fraction, T_{sat} is the saturation temperature, T_f is the liquid temperature and α_S is the slug flow transition void fraction.

For annular/mist flow, TRACE [83], like RELAP [40,65,67,69], divides the interphase friction force calculation into two components, that between the vapor core and the liquid film and that between the vapor core and the entrained liquid droplets. Beginning with the interphase friction between the vapor core and the liquid film, TRACE specifies that the interphase friction force can be determined as:

$$F_{i,film}''' = f_{i,film} A_{i,film}''' \frac{1}{2} \rho_g (v_g - v_{film}) |v_g - v_{film}| \quad 206$$

where $f_{i,film}$ is the friction factor between the vapor core and the liquid film and $A_{i,film}^{'''}$ is the interfacial area per unit volume, and v_{film} is the velocity of the liquid film. [83]

The friction factor between the vapor core and the liquid film is determined using Equation 207: [83]

$$f_{i,film} = 0.005[1 + 75(1 - \alpha)] \quad 207$$

To calculate the interfacial area per unit volume between the liquid film and the vapor core, Equation 208 is used. [83]

$$A_{i,film}''' = \frac{4\sqrt{\alpha}}{D} \quad 208$$

Therefore, the interphase friction force between the vapor core and the liquid film can be summarized as: [83]

$$F_{i,film}''' = \frac{0.01[1 + 75(1 - \alpha)]\rho_g\sqrt{\alpha}}{D}(v_g - v_{film})|v_g - v_{film}| \quad 209$$

The interphase friction coefficient for the liquid film is: [83]

$$C_{i,film} = \frac{0.01[1 + 75(1 - \alpha)]\rho_g\sqrt{\alpha}}{D} \quad 210$$

To calculate the interphase friction force between the liquid droplets and the vapor core, TRACE [83] uses the same drag coefficient that RELAP5/MOD3.3 [40,69] and RELAP5-3D [67] use, but with an altered approach. The interphase friction force for the droplets is calculated as:

$$F_d''' = \frac{1}{2}\rho_g C_d A_d''' {v_{r,d}}^2 = C_{i,drop}{v_{r,d}}^2 \quad 211$$

where C_d is the drag coefficient, $A_d^{'''}$ is the interfacial area per unit volume, $v_{r,d}$ is the terminal velocity of the droplets and $C_{i,drop}$ is the interphase friction coefficient for the droplets, which is given in Equation 200.

$$C_{i,drop} = \frac{1}{2}\rho_g C_d A_d''' \tag{212}$$

The drag coefficient, C_d, and the droplet Reynolds number are calculated the same as is the case with every version of RELAP [40,65,67,68,69], using Equations 105, 122 and 123. However, the mean droplet diameter, d_o, is calculated using a correlation developed by Kataoka, Ishii and Mishima [49] as:

$$d_o = \frac{0.008\sigma}{\rho_g {j_g}^2} {Re_g}^{\frac{2}{3}} \left(\frac{\mu_g}{\mu_f}\right)^{\frac{2}{3}} \left(\frac{\rho_f}{\rho_g}\right)^{\frac{1}{3}} \tag{213}$$

where Re_g is the Reynolds number for the vapor phase and is determined using Equation 152. [83]

The interfacial area per unit volume, $A_d^{'''}$, is determined using Equation 214:

$$A_d''' = \frac{3\alpha\alpha_d}{2d_o(1-\alpha_d)} \tag{214}$$

where α_d represents the liquid fraction of the droplets within the vapor core, and is determined as:

$$\alpha_d = \frac{E_\infty j_f}{j_g} \tag{215}$$

where E_∞ is the fraction of the total liquid flux that is in droplet form, also known as the entrainment fraction. [83]

The entrainment fraction is determined using two different correlations that have been developed, depending on the diameter of the pipe. For pipes with a diameter of less than 1.26 in., TRACE [83] uses a modified form of the correlation developed by Ishii and Mishima [47], given in Equation 216:

$$E_\infty = \tanh\left[7.25 \times 10^{-7} {We_g}^{1.25} \cdot \sqrt[4]{\min\left(6400, Re_f\right)}\right] \tag{216}$$

where We_g is the entrainment Weber number and Re_f is the film Reynolds number, which can be solved using Equation 148. The entrainment Weber number is solved using Equation 217: [83]

$$We_g = \frac{\rho_g {j_g}^2 D}{\sigma} \sqrt[3]{\frac{\rho_f - \rho_g}{\rho_g}} \tag{217}$$

For pipes with a diameter greater than 1.26 in., a modified form of the Steen-Wallis entrainment correlation is used, and is provided in Equation 218: [83]

$$E_\infty = 0.015 + 0.44 \log\left[0.9245 \left(\frac{\pi_2}{2.46 \times 10^{-4}}\right)^2\right] \tag{218}$$

where π_2 is the non-dimensionalized vapor velocity, and is determined as:

$$\pi_2 = \frac{j_g \mu_g}{\sigma} \sqrt{\frac{\rho_g}{\rho_f}} \tag{219}$$

The terminal velocity of the liquid droplets is determined using a correlation developed by Ishii, and is given in Equation 220. [83]

$$v_{r,d} = \begin{cases} 1.718(1-\alpha_d)\sqrt{\dfrac{(1-\alpha_d)(\rho_f - \rho_g) g d_o}{\rho_g}} & if\ d_o \le \sqrt{\dfrac{\sigma}{(\rho_f - \rho_g) g}} \\ (1-\alpha_d)^{1.5} \sqrt{2\sqrt{\dfrac{(\rho_f - \rho_g)\sigma g}{{\rho_g}^2}}} & otherwise \end{cases} \tag{220}$$

Putting the interphase friction force for the liquid film and the droplets together, we get: [83]

$$\begin{aligned} F'''_{i,AM} &= C_{i,film}(v_g - v_{film})|v_g - v_{film}| + C_{i,drop} {v_{r,d}}^2 \\ &= C_{i,AM}(v_g - v_f)|v_g - v_f| \end{aligned} \tag{221}$$

In TRACE [83], it is assumed that the velocity of the liquid is approximately that of the film. Thus, the interphase friction coefficient for annular/mist flow is determined as:

$$C_{i,AM} = C_{i,film} + C_{i,drop}\frac{{v_{r,d}}^2}{\left(v_{g-}v_f\right)^2} \quad 222$$

As a final step of ensuring that there is a smooth transition between bubbly and slug flow to annular flow, the overall interphase friction coefficient in TRACE [83] is calculated as:

$$C_i = \sqrt{{C_{i,BS}}^2 + {C_{i,AM}}^2} \quad 223$$

2.4: Annular Flow Physical Models

Vertical annular two-phase flow presents unique challenges in modeling the interphase friction as opposed to other flow regimes, as the calculations used to predict interphase friction for annular flow are based on the physical interactions between the vapor and liquid. In contrast, the drift flux correlations that have been discussed are used to predict the interphase friction for bubbly and slug flows.

2.4.1: Physical Description of Annular Flow

Annular flow is often studied as two different components, the liquid film and the vapor/droplet core. With regards to interphase friction, the interaction between the vapor core and the liquid film is considered to follow one set of equations, while the interphase friction between the vapor core and the entrained droplets are considered to be the second component.

Liquid film studies have broken down the structure of the liquid film into two categories, ripple waves and disturbance waves. [72] Ripple waves are defined as having small amplitudes and wavelengths, in comparison to the film thickness, and travel at a velocity much closer to that of the liquid film as a whole, than of the vapor core. Meanwhile, disturbance waves are defined by having wave amplitudes that are much larger than ripple waves, and travel at a velocity much closer to that of the vapor core than that of the liquid film.

The disturbance wave crests that break off from the liquid film are considered to be the primary source of entrained liquid droplets within the vapor core. As the wave crests break off from the disturbance waves, they break apart, as the friction force of the vapor core exceeds the surface tension within the crests that works to hold the crests together. [5,36] This results in tiny liquid droplets, which must be small enough so that the drag between the vapor core and the liquid droplets is insufficient to overcome the surface tension within the droplets. The ratio of these two forces is summarized by the Weber number, and it has been established that there exists a critical Weber number by which droplets are limited in size, and also by the Ohnesorge number, *On*, which describes the ratio of the viscous force on a droplet to the surface tension, and is given in Equation 224. [22]

$$On = \frac{\mu_d}{\sqrt{\rho_d d_0 \sigma}} \tag{224}$$

where μ_d is the droplet viscosity, ρ_d is the droplet density, d_0 is the diameter of the diameter and σ is the droplet surface tension.

2.4.2: Annular Flow Interphase Friction Parameters

There are several different parameters that can be examined that would directly impact the interphase friction that occurs between a vapor and a liquid in vertical annular flow. The parameters can be separated into two separate categories, those that directly relate to the interaction between the vapor core and the liquid film, and those that directly relate to the interaction between the vapor core and the entrained liquid droplets. Parameters that relate to the interaction between the vapor core and the liquid film include the interfacial friction factor, f_i, the roughness of the liquid film, C_{ann}, and the film thickness, δ. The parameters that relate to the

interaction between the vapor core and the entrained liquid droplets include the entrainment ratio, E, the droplet drag coefficient, C_D, and the droplet diameter, d_0.

These variables were investigated primarily with modifications to the RELAP5/MOD3.3 source code [40] in mind, and while some are not directly used in the RELAP5/MOD3.3 source code, they can be easily converted into variables that are used in the code. For example, the film thickness, δ, relates to the volume fraction of the liquid film, α_{ff}, as:

$$\alpha_{ff} = 1 - \left(1 - 2\frac{\delta}{D_H}\right)^2 \tag{225}$$

Meanwhile, the liquid volume of droplets within the vapor core, α_{fd}, is commonly studied as the entrainment ratio, E, which is defined as:

$$E = \frac{W_{fe}}{W_f} = \frac{\alpha_{fd}\rho_f v_{fd} A_C}{\alpha_{fd}\rho_f v_{fd} A_C + \alpha_{ff}\rho_f v_{ff} A} \tag{226}$$

where W_{fe} is the mass flow rate of entrained liquid droplets, W_f is the total liquid mass flow rate, v_{fd} is the average velocity of the liquid droplets, v_{ff} is the average velocity of the liquid film and A_C is the cross-sectional area of the vapor core.

Another variable that is investigated is the critical Weber number, which in RELAP5/MOD3.3 is directly related to the average liquid droplet size, d_0.

2.4.2.1: Interfacial Friction Factor, f_i

When considering the research that has taken place regarding f_i between the vapor core and the liquid film, recent research has focused on the case with a vapor core that is experiencing turbulent flow. An early correlation for f_i is that of Wallis [86], which is often used as a comparator to other correlations, and is given as:

$$f_i = 0.005\left[1 + 300\left(\frac{\delta}{D_H}\right)\right] \tag{227}$$

Fore et al [26] found that the Wallis correlation had a tendency to overestimate the interfacial friction factor when the film thickness was less than 0.5% of that of the pipe diameter, D_H, when comparing the correlation to the data from Asali [3] and Fore and Dukler [27], and achieved a much better match when adding a shift shown in Equation 228.

$$f_i = 0.005\left[1 + 300\left(\frac{\delta}{D_H} - 0.0015\right)\right] \tag{228}$$

Fore et al [26] noted that Asali [3] conducted their experiments with air-water in pipes measuring between 0.902 in. and 1.654 in., ranging from 14.70 psia to 29.4 psia, while Fore and Dukler [27] examined air-water and air with a 50% aqueous solution of glycerine in a 2.00 in. pipe at 14.70 psia, which represented a fairly small range of data for comparison. When comparing the shifted Wallis [86] correlation to nitrogen-water data in a 0.2 in. by 4 in. duct obtained by Fore et al, the shifted Wallis correlation proved to underestimate the interfacial friction factor. Also, Fore et al were dissatisfied that the interfacial friction did not asymptotically decrease with increasing Reynolds number, as would be expected with flow in a rough pipe. Thus, Fore et al developed a second correlation that predicted the interfacial shear stress by ±25% for most of the data from all of the studies examined:

$$f_i = 0.005\left\{1 + 300\left[\left(1 + \frac{17500}{Re_G}\right)\frac{\delta}{D_H} - 0.0015\right]\right\} \tag{229}$$

where Re_G is defined as the gas Reynolds number, and is solved as:

$$Re_G = \frac{\rho_g v_g \frac{4A_C}{P_C}}{\mu_g} \tag{230}$$

where A_C is the cross-sectional area of the vapor core and P_C is the perimeter of the vapor core.

Wongwises and Kongkiatwanich [89] found that the correlations that had been developed by Wallis [86] and Fore et al [26], along with those developed by Moeck [53] and Fukano and

Furukawa [28] were primarily developed for annular flow scenarios where the film thickness was thin and a correlation for thicker annular films was necessary. Wongwises and Konkiatwanich performed experiments with air and water in a 1.142 in. diameter pipe made of acrylic glass, and found that none of the above listed correlations matched well with their observations for cases where the ratio of film thickness to pipe diameter was between 0.095 and 0.16. Wongwises and Konkiatwanich found much better agreement with the following empirical equation.

$$f_i = 17.172 {Re_{SG}}^{-0.768} \left(\frac{\delta}{D}\right)^{-0.253} \quad 231$$

$$Re_{SG} = \frac{\rho_g j_g (D - 2\delta)}{\mu_g} \quad 232$$

where Re_{SG} is the superficial gas Reynolds number.

Belt et al [7] disagreed with Fore et al [26] over the need for the interfacial friction factor to include the Reynolds number within the calculation, and found the justification for its inclusion to lack physical reasoning. In their study, Belt et al examined air and water in a 2 in. diameter pipe at atmospheric pressure, and compared the results to the original Wallis correlation and the modified Wallis correlation, shifted by Fore et al. Ultimately, Belt et al concluded that the interfacial friction factor to be:

$$f_i = 1.158 \frac{\delta}{D} + 3.413 \times 10^{-4} \quad 233$$

2.4.2.2: Roughness Parameter, C_{ann}

With regards to the roughness parameter, C_{ann}, there has been extensive discussion regarding the effect of disturbance waves, however this research appears to have focused more on how it relates to the interfacial friction factor, f_i, rather than towards a roughness parameter,

C_{ann}. Therefore at this time, no correlations exist that can be recommended to test against the existing roughness parameter.

2.4.2.3: Film Thickness, δ and Entrainment, E

As α_{ff} and α_{fd} are linked by Equation 118 (and conversely Equation 234), the two are discussed together, even though they represent different components of the interphase friction force.

$$\alpha_{ff} = \frac{\alpha_f - \alpha_{fd}}{1 - \alpha_{fd}} \tag{234}$$

where α_f is the average liquid fraction. [40,69]

As already shown, the volume fraction of the liquid film equates to the average liquid film thickness. Meanwhile, the entrainment ratio, *E*, has been shown to be a function of the liquid fraction of droplets within the vapor core can be determined from the entrainment fraction, using Equation 235.

$$\alpha_{fd} = \frac{E(1-\alpha)v_f}{\alpha v_g(1-E)} \tag{235}$$

Due to the relationships given in Equations 118 and 234, it is important to make sure that when applying a correlation to α_{ff} or α_{fd}, that the other variable is properly accounted. Thus, only one correlation should be applied to either variable at a given time, and each variable should have a maximum value of α_f. Preliminary analyses of these correlations suggested that both variables need to be greater than zero in order for RELAP5/MOD3.3 [40,69] to obtain a converged solution. Therefore, it is recommended that each variable has a maximum value of $\alpha_f - 10^{-4}$.

First, we will examine the average liquid film volume fraction, α_{ff}. In RELAP5/MOD3.3 [40,69], it is determined using the correlation given in Equations 115, 179 and 180. There has

been considerable research to predict the film thickness, which has been shown to be related to the average liquid film volume fraction. In many cases, the correlation that has been proposed by the author has required the knowledge of the interfacial shear, which is not practical for RELAP5/MOD3.3. These studies include, but are not limited to the work of Asali et al [4], Hazuka et al [35], Kosky [50], Okawa et al [57], Schubring and Shedd [77], and Srivastava [79]. However, there have been a few correlations developed that do not require the interfacial shear stress, and use only the thermodynamic and flow properties of the annular flow, including the correlation developed by Hori et al [38], Fukano and Furukawa [28] and Berna et al [8].

The film thickness correlation proposed by Hori et al [38] and cited by Fukano and Furukawa [28] is given in Equation 236, with the definitions of the Reynolds numbers and Froude numbers used to calculate the film thickness given in Equations 237 through 240. The rationale for developing this correlation is unavailable at this time due to the lack of an English translation.

$$\frac{\delta}{D_H} = 0.905 {Re_{gs}}^{-1.45} {Re_{fs}}^{0.90} {Fr_{gs}}^{0.93} {Fr_{fs}}^{-0.68} \left(\frac{\mu_f}{\mu_{H2O}}\right)^{1.06} \quad 236$$

$$Re_{gs} = \frac{\rho_g j_g D_H}{\mu_g} \quad 237$$

$$Re_{fs} = \frac{\rho_f j_f D_H}{\mu_f} \quad 238$$

$$Fr_{gs} = \frac{j_g}{\sqrt{g D_H}} \quad 239$$

$$Fr_{fs} = \frac{j_f}{\sqrt{g D_H}} \quad 240$$

Fukano and Furukawa [28] constructed a test apparatus and studied annular flow with air-water mixed with glycerol at weight percentages of 0.0%, 45%, 53% and 60%. A holdup sensor

measured the liquid film thickness that determined the holdup through measured conductance in brass rings. When the measurements were compared against the correlation developed by Hori et al [38], Fukano and Furukawa showed that Hori et al correlation had a bias to overpredict the film thickness, particularly when the ratio of film thickness to diameter was less than 0.01. However, through trial and error, Fukano and Furukawa developed a similar correlation that is provided in Equation 241, which showed agreement within ±15% for all of their data points.

$$\frac{\delta}{D_H} = 0.0594e^{-0.34{Fr_{gs}}^{0.25}{Re_{fs}}^{0.19}x^{0.6}} \tag{241}$$

where x is the flow quality.

Berna et al [8] proposed a correlation that was empirically derived from the data of Tatterson et al [82], Paras and Karabelas [62], Schubring [76], and Alamu [2]. Tatterson et al measured the liquid film thickness for air-water flow in a horizontal duct that measured 1 in. by 12 in., and included data from Cousins and Hewitt [18], with air-water flowing upward through a 0.374 in. diameter tube, as well as from Wicks and Dukler [87], which had air water flowing down a 5.91 in. by 0.0748 in. duct. Paras and Karabelas studied air-water in a 2 in. diameter horizontal pipe to determine the film thickness for horizontal annular flow. Schubring examined air-water annular flow in both vertical and horizontal settings. For the horizontal flow experiments, tubes with inner diameters of 0.346 in., 0.594 in. and 1.035 in. with pressures ranging from 14.70 to 18.13 psia. Schubring used a quartz tube for his vertical test section that measured 0.921 in., with pressures ranging from 14.41 psia to 15.88 psia. Alamu studied air-water annular flow in vertical pipes that measured 0.748 in. in diameter and were conducted at 21.8 psia.

$$\frac{\delta}{D_H} = 7.165{Re_{gs}}^{-1.07}{Re_{fs}}^{0.48}\left(\frac{Fr_{gs}}{Fr_{fs}}\right)^{0.24} \tag{242}$$

Now we will turn our attention to the volume fraction of the liquid droplets vapor core, α_{fd}. In RELAP5/MOD3.3 [40,69], α_{fd} is determined using Equation 235, after α_{ff} is determined by Equation 118. As has already been discussed, while no direct correlations for α_{fd} appear in the literature, there are several correlations for entrainment available that can be used in RELAP5/MOD3.3

Ishii and Mishima [47] developed the empirical correlation given in Equations 243 through 245, by analyzing the air-water data from Cousins et al [17], Cousins and Hewitt [18], and Steen and Wallis [80]. Cousins et al performed their studies at 40 psia with a 0.374 in. diameter test section, while Steen and Wallis collected air-water data ranging from 14.70 psia to 58.8 psia in test sections that ranged in diameter from 0.421 in. to 0.626 in. More information regarding these experiments, as well as the experiments of Cousins and Hewitt are unavailable at this time.

$$E = \tanh(7.25 \times 10^{-7} We^{1.25} {Re_f}^{0.25}) \quad 243$$

$$We = \frac{\rho_g \langle j_g \rangle^2 D_H}{\sigma} \sqrt[3]{\frac{\rho_f - \rho_g}{\rho_g}} \quad 244$$

$$Re_f = \frac{\rho_f \langle j_f \rangle D_H}{\mu_f} \quad 245$$

Sawant et al [71] examined air-water in a stainless steel pipe with an inner diameter of 0.370 in. at pressures of 17.40 psia, 58.0 psia and 87.0 psia. Two extraction units were used in a series to obtain the amount of liquid flowing through the column. The first extraction unit was intended to measure the amount of liquid that formed the film along the wall, and using a mass balance was also used to estimate the amount of liquid droplets entrained in the vapor core. The second extraction unit was intended to determine the droplet deposition rate. Using the data

obtained from their experiments, Sawant et al [71] developed the following empirical correlation:

$$E = E_m \tanh(aWe^{1.25}) \tag{246}$$

$$E_m = 1 - \frac{Re_{fflim}}{Re_f} \tag{247}$$

$$a = 2.31 \times 10^{-4} {Re_f}^{-0.35} \tag{248}$$

$$Re_{fflim} = 250 \ln(Re_f) - 1265 \tag{249}$$

where Re_{fflim} is the limiting liquid film Reynolds number.

Sawant et al [73] improved upon their earlier correlation by gathering additional data with Freon-113 in a 0.402 in. diameter stainless steel pipe at 40.6 psia, 72.5 psia and 123.3 psia, with the same two extraction units being used for measuring the liquid film thickness, entrainment and droplet deposition rate. From these results, Sawant et al [73] developed the improved correlation given in Equation 250. The viscosity number is described in Equation 251, while the critical Weber number for the correlation of Sawant et al [73] is given in Equation 252, the critical vapor volumetric flux is given in Equation 253 and the liquid film Reynolds number provided by Ishii and Grolmes [43] is given in Equation 254. Equation 255 gives the minimum liquid film Reynolds number for the onset of entrainment in a two-phase annular flow.

$$E = \left(1 - \frac{13{N_{\mu f}}^{-0.5} + 0.3\left(Re_f - 13{N_{\mu f}}^{-0.5}\right)^{0.95}}{Re_f}\right) \times \tanh\left(2.31 \times 10^{-4} {Re_f}^{-0.35} (We - We_{cr})^{1.25}\right) \tag{250}$$

$$N_{\mu f} = \frac{\mu_f}{\sqrt{\rho_f \sigma \sqrt{\frac{\sigma}{g(\rho_f - \rho_g)}}}} \tag{251}$$

$$We_{cr} = \frac{\rho_g \langle j_g \rangle_{cr}{}^2 D_H}{\sigma} \sqrt[4]{\frac{\rho_f - \rho_g}{\rho_g}} \quad 252$$

$$\langle j_g \rangle_{cr} = \begin{cases} \frac{N_{\mu f}{}^{0.8} \sigma}{\mu_f} \sqrt{\frac{\rho_f}{\rho_g}} if\ Re_{ff} \geq 1635 \\ 11.78 \frac{N_{\mu f}{}^{0.8} \sigma}{\mu_f \sqrt[3]{Re_{ff}}} \sqrt{\frac{\rho_f}{\rho_g}} if\ 1635 > Re_{ff} > Re_{ffOE} \end{cases} \quad 253$$

$$Re_{ff} = \frac{4 \rho_f v_{fl} \delta}{\mu_f} \quad 254$$

$$Re_{ffOE} = \frac{13}{\sqrt{N_{\mu f}}} \quad 255$$

2.4.2.5: Droplet Drag Coefficient, C_D

The drag coefficient that has been published by Ishii and Chawla [42] and given in Equation 59 remains the defining drag coefficient for bubbly and droplet flow, with no research seeking to improve upon their work.

2.4.2.6: Droplet Size Diameter, d_0

The critical Weber number, We_{crit}, is used to determine the average droplet diameter, d_0, within the vapor core of the annular flow. In RELAP5/MOD2 [65], RELAP5/MOD3.3 [40,69,70], and RELAP5-3D [67], the critical Weber number for droplets is 3.0, however, in RELAP5/MOD1 [65], We_{crit} is 13.0, while no sources are cited to explain the justification for using either number within the manuals. There have been a few papers that have been written regarding the critical Weber number, which suggest that the critical Weber number is not a constant, but is a function of other parameters.

The first source credited with establishing that the critical Weber number is not constant is Brodkey [9], which stated that the critical Weber number was a function of the Ohnesorge number, and given as:

$$We_{cr} = 12(1 + 1.077Oh^{1.6}) \quad 256$$

Pilch and Erdman [64] and Sazhin [74] state that if the Ohnesorge number is less than 0.1, then the critical Weber number can be approximated as 12, and that droplets that breakup at a Weber number of approximately 12 do so due to vibrations caused by the flow field interacting with the natural vibrations within the droplet. For all cases that RELAP5/MOD3.3 is being tested against, the Ohnesorge number is less than 0.1, thus the Brodkey correlation is not applicable.

Faeth et al [25] identified a critical Weber number of 13 for droplet break up based on work of Hsiang and Faeth [39], where droplets of water, aqueous solutions of glycerol, mercury and heptane were observed in an air filled duct measuring 1.496 in. by 2.52 in, when the Ohnesorge number was less than 0.1. As the Ohnesorge number increased above 0.1, the critical Weber number also increased, with the critical Weber number approximately 100 when the Ohnesorge number is 4, and the critical Weber number approaching 1000, when the Ohnesorge number equaled 10.

When considering modifications to the RELAP5/MOD3.3 code [40], the literature seems to overwhelmingly support an increase in the critical Weber number to 12, from the presently used value of 3. While there is no justification given within the RELAP manuals for setting the critical Weber number equal to 3, it can be assumed that this was initially done to correct a deficiency discovered during the assessment of a previous RELAP5 model.

III. Data Analysis Procedures

The processes which were used to determine the interphase friction force, develop the interphase friction correlations and test the interphase friction correlations against the correlations used in RELAP5/MOD2 [66], RELAP5/MOD3.3 [40.69], RELAP-3D [67], and TRACE [83] are given in the following sections.

3.1: Data Analysis Procedure

The data analysis procedure can be divided into five sections. First, there is the derivation of the interphase friction force, which is described briefly in Section 3.1.1, with a more detailed derivation provided in Appendix A. This is followed by the derivation of the dimensionless parameters used for analyzing the interphase friction and two-phase flow data. The third step was the retrieval and selection of data that was needed for the analysis. The fourth step was the analysis of the two-phase flow data. Finally, the interphase friction correlations were developed using the dimensionless parameters.

3.1.1: Derivation of Interphase Friction Force

The derivation of the interphase friction force is based on a control volume analysis of a small section of pipe, through which the liquid and vapor flow, separated by an interface. The control volume analysis was selected based on data available at the time, where the pressure gradient, test section void fraction and inlet mass flow rates had been provided. The flow regimes were neglected, as Oshinowo [59] was the only study to identify the flow regime for each test case. Initially, only the pressure was allowed to change within the control volume, as it was generally assumed that the void fraction, densities and velocities would be largely unchanged over the control volume. However, when observing the nitrogen-mercury data in Neal [55], it was noticed that the pressure changed significantly, which as a by-product would

also result in large changes in void fraction, vapor density and velocities. Thus, the analysis was modified to account for changes in void fraction, vapor density, vapor velocity and liquid velocity. A force balance diagram showing the different forces that act on both the liquid and vapor phases is shown in Figure 7, and serves as the basis for developing the momentum balance of the control volume, which is used to derive the interphase friction force per unit volume.

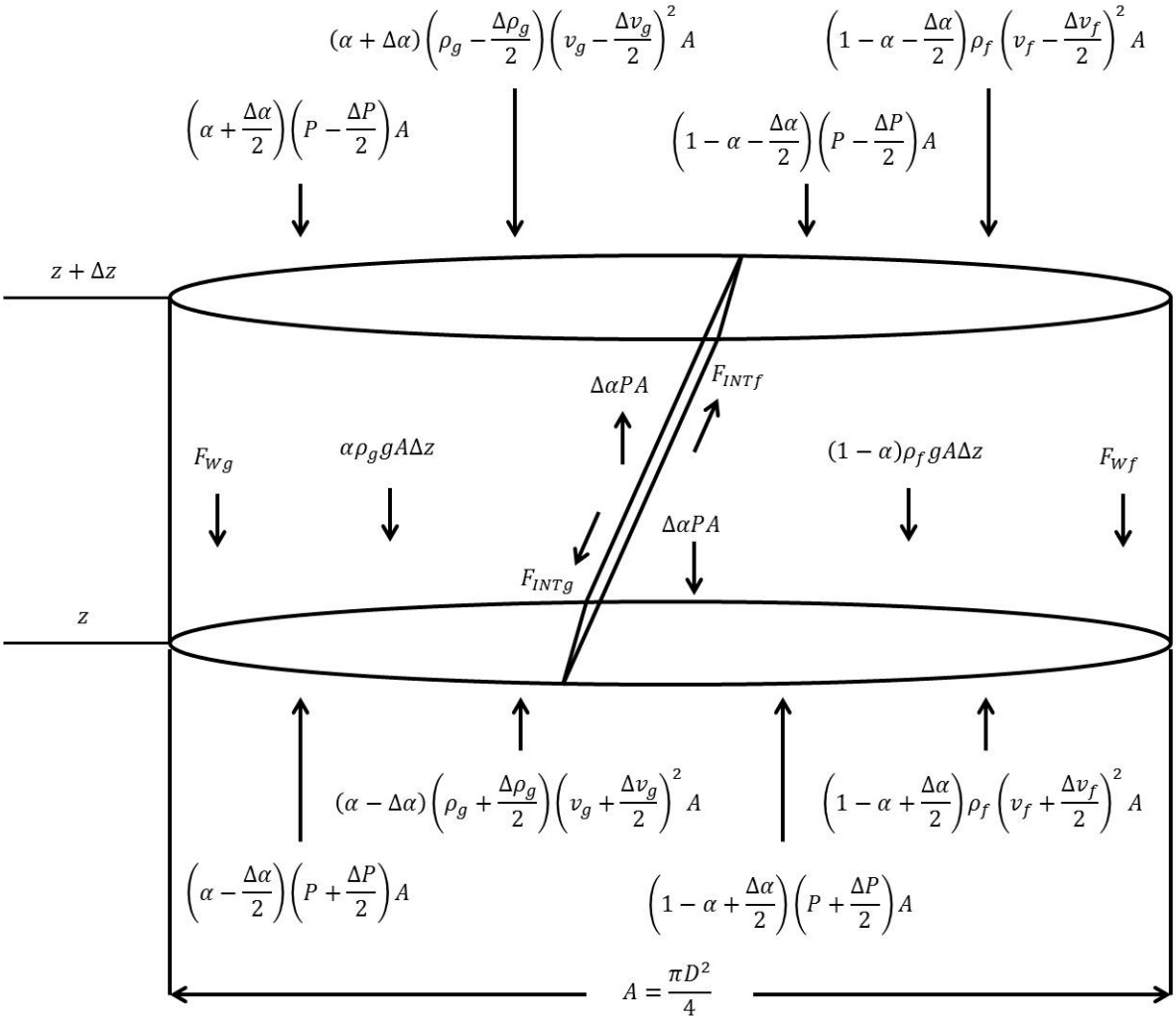

Figure 7: Not-to-Scale Control Volume with Momentum Fluxes and Forces

From the diagram shown in Figure 7, the momentum balance equations for the liquid and vapor phases were developed and are given in Equations 257 and 258.

$$(1-\alpha)\frac{dP}{dz} = (1-\alpha)\rho_f g + F_{Wf} + \rho_f {v_f}^2 \frac{d\alpha}{dz} - F_{INT} \quad (257)$$

$$\alpha\frac{dP}{dz} = \alpha\rho_g g + F_{Wg} + \alpha {v_g}^2 \frac{d\rho_g}{dz} - \rho_g {v_g}^2 \frac{d\alpha}{dz} + F_{INT} \quad (258)$$

The wall friction on the liquid phase is assumed to be significantly larger than that on the vapor phase, and so the wall friction on the vapor phase has been assumed to be negligible and the wall friction calculated for the two-phase flow has been assumed to act entirely on the liquid phase. To solve for the interphase friction force per unit volume, F_{INT}, each momentum balance equation has been rewritten to be solved for the void fraction gradient, $\frac{d\alpha}{dz}$. This results in Equation 257, and can also be found in Appendix A. One final approximation that is made for the vapor density gradient, $\frac{d\rho_g}{dz}$, is that it is assumed to be proportional to the pressure gradient, $\frac{dP}{dz}$, by way of the ideal gas law:

$$F_{INT} = \frac{\left[(1-\alpha)\left(\rho_f g - \frac{dP}{dz}\right) + F_{wf}\right]\left(\rho_g {v_g}^2\right) + \left[\frac{\alpha {\rho_g}^2}{R_g T}\frac{dP}{dz} - \alpha\left(\frac{dP}{dz} - \rho_g g\right)\right]\left(\rho_f {v_f}^2\right)}{\rho_g {v_g}^2 - \rho_f {v_f}^2} \quad (259)$$

where R_g is the ideal gas constant for the given vapor phase, and T is the temperature of the vapor.

3.1.2: Derivation of Dimensionless Parameters

As it was the goal of this study to develop a correlation using data from multiple sources, it was determined that the only way to determine any trends amongst the data was to non-dimensionalize the interphase friction force and compare it against other non-dimensional parameters.

According to the Buckingham Pi Theorem, for a given number of variables, *k*, that are independent and have a unique set of *r* dimensions, there are *k*-*r* non-dimensional Π terms that can be derived from which a function can be determined. [52] In order to apply the Buckingham Pi Theorem to the interphase friction, the first step was to identify the different variables that can be applied to calculate the interphase friction force.

Wallis [84] states that when studying a vapor bubble moving through a stationary liquid, an investigator must be concerned with the inertia, viscosity and density of each phase, as well as surface tension of the liquid and any possible surface contamination. When applied to two-phase flow, the inertia is quantified as the velocity of each phase. Surface contamination is described as any substance that may be dissolved or mixed with the liquid or vapor, and has been neglected for the purpose of this study since no study available provided any information regarding contamination, and each study assumed the vapor and liquid to be homogeneous pure substances within the phase. Balasubramianiam et al [6] used the superficial velocities of the liquid and vapor, j_f and j_g, respectively, the liquid and vapor viscosities, μ_f and μ_g, the liquid and vapor densities, ρ_f and ρ_g, the surface tension of the liquid, σ, the pipe diameter, D_H, the gravitational acceleration, g and the inclination angle of the flow, ϕ.

For this analysis, we will use the actual velocities of the vapor and liquid, v_g and v_f, respectively, and the void fraction α. Since we are focusing on vertical upflow only, ϕ has been set constant for this exercise and will not be used. Therefore, for the Buckingham Pi Theorem to be applied, it has been determined that:

$$F_{INT} = f\left(\rho_f, \rho_g, v_f, v_g, \mu_f, \mu_g, \sigma, D_H, g, \alpha\right) \qquad 260$$

For the eleven variables that are listed, there are three dimensions (mass, length and time), which results in eight Π terms. Thus we need eight non-repeating variables and three

repeating variables, which can be tricky to determine, given that there are three variables with the same dimensions. However, considering that we are examining the interaction between two phases, it may be better to consider the differences in properties between the liquid and vapor phases rather than the actual properties of one phase or the other. Thus, instead of using the liquid density and liquid velocity, the density difference, ρ_f-ρ_g, and the velocity difference, v_g-v_f, will be used.

The simplest dimensionless parameter to derive is the void fraction, α, and will serve as the first non-repeating variable. From Balasubramianiam et al [6], we find that the ratios of the density, viscosity and velocity are all worth considering as well, for which the vapor density, ρ_g, vapor viscosity, μ_g, and vapor velocity, v_g, will serve as non-repeating variables. Also, a Reynolds number, a Weber number and a Froude number need to be developed, which will use the liquid viscosity, μ_f, liquid surface tension, σ, and gravity, g, as their respective non-repeating variables. The most important dimensionless parameter is the dimensionless interphase friction force, with the interphase friction force, F_{INT}, serving as the non-repeating variable. This leaves the density difference, ρ_f-ρ_g, the velocity difference, v_g-v_f, and the pipe diameter, D_H, as the repeating variables. Applying dimensional analysis to each non-repeating variable as a product with the repeating variables, we establish the following dimensionless properties:

$$\frac{F_{INT}D_H}{(\rho_f-\rho_g)(v_f-v_g)^2} \qquad Re=\frac{(\rho_f-\rho_g)|v_g-v_f|D_H}{\mu_f}$$

$$We=\frac{(\rho_f-\rho_g)(v_g-v_f)^2D_H}{\sigma} \qquad Fr=\frac{(v_g-v_f)^2}{gD_H}$$

$$\frac{\rho_g}{\rho_f} \qquad \frac{v_g}{v_f}$$

$\frac{\mu_g}{\mu_f}$ α

As Balasubramianiam et al [6] noted, there may be other dimensionless parameters worth considering, as the desired results may not come from the list shown above. That is why a second dimensionless interphase friction force has been considered in the form of $F_{INT}/(\rho_f-\rho_g)g$. Also notable of dimensionless parameters examined is the mixture Froude number that was used by Kozloff [51], Griffith and Wallis [33] and Oshinowo and Charles [59,60].

3.1.3: Experimental Data Selection

As the proposed correlation should be applicable for a wide range of applications, it was necessary to accumulate as many data sources as possible that accounted for many different conditions. The data that has been used does not constitute as complete of a data set as desired, but is the most data that could be retrieved through all means available. The different studies that are discussed have provided varying levels of insight into two-phase flow, although only the data attributed to Govier et al [11,31,32], Turner [84], Gill, Hewitt and Lacey [29], Runge [84], Oshinowo [59] and Schlegal [75] proved to be useful for the purposes of this study. Therefore, these are discussed before and in more detail than the research of Petrick [63], Smissaert [78] and Neal [55].

3.1.3.1: Govier et al

Govier et al represents a group of three different papers published by Govier, Radford and Dunn [31] in 1957, Govier and Shortt [32] in 1958, and Brown, Sullivan and Govier [11] in 1960, which used air and water on an apparatus that was slightly modified for different experiments with the intent of studying the effect of liquid and vapor mass flow rates, pipe diameter, and the vapor density on flow pattern, void fraction and pressure drop in a vertical

pipe. A subset of the collected data was published in these three journal articles, with the complete data made available at the now-defunct American Document Institute. Attempts through several different avenues were made to try to locate and retrieve the complete data but ultimately proved unsuccessful; however, the data made available in the journal articles was still used to help derive the correlation. [11,31,32]

Air and water would be combined in a simple mixing tee before rising two feet through a galvanized iron pipe with a 1 in. diameter, and into the test section. The test section consisted of 30 ft. of piping, with a second section of galvanized iron piping connected to its outlet. Each section of galvanized iron pipe included a plug valve that could be opened or closed with a 90° turn. The valve handles were connected by an aluminum rod, which would allow for the plug valves to be opened or closed simultaneously. Three pressure taps were drilled into the tubing, with the bottom pressure tap approximately 8 ft. above the mixing tee, the top pressure tap 22.88 ft. above the bottom pressure tap, and the third placed in the middle. The middle pressure tap was used to ensure that the pressure of the system was that prescribed by the study, while the top and bottom pressure taps were used to measure pressure gradient. A diagram of the test section used for the experiments is shown in Figure 8. [11,31,32]

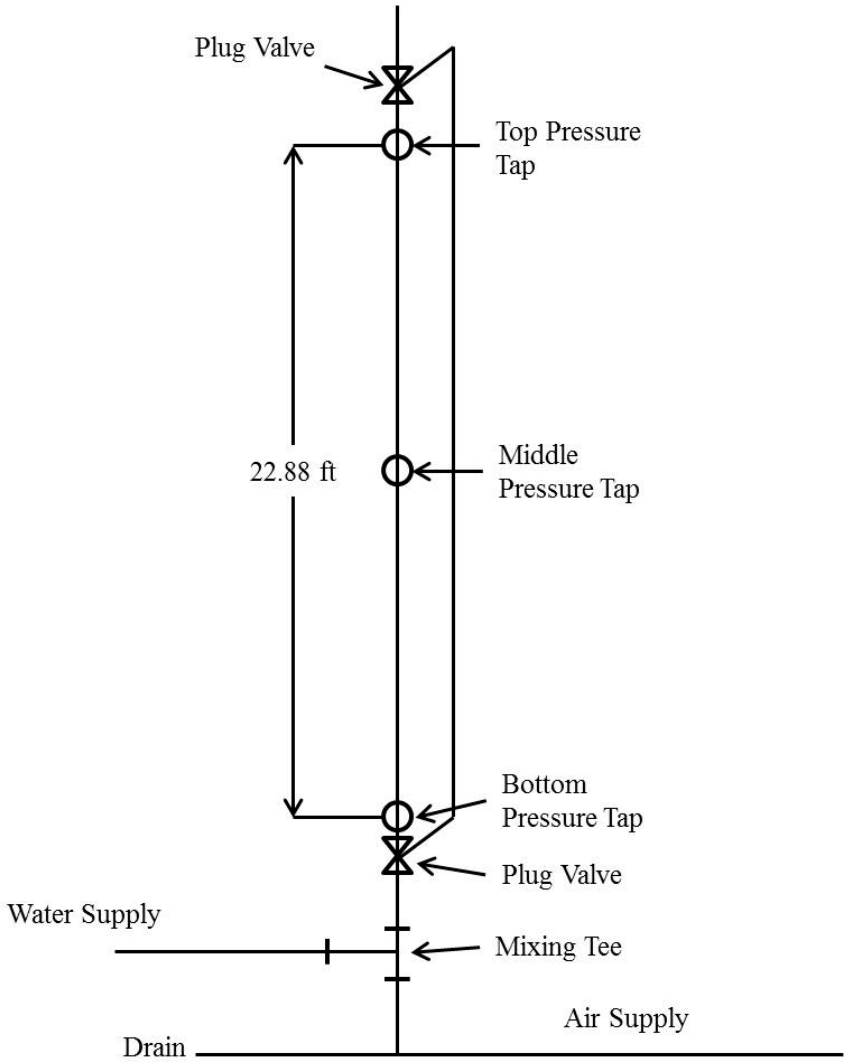

Figure 8: Test Section Diagram for Govier et al [11,31,32] Air-Water Studies

In Govier, Radford and Dunn [31], the test section was comprised of cellulose acetate-butyrate plastic tubing, and had an inner diameter of 1.025 in. The pressure at the middle tap was 36 psia for all test runs, while the temperature ranged from 67°F to 75°F. Volumetric flow rates for water ranged from 4 x 10^{-4} ft^3/s to 0.0421 ft^3/s, while the volumetric flow rates for air ranged from 0 ft^3/s to 0.158 ft^3/s.

Govier and Short [32] expanded on the work of Govier, Radford and Dunn [31] by incorporating three additional test sections, along with conducting experiments with the original

1.025 in. diameter cellulose-acetate-butyrate tubing. Tests were conducted with a cellulose-acetate-butyrate tubing with an inner diameter of 0.630 in., a 1.50 in. diameter copper pipe and a 2.50 in. carbon black loaded polythene tube. The pressure at the middle of the test section was held at 36.0 psia, while the temperature ranged from 62°F to 81°F. Volumetric flow rate of water ranged from 0.00183 ft^3/s to 0.0296 ft^3/s, while the volumetric flow rate of air ranged from 4.26 x 10^{-3} ft^3/s to 0.510 ft^3/s.

Brown, Sullivan and Govier [11] studied the effect of the vapor density by adjusting the pressure at the middle of the test section, which consisted 1.50 in. diameter copper piping. The pressure ranged from 18.0 psia to 110.0 psia, while the temperature ranged from 67°F to 95°F. While the volumetric flow rate of the water was held constant at 0.0107 ft^3/s, the volumetric flow rate of air ranged from 0.0215 ft^3/s to 0.389 ft^3/s.

3.1.3.2: Turner

Turner [84] provided three different data sets: one from his own research; one work by Runge that was otherwise unavailable; and one from a study by Gill, Hewitt and Lacey. The data from Gill, Hewitt and Lacey [29] was found in a separate report, which was considered to be more comprehensive than that provided in Turner. Therefore, the data from the report by Gill, Hewitt and Lacey was used instead of that provided in Turner.

Turner [84] published in 1965 research that he had conducted on two-phase annular flow with air and water, as well as with air and heptane. The two-phase flow mixture would enter into the bottom of an 18 ft. pipe, with the first 12 ft. representing the calming length, and the final 6 ft. representing the test section. For air-water experiments, Plexiglas tubing was used to observe the annular flow, but copper tubing had to be used with air-heptane as the heptane reacted with the Plexiglas to make it exceptionally brittle. For many runs with the same mass flow rates of

water and air, Turner provides multiple measurements of pressure gradient and void fraction. These measures have been ensemble averaged together to provide a single data point for analysis.

3.1.3.3: Gill, Hewitt and Lacey

Gill, Hewitt and Lacey [29] published in 1963 their experimental research on annular two-phase flow with air and water within a 1.25 in. diameter acrylic resin pipe. Air entered the apparatus at the bottom, and flowed upward through 6 feet of piping that served as a calming section before water was injected by a porous sinter tube. The pressure gradient was measured using pressure taps at 13.92 ft. and 17.83 ft. above the liquid injection point. At 17.42 ft. above the water injection point, a sampling probe was placed that measured the liquid holdup at 15 different points along the radius of the pipe. Conductance probes were placed 3 inches above the sampling probe to measure the thickness of the film of water along the wall.

Gill, Hewitt and Lacey [29] varied the air mass flow rate between 0.0278 lb_m/s and 0.1667 lb_m/s, and varied the water mass flow rate between 0.00833 lb_m/s and 0.347 lb_m/s. However, it was found that when the air mass flow rate was 0.0278 lb_m/s that the maximum water mass flow rate that could be used was 0.1389 lb_m/s, or else the flow regime would switch to churn-turbulent flow, which was not the object of their study. Also, it was mentioned that at an air mass flow rate of 0.1667 lb_m/s, liquid mass flow rates were limited by two different factors. Results for liquid mass flow rates at 0.00833 lb_m/s could not be obtained as the wall dried out, while the water pump could not pump out more than 0.1389 lb_m/s due to high back pressure in the apparatus.

3.1.3.4: Runge

The data that is attributed to Runge was first published by Turner [84], and was expected to be published in a future report that cannot be found. Therefore, all knowledge of the Runge experiments is based solely on the summary provided by Turner. Runge studied steam-water flow through a 1.049 in. diameter pipe at pressures of 65, 135, 215, 400 and 600 psia. Steam would be added to pressurized liquid water at 100-150 psi greater than the pressure of the water, and then would flow with the water through a 5 ft. calming section, before entering the 5.17 ft. test section. The pressure gradient was measured using a differential manometer that was connected to several pressure taps within the test section. To measure the void fraction when the operating pressure of the system was 65, 135 and 215 psia, the test section would be closed off by using two quick-closing valves. Once the liquid had settled to the bottom of the test section, a gamma-ray attenuation apparatus was used to determine the liquid level. At 400 and 600 psia, the flow was allowed to continue without interruption, and the void fraction was determined using gamma-ray attenuation. However, the method of using gamma-ray attenuation cited by Turner is from a report by Hooker and Popper [37], which describes void fraction measurements in a square channel, not a circular channel. As a clearer description of how the gamma-ray attenuation approach was used for Runge is not available, the data at 400 and 600 psi has been neglected from this study, and only the data at 65, 135 and 215 psia is used for analysis.

3.1.3.5: Oshinowo

Oshinowo [59,60,61] published in 1971 his study of flow regimes, liquid holdup and pressure drop of two-phase flow using an apparatus that consisted of a riser (called 1/Riser by Oshinowo), followed by a downcomer and then a second riser (called 2/Riser). As shown in Figure 9, the air and liquid would mix in a simple tee connection before rising through 5 feet of 1

inch diameter copper tubing that served as a calming length, before passing the first ball valve into 1/Riser. A total of 8.25 ft. were traveled before passing the first pressure tap. The risers and the downcomer were made form Lucite tubing and were connected by "U-bends" that were also made of Lucite. For most experiments, a U-bend tube with a 6-inch turning radius was used, while for some air-water studies, a U-bend tube with a 3-inch turning radius was used to compare against the 6-inch turning radius U-bends. The pressure in the system was regulated using a pressure control system that was placed downstream of 2/Riser, before the air was separated from the liquid. Pressure taps were drilled into the Lucite tubing in order to measure the pressure gradients in each test section once the system had attained a steady state. After the pressure gradient was measured, ball valves at the beginning and end of each test section would be shut simultaneously to trap the air-liquid mixture in each test section. The liquid was allowed sufficient time to drain to the bottom of the test section before the liquid fraction was measured. To account for liquid that remained alongside the walls, a correction factor was developed by filling a Lucite pipe completely with the liquid and measuring the amount that drained. Dimensions of Oshinowo's apparatus are provided in Table 4.

Table 4: Apparatus Dimensions for Oshinowo [59,60,61]

	1/Riser	Downcomer	2/Riser
Inside Diameter (in)	0.992	0.983	0.994
Pressure Tap Distance (ft.)	12.990	12.840	12.860
Ball Valve Distance (ft.)	17.300	17.300	17.300

Oshinowo [59,60,61] studied two-phase flow of air and water with varying concentrations of glycerol (0.0%, 16.0%, 35.0%, 56.0% and 60.5% by volume). The properties of water and the varying concentrations of glycerol solutions are provided in Table 5.

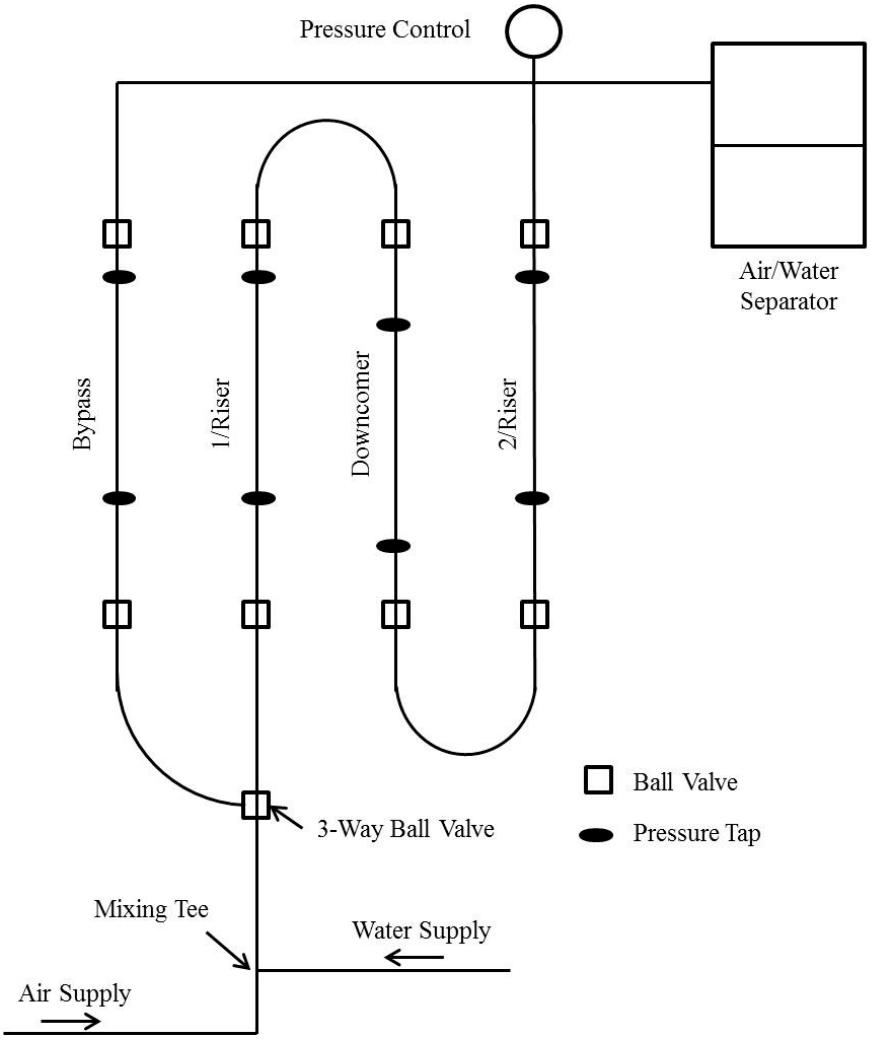

Figure 9: Diagram of the Apparatus Used by Oshinowo and Charles [59,60,61]

Table 5: Properties of the Liquids Used in Oshinowo at 14.696 psia and 70°F [59,60]

Fluid	Density (lb_m/ft^3)	Viscosity ($lb_m/ft\text{-}s$)	Surface Tension (lb_m/s^2)
Water	62.3013	6.55E-04	0.1600
16.0% Glycerol	64.7934	1.18E-03	0.1580
35.0% Glycerol	67.9084	2.16E-03	0.1545
56.0% Glycerol	71.2104	5.73E-03	0.1501
60.5% Glycerol	71.9580	7.40E-03	0.1490

Only data from the first riser was used for this data analysis due to concerns over entrance effects as the two-phase flow transitioned to downflow and upflow again.

3.1.3.6: Schlegal

Schlegal [75] represents the most recent, having been published in 2009, and perhaps most sophisticated data set that was used for data analysis. Air and water were mixed together and flowed up two different risers, one with a diameter of 0.4987 ft. and the other 0.6660 ft. Each test section had pressure taps and impedance probes placed at five different heights along the test section, with the pressure taps being used to measure the pressure gradient and the impedance probes used to measure the area-averaged void fraction. For the 0.4987 ft. diameter test section, the pressure and void fraction measurements were taken at heights of 0.00, 3.63, 7.73, 11.42 and 14.41 ft., while for the 0.6660 ft. diameter test section, the measurements were taken at heights of 5.49, 8.92, 12.59, 16.98 and 19.78 ft.

With Schlegal [75], there is some concern with the uncertainties, particularly with the void fraction measurement. Most of Schlegal's equipment has been calibrated to the extent that the uncertainty is less than 1%. For example, the electromagnetic flowmeters used by Schlegal for measuring the flow of the water had an overall uncertainty of 0.9%, while the air flow meters were calibrated by their manufacturer to have an uncertainty of 0.1%. Within the test section, the pressure transducers were calibrated independently and were found to have an uncertainty in pressure reading of 0.5%. However, there is an inherent weakness in the impedance probe measurement because it is calibrated against its measurement at a void fraction of 0.0. Schelgal reports that the calibration has an uncertainty of 1%, but when applied to a two-phase flow with a void fraction of 0.2 the error can be greater than 10%, and it can be greater than 5% for void fractions up to 0.4.

For this project, the data provided by Schlegal [75] for each test run was broken into four different data points, with the pressure and void fraction measurement points serving as the

boundaries for each interval. The pressure measurements were used to derive the pressure gradient and average pressure of the interval, while the void fraction measurements at the inlet and outlet of each interval were averaged to produce a volume-averaged void fraction for the interval. Although Schlegal does not indicate any calming length for the two-phase mixture prior to entering the test section, the data for the first interval of both test sections proved to be consistent in pressure gradient and void fraction measurement with that of the three downstream intervals, indicating that the two-phase flow was fully developed prior to entering the test section.

3.1.3.7: Neal

Neal [55] published in 1963 research on mercury-nitrogen two-phase vertical upflow, using both an electric probe to measure void fractions at several points along the radius of the flow along with pressure taps used to measure pressure gradients. The test section was 5 ft. long and made of a stainless steel, 1 in. diameter schedule 40 pipe. Pressure and void fraction measurements took place at heights of 0.499 ft., 1.496 ft., 2.49 ft. and 4.51 ft.

Neal's [55] data showed how the pressure could change significantly over a small change in height due to the high density of the mercury. Assuming nitrogen to be an ideal gas, this implied that the density of the nitrogen would change proportionately over the same interval. While the change in pressure with respect to height is significantly smaller in cases of air-water and steam-water two-phase flow cases, the net change in height in the air-water and steam-water is much larger in many of the studies that have been reviewed for this project. This observation in the data led to the additional consideration of variable density, void fraction and velocities in the derivation of interphase friction.

Neal's [55] data was not used as part of the final analysis of all data due to concerns over wall wetting. Mercury has a contact angle of 133° with stainless steel [24], indicating that on a horizontal surface, mercury would retain the form of a droplet, rather than spread out into a thin layer, like one would expect from water. Neal's void fraction data suggests that there is a higher void fraction near the wall than in the center of the pipe, indicating that a non-wetted wall is the case. Thus, the Neal experiments were not used in the data analysis used to derive the interphase friction correlation.

3.1.3.8: Petrick

Published in 1962, Petrick [63] studied two-phase flow with both air-water and with steam-water. Although different apparatuses were used for study, due to the differences in pressure and temperature between the air-water and steam-water experiments, the basic concept of both apparatuses was the same. Liquid and vapor would rise through the inside pipe of an annulus until reaching a plenum. In the separation plenum, the vapor would either separate from the liquid, or be carried under by liquid falling through the outer ring of the annulus.

In the case of air-water, a mixing section was built that consisted of two pipes, one with an inner diameter of 0.427 ft. placed concentrically inside the second with an inner diameter. The air was fed through the outer pipe, also known as the annular plenum, while the inner pipe contained 300 holes that were randomly distributed throughout the mixing section. Air that was carried under in the separation plenum was later separated when the two-phase flow reached the bottom of the apparatus and was flowing horizontally on the return leg to the water pump. [63]

For the steam-water experiments, steam was generated by passing water through a heated section that consisted of water passing inside a 1.5 in., schedule 40 stainless steel pipe that was electrically heated by brazed copper plates that were attached at each end. Steam that did not

separate from the water in the separation plenum, was condensed in a parallel flow heat exchanger. [63]

For the air-water experiments, Petrick [62] assumed that the change in pressure with respect to height was purely hydrostatic. Therefore, only the pressure gradient was measured, and only the corresponding void fraction was provided by Petrick, as derived using Equation 261.

$$\alpha = \frac{\rho_f g - \frac{dP}{dz}}{(\rho_f - \rho_g)g} \tag{261}$$

In the case of steam-water, Petrick [63] employed three different techniques, including a Potter meter, gamma-ray traversing and using the differential pressure as was done with the air-water experiments. Comparing the results, Petrick concluded that the void fraction measurements agreed sufficiently well, and chose to use and report the void fraction based on the differential pressure.

The data from Petrick [63] was not used for evaluating the interphase friction force due to the fact that the void fraction was not measured independently of the pressure gradient. Petrick assumes that the pressure gradient is wholly hydrostatic, and thus the change in pressure due to wall friction and acceleration are assumed to be negligible. However, Equation 259 requires the wall friction and accelerational terms in order for the interphase friction force to be calculated, which requires that the void fraction and pressure gradient must be measured independently.

3.1.3.9: Smissaert

Smissaert [78] studied two-phase concurrent upflow involving several different fluids, including nitrogen-mercury, air-water and mitrogen-Freon-113. Each experiment was conducted at atmospheric pressure with the temperature being between 68°F and 70°F. The same test

apparatus was used for the air-water and nitrogen-Freon-113 experiments, while a slightly modified apparatus was used for the nitrogen-mercury experiments.

For the air-water and nitrogen-Freon-113 experiments, the liquid and vapor would enter into a pipe tee at the bottom of the apparatus. The vapor would enter through a mesh that was shaped in a cone in order to make the bubble size and distribution more uniform in the two-phase mixture as it entered the test section. The two-phase mixture then would rise through the test section, which consisted of 10.46 ft. of Lucite pipe, with an inner diameter of 2.75 in. The top 0.792 ft. of the pipe entered into a separation tank at the top of the apparatus, where the liquid level was kept at a minimum of 1 in. above the pipe outlet. This was done to minimize any effects that the separator may have had on the test data. [78]

The first 5.04 ft. of the test section used for the air-water and nitrogen-Freon-113 experiments served as a calming section, before the bottom of five pressure taps was encountered. Pressure taps were also placed 1 ft., 2 ft., and 3 ft. above the first pressure tap. The final pressure tap was placed on the separation tank, at the height of the pipe outlet. A gamma traversing system was installed at a height of 9.5 in. above the second pressure tap. [78]

A similar apparatus was used for the nitrogen-mercury, although special emphasis had to be made to account for the difficulty in achieving a wetted wall with mercury. Smissaert [78] found that a nickel-plated surface treated with diluted hydrochloric acid would stay wetted by mercury for up to an hour, provided that the surface did not have enough time to dry after acid treatment. Thus the test section was made of nickel-plated pipe with a total length of 6 ft. and a diameter of 2 in. The first 2.50 ft. of the test section represented the calming section of the pipe, with pressure taps placed at heights of 2.50 ft., 3.00 ft., 3.50 ft., 4.50 ft., 5.00 ft. and 5.50 ft.

Smissaert [78] used both a gamma traversing system and the differential pressure to determine the void fraction for the air-water and nitrogen-Freon-113 experiments. However, it was found that the gamma traversing system had several inaccuracies. Since the void fractions obtained from the gamma traversing system proved to be inconsistent with the pressure gradient data, Smissaert chose to use the pressure gradient to evaluate the void fraction in the same manner as Petrick [63] did. As discussed in Section 3.1.3.8: Petrick, the lack of an independently measured void fraction with the measured pressure gradient means that the data from Smissaert is not conducive for analysis with the interphase friction force equation, and thus was not used to derive the interphase friction force correlations.

3.1.4: Data Processing and Analysis

Each of the studies that are discussed in the previous data set had provided tabulated data in one or more of the publications that are cited. As each study examined different phenomena related to two-phase flow, no two data sets contained the exact same data. Thus each data set had to be processed individually in Microsoft (MS) Excel™ spreadsheets before they could be merged into a single spreadsheet where the data sets could be compared against each other.

Each data set provided different values regarding the two-phase flow experiments that were performed. It was necessary to know average pressure and temperature for which each experiment operated in order for the densities of the vapor and the liquid, viscosities of the vapor and the liquid and the surface tension of the liquid to be determined. The thermodynamic properties of air, nitrogen, Freon-113, heptane and water were determined using the Xprops [58] add-on for MS Excel™. Properties for the glycerol concentrations used by Oshinowo were determined by finding the properties of water at the given pressure and temperature, and using multipliers that were provided by Oshinowo and Charles. [59,60,61]

Each data set had to provide some form of data that allowed for the calculation of the average velocities of the liquid and vapor within the test section. In most cases, this was determined from the mass flow rates of each phase. Using the densities of the liquid and vapor, the volumetric flow rates could be calculated. Given the diameter of the test section, the volumetric fluxes could be derived from the volumetric flow rates. The velocities would then be solved for using the volumetric fluxes and the void fraction that had been obtained from the data.

The void fraction and the pressure gradient proved to be two very critical pieces of data necessary to calculate the interphase friction. Initial calculations allowed for cases where void fraction was derived from the pressure gradient, rather than being directly measured. However, with the derivation of the interphase friction taking on the role of changing void fraction, vapor density and liquid and vapor velocities, the assumption that the void fraction was directly related to the pressure gradient was no longer valid. This led to the exclusion of data from Petrick [63] and Smissaert [78], along with other data sources not mentioned above.

Early wall friction calculations were determined using a force balance that neglected the pressure drop due to acceleration. However, when accounting for changes in vapor density, void fraction, liquid velocity and vapor velocity, the accelerational pressure drop becomes a necessary term for analysis. Thus, the wall friction needed to be calculated independently of the force balance. Several correlations exist for calculating the wall friction of two-phase flow, but none are more widely used than the Lockhart-Martinelli [52] correlation that has been discussed. One weakness of the Lockhart-Martinelli parameter is that the correlation exists primarily as a table of point values, where for a given value of X, there is a corresponding Φ_f and Φ_g. There is no explicit function provided by Lockhart and Martinelli that shows Φ_f or Φ_g as a function of X only.

For this dissertation, a correlation was developed where the parameter Φ_f could be predicted within 5% of the published value of Φ_f as a function of X, using Equation 262.

$$\Phi_f = A \cdot 10^{B\left(e^{C\log(X)}\right)} \quad 262$$

where the values A, B and C are coefficients defined in Table 6.

Table 6: Coefficients for Lockhart-Martinelli Function

Φ_f	$X \geq 40$			$40 > X \geq 1$			$X < 1$		
Category	A	B	C	A	B	C	A	B	C
tt	0.6699	0.8100	-0.6536	0.6699	0.8100	-0.6536	0.1862	1.3778	-0.3658
vt	0.0119	2.2506	-0.0668	0.0083	2.6093	-0.1396	0.0046	2.8219	-0.2237
tv	0.0119	2.2506	-0.0668	0.0091	2.5526	-0.1218	0.0064	2.6650	-0.2328
vv	0.0119	2.2506	-0.0668	0.0115	2.3297	-0.0985	0.0042	2.7293	-0.2397

In Table 6, the four flow categories; tt, tv, vt and vv, represent whether the liquid and vapor phases are experiencing turbulent or viscous flow, respectively. The liquid and vapor phases are determined to be turbulent or viscous by calculating the Reynolds number for each phase, specified in Equations 21 and 22. While Lockhart and Martinelli [52] specified that each phase experienced viscous flow for its phasic Reynolds number being less than 1000, for this analysis, it was assumed for simplicity that all phasic flows with a phasic Reynolds number less than 2000 were viscous.

The form of Equation 262 was selected because when the Lockhart-Martinelli [52] parameters are plotted on a log-log chart, the function, $\Phi_f(X)$, resembles an exponential curve. However, when a singular curve for all values of X was attempted for each Φ_f, the function would only match within 5% of the Lockhart-Martinelli value for a small range. Thus, the function was broken up into three different curves, where each curve was able to match the Lockhart-Martinelli value within ±5% for the entire range of values for X. With Φ_f determined, the wall friction could be determined using the equations discussed in Section 2.1.1.4. The wall

friction was calculated using the properties of both the vapor and the liquid, so as to ensure that the end result was consistent with the data.

Once the wall friction had been calculated, the accelerational pressure gradient was determined using a force balance with the overall pressure gradient, the hydrostatic pressure gradient and the frictional pressure gradient, as shown in Equation 263.

$$\left(\frac{dP}{dz}\right)_A = \frac{dP}{dz} - \left\{\left[\alpha\rho_g + (1-\alpha)\rho_f\right]g + F_W\right\} \qquad 263$$

where the subscript *A* stands for acceleration, and F_W represents the total pressure drop for wall friction.

The accelerational pressure gradient allowed for the calculation of the void fraction gradient, using Equation 264 below.

$$\frac{d\alpha}{dz} = \frac{\left(\frac{dP}{dz}\right)_A - \alpha {v_g}^2 \frac{d\rho_g}{dz}}{\rho_f {v_f}^2 - \rho_g {v_g}^2} \qquad 264$$

The vapor density gradient was approximated for all data sets using the overall pressure gradient and the ideal gas law, as shown in Equation 265.

$$\frac{d\rho_g}{dz} = \frac{1}{R_g T}\frac{dP}{dz} \qquad 265$$

The interphase friction was calculated using the equations derived from the vapor momentum balance, the liquid momentum balance and the overall momentum balance shown in Equations 266, 267 and 259, respectively, to ensure that the results were consistent and that no errors had been made in calculating the interphase friction. Any differences found between the three values were always fixed by correcting errors in data entry or formulae entered into the MS Excel™ spreadsheet.

$$F_{INT} = \alpha\left(\frac{dP}{dz} - \rho_g g\right) - \alpha {v_g}^2 \frac{d\rho_g}{dz} + \rho_g {v_g}^2 \frac{d\alpha}{dz} \quad 266$$

$$F_{INT} = (1-\alpha)\left(\rho_f g - \frac{dP}{dz}\right) + F_W + \rho_f {v_f}^2 \frac{d\alpha}{dz} \quad 267$$

Data points that resulted in negative interphase friction values were discarded. Because of the use of a correlation to predict wall friction, rather than a measurement, the sensitivity of the interphase friction to the wall friction was determined. The sensitivity of the interphase friction to wall friction was found by finding the derivative of the interphase friction force with respect to the wall friction, and is given in Equation 268. Using the sensitivity, the error in the interphase friction force that would be produced by a 50% error in the wall friction calculation was determined, using Equation 269. Data points for which a 50% error in wall friction results in an error in the wall friction correlation of greater than or equal to 50% were also discarded.

$$\frac{dF_{INT}}{dF_W} = \frac{\rho_g {v_g}^2}{\rho_g {v_g}^2 - \rho_f {v_f}^2} \quad 268$$

$$\%\, Error = 0.5 \frac{F_W}{F_{INT}} \frac{dF_{INT}}{dF_W} \quad 269$$

3.1.5: Correlation Development

The first step is to compare the non-dimensionalized interphase friction forces that have been developed against the dimensionless values to determine which non-dimensionalized interphase friction force provides the best correlation. This is done by examining the values of the non-dimensionalized interphase friction forces and comparing the values to the dimensionless parameters to determine which set of values best characterizes the physics of interphase friction with two-phase flow.

Once the most appropriate non-dimensionalized interphase friction force, f_{INT}, is selected, it will be compared against the various non-dimensional parameters that have been derived and discussed, with the emphasis placed on developing a correlation between the interphase friction force and the non-dimensional parameter. All plots, with the exception of those involving void fraction, where there is a known minimum value of 0 and maximum value of 1, are log-log (i.e. both the x and y axes are logarithmic), and are semi-log when the non-dimensionalized interphase friction force (plotted along a logarithmic axis) is compared to the void fraction (plotted on a linear axis).

When appropriate, the author has attempted to develop the correlation by analyzing plots of the data to determine which curves would best fit the data. If the data appears to fit a straight line, regardless of the type of plot, then the author has used visual observation to determine the coordinates of the line and derived the correlation from those observations. Where a curved line is more appropriate, the author has used the shape of the curve to assume a basic form, and employed a least squares error data solver to determine the coefficients that produce the minimum root mean square error, determined using Equation 270:

$$RMS = \sqrt{\sum_{i=1}^{N} \left(f_{INT_i} - f(\Pi_i) \right)^2} \qquad 270$$

where *RMS* is the root mean square error, *N* is the total number of data points, and *f(Π)* represents the correlation of a given dimensionless parameter, *Π*.

To determine the accuracy of the correlation in predicting the non-dimensionalized interphase friction, the error percentage for each data point is calculated as:

$$Percent\ Error = \frac{|f_{INT} - f(\Pi)|}{f_{INT}} \times 100\% \qquad 271$$

With the error percentage calculated for each point, attention will be focused on the mean and median average error percentages, the maximum percent error, as well as the number of points that fall within a ±20% error and a ±50% error.

After an initial correlation has been developed, the non-dimensionalized interphase friction will be normalized by the correlation, so as to produce a random distribution of points about a mean value, with which the standard deviation could be determined. As the standard deviation is being determined using what can only be safely called a sample of the entire population of potential data, it will be calculated using Equation 272.

$$\sigma = \sqrt{\frac{\sum_{i=1}^{N}\left(f_{int_i} - \overline{f_{int}}\right)}{N-1}} \qquad 272$$

where σ is the standard deviation, f_{int} is the non-dimensionalized interphase friction force normalized by the correlation, with the barred f_{int} representing the mean average and N is the total number of data points that are being analyzed.

In order to gain a greater statistical understanding of the correlation, the skewness and kurtosis of the distribution has also been studied. As discussed by Vince and Lahey [85], the skewness provides a statistical description of how a population is distributed along its mean, with the coefficient of skewness solved by using Equation 273:

$$C_s = \frac{\sum_{i=1}^{N}\left(f_{int_i} - \overline{f_{int}}\right)^3}{\left(\sum_{i=1}^{N}\left(f_{int_i} - \overline{f_{int}}\right)^2\right)^{1.5}} \qquad 273$$

where C_s is the coefficient of skewness. Ideally, the coefficient of skewness would have a value of 0, indicating that the data is evenly distributed around the mean average. If $C_s > 0$, it is known as positive skewness, and would indicate that there are more f_{int} values that are greater than the mean than less than the mean.

The kurtosis is used to describe the concentration of data points near the mean value, and is quantified by the coefficient of kurtosis, C_k, given in Equation 274. A normal distribution would have $C_k = 3$, while $C_k < 3$ indicates a flatter distribution curve and $C_k > 3$ indicates a more peaked distribution. [83]

$$C_k = \frac{\sum_{i=1}^{N}\left(f_{int_i} - \overline{f_{int}}\right)^4}{\left(\sum_{i=1}^{N}\left(f_{int_i} - \overline{f_{int}}\right)^2\right)^2} \qquad 274$$

Normalized data points that are within 2 standard deviations of the mean normalized value will be used to re-evaluate the interphase friction correlation, eliminating the effect of statistically insignificant outliers, to determine the final correlation with respect to the given parameter. The process will be repeated with the other non-dimensional parameters until the standard deviation is no longer decreasing with the addition of a new parameter.

3.2: Model Comparison Procedures

With the development of the interphase friction correlations from the data, it is necessary to compare the correlations against those that are used by RELAP5/MOD2 [66], RELAP5/MOD3.3 [69], RELAP5-3D [67] and TRACE [83]. First, the interphase friction force that is calculated using the force balance equation is compared to the developed correlations and the equations provided in the manuals of RELAP5/MOD2, RELAP5/MOD3.3, RELAP5-3D and TRACE. As the source code is also available for RELAP5/MOD3.3 [40], additional comparisons are made to the RELAP5/MOD3.3 source code, as well as the output of executed RELAP5/MOD3.3. The RELAP5/MOD3.3 source code is then modified so as to calculate the interphase friction force using the correlations that have been developed. Additional modifications are made to the RELAP5/MOD3.3 source code to test the effectiveness of

individual physical correlations for annular flow to improve the modeling of the annular flow data points.

3.2.1: Comparisons of Nuclear Thermal Hydraulic Code Manuals

To compare the correlation that has been developed against those that are used by RELAP5/MOD2 [66], RELAP5/MOD3.3 [69], RELAP5-3D [67] and TRACE [83] requires calculating the interphase friction that is predicted by the equations used in each model. The correlation should allow for a fairly easy calculation of the interphase friction, by using the non-dimensional correlation that has been developed and multiplying it by the variables against which the interphase friction force has been non-dimensionalized.

Comparisons of the correlation are made to all four models, using the equations that are provided in each thermal-hydraulic codes user manual, and the data that has been used to develop the correlation. These calculations were performed in a MS Excel™ spreadsheet. As the executable version of RELAP5/MOD2, RELAP5-3D and TRACE were unavailable, comparisons can only be made with the interphase friction that is predicted based on the equations provided in their respective manuals.

3.2.2: Comparisons of the RELAP5/MOD3.3 Manual and Source Code

With the source code for RELAP5/MOD3.3 [40] available, the equations for interphase friction provided in the manual [69,70] were compared to those found in the source code. As several differences between the two sources were noticed, it was determined that the interphase friction force needed to be calculated both ways, and to have the results compared.

3.2.3: Comparisons of the RELAP5/MOD3.3 Executable

Comparing the interphase friction force that is calculated by using the equations in the manual and the source code only provide a theoretical prediction of how RELAP5/MOD3.3 [40] will model two-phase vertical upflow. The interphase friction force that is calculated using the equations in the manual and in the source code assume that the pressure, temperature, pressure gradient, void fraction, phasic velocities and other parameters will remain constant. When RELAP5/MOD3.3 is executed, all of these variables are allowed to change, to allow RELAP to achieve what it considers to be a converged solution.

To model the vapor-liquid scenarios in RELAP5/MOD3.3 [40], a prototypical input file was developed to replicate the test apparatuses used for all studies, and could be easily modified so both steam-water and air-water cases could be replicated. No RELAP model runs were conducted with other liquids, such as heptane or varying concentrations of glycerol. Data from Schlegal [75] was not modeled as Schelgal's data represented four different intervals within the same trial run, with no entrance length specified before the air-water mixture entered the bottom test interval.

Each phase would start in a time dependent volume positioned at the bottom of the simulated apparatus. From their respective time dependent volumes, each phase would empty into a branch connection, where the vapor and liquid would mix, with diameter specified by the study from which that model was replicating. The two-phase mixture would then rise through an entrance length, modeled as two pipe volumes with a total length specified by the study, before entering the test section. The test section was modeled as five volumes, with a total combined length equal to that specified in each study. The two-phase mixture would then flow through an exit region, consisting of two pipe volumes measuring 2.5 ft. each in length, followed by an exit

time dependent volume measuring 15.0 ft. in length. A schematic of the input file is provided in Figure 10.

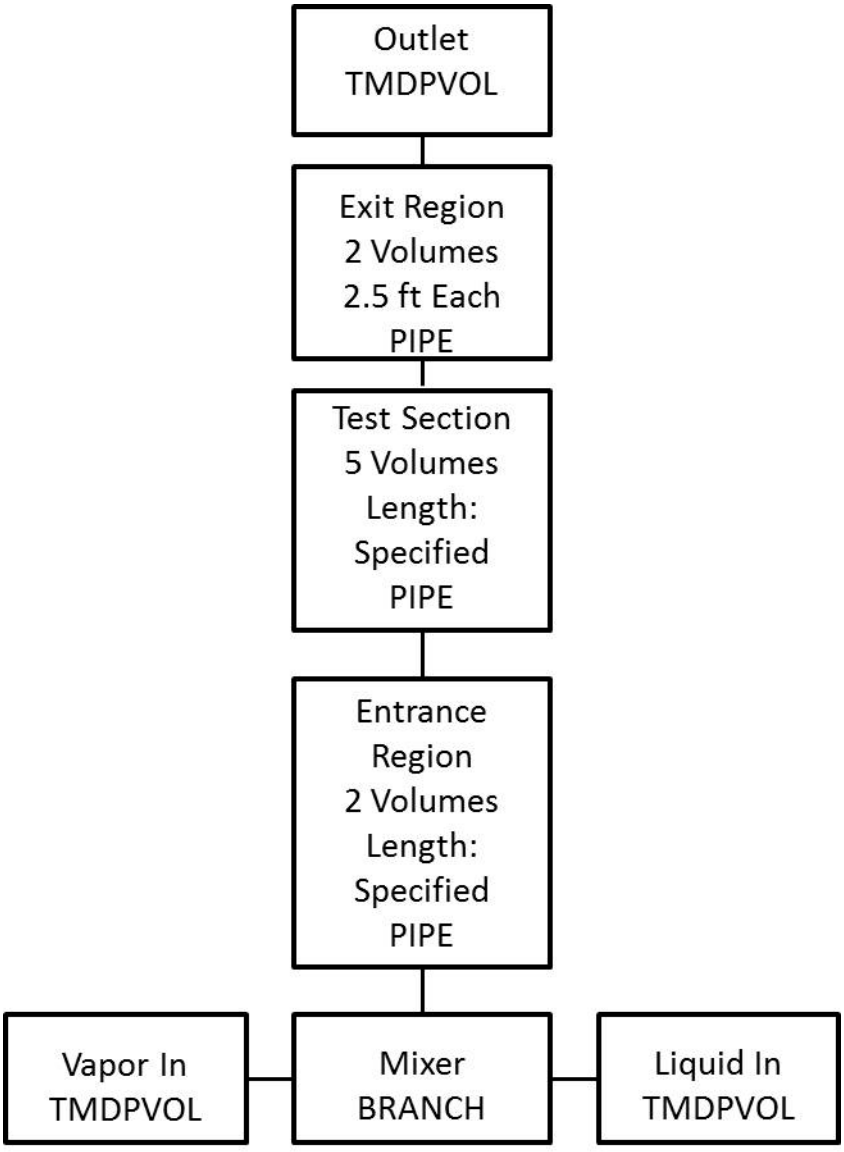

Figure 10: Schematic of RELAP5/MOD3.3 Input File Apparatus Setup

For steam-water test cases, the vapor and liquid were held at a quality of 1.0 and 0.0, respectively, within the time dependent volumes at the bottom of the test apparatus. However, for air-water test cases, it was found that setting the quality within the liquid time dependent volume forced RELAP to assume that the air was dry throughout the test apparatus, and resulted in simulations that largely kept the water from rising through the test section. By increasing the

quality within the liquid time dependent volume to a nominal value of 10^{-8}, RELAP was able to model the air with saturated water vapor, and assured that mass was conserved throughout the test section.

3.2.3: Comparisons with RELAP5/MOD3.3 Modified by the Developed Correlations

The source code that was provided by RSICC of RELAP5/MOD3.3 [40] could only be compiled using shell programs that were written for Linux or Cygwin in 2003. Many attempts were made to update the commands within these shell programs so that RELAP5/MOD3.3 could be compiled on a computer with a current version of Linux or Cygwin, but these attempts proved to be time consuming and unsuccessful. A Toshiba™ Satellite™ laptop computer built in 2002 was acquired, with Red Hat Linux™ 9.0 installed proved to be the only available computer that was capable of compiling the RELAP5/MOD3.3 source code, along with any version of RELAP5/MOD3.3 that was modified to include the correlations developed by this study, or any correlation found in the literature that was tested in RELAP5/MOD3.3.

In order to implement the correlations into RELAP5/MOD3.3, three different subroutines were modified: bubdrag, slugdrag and amistdrag. The subroutine bubdrag calculates the interphase friction for the bubbly flow regime, while slugdrag and amistdrag calculate the interphase friction for the slug and annular flow regimes, respectively. The subroutine dispdrag, which calculates the interphase friction for the mist pre-CHF flow regime was not modified, as the correlation could not be benchmarked for void fractions greater than or equal to 0.9999. Also, when the dispdrag subroutine was modified with the correlations, RELAP5/MOD3.3 was unable to achieve a converged solution for each of the test cases, with nearly all test cases resulting in errors.

In the subroutines bubdrag, slugdrag and amistdrag, the interphase friction factor is calculated, rather than the interphase friction force. Therefore, in order to implement the correlation into RELAP5/MOD3.3, the interphase friction force is calculated using the correlations derived, but then needs to be divided by the square of a velocity difference in the RELAP5/MOD3.3 source code in order to obtain the interphase friction factor. For the bubdrag and slugdrag subroutines, the interphase friction force calculated by the correlation is divided by the square of the vapor drift velocity, which is found by finding the difference between the vapor velocity and the total volumetric flux for the given time step within those subroutines. For the subroutine amistdrag, the correlation interphase friction force is divided by the square of the velocity difference between the vapor and liquid phases.

3.2.4: Comparisons with RELAP5/MOD3.3 Modified by the Annular Flow Physical Models

In addition to developing correlations through statistical analysis of dimensionless variables, and evaluating those correlations in RELAP5/MOD3.3 [40], individual physical correlations for annular flow were studied and selected to be tested in RELAP5/MOD3.3. Air-water and steam-water test data points that were identified as being in the annular flow regime using the RELAP5/MOD3.3 source code flow regime map were run.

IV. Results

The following results have been obtained from the data analysis procedures that have been described in Chapter III. Several plots are shown with dotted, dashed and/or solid lines. If the axes of the plot are on a logarithmic scale, only a solid line will be shown, which is used to represent that the value of the y-axis is equal to that of the x-axis. When the axes of a plot are on a normal scale, a solid line will also represent equality. Dotted lines will represent the y-axis value being ±50% of the x-axis value, while dashed lines represent y-axis values that are ±20% of the x-axis value, and are only shown when the plot is on a normal scale.

4.1: Data Analysis Results

4.1.1: Comparison of Dimensionless Parameters

First, the non-dimensionalized interphase friction force against the inertial force, $F_{INT}D_H/(\rho_f - \rho_g)(v_g - v_f)^2$, shall be compared against the dimensionless parameters that have been derived. The goal of analyzing each chart is to determine if a relationship exists between the dimensionless parameter and the non-dimensionalized interphase friction force. Such a relationship should appear in the form of a curve that the data follows along, which would allow for the non-dimensionalized interphase friction force to be described as a function of the dimensionless parameter.

The initial Reynolds number for which the non-dimensionalized interphase friction is compared against is that for the differential flow listed in Section 3.1.2. In Figure 11, it is shown that the interphase friction data follows along several lines with respect to the Reynolds number. This would indicate that there is either a missing variable or an extra variable in the calculation of the Reynolds number which is causing the data to split into several groups. Figure 12 shows that each study appears to fall along its own line. The differentiation of the Oshinowo [59] data

would indicate that the primary driver of differences between each line would be the properties of the liquid. However, with Schlegal [75] comprising of air-water data that does not fit with the rest of the data sets, then the attention turns to the diameter of the pipe as another potential reason why the data does not fit along a single curve. This is further shown in Figure 13 where the Schlegal data is broken down by test section diameter. The Schlegal experiments conducted with a diameter of 0.4987 ft. have smaller dimensionless interphase friction values with respect to Reynolds number than the experiments with a diameter of 0.6660 ft., indicating that there may also be sensitivity to the pipe diameter. There is also the possibility that such sensitivity to the diameter is manufactured by the inclusion of the pipe diameter in the non-dimensionalized interphase friction.

There is also concern over the large range of values for the non-dimensionalized interphase friction force, as it appears to be spread across nine orders of magnitude. However, when examining the actual interphase friction force, values only range by two orders of magnitude in units of lb_f/ft^3. Non-dimensionalization of the interphase friction force should not increase the orders of magnitude so significantly, and suggests that the inertial force may not be appropriate for non-dimensionalizing the interphase friction force, because the effect of the inertial force is masking the effect of the interphase friction force that is being studied.

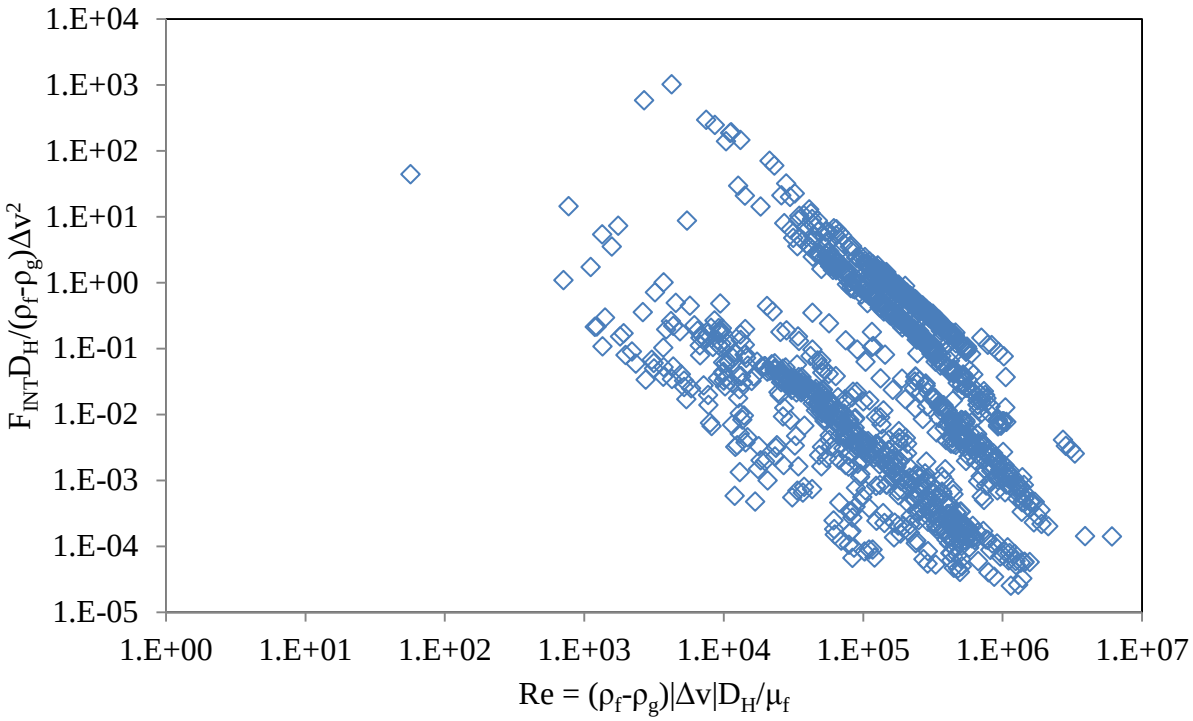

Figure 11: Comparison of the Interphase Friction Force Non-Dimensionalized by the Inertial Force Compared Against the Flow Difference Reynolds Number

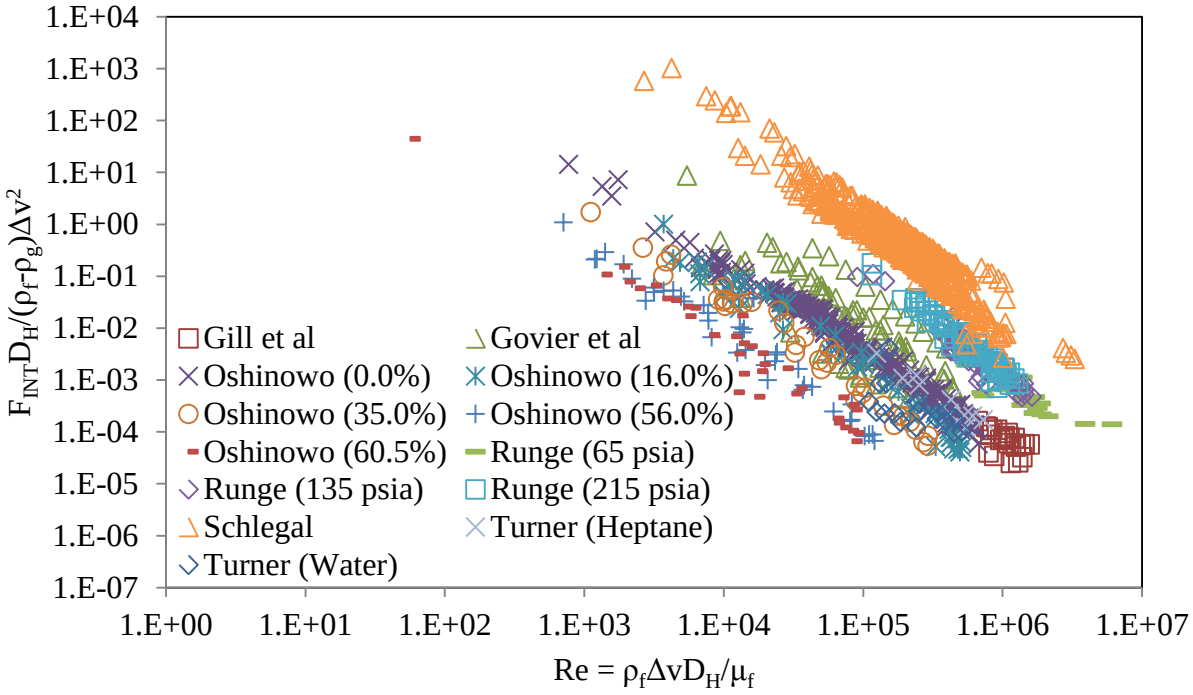

Figure 12: Comparison of the Interphase Friction Force Non-Dimensionalized by the Inertial Force against the Flow Differential Reynolds Number with Studies Specified

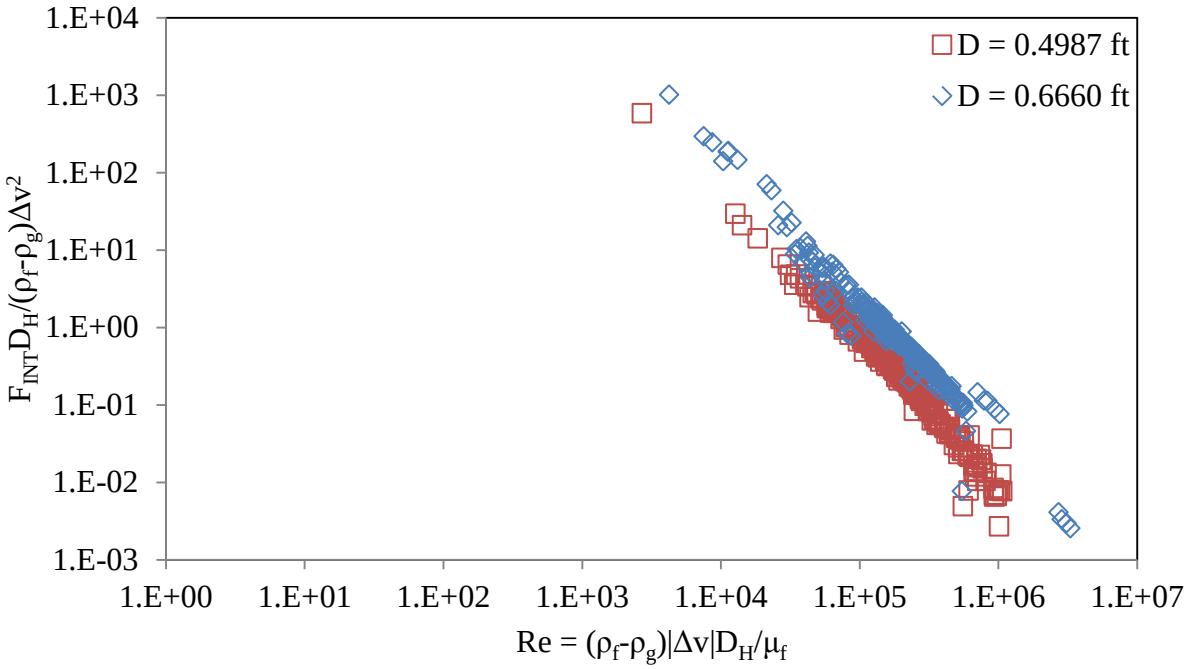

Figure 13: Comparison of the Interphase Friction Force Non-Dimensionalized by the Inertial Force against the Flow Differential Reynolds Number Using Schlegal's [75] Data

In Figure 14 and Figure 15, the interphase friction force non-dimensionalized by the inertial force is compared against the particle Reynolds number for a continuous liquid phase. In both of these charts, there appears to be a general trend of increasing interphase friction with increasing particle Reynolds number. There appears to be three separate curves for which the data follows along, with the line with higher interphase friction made up mostly of Schelgal [75] data, the middle line consists of Oshinowo [59] data and the bottom line appears to consist of data from Gill et al [29], Runge and Turner [84]. Ideally, there should be two curves instead, one that fits data with a continuous liquid phase and another for a continuous vapor phase.

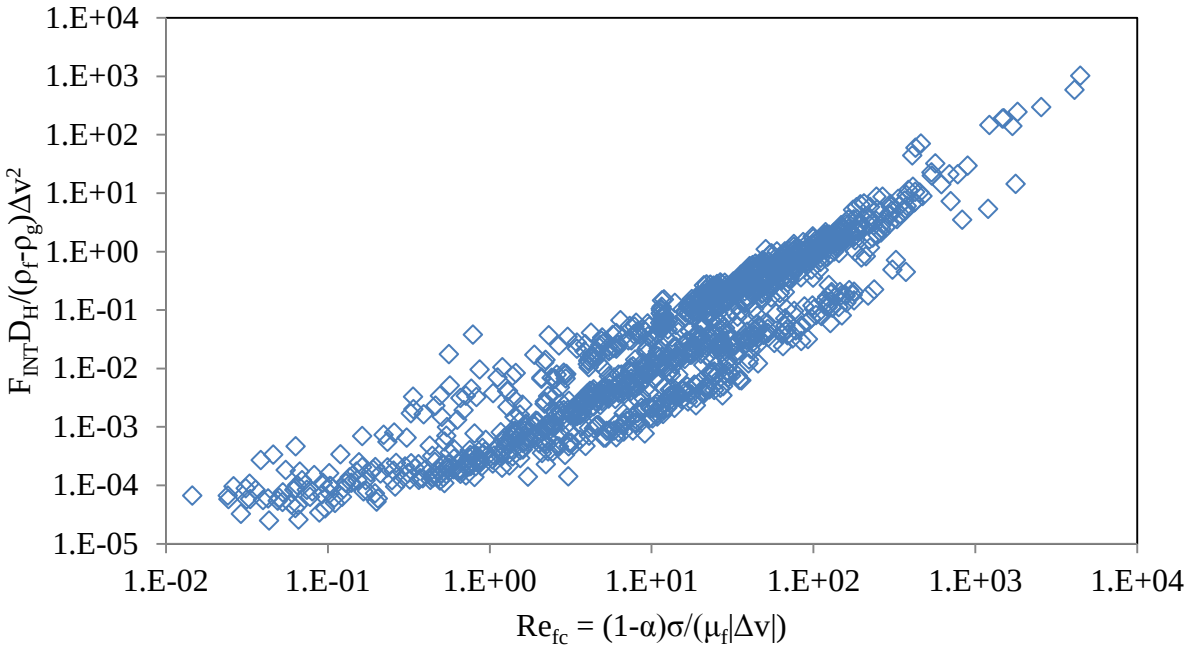

Figure 14: Comparison of the Interphase Friction Force Non-Dimensionalized by the Inertial Force to the Particle Reynolds Number for a Continuous Liquid Phase

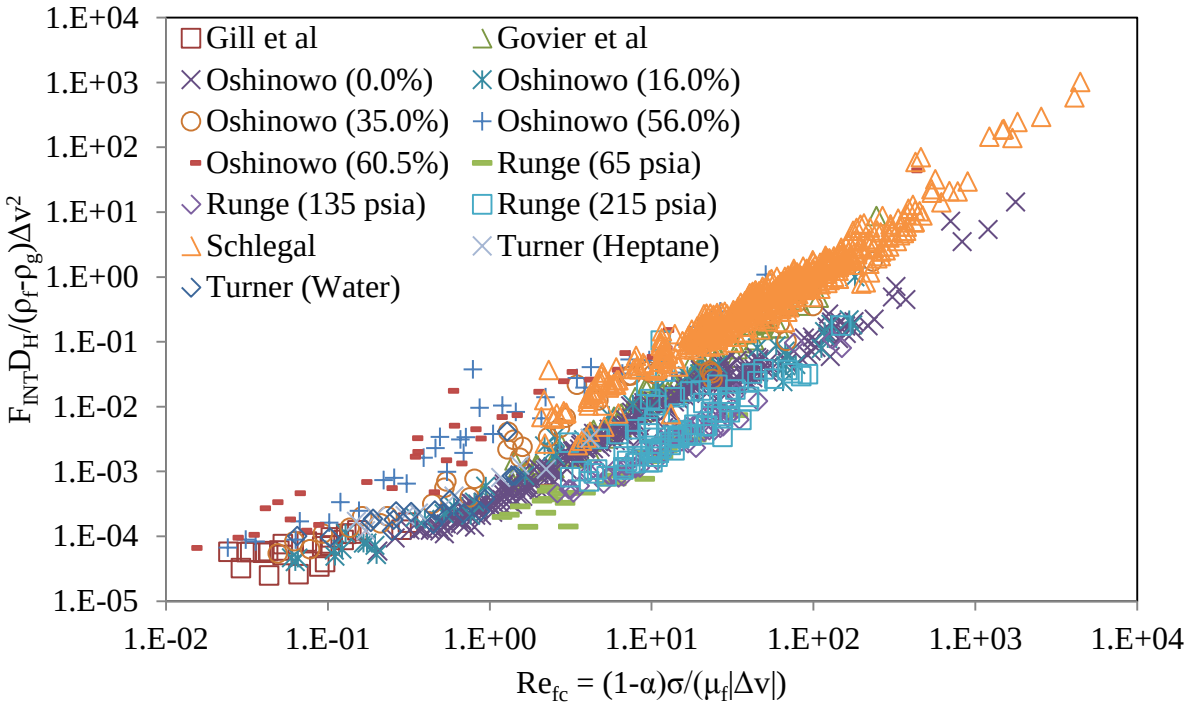

Figure 15: Comparison of the Interphase Friction Force Non-Dimensionalized by the Inertial Force against the Particle Reynolds Number for a Continuous Liquid Phase with Studies Specified

In Figure 16, the interphase friction force is compared against the particle Reynolds number for a continuous vapor phase. There appears to be a hook along which the data fits along, but this particular variable is meant to link the data from Gill et al [29], Runge and Turner [84] together, as those are the studies for which most of the data was documented as annular flow. Most of those data sets are obscured in Figure 17, although they appear to be concentrated between Re_{gc} = 100 and 1000. Figure 18 shows the data from Gill et al, Runge and Turner, and the results appear to resemble a mass rather than a curve, making the determination of a curve difficult without further investigation. This can only be done with the implementation of a flow regime map that decides whether the liquid or vapor phase is continuous.

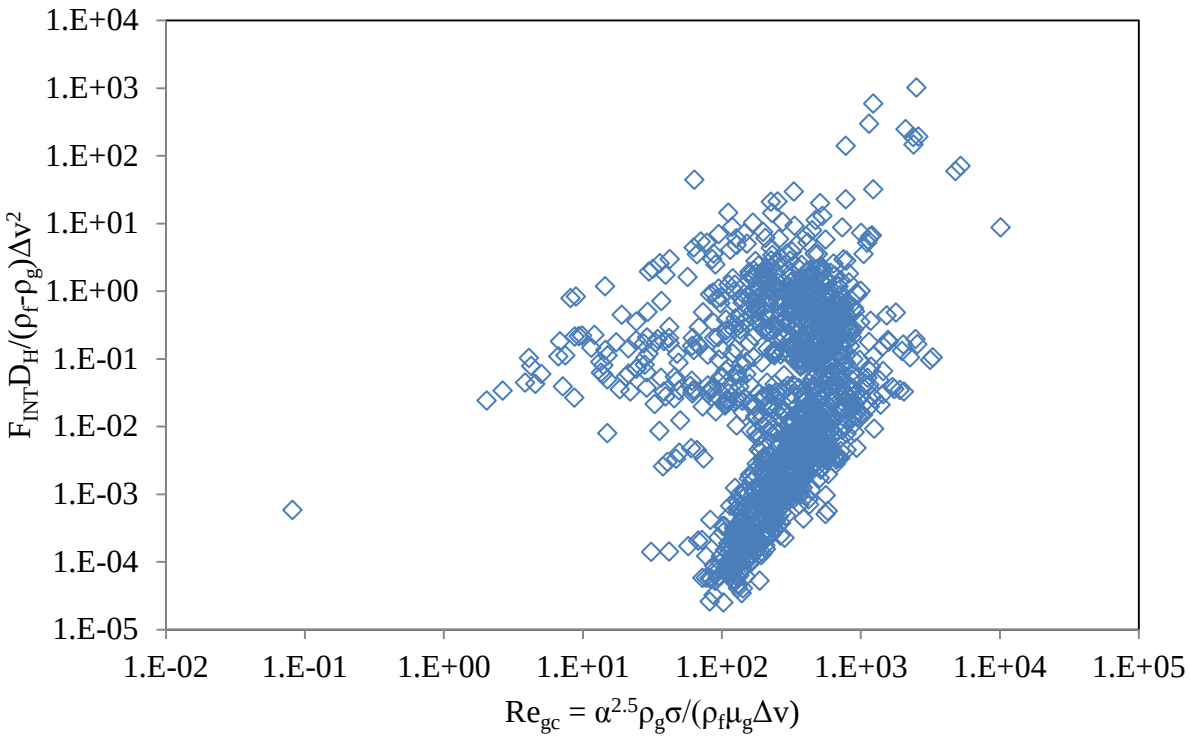

Figure 16: Comparison of the Interphase Friction Force Non-Dimensionalized by the Inertial Force against the Particle Reynolds Number for a Continuous Vapor Phase

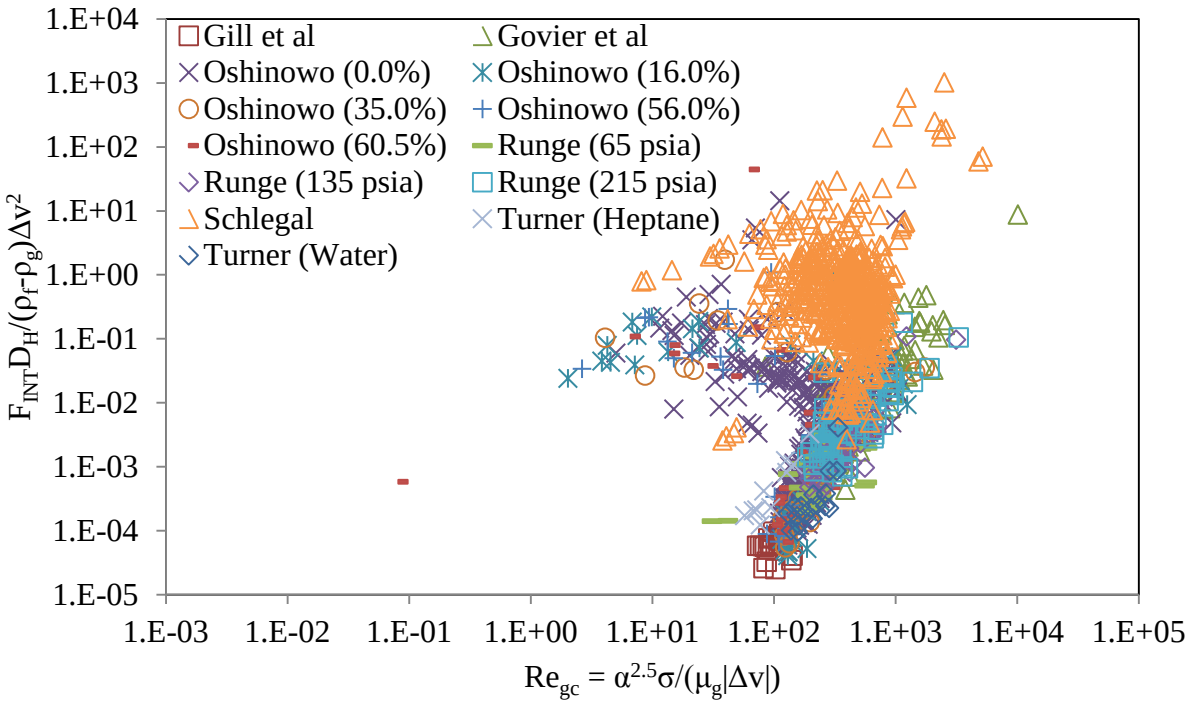

Figure 17: Comparison of the Interphase Friction Force Non-Dimensionalized by the Inertial Force against the Particle Reynolds Number for a Continuous Vapor Phase with Studies Specified

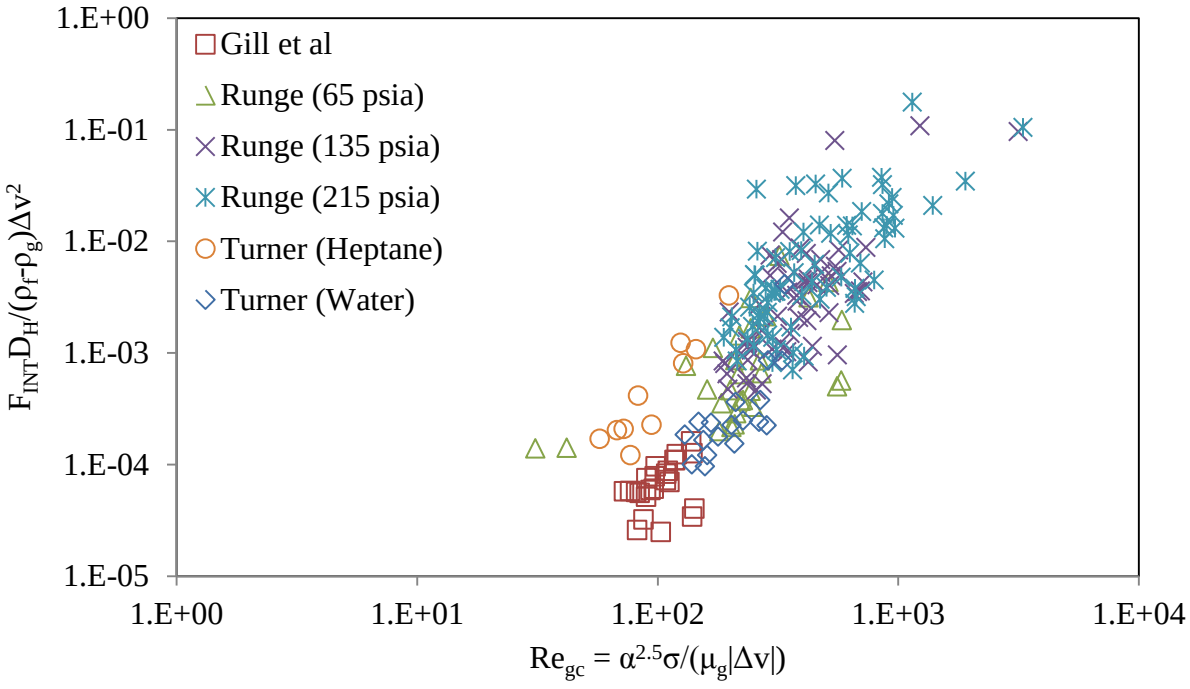

Figure 18: Comparison of the Interphase Friction Force Non-Dimensionalized by the Inertial Force against the Particle Reynolds Number for a Continuous Vapor Phase with Data from Gill et al [29], Runge and Turner [84]

Next, the interphase friction force is compared against the Weber number, which Figure 19 shows is a very interesting relationship. Two definitive curves appear that the data appears to fall along. This could be very useful if it were to also correlate with the continuous phase or with a change in the fluid properties that could be used to predict interphase friction under a wide set of conditions. However, as Figure 20 shows, the difference between the two lines is that the higher interphase friction line is made exclusively of data points from Schlegal [75], while the rest of the data points fall along the line with lower interphase friction values. The most significant difference between the Schlegal data and the rest of the data is that Schlegal conducted experiments with a significantly larger pipe diameter than the rest, which indicates that the pipe diameter may be a factor in interphase friction, although it may also be related to the presence of pipe diameter in both the non-dimensionalized interphase friction and the Weber number calculation.

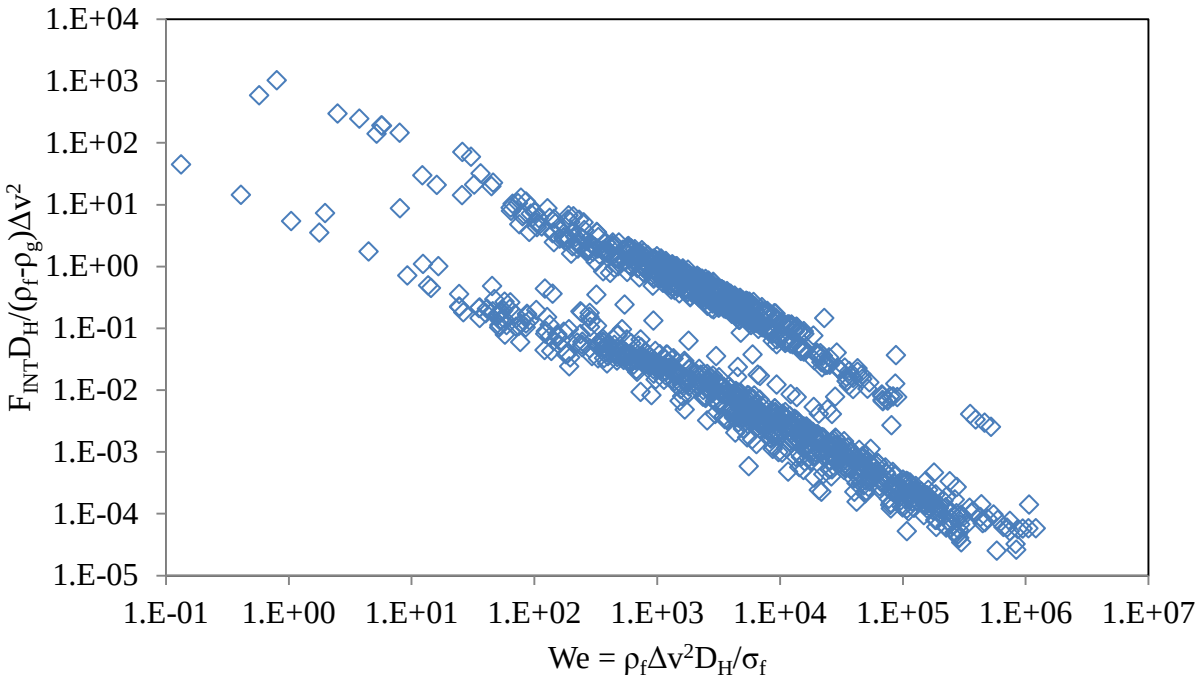

Figure 19: Comparison of the Interphase Friction Force Non-Dimensionalized by the Inertial Force against the Weber Number

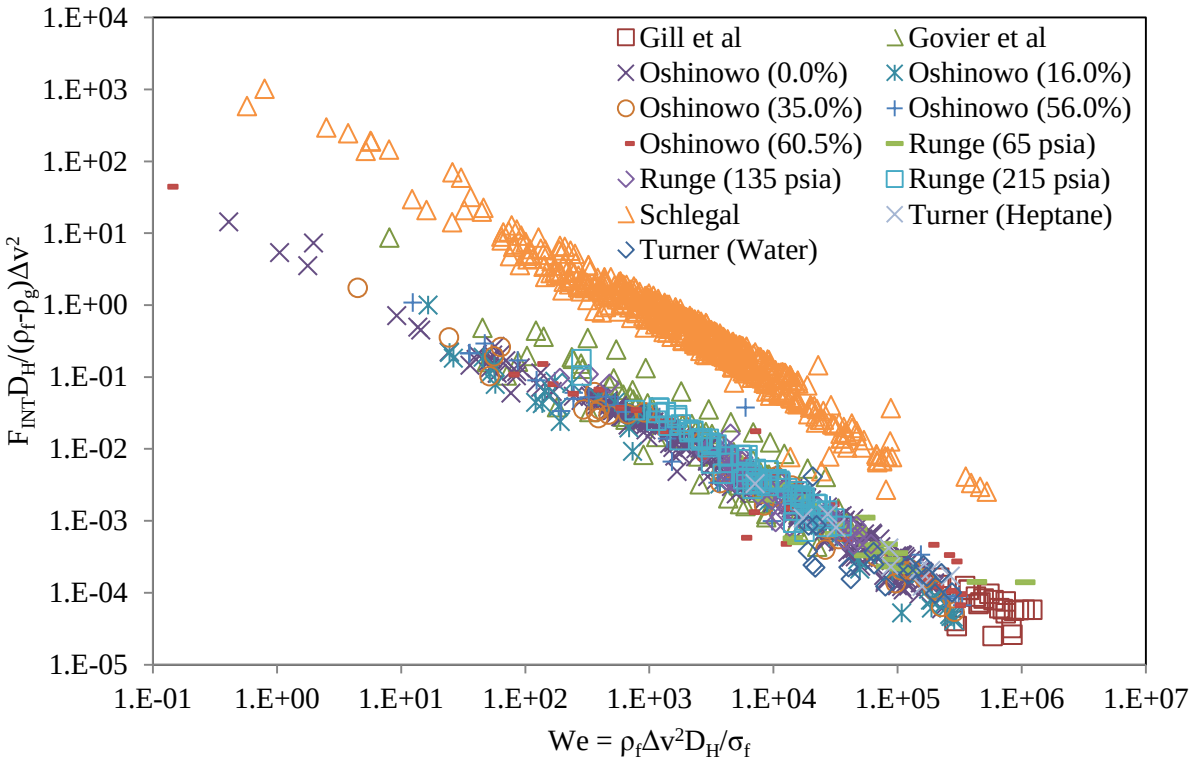

Figure 20: Comparison of the Interphase Friction Force Non-Dimensionalized by the Inertial Force against the Weber Number with Studies Specified

Next, the non-dimensionalized interphase friction force is compared against the Froude number. In Figure 21, we find that the data fits extremely well along what appears to be a straight line. Considering that Figure 21 is a log-log plot, the data appears to fit a correlation resembling Equation 275.

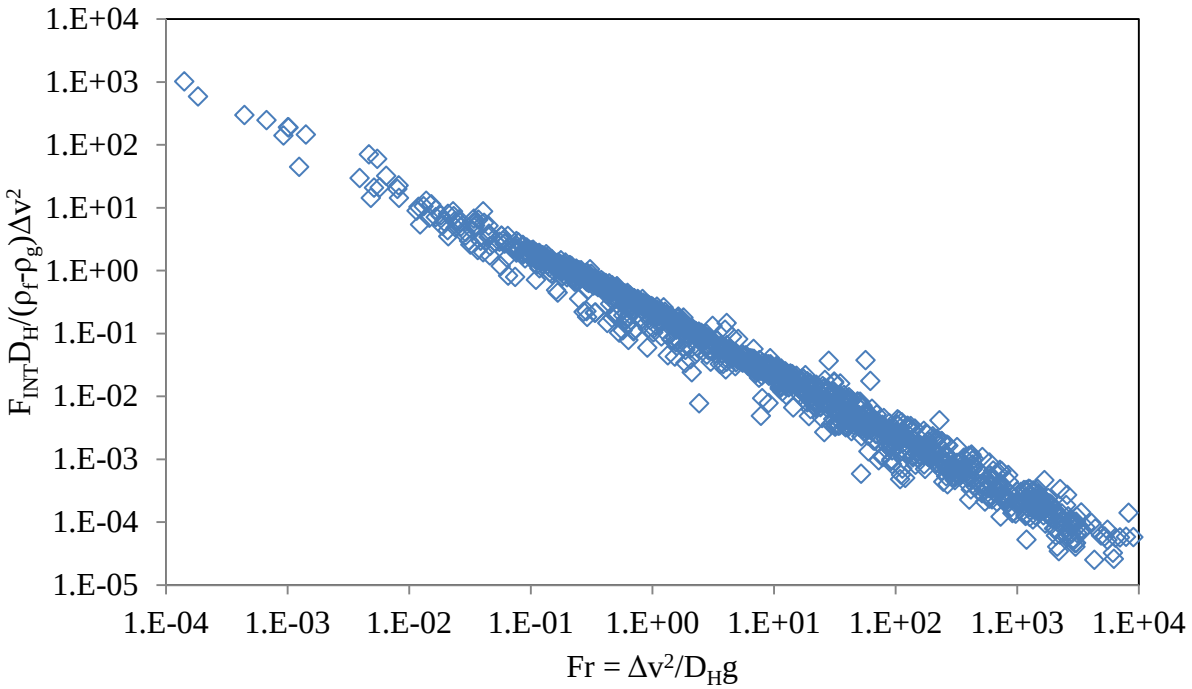

Figure 21: Comparison of the Interphase Friction Force Non-Dimensionalized by the Inertial Force against the Froude Number

$$\frac{F_{INT}D_H}{(\rho_f-\rho_g)(v_g-v_f)^2} = AFr^B \tag{275}$$

In Figure 22, the values for *A* and *B* in Equation 275 have been solved for by finding the values that produce the least squares error between the correlation and the data. The result is a value of 0.1859 for *A* and -0.961 for *B*, with a least squares error of 5.83.

While Figure 22 appears to show a correlation that fits the data fairly well, there are some physical considerations that need to be taken into account. Since the Froude number is raised to a power of approximately -1, we find that the velocity difference is raised to a power of approximately -2. However, the velocity difference appears in the non-dimensionalized interphase friction in the denominator, raised to a power of 2. Thus, the real meaning of Figure 22 becomes that the velocity difference squared equals itself, and all other variables are negligible in comparison to the velocity difference squared. This also demonstrates the wide

range of non-dimensionalized interphase friction values as largely being the result of the velocity difference, rather than resulting from a large range in interphase friction.

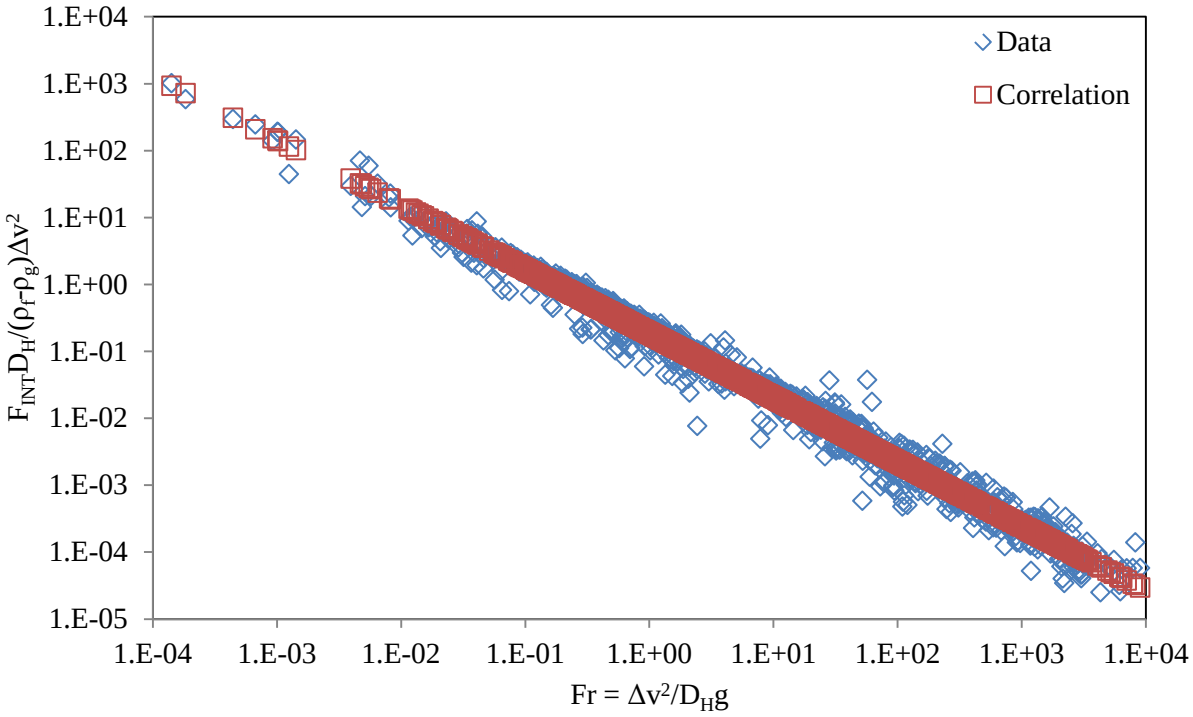

Figure 22: Comparison of the Interphase Friction Force Non-Dimensionalized by the Inertial Force against the Froude number with Correlation

Further comparisons of the interphase friction force non-dimensionalized by the inertial force against other dimensionless parameters may still show a relationship with interphase friction. In Figure 23, the interphase friction is compared against the mixture Froude number, which shows what appears to be a main correlation with several bifurcations. Figure 24 shows the relationship between the non-dimensionalized interphase friction and the velocity ratio. However, as the velocity ratio approaches 1, the non-dimensionalized interphase friction approaches ∞, with decreasing non-dimensionalized interphase friction as the velocity ratio moves away from 1, further signifying the effect of the inertial force on the non-dimensionalized interphase friction. The density ratio is compared against the non-dimensionalized interphase friction in Figure 25, although the chart shows that there is no significant relationship between

the density ratio and the non-dimensionalized interphase friction. Figure 26 shows the relationship between the non-dimensionalized interphase friction and the void fraction. It would be expected that the interphase friction would be 0 when the void fraction equaled 0 or 1, as those values correspond to the lack of a second phase. However, that does not appear to be the case in Figure 26, as the non-dimensionalized interphase friction appears to approach a median value of 1 when the void fraction approaches 0.

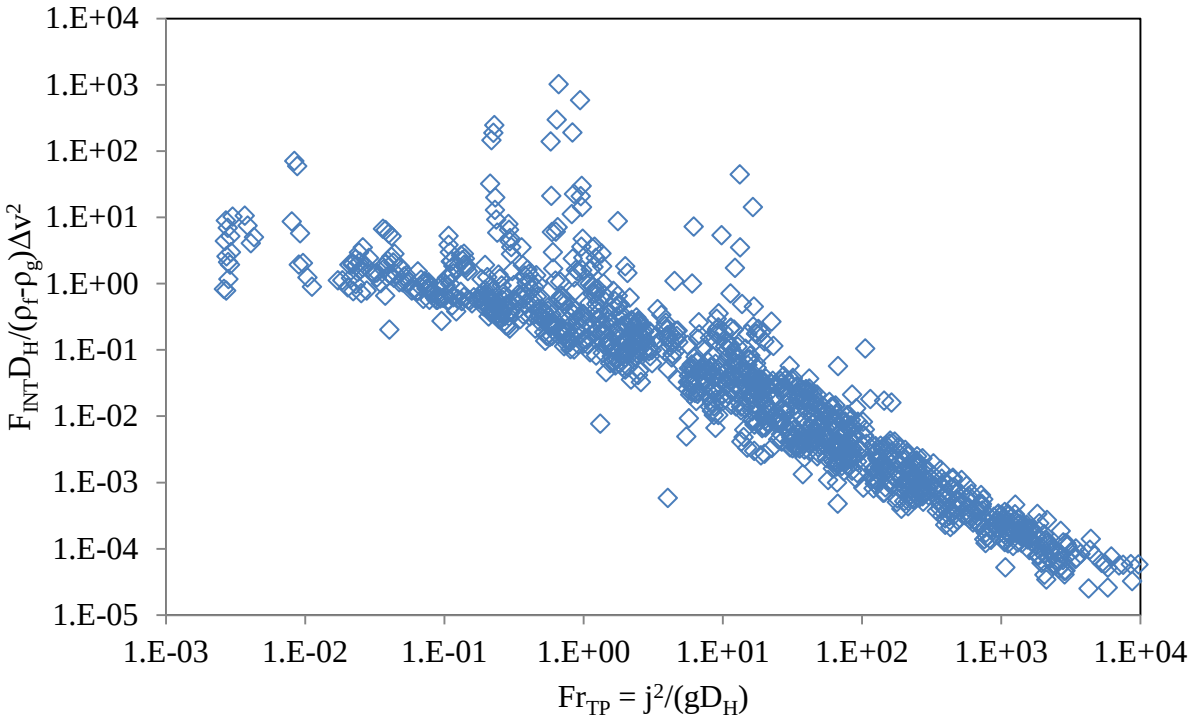

Figure 23: Comparison of the Interphase Friction Force Non-Dimensionalized by the Inertial Force against the Mixture Froude Number

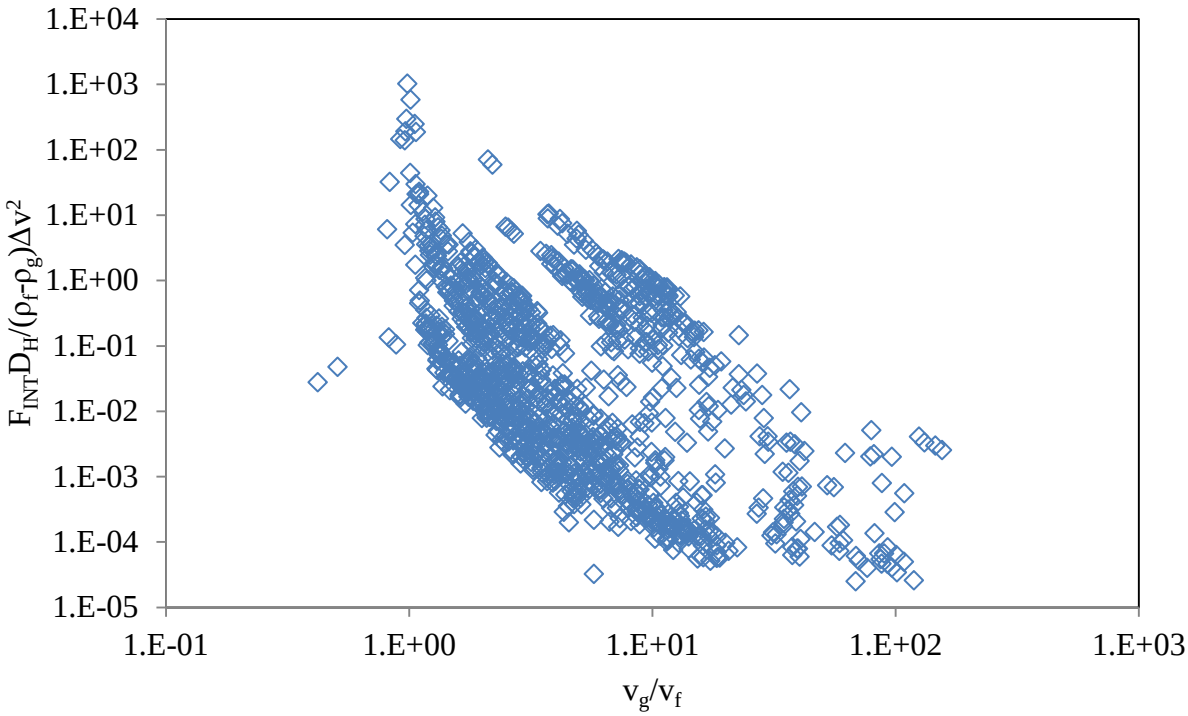

Figure 24: Comparison of the Interphase Friction Force Non-Dimensionalized by the Inertial Force against the Velocity Ratio

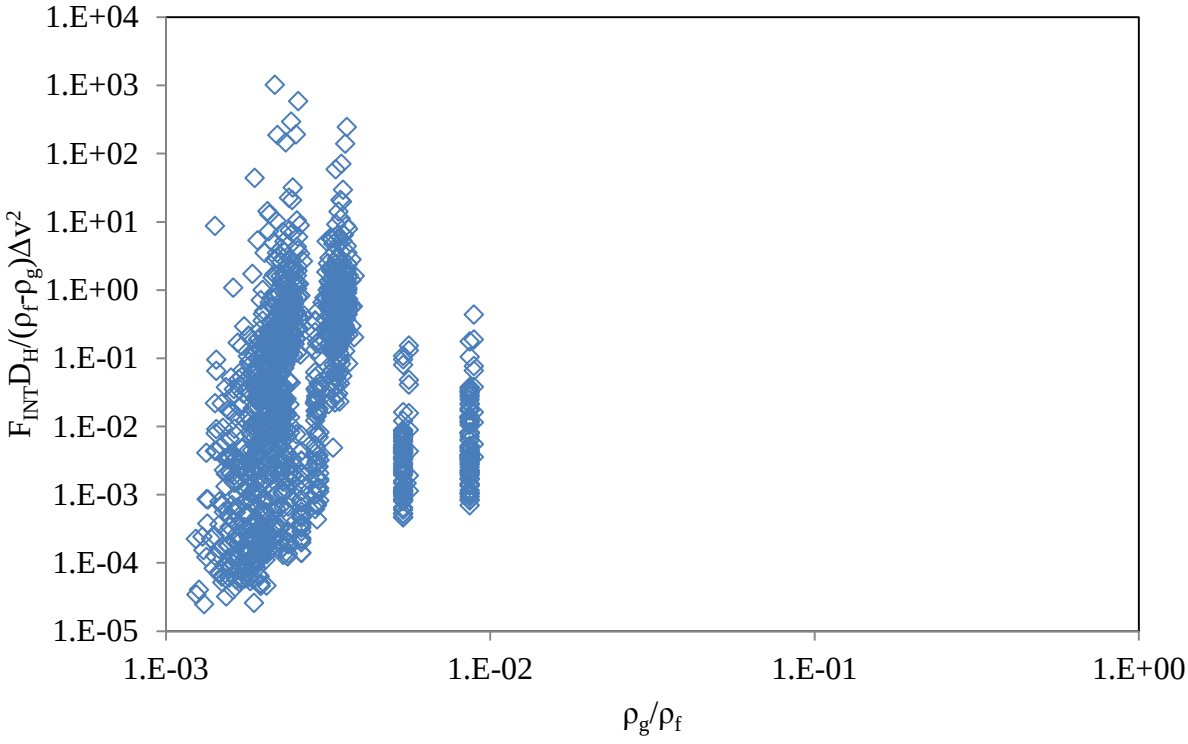

Figure 25: Comparison of the Interphase Friction Force Non-Dimensionalized by the Inertial Force against the Density Ratio

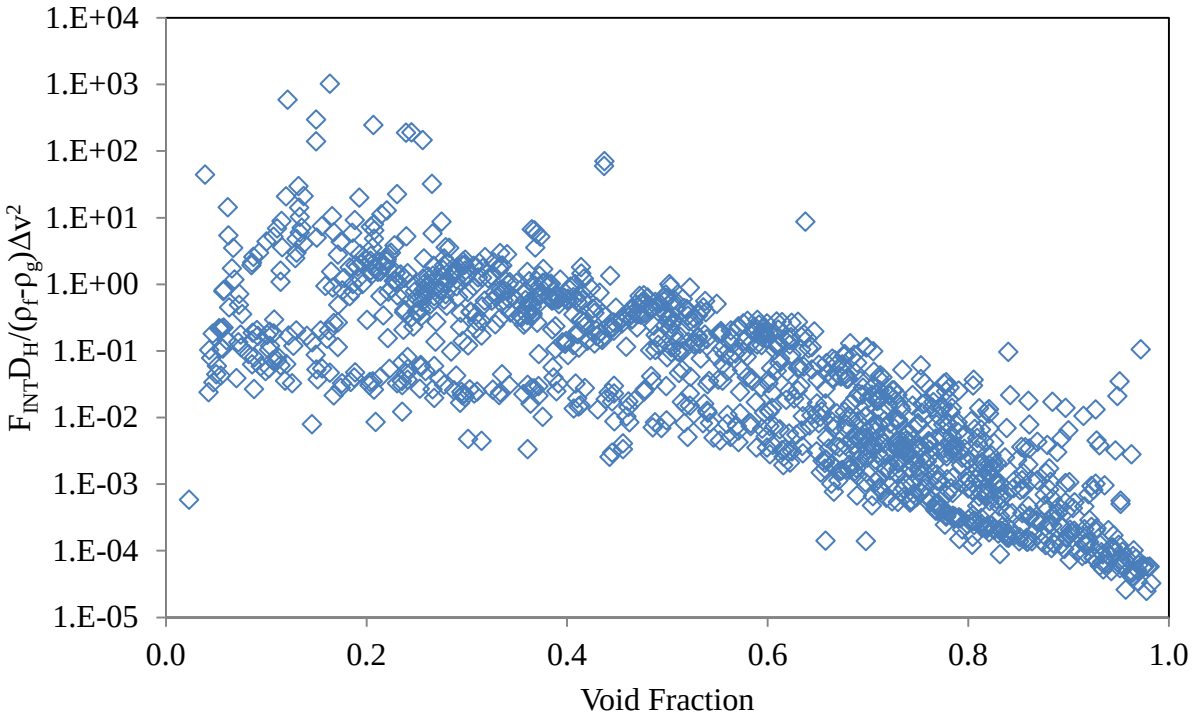

Figure 26: Comparison of the Interphase Friction Force Non-Dimensionalized by the Inertial Force against the Void Fraction

In the preceding analysis, it is shown that the inertial force dominates over the interphase friction force, and that using the inertial force to non-dimensionalize the interphase friction may not be appropriate. Instead, using a force that is more proportional to the interphase friction force would be more suitable. Since the densities of the liquid and vapor phases are generally the same order of magnitude as the interphase friction, then the density difference, $(\rho_f - \rho_g)$, may yield results where the dimensionless parameters are weighed against the interphase friction force.

In Figure 27, the interphase friction force is non-dimensionalized by the density difference and is compared to the Reynolds number. There does not appear to be a correlation between the Reynolds number and the non-dimensionalized interphase friction force, and this

appears to also be the case for the particle Reynolds numbers for continuous liquid and vapor, as shown in Figure 28 and Figure 29, respectively.

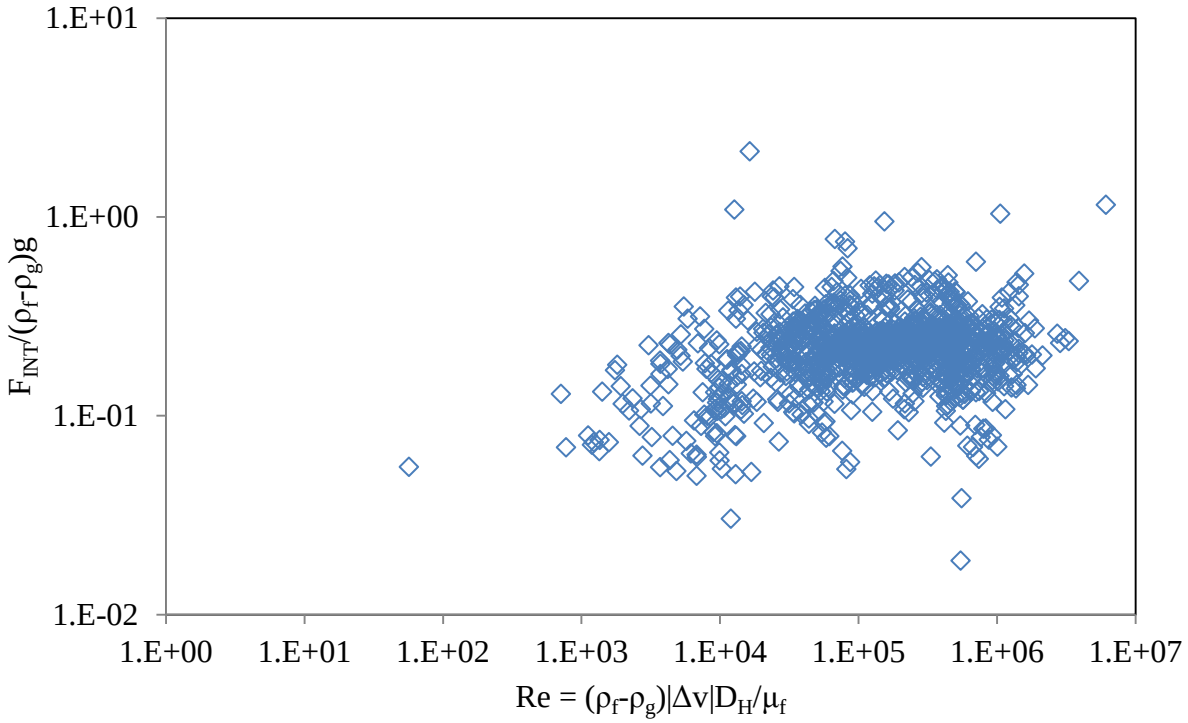

Figure 27: Comparison of the Interphase Friction Force Non-Dimensionalized by the Density Difference against the Reynolds Number

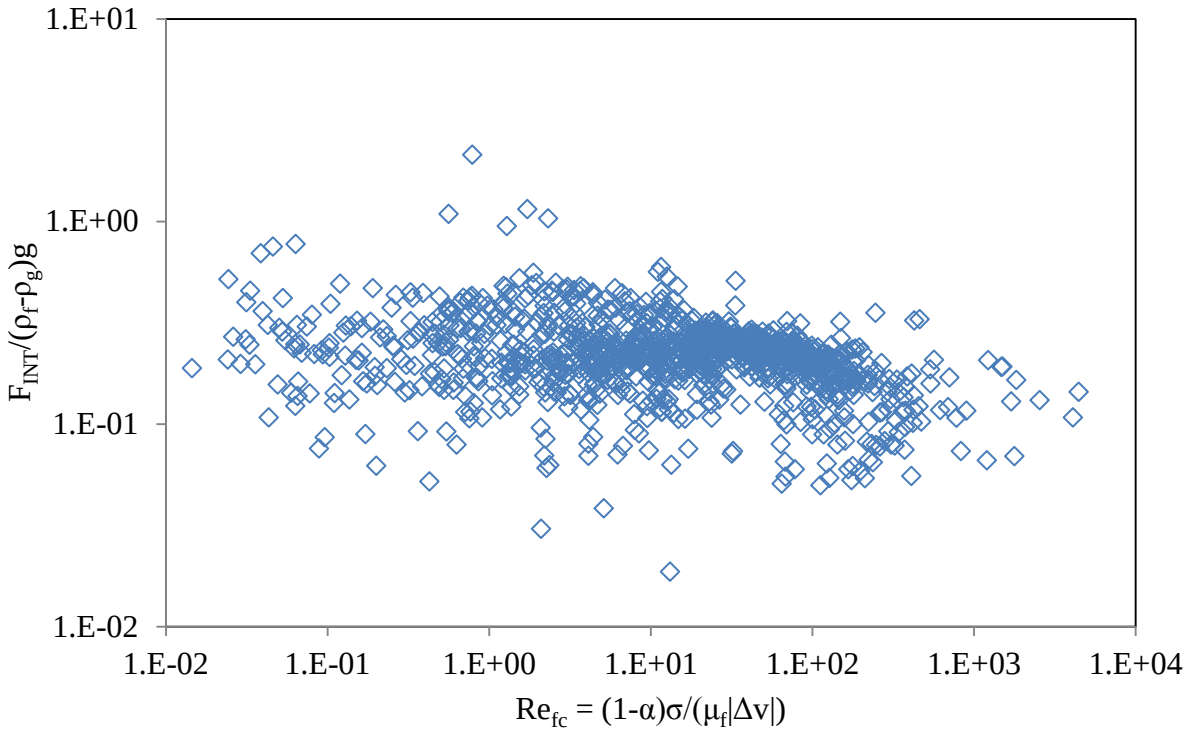

Figure 28: Comparison of the Interphase Friction Force Non-Dimensionalized by the Density Difference against the Particle Reynolds Number for a Continuous Liquid Phase

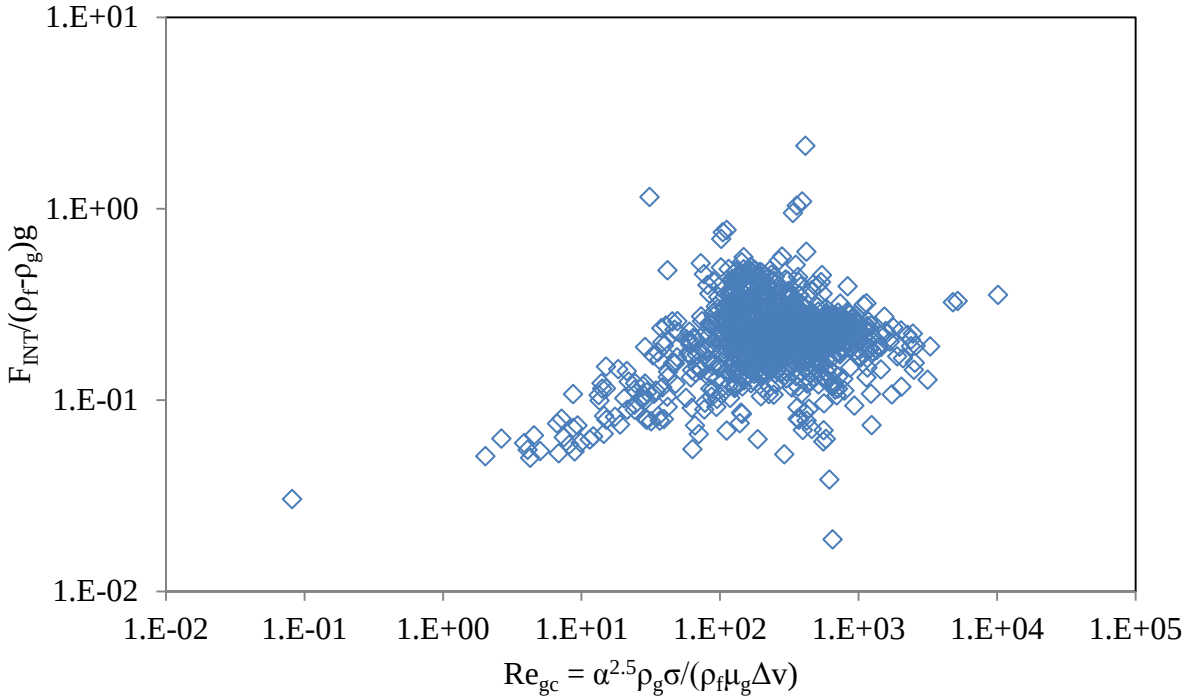

Figure 29: Comparison of the Interphase Friction Force Non-Dimensionalized by the Density Difference against the Particle Reynolds Number for a Continuous Vapor Phase

In Figure 30, the non-dimensionalized interphase friction force is compared against the Weber number. Similar to the results with the Reynolds numbers, there does not appear to be any correlation between the non-dimensionalized interphase friction and the Weber number. Similarly, in Figure 31 and Figure 32, there does not appear to be a correlation between the non-dimensionalized interphase friction force and either version of the Froude number.

It is interesting to note that in Figure 33 that the non-dimensionalized interphase friction force does not approach ∞ as the velocity ratio approaches 1, as was the case in Figure 24. This suggests that the interphase friction may not be as directly related to the velocity difference as has been previously expected, or at least that it is not as obvious of a correlation as would be expected.

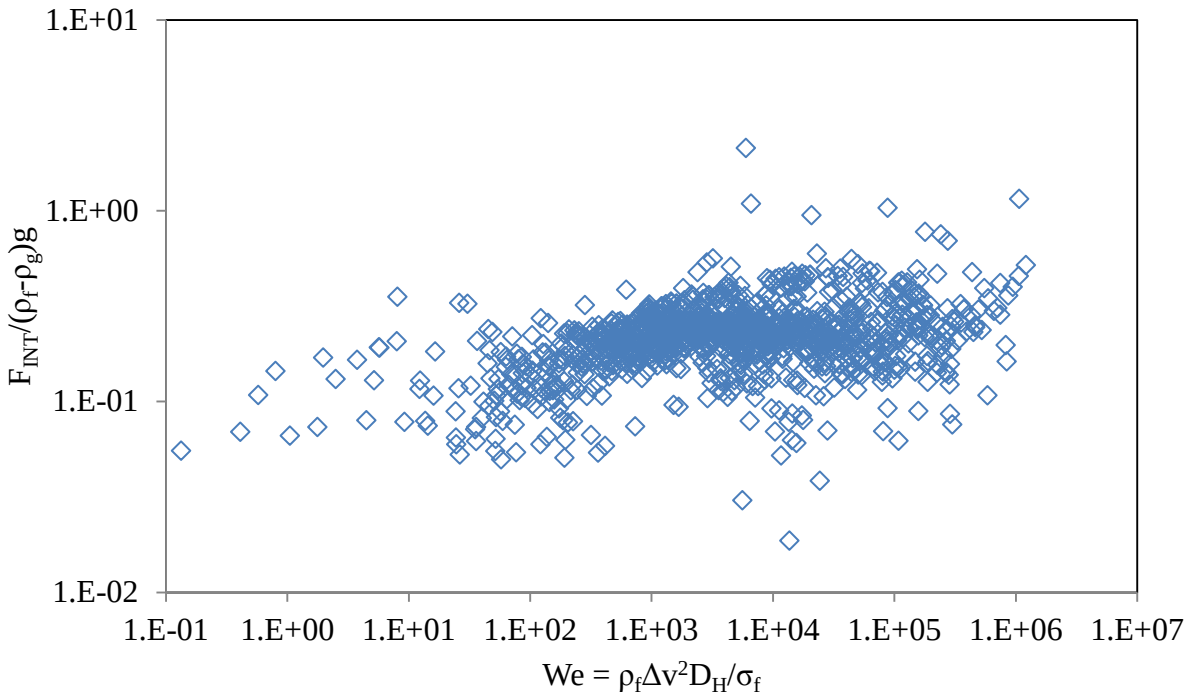

Figure 30: Comparison of the Interphase Friction Force Non-Dimensionalized by the Density Difference against the Weber Number

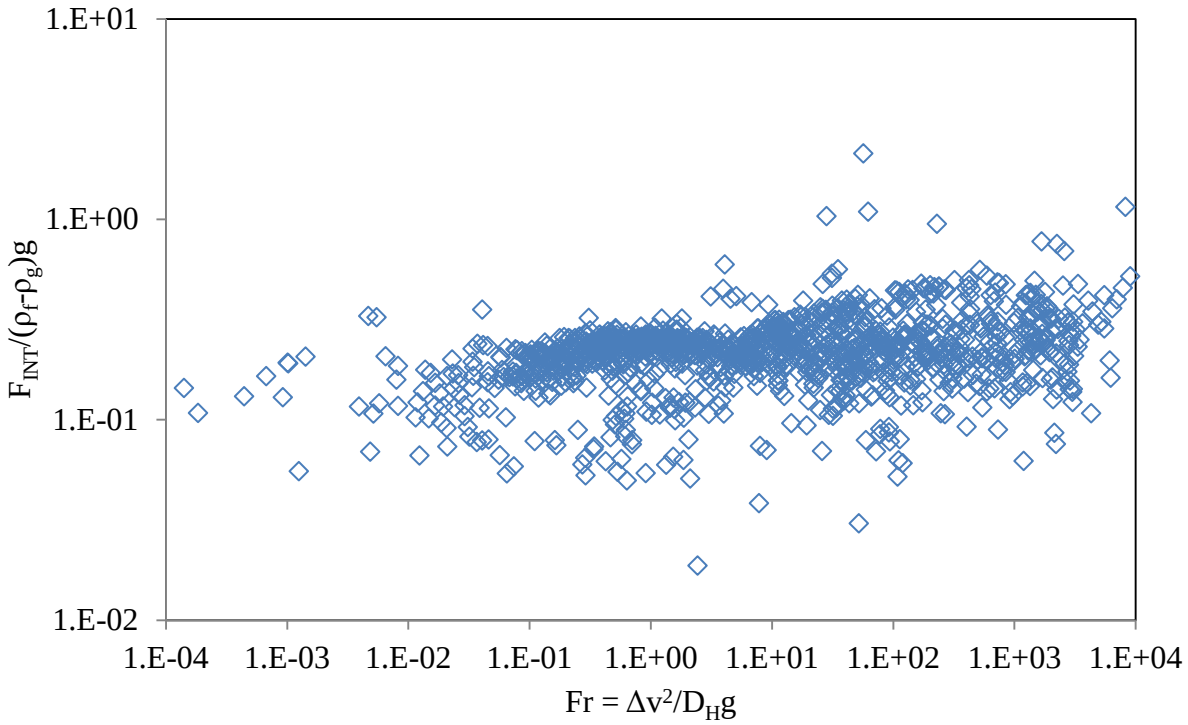

Figure 31: Comparison of the Interphase Friction Force Non-Dimensionalized by the Density Difference against the Froude Number

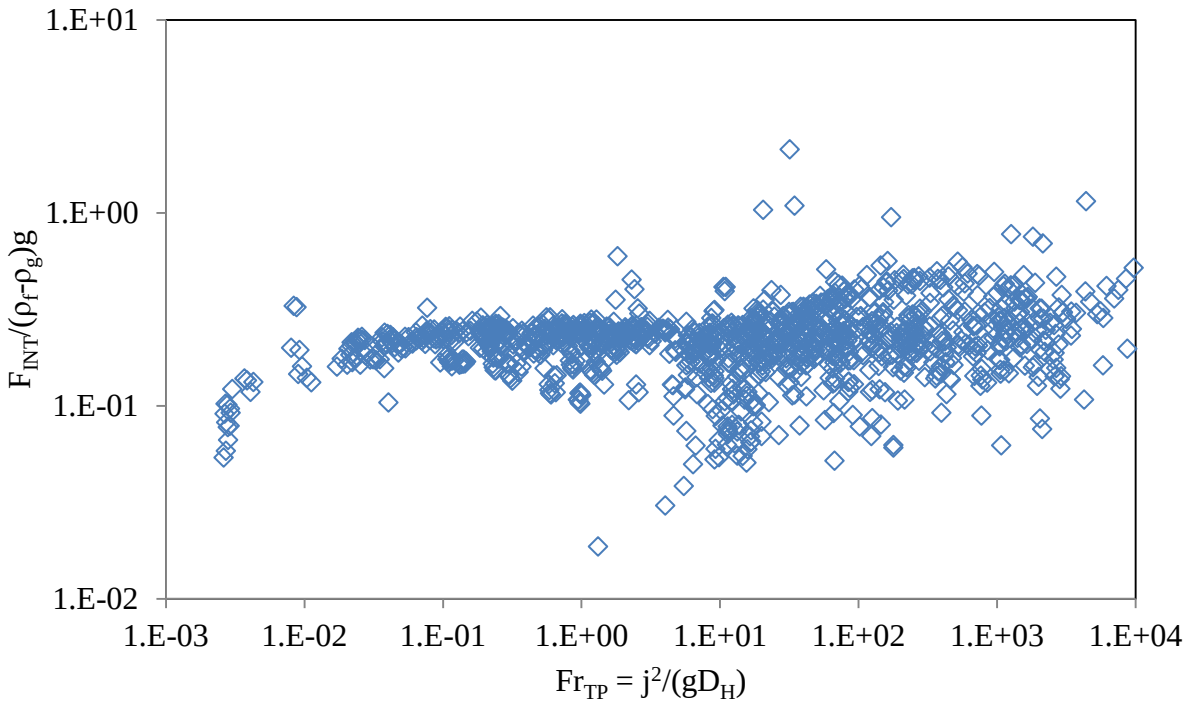

Figure 32: Comparison of the Interphase Friction Force Non-Dimensionalized by the Density Difference against the Mixture Froude Number

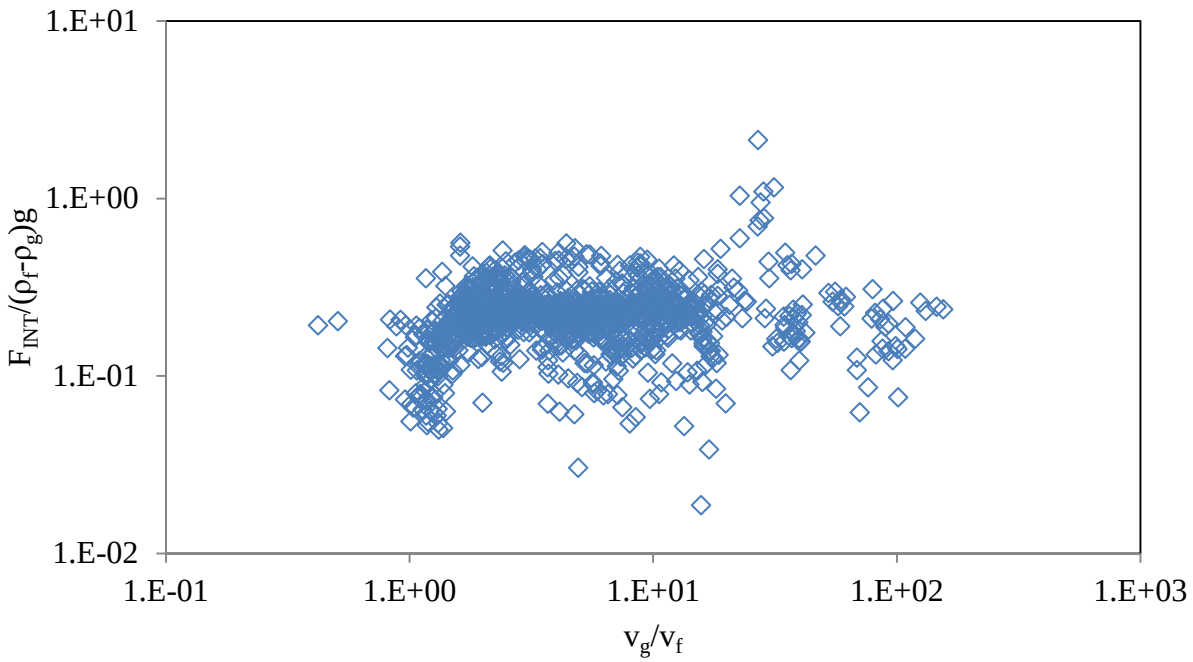

Figure 33: Comparison of the Interphase Friction Force Non-Dimensionalized by the Density Difference against the Velocity Ratio

In Figure 34, the non-dimensionalized interphase friction is compared to the density ratio. Since the density ratio does not exceed 0.01 for any data points, it is not possible to tell if the non-dimensionalized interphase friction would approach ∞ if the density ratio approached 1. More importantly, is the discovery that the density ratio does not seem to correlate at all with the non-dimensionalized interphase friction, as within each study that has been examined, the density ratio is largely unchanged, but the interphase friction force may vary depending on the other conditions. The density ratio may be useful in conjunction with another correlation, but when compared directly to the interphase friction force, development of a correlation is futile.

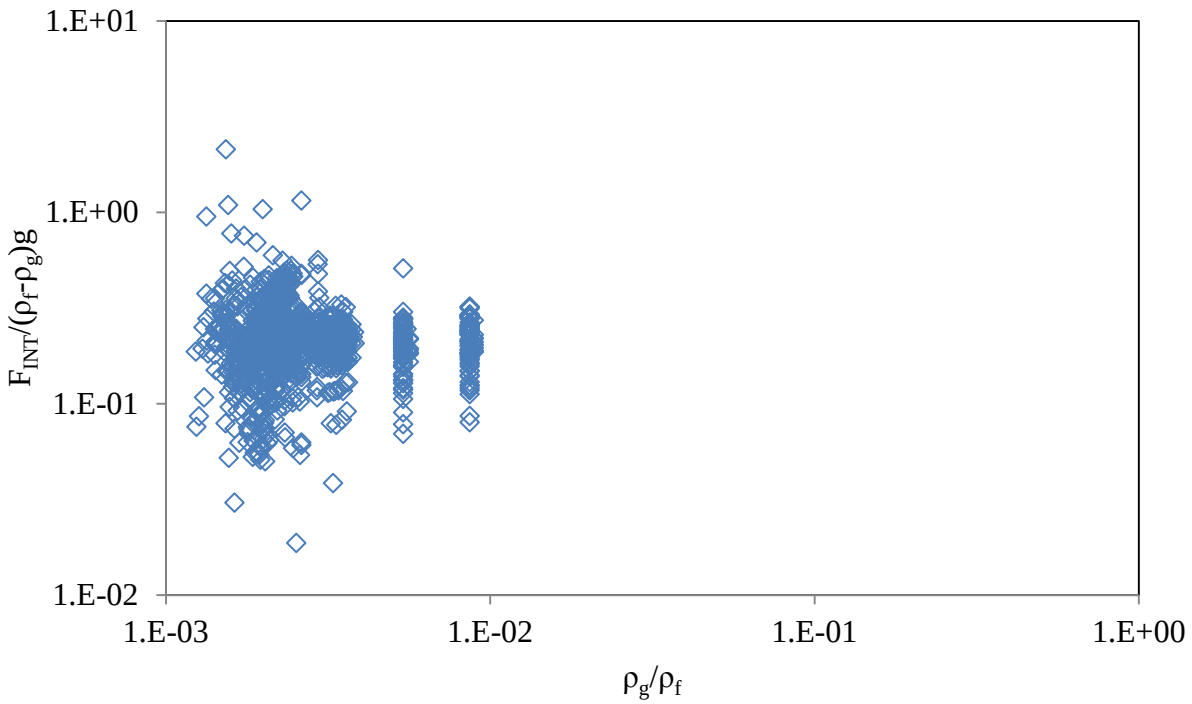

Figure 34: Comparison of the Interphase Friction Force Non-Dimensionalized by the Density Difference against the Density Ratio

Comparing the non-dimensionalized interphase friction force to the void fraction yields a far more interesting result than has been depicted thus far. In Figure 35, there appears to be a curve such that when the void fraction approaches 0 or 1, the non-dimensionalized interphase friction approaches 0. Also, there appears to be a maximum in the interphase friction at a void fraction of approximately 0.5. The data appears to fit a curve more tightly for void fraction values less than 0.5, while there is considerably more spread above 0.5.

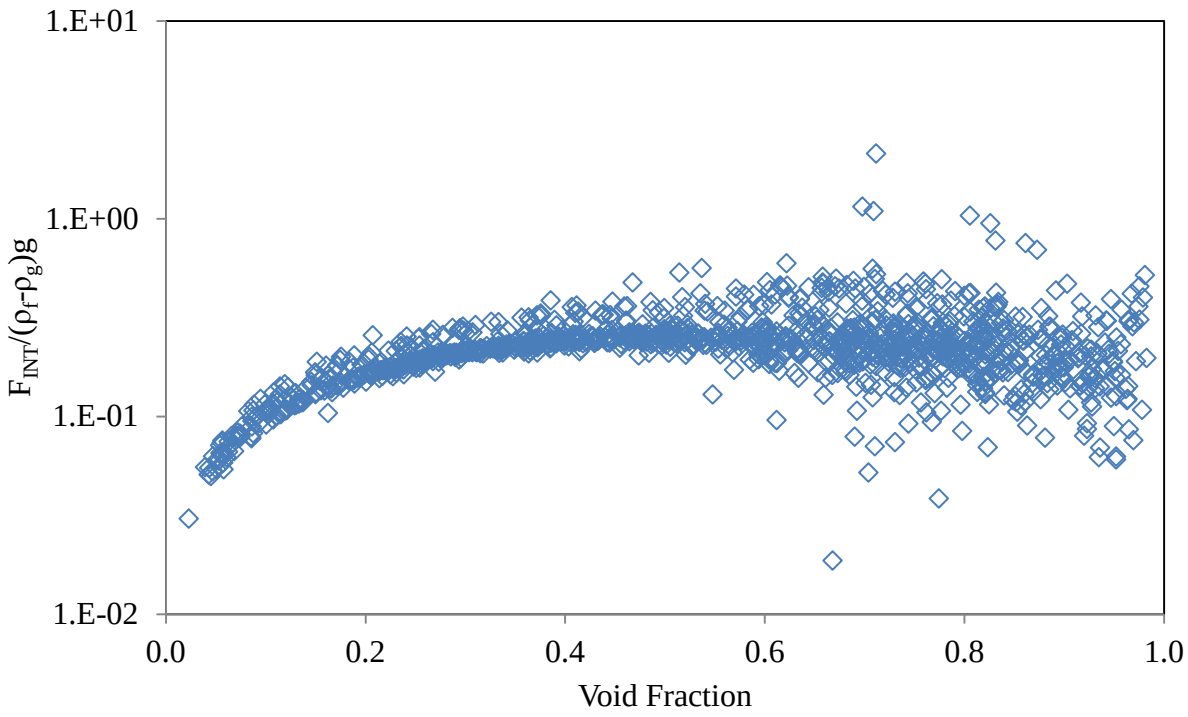

Figure 35: Comparison of the Interphase Friction Force Non-Dimensionalized by the Density Difference against the Void Fraction

Nonetheless, there are two different options to consider when deciding on how to approach the correlation. The data appears to fit a curve roughly equal to $\alpha(1-\alpha)$, which if implemented into the non-dimensionalization would result in the term $F_{INT}/\alpha(1-\alpha)(\rho_f-\rho_g)g$, which would be considered non-dimensionalization against the buoyancy force. As shown in Equations 73, 74 and 75, this non-dimensionalized interphase friction value would be physically meaningful. The other option would be to find the values for *A*, *B* and *C* such that:

$$\frac{F_{INT}}{(\rho_f-\rho_g)g} = A\alpha^B(1-\alpha)^C \qquad 276$$

While the second option would produce a more mathematically accurate solution to the non-dimensionalized interphase friction force, the first option produces a more physically sound solution that can be explored further. Therefore, the non-dimensionalized interphase friction force will now be determined using Equation 277.

$$f_{INT} = \frac{F_{INT}}{\alpha(1-\alpha)(\rho_f - \rho_g)g} \quad 277$$

For this phase of the analysis, we begin by comparing the non-dimensionalized interphase friction force to the Reynolds number in Figure 36 and Figure 37. In this comparison, there does not appear to be a solid correlation that relates the non-dimensionalized interphase friction force to the Reynolds number. It appears that the data follows along the line $f_{INT} = 1$ until roughly a Reynolds number value of 50000, where the data diverges along three different lines. Figure 37 shows that the first line features data from Turner [84], and peaks at $f_{INT} = 9$. The second line is attributed to the Gill et al [29] data, and peaks at $f_{INT} = 28$, while the third line follows the Runge data at 65 psia and peaks at $f_{INT} = 5.5$. These three studies all featured annular flow data predominantly, and would be expected to all follow along one line rather than diverge into three.

Perhaps a different interpretation of the Reynolds number will yield better results, and so the non-dimensionalized interphase friction is compared to the continuous liquid phase Reynolds number in Figure 38 and Figure 39, and the continuous vapor phase Reynolds number in Figure 40 and Figure 41. The comparison to the continuous liquid phase Reynolds number, Re_{fc}, shows a very interesting curve with f_{INT} values of approximately 1 for $Re_{fc} \geq 10$. Then as Re_{fc} decreases, f_{INT} increases, but there is also an increasing amount of spread in the data as Re_{fc} approaches 0.01.

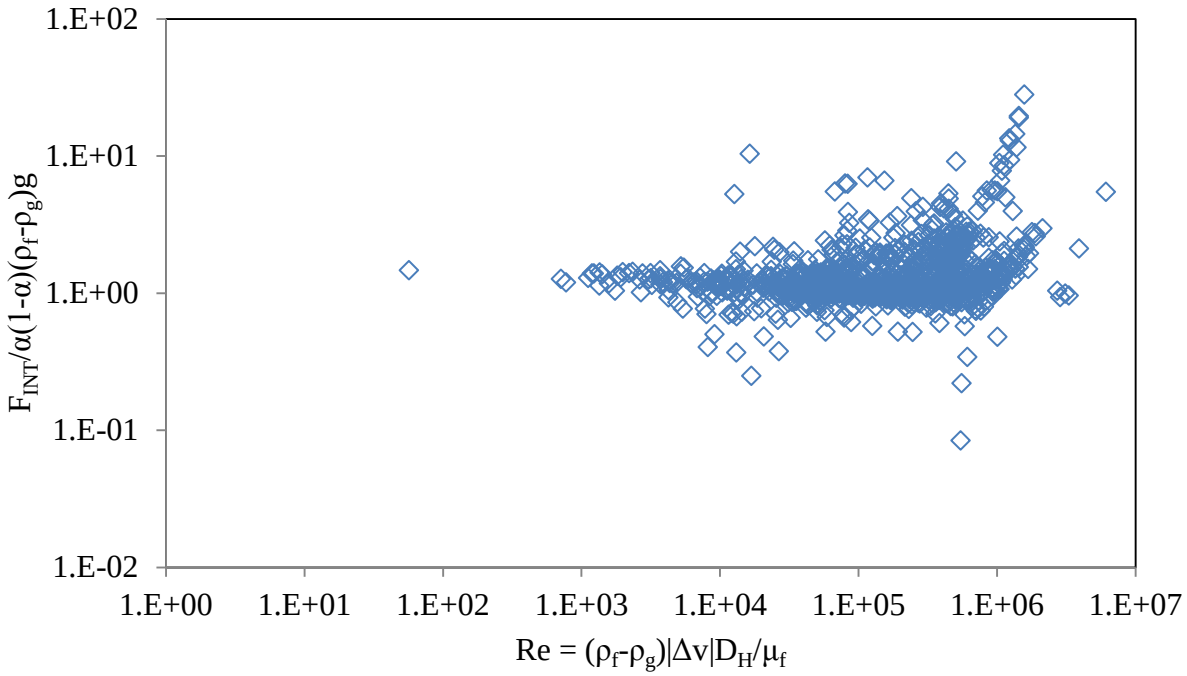

Figure 36: Comparison of the Non-Dimensionalized Interphase Friction Force against the Reynolds Number

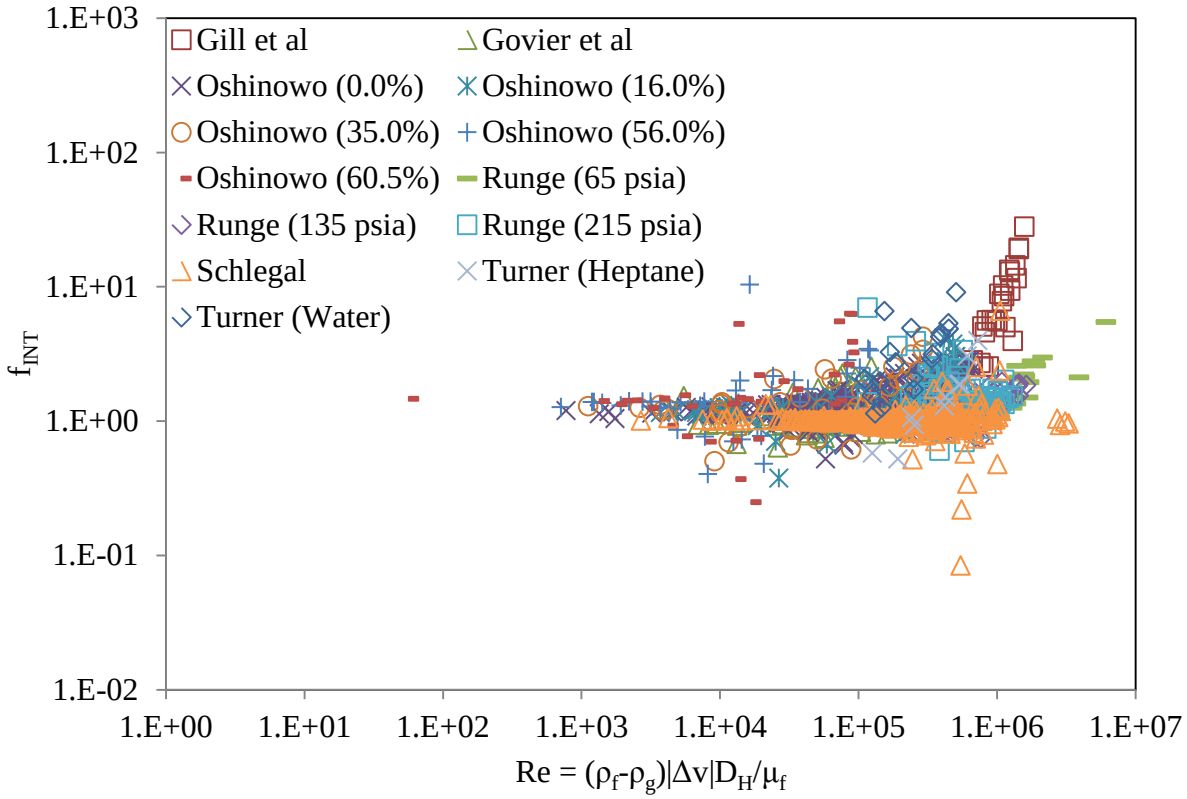

Figure 37: Comparison of the Non-Dimensionalized Interphase Friction Force against the Reynolds Number

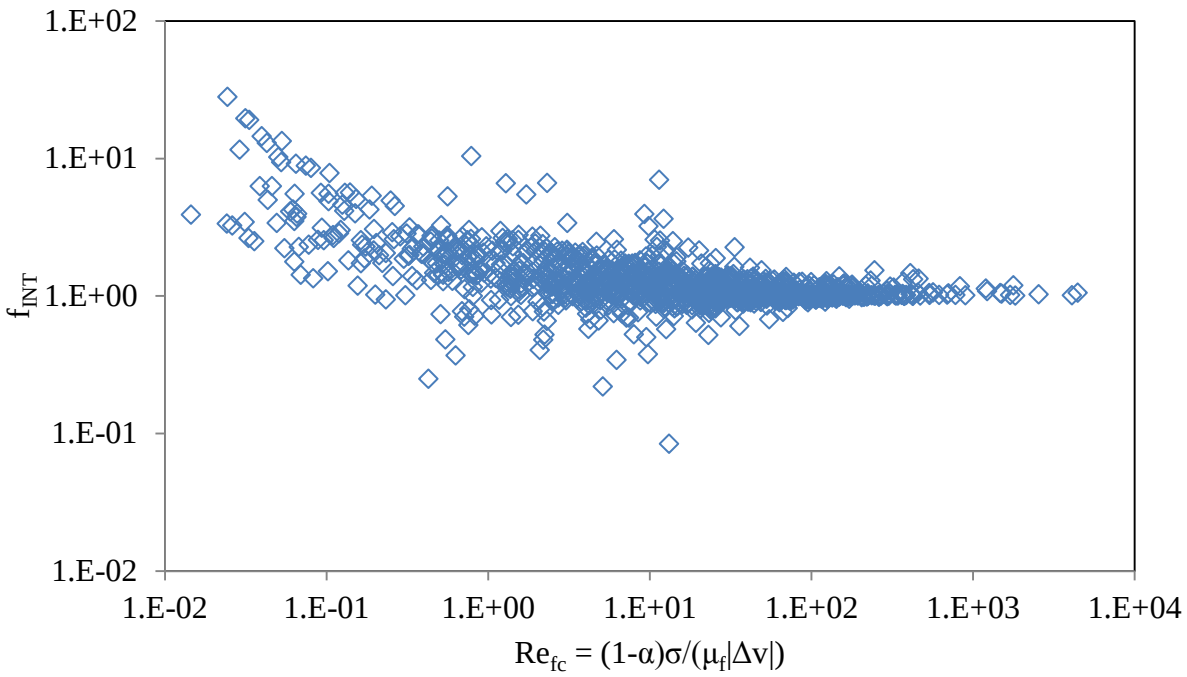

Figure 38: Comparison of the Non-Dimensionalized Interphase Friction Force against the Particle Reynolds Number for a Continuous Liquid Phase

In Figure 39, we see that the data points for which $Re_{fc} \geq 10$ are largely made up of the Schlegal data, along with a few data points from Oshinowo [59] with 0.0% glycerol concentration. While the data points with Re_{fc} approaching 0.01 are mainly from Gill et al [29], Turner [84] and Oshinowo at glycerol concentrations of 56.0% and 60.5%. Notice that the Gill et al and Turner data appear to follow along a curve with higher non-dimensionalized interphase friction force values than that with the Oshinowo data over the range $1 \geq Re_{fc} \geq 0.01$. At such a low Re_{fc} value, it can be expected that the flow regime is annular, and the particle Reynolds number for a continuous liquid phase may not suit the data as well as that for a continuous vapor phase.

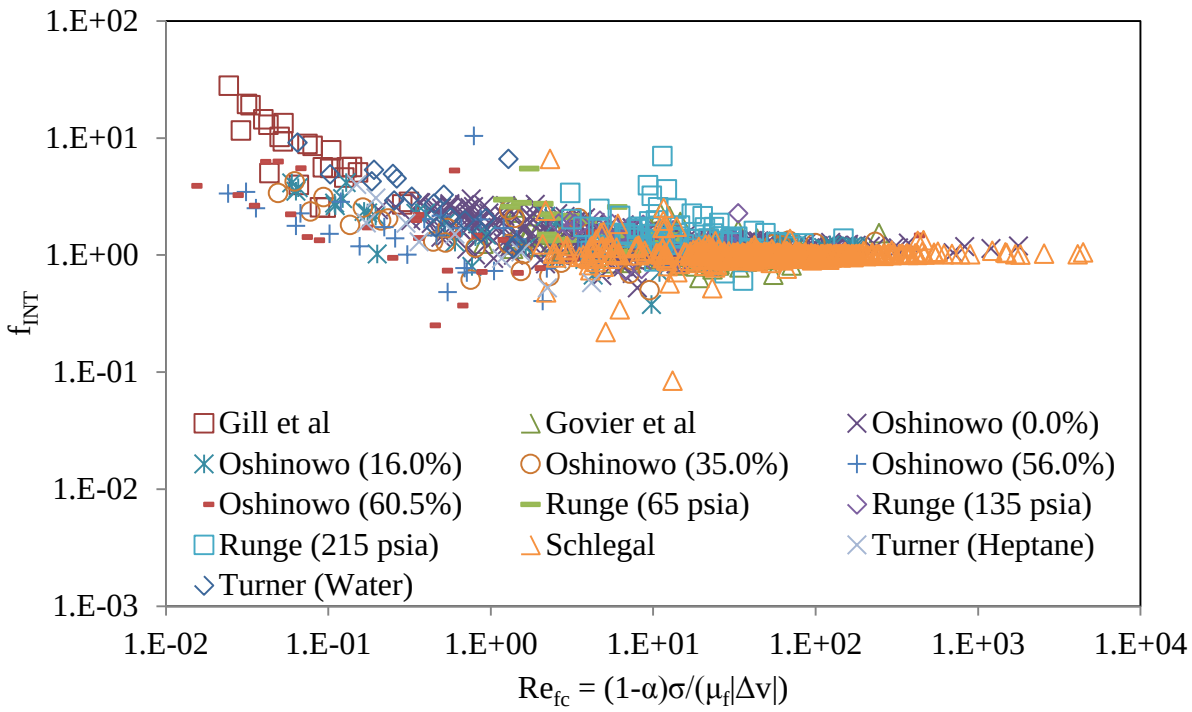

Figure 39: Comparison of the Non-Dimensionalized Interphase Friction Force against the Particle Reynolds Number for a Continuous Liquid Phase with Studies Specified

In Figure 40, we see that there are two separate lines along which the majority of the data fits. Spanning from $0.1 \leq Re_{gc} \leq 10000$, there is a large swath of points where the non-dimensionalized interphase friction force is roughly equal to 1. However, there is a spike that comes from this swath at approximately $Re_{gc} = 300$, where the non-dimensionalized interphase friction rapid increases to 28 as Re_{gc} approaches 70. In Figure 41, it is shown that this spike is largely attributed to the Gill et al data, along with a few data points from Turner with water as the working fluid.

Due to the range of Re_{gc} values for which $f_{INT} = 1$, Re_{gc} on its own would not serve as a useful variable for predicting interphase friction. Combined, Re_{fc} and Re_{gc} may serve as a function for predicting interphase friction. The Reynolds number for a continuous liquid phase is useful in determining which phase is continuous, as it appears to have separate regimes corresponding to different value range of Re_{fc}. For $Re_{fc} \geq 10$, f_{INT} is approximately 1, and does

not even appear to be a function of Re_{fc}. However, as Re_{fc} decreases below 10, there is an increasing amount of spread in the data and f_{INT} increases above 1. When $Re_{fc} \leq 1$, the data points appear to fit along the spike noticed in Figure 40 and Figure 41. For $10 \geq Re_{fc} \geq 1$, there appear to be a transition region where some form of interpolation would need to occur to find a correlation that fit the data within that range. These three regions of data may also be apparent when the non-dimensionalized interphase friction force is compared against other dimensionless parameters, and may prove to be more useful than a combined Re_{fc} and Re_{gc} correlation.

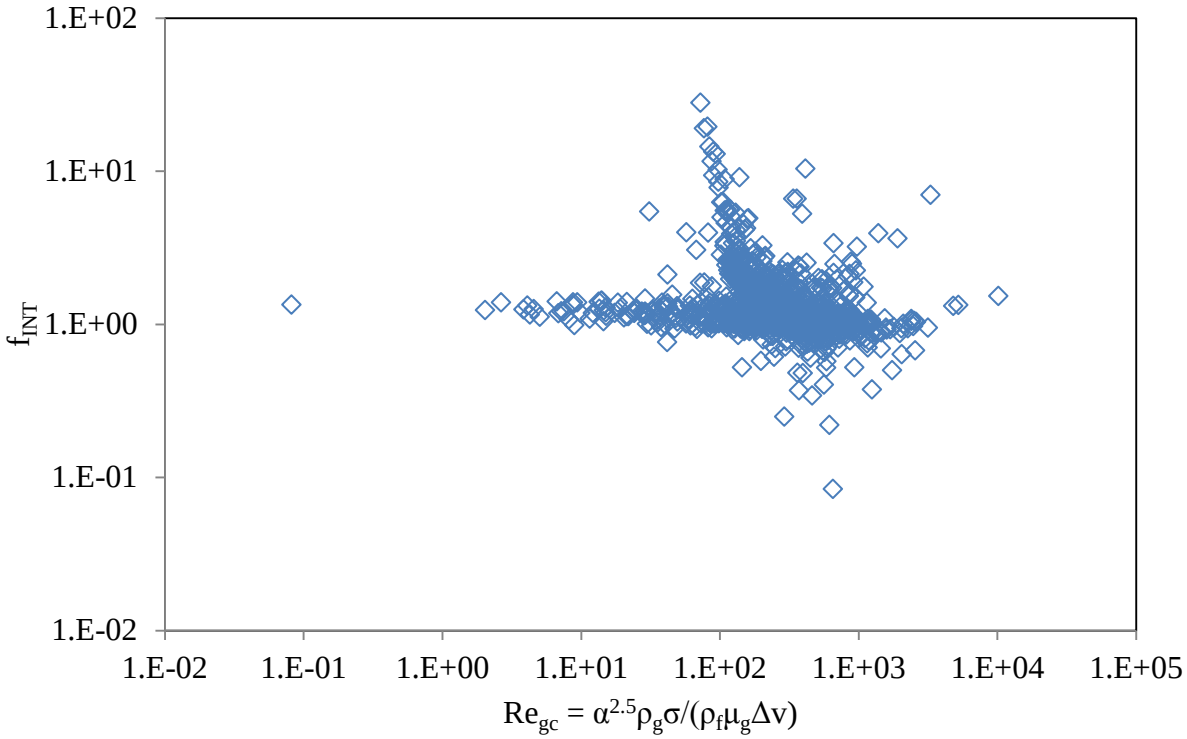

Figure 40: Comparison of the Non-Dimensionalized Interphase Friction Force against the Particle Reynolds Number for a Continuous Vapor Phase

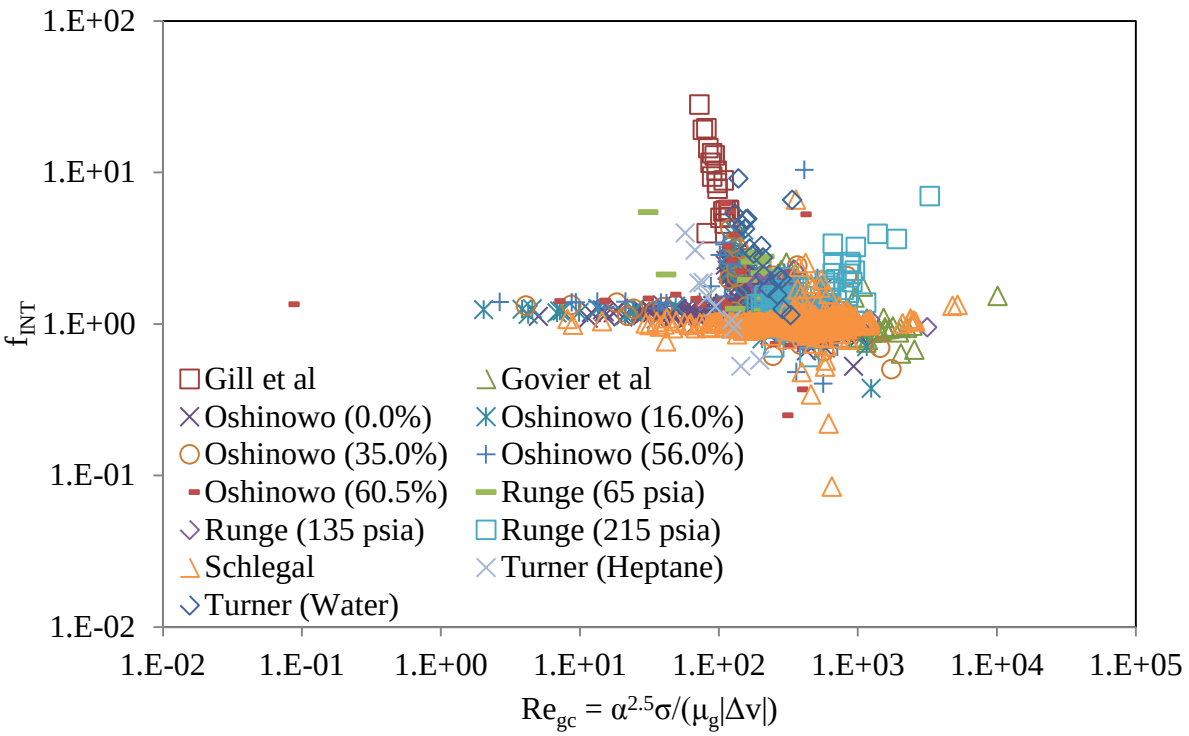

Figure 41: Comparison of the Non-Dimensionalized Interphase Friction Force against the Particle Reynolds Number for a Continuous Vapor Phase

Next, the non-dimensionalized interphase friction force is compared against the Weber number, as shown in Figure 42. As seen in the previous analysis of the particle Reynolds numbers, there appears to be three different regions where the non-dimensionalized interphase friction force correlates with the Weber number. First, there is the region where f_{INT} is approximately 1, which occurs for $We < 10{,}000$. Then, for $We > 250{,}000$, there is a set of data points for which f_{INT} follows a second straight line, where f_{INT} is a function of the Weber number. In between, where $10{,}000 < We < 250{,}000$, the data appears to fit a curve along which f_{INT} is a separate function of the Weber number. Figure 43 shows that the regime for $We \geq 250{,}000$ largely consists of the Gill et al [29] data, while the other regions appear to include data points from several studies. Also noticeable is how the Schlegal [75] data seems to fit $f_{INT} = 1$ perfectly for many data points, but there are also a few significant outliers from the general trend.

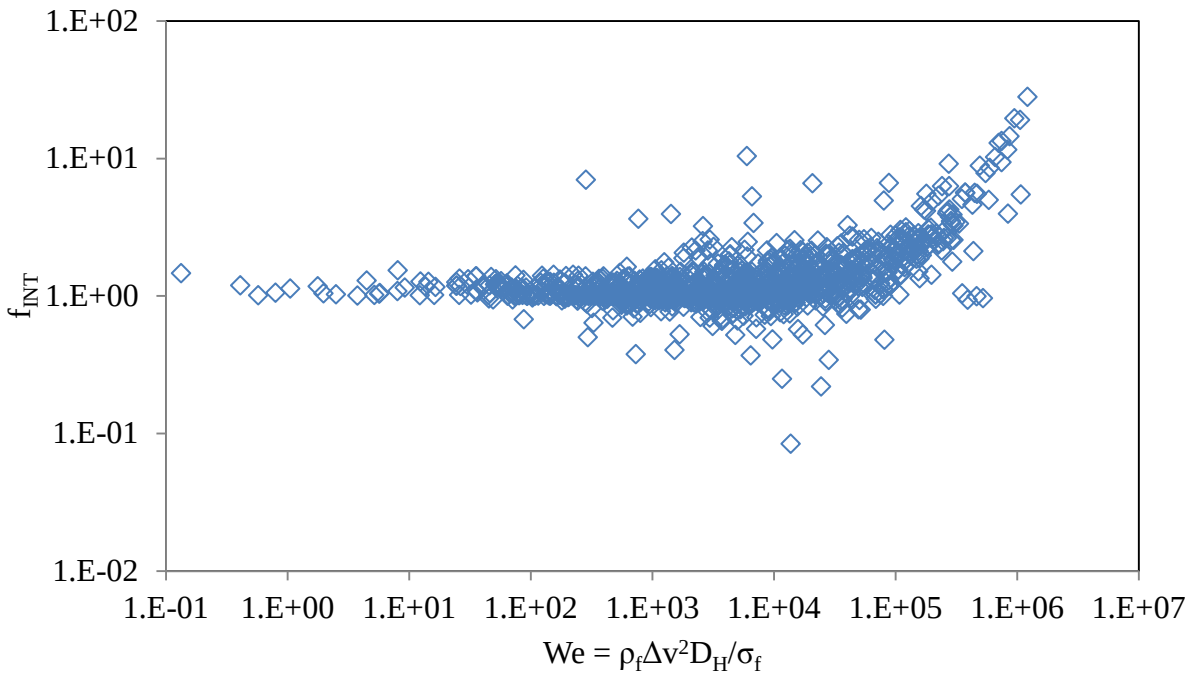

Figure 42: Comparison of the Non-Dimensionalized Interphase Friction Force against the Weber Number

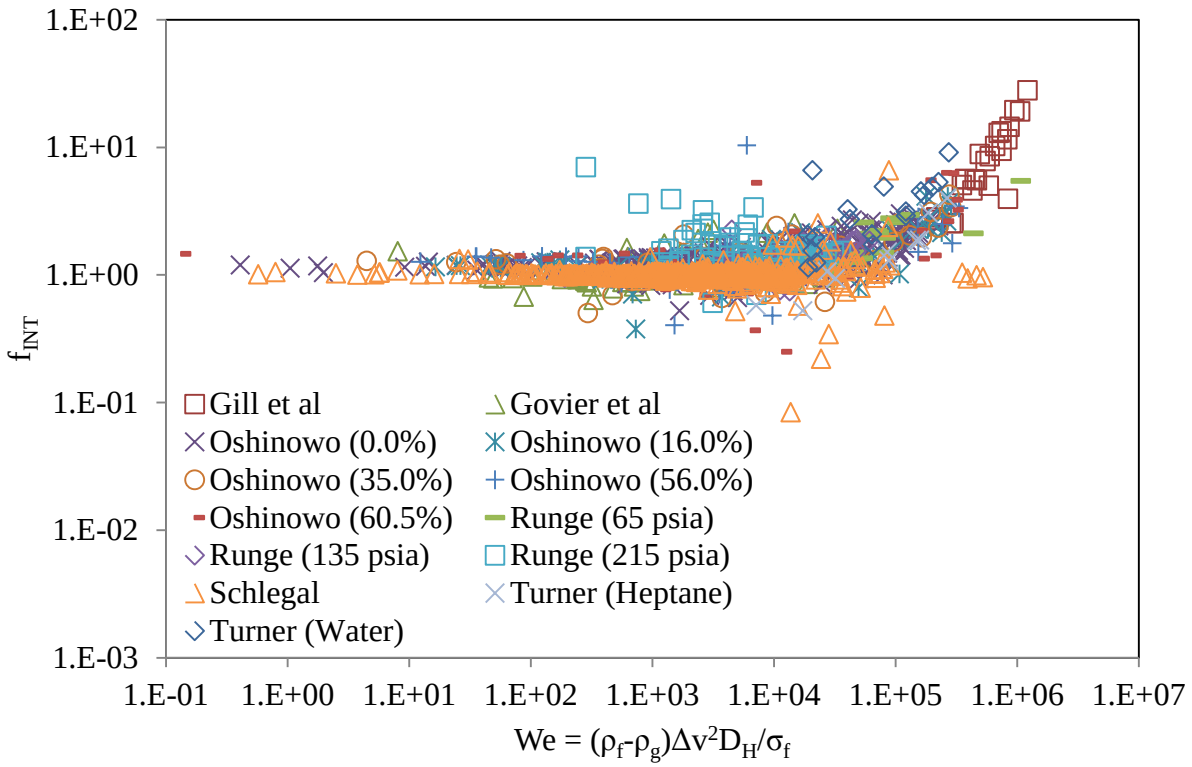

Figure 43: Comparison of the Non-Dimensionalized Interphase Friction Force against the Weber Number with Studies Specified

In Figure 44 and Figure 45, the non-dimensionalized interphase friction force is compared against the Froude number calculated with the velocity difference. Figure 44 shows a similar curve as was seen with the Weber number in Figure 42. This would indicate that the curve is chiefly related to the velocity difference, as opposed to the other variables that comprise of the dimensionless parameters. As the Froude number contains the fewest variables of the dimensionless parameters, the usage of the Froude number would produce a simpler correlation, which implies easier implementation.

The non-dimensionalized interphase friction force is roughly equal to 1 for Fr approximately less than 5, while it appears to fit a straight line when the Froude number is approximately greater than 3000. Meanwhile, in between the Froude number values of 5 and 3000, the data appears to fit a curve that would make the entire function continuous throughout the range of Froude number values. Figure 45 shows that the data with the highest Froude numbers is almost entirely from the Gill et al [29] data set, indicating that the high Froude numbers correlate mostly with annular flow with very high void fraction.

This observation that the interphase friction force may be a function of the Froude number, where the equation may change with the Froude number, indicates that the physics of interphase friction change with increasing Froude number. It implies that there may be a regime change that occurs as the Froude number increases, not unlike changes in flow regime that occur with changing conditions. However, the Froude number used in Figure 44 and Figure 45, has not been documented as an indicator in changing flow regimes. The mixture Froude number, defined in Equation 50, has been used by Kozloff [51], Griffith and Wallis [33] and Oshinowo and Charles [59,60] as a variable that can determine flow regimes, and may also provide insight into the interphase friction force.

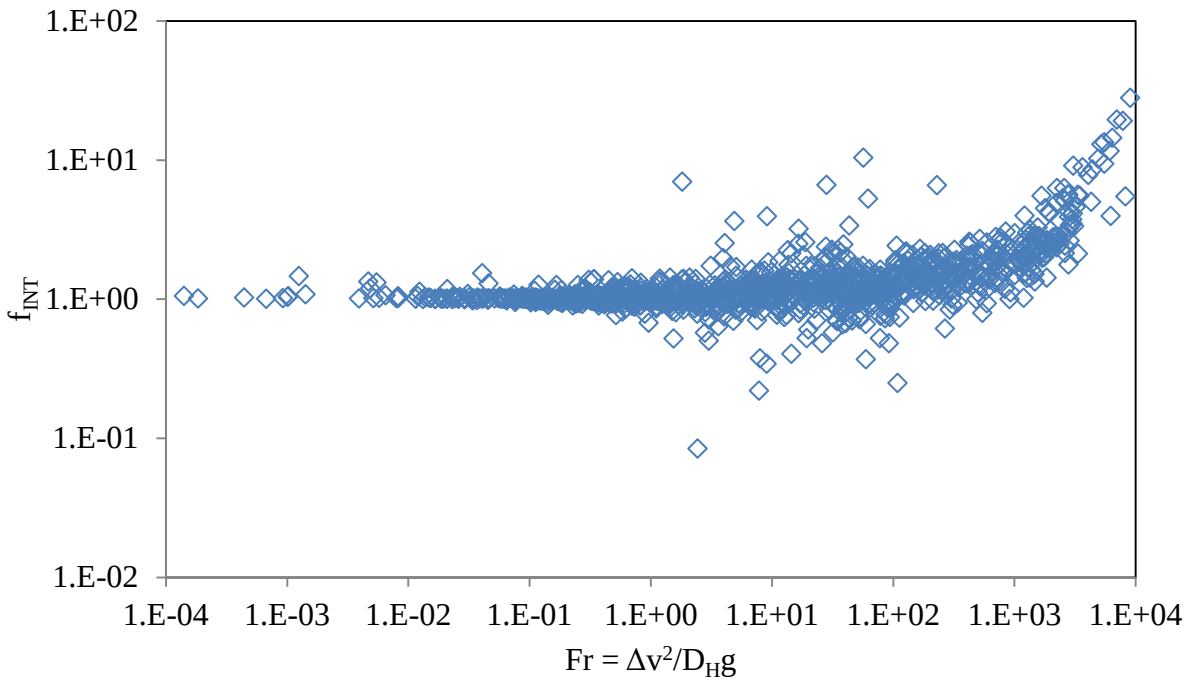

Figure 44: Comparison of the Non-Dimensionalized Interphase Friction Force against the Froude Number

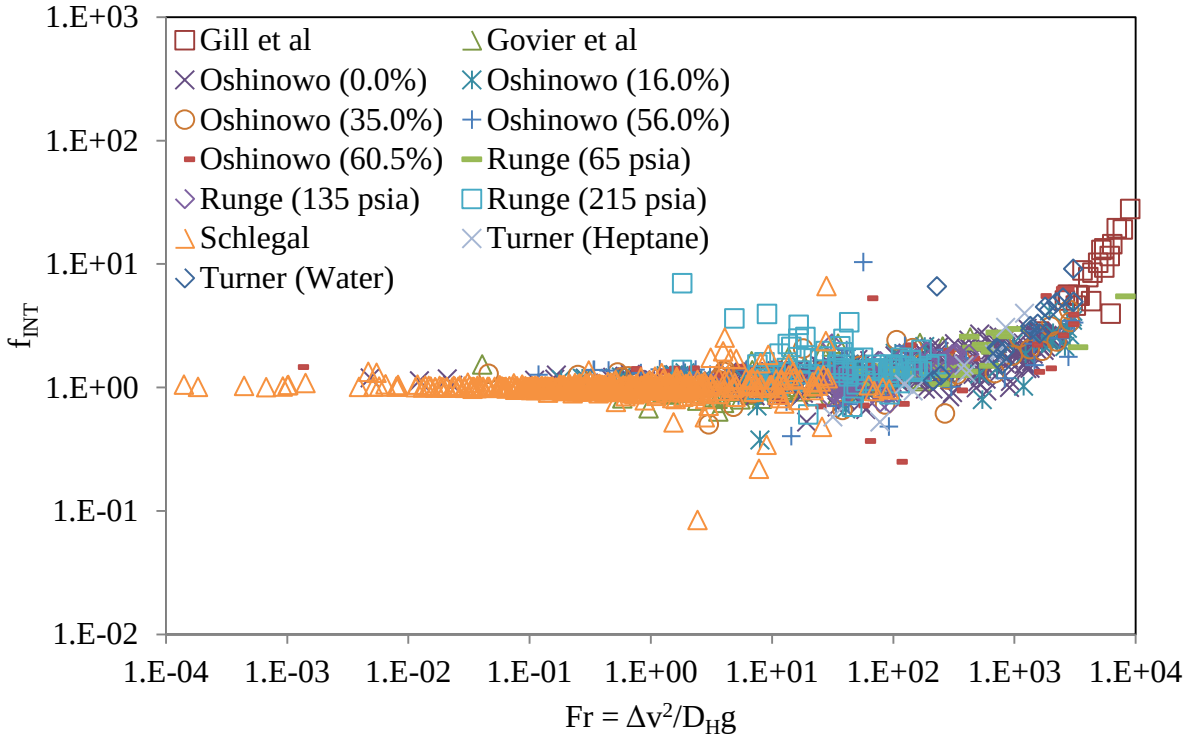

Figure 45: Comparison of the Non-Dimensionalized Interphase Friction Force against the Froude Number with Studies Specified

In Figure 46 and Figure 47, the non-dimensionalized interphase friction force is compared against the mixture Froude number, which serves as the basis of the flow regime maps produced by Kozloff [51], Griffith and Wallis [33] and Oshinowo and Charles. [59,60] In each case, the investigator showed that the flow regime was a function of the mixture Froude number. Figure 46 shows a similar pattern as was seen with the Froude number in Figure 44, where there appear to be a set of data points where $Fr_m < 5$ for which $f_{INT} \approx 1$, and then for $Fr_m > 1500$ we find that the non-dimensionalized interphase friction fits a curve that resembles a straight line on a log-log plot. In Figure 47, it is shown that most of the data points for which $Fr_m < 5$ are from the Schlegal [75] data set, while most points for which $Fr_m > 1500$ are from Gill, Hewitt and Lacey [29].

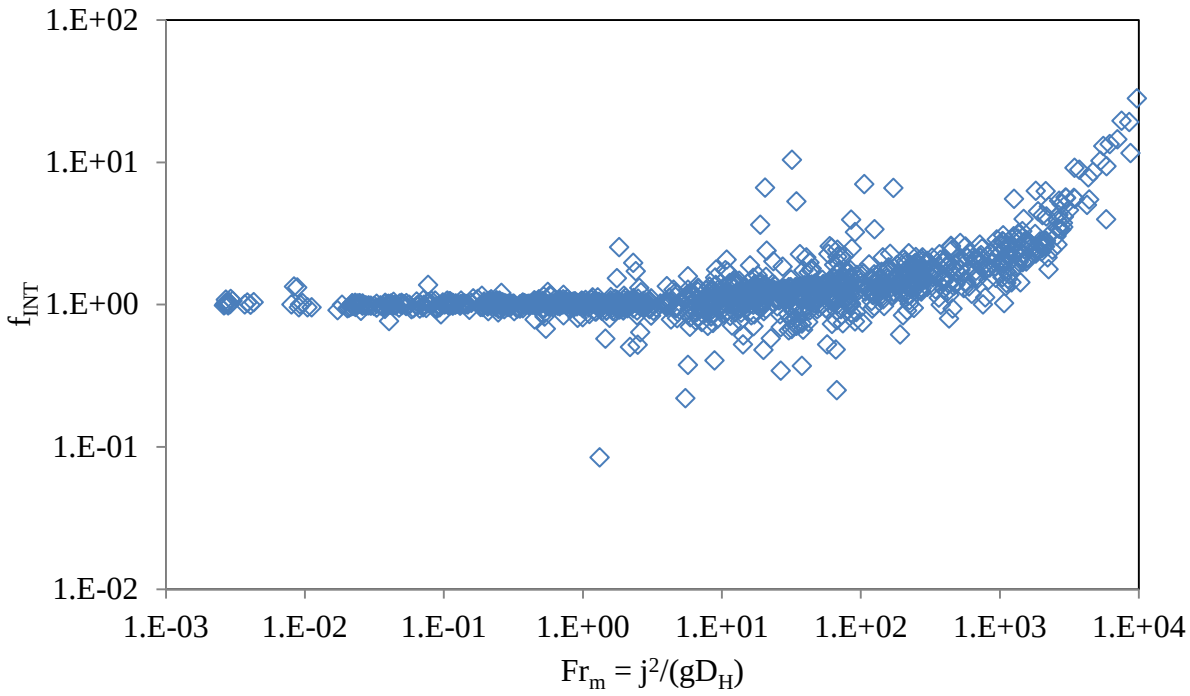

Figure 46: Comparison of the Non-Dimensionalized Interphase Friction Force against the Mixture Froude Number

The fact that Figure 44 and Figure 46 resemble each other may be an indication that the deciding factor in separating the different interphase friction regimes may not be the velocity

difference or the total volumetric flux, but is more directly related to the volumetric flux of the vapor phase, as that would be the dominant term in both the velocity difference and total volumetric flux. Whether the velocity or volumetric flux of the liquid phase is added or subtracted appears to make little difference on how the Froude number relates to the interphase friction. However, Figure 44 and Figure 46 show that as the flow of the vapor phase increases, there is an increasing amount of interphase friction beyond what can be accounted for through buoyancy alone.

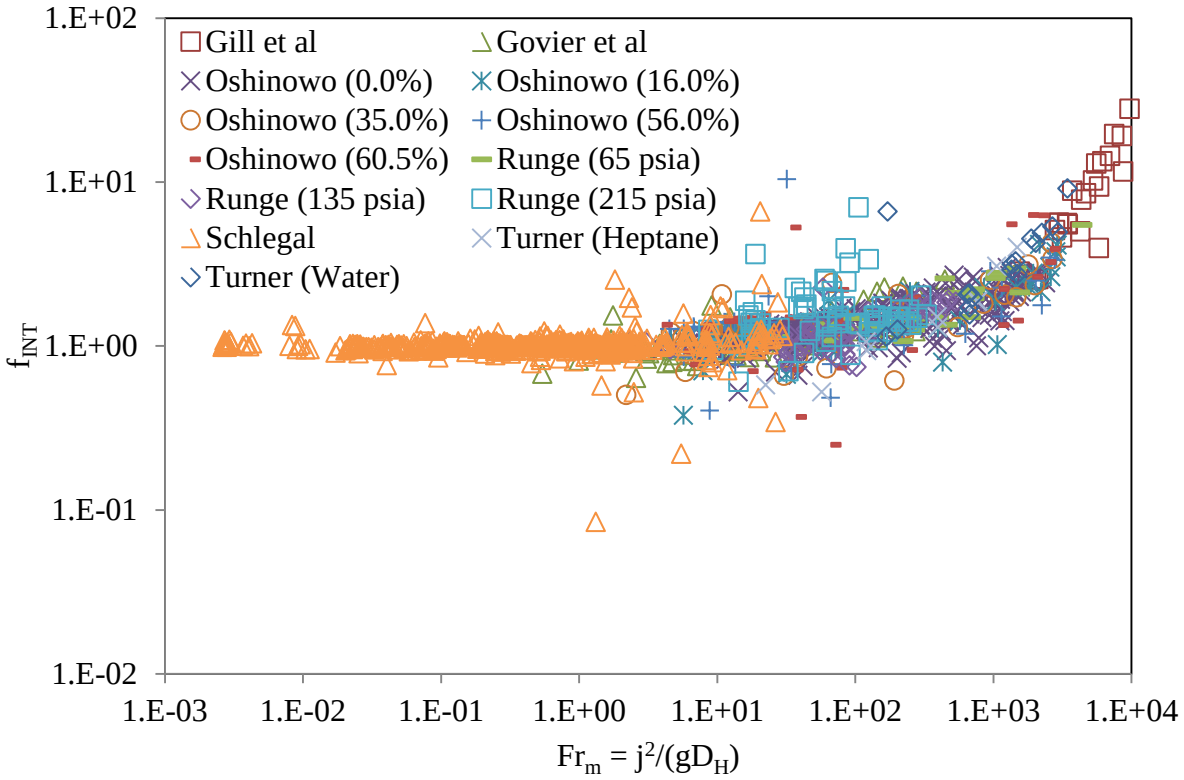

Figure 47: Comparison of the Non-Dimensionalized Interphase Friction Force against the Mixture Froude Number with Studies Specified

In Figure 48, we see the non-dimensionalized interphase friction compared against the velocity ratio. It is surprising to find that the data points where the ratio between the vapor velocity and liquid velocity are highest do not appear to coincide with the data points that have the highest non-dimensionalized interphase friction force. Figure 49 shows that the data points

with a velocity ratio on the order of 100 are representative of several different studies, although it can be assumed that for most of these data points, the flow regime is annular.

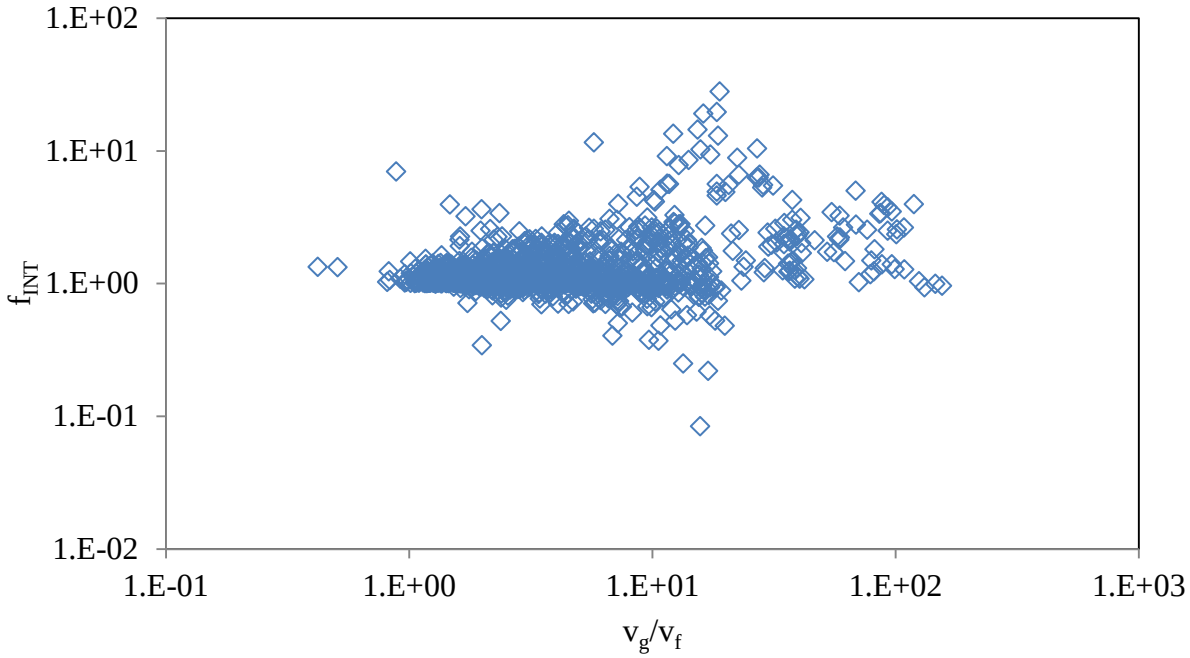

Figure 48: Comparison of the Non-Dimensionalized Interphase Friction Force against the Velocity Ratio

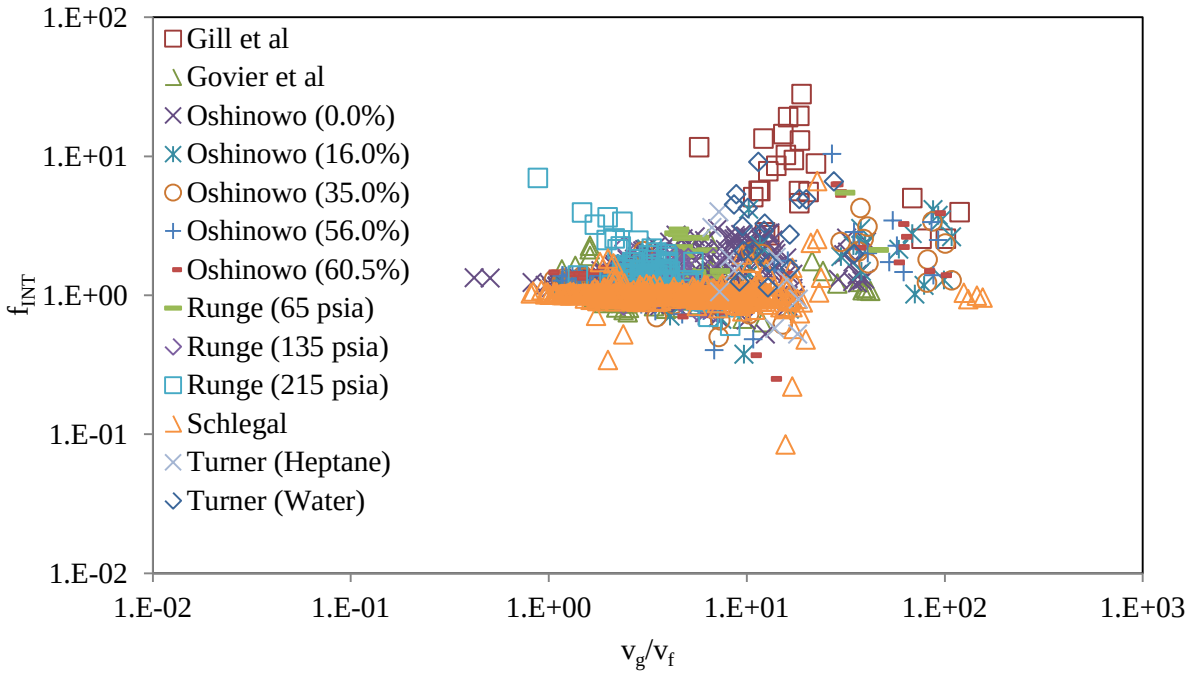

Figure 49: Comparison of the Non-Dimensionalized Interphase Friction Force against the Velocity Ratio with Studies Specified

The Froude number using velocity difference and the mixture Froude number indicated that there was a strong relationship between the non-dimensionalized interphase force and the flow of the vapor phase. However, as Figure 48 and Figure 49 indicate, that relationship does not appear to exist with the vapor velocity. In Figure 50, we find that there does appear to be a relationship between the ratio of the volumetric fluxes and the non-dimensionalized interphase friction force. The data does not fit a singular curve, as there is increasing spread in the non-dimensionalized interphase friction force values as the volumetric flux ratio increases. With the volumetric flux ratio being less than 1, most data points appear to fall within a small range of $f_{INT} = 1$, and as the ratio increases to approximately 100, the non-dimensionalized interphase friction force values spread out, but remain within a single range. Only as the volumetric flux ratio increases above 100, does there appear to be a split, where the data follows along two different trend lines, one increasing more with increasing volumetric flux than the other. Figure 51 shows that the majority of data points along the higher trend line are from Gill, Hewitt and Lacey while the lower trend line is from several different sources.

The clearest indication of how the distribution of liquid and vapor relate to the interphase friction occurs in Figure 52, which shows that the non-dimensionalized interphase friction force is approximately 1 for void fractions below 0.5. This range void fraction values is normally associated with bubbly flow and some slug flow. For void fractions between 0.5 and 0.95, the non-dimensionalized interphase friction force follows a gently increasing curve, which appears to straddle both the slug flow and annular flow regimes. Only when the void fraction goes above 0.95, does the interphase friction force appear to follow a linear trajectory, increasing with increasing void fraction. Void fractions between 0.95 and 1.0 are associated with annular flow and the transition to mist flow as the void fraction approaches 1.0.

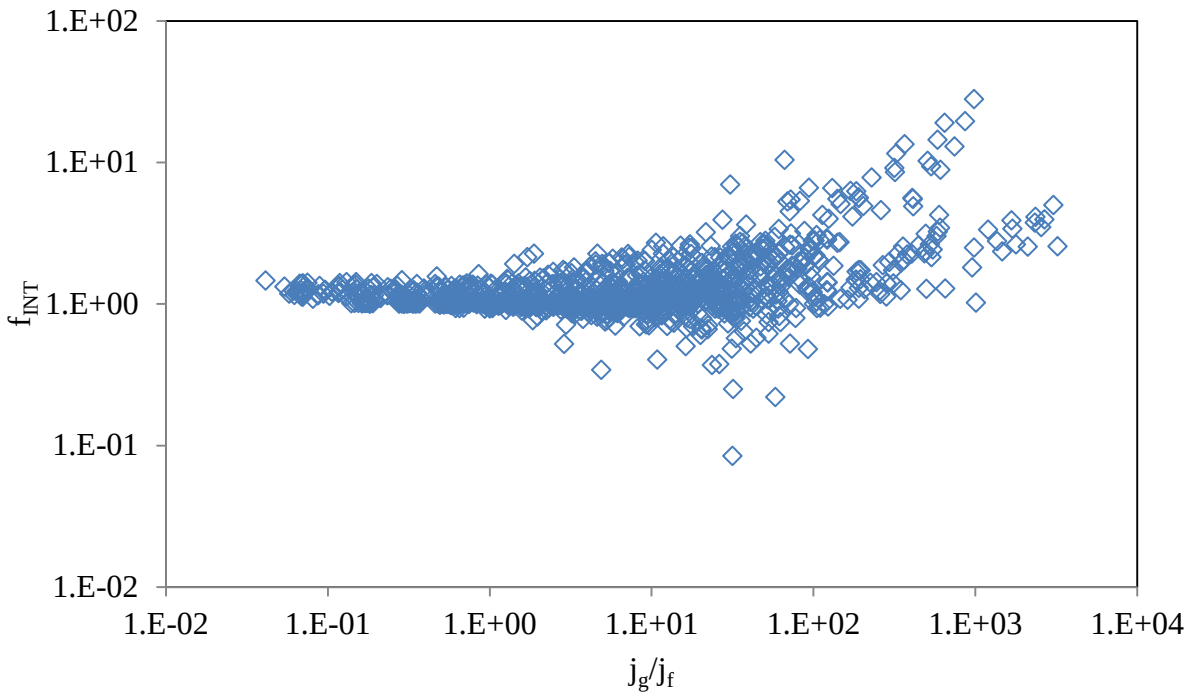

Figure 50: Comparison of the Non-Dimensionalized Interphase Friction Force against the Volumetric Flux Ratio

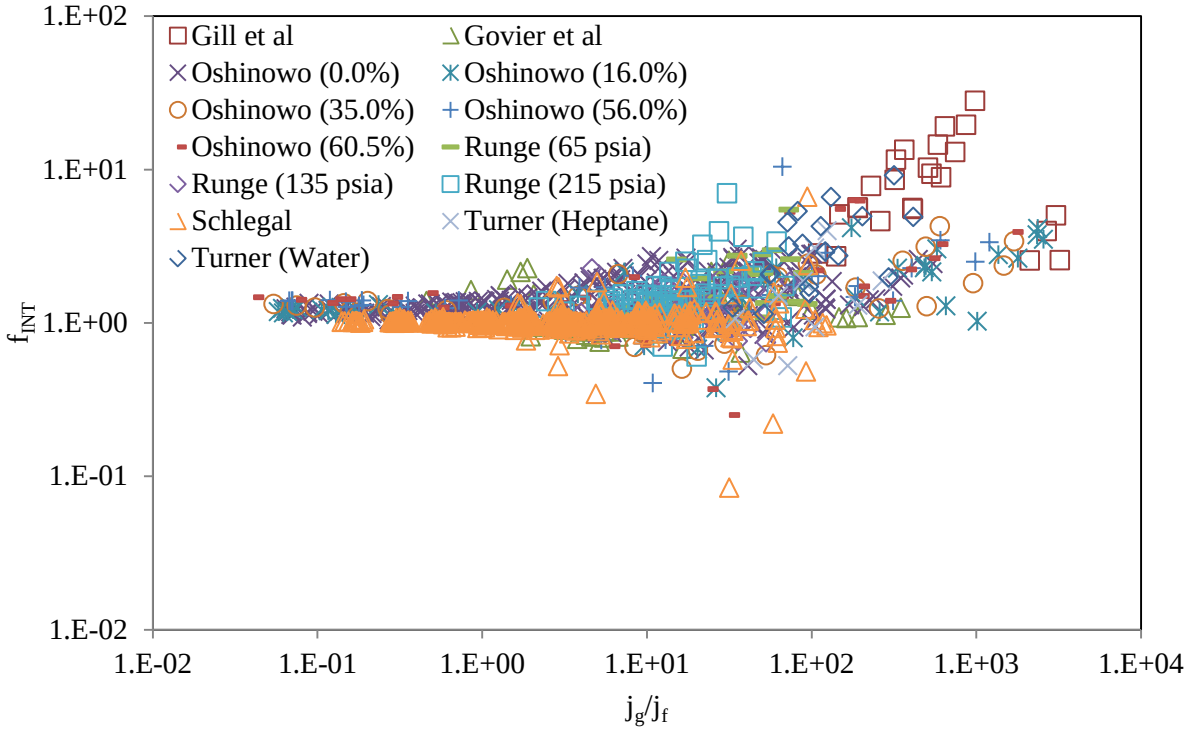

Figure 51: Comparison of the Non-Dimensionalized Interphase Friction Force against the Volumetric Flux Ratio with Studies Specified

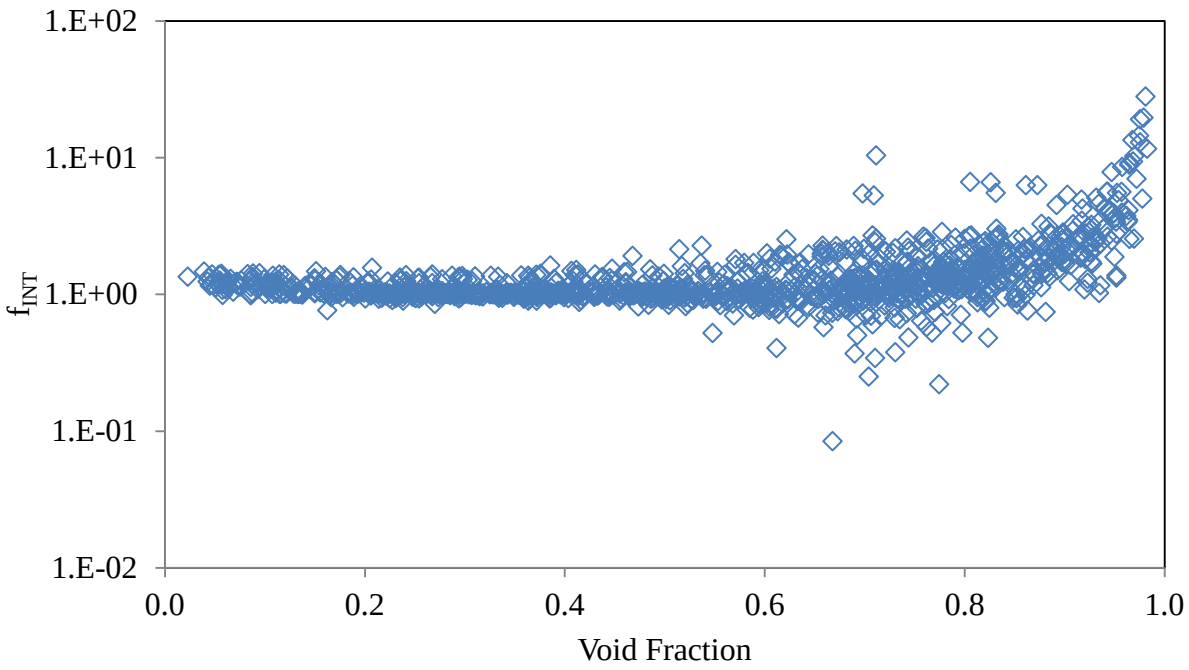

Figure 52: Comparison of the Non-Dimensionalized Interphase Friction Force against the Void Fraction

Figure 54 shows how the non-dimensionalized interphase friction force compares with the void fraction for the various studies. Not surprisingly, given earlier analysis of the data, the Schlegal [75] data represents the majority of the data with a void fraction less than 0.5 where $f_{INT} \approx 1$. Meanwhile, the data with the highest void fraction values comes predominantly from Gill, Hewitt and Lacey [29], along with a few data points from Turner [84]. The spread in the data seems to largely come from the data of Oshinowo [59] and Runge [84].

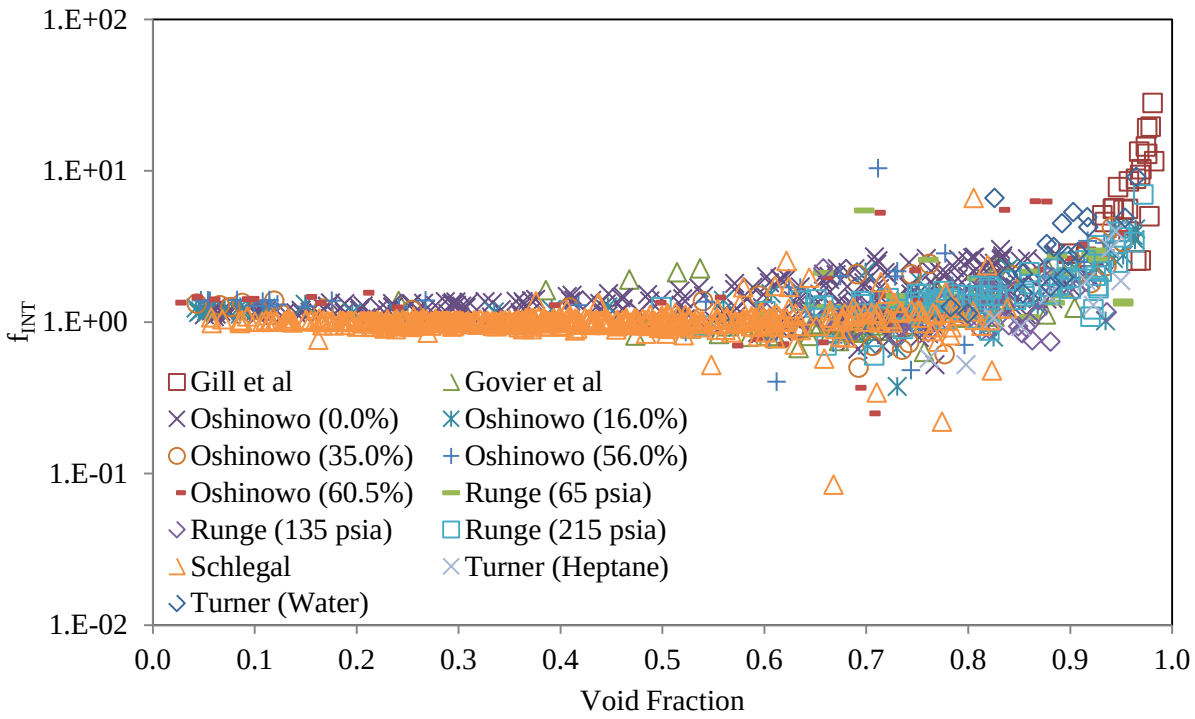

Figure 53: Comparison of the Non-Dimensionalized Interphase Friction Force against the Void Fraction with Studies Specified

4.1.2: Developing the Correlation

Having compared the non-dimensionalized interphase friction force against several derived and published dimensionless parameters, there appear to be a few that are worth further analysis, and for which a correlation may be drawn that can be used to predict the interphase friction force. So far it has been determined that the most appropriate non-dimensionalization of the interphase friction force is satisfied by Equation 277. A particular strong relationship has been shown between f_{INT} and the Weber number, Froude number using velocity difference and the mixture Froude number described in Equation 54.

First, the relationship between the non-dimensionalized interphase friction force and the Weber number will be investigated. We begin by looking at Figure 42, and examining how the data fits a potential curve. As discussed, it appears that for $We \leq 10{,}000$, $f_{INT} \approx 1$, and that for $We \geq 250{,}000$, the data fits along a straight line, when plotted on a log-log plot.

In Figure 54, the comparison of non-dimensionalized interphase friction force to the Weber number is shown, with lines drawn meant to serve as axes that would fit a correlation between the two dimensionless parameters. A horizontal line is drawn along f_{INT} = 1 which shows a trend of data points falling along the line up to *We* = 10,000.

A second line has been drawn that follows several data points between *We* = 450,000 and *We* = 1,200,000. For *We* = 1,000,000, we find that this line has f_{INT} = 20, and for *We* = 200,000, f_{INT} = 1. Since we are using a log-log plot to depict the curve, then the line would fit an equation similar to:

$$\log(f_{INT}) = A\log(We) + B \tag{278}$$

where *A* and *B* are constants. Using the boundary values for f_{INT} and *We* that have been described, *A* has been found to equal 1.861 and *B* equal to -9.87. This translates to a final equation for *We* ≥ 450,000:

$$f_{INT} = 1.358 \times 10^{-10} We^{1.861} \tag{279}$$

One key observation that will be worth investigating deeper with respect to the Froude number is that the Weber number is raised to a power of 1.861 for this set of data points. This may indicate that the interphase friction force is proportional to the velocity difference to a power higher than 2, in this case 3.72.

For 10,000 < We < 450,000, it appears that the non-dimensionalized interphase friction force follows an exponential function of the Weber number. Given this information, we can determine that the non-dimensionalized interphase friction force can be described as a function of the Weber number using Equation 280.

$$f_{INT} = \begin{cases} 1 \; if \; We \; \leq 10{,}000 \\ Ae^{BWe} \; if \; 10{,}000 > We > 450{,}000 \\ 1.358 \times 10^{-10} We^{1.861} if \; We \; \geq 450{,}000 \end{cases} \tag{280}$$

where *A* and *B* are constants that are determined using a least squares solution.

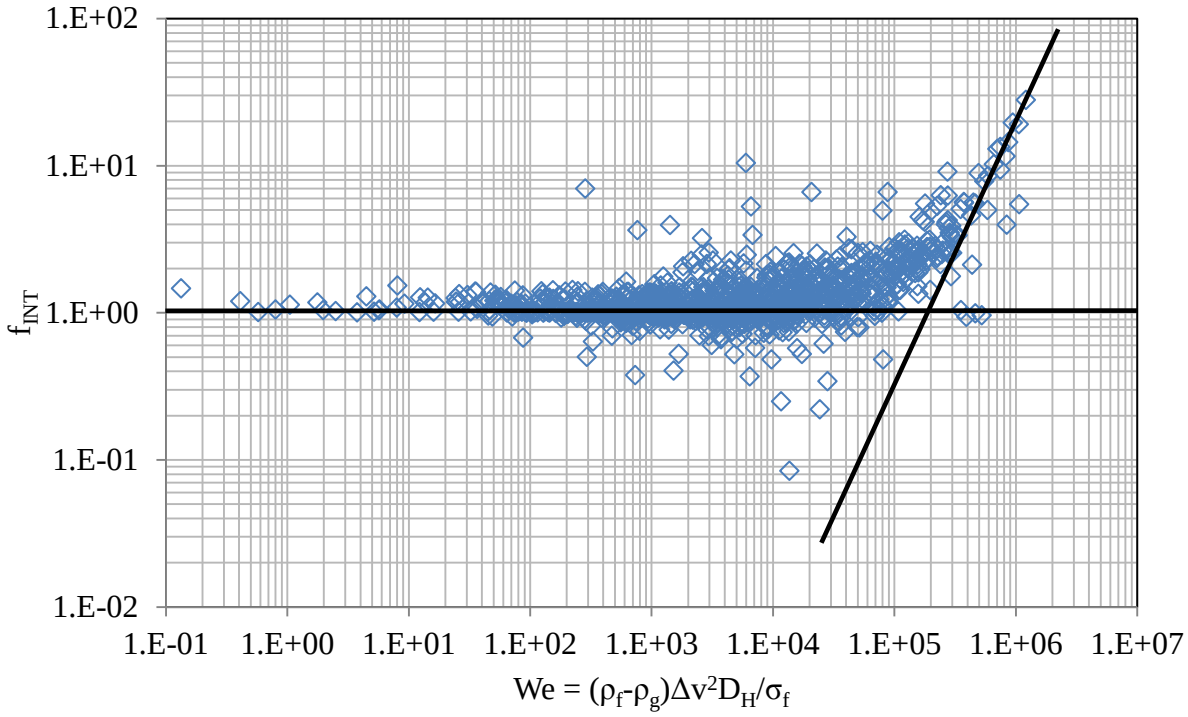

Figure 54: Weber Number Comparison to the Non-Dimensionalized Interphase Friction Force, with Correlation Axes

In Figure 55, the correlation proposed in Equation 281, is shown in comparison to the data that has been shown in Figure 54. Using a least squares analysis of the data, the coefficients for the correlation in Equation 280 are $A = 0.966$ and $B = 3.43\text{x}10^{-6}$. Thus, the final equation can be written as:

$$f_{INT} = \begin{cases} 1 \; if \; We \; \leq 10{,}000 \\ 0.966e^{3.43\times10^{-6}We} \; if \; 10{,}000 < We < 450{,}000 \\ 1.358 \times 10^{-10} We^{1.861} if \; We \; \geq 450{,}000 \end{cases} \quad 281$$

The root mean square error for the entire correlation in Equation 281 is 0.941. The mean average error of correlation for all data points is 21.0%, while the median average error is 12.58%. Of the 1262 data points for which the correlation was matched against, 797 were within ±20% error, accounting for 63.2% of the data points, while 1182 were within ±50% error,

accounting 93.7% of the data points. The maximum error for the correlation amongst all data points was 1103%.

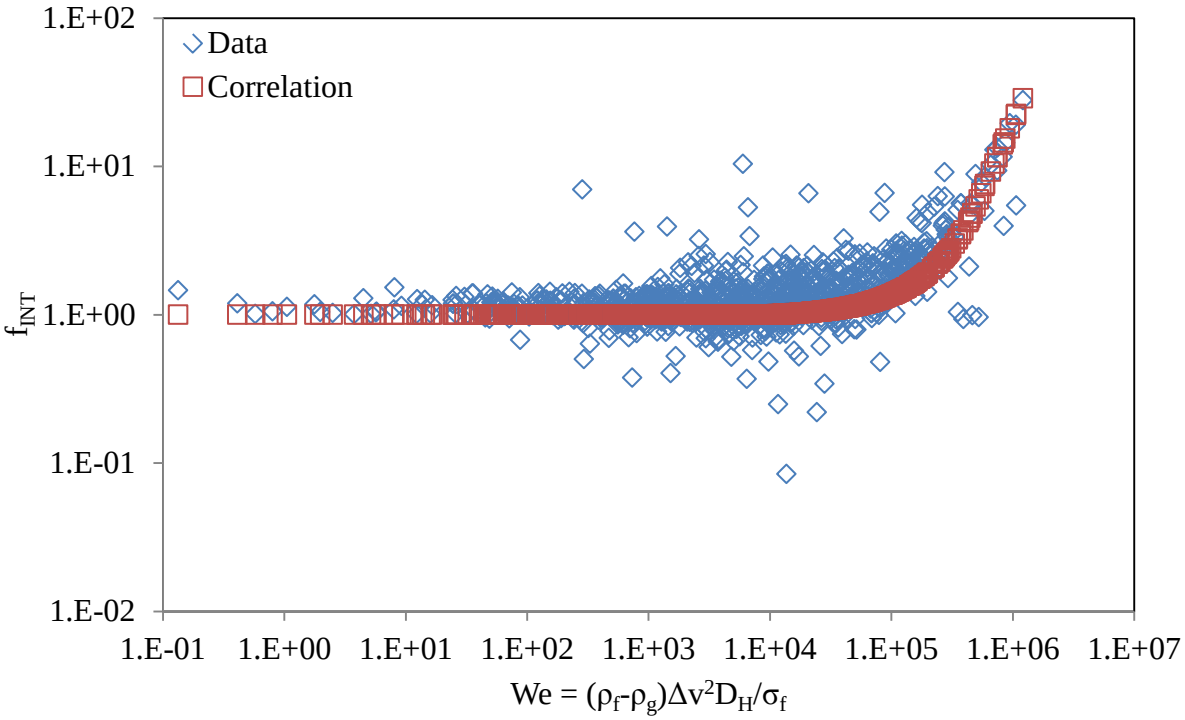

Figure 55: Comparison of the Non-Dimensionalized Interphase Friction Force to the Weber Number and Correlation Developed Through Analysis and Least Squares Solution

Figure 56 shows the non-dimensionalized interphase friction force normalized by the Weber number correlation. The mean average value for the normalized interphase friction force is 1.208, which is significantly higher than the desired value of 1.0. The standard deviation for the normalized interphase friction force is 0.536. Data points marked with a blue diamond are within 2 standard deviations of the mean value, while data points outside two standard deviations are marked as red squares. There were 1233 of 1262 data points, accounting for 97.7%, within 2 standard deviations of the mean average value for normalized interphase friction. The coefficient of skewness, C_s, is 7.09, which is reflected by the greater number of statistical outliers that are greater than the mean value then there are less than the mean value. Nonetheless, we

have a very peaked distribution of data points, as indicated by the coefficient of kurtosis, C_k, is 94.1.

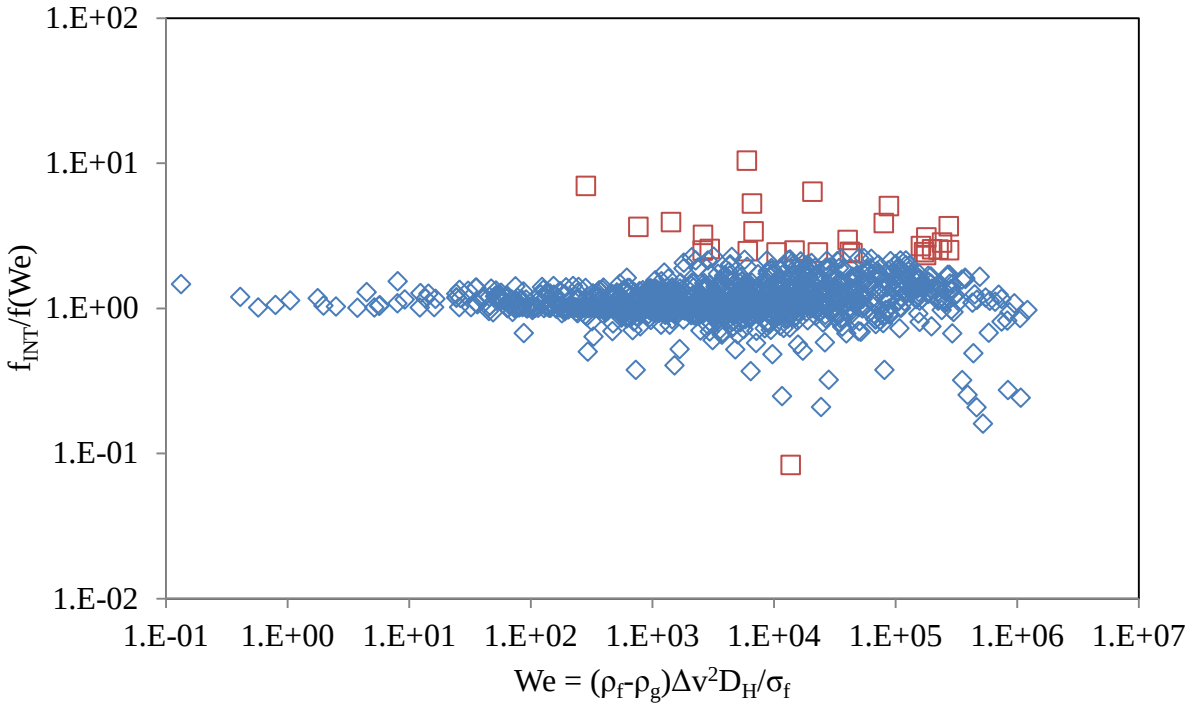

Figure 56: Non-Dimensionalized Interphase Friction Force Normalized by the Weber Number Correlation

There are two different steps that can be taken to improve upon the correlation with the Weber number. First, the correlation can be re-evaluated with only data points that are within two standard deviations of the current correlation. Also, the boundaries between the equations used for the current correlation can be adjusted, which may produce a more accurate solution. When changing the boundaries, it is necessary to allow the equation for the middle region to change to adjust to the increasing or decreasing data points that are being factored into its derivation. Thus, a least squares solution was attempted allowing for both the boundaries to change and the coefficients of the middle equation to change simultaneously, using only the data points within 2 standard deviations of the original Weber number correlation. However, the data

solver was unable to improve on the Weber number correlation, as all variables were held constant.

Another possibility that exists with the Weber number is to adjust the function by which the middle region. Instead of the non-dimensionalized interphase friction being an exponential function of the Weber number, perhaps it is a log-log linear function instead. Thus we consider the case of Figure 54, and draw a third line that follows the data and bridges the two previously identified lines. Using a data solver to find the least squares error between such a correlation and the data results in Equation 282, and is depicted in Figure 57.

$$f_{INT} = \begin{cases} 1 \; if \; We \; \leq 10{,}290 \\ 0.0357We^{0.361} \; if \; 10{,}288 < We < 408{,}200 \\ 1.358 \times 10^{-10} We^{1.861} if \; We \; \geq 408{,}200 \end{cases} \quad 282$$

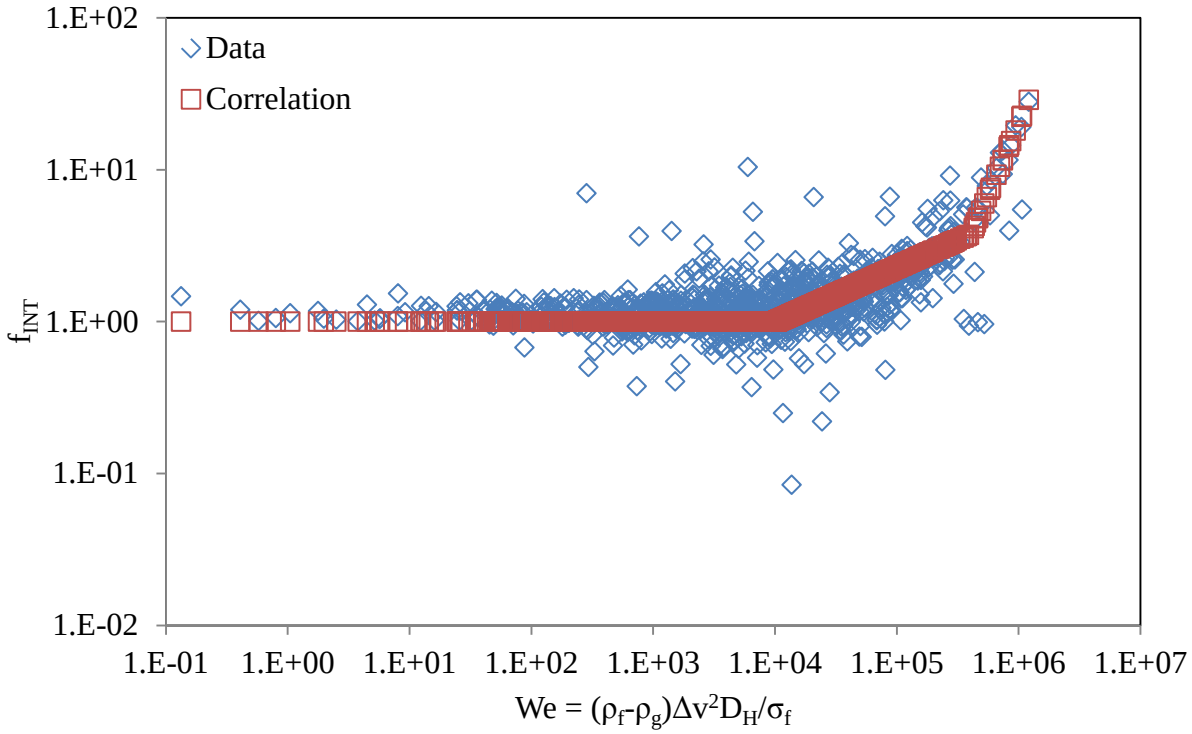

Figure 57: Comparison of the Non-Dimensionalized Interphase Friction Force to the Weber Number Correlation with Respect to the Weber Number

Statistically, this new Weber number correlation is an improvement over the earlier correlation. The RMS error has decreased from 0.941 to 0.889, and while the mean average error is up from 21.0% to 21.6%, the median average error has decreased from 12.58% to 11.25%. The number of data points with an error of less than ±20% has increased from 797 to 833, although the number of data points with an error of less than ±50% has decreased from 1182 to 1171. The maximum error increased from 1103% to 1218%.

When the non-dimensionalized interphase friction force is normalized against the correlation, the mean value decreased from 1.208 to 1.097, while the median value decreased from 1.065 to 1.018. The standard deviation decreased from 0.536 to 0.482, indicating that the new formulation is more precise than the previous correlation. Also, the coefficient of skewness increased from 7.09 to 8.78, which indicates that the new formulation has a greater bias to underestimate the non-dimensionalized interphase friction force than the earlier correlation. Meanwhile, the coefficient of kurtosis increased from 94.1 to 139.0, suggesting that the new correlation is much stronger than the earlier correlation.

Physically, this correlation shows that the interphase friction force is related only to buoyancy up to a Weber number of about 10,288. Between Weber number values of 10,288 and 408,200, it appears that the interphase friction force is related to the velocity difference raised to a power of approximately 0.72, which is insufficient to call it a drag region, as one would expect the drag to be proportional to the velocity difference squared. This region appears to have something that inhibits a pure form of drag to take place between the vapor and liquid, which may be the surface tension that is being factored in through the Weber number. A closer look with the Froude number should provide a more direct relationship between the velocity difference and the interphase friction force. For Weber number values above 408,200, the

velocity difference is raised to the power of 3.7, indicating that in addition to drag, there are other factors adding to the interphase friction. This will also be further investigated with the Froude number.

The Froude number that includes the velocity difference will first be considered for analysis. Similar to the analysis that was conducted with the Weber number, we consider Figure 44, only this time with minor grid lines included, along with lines following the data on the log-log plot. In Figure 58, two lines have been drawn that appear to fit well with the data on the log-log plot. For $Fr \leq 10$, it appears that $f_{INT} \approx 1$. Meanwhile, for data points where Fr $\geq$ 3000, it appears that the data fits along the second line that has been drawn. This second line fits a curve such that for Fr = 1000, f_{INT} = 1, and when Fr = 10,000, f_{INT} = 30. The line corresponds to Equation 283.

$$f_{INT} = 3.70 \times 10^{-5} Fr^{1.477} \tag{283}$$

For the range $10 < Fr < 3000$, there appears to be an exponential curve along which the data fits. However, as has been shown with the Weber number, a power curve will likely fit the data better, and would also be easier to compare against the results from the Weber number. Therefore, the Froude number correlation for which the data solver will be used to determine the best fitting coefficients will be:

$$f_{INT} = \begin{cases} 1 \; if \; Fr \; \leq Fr_1 \\ AFr^B \; if \; Fr_1 < Fr < Fr_2 \\ 3.70 \times 10^{-5} Fr^{1.477} if \; Fr \; \geq Fr_2 \end{cases} \tag{284}$$

where A and B are coefficients for the intermediate region of Froude numbers, while Fr_1 and Fr_2 represent the boundary values between each region. Each of the four parameters will be determined through the data solver.

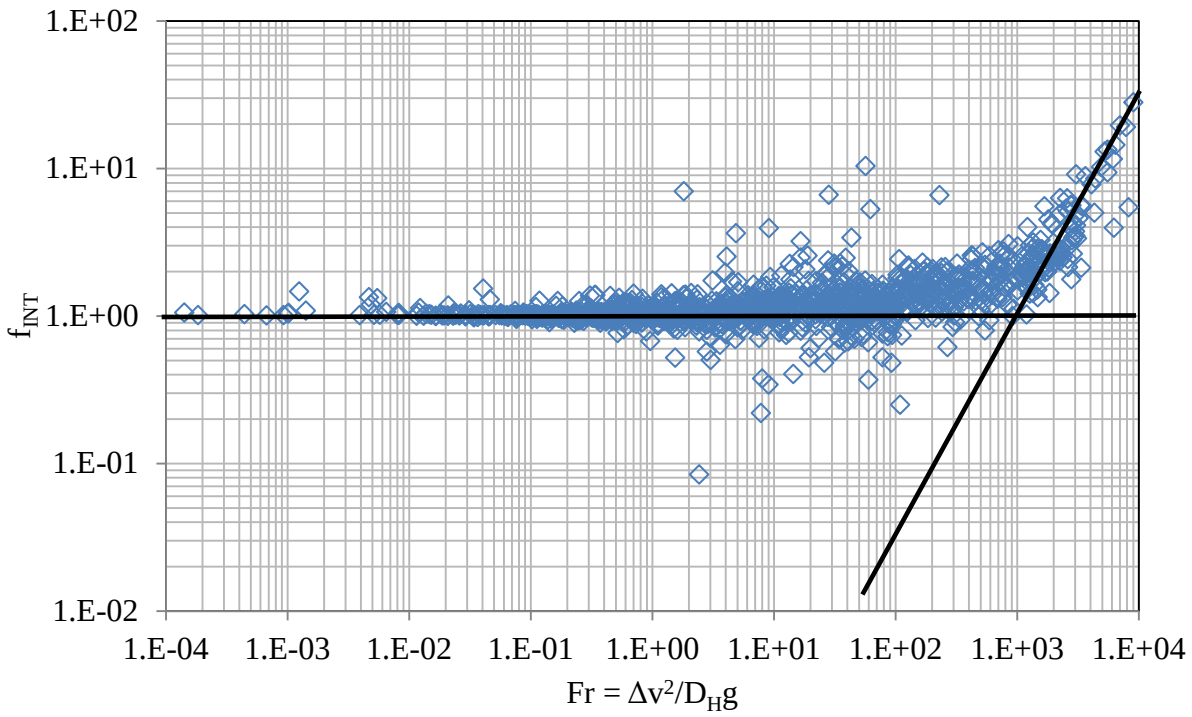

Figure 58: Comparison of the Non-Dimensionalized Interphase Friction Force against the Froude Number with Correlation Lines Drawn

Using the data solver to find the least squares error for the correlation, it was determined that the Froude number correlation that best fit the data was:

$$f_{INT} = \begin{cases} 1 \; if \; Fr \leq 6.50 \\ 0.758 Fr^{0.1477} \; if \; 6.50 < Fr < 1750 \\ 3.70 \times 10^{-5} Fr^{1.477} if \; Fr \geq 1750 \end{cases} \quad 285$$

and has been depicted in Figure 59.

The Froude number correlation at this point appears to be statistically improved from the Weber number correlation. The RMS error is 0.851, while the mean average error is 20.1% and the median average error is 10.13%. Of the 1262 total data points, 897, or 71.1%, were within ±20% error, while 1166, or 92.4%, were within ±50% error. The maximum error was 1088%.

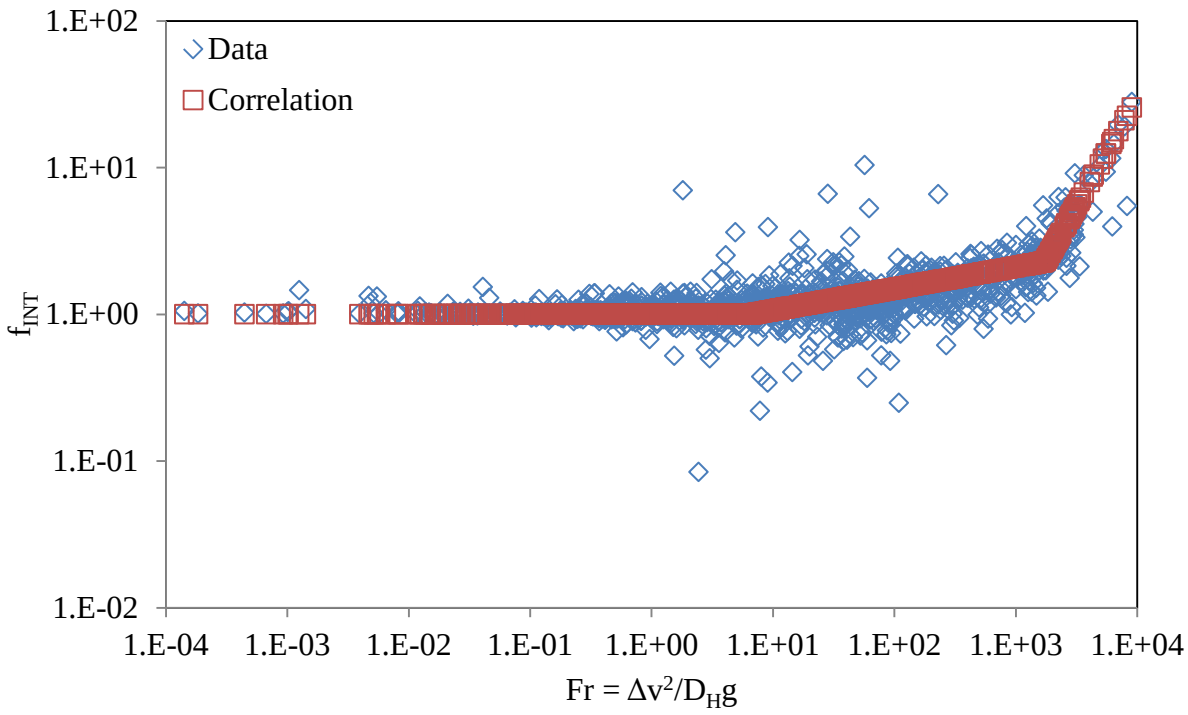

Figure 59: Comparison of the Non-Dimensionalized Interphase Friction Force to the Froude Number Correlation

In Figure 60, the non-dimensionalized interphase friction force is normalized by the Froude number correlation given in Equation 285. The mean average value for the normalized non-dimensionalized interphase friction force is 1.023, while the median average value is 1.004, with a standard deviation of 0.404. Data points within 2 standard deviations of the mean value number 1238, and are marked with a blue square in Figure 60, while data points outside two standard deviations are marked with red diamonds. The skewness coefficient is 8.07 and the kurtosis coefficient is 110.2, indicating that the correlation is not as centered on the mean as the Weber number correlation, nor is it as likely to underpredict the interphase friction force.

If the statistical outliers are omitted from the analysis, then the correlation shown in Equation 286, and depicted in Figure 62 would be the result. The RMS error for the new Froude number correlation would be 0.853, which is a slight increase from 0.851 for all data points; however it decreased from 0.731 to 0.729 for data points within two standard deviations of the

original Froude number correlation. The mean average error improved from 20.1% to 18.96%, while the median average error improved from 10.13% to 9.98%. While the number of points within ±20% error decreased from 897 to 893, the number of data points within ±50% error increased from 1166 to 1179. The maximum error percentage remained 1088%. When the non-dimensionalized interphase friction force is normalized by the new Froude number correlation, the mean average value of the normalized interphase friction force is 1.063, an increase from 1.023, and the median average value is 1.012, increased from 1.004. The standard deviation increased from 0.404 to 0.436, while the coefficient of skewness increased from 8.07 to 8.34 and the coefficient of kurtosis increased from 110.2 to 114.4.

$$f_{INT} = \begin{cases} 1 \; if \; Fr \; \leq 17.71 \\ 0.596 Fr^{0.1799} \; if \; 17.71 < Fr < 1749 \\ 3.70 \times 10^{-5} Fr^{1.477} if \; Fr \; \geq 1749 \end{cases} \quad 286$$

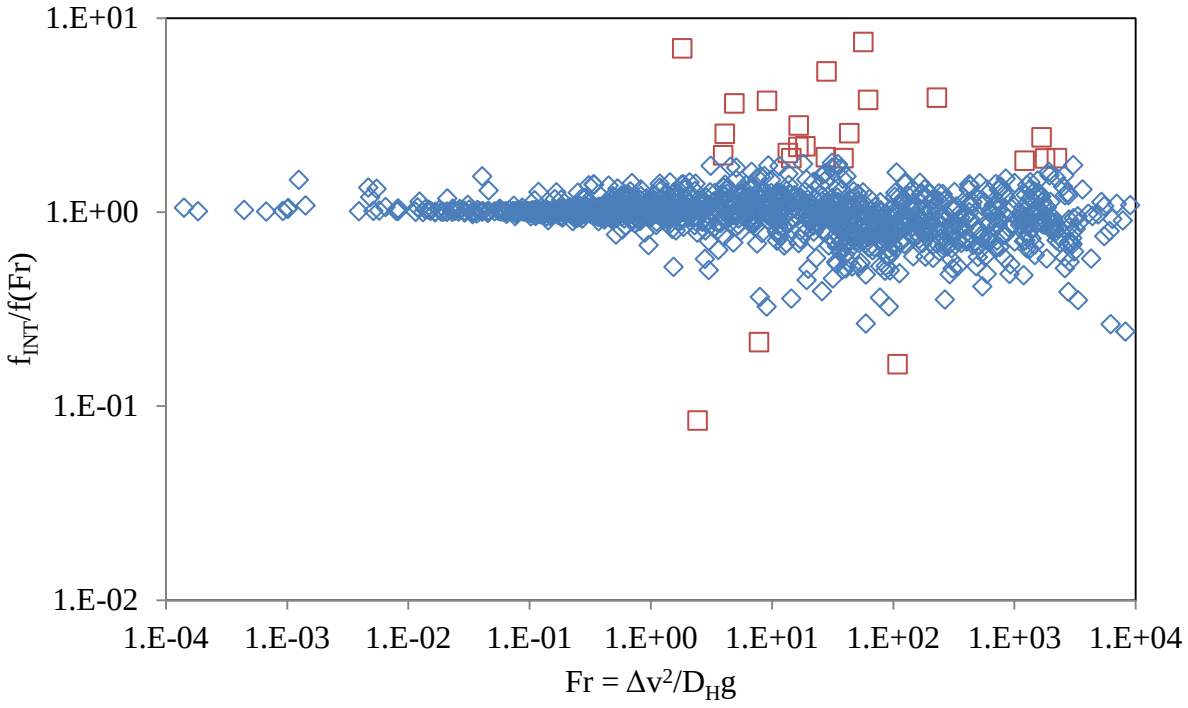

Figure 60: Non-Dimensionalized Interphase Friction Force Normalized by Froude Number Correlation

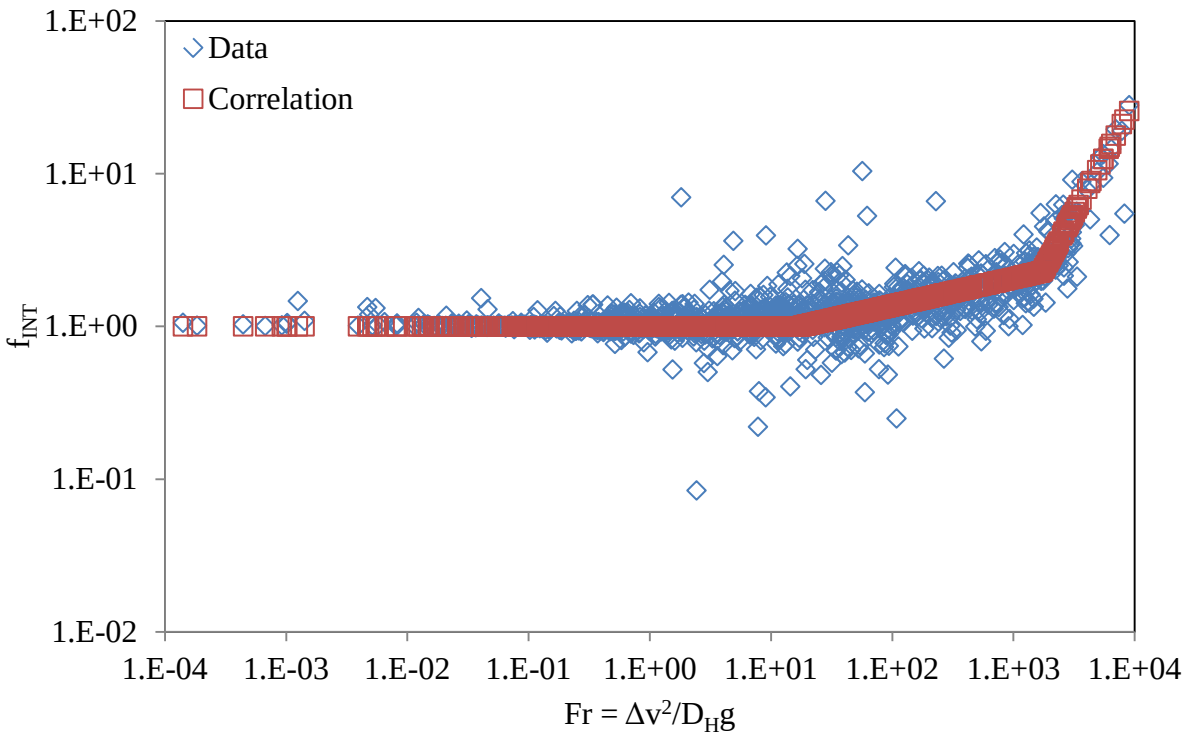

Figure 61: Comparison of the Non-Dimensionalized Interphase Friction Force to the Froude Number Correlation Reanalyzed without Outliers

The original Froude number correlation given in Equation 283 and the reanalyzed Froude number correlation given in Equation 286, do not appear to be significantly different from each other in terms of statistical analysis. However, when considering the appearance of Figure 59 in relation to Figure 61, and considering that the reanalyzed correlation omitted data points that were considered to be statistical outliers, the reanalyzed correlation should be considered the more desirable solution to this particular problem.

As seen with the Weber number, there are some interesting physical interpretations that can be drawn from studying the Froude number correlation. Like the Weber number correlation, there appear to be three regions where the interphase friction force data appears to fit along the same correlations. For $Fr \leq 17.71$, the interphase friction force appears to be purely a function of buoyancy, and independent of the velocity difference. When the Froude number is between a value of 17.71 and 1749, we find that the interphase friction force is proportional to the velocity

difference raised to a power of 0.36, based on the Froude number correlation. With the Weber number, the middle region showed that it was proportional to velocity difference raised to a power of 0.72. However, since the Froude number is a more direct representation of the velocity difference, it may be more accurate to consider that for this intermediate region that the interphase friction force is proportional to the velocity difference raised to the 0.36 power. Nonetheless, this is still significantly less than that of the drag force, which would be expected to be proportional to the square of the velocity difference, and indicates that other factors may be affecting the interphase friction force. For $Fr > 1749$, we find that the interphase friction force is proportional to the velocity difference raised to the power of 2.95. Since it is a higher power than the expect value of 2 for interphase drag, then it is suggested that there are other factors in addition to the velocity difference contributing to the interphase friction force.

With the observation that the non-dimensionalized interphase friction force appears to fit within three different regions, then it is pondered if what is being identified are flow regimes, where the interphase friction force is known to change as the flow regimes change. However, there is no documented case of the flow regime being correlated to either the Weber number or the Froude number calculated using the velocity difference. However, there are documented flow regime maps that use the mixture Froude number, which is shown in Figure 46 to have a similar relationship to the non-dimensionalized interphase friction force as the Weber number and the velocity difference Froude number.

If we consider the non-dimensionalized interphase friction force as a three-part function of the mixture Froude number, then it would likely resemble that drawn in Figure 62. For $Fr_m < 20$ approximately, we find that $f_{INT} \approx 1$. At $Fr_m = 20$, the non-dimensionalized interphase friction force data follows a gently sloping line, until reaching the steeper sloping line at $Fr_m \approx 1750$.

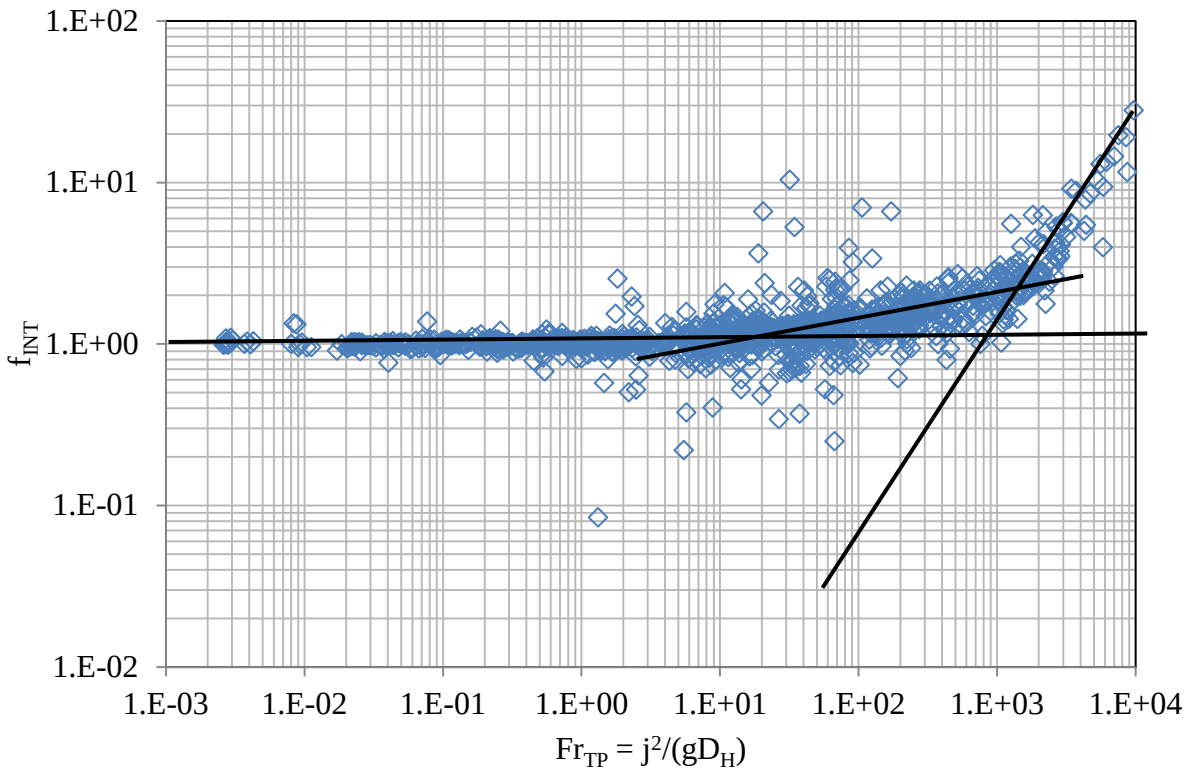

Figure 62: Comparison of the Non-Dimensionalized Interphase Friction Force against the Mixture Froude Number

For the higher Fr_m region, we find that the line fits the curve given in Equation 287, which coincidentally is the same equation that fits the velocity difference Froude number for $Fr \geq 1749$. The middle region, along with the region boundaries are determined by the data solver.

$$f_{INT} = 3.70 \times 10^{-5} {Fr_m}^{1.477} \tag{287}$$

In Equation 288, the best fitting correlation between the mixture Froude number and the non-dimensionalized interphase friction is given, while it is graphically shown in Figure 64.

$$f_{INT} = \begin{cases} 1 \; if \; Fr_m \leq 5.88 \\ 0.778 {Fr_m}^{0.1414} \; if \; 5.88 < Fr_m < 1723 \\ 3.70 \times 10^{-5} {Fr_m}^{1.477} if \; Fr_m \geq 1723 \end{cases} \tag{288}$$

Statistically, the mixture Froude number correlation compares very well with the previously developed correlations, as it has an RMS error of 0.755. The mean average error for

the correlation is 17.54% while the median average error is 7.24% and the maximum error is 1088%. A total of 932 data points were within ±20% error of the between the correlation and the data point, accounting for 73.9% of all data points, while 1179 data points were within ±50% error. When the non-dimensionalized interphase friction force is normalized by the mixture Froude number correlation, as shown in Figure 65, we find that the mean average value is 1.004, while the median average value is 1.000. The standard deviation is 0.372, while the coefficient of skewness is 9.24 and the kurtosis coefficient is 145.0. Of the 1262 data points, 1239 are within two standard deviations, accounting for 98.2% of all of the data points.

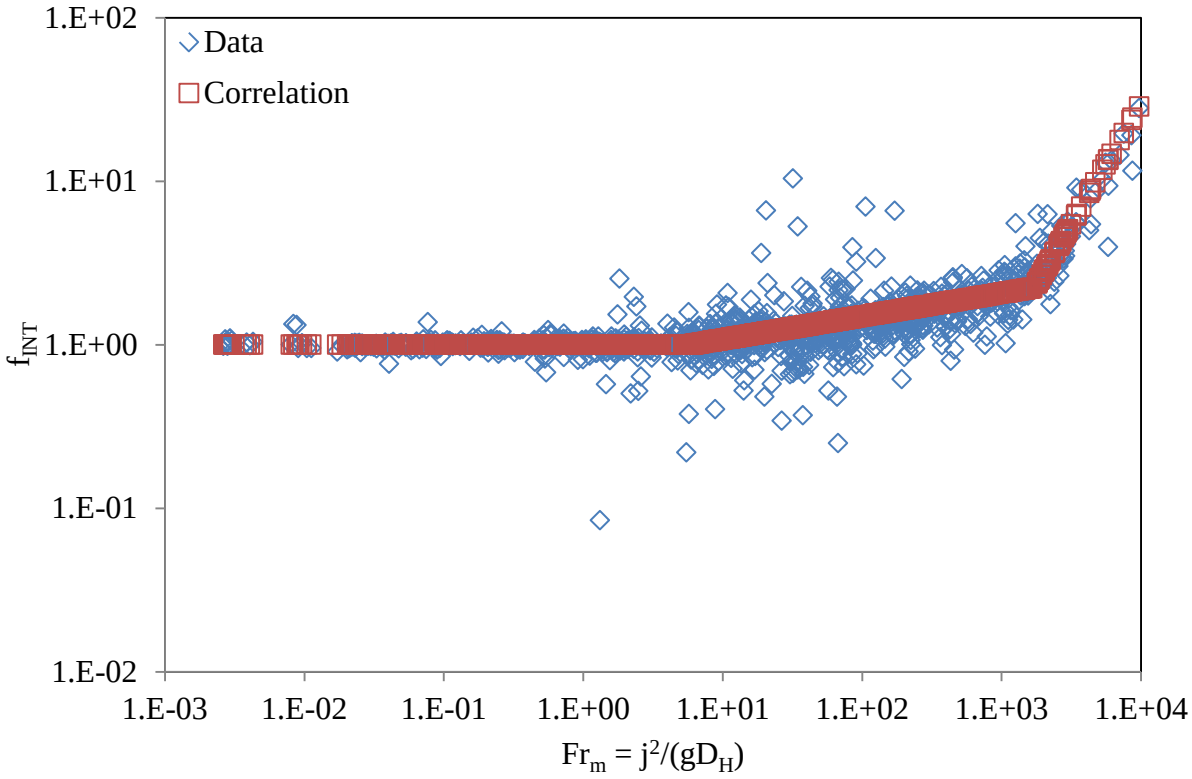

Figure 63: Comparison of the Non-Dimensionalized Interphase Friction Force to the Mixture Froude Number Correlation against the Mixture Froude Number

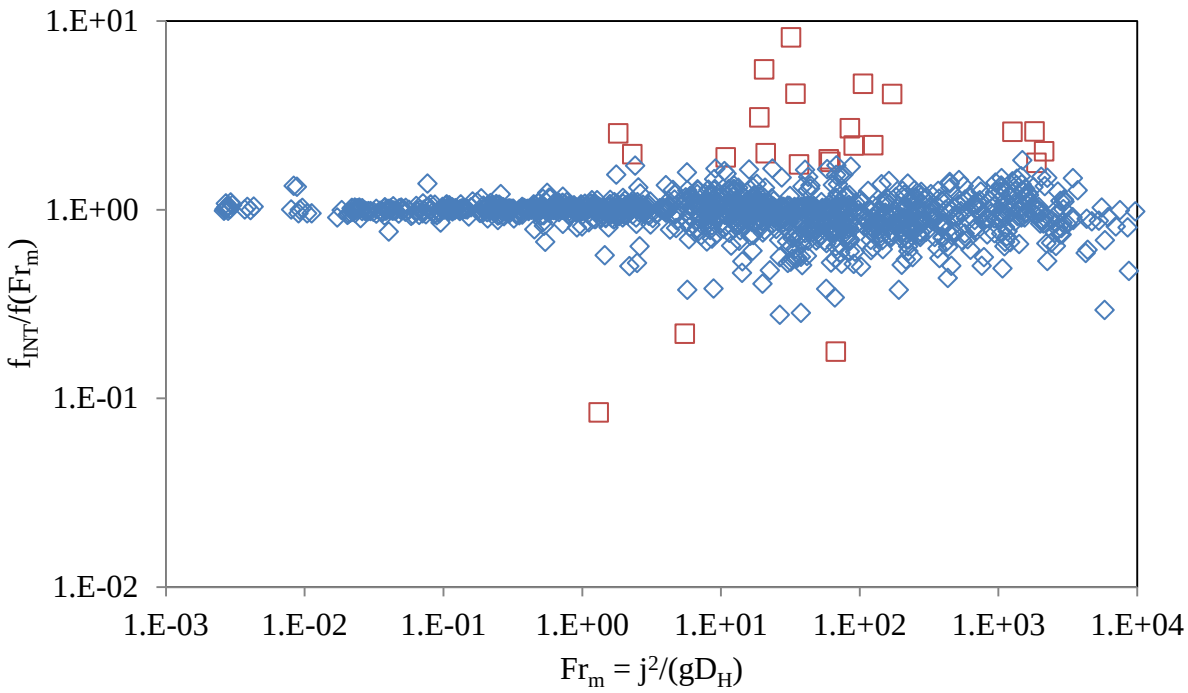

Figure 64: Non-Dimensionalized Interphase Friction Normalized by the Mixture Froude Number Correlation

If we rerun the data solver only for the points that fall within two standard deviations of the correlation, we find that the correlation will adjust to the following equation:

$$f_{INT} = \begin{cases} 1 \; if \; Fr_m \leq 12.73 \\ 0.660 {Fr_m}^{0.1631} \; if \; 12.73 < Fr_m < 1719 \\ 3.70 \times 10^{-5} {Fr_m}^{1.477} if \; Fr_m \geq 1719 \end{cases} \quad 289$$

The most significant change is that the boundary between the first and second regions moves from Fr_m = 5.88 to 12.73, while the multiplier for the middle section decreased from 0.778 to 0.660 and the exponent increased from 0.1414 to 0.1631. However, there appears to be very little difference between the two correlations when comparing the original correlation shown in Figure 63 to the reanalyzed correlation in Figure 65.

For all data points, the RMS error increased slightly from 0.755 to 0.757. While the mean average error improved from 17.54% to 16.87%, the median average error increased from 7.24% to 8.67%, while the maximum error remained at 1088%. The number of data points for

which the correlation was within ±20% of the data points increased from 932 to 955, and for ±50%, the number increased from 1179 to 1186. When the non-dimensionalized interphase friction force is normalized by the new mixture Froude number correlation, as shown in Figure 66, the mean value increases from 1.004 to 1.041, while the median value increases from 1.000 to 1.009. The standard deviation increases from 0.372 to 0.402, with 1240 data points within two standard deviations of the mean average value. Meanwhile, the coefficient of skewness increases from 9.24 to 9.73 and the coefficient of kurtosis increases from 145.0 to 155.8. While the kurtosis suggests that the reanalyzed correlation is stronger than the original, the standard deviation and skewness suggest that the reanalyzed correlation may not be as accurate as the original correlation. However, the desire to have as many data points to be within ±20% and ±50% of the correlation makes the reanalyzed correlation more desirable for the purposes of this study.

The correlation for the interphase friction force using the mixture Froude number requires a different physical interpretation than the velocity difference Froude number. As has been noted, when $f_{INT} = 1$, then the buoyancy of the vapor phase in the liquid is the driver of the interphase friction. When the correlation shows that the non-dimensionalized interphase friction force is a function of the mixture Froude number raised to a power of 0.1631, then it suggests that the interphase friction is a function of the total volumetric flux raised to a power of 0.326. If it is assumed that these are the mostly the same data points for which the non-dimensionalized interphase friction was a function of the velocity difference Froude number raised to a power of 0.1799, then we find that for these data points, the interphase friction force is proportional to the total volumetric flux raised to a power of 0.326, and the velocity difference raised to a power of 0.360. Since the velocity difference and the total volumetric flux are raised to nearly the same

exponent, it implies that one phase's velocity is likely dominating over the other as a factor of interphase friction. In this case, it would seem likely that the vapor velocity is the dominant phasic velocity because the liquid velocity is being subtracted from the vapor velocity in the velocity difference calculation, while the liquid volumetric flux is being added to that of the vapor phase for the mixture Froude number, accounting for the small difference in exponentials. The same can be said for the third region, where both the mixture Froude number and the velocity difference Froude number are raised to a power of 1.477 indicating that for these data points, the effect of the liquid velocity is negligible compared to the vapor velocity.

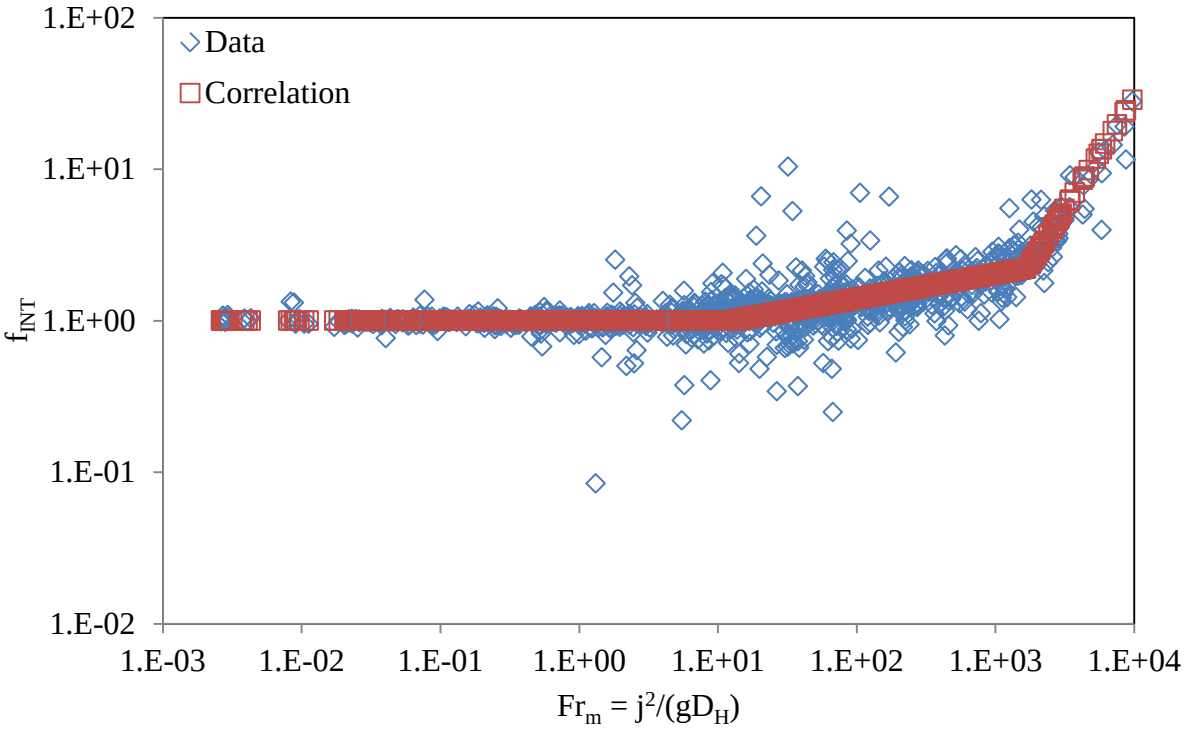

Figure 65: Comparison of the Non-Dimensionalized Interphase Friction Force to the Reanalyzed Mixture Froude Number Correlation with Respect to the Mixture Froude Number

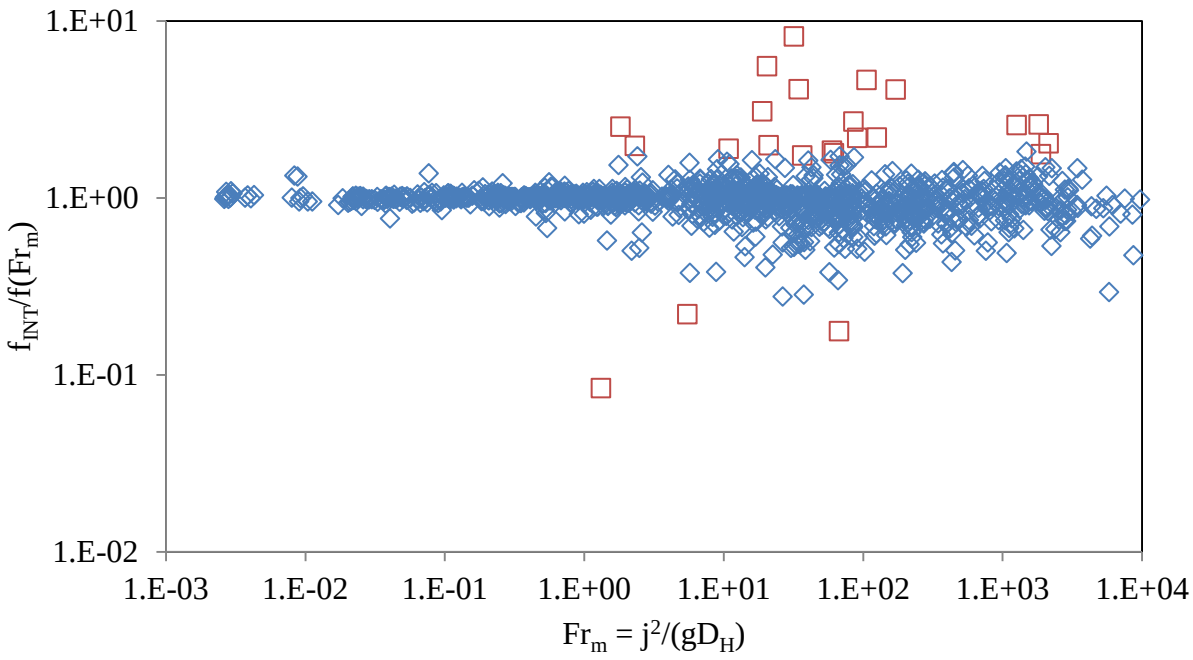

Figure 66: Non-Dimensionalized Interphase Friction Normalized by the Reanalyzed Mixture Froude Number Correlation

In summary, at this point, three different correlations have been developed for the interphase friction force using the Weber number, the velocity difference Froude number and the mixture Froude number as independent variables, and are shown in Equations 282, 286 and 289. As the residual of each correlation does not show any patterns, there does not appear to be any possibility that a secondary correlation will improve upon the existing correlations. The statistical accuracy of these correlations is compared in Table 7 and Table 8. Table 7 shows how well each correlation matches with the non-dimensionalized interphase friction force, while Table 8 shows the precision and accuracy of the non-dimensionalized interphase friction force normalized by the respective correlations. The mixture Froude number correlation is the most accurate of the three correlations that have been developed.

Table 7: Summary of Correlation Accuracy Statistics

	$f(We = (\rho_f-\rho_g)\Delta v^2 D_H/\sigma_f)$	$f(Fr = \Delta v^2/D_H g)$	$f(Fr_m = j^2/D_H g)$
RMS Error	0.889	0.853	0.757
Mean Error	21.60%	18.69%	16.87%
Median Error	11.25%	9.98%	8.67%
±20% Error	833	893	955
- (Percentage)	66.0%	70.8%	75.7%
±50% Error	1171	1179	1186
- (Percentage)	92.8%	93.4%	94.0%
Maximum Error	1218%	1088%	1088%

Table 8: Summary of Normalized Interphase Friction Correlation Statistics

	$f_{INT}/f(We)$	$f_{INT}/f(Fr)$	$f_{INT}/f(Fr_m)$
Mean Average	1.097	1.063	1.041
Median Average	1.018	1.012	1.009
Standard Deviation	0.482	0.436	0.402
Skewness Coefficient	8.78	8.34	9.73
Kurtosis Coefficient	139.0	114.4	155.8

4.1.3: Flow Regime Comparison

As we have seen with the three correlations that have been developed to predict the interphase friction force, each correlation can be divided into three components. However, there does not appear to be a clear physical explanation as to why the data fits into these three groups or how these three groups relate to the physics of one-dimensional vertical two-phase flow. By comparing the results to some of the published flow regime maps, a greater understanding of the correlations and their physical meaning can be gained.

First, consider the three components of each correlation. The first component is always $f_{INT} = 1$, which suggests that for this particular component, that the interphase friction force is the result of buoyancy, and that there is no additional force on the vapor of liquid that is affecting the interphase friction. It has been suggested that for the second component, the velocity of the

vapor is increasingly more important in calculating the interphase friction force than the liquid velocity, while in the third region; the effect of the liquid velocity is negligible. For each correlation, the region shall be known as the "Buoyancy Regime," to reflect the importance of buoyancy with these data points. The third region shall be referred to as the "Vapor Drag Regime," as it appears that for these data points, the vapor velocity or volumetric flux is exceedingly dominant over the liquid velocity or volumetric flux in determining the interphase friction force. The second region, which is in between the "Buoyancy Regime" and the "Vapor Drag Regime," will be referred to as the "Transition Regime."

First, we will consider each point, with respect to the other correlations, to determine how well the flow regimes agree with each other. Comparing the groups within each correlation shows that for 838 of the 1262 data points, or 66.4%, the three correlations are unanimous in their agreement of the interphase friction regime, while at least two of the three correlations agree on the remaining 424 data points, or 33.6%. For 290 of the 424 data points, the velocity difference Froude number correlation agreed with the mixture Froude number correlation on the regime, while for 116 data points, the agreement was between the Weber number correlation and the velocity difference Froude number correlation. Only for 18 data points did the Weber number correlation agree on the friction regime with the mixture Froude number correlation, but not with the velocity difference Froude number.

Now, we shall consider how each correlations friction regime compares to the flow regimes that have been published and previously discussed. The Vince and Lahey [85] flow regime map is specific to air and water flowing in a singular diameter pipe, and thus will not be considered for comparison as all data will be applied to a singular map. With regards to the Taitel et al [81] flow regime map, we need to determine the flow regime for each data point

using Equations 38 through 44, and draw a flow regime map accordingly, instead of using the flow regime map shown in Figure 2, as it is also specified for only air-water in a one-inch diameter pipe at atmospheric pressure and room temperature. We find that for all data points, the Taitel et al flow regime map resembles that shown in Figure 67. The lines that have been drawn represent approximate demarcations between the flow regimes identified by Taitel et al. Note that the churn-turbulent flow data points appear to be interspersed amongst the slug flow regime, thus they have been merged into a single grouping.

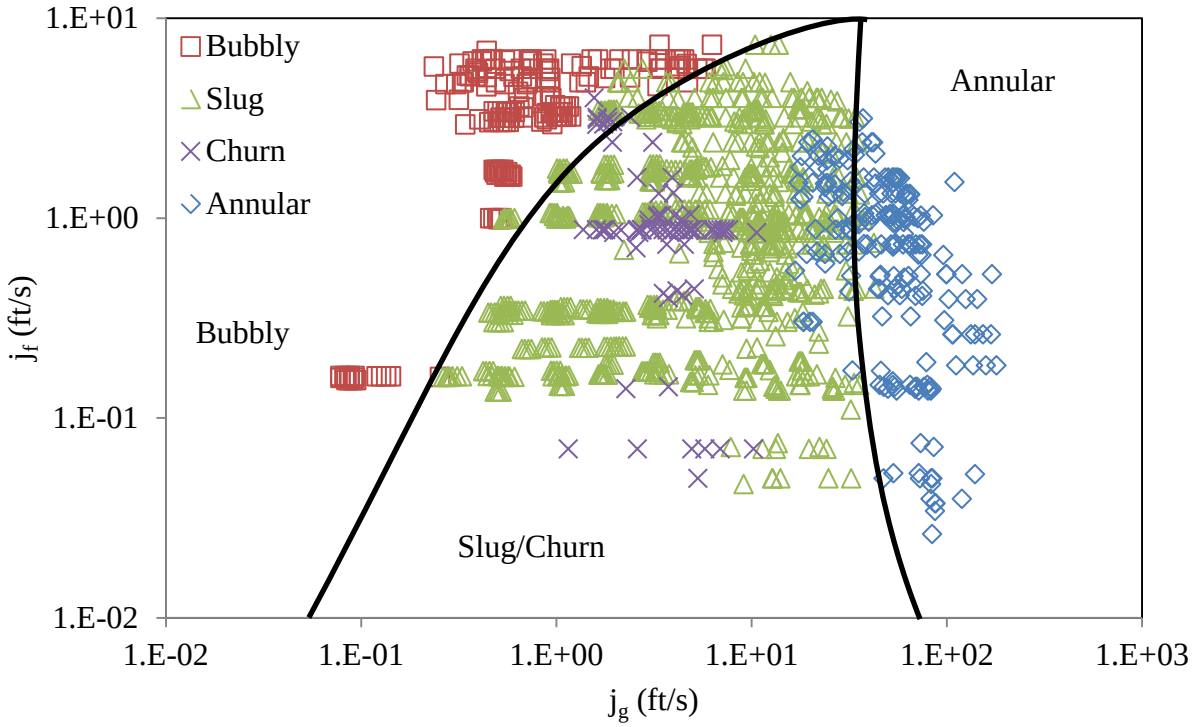

Figure 67: Taitel et al [81] Flow Regime Map

If we apply the flow regime map that has been drawn in Figure 67 to the friction regimes identified for each correlation, then we may be able to draw some conclusions regarding the interphase friction force correlations and their physical meanings. In Figure 68, the Taitel et al [81] flow regime map is compared against the Weber number correlation interphase friction regimes. Figure 69 shows the Taitel et al flow regime map compared to the velocity difference

Froude number correlation interphase friction regimes, and Figure 70 shows the comparison with the mixture Froude number correlation interphase friction regimes. What we see in each of these comparisons is that the buoyancy regime appears to include both the bubbly and slug flow regimes, while the transitional regime includes both the slug flow regime and the annular flow regime. The vapor drag regime is almost exclusively within the annular flow regime, with the exception of a few data points with the Weber number correlation. Also, there does not appear to be a smooth transition from the buoyancy regime to the transitional regime, when comparing the volumetric fluxes of each phase. It appears that the transition from buoyancy to transitional occurs over a range of vapor volumetric fluxes, and does not appear to correspond to a particular function of the liquid volumetric flux. There does appear to be a more definitive boundary between the transitional and vapor drag regimes, as the boundary between the two regimes appears at j_g = 100 ft/s for the Weber number correlation, and j_g = 70 ft/s for the velocity difference and mixture Froude numbers. The vapor drag regime appears to be a subset of the annular flow, encompassing the data points with the highest vapor volumetric fluxes. This implies that the vapor drag regime represents cases of annular flow where the liquid film along the pipe wall is likely very small, with the main source of interphase friction being the liquid droplets entrained in the vapor core.

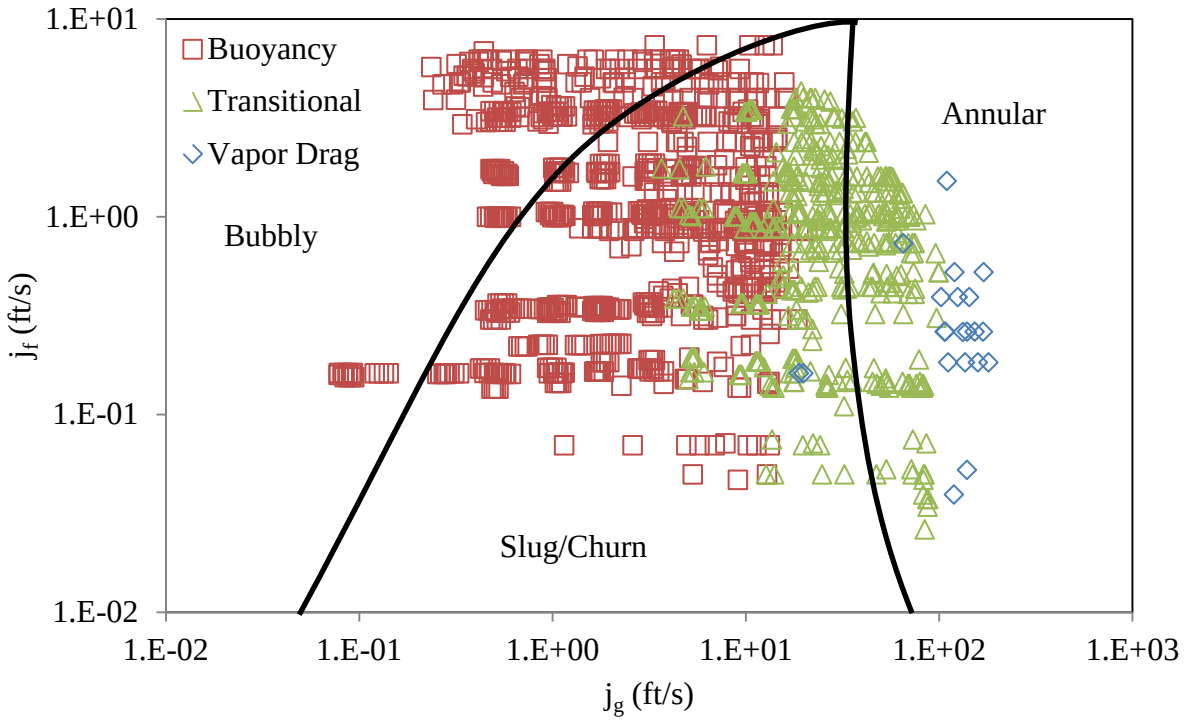

Figure 68: Comparison of the Taitel et al [81] Flow Regime Map to the Weber Number Correlation Interphase Friction Regime

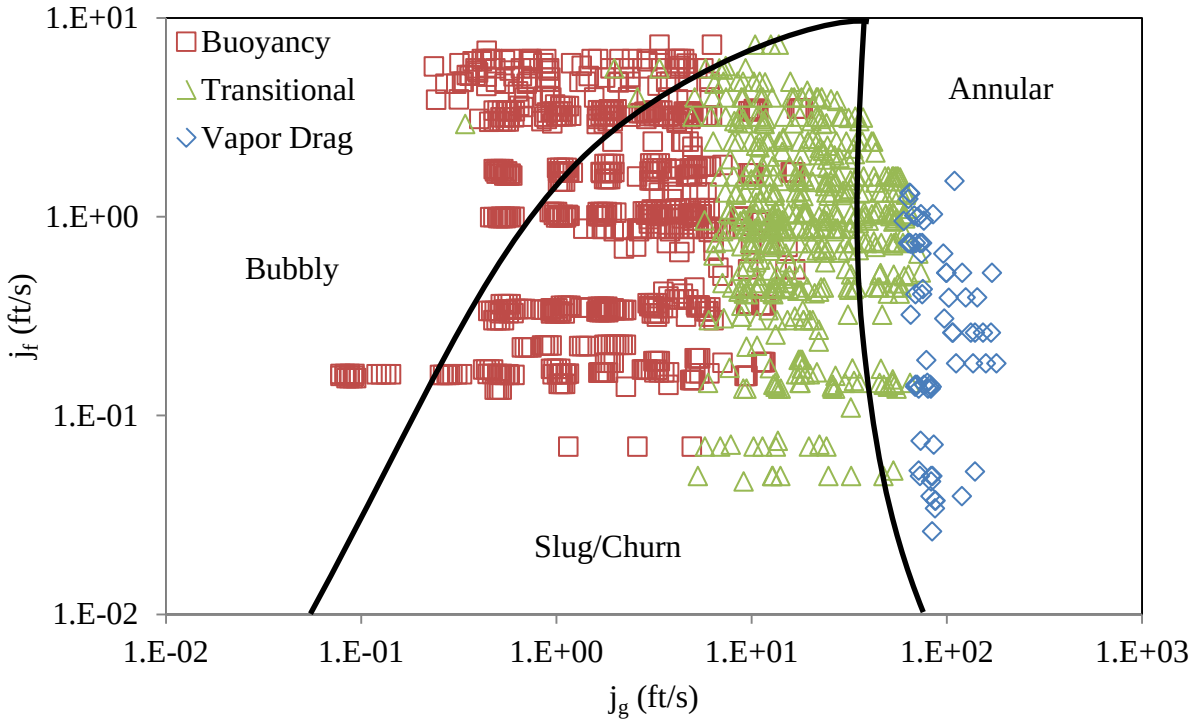

Figure 69: Comparison of the Taitel et al [81] Flow Regime Map to the Velocity Difference Froude Number Correlation Interphase Friction Regime

One difference between the mixture Froude number comparison and those for the Weber number and velocity difference Froude number correlations involves a set of data points with relatively high liquid volumetric fluxes. Notice in Figure 68 and Figure 69 that there for all data points with a liquid volumetric flux greater than 4 ft/s, they are classified as being in the buoyancy regime, whereas the mixture Froude number correlation shows in Figure 70 that those data points are part of the transitional regime. Since these data points would have relatively large liquid velocities, their velocity differences would be relatively small, as would their respective Weber number and velocity difference Froude number. However, they would consequentially have larger total volumetric fluxes, giving them larger mixture Froude numbers, bumping these data points into the transitional flow regime.

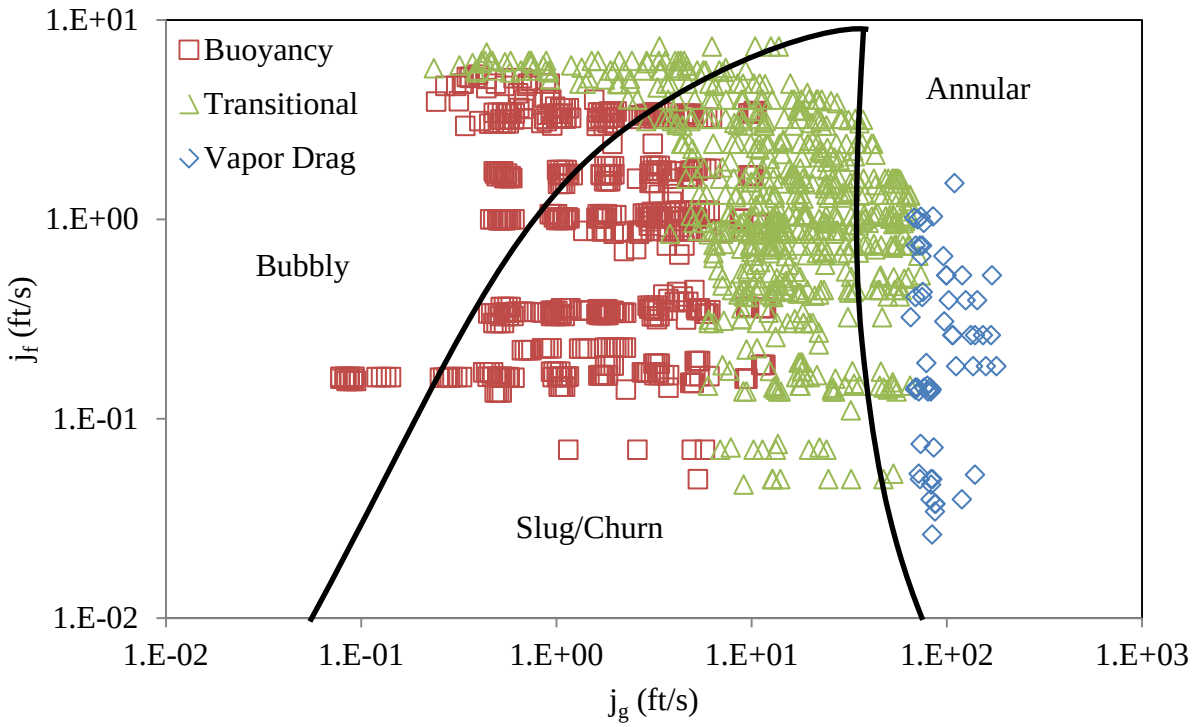

Figure 70: Comparison of the Taitel et al [81] Flow Regime Map to the Mixture Froude Number Correlation Interphase Friction Regime

Figure 71 offers a comparison of the non-dimensionalized interphase friction force to the correlation predicted value for this set of data points. Each data point had the Weber number

correlation and the velocity difference Froude number correlation agreeing that the interphase friction regime was in the buoyancy regime, while the mixture Froude number correlation considered the flow to be in the transitional regime. Also, for each case, the liquid volumetric flux, j_f, was greater than or equal to 3.5 ft/s. The solid line represents data points where the non-dimensionalized interphase friction force is equal to the correlation value, while dashed lines represent ±20% difference. Figure 71 shows that for these particular data points, the mixture Froude number correlation provides a closer approximation to the non-dimensionalized interphase friction force than the other two correlations, as the majority of the data points fall within the ±20% range.

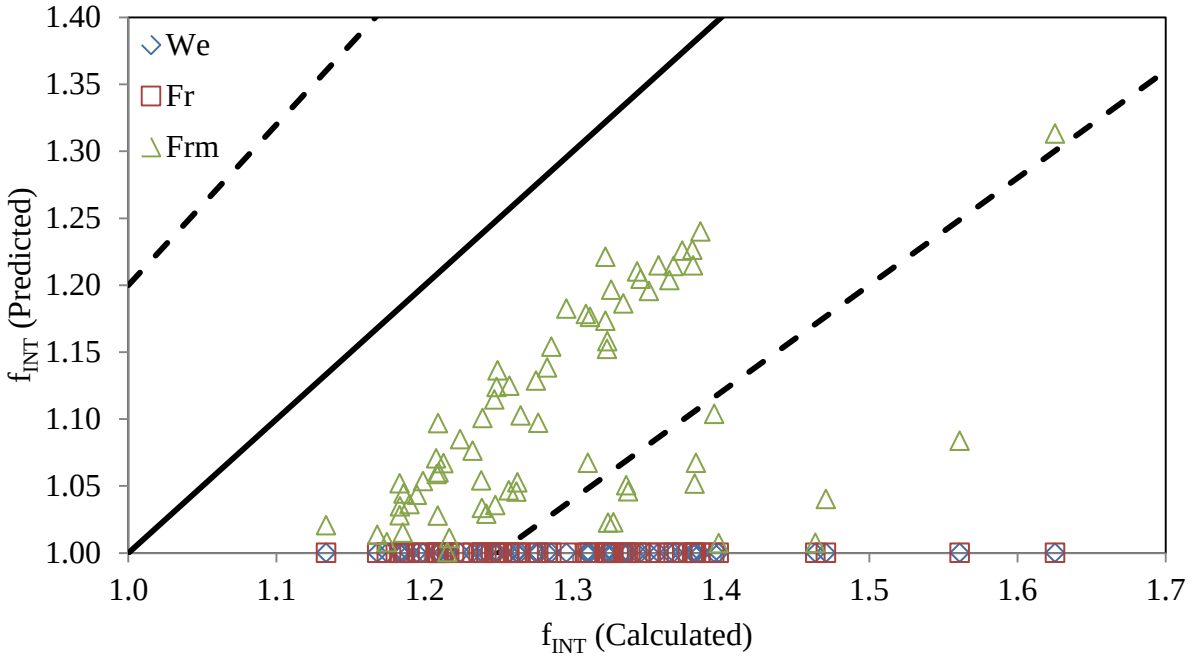

Figure 71: Comparison of Non-Dimensionalized Interphase Friction Force Predictions for Data Points with j_g > 3.5 ft/s

More conclusions may be drawn if the correlations are compared against the flow regime maps with dimensionless properties serving as axes. First, if we consider the flow regime map of Kozloff [51], where the flow regimes are considered a function of the mixture flow regime and flow void fraction. Note that the mixture Froude number used by Kozloff differs slightly from

that used by Griffith and Wallis [33], Oshinowo and Charles [59,60] and for the mixture Froude number correlation.

Figure 72, Figure 73 and Figure 74 show how the Weber number correlation, velocity difference Froude number correlation and mixture Froude number correlation regimes compare to the Kozloff [51] flow regime map. We find that the buoyancy regime in each case appears to stretch across all six of Kosloff's flow regimes, which is surprising given that Kozloff identifies the highest flow regime to be drop flow, where the vapor drag regime would be expected. The transitional flow regime is largely confined to the film emulsion and drop flow regimes for the Weber number correlation, while it expands into the plug flow regimes for the velocity difference flow regime and to the bubbly flow regime for the mixture Froude number correlation. The vapor drag regime to the higher regions of the film emulsion flow regime.

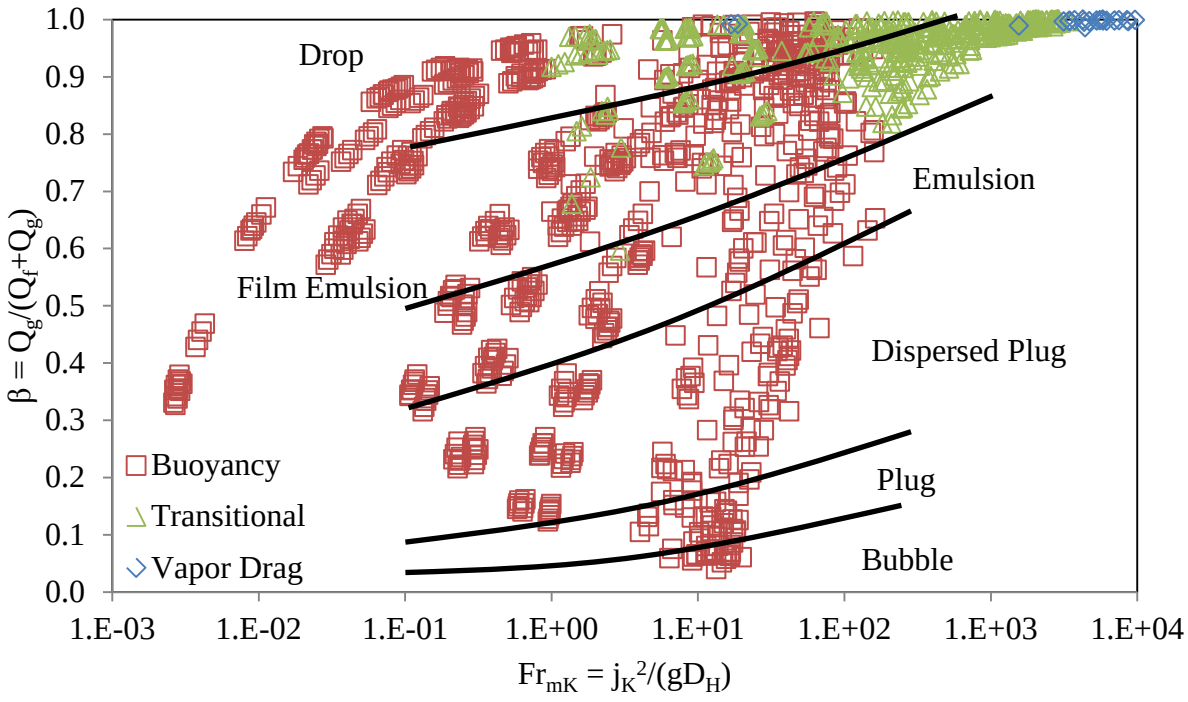

Figure 72: Comparison of the Weber Number Correlation Interphase Friction Regimes to the Kozloff [51] Flow Regime Map

The Kozloff [51] flow regime map was primarily designed for air-water at near atmospheric pressure in a 1 in. diameter pipe. Kozloff assumed that the flow regime map may be useful for pipe diameters up to 4 inches, with modifications, but did not provide any clues as to how the map would need to be modified accordingly. While the map was developed using air-water data, Kozloff intended the flow regime map to be applicable to other scenarios, including in boilers and petroleum wells, thus the comparisons with different liquids and vapors should not be a factor in why the Kozloff flow regime map does not compare favorably to the interphase friction regimes.

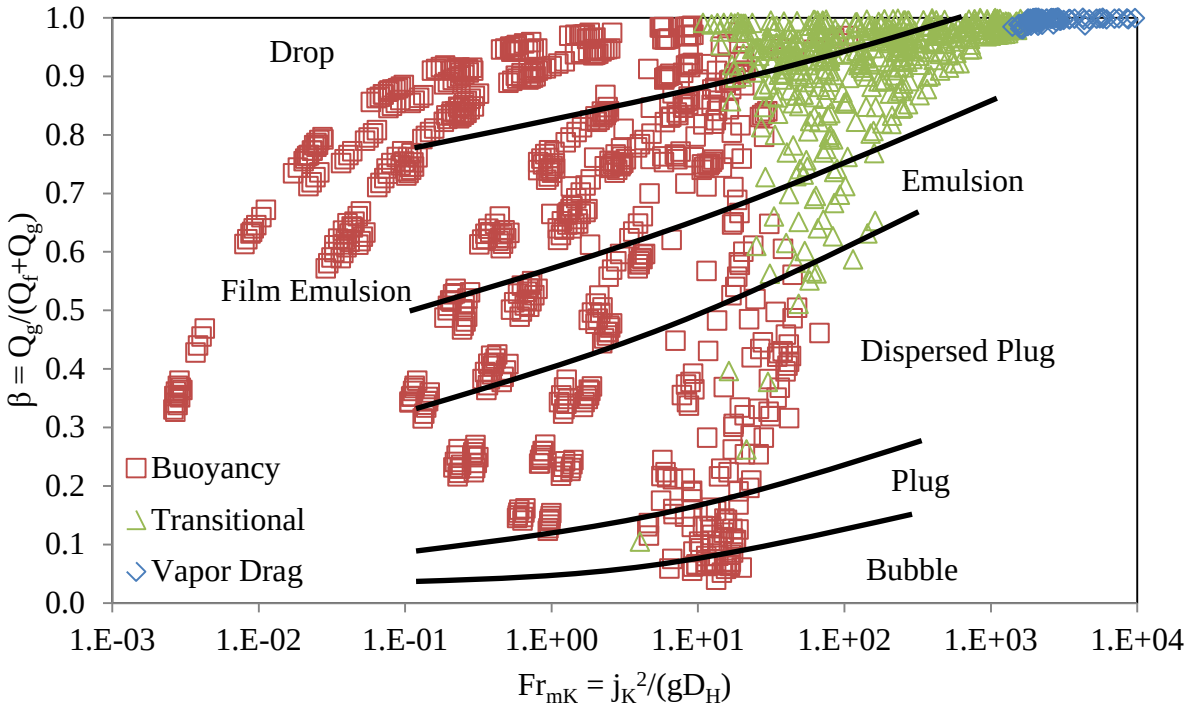

Figure 73: Comparison of the Velocity Difference Froude Number Correlation Interphase Friction Regimes to the Kozloff [51] Flow Regime Map

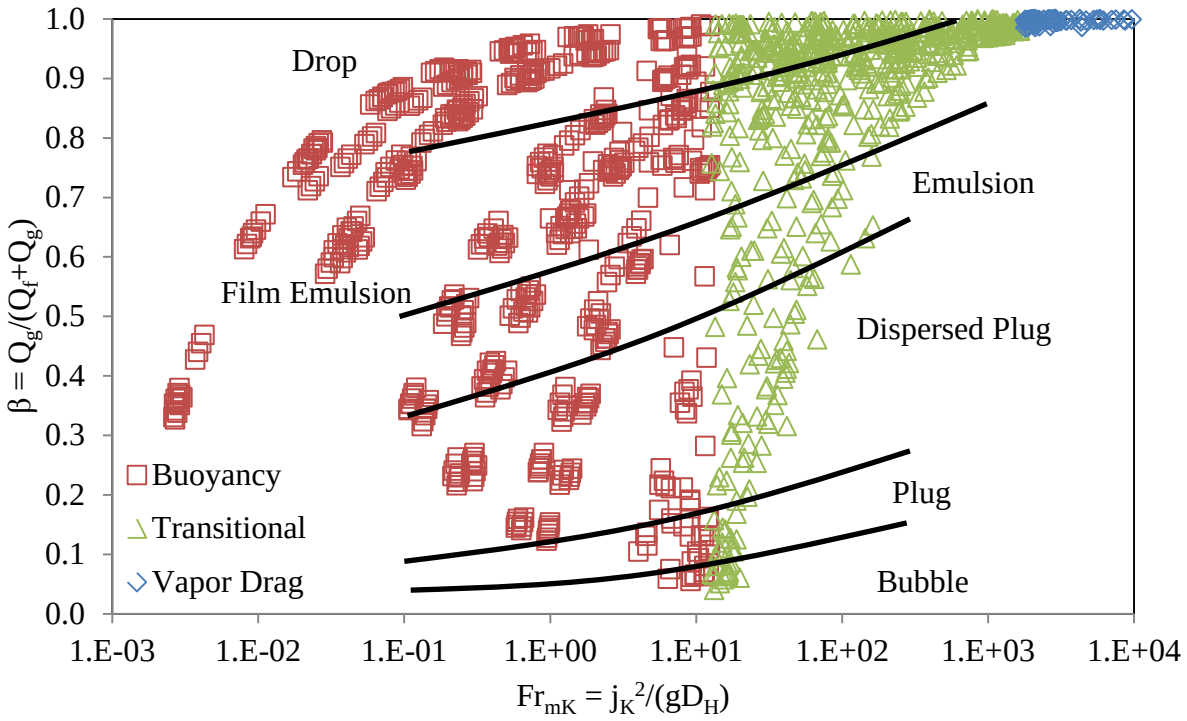

Figure 74: Comparison of the Mixture Froude Number Correlation Interphase Friction Regimes to the Kozloff [51] Flow Regime

The interphase friction regimes are compared to the Griffith and Wallis [33] flow regime map in Figure 75, Figure 76 and Figure 77. In Figure 75, it is shown that the buoyancy regime can be experienced with bubbly, slug and annular flow, while Figure 76 and Figure 77 show that the buoyancy regime is limited to only the bubbly and slug flow regimes. When comparing the velocity difference Froude number correlation regimes to the Griffith and Wallis flow regime map, the boundary between slug and annular flow matches very well with the boundary between the buoyancy and transitional regimes. This would suggest that buoyancy would be dominant for all bubbly and slug flows, while the transition to vapor drag only occurs within the annular flow regime. However, the mixture Froude number correlation suggests that the transition occurs within the slug flow regime. With each correlation, the vapor drag regime is confined to the higher flow void fraction values of the annular flow regime.

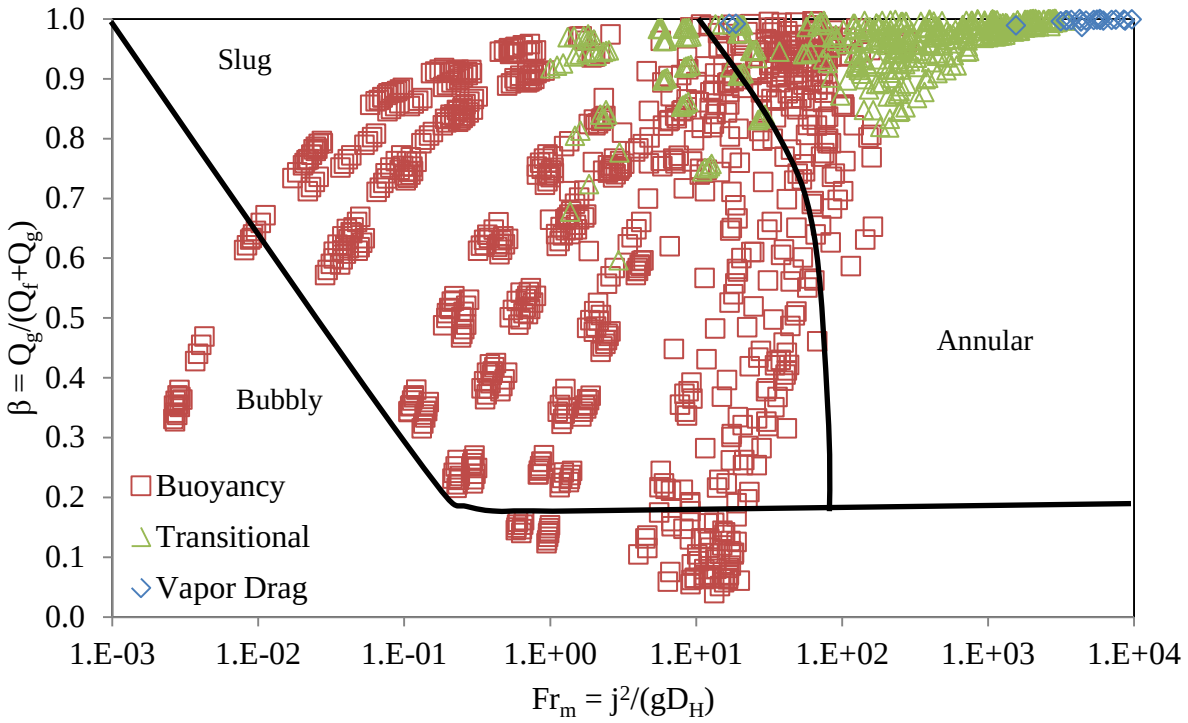

Figure 75: Comparison of the Weber Number Correlation Interphase Friction Regimes to the Griffith and Wallis [33] Flow Regime Map

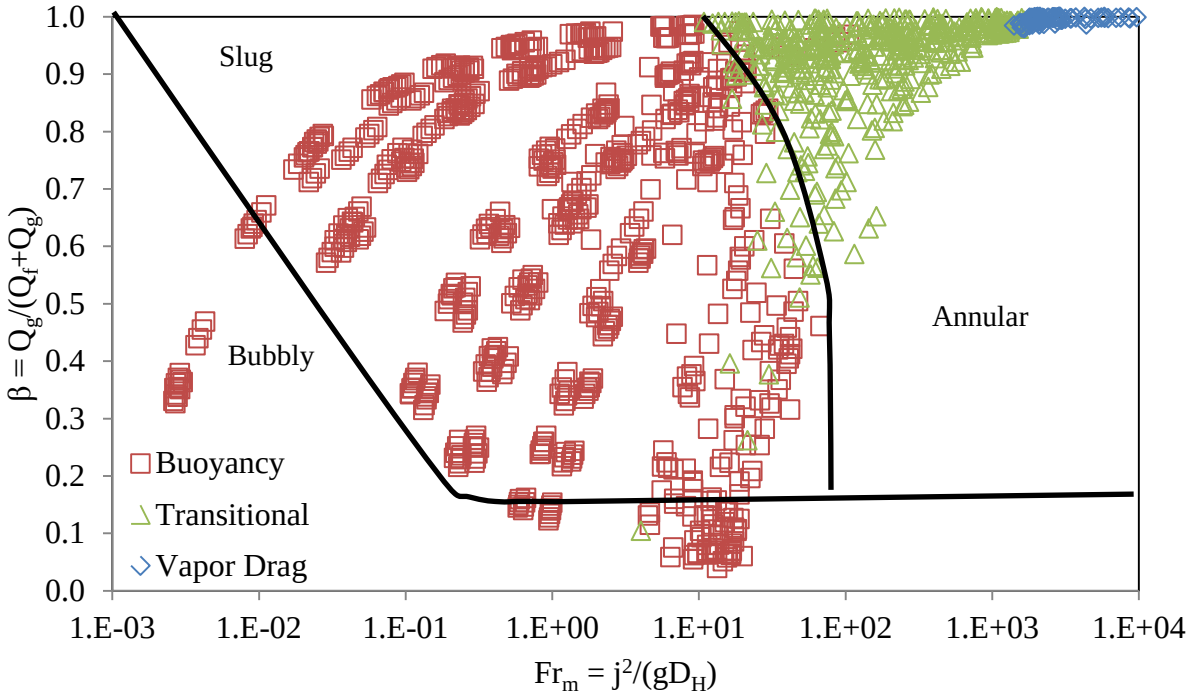

Figure 76: Comparison of the Velocity Difference Froude Number Correlation Interphase Friction Regimes to the Griffith and Wallis [33] Flow Regime Map

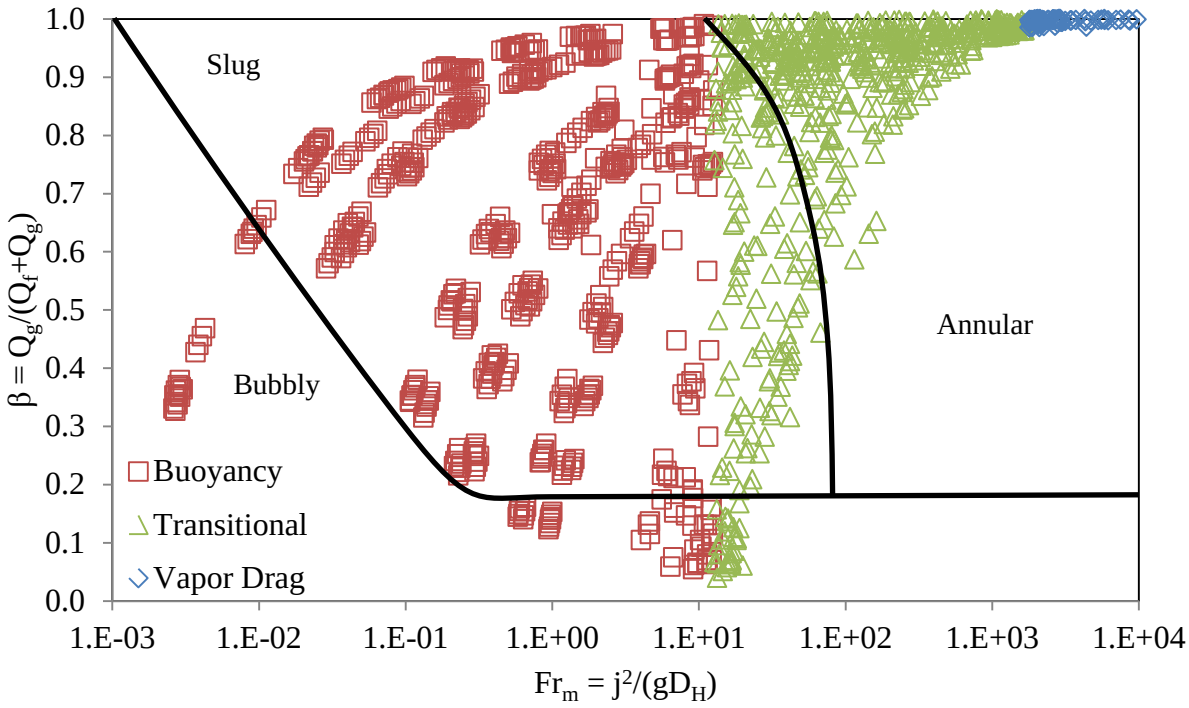

Figure 77: Comparison of the Mixture Froude Number Correlation Interphase Friction Regimes to the Griffith and Wallis [33] Flow Regime Map

Lastly, the interphase friction regimes will be compared to the flow regime map developed by Oshinowo and Charles [59,60], as shown in Figure 78, Figure 79 and Figure 80. In Figure 78, the border between the buoyancy regime and the transitional regime appear to coincide generally with the boundary between frothy slug and froth flow. However, there do appear to be a few transitional data points that fall within the dispersed slug and frothy slug flow regimes. With the exception of two data points in the frothy slug flow regime, the vapor drag regime with the Weber number correlation appears to be largely within the annular flow regime. The velocity difference Froude number correlation shown in Figure 79 shows a very distinct transition from the buoyancy regime to the transitional regime that falls within Oshinowo and Charles' frothy slug regime. Meanwhile, the vapor drag interphase friction regime from the velocity difference Froude number correlation encompasses most of the annular flow data points. The mixture Froude number correlation shown in Figure 80 reveals that the transition from

buoyancy to transitional occurs much closer to the transition from the dispersed slug to frothy slug flow regime, while like the velocity difference Froude number correlation, most of the data points in the annular flow regime are from the vapor drag interphase friction regime.

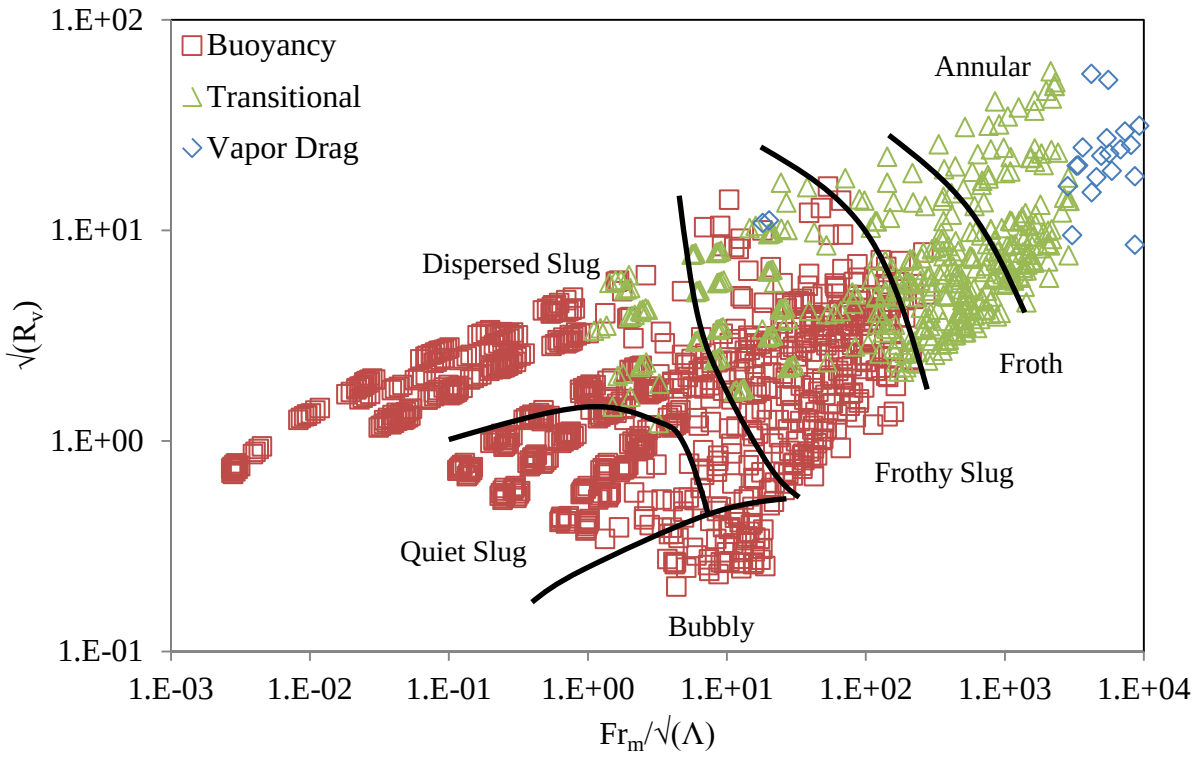

Figure 78: Comparison of the Weber Number Correlation Interphase Friction Regimes to the Oshinowo and Charles [59,60] Flow Regime Map

In general, it can be concluded that from comparing the interphase friction regimes to the various flow regime maps is that for bubbly and slug flow, it appears that the interphase friction is purely based on the buoyancy of the vapor bubbles within the liquid. However, there appears to be a point within the slug flow regime where the interphase friction becomes a function of the velocity difference itself, and appears to occur when the volumetric flux of the vapor phase exceeds a certain threshold. Perhaps this is where the transition from slug flow to the less stable churn-turbulent flow occurs. This transitional region appears to hold true into the annular flow regime, but within the annular flow regime, the interphase friction regime changes to the vapor

drag region, with the interphase friction increasing at an increased rate with respect to increasing vapor flow. This indicates that when there is annular flow, but the vapor volumetric flux is below a certain threshold, the interphase friction may behave more similarly to churn-turbulent flow, even though the Taitel et al [81] map did not indicate that was the case. Kozloff [51] described this flow pattern as film emulsion flow, meanwhile the vapor drag regime sounds more consistent with what Kozloff described as drop flow, even though as shown in Figure 72, Figure 73 and Figure 74, the Kozloff flow regime map does not appear to reflect this observation.

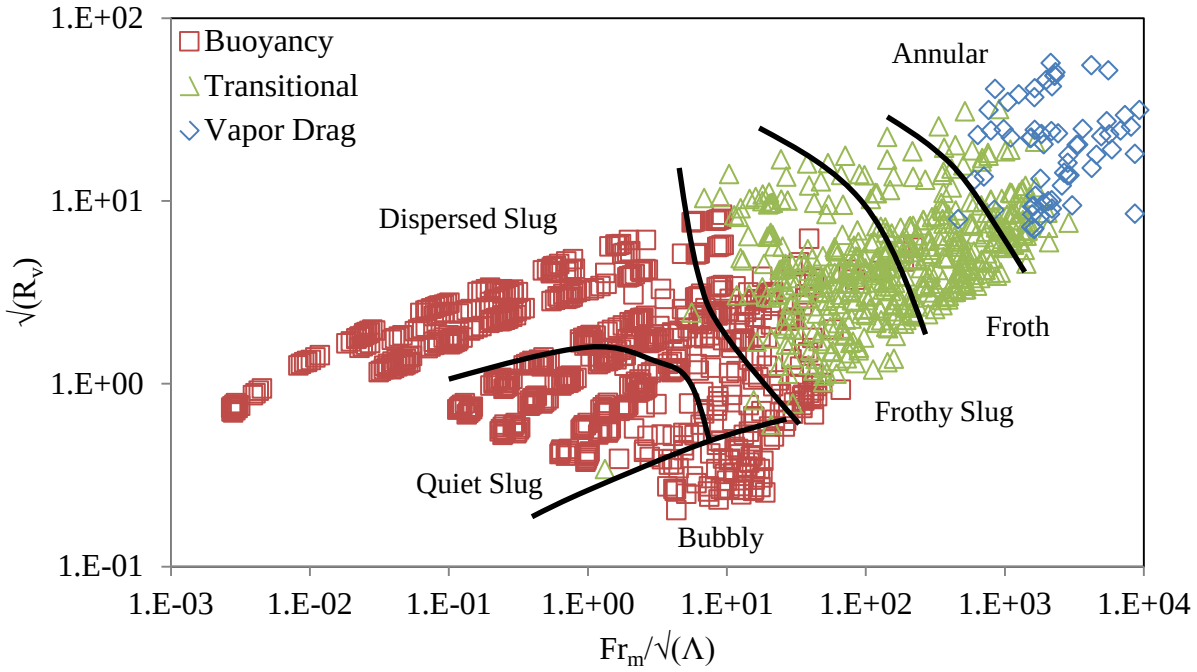

Figure 79: Comparison of the Velocity Difference Froude Number Correlation Regimes to the Oshinowo and Charles [59,60] Flow Regime Map

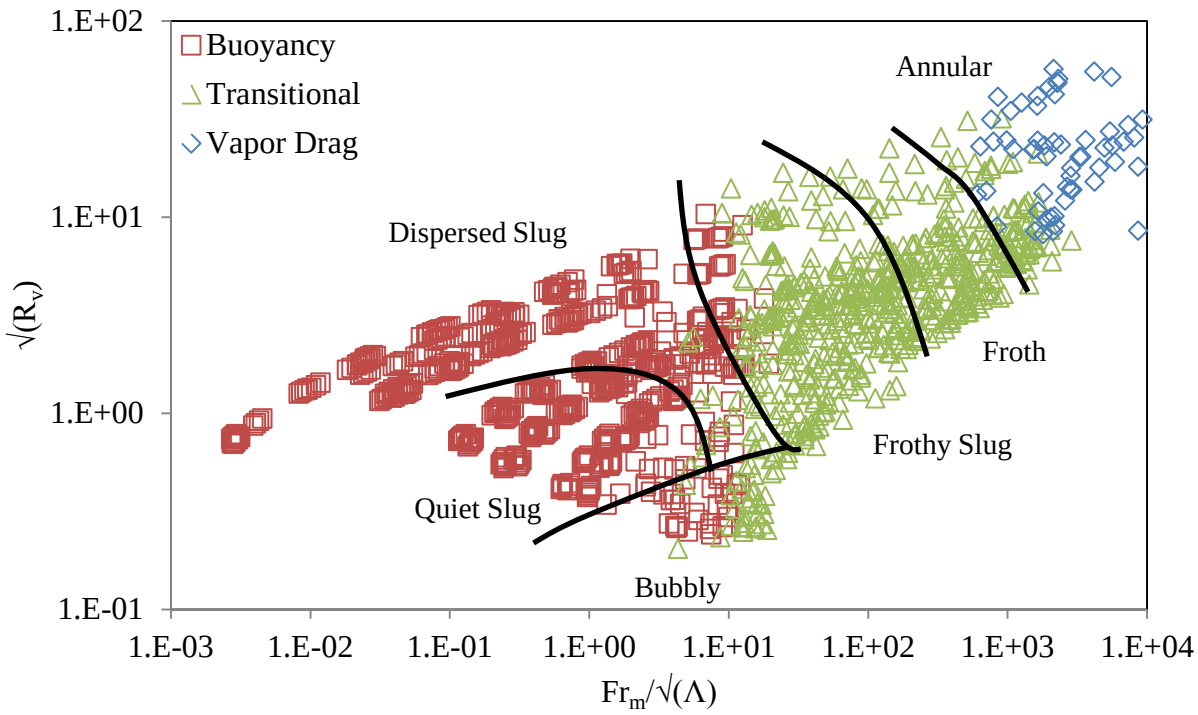

Figure 80: Comparison of the Mixture Froude Number Correlation Interphase Friction Regimes to the Oshinowo and Charles [59,60] Flow Regime Map

4.1.4: Concluding Remarks of Correlation Development

After reviewing all of the data and comparisons, the mixture Froude number correlation provides the most accurate prediction of the non-dimensionalized interphase friction. However, all three correlations will be tested in RELAP5/MOD3.3 [40,69] to determine how well each correlation performs.

One disappointment regarding the correlations is that for the buoyancy regime of data points, where the dimensionless interphase friction, f_{int} = 1, there is no discernible relationship between the velocity difference and the interphase friction force. Since no such relationship can be determined through this analysis, when the correlations are implemented into RELAP5/MOD3.3 [40], the interphase friction factor calculation will remain unchanged in RELAP5/MOD3.3 when the data suggests that the buoyancy regime is present.

In comparing the correlations to the flow regime maps of Taitel et al [81], Kozloff [51], Griffith and Wallis [33] and Oshinowo [59,60], it appears that the correlation would be most applicable to annular flow, and may also be applicable to slug flow. For the sake of simplicity, this dissertation will only explore the effect of the correlation on annular flow, as the flow regime maps indicate that for some slug flow data points, the correlations may not be applicable at all. Even though this study will focus on annular flow data points, the correlation needs to be substituted into the interphase friction subroutines bubdrag and slugdrag, in the even that RELAP5/MOD3.3 [40] were to change the flow regime to bubbly or slug flow within the test section.

The interphase friction factor, *fint*, using the correlations in the RELAP5/MOD3.3 [40] subroutines bubdrag and slugdrag is calculated as:

$$fint = \begin{cases} RELAP\ Calculation\ for\ We\ \leq 10{,}290 \\ \dfrac{0.0357\alpha(1-\alpha)(\rho_f-\rho_g)gWe^{0.361}}{(v_g-j)^2}\ for\ 10{,}290 < We < 408{,}000 \\ \dfrac{(1.358\times10^{-10})\alpha(1-\alpha)(\rho_f-\rho_g)gWe^{1.861}}{(v_g-j)^2}\ for\ We\ \geq 408{,}000 \end{cases} \quad (290)$$

$$fint = \begin{cases} RELAP\ Calculation\ for\ Fr\ \leq 17.71 \\ \dfrac{0.596\alpha(1-\alpha)(\rho_f-\rho_g)gFr^{0.1799}}{(v_g-j)^2}\ for\ 17.71 < Fr < 1749 \\ \dfrac{(3.70\times10^{-5})\alpha(1-\alpha)(\rho_f-\rho_g)gFr^{1.477}}{(v_g-j)^2}\ for\ Fr\ \geq 1749 \end{cases} \quad (291)$$

$$fint = \begin{cases} RELAP\ Calculation\ for\ Fr_m\ \leq 12.73 \\ \dfrac{0.660\alpha(1-\alpha)(\rho_f-\rho_g)gFr_m{}^{0.1631}}{(v_g-j)^2}\ for\ 12.73 < Fr_m < 1719 \\ \dfrac{(3.70\times10^{-5})\alpha(1-\alpha)(\rho_f-\rho_g)gFr_m{}^{1.477}}{(v_g-j)^2}\ for\ Fr_m\ \geq 1719 \end{cases} \quad (292)$$

For the RELAP5/MOD3.3 [40] subroutine amistdrag, the interphase friction factor is calculated as:

$$fint = \begin{cases} RELAP\ Calculation\ for\ We\ \leq 10{,}290 \\ \dfrac{0.0357\alpha(1-\alpha)(\rho_f-\rho_g)gWe^{0.361}}{(v_g-v_f)^2}\ for\ 10{,}290 < We < 408{,}000 \\ \dfrac{(1.358\times10^{-10})\alpha(1-\alpha)(\rho_f-\rho_g)gWe^{1.861}}{(v_g-v_f)^2}\ for\ We\ \geq 408{,}000 \end{cases} \quad (293)$$

$$fint = \begin{cases} RELAP\ Calculation\ for\ Fr\ \leq 17.71 \\ \dfrac{0.596\alpha(1-\alpha)(\rho_f-\rho_g)gFr^{0.1799}}{(v_g-v_f)^2}\ for\ 17.71 < Fr < 1749 \\ \dfrac{(3.70\times10^{-5})\alpha(1-\alpha)(\rho_f-\rho_g)gFr^{1.477}}{(v_g-v_f)^2}\ for\ Fr\ \geq 1749 \end{cases} \quad (294)$$

$$fint = \begin{cases} RELAP\ Calculation\ for\ Fr_m\ \leq 12.73 \\ \dfrac{0.660\alpha(1-\alpha)(\rho_f-\rho_g)gFr_m{}^{0.1631}}{(v_g-v_f)^2}\ for\ 12.73 < Fr_m < 1719 \\ \dfrac{(3.70\times10^{-5})\alpha(1-\alpha)(\rho_f-\rho_g)gFr_m{}^{1.477}}{(v_g-v_f)^2}\ for\ Fr_m\ \geq 1719 \end{cases} \quad (295)$$

4.2: Comparisons to Nuclear Thermal Hydraulic Code Models

Now, we will begin comparing the derived interphase friction correlation to those that are published in the manuals of RELAP5/MOD2 [66], RELAP5/MOD3.3 [69], RELAP5-3D [67] and TRACE [83]. The utmost care has been taken to try to replicate the results as close as

possible to those that are published in the manuals of the respective nuclear thermal hydraulic codes, with the formulae being followed as closely as possible to those that were published in their respective manuals, and provided in Section 2.3.

4.2.1: Comparisons to RELAP5/MOD2

The interphase friction force for each data point has been calculated using both the mixture Froude number correlation and the RELAP5/MOD2 [66] interphase friction force equations that are described in Section 2.3.1.3. In Figure 81, the predicted interphase friction force using both the RELAP5/MOD2 equations and the mixture Froude number correlation are shown, and plotted against the interphase friction force that was calculated from the force balance in Equation 259. A solid black line has been added to show where the predicted interphase friction force would equal the force balance interphase friction. For 38 cases in the annular flow regime, the RELAP5/MOD2 equations were unable to calculate the interphase friction because RELAP5/MOD2 calculated the film void fraction, α_{ff}, in Equation 115 was greater than 1. The manual does not offer any indication as to how RELAP5/MOD2 would approach such a situation, and so those points have been neglected. Nonetheless, Figure 81 shows that the RELAP5/MOD2 equations significantly overpredict the interphase friction in the majority of cases.

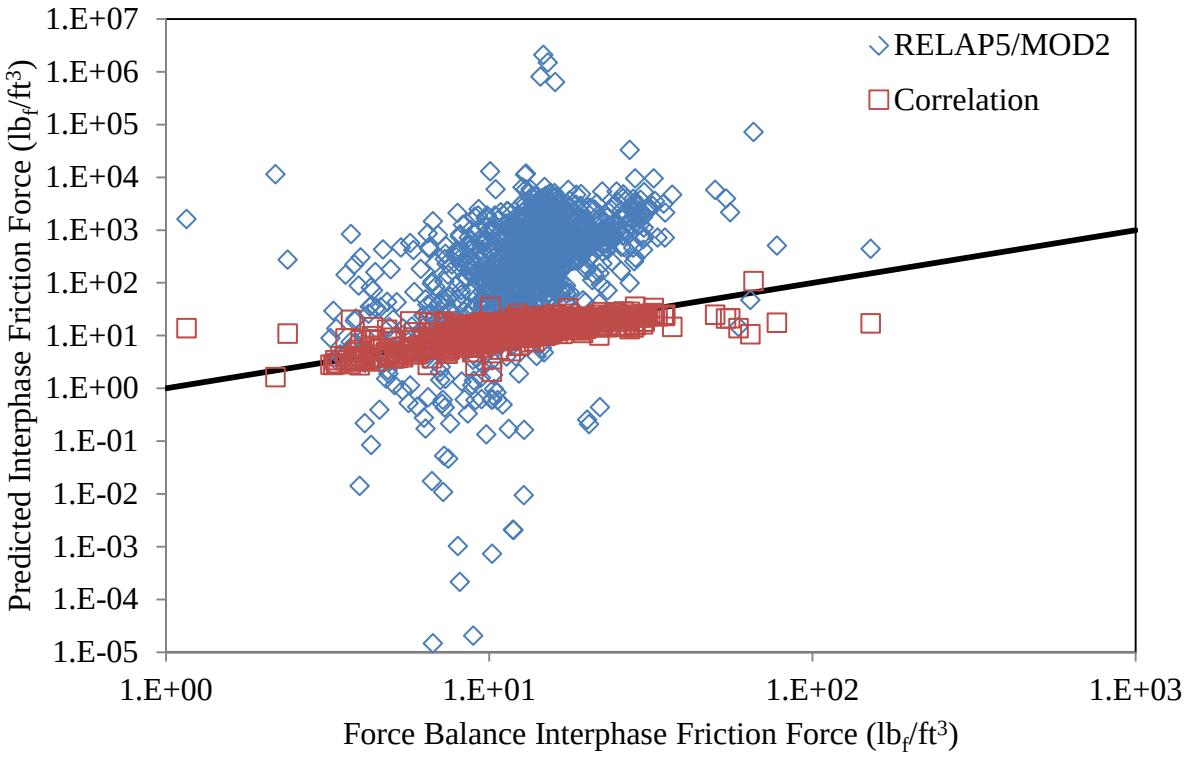

Figure 81: Comparison of the RELAP5/MOD2 [66] Predicted Interphase Friction Force to the Mixture Froude Number Correlation

Figure 83 shows how the mixture Froude number correlation interphase friction prediction compares to that by RELAP5/MOD2 [66] for data points where RELAP5/MOD2 identifies the flow regime as bubbly flow. This accounts for 105 of the 1262 data points. The mixture Froude number correlation appears to be a very close approximation to the force balance values for bubbly flow, while RELAP5/MOD2 seems to have a very inconsistent pattern of errantly predicting the interphase friction force.

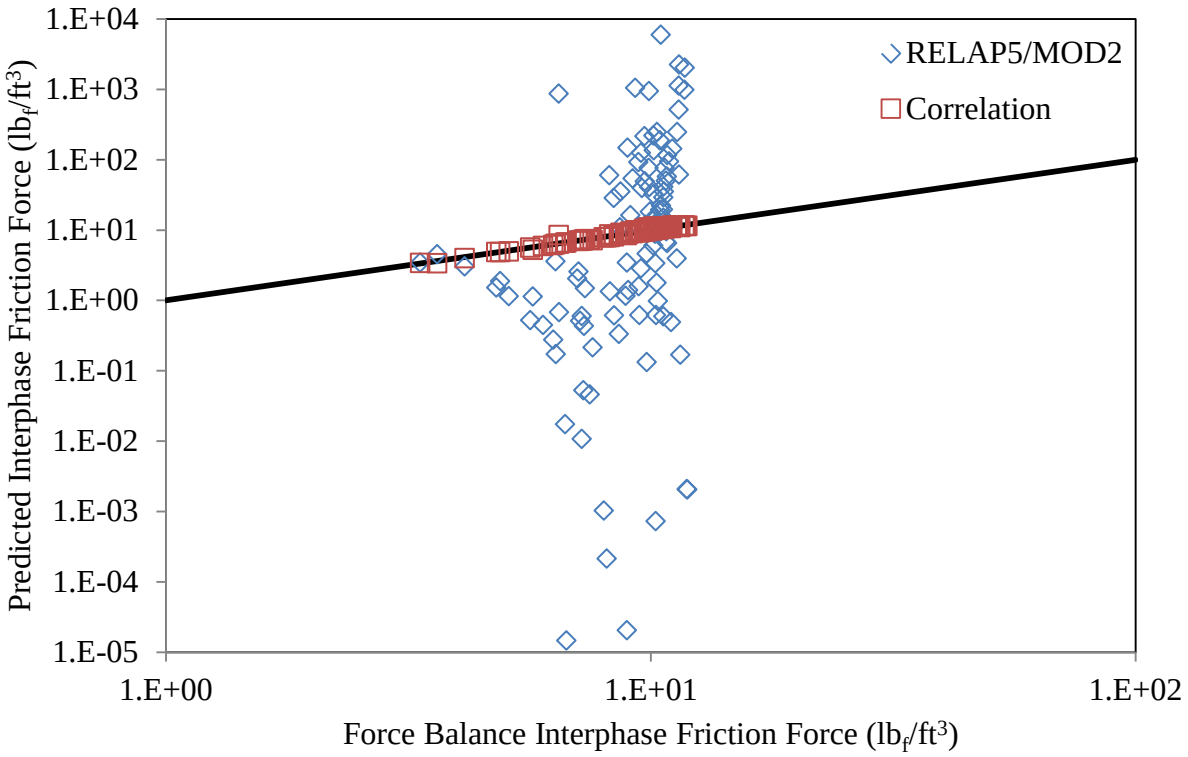

Figure 82: Comparison of the RELAP5/MOD2 [66] Interphase Friction Calculation to the Mixture Froude Number Correlation for RELAP5/MOD2 Bubbly Flow

The interphase friction force predictions for 851 data points that RELAP5/MOD2 [66] identifies as slug flow is compared in Figure 84. While the RELAP5/MOD2 prediction errs significantly from the force balance value, it appears that for most cases, RELAP5/MOD2 overpredicts the interphase friction force by several orders of magnitude.

Figure 85 shows the data points which RELAP5/MOD2 [66] identifies as annular flow. There are 306 data points shown representing the interphase friction force predicted using the mixture Froude number correlation, but only 265 data points shown using the RELAP5/MOD2 equations. Along with the 38 data points for which the RELAP5/MOD2 equations could not predict the interphase friction, there are three data points for which the equations produced an interphase friction force less than 0 lb_f/ft^3. For the data points shown, RELAP5/MOD2 shows a

bias to overpredict the interphase friction force by several orders of magnitude over the force balance value.

Table 9 shows how the RELAP5/MOD2 [66] equations for predicting interphase friction force compare against the mixture Froude number correlation, from a more quantitative perspective. It shows that for both the overall case, as well as for the cases of each individual flow regime, the mixture Froude number correlation is a significant improvement over the RELAP5/MOD2 interphase friction force equations. Note that for the annular flow case, the RELAP5/MOD2 averages and errors are for the 268 data points for which results could be retrieved (including the three data points that RELAP5/MOD2 predicts have negative interphase friction), while the mixture Froude number averages and errors are taken over all 306 data points.

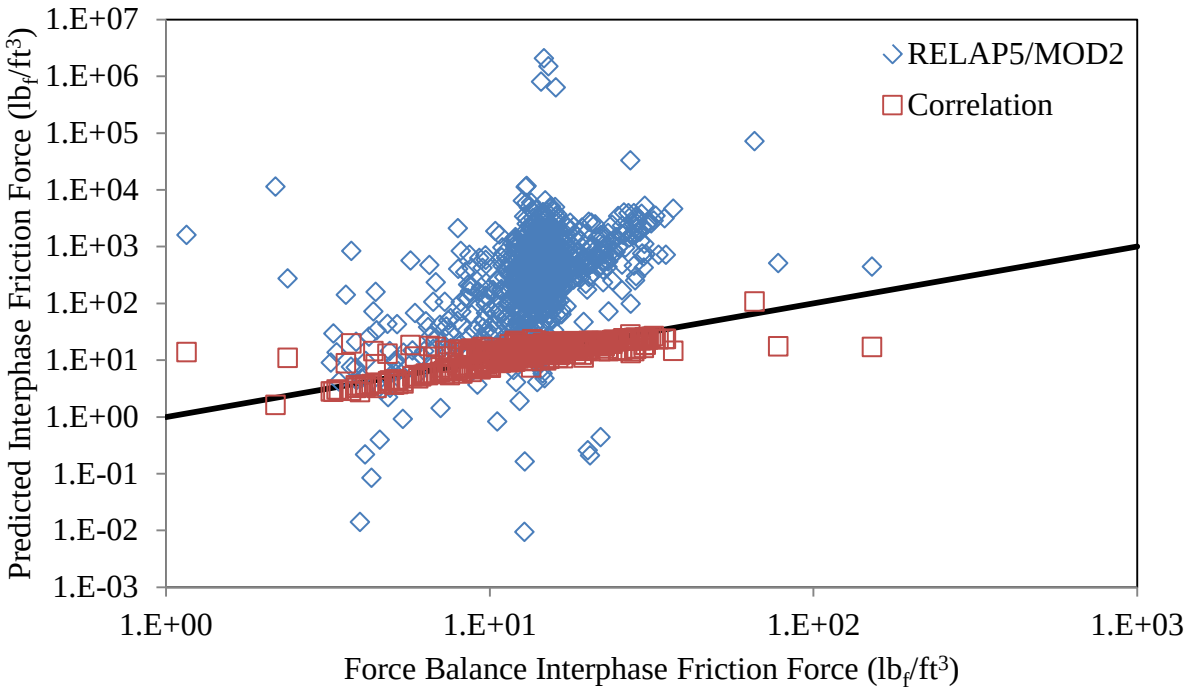

Figure 83: Comparison of the RELAP5/MOD2 [66] Interphase Friction Calculation to the Mixture Froude Number Correlation for RELAP5/MOD2 Slug Flow

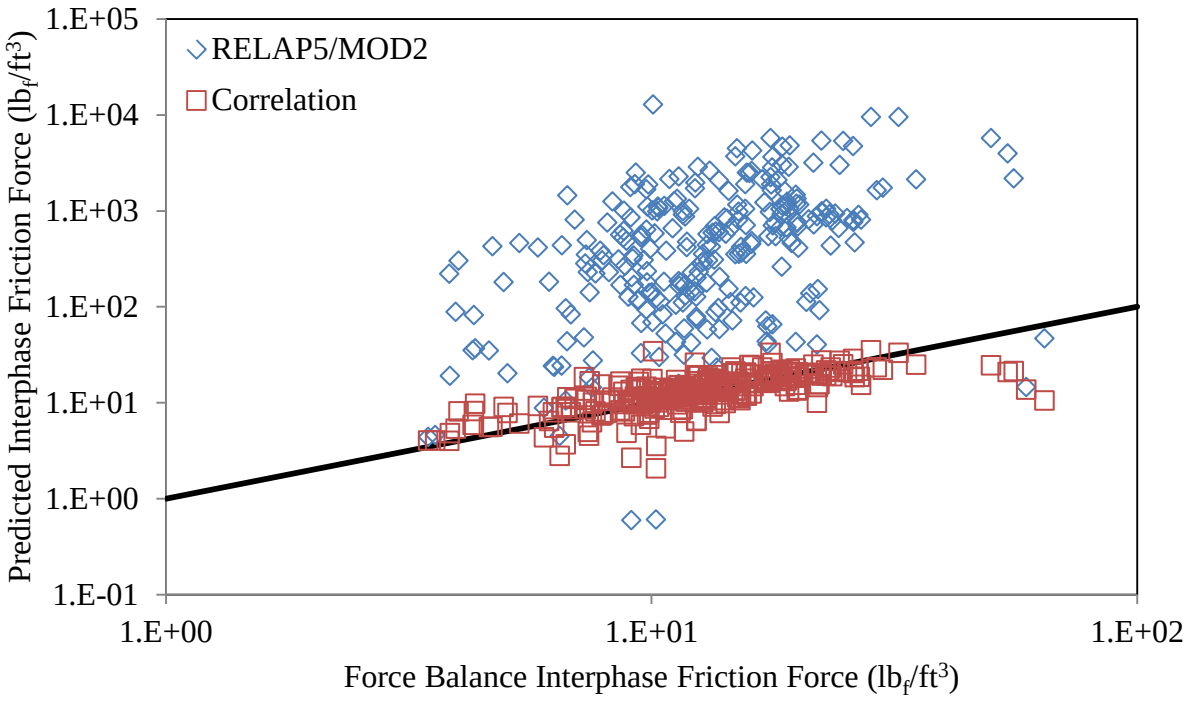

Figure 84: Comparison of the RELAP5/MOD2 [66] Interphase Friction to the Mixture Froude Number Correlation Interphase Friction for RELAP5/MOD2 Annular Flow

Table 9: Statistical Comparison of the Mixture Froude Number Correlation Interphase Friction Force Prediction to the RELAP5/MOD2 [66] Interphase Friction Prediction

	Overall		Bubbly		Slug		Annular	
	$f(Fr_m)$	RELAP5/ MOD2	$f(Fr_m)$	RELAP5/ MOD2	$f(Fr_m)$	RELAP5/ MOD2	$f(Fr_m)$	RELAP5/ MOD2
RMS Error (lb_f/ft^3)	5.93	$7.86x10^4$	0.350	687	6.09	94300	6.47	1773
Mean Average Error (%)	16.87	$3.25x10^4$	2.51	1701	15.75	44600	24.9	6140
Median Average Error (%)	8.67	21.2	1.475	97.2	8.02	2170	17.01	3420
±20% Error	955	21	104	5	683	15	168	1
- (Percentage)	75.7	1.7	99.0	0.0	80.3	1.76	54.9	0.33
±50% Error	1186	53	105	16	815	30	266	7
- (Percentage)	94.0	4.2	100.0	15.24	95.8	3.525	86.9	2.29
Maximum Error (%)	1088	$1.410x10^7$	30.8	56400	1088	$1.410x10^7$	241	127500

4.2.2: Comparisons to RELAP5/MOD3.3

Next, the interphase friction force prediction from the RELAP5/MOD3.3 manual [69] is compared to the prediction from the mixture Froude number correlation. Figure 86 shows how the two methods compare for all 1262 data points. In general, we find that the RELAP5/MOD3.3 correlations vary greatly in predicting the interphase friction force, with values ranging over by nine orders of magnitude for data points that the force balance suggests should be much closer in value. Not shown in Figure 86 are the 241 data points for which the RELAP5/MOD3.3 correlations produce an interphase friction force value less than 0. In each of these cases the relative velocity, v_R, was determined to be less than 0, which results in the interphase friction force being calculated as less than 0.

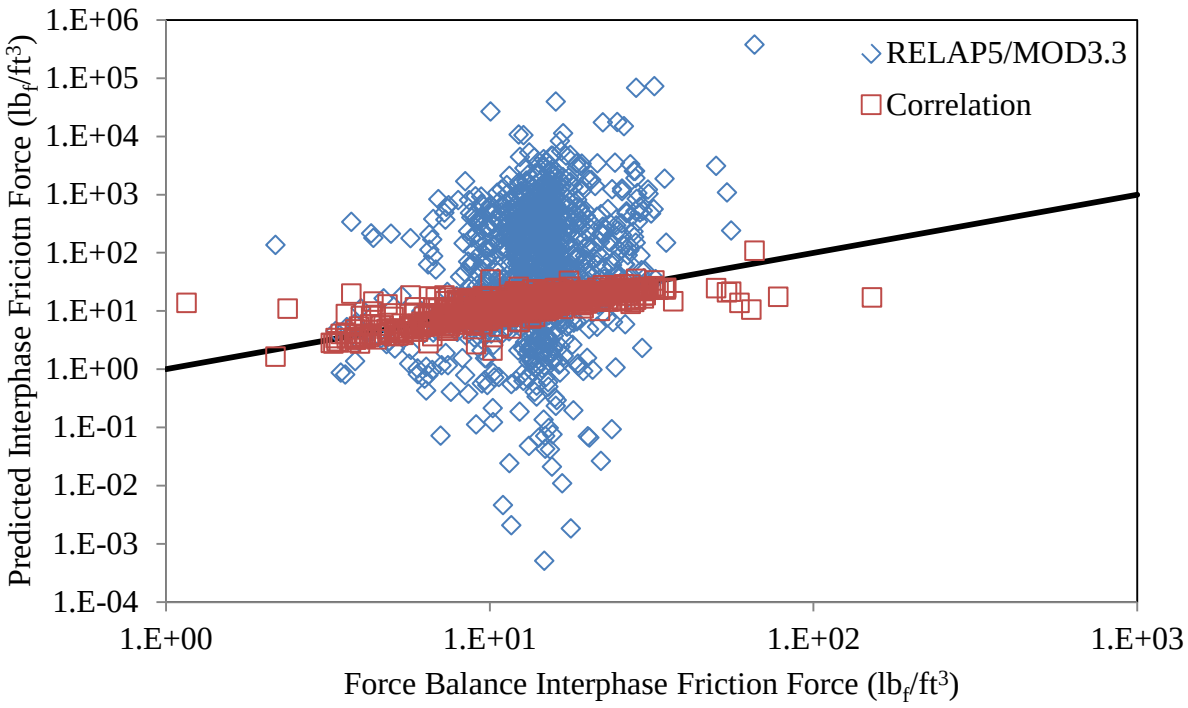

Figure 85: Comparison of the RELAP5/MOD3.3 [69] Interphase Friction to the Mixture Froude Number Correlation

For the 106 data points that RELAP5/MOD3.3 [40,69] identifies as bubbly flow, it appears that while there is very good agreement between the mixture Froude number correlation

and the force balance calculation, the RELAP5/MOD3.3 prediction varies over six orders of magnitude as shown in Figure 87. It appears that the likely cause for the large range in values for the interphase friction force can be attributed to the relative velocity calculation given in Equation 141. When the relative velocity is calculated as in Equation 142, the interphase friction force is much closer to that of the force balance value, as shown in Figure 88. The end result is that the interphase friction force is calculated using Equation 75, and is equivalent to the mixture Froude correlation for $Fr_m \leq 12.73$.

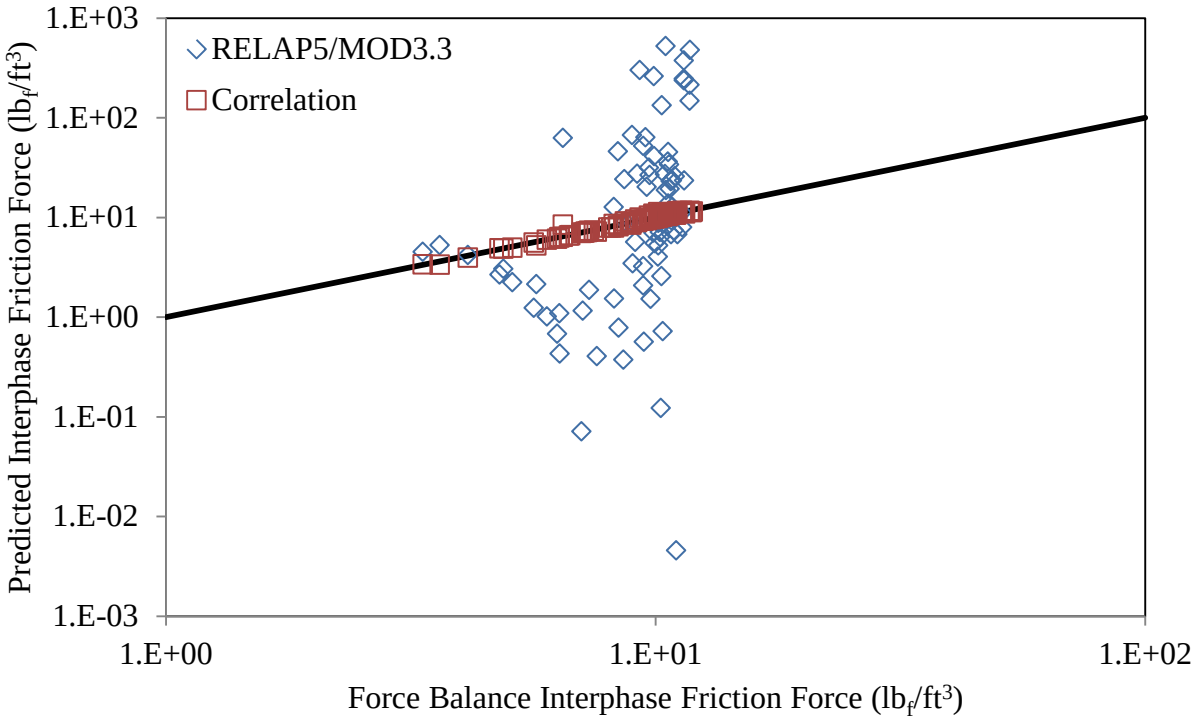

Figure 86: Comparison of the RELAP5/MOD3.3 [69] Interphase Friction to the Mixture Froude Number Correlation for RELAP5/MOD3.3 Bubbly Flow

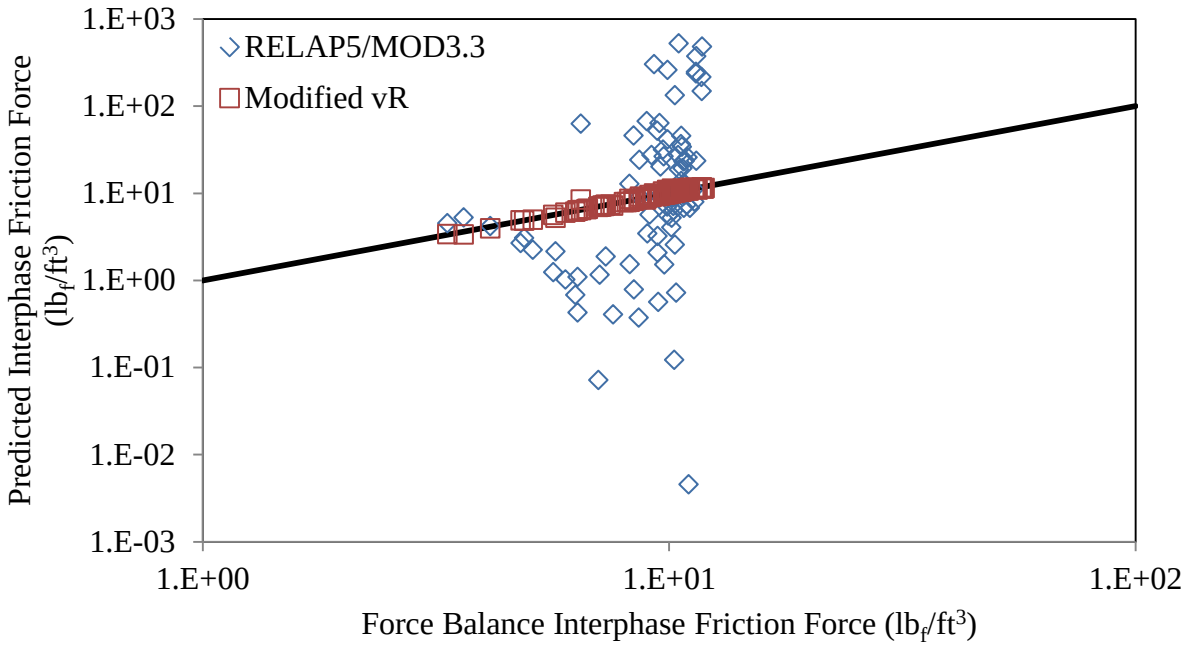

Figure 87: Comparison of the RELAP5/MOD3.3 [69] Interphase Friction for Bubbly Flow with the Original Relative Velocity Calculation to the Modified Relative Velocity Calculation

For the 946 data points that RELAP5/MOD3.3 [69] identifies as slug flow, the interphase friction force predictions using the drift flux correlations in the RELAP5/MOD3.3 source code are compared to the mixture Froude number correlation in Figure 88. Similar to the case with bubbly flow, we find that interphase friction force prediction of RELAP5/MOD3.3 varies over nine orders of magnitude when the force balance interphase friction force suggests that values should be within one order of magnitude.

In Figure 89, the interphase friction force is calculated using the two different relative velocity formulations given in Equations 141 and 142. The formulation that uses the distribution parameters, which is used in the RELAP5/MOD3.3 code [40] (Equation 141) produces an interphase friction force calculation that ranges over nine orders of magnitude. Meanwhile, the formulation in Equation 142, which is supposed to be the equivalent of the distribution parameter correlation, produces a result much closer to the force balance interphase friction force value.

The relative velocity that is calculated using the distribution parameters in Equation 141 is supposed to be the same as that calculated using Equation 142. However, the results shown in Figure 88 and Figure 90 show that is not the case. The interphase friction force should closely match the force balance value, but when using the distribution parameters to calculate the relative velocity that does not appear to be the case. It would appear that a more consistent approach for calculating the relative velocity, that better matches the relative velocity given in Equation 142, is necessary in order to improve the interphase friction calculation in RELAP5/MOD3.3 [40,69]. In Table 10, the accuracy of each method for predicting the interphase friction is compared, showing that a method that more closely approximates the vapor drift velocity would provide a more accurate interphase friction force prediction.

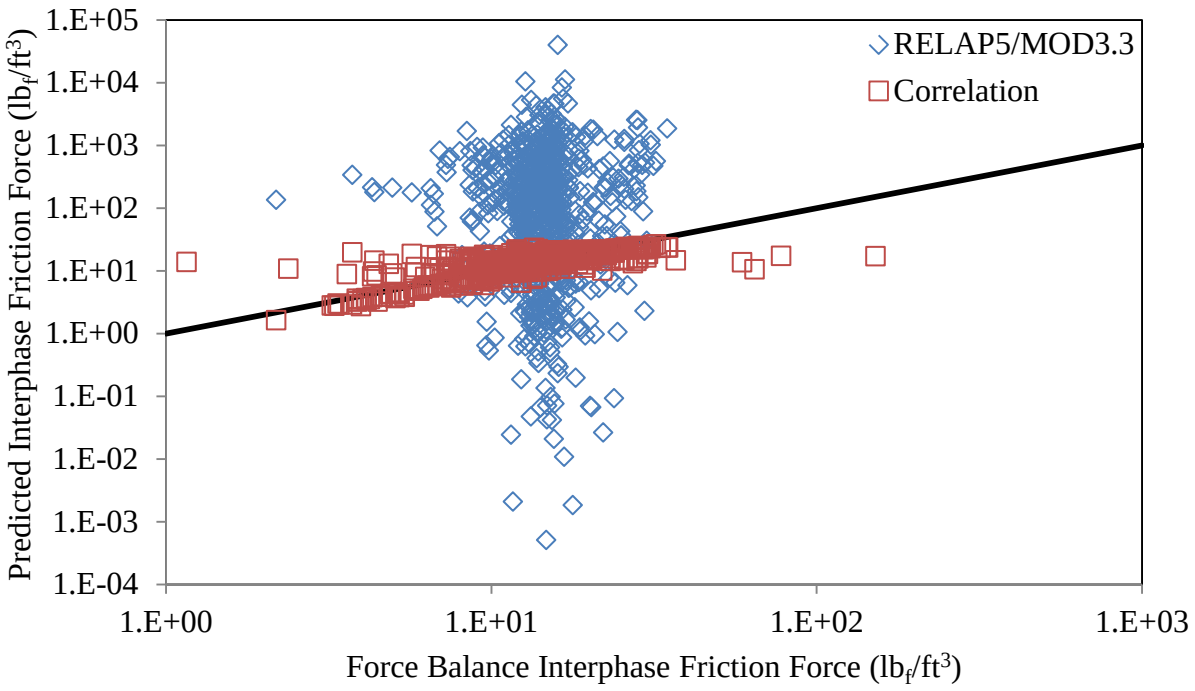

Figure 88: Comparison of the RELAP5/MOD3.3 [69] Interphase Friction to the Mixture Froude Number Correlation for RELAP5/MOD3.3 Slug Flow

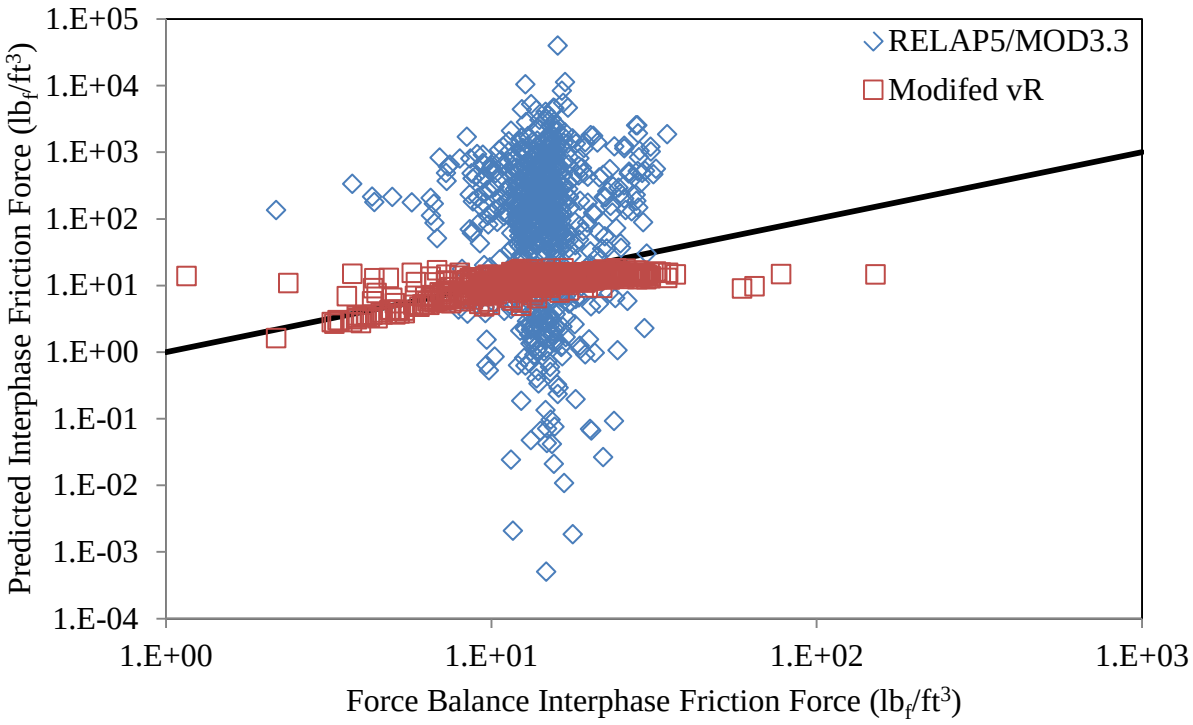

Figure 89: Comparison of the RELAP5/MOD3.3 [69] Interphase Friction for Slug Flow with the Original Relative Velocity Calculation to the Modified Relative Velocity Calculation

Table 10: Comparison of Interphase Friction Force Accuracy Using Distribution Parameters Versus Vapor Drift Velocity for Relative Velocity [69]

	Bubbly		Slug	
	C_1v_g-C_0v_f	$v_{gj}/(1-\alpha)$	C_1v_g-C_0v_f	$v_{gj}/(1-\alpha)$
RMS Error (lb_f/ft^3)	96.8	0.349	2840	6.94
Mean Average Error (%)	385	2.49	4340	18.13
Median Average Error (%)	98.9	1.457	637	10.93
±20% Error	13	105	13	626
- (Percentage)	12.26	99.1	1.374	66.2
±50% Error	28	106	46	868
- (Percentage)	26.4	100.0	4.86	91.8
Maximum Error (%)	4900	30.8	24700	1088

Figure 91 shows the comparison of the interphase friction force predictions between the RELAP5/MOD3.3 [69] equations and the mixture Froude number against the force balance calculated interphase friction force, for the 210 data points that RELAP5/MOD3.3 identifies as annular flow. The RELAP5/MOD3.3 equations appear to follow a spectrum of both overpredicting and underpredicting the interphase friction by several orders of magnitude, while the mixture Froude number remains much closer to the force balance calculated interphase friction.

Table 11 provides a quantifiable description of how the RELAP5/MOD3.3 [69] equations predict the interphase friction, in comparison to the mixture Froude number correlation. The correlation is superior to the RELAP5/MOD3.3 predicted interphase friction force, and when broken down by flow regime, it appears that it most significantly improves the interphase friction force prediction for the annular flow regime. While the correlation stands to also improve upon the drift flux correlations used by RELAP5/MOD3.3 for bubbly and slug flow, it appears that the error with those calculations lie with the distribution parameters, and their application in modeling the interphase friction force.

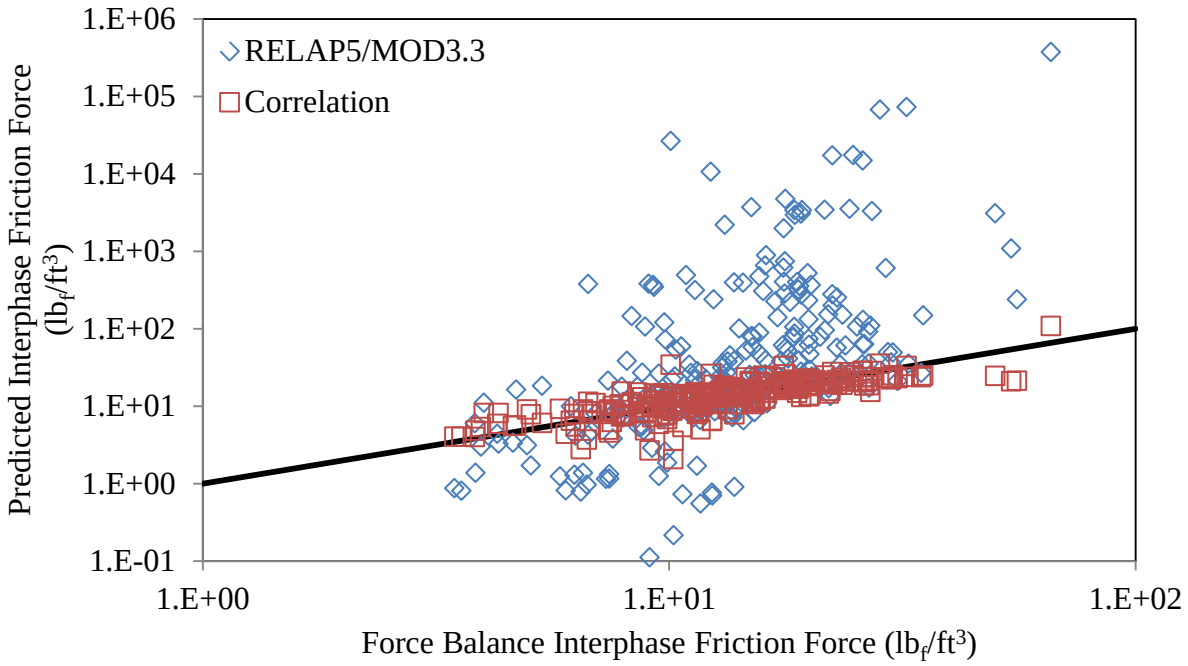

Figure 90: Comparison of the RELAP5/MOD3.3 [69] Interphase Friction to the Mixture Froude Number Correlation for RELAP5/MOD3.3 Annular Flow

Table 11: Statistical Comparison of the RELAP5/MOD3.3 [69] Interphase Friction Prediction to the Mixture Froude Number Correlation

	Overall		Bubbly		Slug		Annular	
	$f(Fr_m)$	RELAP5/ MOD3.3	$f(Fr_m)$	RELAP5/ MOD3.3	$f(Fr_m)$	RELAP5/ MOD3.3	$f(Fr_m)$	RELAP5/ MOD3.3
RMS Error (lb_f/ft^3)	5.93	11250	0.349	96.8	6.17	2840	6.30	25000
Mean Average Error (%)	16.87	4780	2.49	385	17.22	4340	22.5	8960
Median Average Error (%)	8.67	398	1.457	98.9	8.71	637	15.72	136.8
±20% Error	955	58	105	13	727	13	123	32
- (Percentage)	75.7	4.6	99.1	12.26	76.8	1.374	58.6	15.24
±50% Error	1186	145	106	28	892	46	188	71
- (Percentage)	94.0	11.5	100.0	26.42	94.3	4.86	89.5	33.8
Maximum Error (%)	1088	$5.69x10^5$	30.8	4900	1088	24700	241	$5.69x10^5$

4.2.3: Comparisons to RELAP5-3D

The equations used to predict the interphase friction force in RELAP5-3D [67] are subtly different than those used in RELAP5/MOD3.3 [69], and consequentially, there are some subtle differences in the results. However, the general trends remain true that the interphase friction force for bubbly and slug flow is not predicted well, largely because the distribution parameters do not produce a consistent solution for the relative velocity. Thus, it is not surprising that Figure 91, which compares the interphase friction force prediction of RELAP5-3D to that of the mixture Froude number correlation, bears a strong resemblance to Figure 85, with interphase friction force calculations of RELAP5-3D ranging over eleven orders of magnitude while the force balance interphase friction force only varies over a range of 2.5 orders of magnitude.

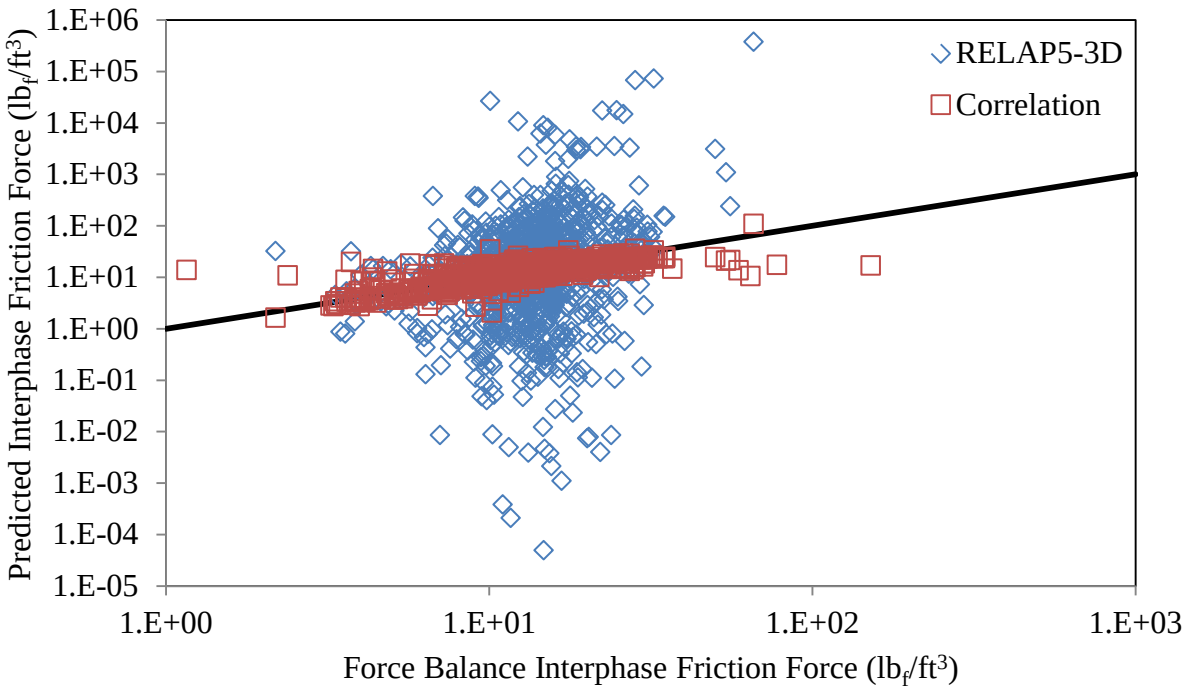

Figure 91: Comparison of the RELAP5-3D [67] Interphase Friction to the Mixture Froude Number Correlation

Similar to the case with RELAP5/MOD3.3 [69] in Figure 86 and Figure 88, we find that the interphase friction force prediction for RELAP5-3D [67] for bubbly and slug flow to be

spread over a range of several orders of magnitude greater than the force balance interphase friction force would indicate in Figure 92 and Figure 94. Similar to the case with RELAP5/MOD3.3, this appears to be largely the result of the distribution parameters being used to calculate the relative velocity; with different results than the vapor drift velocity would indicate. For the annular flow, the interphase friction force that is predicted by RELAP-3D in Figure 94 yields very similar results to that for RELAP5/MOD3.3 in Figure 91. Overall, the RELAP5-3D interphase friction force equations are less accurate than those in RELAP5/MOD3.3 as can be seen in Table 12.

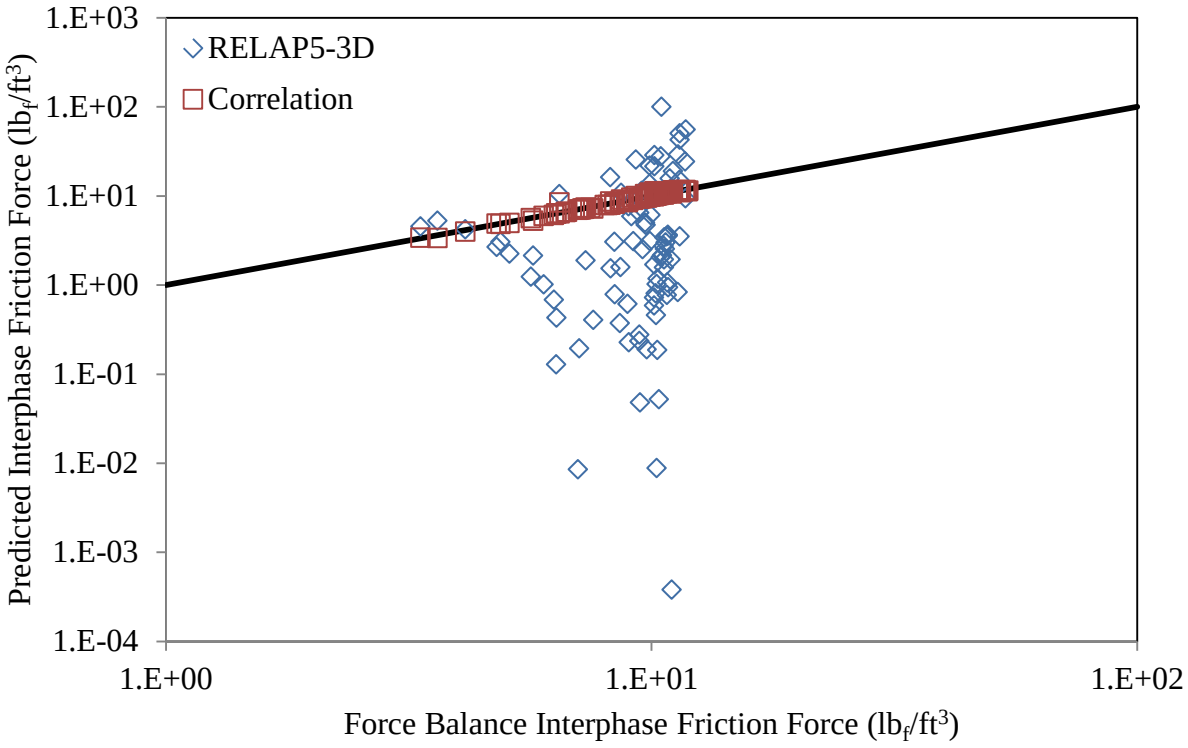

Figure 92: Comparison of the RELAP5-3D [67] Interphase Friction to the Mixture Froude Number Correlation for RELAP5-3D Bubbly Flow

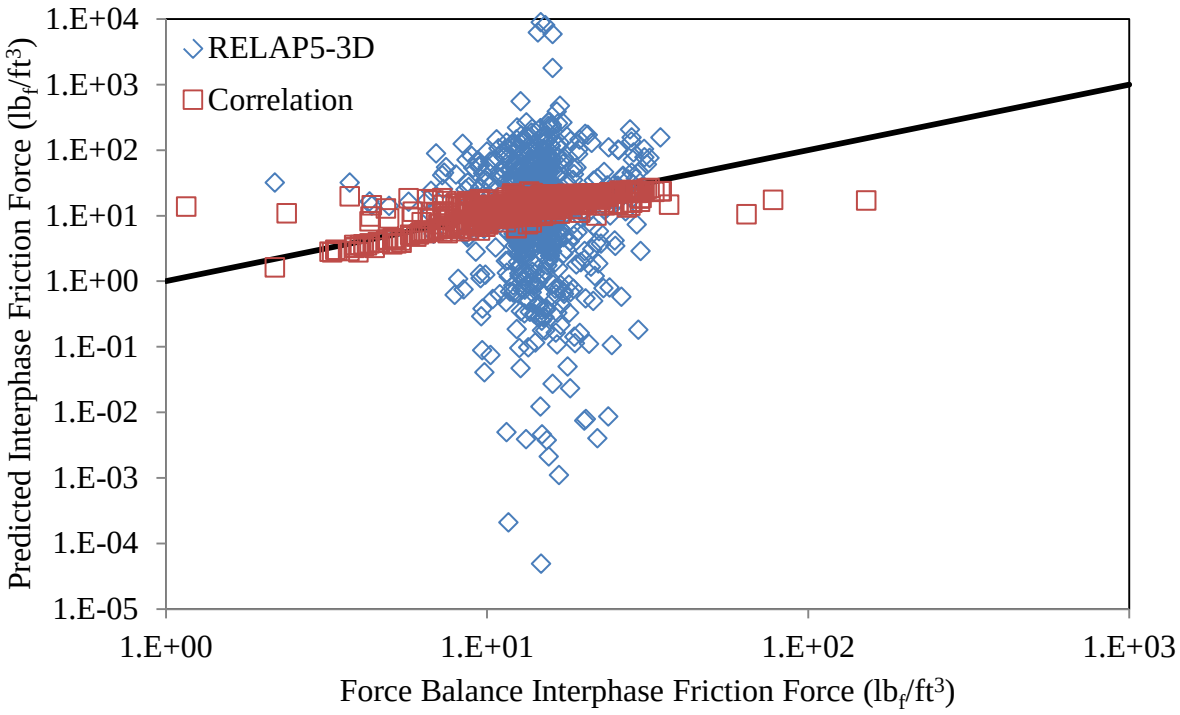

Figure 93: Comparison of the RELAP5-3D [67] Interphase Friction to the Mixture Froude Number Correlation for RELAP5-3D Slug Flow

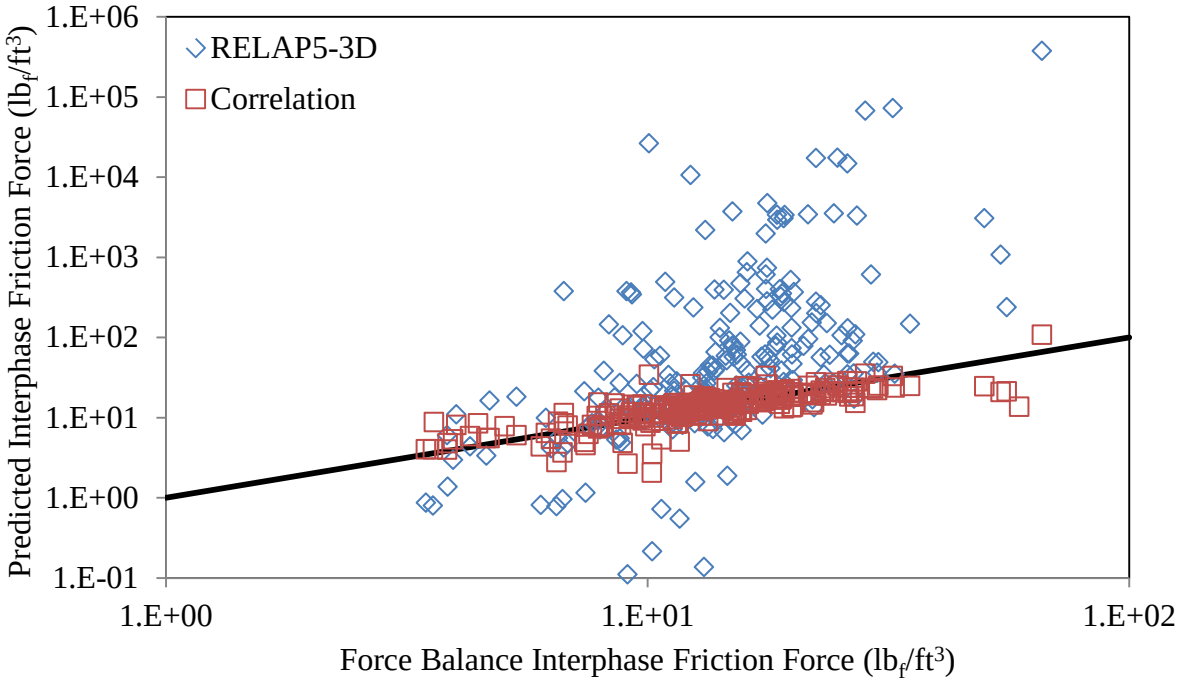

Figure 94: Comparison of the RELAP5-3D [67] Interphase friction to the Mixture Froude Number Correlation for RELAP5-3D Annular Flow

Table 12: Statistical Comparison of the RELAP5-3D [67] Interphase Friction Prediction and the Mixture Froude Number Correlation

	Overall		Bubbly		Slug		Annular	
	$f(Fr_m)$	RELAP5-3D	$f(Fr_m)$	RELAP5-3D	$f(Fr_m)$	RELAP5-3D	$f(Fr_m)$	RELAP5-3D
RMS Error (lb_f/ft^3)	5.93	$3.55x10^5$	0.349	14.19	6.17	$4.10x10^5$	6.30	26900
Mean Error (%)	16.87	$1.81x10^5$	2.49	103.4	17.22	$2.39x10^5$	22.5	8960
Median Error (%)	8.67	99.4	1.457	92.8	8.71	99.7	15.72	136.8
±20% Error	955	115	105	4	727	79	123	32
- (Percentage)	75.7	9.11	99.1	3.8	76.85	8.35	58.6	15.24
±50% Error	1186	282	106	17	892	194	188	71
- (Percentage)	94.0	22.3	100.00	16.04	94.3	20.5	89.5	33.81
Maximum Error (%)	1088	$4.90x10^7$	30.8	855	1088	$4.90x10^7$	241	$5.69x10^5$

4.2.4: Comparisons to TRACE

Lastly, the interphase friction force prediction of TRACE [83] is compared against the mixture Froude number correlation. Since TRACE does not base its interphase friction calculation on a flow regime map, the comparison will not be broken down by regimes. Instead, only the TRACE correlation as a whole will be studied, as shown in Figure 95. As can be seen, TRACE appears to generally overpredict the interphase friction force for all data points, although there are a few for which TRACE also underpredicts.

Statistically, TRACE [83] and RELAP5/MOD3.3 [69] appear to be overall more accurate than RELAP5/MOD2 [65] and RELAP5-3D [67], as shown in Table 13. While TRACE has a lower RMS error for predicting the interphase friction force, RELAP5/MOD3.3 has lower mean and median average percentage errors.

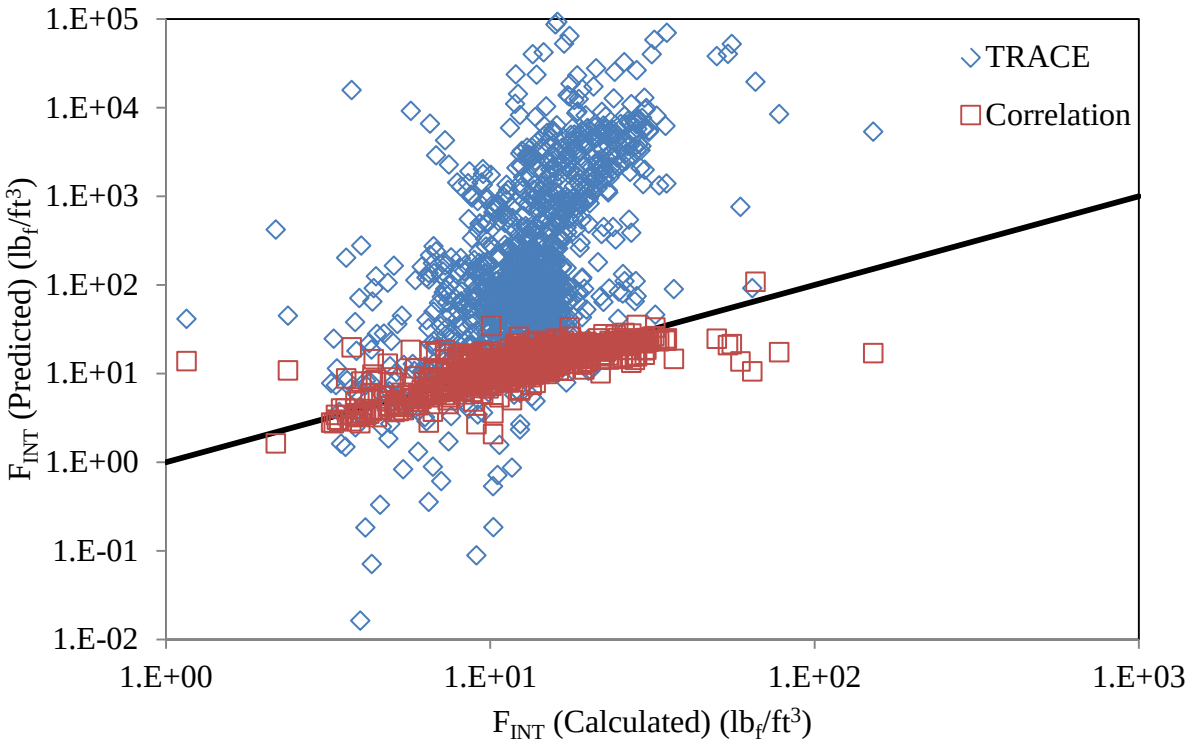

Figure 95: Comparison of the TRACE [83] Interphase Friction to the Mixture Froude Number Correlation

Table 13: Statistical Comparison of the Mixture Froude Number to the Nuclear Thermal Hydraulic Codes Interphase Friction Force Predictions

	$f(Fr_m)$	RELAP5/ MOD2	RELAP5/ MOD3.3	RELAP5 -3D	TRACE
RMS Error (lb_f/ft^3)	5.93	$7.86x10^4$	11250	3.55x105	6490
Mean Average Error (%)	16.87	$3.25x10^4$	4780	1.81x105	8530
Median Average Error (%)	8.67	21.2	398	99.4	666
±20% Error	955	21	58	115	35
- (Percentage)	75.7	1.7	4.6	9.11	2.8
±50% Error	1186	53	145	282	79
- (Percentage)	94.0	4.2	11.5	22.3	6.3
Maximum Error (%)	1088	$1.410x10^7$	5.69x105	4.90x107	573000

4.3: Comparisons of the Correlations to the RELAP5/MOD3.3 Source Code and Executable

For the remainder of this dissertation, analysis of nuclear thermal hydraulic codes will focus solely on RELAP5/MOD3.3 [40], and when RELAP is mentioned, it only refers to RELAP5/MOD3.3, unless otherwise specified. First, the interphase friction calculation from the manual will be compared against the source code, which was found to differ when the source code was studied. Then the calculations from the source code will be compared results obtained from running the executable version of RELAP.

4.3.1: Comparisons of Data to the RELAP5/MOD3.3 Source Code

As had been noted in Section 2.3.2.3, there were several differences noticed in the interphase friction force equations between the RELAP manual [69] and source code [40]. While many of these differences appear to be subtle, the different interpretations that results from reading the manual alone, versus examining the manual with the source code can result in very different calculations of the interphase friction force. Thus, it is important to examine the differences between these two different sets of equations.

Beginning with the bubbly flow data points, we find in Figure 96, the source code generally provides a slightly lower prediction of the interphase friction force when the force balance value is greater than 6.4, and a slightly higher prediction of the interphase friction force when the force balance value is less than 6.4. In general, the manual calculations reveal that the data points where the source code is producing a slightly smaller interphase friction force coincides with the data points where the Chexal-Lellouche [12] drift flux correlation is used for the vapor drift velocity and the distribution parameter, while the data points where the source code is producing a slightly higher interphase friction use the Kataoka-Ishii [48] and Churn-

Turbulent drift flux correlations. The most significant difference between the source code and the manual regarding the Chexal-Lellouche drift flux correlation involves the likely typographical error in the manual where the constant C_9 is multiplied by the variable B_1 rather than raised to the power of B_1, as is done in the source code, and likely is the cause for some difference in those calculations. Meanwhile, the different formulae for calculating C_∞ in the manual and in the source code is the most likely reason why there is a difference between in the interphase friction force calculations that use the Kataoka-Ishii and Churn-Turbulent drift flux correlations. [40]

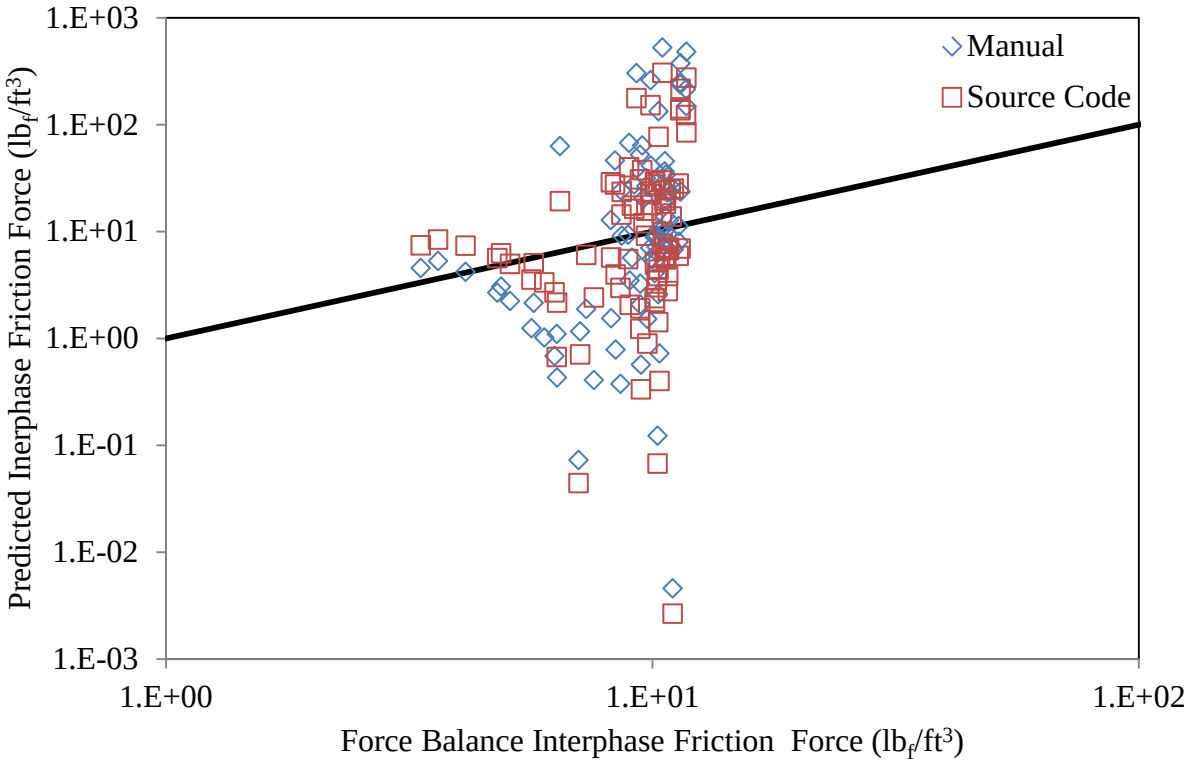

Figure 96: Comparison of the RELAP5/MOD3.3 Manual [69] Interphase Friction Force Equations to the Source Code [40] Equations for Bubbly Flow

In Figure 97, the interphase friction force values that are achieved using both the manual equations and the source code equations is shown, plotted against the force balance interphase friction force values. With 946 data points, it is very difficult to distinguish those data points for

which the different drift flux correlations are being used, although it can be presumed that the same differences in interphase friction force prediction that are noticed with bubbly flow can be presumed with slug flow. Additionally, there will be differences to be considered with the additional terms *fslug* and *fanm*, which are used as exponential terms that are applied to the interphase friction factor in the slug and annular flow regimes within the code [40], and would be expected to decrease the interphase friction force in magnitude.

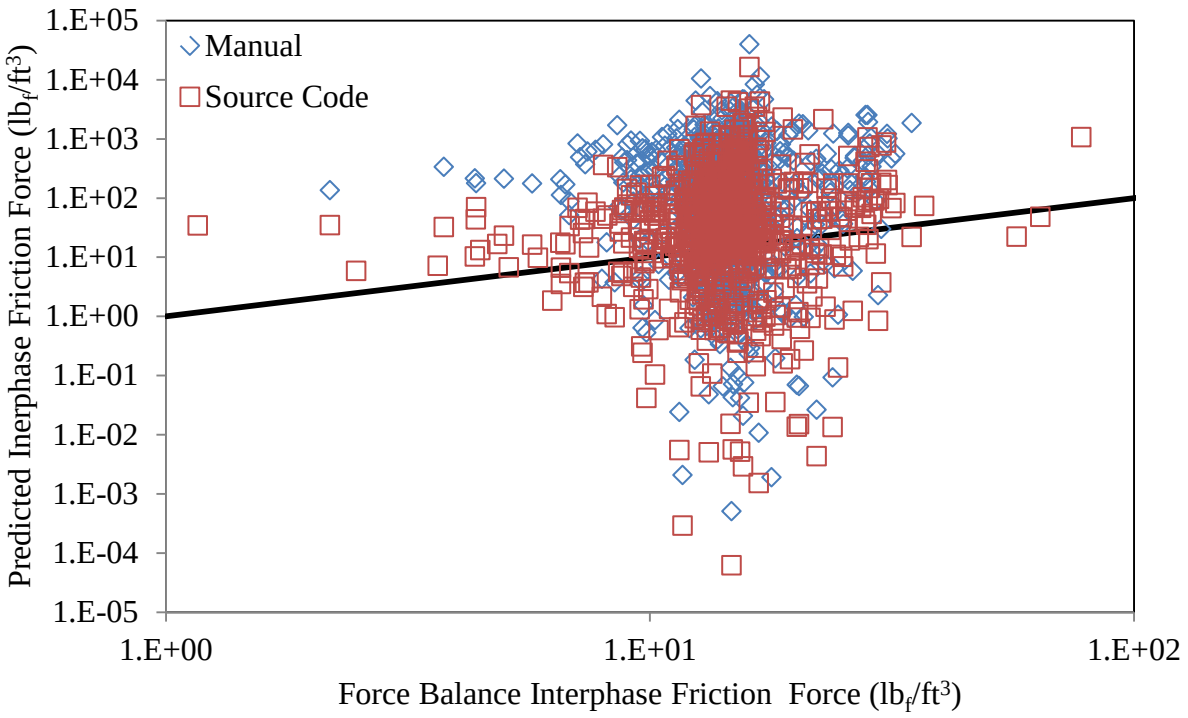

Figure 97: Comparison of the RELAP5/MOD3.3 Interphase Friction Force Calculation Using the Manual [69] Equations to the Source Code [40] Equations for Slug Flow

Figure 99 shows how the RELAP manual [69] calculation for interphase friction force with annular flow compares to that for the RELAP source code [40]. Even though both sets of equations are shown to deviate from the force balance interphase friction by several orders of magnitude, the RELAP predicted interphase friction force shows a more encouraging trend of increasing the interphase friction force prediction as the force balance interphase friction

indicates that it should be increasing. This is in contrast to the values seen for bubbly and slug flow, where there is more randomness to the interphase friction force predictions. While the manual calculation matches the source code value in many cases, there appear to be a handful of data points where the manual predicts an interphase friction force up to two orders of magnitude greater than the source code. The difference appears to be additional steps that the RELAP source code takes to calculate the velocity difference, which is then used to calculate the droplet size. When broken down by component, the difference between the interphase friction force calculation using the RELAP manual and the source code takes place with the liquid droplets in the vapor core, as the calculations for the interphase friction force between the liquid film and the vapor core is the same for all data points.

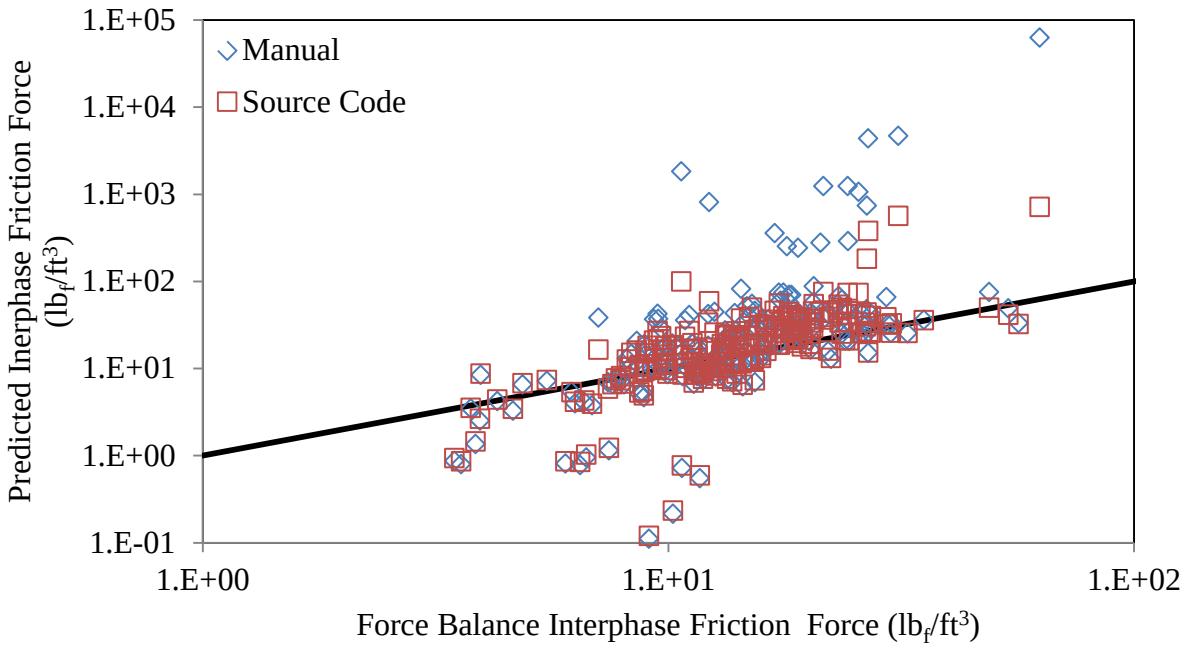

Figure 98: Comparison of the RELAP5/MOD3.3 Interphase Friction Force Calculation Using the Manual [69] Equations to the Source Code [40] Equations for Annular Flow

In Table 14, the interphase friction force calculation from the manual [69] and the source code [40] are compared from a statistical perspective for all data points, as well as for each flow regime. In general, it is shown that the source code is much more accurate at predicting the

interphase friction force than the manual. The code appears to be most accurate in predicting the interphase friction force for the annular flow regime, although there is still a significant amount of error.

Table 14: Statistical Comparison of the Interphase Friction Force RELAP5/MOD3.3 Manual [69] Equations to the Source Code [40] Equations

	Overall		Bubbly		Slug		Annular	
	Manual	Code	Manual	Code	Manual	Code	Manual	Code
RMS Error (lb_f/ft^3)	3010	592	96.8	54.8	2820	683	4340	65.3
Mean Average Error (%)	3440	784	385	243	4340	1000	919	81.7
Median Average Error (%)	292	100.1	98.9	96.3	636	120.1	48.0	42.2
± 20% Error	79	125	13	5	13	59	53	61
- Percentage	6.25	9.89	12.26	4.72	1.374	6.24	25.2	29
± 50% Error	181	317	28	24	46	174	107	119
- Percentage	14.32	25.0	26.4	22.6	4.86	18.39	51.0	56.7
Maximum Error (%)	247000	101700	4900	2790	247000	101700	99800	1705

4.3.2: Comparisons of the Data to the RELAP5/MOD3.3 Executable

In this comparison of data from the RELAP executable [40] to data previously obtained from calculations, only air-water and steam-water was simulated, as the properties of those fluids are included within RELAP. Simulations of the Schlegal [75] air-water data were not conducted, as the Schlegal data was taken from several intervals within a single run, and no entrance length was provided for the Schlegal apparatus. Thus a total of 572 air-water and steam-water tests were run in RELAP, with 9 air-water data points ending in transient failures, producing 563 viable data points for analysis. As only data points from Schlegal were predicted to be bubbly flow through calculations with the RELAP flow regime map, all data points that were modeled were expected to be either slug flow or annular flow.

The data is broken down by the flow regime determined through calculations of the RELAP [40] flow regime map, which was not always in agreement with the flow regime reported in the RELAP executable output. The flow regime reported by the RELAP executable is an ensemble-average over the 4 junctions between the five volumes within the test section, when the model run achieved steady-state. In cases where the model run did not achieve steady-state, the flow regime in each volume is time-averaged over the last 50 seconds of the model run before the four junctions are ensemble-averaged. While RELAP gives a whole number (4 for bubbly flow, 5 for slug flow and 6 for annular flow) [40,69] for the flow regime at each junction,

In Figure 99, we see the pressure gradient that is determined using the data output of RELAP [40] compared against the observed pressure gradients for all air-water and steam-water data for which RELAP model runs were performed. The RELAP executable determined that 14 data points from Oshinowo [59] were bubbly flow rather than slug flow. Generally, it appears that RELAP is within ±50% of the observed pressure gradient for most of the model runs. However, one trend that is noticed in the chart below that cannot be explained at this time is an offshoot of slug flow data points, where RELAP has underpredicted the pressure gradient by at least 20%, and as much as 76.1%. This data appears to be a subset of the Oshinowo air-water data, where Oshinowo placed downstream of the test section a tube bend with a 3 in. turning radius. However, as shown in Figure 100, there are more data points from Oshinowo's observations for which the pressure gradient from the RELAP data matches well with that reported by Oshinowo.

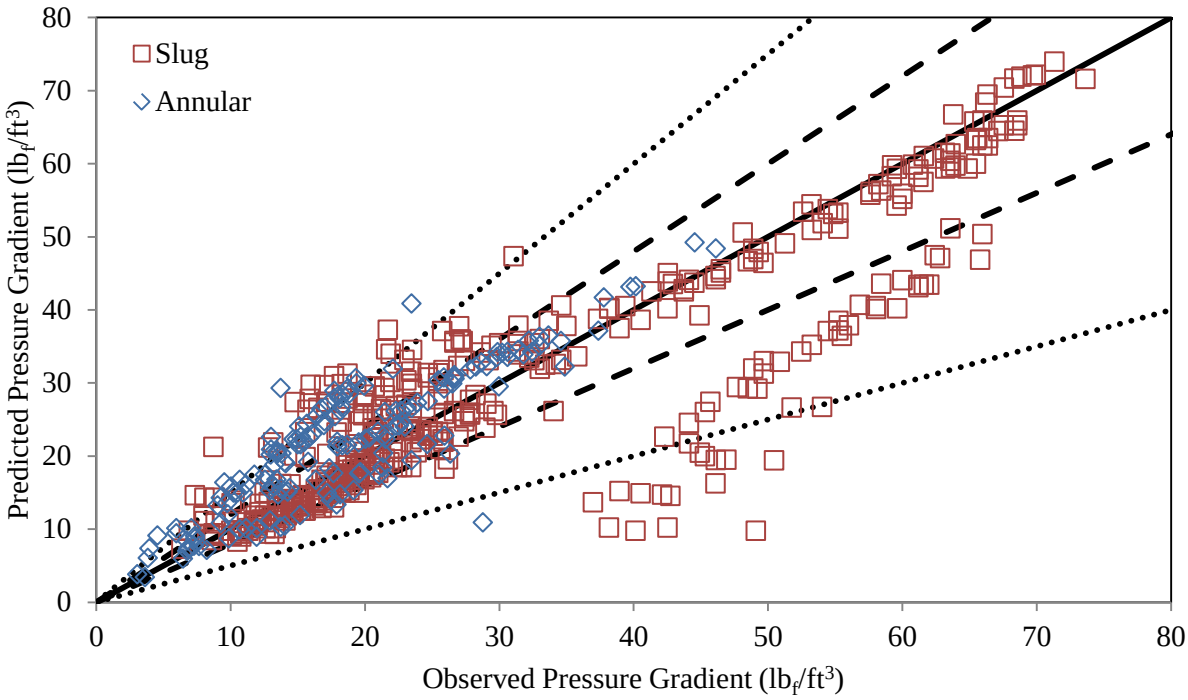

Figure 99: Comparison of the RELAP5/MOD3.3 [40] Pressure Gradient to the Observed Pressure Gradient

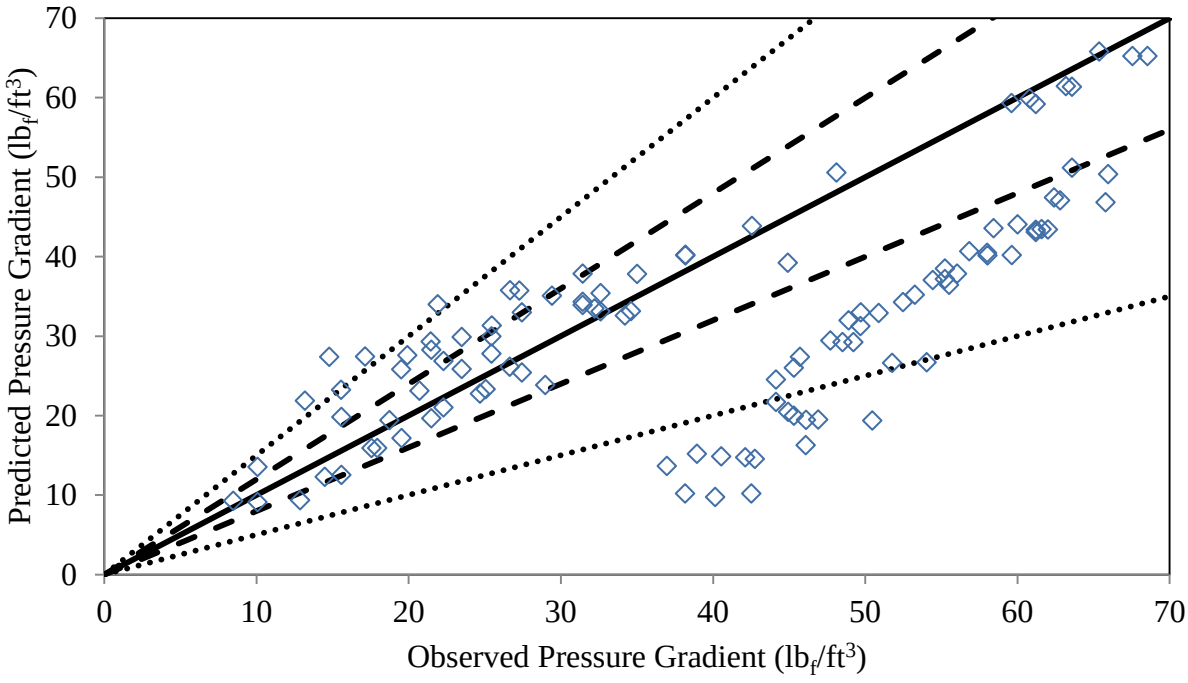

Figure 100: Comparison of the RELAP5/MOD3.3 [40] Pressure Gradient to the Pressure Gradient Observed by Oshinowo [59] for Air-Water Test Runs with a 3 in. Turning Radius Bend Downstream

In Figure 101, the average void fraction throughout the test section according to the RELAP [40] data is compared to the observed void fraction from their respective studies. For the 14 data points that RELAP predicted to be bubbly flow instead of slug flow, RELAP gives predicted void fractions very close to zero. For slug flow, RELAP appears to have a wide spread in predicting the average void fraction in comparison to the observed values, with the void fraction being overpredicted by greater than 50% in many cases. For annular flow, RELAP appears to predict void fractions that are much closer to the expected value, but this may also be due to the limited range with which RELAP can predict the void fraction.

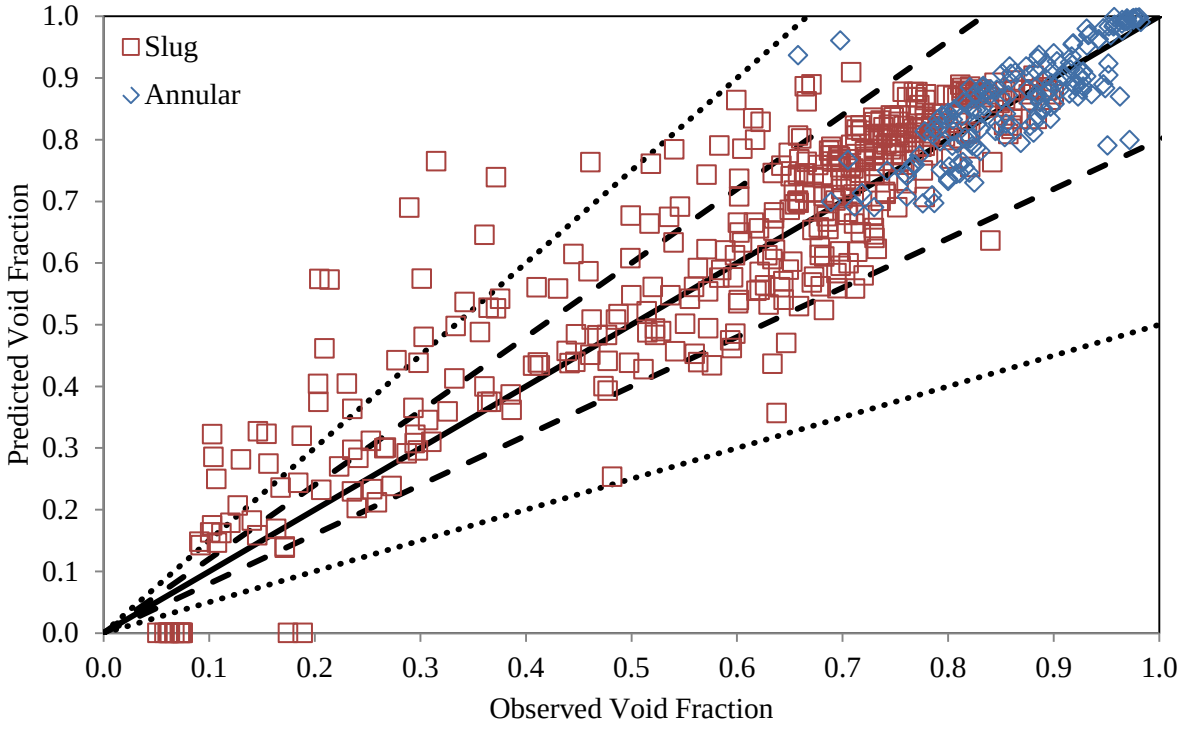

Figure 101: Comparison of the RELAP5/MOD3.3 [40] Void Fraction to the Observed Void Fraction

When comparing the liquid velocity that is predicted by RELAP [40] to the liquid velocity that is derived from the observations in Figure 102, it is shown that generally, RELAP matches well with the observed data for slug flow, but for some of the annular flow data points, the liquid velocity appears to be significantly overpredicted. This is likely the result of RELAP

predicting that the flow regime is close to the transition to mist flow, where most of the liquid in the two-phase mixture has taken the form of entrained droplets. In these cases, the liquid flows at a velocity closer to that of the vapor phase, as opposed to the liquid film, which flows along the pipe wall at a much slower rate.

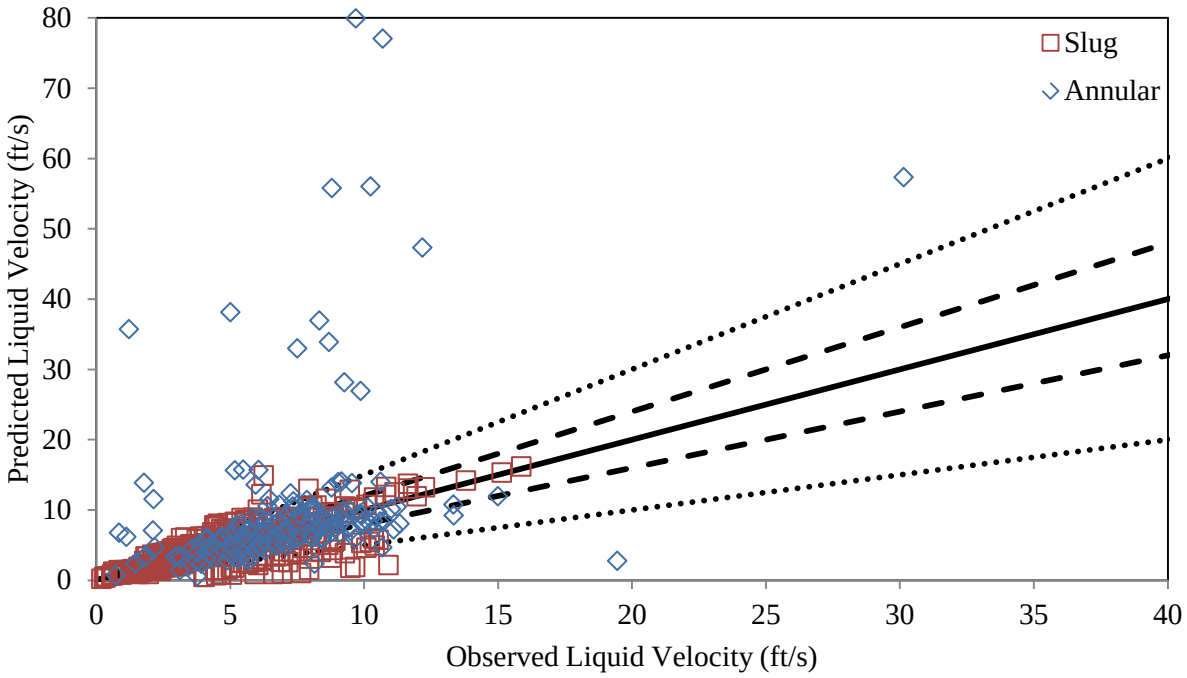

Figure 102: Comparison of the RELAP5/MOD3.3 [40] Liquid Velocity to the Observed Liquid Velocity

Figure 103 shows the comparison of the vapor velocity from RELAP [40] to that based on the observed data. In general, the vapor velocities predicted by RELAP match very well with the vapor velocities determined from the observed void fraction and vapor mass flow rate, with just a few data points from the annular flow regime falling outside the ±20% error region.

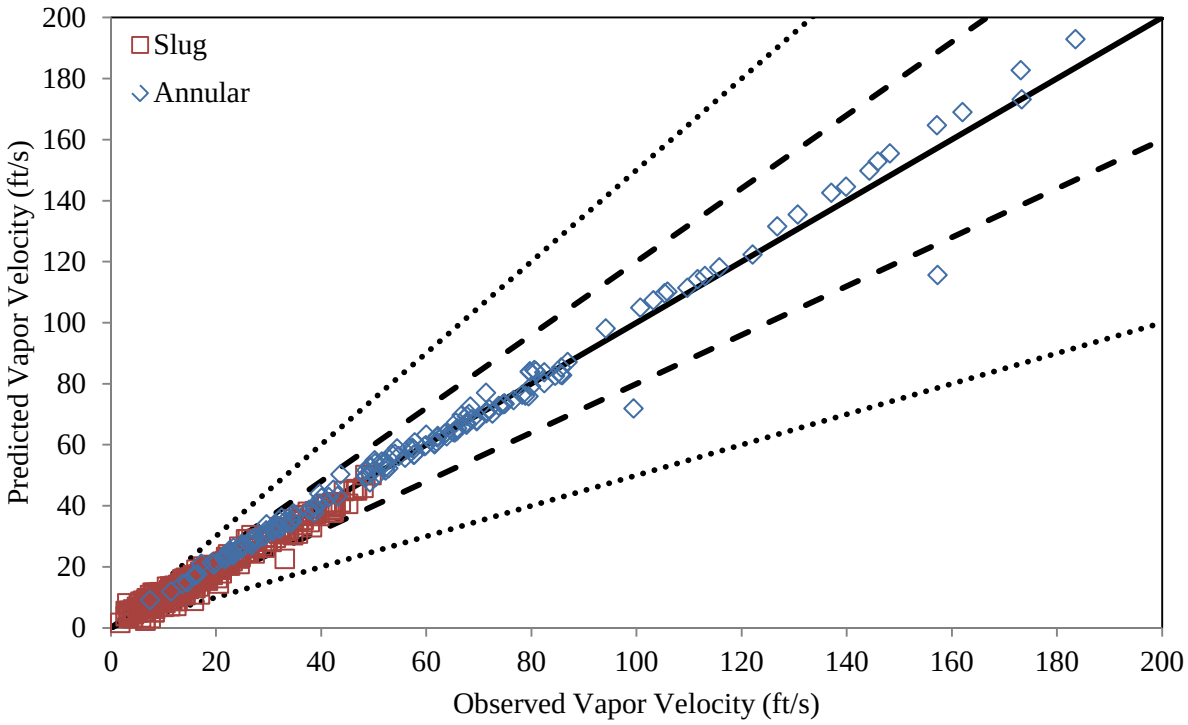

Figure 103: Comparison of the RELAP5/MOD3.3 [40] Vapor Velocity to the Observed Vapor Velocity

Finally, the interphase friction force that is determined from RELAP [40] is compared against the force balance interphase friction force in Figure 104. The general trend that is noticed is that the interphase friction force for slug flow is underpredicted compared to the force balance value, while the annular flow interphase friction force is close to the expected value. However, there are several significant outliers within the slug flow regime that are not shown in Figure 104. The most significant outlier predicted by RELAP is 3970 lb_f/ft^3, while the force balance value indicates that the interphase friction force should be 15.35 lb_f/ft^3. Meanwhile, for annular flow, most data points fall within the ±50% range, although a few data points exist outside that range. Data points that are identified as annular flow, but have interphase friction force values close to zero are the result of RELAP adjusting the void fraction such that the flow regime became slug flow, rather than the predicted annular flow. These few data points will continue to be analyzed as annular flow points as it is hoped that with modifications to the

interphase friction correlations will result in RELAP identifying these data points as annular flow rather than slug flow.

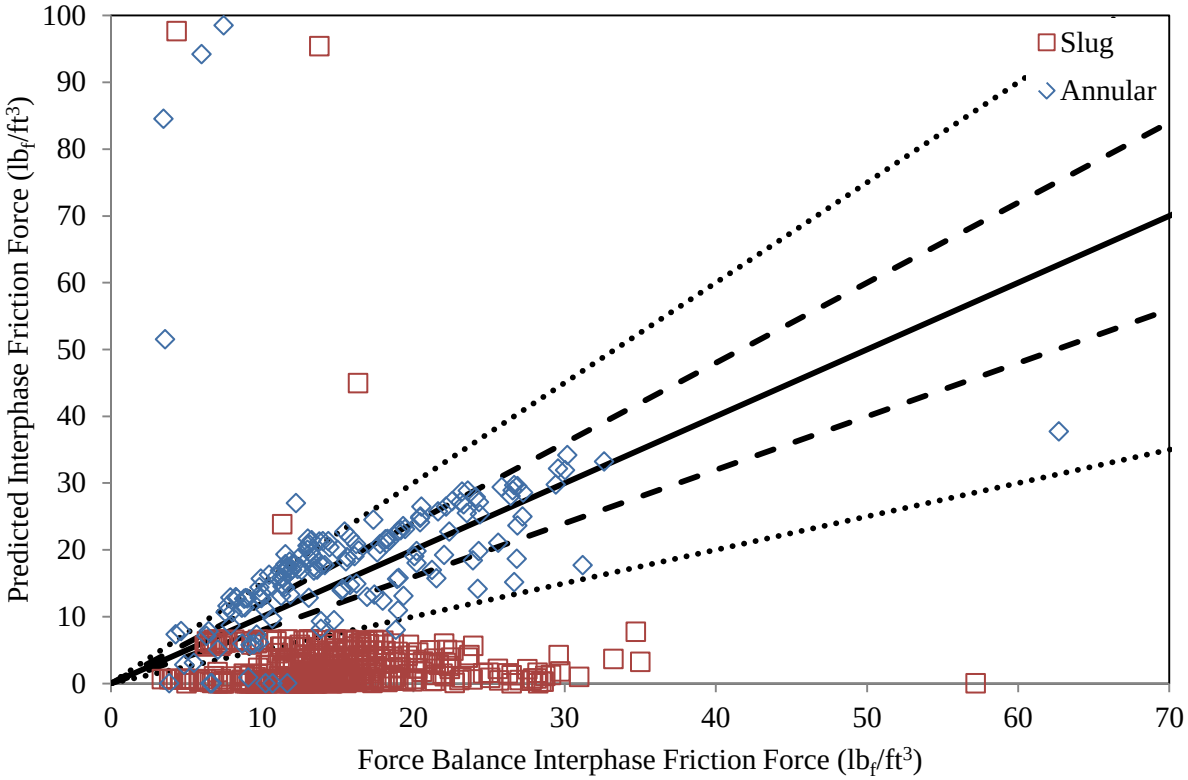

Figure 104: Comparison of the RELAP5/MOD3.3 [40] Interphase Friction Force to the Force Balance Interphase Friction Force

A comparison of the RELAP [40] errors for all data points is shown in Table 15. It shows that even though RELAP does not appear to accurately model the interphase friction force, it has a fairly good handle on modeling the pressure gradient, void fraction and the phasic velocities. Table 16 shows that for slug flow, an inaccurate prediction of the interphase friction appears to still result in surprisingly accurate predictions of pressure gradient, void fraction, and the phasic velocities. However, for annular flow, the results indicate in Table 17 that the interphase friction force prediction is much more accurate than for slug flow. However, RELAP is less accurate with the pressure gradient and liquid velocity predictions than with slug flow.

Table 15: Average Percentage Errors of RELAP5/MOD3.3 [40] against Observed Data

	Pressure Gradient	Void Fraction	Liquid Velocity	Vapor Velocity	Interphase Friction Force
Mean Average Error (%)	21.6	16.09	45.4	9.21	164.1
Median Average Error (%)	14.09	6.46	23.3	5.39	83.5
±20% Error	358	465	245	500	62
- Percentage	63.6	82.6	43.5	88.8	11.01
±50% Error	494	520	444	556	151
- Percentage	87.7	92.4	78.9	98.8	26.8
Maximum Error (%)	143.5	213	2820	153.6	25800

Table 16: Average Percentage Errors of RELAP5/MOD3.3 [40] against Observed Data for Slug Flow

	Pressure Gradient	Void Fraction	Liquid Velocity	Vapor Velocity	Interphase Friction Force
Mean Average Error (%)	19.15	20.80	27.7	11.13	188.2
Median Average Error (%)	11.49	9.23	21.7	6.60	91.7
±20% Error	272	303	188	340	9
- Percentage	68.2	75.9	47.1	85.2	2.26
±50% Error	362	356	321	392	22
- Percentage	90.7	89.2	80.5	98.2	5.51
Maximum Error (%)	143.5	213	137.8	153.6	25800

Table 17: Average Percentage Errors of RELAP5/MOD3.3 [40] against Observed Data for Annular Flow

	Pressure Gradient	Void Fraction	Liquid Velocity	Vapor Velocity	Interphase Friction Force
Mean Average Error (%)	27.7	4.53	88.5	4.54	105.7
Median Average Error (%)	18.83	3.62	26.4	3.58	30.5
±20% Error	86	162	57	160	53
- Percentage	52.4	98.8	34.8	97.6	32.3
±50% Error	132	164	123	164	129
- Percentage	80.5	100.0	75.0	100.0	78.7
Maximum Error (%)	113.3	42.4	2820	27.8	2970

4.4: Analyses of the RELAP5/MOD3.3 Source Code Modified by the Correlation

In this section, the RELAP source code [40] has been modified to calculate the interphase friction using the correlations developed in Section 4.1, that utilize the Weber number, the Froude number and the mixture Froude number, and shown in Equations 290 through 295. Here we will look at the results of running RELAP with the modifications to the source code, and compare those results against the unmodified RELAP output. The correlation that provides the most accurate prediction of pressure gradient, void fraction and phasic velocities was selected to explore further modifications with a multiplier to determine if adjusting the multiplier would improve upon the RELAP model.

4.4.1: Analysis of the Weber Number Correlation

First, the Weber number correlation is tested in RELAP [40], and is compared to the original RELAP data. Of the original 164 data points that were identified as annular flow by the RELAP flow regime map, 6 model runs resulted in transient errors when the Weber number correlation was implemented. Transient errors occur when the properties in one or more of the volumes of the RELAP model diverges to an unrealistic solution. Given that most of the data points produced a viable solution, this would indicate there was likely some incompatibility between the correlation and the 6 data points.

Examining the data points for which a result could be obtained, we find that in general the Weber number correlation appears to slightly overpredict the pressure gradient, especially in comparison to the original RELAP [40] prediction, as seen in Figure 105. As one might expect with an overprediction of pressure gradient, there is a slight underprediction of the void fraction that is noticeable in Figure 106. The liquid velocity prediction by RELAP with the Weber number correlation appears to be greatly improved over the original model in Figure 107, while

the vapor velocity appears to be close to the given value and that predicted by the unmodified RELAP in Figure 108.

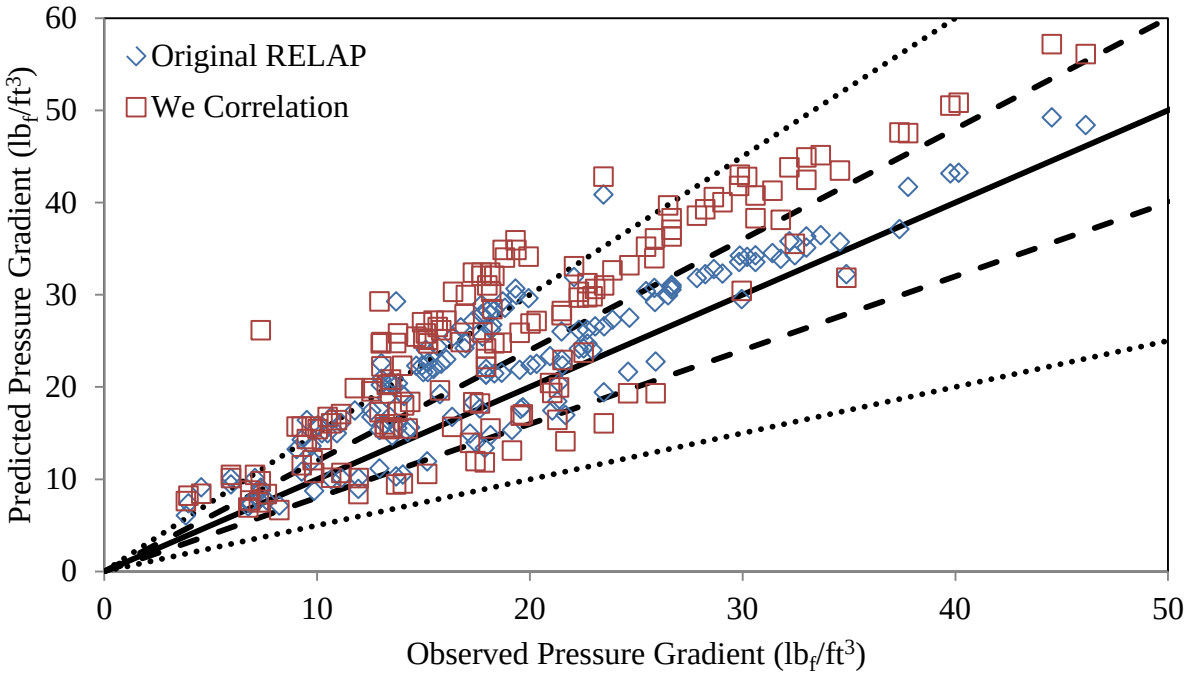

Figure 105: Comparison of the Pressure Gradient Prediction of the Original RELAP5/MOD3.3 Model [40] to the Weber Number Correlation

The interphase friction prediction appears to be relatively unchanged for most data points when viewed in Figure 109, however, as Table 18 indicates, there has been a significant reduction in the error of outliers. This has resulted in lower mean average errors with the interphase friction force when using the Weber number correlation, for both air-water and steam-water, but does not appear to have improved the overall pattern with higher median average errors. Table 18 also indicates that the liquid velocity prediction has significantly improved, particularly for the air-water data.

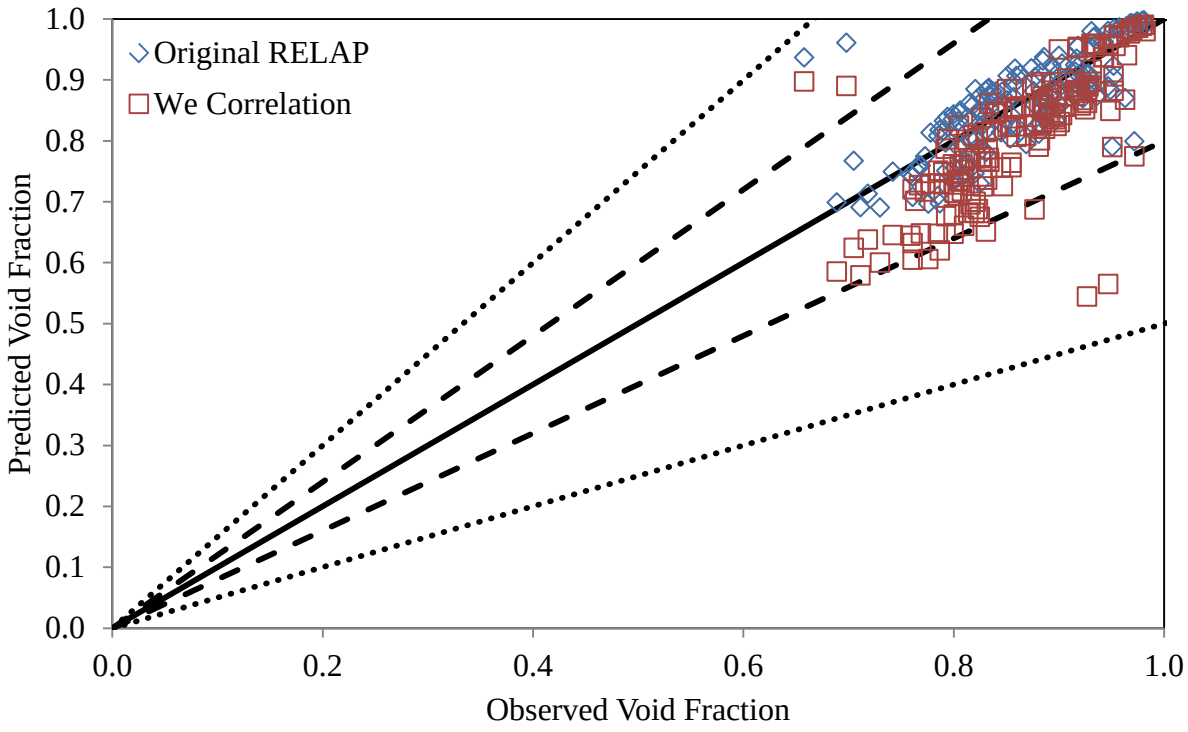

Figure 106: Comparison of the Void Fraction Prediction of the Original RELAP5/MOD3.3 Model [40] to the Weber Number Correlation

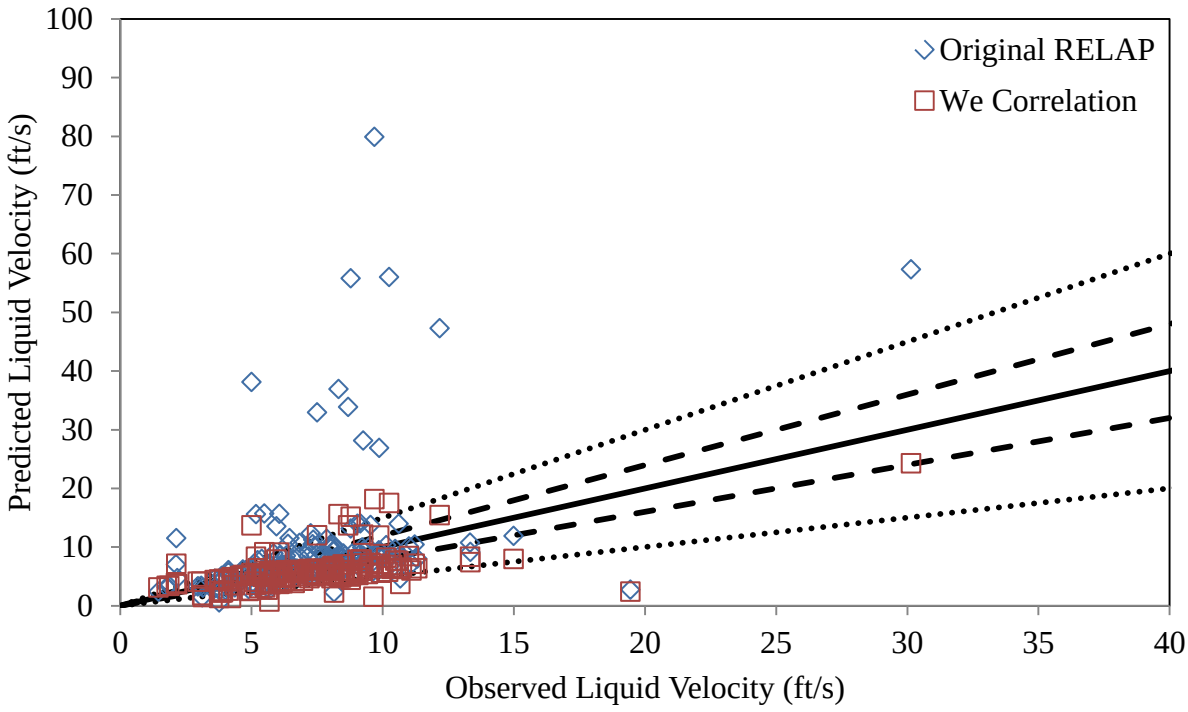

Figure 107: Comparison of the Liquid Velocity Prediction of the Original RELAP5/MOD3.3 Model [40] to the Weber Number Correlation

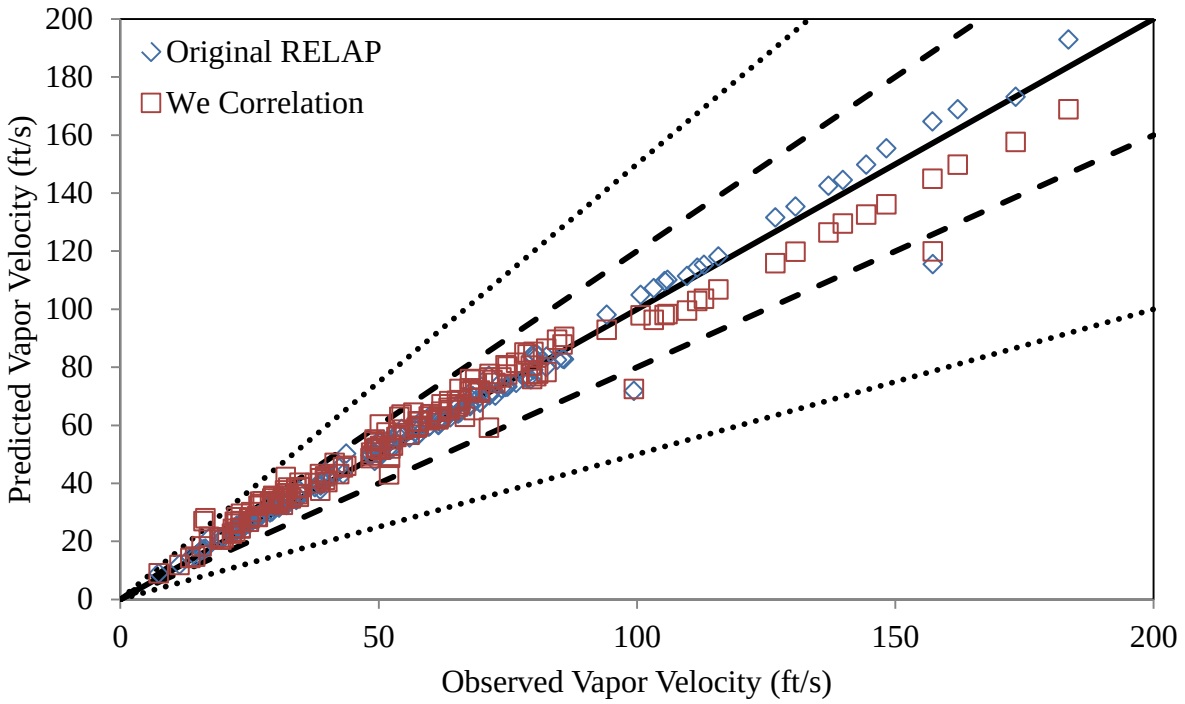

Figure 108: Comparison of the Vapor Velocity Prediction of the Original RELAP5/MOD3.3 Model [40] to the Weber Number Correlation

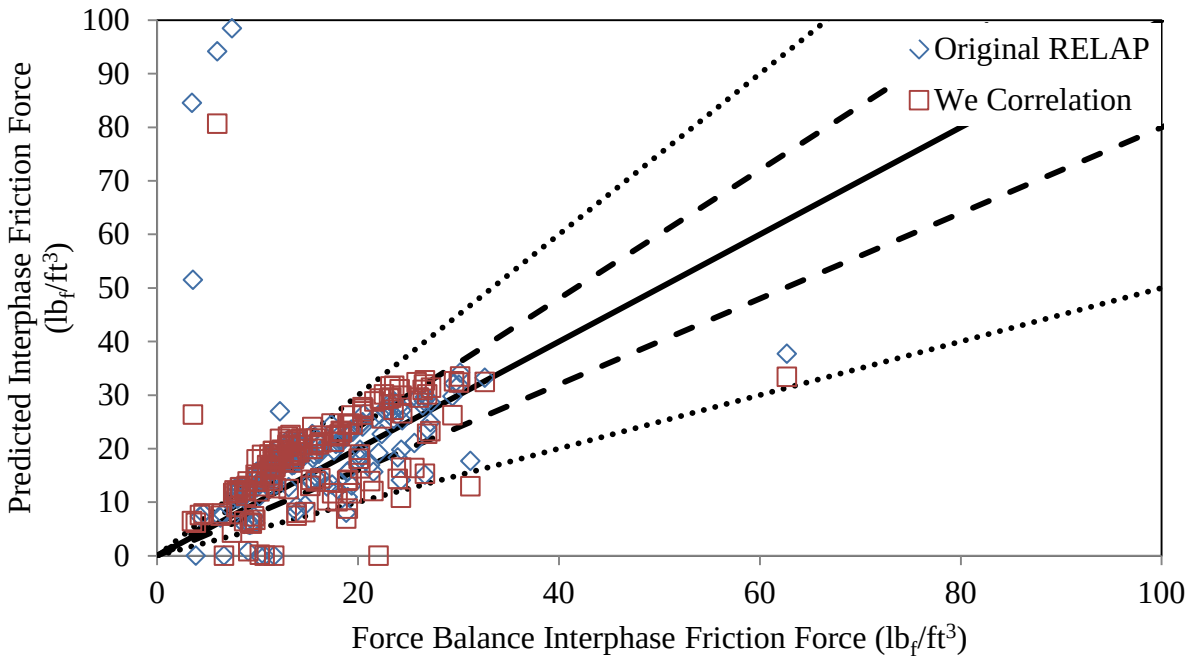

Figure 109: Comparison of the Interphase Friction Force Prediction of the Original RELAP5/MOD3.3 Model [40] to the Weber Number Correlation

Table 18: Comparison of Errors of the Original RELAP5/MOD3.3 Model [40] to the Weber Number Correlation

			Original RELAP					Weber Number Correlation				
			dP/dz	α	v_f	v_g	F_{int}	dP/dz	α	v_f	v_g	F_{int}
All Annular	158	Mean Average	27.83%	4.61%	58.55%	4.64%	108.06%	43.53%	7.68%	34.84%	9.29%	51.19%
		Median Average	18.78%	3.81%	26.06%	3.61%	30.14%	34.90%	5.71%	32.11%	6.84%	38.28%
		± 20%	84	156	56	154	52	29	148	52	144	26
		- Percentage	53.16%	98.73%	35.44%	97.47%	32.91%	18.35%	93.67%	32.91%	91.14%	16.46%
		± 50%	127	158	122	158	124	104	158	134	156	112
		- Percentage	80.38%	100.00%	77.22%	100.00%	78.48%	65.82%	100.00%	84.81%	98.73%	70.89%
		Maximum	113.29%	42.36%	724.75%	27.78%	2965.69%	254.84%	41.30%	233.55%	69.30%	1242.02%
Air-Water	89	Mean Average	13.73%	3.39%	72.37%	2.99%	85.30%	27.13%	4.54%	27.89%	6.54%	29.91%
		Median Average	12.11%	3.13%	29.03%	2.52%	19.24%	29.98%	3.03%	19.50%	5.81%	28.84%
		± 20%	75	89	30	89	47	22	87	45	88	21
		- Percentage	84.27%	100.00%	33.71%	100.00%	52.81%	24.72%	97.75%	50.56%	98.88%	23.60%
		± 50%	88	89	61	89	84	88	89	74	89	81
		- Percentage	98.88%	100.00%	68.54%	100.00%	94.38%	98.88%	100.00%	83.15%	100.00%	91.01%
		Maximum	113.29%	8.74%	724.75%	9.97%	2965.69%	80.48%	21.65%	114.94%	31.67%	99.92%
Steam-Water	69	Mean Average	46.01%	6.17%	40.72%	6.77%	137.42%	64.69%	11.74%	43.80%	12.85%	78.64%
		Median Average	47.61%	4.77%	22.14%	6.14%	46.86%	68.36%	10.29%	37.72%	10.72%	53.94%
		± 20%	9	67	26	65	5	7	61	7	56	5
		- Percentage	13.04%	97.10%	37.68%	94.20%	7.25%	10.14%	88.41%	10.14%	81.16%	7.25%
		± 50%	39	69	61	69	40	16	69	60	67	31
		- Percentage	56.52%	100.00%	88.41%	100.00%	57.97%	23.19%	100.00%	86.96%	97.10%	44.93%
		Maximum	99.95%	42.36%	660.97%	27.78%	2335.38%	254.84%	41.30%	233.55%	69.30%	1242.02%

4.4.2:Analysis of the Froude Number Correlation

For this section, the Froude number correlation given in Equations 291 and 294, has been inserted into the RELAP source code [40] and the resulting data has been compared against the unmodified RELAP results. Based on the data analysis that went into developing each of these correlations, one would expect that the Froude number correlation would perform better than the Weber number correlation.

In Figure 110, the pressure gradient prediction of the unmodified RELAP [40] is compared to the model results when the Froude number correlation has been inserted into

RELAP. Comparing the Froude number correlation results to those of the Weber number in Figure 105, shows that the Froude number correlation has a slightly larger spread in the pressure gradient prediction than either the unmodified RELAP or the Weber number correlation. This is particularly evident with the set of data points where the observed pressure gradient was between 10 and 20 lb_f/ft^3, and the Froude number correlation has overpredicted the pressure gradient by more than 50%.

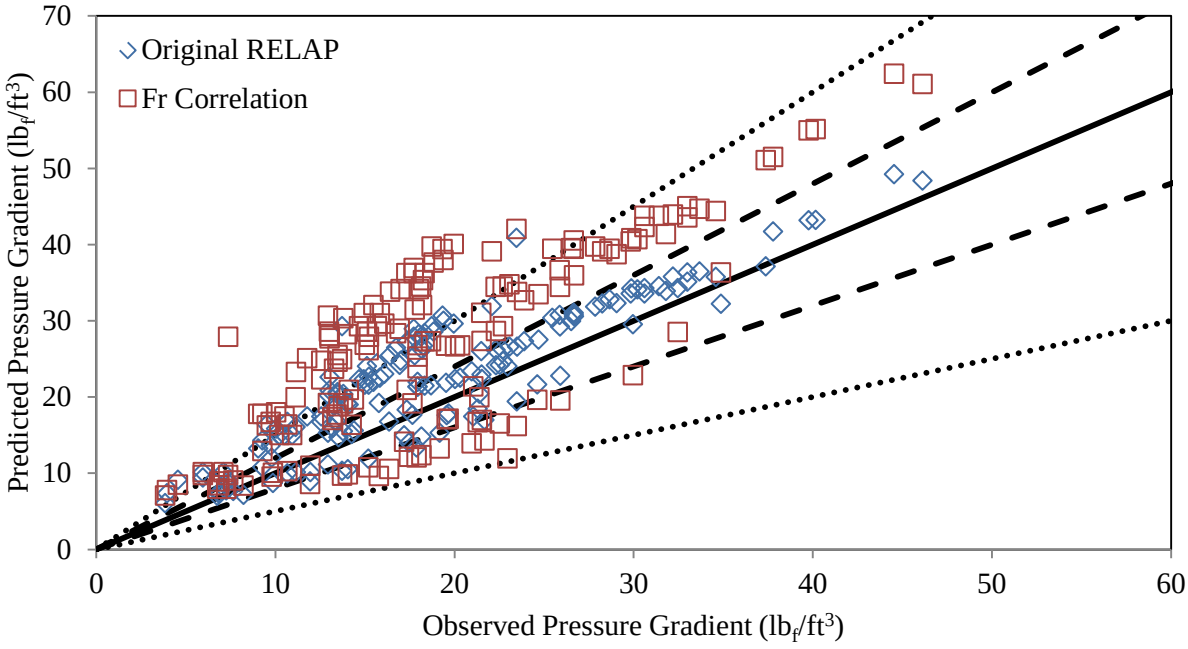

Figure 110: Comparison of the Pressure Gradient Prediction of the Original RELAP5/MOD3.3 Model [40] with the Froude Number Correlation

With overprediction of the pressure gradient, it would then be expected that the void fraction would be underpredicted. As Figure 111 shows, that is the case. While most data points are still within 20% of the observed value, and all are within 50%, the Froude number correlation shows a bias toward underpredicting the void fraction.

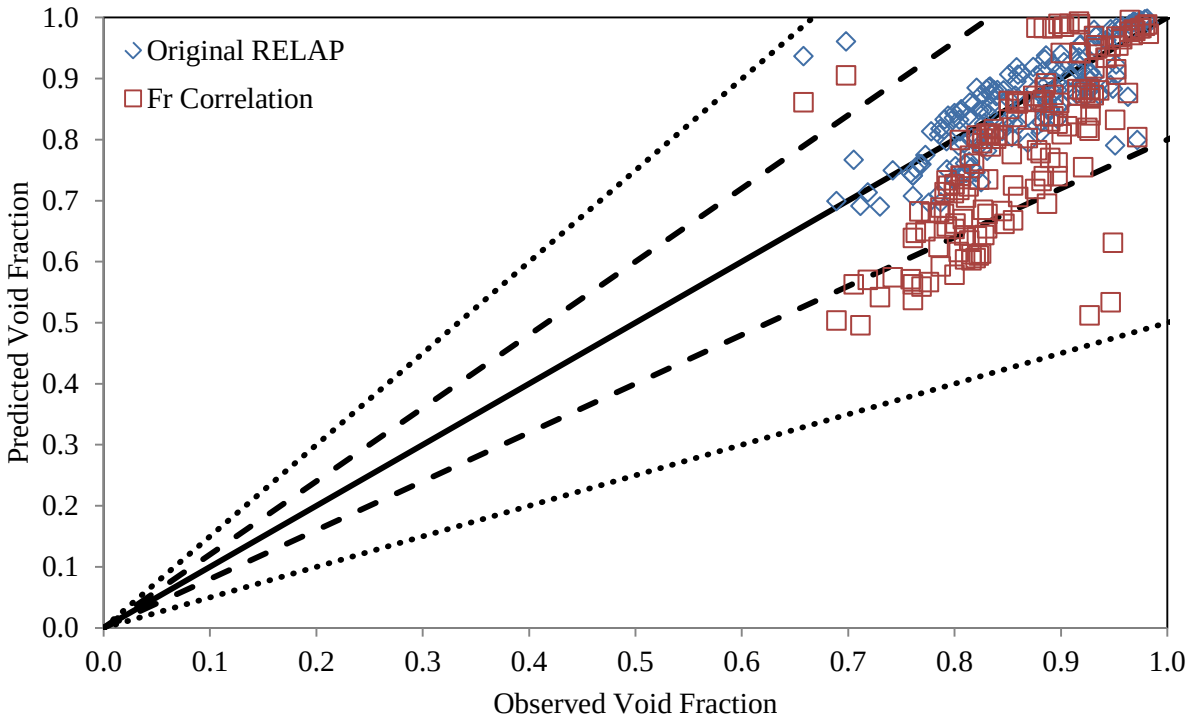

Figure 111: Comparison of the Void Fraction Prediction of the Original RELAP5/MOD3.3 Model [40] with the Froude Number Correlation

A smaller void fraction would indicate that there is more liquid within the test section, and that for data points where the void fraction is underpredicted and the pressure gradient is overpredicted, the liquid velocity should be underpredicted, so as to maintain the conservation of mass. In Figure 112, this appears to be the case for most data points. There are a few cases where RELAP [40] with the Froude number correlation has liquid velocities that are significantly higher than the observed value. These correspond with several air-water data points from Turner [84], where RELAP has predicted very high void fractions that are just below the threshold for mist flow. The decreased void fraction does not appear to have had a significant impact on the vapor velocity, as shown in Figure 113. To maintain continuity, RELAP with the Froude correlation does have an inverse relationship between the void fraction and vapor velocity, with void fraction overprediction implying vapor velocity underprediction and vice versa.

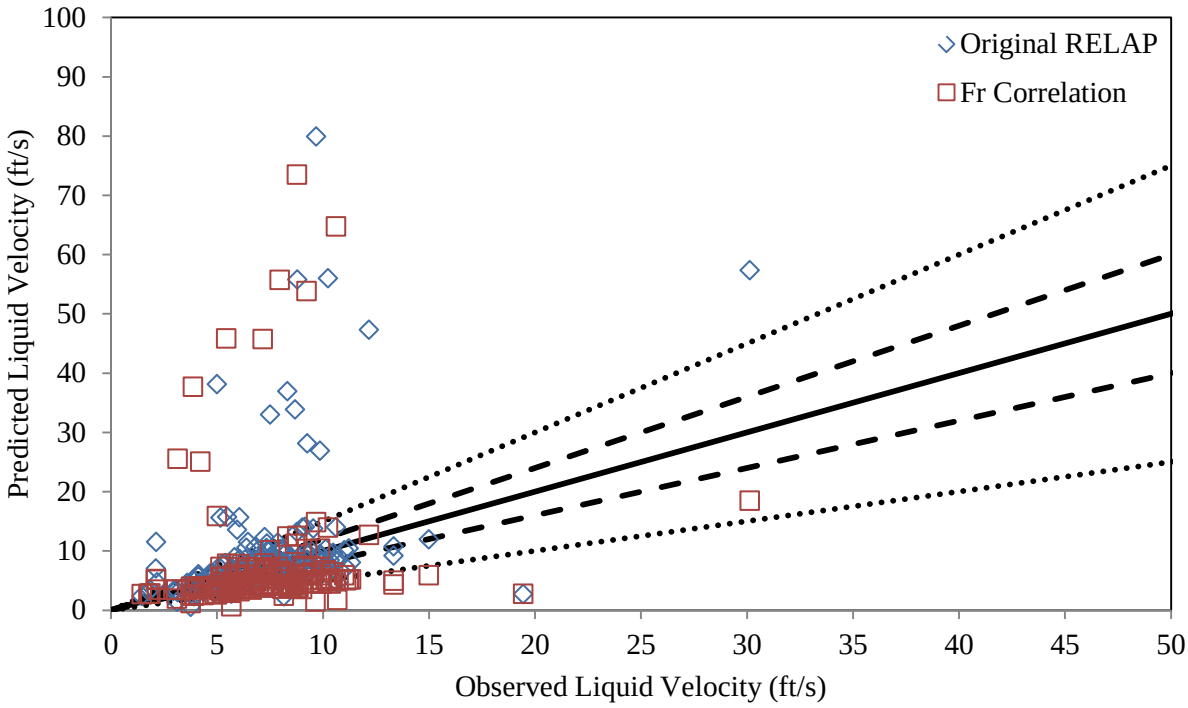

Figure 112: Comparison of the Liquid Velocity Prediction of the Original RELAP5/MOD3.3 Model [40] to the Froude Number Correlation

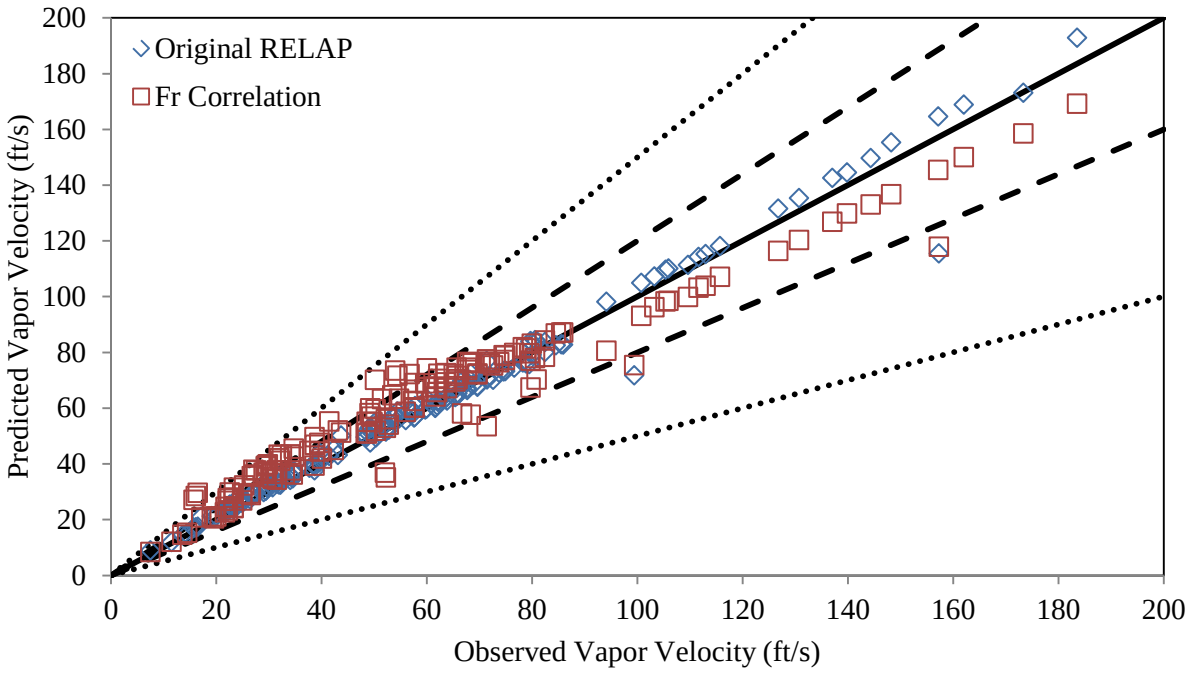

Figure 113: Comparison of the Vapor Velocity Prediction of the Original RELAP5/MOD3.3 Model [40] to the Froude Number Correlation

In Figure 114, the interphase friction force prediction of unmodified RELAP [40] is compared to the Froude number correlation, with respect to the interphase friction force that was derived from the force balance of the data. The chart does not seem to indicate that the Froude number correlation is not an improvement over the original RELAP prediction of the interphase friction, as the Froude number correlation appears to be split on overpredicting and underpredicting the interphase friction for the data points for which the original RELAP model is within the ±50% range of the force balance value. What Figure 114 does not show are the several data points for which the original RELAP model run significantly overpredicts the interphase friction force and the Froude number correlation has offered a correction that brings the interphase friction force within an order of magnitude of the force balance value.

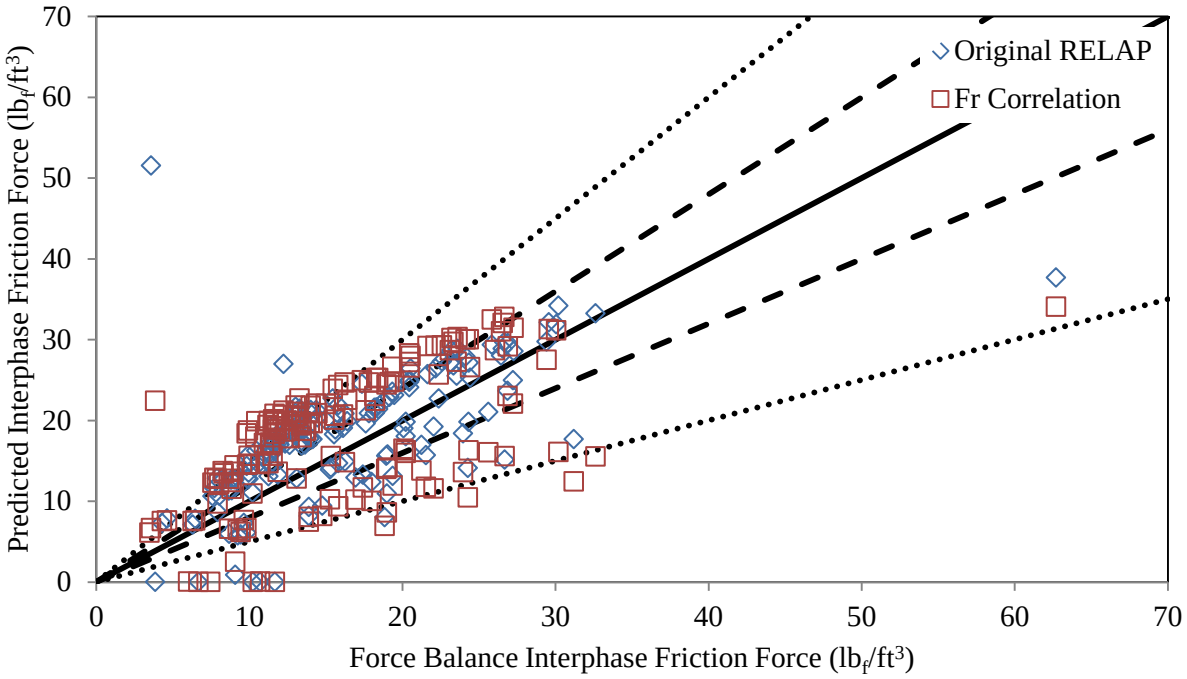

Figure 114: Comparison of the Interphase Friction Force of the Original RELAP5/MOD3.3 Model [40] to the Froude Number Correlation

Table 19 offers a numerical comparison of the errors that the original RELAP model [40] and the Froude number correlation in predicting the behavior that was either observed or directly

derived from observations. For all of the annular data points, the Froude number correlation is less accurate than the original RELAP model for predicting pressure gradient, void fraction and the phasic velocities. The mean average error of the interphase friction force appears to have improved with the utilization of the Froude number correlation, but is largely the product of improving a few outliers of the original RELAP model. As the median error suggests, along with the count of data points within ±20% and ±50% error, the Froude number correlation produces a less accurate interphase friction force prediction for most data points.

Table 19: Comparison of Errors of the Original RELAP5/MOD3.3 Model [40] to the Froude Number Correlation

			Original RELAP					Froude Number Correlation				
			dP/dz	α	v_f	v_g	F_{int}	dP/dz	α	v_f	v_g	F_{int}
All Annular	158	Mean Average	27.83%	4.61%	58.55%	4.64%	108.06%	54.67%	11.34%	72.26%	15.03%	46.83%
		Median Average	18.78%	3.81%	26.06%	3.61%	30.14%	40.44%	9.13%	39.47%	10.47%	41.47%
		± 20%	84	156	56	154	52	17	124	34	115	21
		- Percentage	53.16%	98.73%	35.44%	97.47%	32.91%	10.76%	78.48%	21.52%	72.78%	13.29%
		± 50%	127	158	122	158	124	95	158	112	155	98
		- Percentage	80.38%	100.00%	77.22%	100.00%	78.48%	60.13%	100.00%	70.89%	98.10%	62.03%
		Maximum	113.29%	42.36%	724.75%	27.78%	2965.69%	278.50%	44.77%	873.07%	79.86%	481.40%
Air-Water	89	Mean Average	13.73%	3.39%	72.37%	2.99%	85.30%	33.41%	6.48%	86.45%	10.12%	32.20%
		Median Average	12.11%	3.13%	29.03%	2.52%	19.24%	33.59%	3.89%	26.86%	7.59%	32.03%
		± 20%	75	89	30	89	47	11	82	34	79	16
		- Percentage	84.27%	100.00%	33.71%	100.00%	52.81%	12.36%	92.13%	38.20%	88.76%	17.98%
		± 50%	88	89	61	89	84	83	89	75	89	79
		- Percentage	98.88%	100.00%	68.54%	100.00%	94.38%	93.26%	100.00%	84.27%	100.00%	88.76%
		Maximum	113.29%	8.74%	724.75%	9.97%	2965.69%	81.82%	30.35%	873.07%	39.69%	73.10%
Steam-Water	69	Mean Average	46.01%	6.17%	40.72%	6.77%	137.42%	82.09%	17.61%	53.95%	21.37%	65.70%
		Median Average	47.61%	4.77%	22.14%	6.14%	46.86%	86.04%	17.31%	48.60%	19.39%	58.22%
		± 20%	9	67	26	65	5	6	42	0	36	5
		- Percentage	13.04%	97.10%	37.68%	94.20%	7.25%	8.70%	60.87%	0.00%	52.17%	7.25%
		± 50%	39	69	61	69	40	12	69	37	66	19
		- Percentage	56.52%	100.00%	88.41%	100.00%	57.97%	17.39%	100.00%	53.62%	95.65%	27.54%
		Maximum	99.95%	42.36%	660.97%	27.78%	2335.38%	278.50%	44.77%	216.94%	79.86%	481.40%

4.4.3: Analysis of the Mixture Froude Number Correlation

The last correlation that has been developed that is to be tested in RELAP [40] is the mixture Froude number correlation. The statistical analysis of the correlation that was performed during its development suggested that the mixture Froude number correlation would be the most accurate of the correlations that were developed. However, only in testing all three correlations in RELAP would it be known for certain which correlation produces the best results.

Figure 115 shows how the mixture Froude number correlation compares to the original RELAP model [40] in predicting the pressure gradient. For most points, it appears that the pressure gradient is being overpredicted. This would further imply underpredicted void fraction, underpredicted liquid velocity with overpredicted vapor velocity, which is seen in Figure 116 through Figure 118, respectively. Underpredicted liquid velocity and overpredicted vapor velocity would also imply an overpredicted interphase friction force, which is evident in Figure 119.

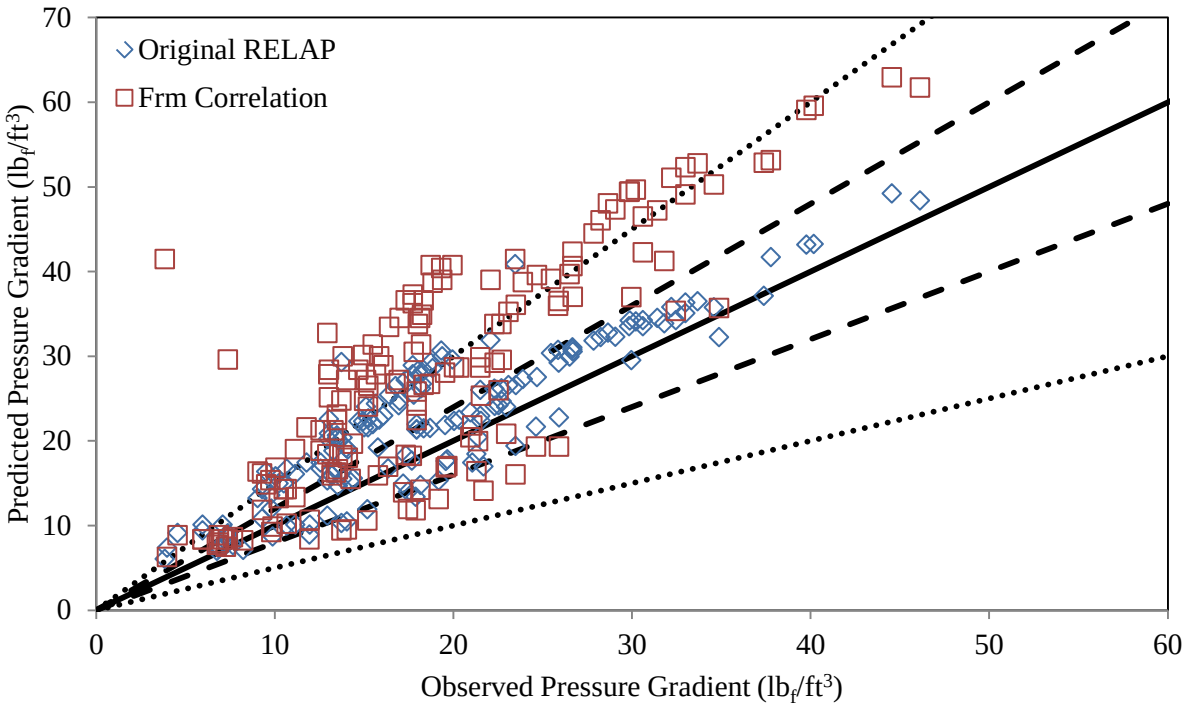

Figure 115: Comparison of the Pressure Gradient Prediction of the Original RELAP5/MOD3.3 Model [40] to the Mixture Froude Number Correlation

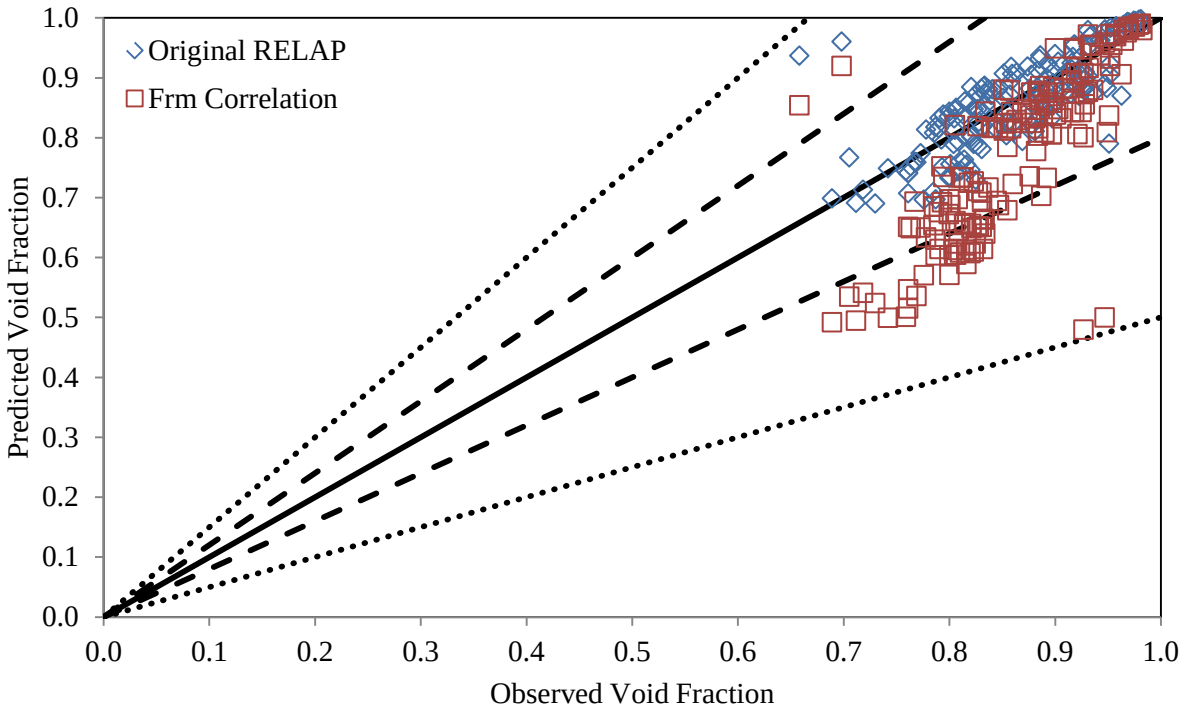

Figure 116: Comparison of the Void Fraction Prediction of the Original RELAP5/MOD3.3 Model [40] to the Mixture Froude Number Correlation

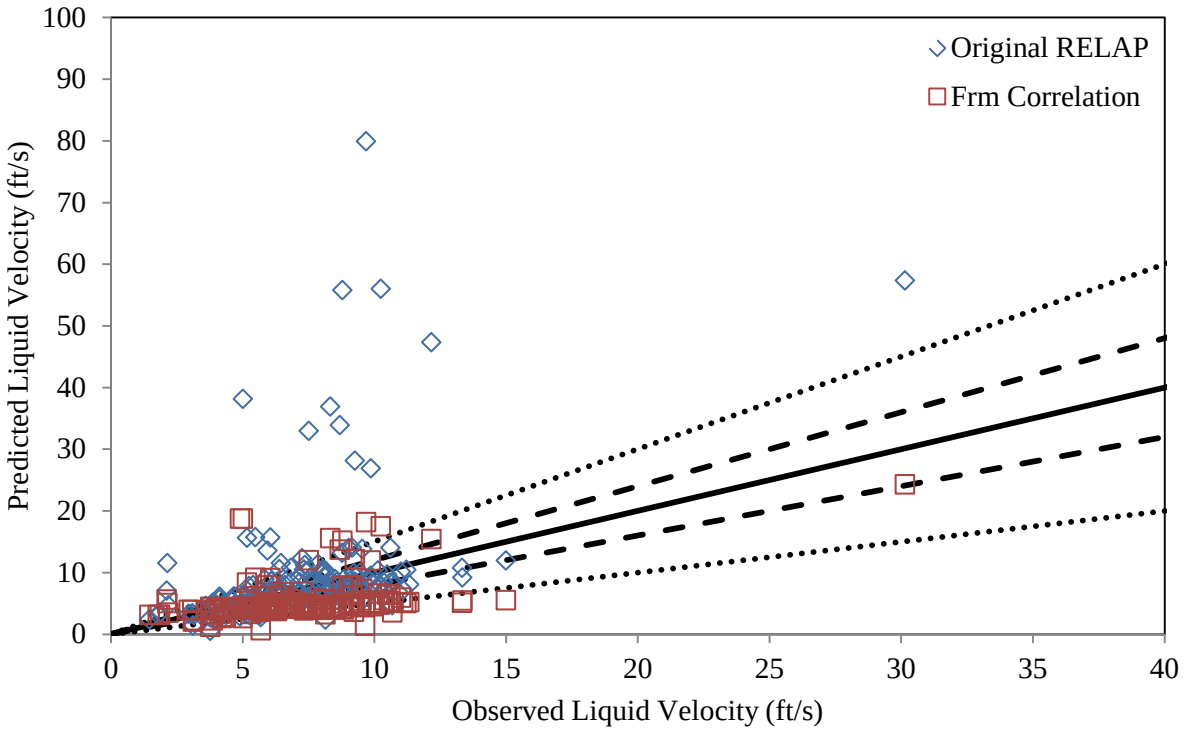

Figure 117: Comparison of the Liquid Velocity Prediction of the Original RELAP5/MOD3.3 Model [40] to the Mixture Froude Number Correlation

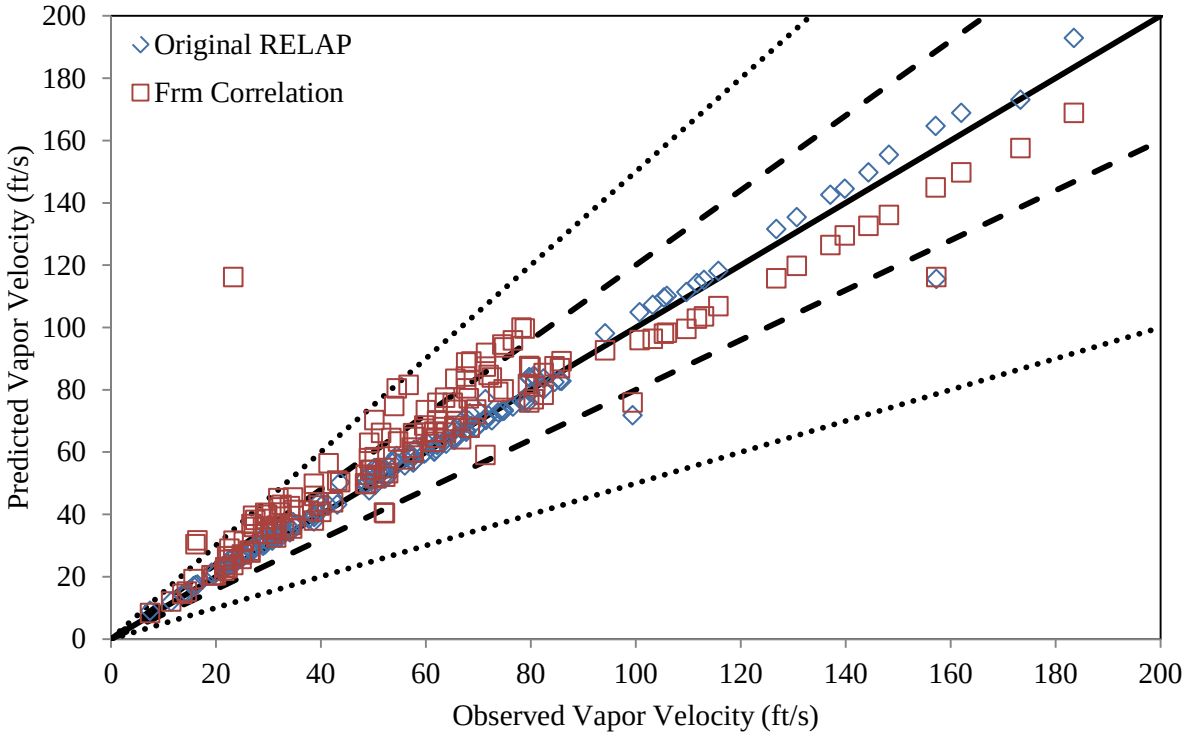

Figure 118: Comparison of the Vapor Velocity Prediction of the Original RELAP5/MOD3.3 Model [40] to the Mixture Froude Number Correlation

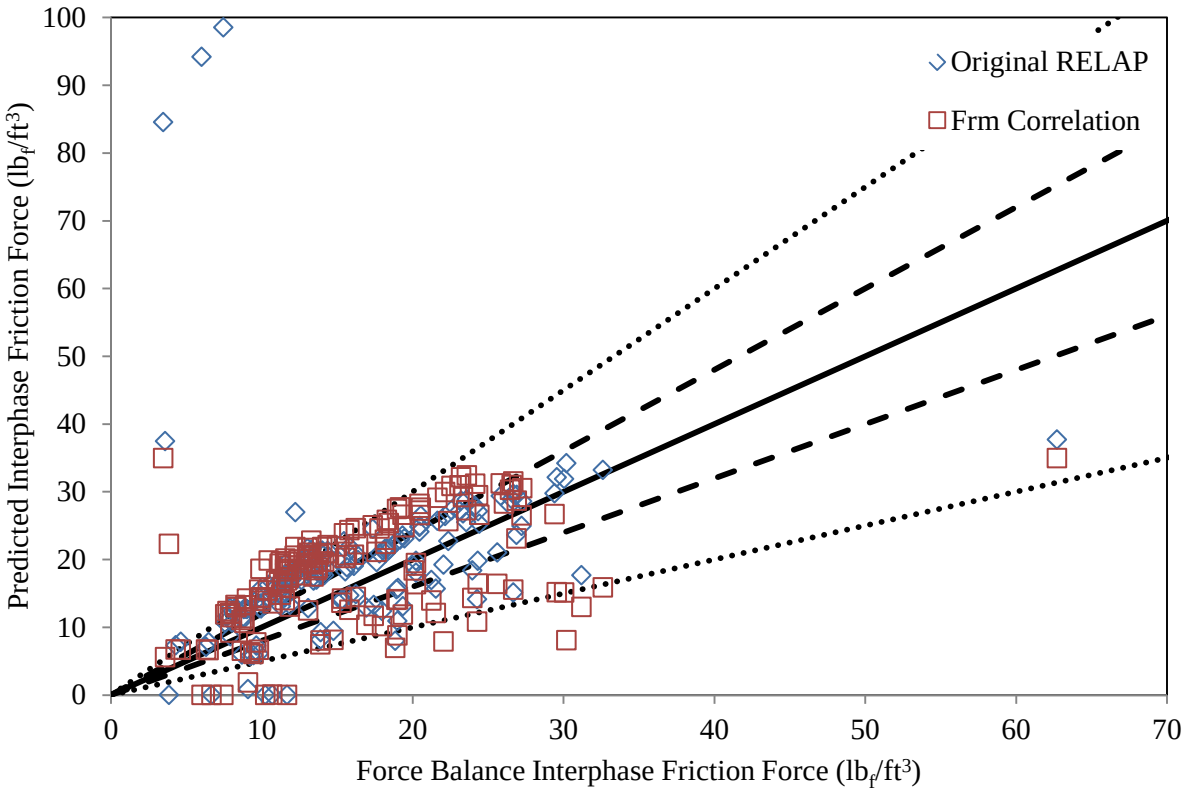

Figure 119: Comparison of the Interphase Friction Force Prediction of the Original RELAP5/MOD3.3 Model [40] to the Mixture Froude Number Correlation

The errors of the original RELAP model [40] are compared against the errors of the mixture Froude number correlation in Table 20. Despite expectations that the mixture Froude number correlation would be the best performing correlation of the three general interphase friction correlations developed, the errors show that is not the case. In fact, the mixture Froude number has the highest mean and median average errors for pressure gradient, and the highest mean average error for void fraction, of the three correlations. While the mixture Froude number correlation is better than the RELAP model for predicting the interphase friction force, it is not as good as the Froude number correlation based on velocity difference.

Table 20: Comparison of Errors of the Original RELAP5/MOD3.3 Model [40] to the Mixture Froude Number Correlation

	Total		Original RELAP					Mixture Froude Number Correlation				
			dP/dz	α	v_f	v_g	F_{int}	dP/dz	α	v_f	v_g	F_{int}
All Annular	157	Mean Average	27.77%	4.52%	58.37%	4.53%	106.20%	57.69%	11.90%	42.91%	17.79%	50.53%
		Median Average	18.75%	3.78%	26.03%	3.60%	30.34%	45.34%	9.10%	38.93%	9.62%	41.73%
		± 20%	84	155	56	154	51	28	117	30	108	25
		- Percentage	53.50%	98.73%	35.67%	98.09%	32.48%	17.83%	74.52%	19.11%	68.79%	15.92%
		± 50%	126	157	122	157	123	85	157	115	154	105
		- Percentage	80.25%	100.00%	77.71%	100.00%	78.34%	54.14%	100.00%	73.25%	98.09%	66.88%
		Maximum	113.29%	42.36%	724.75%	27.78%	2965.69%	978.43%	48.27%	282.13%	398.63%	907.37%
Air-Water	89	Mean Average	13.73%	3.39%	72.37%	2.99%	85.30%	35.25%	9.08%	35.77%	12.58%	32.78%
		Median Average	12.11%	3.13%	29.03%	2.52%	19.24%	34.60%	4.01%	32.12%	8.11%	33.97%
		± 20%	75	89	30	89	47	19	72	26	67	20
		- Percentage	84.27%	100.00%	33.71%	100.00%	52.81%	21.35%	80.90%	29.21%	75.28%	22.47%
		± 50%	88	89	61	89	84	68	89	73	89	78
		- Percentage	98.88%	100.00%	68.54%	100.00%	94.38%	76.40%	100.00%	82.02%	100.00%	87.64%
		Maximum	113.29%	8.74%	724.75%	9.97%	2965.69%	80.48%	33.97%	163.15%	47.72%	78.48%
Steam-Water	68	Mean Average	46.14%	6.00%	40.05%	6.55%	133.55%	87.07%	15.59%	52.25%	24.60%	73.76%
		Median Average	47.72%	4.74%	22.08%	6.07%	46.87%	75.24%	13.84%	46.93%	15.07%	55.13%
		± 20%	9	66	26	65	4	9	45	4	41	5
		- Percentage	13.24%	97.06%	38.24%	95.59%	5.88%	13.24%	66.18%	5.88%	60.29%	7.35%
		± 50%	38	68	61	68	39	17	68	42	65	27
		- Percentage	55.88%	100.00%	89.71%	100.00%	57.35%	25.00%	100.00%	61.76%	95.59%	39.71%
		Maximum	99.95%	42.36%	660.97%	27.78%	2335.38%	978.43%	48.27%	282.13%	398.63%	907.37%

4.4.4: Parametric Study of the Weber Number Correlation

Even though the original analysis of the interphase friction force correlations suggested that the mixture Froude number correlation should provide the most accurate prediction of interphase friction, the Weber number generally appears to have performed better of the three correlations that were developed. Thus, a parametric study was conducted with the Weber number correlation where a multiplier was added to the correlation to determine if increasing or decreasing the magnitude of the correlation would improve the prediction of pressure gradient, void fraction, the phasic velocities and interphase friction. Model runs were carried out with

multipliers of 50%, 75%, 125%, 150%, 175% and 200%, and were applied in the source code as shown in Equation 296 for the subroutine bubdrag and slugdrag and Equation 297 for the subroutine amistdrag:

$$fint = \begin{cases} RELAP\ Calculation\ for\ We \leq 10{,}290 \\ M \times \dfrac{0.0357\alpha(1-\alpha)(\rho_f - \rho_g)gWe^{0.361}}{(v_g - j)^2}\ for\ 10{,}290 < We < 408{,}000 \\ M \times \dfrac{(1.358 \times 10^{-10})\alpha(1-\alpha)(\rho_f - \rho_g)gWe^{1.861}}{(v_g - j)^2}\ for\ We \geq 408{,}000 \end{cases} \quad (296)$$

$$fint = \begin{cases} RELAP\ Calculation\ for\ We \leq 10{,}290 \\ M \times \dfrac{0.0357\alpha(1-\alpha)(\rho_f - \rho_g)gWe^{0.361}}{(v_g - v_f)^2}\ for\ 10{,}290 < We < 408{,}000 \\ M \times \dfrac{(1.358 \times 10^{-10})\alpha(1-\alpha)(\rho_f - \rho_g)gWe^{1.861}}{(v_g - v_f)^2}\ for\ We \geq 408{,}000 \end{cases} \quad (297)$$

where *M* represents the percentage multiplier that is being applied in each test case.

The errors of each of the multipliers with the Weber number correlation will be compared in table form first, before selecting the most accurate multiplier for graphical analysis of data plots. One interesting note in looking at all of the data is that when RELAP [40] is recompiled with the multiplier, it was noticed that for all multipliers that transient errors occurred for three fewer air-water cases with each multiplier than had occurred when the unmodified Weber number correlation was used. As a result, each case of the parametric study has 92 air-water data points and 161 total data points to compare results against, rather than 89 air-water data points and 158 total data points which had been the case for the original Weber number correlation. It is not clear at this time why the original Weber number correlation had three more data points trigger transient errors, as the only change in the source code and model was the addition of the

multiplier. The data points with which transient errors occurred were all test cases with high observed void fraction values, and the same data points triggered transient errors for all multipliers.

In Table 21, the errors with respect to the observed and calculated data of the original RELAP model [40] and 50% of the Weber number correlation are given. In general, it is shown that when the interphase friction calculation of the Weber number correlation is reduced by 50%, RELAP produces a less accurate modeling of the observed conditions as the errors are larger for the pressure gradient, void fraction and vapor velocity. The mean average error of the liquid velocity only appears to be an improvement over the original RELAP model because the error of an outlier has diminished significantly, but the median error for liquid velocity has increased. When compared to the results in Table 18, we find that the 50% Weber number correlation has higher average errors than the unmodified Weber number correlation.

Table 22 shows how 75% of the Weber number correlation compares to the original RELAP model [40]. At 75%, as was the case at 50% in Table 21, the Weber number correlation produces greater errors with respect to the observed pressure gradient, void fraction and vapor velocity than the original RELAP model, and the decreased liquid velocity mean average error can be attributed to the sharp decrease in error of an outlier. In comparison to the errors produced by the unmodified Weber number correlation in Table 18, the Weber number correlation at 75% produces higher errors for pressure gradient, void fraction and the phasic velocities.

Table 21: Comparison of Errors of the Original RELAP5/MOD3.3 Model [40] to 50% of the Weber Number Correlation

	Total		Original RELAP					50% Weber Correlation				
			dP/dz	α	v_f	v_g	F_{int}	dP/dz	α	v_f	v_g	F_{int}
All Annular	161	Mean Average	27.89%	4.58%	81.96%	4.59%	106.56%	108.40%	28.74%	59.29%	42.54%	116.50%
		Median Average	18.82%	3.78%	26.26%	3.60%	29.95%	103.86%	33.93%	61.08%	45.72%	64.33%
		± 20%	85	159	56	157	53	14	38	9	42	17
		- Percentage	52.80%	98.76%	34.78%	97.52%	32.92%	8.70%	23.60%	5.59%	26.09%	10.56%
		± 50%	129	161	122	161	127	35	161	33	87	60
		- Percentage	80.12%	100.00%	75.78%	100.00%	78.88%	21.74%	100.00%	20.50%	54.04%	37.27%
		Maximum	113.29%	42.36%	2816.63%	27.78%	2965.69%	403.18%	49.32%	202.26%	96.82%	5849.47%
Air-Water	92	Mean Average	14.31%	3.38%	112.88%	2.95%	83.42%	73.42%	24.33%	53.17%	32.72%	54.72%
		Median Average	12.17%	3.10%	31.24%	2.48%	19.40%	80.91%	30.11%	58.40%	37.91%	49.49%
		± 20%	76	92	30	92	48	11	29	7	32	15
		- Percentage	82.61%	100.00%	32.61%	100.00%	52.17%	11.96%	31.52%	7.61%	34.78%	16.30%
		± 50%	87	89	58	89	84	27	89	26	61	47
		- Percentage	94.57%	96.74%	63.04%	96.74%	91.30%	29.35%	96.74%	28.26%	66.30%	51.09%
		Maximum	113.29%	8.74%	2816.63%	9.97%	2965.69%	165.75%	43.77%	202.26%	79.68%	135.53%
Steam-Water	69	Mean Average	46.01%	6.17%	40.72%	6.77%	137.42%	155.03%	34.63%	67.46%	55.63%	198.87%
		Median Average	47.61%	4.77%	22.14%	6.14%	46.86%	148.12%	38.35%	68.24%	59.90%	99.98%
		± 20%	9	67	26	65	5	3	9	2	10	2
		- Percentage	13.04%	97.10%	37.68%	94.20%	7.25%	4.35%	13.04%	2.90%	14.49%	2.90%
		± 50%	40	70	62	70	41	7	70	5	24	11
		- Percentage	57.97%	101.45%	89.86%	101.45%	59.42%	10.14%	101.45%	7.25%	34.78%	15.94%
		Maximum	99.95%	42.36%	660.97%	27.78%	2335.38%	403.18%	49.32%	94.91%	96.82%	5849.47%

When the Weber number correlation is multiplied by 125%, the predictions of the model improve over the original Weber number correlation, and yield modestly favorable results for improving upon the original RELAP model [40], as shown in Table 23. While increasing the Weber number correlation has increased the liquid velocity mean average error from the original Weber number correlation, it has improved the median error. At 125% of the Weber number correlation, the most noticeable improvements over the unmodified Weber number correlation is the pressure gradient and void fraction, and with more improvements noticed with the steam-water data than with the air-water data.

Table 22: Comparison of Errors of the Original RELAP5/MOD3.3 Model [40] to 75% of the Weber Number Correlation

			Original RELAP					75% Weber Correlation				
	Total		dP/dz	α	v_f	v_g	F_{int}	dP/dz	α	v_f	v_g	F_{int}
All Annular	161	Mean Average	27.89%	4.58%	81.96%	4.59%	106.56%	67.32%	15.69%	46.64%	19.81%	66.81%
		Median Average	18.82%	3.78%	26.26%	3.60%	29.95%	58.47%	16.56%	44.13%	17.21%	48.12%
		± 20%	85	159	56	157	53	22	105	18	96	22
		- Percentage	52.80%	98.76%	34.78%	97.52%	32.92%	13.66%	65.22%	11.18%	59.63%	13.66%
		± 50%	129	161	122	161	127	65	161	96	155	84
		- Percentage	80.12%	100.00%	75.78%	100.00%	78.88%	40.37%	100.00%	59.63%	96.27%	52.17%
		Maximum	113.29%	42.36%	2816.63%	27.78%	2965.69%	313.41%	48.65%	284.88%	93.69%	1295.18%
Air-Water	92	Mean Average	14.31%	3.38%	112.88%	2.95%	83.42%	41.55%	11.05%	37.78%	13.62%	36.11%
		Median Average	12.17%	3.10%	31.24%	2.48%	19.40%	45.21%	9.73%	36.40%	9.35%	37.16%
		± 20%	76	92	30	92	48	16	77	17	72	20
		- Percentage	82.61%	100.00%	32.61%	100.00%	52.17%	17.39%	83.70%	18.48%	78.26%	21.74%
		± 50%	87	89	58	89	84	55	89	79	88	69
		- Percentage	94.57%	96.74%	63.04%	96.74%	91.30%	59.78%	96.74%	85.87%	95.65%	75.00%
		Maximum	113.29%	8.74%	2816.63%	9.97%	2965.69%	83.83%	40.32%	284.88%	71.41%	99.99%
Steam-Water	69	Mean Average	46.01%	6.17%	40.72%	6.77%	137.42%	101.69%	21.88%	58.46%	28.07%	107.74%
		Median Average	47.61%	4.77%	22.14%	6.14%	46.86%	107.78%	23.13%	56.32%	27.83%	67.67%
		± 20%	9	67	26	65	5	6	28	1	24	2
		- Percentage	13.04%	97.10%	37.68%	94.20%	7.25%	8.70%	40.58%	1.45%	34.78%	2.90%
		± 50%	40	70	62	70	41	9	70	17	65	13
		- Percentage	57.97%	101.45%	89.86%	101.45%	59.42%	13.04%	101.45%	24.64%	94.20%	18.84%
		Maximum	99.95%	42.36%	660.97%	27.78%	2335.38%	313.41%	48.65%	149.29%	93.69%	1295.18%

At 150% of the Weber number correlation, a trend is noticed that as the Weber number correlation is increased in magnitude, the errors in pressure gradient, void fraction and interphase friction decrease, when comparing the errors in Table 24 with those in Table 23. The gains that are made by increasing the Weber number correlation by 150% appear to largely be made with the steam-water data. For steam-water, the mean and median errors for pressure gradient, void fraction, the phasic velocities and interphase friction force are all improvements over the existing RELAP model [40], and are also significantly improved over the prediction at 125% of the Weber number correlation.

Table 23: Comparison of Errors of the Original RELAP5/MOD3.3 Model [40] to 125% of the Weber Number Correlation

			Original RELAP					125% Weber Correlation				
	Total		dP/dz	α	v_f	v_g	F_{int}	dP/dz	α	v_f	v_g	F_{int}
All Annular	161	Mean Average	27.89%	4.58%	81.96%	4.59%	106.56%	31.40%	4.36%	35.73%	5.44%	51.22%
		Median Average	18.82%	3.78%	26.26%	3.60%	29.95%	25.44%	2.73%	21.26%	2.79%	34.14%
		± 20%	85	159	56	157	53	56	156	75	154	32
		- Percentage	52.80%	98.76%	34.78%	97.52%	32.92%	34.78%	96.89%	46.58%	95.65%	19.88%
		± 50%	129	161	122	161	127	133	161	135	159	130
		- Percentage	80.12%	100.00%	75.78%	100.00%	78.88%	82.61%	100.00%	83.85%	98.76%	80.75%
		Maximum	113.29%	42.36%	2816.63%	27.78%	2965.69%	216.99%	39.49%	421.56%	55.02%	1207.23%
Air-Water	92	Mean Average	14.31%	3.38%	112.88%	2.95%	83.42%	20.65%	2.76%	39.55%	4.68%	28.66%
		Median Average	12.17%	3.10%	31.24%	2.48%	19.40%	20.75%	2.13%	22.69%	2.71%	26.74%
		± 20%	76	92	30	92	48	44	91	41	89	25
		- Percentage	82.61%	100.00%	32.61%	100.00%	52.17%	47.83%	98.91%	44.57%	96.74%	27.17%
		± 50%	87	89	58	89	84	87	89	71	89	82
		- Percentage	94.57%	96.74%	63.04%	96.74%	91.30%	94.57%	96.74%	77.17%	96.74%	89.13%
		Maximum	113.29%	8.74%	2816.63%	9.97%	2965.69%	81.48%	20.34%	421.56%	30.40%	76.42%
Steam-Water	69	Mean Average	46.01%	6.17%	40.72%	6.77%	137.42%	45.73%	6.50%	30.64%	6.46%	81.29%
		Median Average	47.61%	4.77%	22.14%	6.14%	46.86%	44.25%	4.07%	20.22%	3.18%	45.67%
		± 20%	9	67	26	65	5	12	65	34	65	7
		- Percentage	13.04%	97.10%	37.68%	94.20%	7.25%	17.39%	94.20%	49.28%	94.20%	10.14%
		± 50%	40	70	62	70	41	44	70	62	68	47
		- Percentage	57.97%	101.45%	89.86%	101.45%	59.42%	63.77%	101.45%	89.86%	98.55%	68.12%
		Maximum	99.95%	42.36%	660.97%	27.78%	2335.38%	216.99%	39.49%	315.95%	55.02%	1207.23%

Increasing the multiplier of the Weber number correlation to 175% shows that the trends noticed at 150% have a limit. While the errors for the pressure gradient and interphase friction force prediction have continued to decrease, the mean and median errors of the void fraction, liquid velocity and vapor velocity increased, when comparing the errors reported in Table 25 with Table 24. The 175% multiplier does still appear to be a viable improvement of the original RELAP model [40], particularly for the pressure gradient, but the void fraction and phasic velocities, it does not appear to give a better overall prediction than the 150% multiplier.

Table 24: Comparison of Errors of the Original RELAP5/MOD3.3 Model [40] to 150% of the Weber Number Correlation

	Total		Original RELAP					150% Weber Correlation				
			dP/dz	α	v_f	v_g	F_{int}	dP/dz	α	v_f	v_g	F_{int}
All Annular	161	Mean Average	27.89%	4.58%	81.96%	4.59%	106.56%	23.97%	4.03%	45.93%	4.66%	44.53%
		Median Average	18.82%	3.78%	26.26%	3.60%	29.95%	20.75%	2.80%	27.15%	2.93%	29.91%
		± 20%	85	159	56	157	53	78	158	63	155	39
		- Percentage	52.80%	98.76%	34.78%	97.52%	32.92%	48.45%	98.14%	39.13%	96.27%	24.22%
		± 50%	129	161	122	161	127	147	161	117	161	139
		- Percentage	80.12%	100.00%	75.78%	100.00%	78.88%	91.30%	100.00%	72.67%	100.00%	86.34%
		Maximum	113.29%	42.36%	2816.63%	27.78%	2965.69%	91.15%	41.50%	481.83%	46.35%	1175.55%
Air-Water	92	Mean Average	14.31%	3.38%	112.88%	2.95%	83.42%	17.77%	4.03%	61.11%	5.32%	27.68%
		Median Average	12.17%	3.10%	31.24%	2.48%	19.40%	16.50%	3.43%	42.68%	4.17%	26.48%
		± 20%	76	92	30	92	48	61	92	14	89	27
		- Percentage	82.61%	100.00%	32.61%	100.00%	52.17%	66.30%	100.00%	15.22%	96.74%	29.35%
		± 50%	87	89	58	89	84	87	89	51	89	83
		- Percentage	94.57%	96.74%	63.04%	96.74%	91.30%	94.57%	96.74%	55.43%	96.74%	90.22%
		Maximum	113.29%	8.74%	2816.63%	9.97%	2965.69%	80.48%	12.59%	481.83%	20.15%	78.04%
Steam-Water	69	Mean Average	46.01%	6.17%	40.72%	6.77%	137.42%	32.24%	4.03%	25.69%	3.79%	67.00%
		Median Average	47.61%	4.77%	22.14%	6.14%	46.86%	31.22%	1.90%	10.64%	1.57%	38.63%
		± 20%	9	67	26	65	5	17	66	49	66	12
		- Percentage	13.04%	97.10%	37.68%	94.20%	7.25%	24.64%	95.65%	71.01%	95.65%	17.39%
		± 50%	40	70	62	70	41	58	70	64	70	54
		- Percentage	57.97%	101.45%	89.86%	101.45%	59.42%	84.06%	101.45%	92.75%	101.45%	78.26%
		Maximum	99.95%	42.36%	660.97%	27.78%	2335.38%	91.15%	41.50%	395.71%	46.35%	1175.55%

Lastly, in Table 26, the errors of the original RELAP model [40] are compared to the errors of the Weber correlation when multiplied by 200%. For all annular flow data points, the 200% Weber number correlation provides an improved prediction of the pressure gradient and interphase friction force, but does not fare as well with the void fraction and the phasic velocities. The 200% Weber number correlation is not as accurate with the void fraction as the 150% Weber number correlation proved to be, and the pressure gradient prediction is not significantly better than the prediction with the 150% Weber number correlation model. It also appears that with increasing the Weber number correlation, the error in the liquid velocity is

increasing, further demonstrating that the best multiplier for the Weber number correlation is 150%.

Table 25: Comparison of Errors of the Original RELAP5/MOD3.3 Model [40] to 175% of the Weber Number Correlation

			Original RELAP					175% Weber Correlation				
	Total		dP/dz	α	v_f	v_g	F_{int}	dP/dz	α	v_f	v_g	F_{int}
All Annular	161	Mean Average	27.89%	4.58%	81.96%	4.59%	106.56%	20.77%	5.05%	62.27%	5.51%	42.88%
		Median Average	18.82%	3.78%	26.26%	3.60%	29.95%	17.67%	4.04%	42.72%	4.34%	27.92%
		± 20%	85	159	56	157	53	88	158	44	155	47
		- Percentage	52.80%	98.76%	34.78%	97.52%	32.92%	54.66%	98.14%	27.33%	96.27%	29.19%
		± 50%	129	161	122	161	127	156	161	95	161	142
		- Percentage	80.12%	100.00%	75.78%	100.00%	78.88%	96.89%	100.00%	59.01%	100.00%	88.20%
		Maximum	113.29%	42.36%	2816.63%	27.78%	2965.69%	80.14%	42.90%	538.47%	40.50%	1191.47%
Air-Water	92	Mean Average	14.31%	3.38%	112.88%	2.95%	83.42%	16.50%	5.53%	83.33%	6.38%	26.96%
		Median Average	12.17%	3.10%	31.24%	2.48%	19.40%	14.39%	5.60%	66.45%	5.82%	25.79%
		± 20%	76	92	30	92	48	62	92	10	89	31
		- Percentage	82.61%	100.00%	32.61%	100.00%	52.17%	67.39%	100.00%	10.87%	96.74%	33.70%
		± 50%	87	89	58	89	84	87	89	33	89	84
		- Percentage	94.57%	96.74%	63.04%	96.74%	91.30%	94.57%	96.74%	35.87%	96.74%	91.30%
		Maximum	113.29%	8.74%	2816.63%	9.97%	2965.69%	80.14%	12.89%	538.47%	13.52%	79.25%
Steam-Water	69	Mean Average	46.01%	6.17%	40.72%	6.77%	137.42%	26.46%	4.41%	34.18%	4.35%	64.11%
		Median Average	47.61%	4.77%	22.14%	6.14%	46.86%	24.46%	2.61%	20.94%	2.65%	34.31%
		± 20%	9	67	26	65	5	26	66	34	66	16
		- Percentage	13.04%	97.10%	37.68%	94.20%	7.25%	37.68%	95.65%	49.28%	95.65%	23.19%
		± 50%	40	70	62	70	41	67	70	60	70	56
		- Percentage	57.97%	101.45%	89.86%	101.45%	59.42%	97.10%	101.45%	86.96%	101.45%	81.16%
		Maximum	99.95%	42.36%	660.97%	27.78%	2335.38%	77.69%	42.90%	472.51%	40.50%	1191.47%

Based on the errors reported in Table 18 and Table 21 through Table 26, the multiplier that appears to give the prediction that best matches the observed data and improves RELAP is 150%. As Table 24 shows, the errors for both the pressure gradient and void fraction are improved over the original RELAP model [40] at 150% of the Weber number correlation.

Table 26: Comparison of Errors of the Original RELAP5/MOD3.3 Model [40] to 200% of the Weber Number Correlation

			Original RELAP					200% Weber Correlation				
	Total		dP/dz	α	v_f	v_g	F_{int}	dP/dz	α	v_f	v_g	F_{int}
All Annular	161	Mean Average	27.89%	4.58%	81.96%	4.59%	106.56%	18.94%	6.04%	80.04%	6.42%	40.38%
		Median Average	18.82%	3.78%	26.26%	3.60%	29.95%	15.96%	4.83%	58.85%	5.45%	26.56%
		± 20%	85	159	56	157	53	97	158	23	155	50
		- Percentage	52.80%	98.76%	34.78%	97.52%	32.92%	60.25%	98.14%	14.29%	96.27%	31.06%
		± 50%	129	161	122	161	127	156	161	69	161	146
		- Percentage	80.12%	100.00%	75.78%	100.00%	78.88%	96.89%	100.00%	42.86%	100.00%	90.68%
		Maximum	113.29%	42.36%	2816.63%	27.78%	2965.69%	79.81%	43.94%	592.14%	36.27%	1175.56%
Air-Water	92	Mean Average	14.31%	3.38%	112.88%	2.95%	83.42%	15.90%	6.71%	105.57%	7.20%	26.55%
		Median Average	12.17%	3.10%	31.24%	2.48%	19.40%	13.05%	6.69%	87.26%	7.01%	25.49%
		± 20%	76	92	30	92	48	65	92	7	89	32
		- Percentage	82.61%	100.00%	32.61%	100.00%	52.17%	70.65%	100.00%	7.61%	96.74%	34.78%
		± 50%	87	89	58	89	84	87	89	12	89	84
		- Percentage	94.57%	96.74%	63.04%	96.74%	91.30%	94.57%	96.74%	13.04%	96.74%	91.30%
		Maximum	113.29%	8.74%	2816.63%	9.97%	2965.69%	79.81%	14.35%	592.14%	11.84%	80.19%
Steam-Water	69	Mean Average	46.01%	6.17%	40.72%	6.77%	137.42%	22.99%	5.16%	46.00%	5.36%	58.83%
		Median Average	47.61%	4.77%	22.14%	6.14%	46.86%	22.02%	3.54%	33.37%	3.69%	31.24%
		± 20%	9	67	26	65	5	32	66	16	66	18
		- Percentage	13.04%	97.10%	37.68%	94.20%	7.25%	46.38%	95.65%	23.19%	95.65%	26.09%
		± 50%	40	70	62	70	41	67	70	55	70	60
		- Percentage	57.97%	101.45%	89.86%	101.45%	59.42%	97.10%	101.45%	79.71%	101.45%	86.96%
		Maximum	99.95%	42.36%	660.97%	27.78%	2335.38%	75.47%	43.94%	546.23%	36.27%	1175.56%

In Figure 120, the pressure gradient prediction of the original RELAP model is compared to that of the Weber number correlation at 150%. The general trend from the chart shows that the Weber correlation at 150% matches well with the original RELAP model in predicting the pressure gradient, but does not appear to be a very significant improvement over the original RELAP model. However, examining the void fraction predictions in Figure 121 shows that the Weber number correlation at 150% does present a more accurate void fraction prediction, as the data points appear to be more aligned along the equality line with the observed values than the original RELAP model, with a small overprediction for most data points.

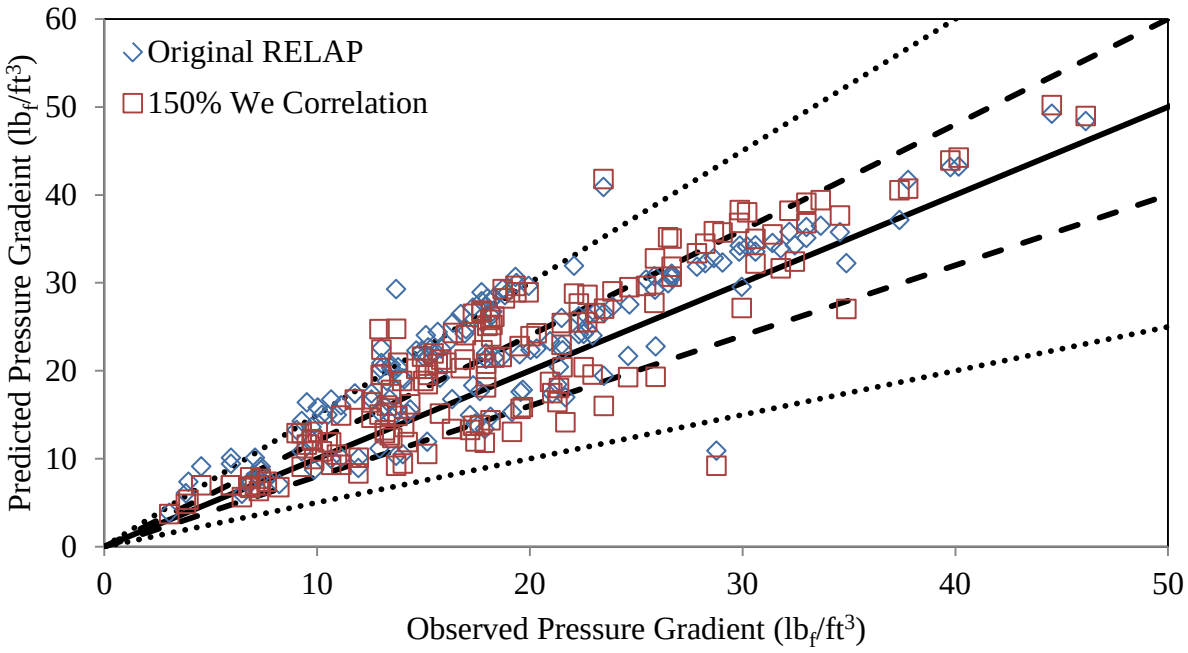

Figure 120: Comparison of Pressure Gradient Prediction of the Original RELAP5/MOD3.3 Model [40] and 150% of the Weber Number Correlation

With the pressure gradient and void fraction predictions showing improvement with the 150% Weber number correlation, the predicted velocities of the liquid and vapor appear to be much closer to their observed values, based on the comparisons made in Figure 122 and Figure 123, respectively.

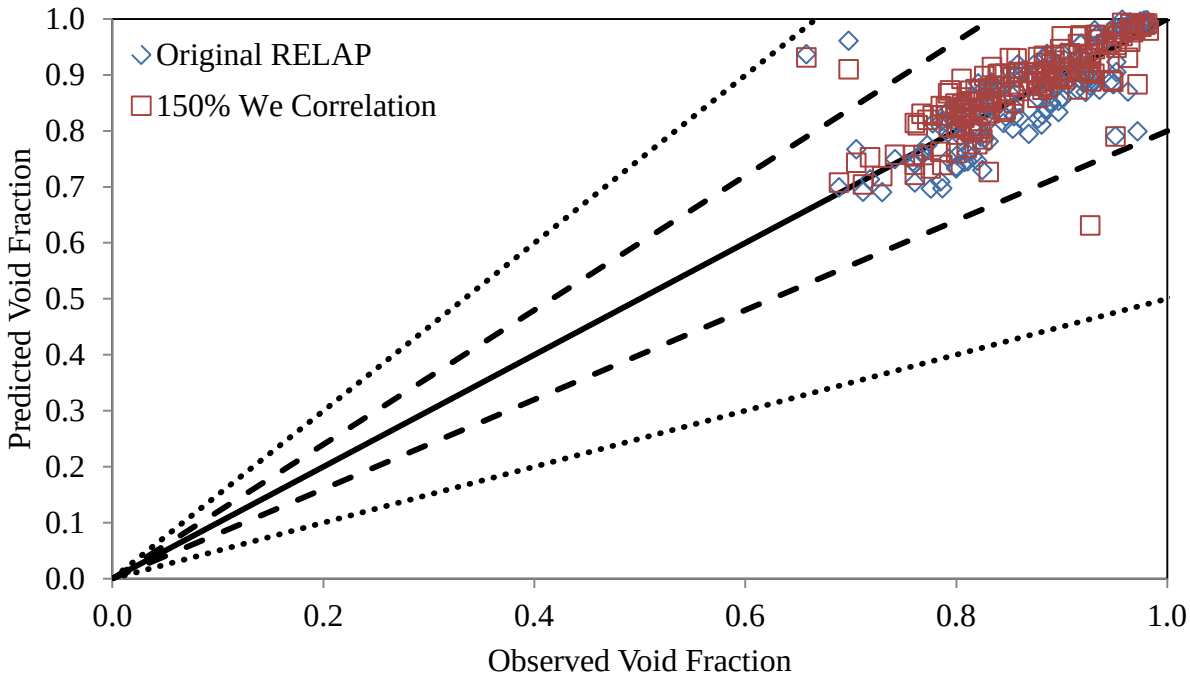

Figure 121: Comparison of the Void Fraction Prediction of the Original RELAP5/MOD3.3 Model [40] and 150% of the Weber Number Correlation

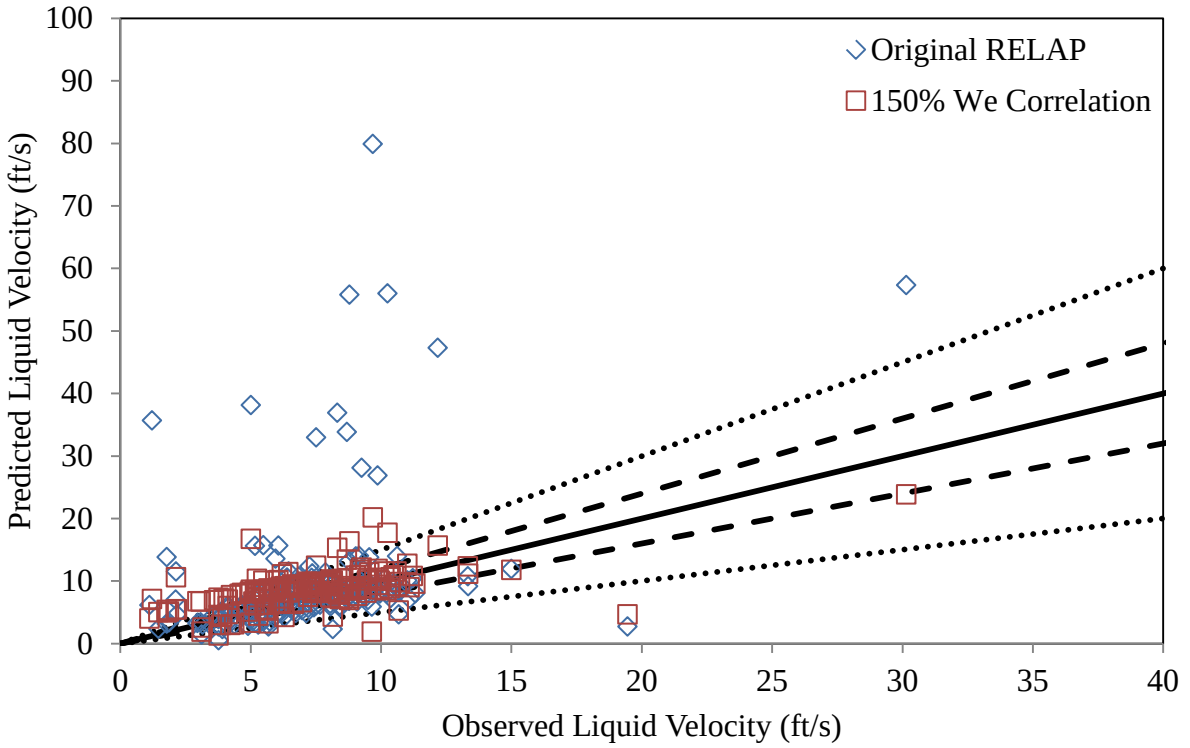

Figure 122: Comparison of the Liquid Velocity Prediction of the Original RELAP5/MOD3.3 Model [40] and 150% of the Weber Number Correlation

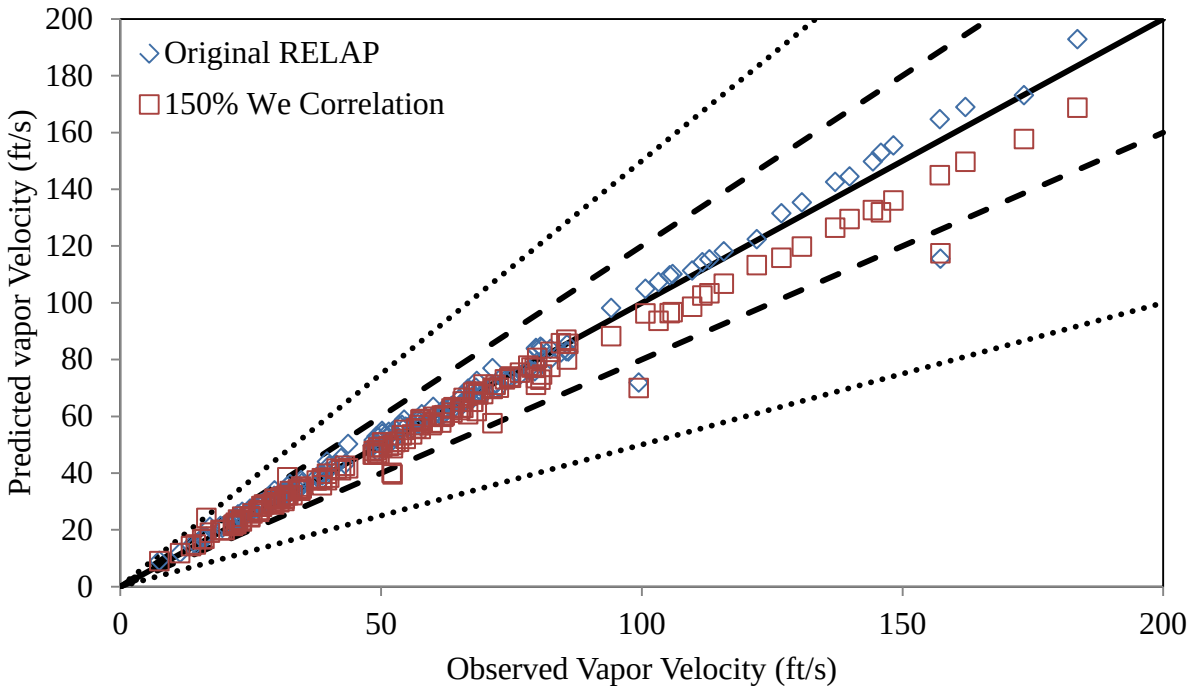

Figure 123: Comparison of the Vapor Velocity Prediction of the Original RELAP5/MOD3.3 Model [40] and 150% of the Weber Number Correlation

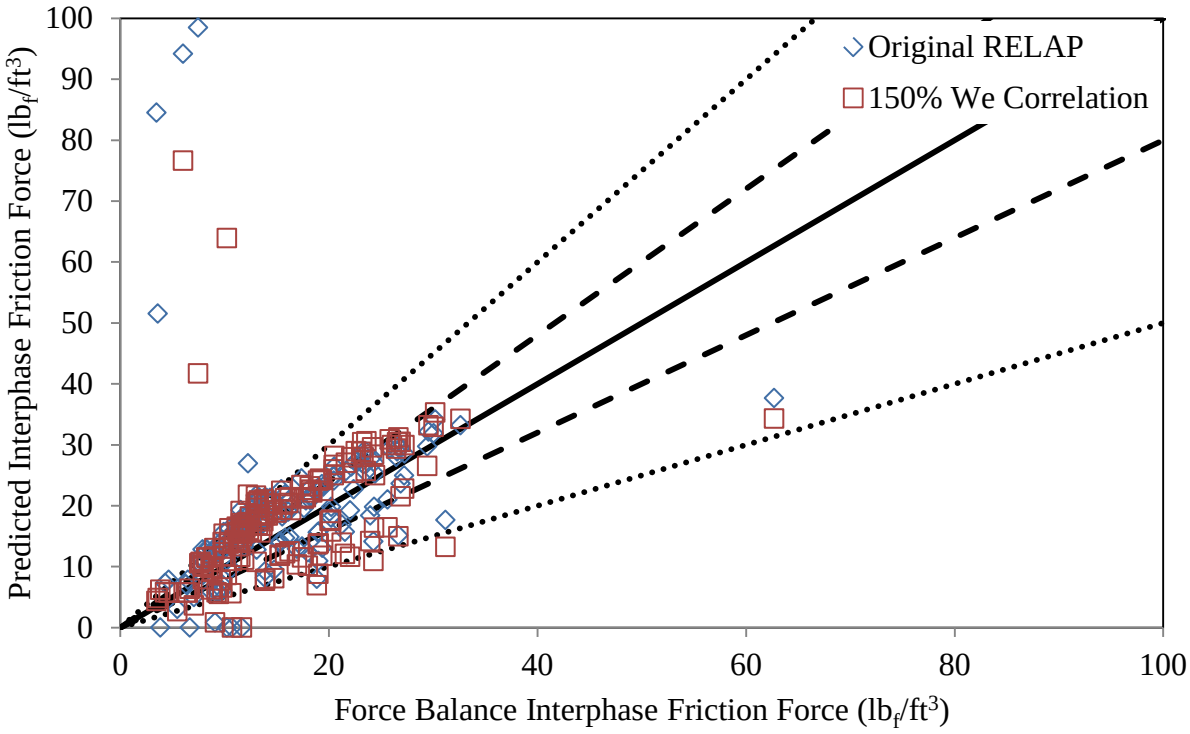

Figure 124: Comparison of the Interphase Friction Force Prediction of the Original RELAP5/MOD3.3 Model [40] and 150% of the Weber Number Correlation

4.5: Analyses of the Annular Flow Physical Models

The development of a general correlation for interphase friction has one significant drawback as it is not accountable to any particular physics of two-phase vertical flow. Instead, the correlation is purely empirical, and does not necessarily represent the best correlation for all scenarios, only those that have been studied. Thus, in addition to developing and testing the general interphase friction force correlations in RELAP5/MOD3.3 [40,69], correlations that have been developed to more directly examine individual phenomena relevant to the interphase friction force and annular flow has been investigated. The correlations that have been chosen for testing were previously discussed in Section 2.4.2.

4.5.1: Analyses of the Interfacial Friction Factor, f_i, Model

First, the interfacial friction factor, f_i, is investigated to determine if any of the correlations that have been developed would improve upon the existing calculations within RELAP5/MOD3.3. The focus of this investigation has been on the interfacial friction factor when the vapor flow is considered turbulent, as defined by Equation 182.

4.5.1.1: The Wallis f_i Correlation

The Wallis [86] f_i correlation serves as the basis for the correlation used in RELAP5/MOD3.3. Assessments of RELAP determined that multiplying the Wallis correlation by a factor of 4 provided the best results for modeling the interphase friction for annular flow. [69] While the Wallis f_i correlation has a lower magnitude than the correlation used in RELAP, the data suggests that in many cases the interphase friction force is increased rather than decreased.

Beginning with the pressure gradient prediction in Figure 126, it appears that the Wallis [86] correlation leads to an overprediction of the pressure gradient for many data points, both with respect to the observed value and that of the original RELAP, although for a select few, the pressure gradient is underpredicted. This corresponds with a trend of underpredicting the void fraction for most data points, with a few having the void fraction overpredicted, as noticed in Figure 127. Decreased void fraction values would indicate more liquid in the test section, implying a reduced liquid velocity in order to ensure continuity, and can be seen for most data points in Figure 128. Additionally, this should increase the velocity of the vapor, which is seen to take place in Figure 129 only for cases where the observed vapor velocity is less than 85 ft/s. Data points where the observed vapor velocity is greater than 85 ft/s, and show a slight underprediction of vapor velocity in Figure 129 correspond to data points with overpredicted liquid velocity in Figure 128, overpredicted void fraction in Figure 127 and underpredicted pressure gradient in Figure 126.

If all other parameters were held constant, the modification of RELAP with the Wallis [86] interfacial friction factor would produce a decrease in the interphase friction force, as the Wallis correlation has a lower magnitude than the original RELAP correlation. However, when considering the impact that this would carry on other parameters, as RELAP does, we find that it is not so simple, as the interphase friction force may both increase or decrease as a result of the correlation.

A decreased interfacial friction factor implies that at first, the vapor core should be able to be able to move faster with respect to the liquid film and a faster vapor core with slower liquid film would ultimately mean a higher interphase friction force. As the interphase friction force increases, the disturbance waves of the liquid film would become more pronounced, and break

off producing more entrained droplets within the vapor core. More entrained droplets would imply a higher liquid velocity, which would then lower the overall interphase friction force. Thus, it is possible for the Wallis correlation to produce mixed results.

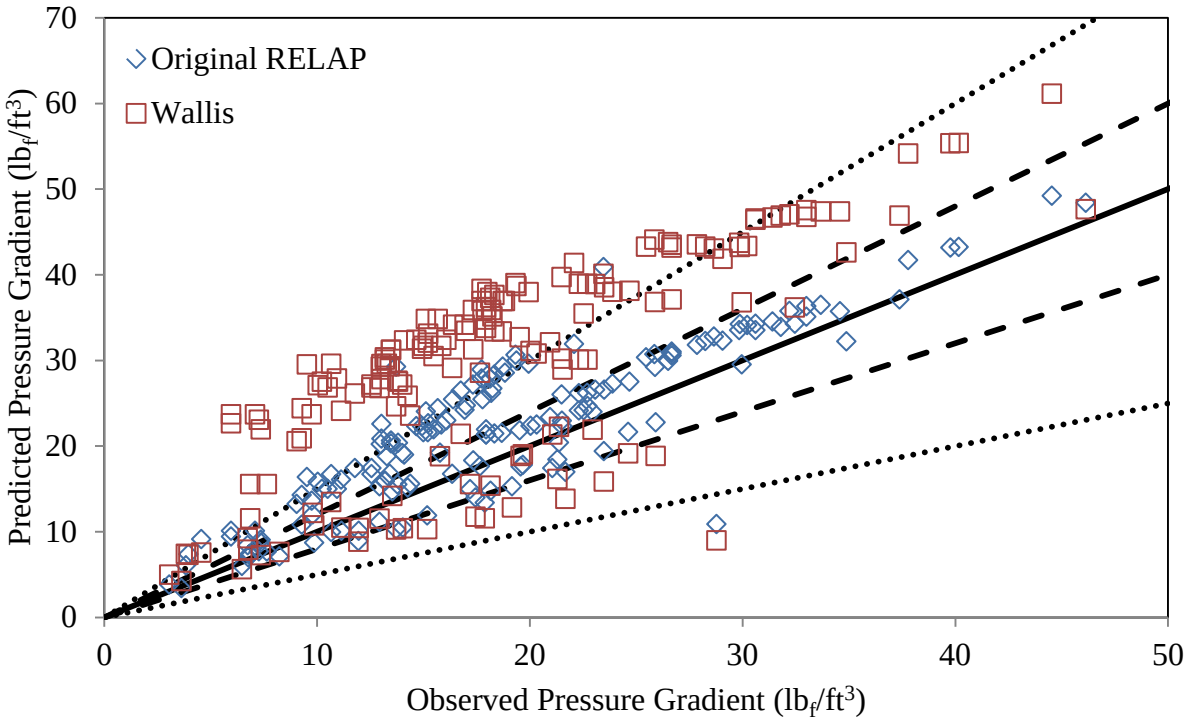

Figure 125: Comparison of the Pressure Gradient Prediction using the RELAP5/MOD3.3 [40] Interfacial Friction Factor Correlation to the Wallis [86] Interfacial Friction Factor Correlation

Based on the observations of the Wallis [86] correlation modified RELAP data, it appears that for cases where the observed void fraction was less than 0.95, RELAP expects the decrease in interphase friction between the vapor core and liquid film to result in a thicker liquid film with fewer emulsions. This would explain the lower void fractions and decreased liquid velocity. With more liquid film along the wall, and fewer entrained droplets, the vapor core has a higher velocity, and this produces a higher interphase friction force, as seen in Figure 130.

When the observed void fraction is greater than 0.95, the Wallis [86] modified RELAP follows a different flow pattern. An increased void fraction means that there is more vapor

within the test section, and combined with higher liquid velocities, implies that the liquid film is thinner, with a greater amount of liquid being entrained as droplets in the vapor core. With a higher void fraction, the vapor velocity decreases, and the resulting difference in phasic velocities produces a smaller interphase friction force, which appears as the few underpredicted data points in Figure 130.

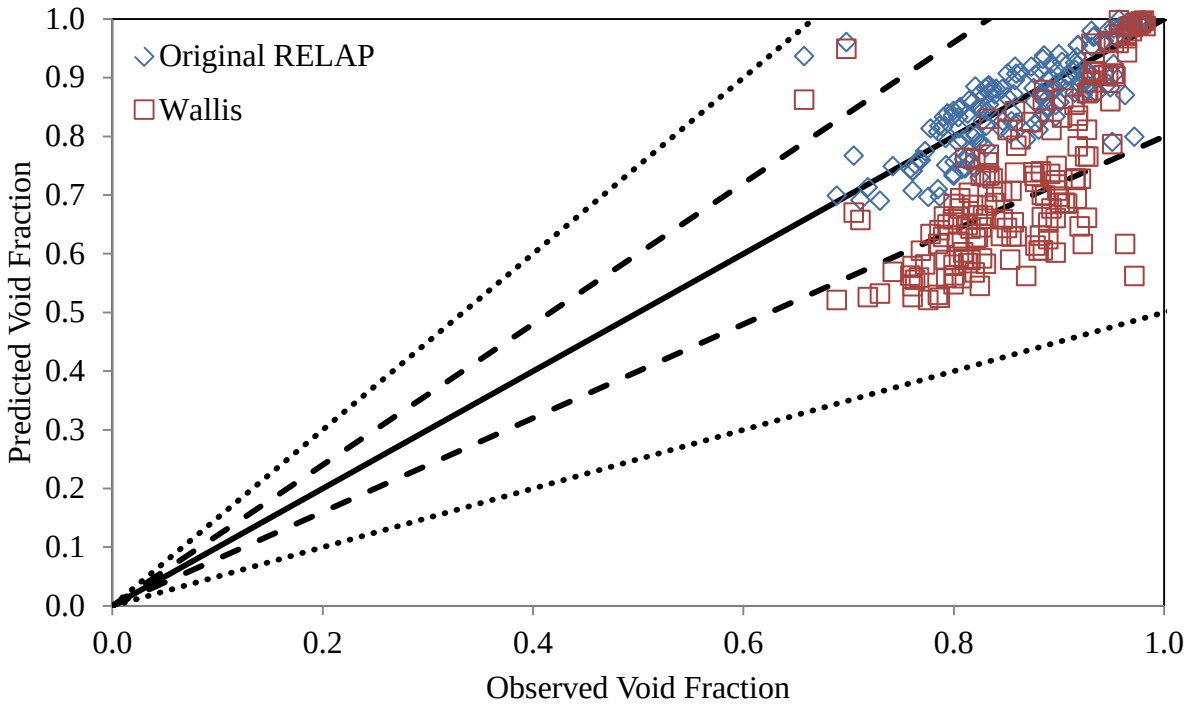

Figure 126: Comparison of the Void Fraction Prediction using the RELAP5/MOD3.3 [40] Interfacial Friction Factor Correlation to the Wallis [86] Interfacial Friction Factor Correlation

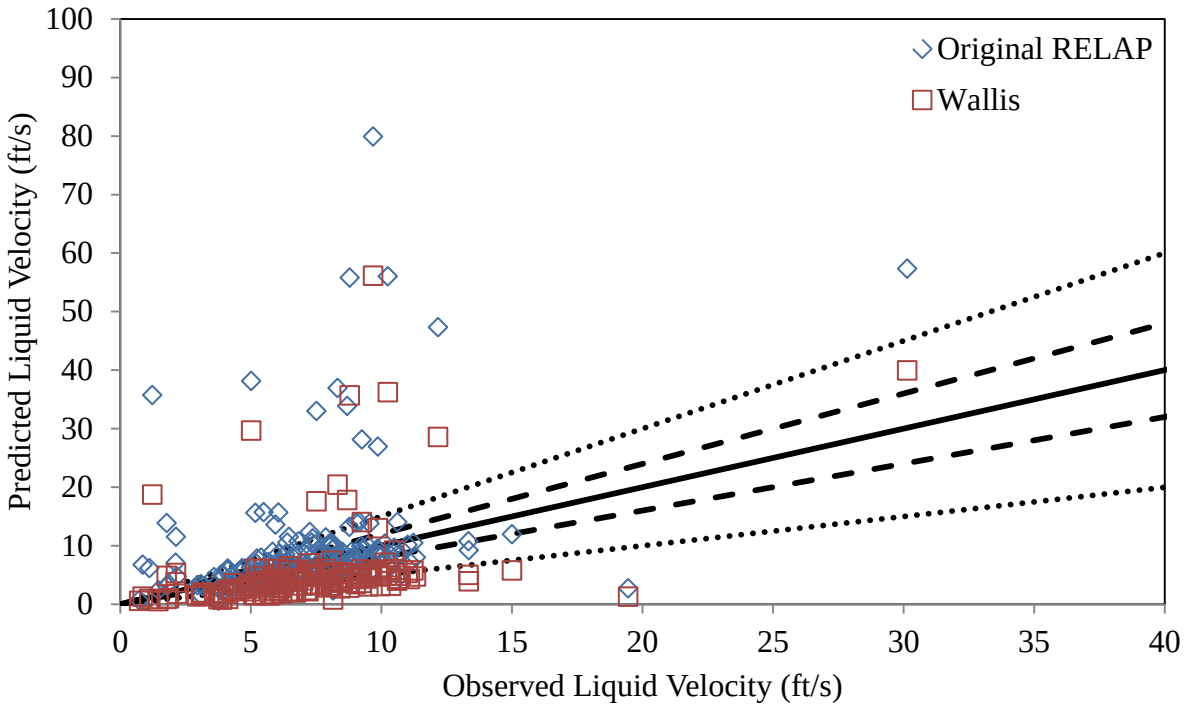

Figure 127: Comparison of the Liquid Velocity Prediction using RELAP5/MOD3.3 [40] Interfacial Friction Factor Correlation to the Wallis [86] Interfacial Friction Factor Correlation

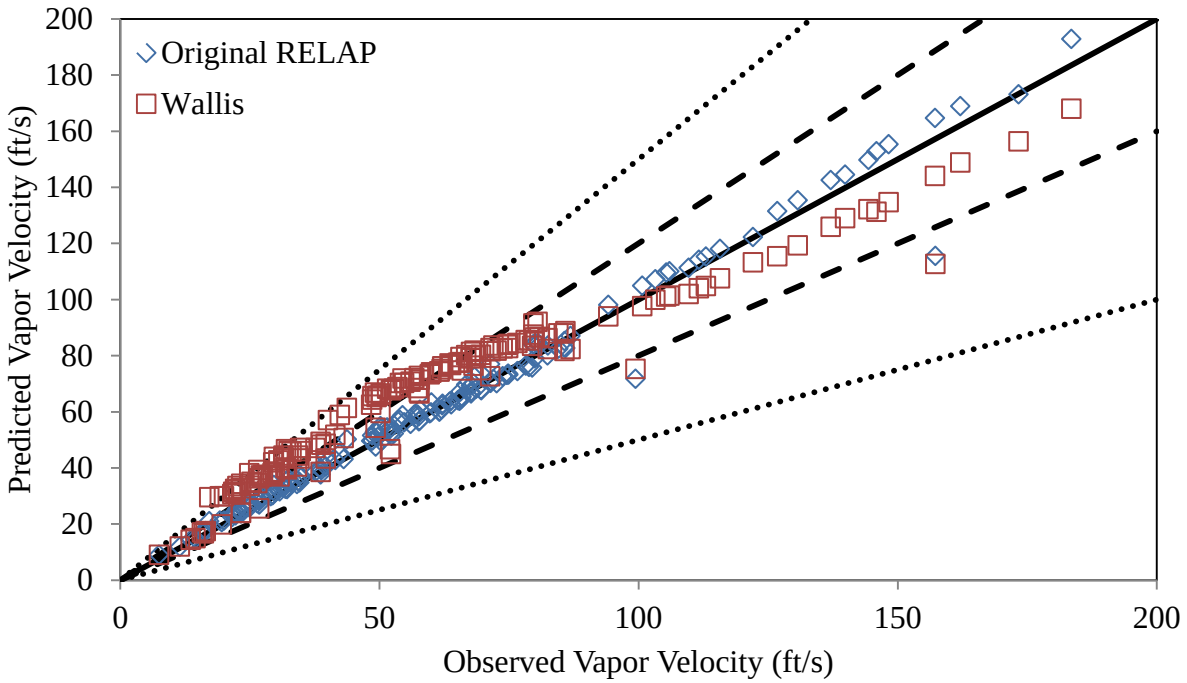

Figure 128: Comparison of the Vapor Velocity Prediction using the RELAP5/MOD3.3 [40] Interfacial Friction Factor Correlation to the Wallis [86] Interfacial Friction Factor Correlation

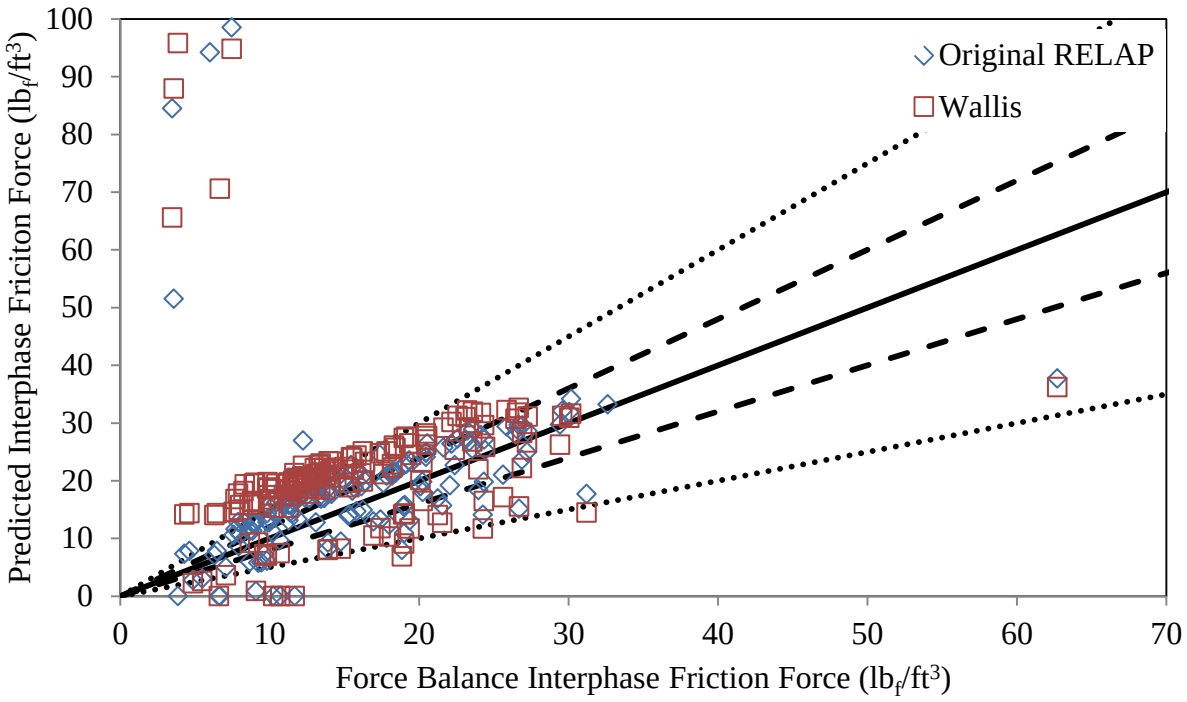

Figure 129: Comparison of the Interphase Friction Force Prediction using the RELAP5/MOD3.3 [40] Interfacial Friction Factor Correlation to the Wallis [86] Interfacial Friction Factor Correlation

As we look at the errors that are produced by both the unmodified RELAP code and the Wallis [86] f_i correlation that has been inserted into the RELAP code in Table 27, the general trend is that there is not an improvement in the RELAP model with the Wallis correlation. The pressure gradient prediction is less accurate with the Wallis correlation by all measures, and only appears to slightly reduce a maximum error for the void fraction. The reduction in the liquid velocity error appears to be largely attributed to reducing the errors of outliers with the original RELAP code, while the errors have increased for the vapor velocity and the interphase friction. It is expected that the Wallis correlation would be less accurate than the original RELAP model, as the original RELAP model is a modified version of the Wallis correlation, based on assessment results. [69]

Table 27: Comparison of Errors of the Original RELAP5/MOD3.3 [40] Interphase Friction Factor Correlation to the Wallis [86] Interphase Friction Factor Correlation

			Original RELAP					Wallis f_i Correlation				
Total			dP/dz	α	v_f	v_g	F_{int}	dP/dz	α	v_f	v_g	F_{int}
All Annular	163	Mean Average	27.74%	4.54%	85.21%	4.53%	106.13%	76.42%	17.23%	67.30%	21.54%	713.41%
		Median Average	18.82%	3.70%	26.26%	3.55%	30.34%	68.59%	18.23%	49.00%	20.08%	51.84%
		± 20%	86	161	57	159	53	20	88	13	79	19
		- Percentage	52.76%	98.77%	34.97%	97.55%	32.52%	12.27%	53.99%	7.98%	48.47%	11.66%
		± 50%	131	163	123	163	128	60	163	85	160	78
		- Percentage	80.37%	100.00%	75.46%	100.00%	78.53%	36.81%	100.00%	52.15%	98.16%	47.85%
		Maximum	113.29%	42.36%	2816.63%	27.78%	2965.69%	297.77%	42.20%	1428.78%	71.86%	34535.95%
Air-Water	94	Mean Average	14.33%	3.35%	117.88%	2.89%	83.17%	52.47%	12.63%	69.24%	15.36%	792.53%
		Median Average	12.17%	3.05%	31.24%	2.44%	19.58%	46.31%	13.29%	41.92%	13.66%	36.02%
		± 20%	77	94	31	94	48	13	70	11	65	18
		- Percentage	81.91%	100.00%	32.98%	100.00%	51.06%	13.83%	74.47%	11.70%	69.15%	19.15%
		± 50%	92	94	62	94	88	50	94	67	94	68
		- Percentage	97.87%	100.00%	65.96%	100.00%	93.62%	53.19%	100.00%	71.28%	100.00%	72.34%
		Maximum	113.29%	8.74%	2816.63%	9.97%	2965.69%	217.38%	30.94%	1428.78%	45.71%	34535.95%
Steam-Water	69	Mean Average	46.01%	6.17%	40.72%	6.77%	137.42%	109.04%	23.50%	64.67%	29.97%	605.62%
		Median Average	47.61%	4.77%	22.14%	6.14%	46.86%	108.26%	25.54%	56.49%	29.91%	72.85%
		± 20%	9	67	26	65	5	7	18	2	14	1
		- Percentage	13.04%	97.10%	37.68%	94.20%	7.25%	10.14%	26.09%	2.90%	20.29%	1.45%
		± 50%	39	69	61	69	40	10	69	18	66	10
		- Percentage	56.52%	100.00%	88.41%	100.00%	57.97%	14.49%	100.00%	26.09%	95.65%	14.49%
		Maximum	99.95%	42.36%	660.97%	27.78%	2335.38%	297.77%	42.20%	491.95%	71.86%	26802.23%

4.5.1.2: The First Fore, Beus and Bauer fi Correlation

The first f_i correlation proposed by Fore et al [26], is simply a shift of the correlation originally proposed by Wallis [86], and is given in Equation 228. Even though the data used by Fore et al suggested that this shift in Wallis correlation matched better than the original correlation, such a shift would not be expected to produce significantly different results when inserted into RELAP.

In Figure 131, we find the pressure gradient prediction of RELAP, modified to use the first Fore et al [26] f_i correlation compared to the original RELAP correlation. Similar to the results with the Wallis [86] correlation shown in Figure 125, we find that the pressure gradient is

generally overpredicted for most points, with a handful of data points experiencing pressure gradient underprediction.

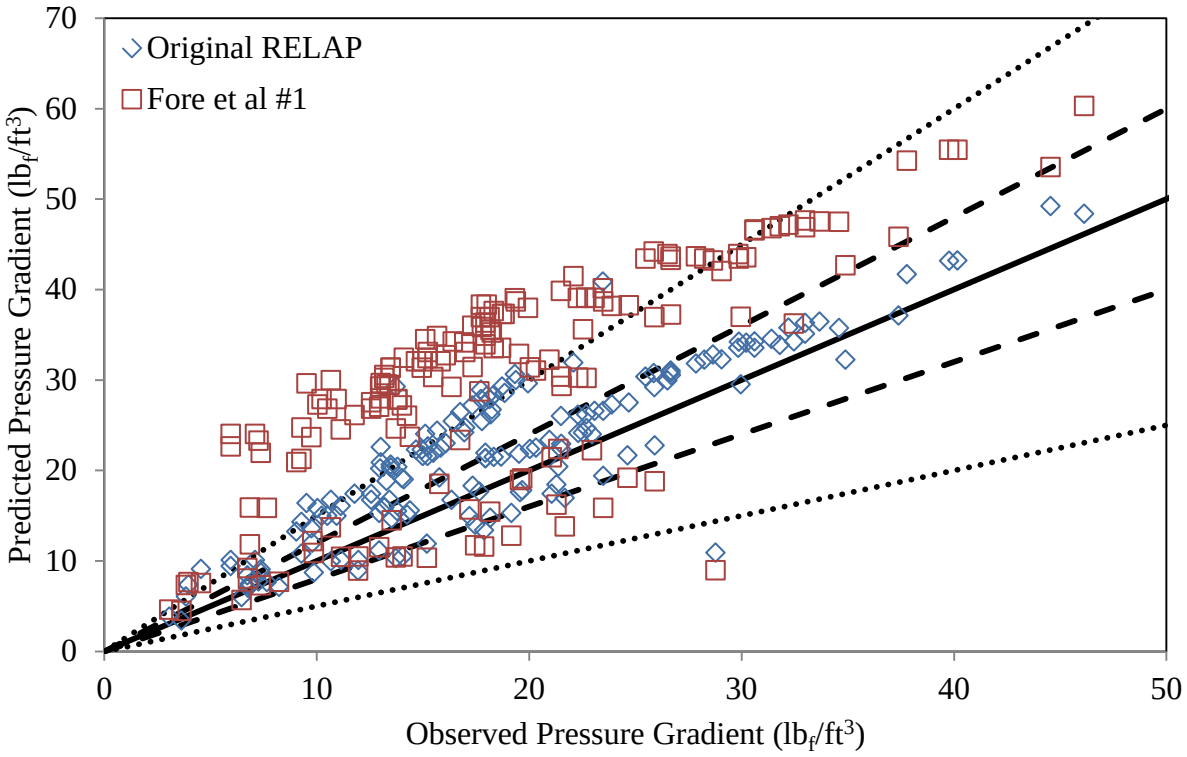

Figure 130: Comparison of the Pressure Gradient Prediction of the RELAP5/MOD3.3 [40] Interfacial Friction Factor Correlation to the First Fore et al [26] Interfacial Friction Factor Correlation

Figure 132 compares the void fraction prediction of the original RELAP with that of RELAP modified by the first Fore et al [26] f_i correlation. As was the case with pressure gradient, the void fraction prediction of RELAP using the first Fore et al f_i correlation is very similar to that seen with the Wallis [86] correlation. The similarities with Wallis correlation results are also noticeable with the liquid velocity shown in Figure 133, the vapor velocity shown in Figure 134 and the interphase friction force shown in Figure 135.

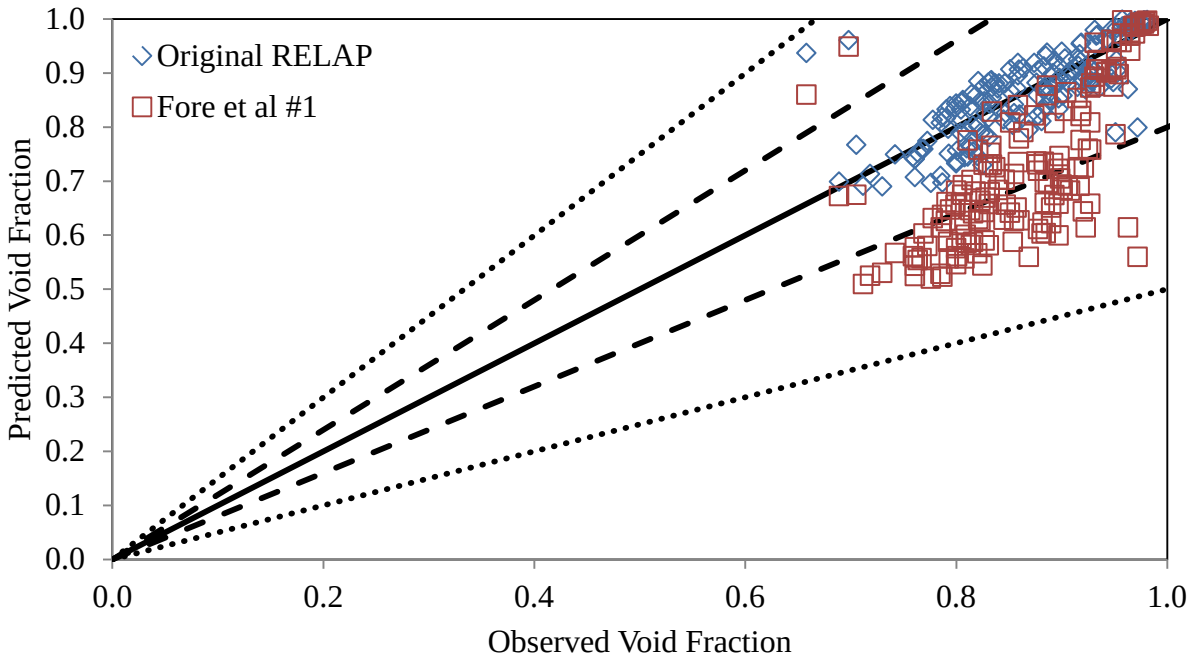

Figure 131: Comparison of the Void Fraction Prediction of the RELAP5/MOD3.3 [40] Interfacial Friction Factor Correlation to the First Fore et al [26] Interfacial Friction Factor Correlation

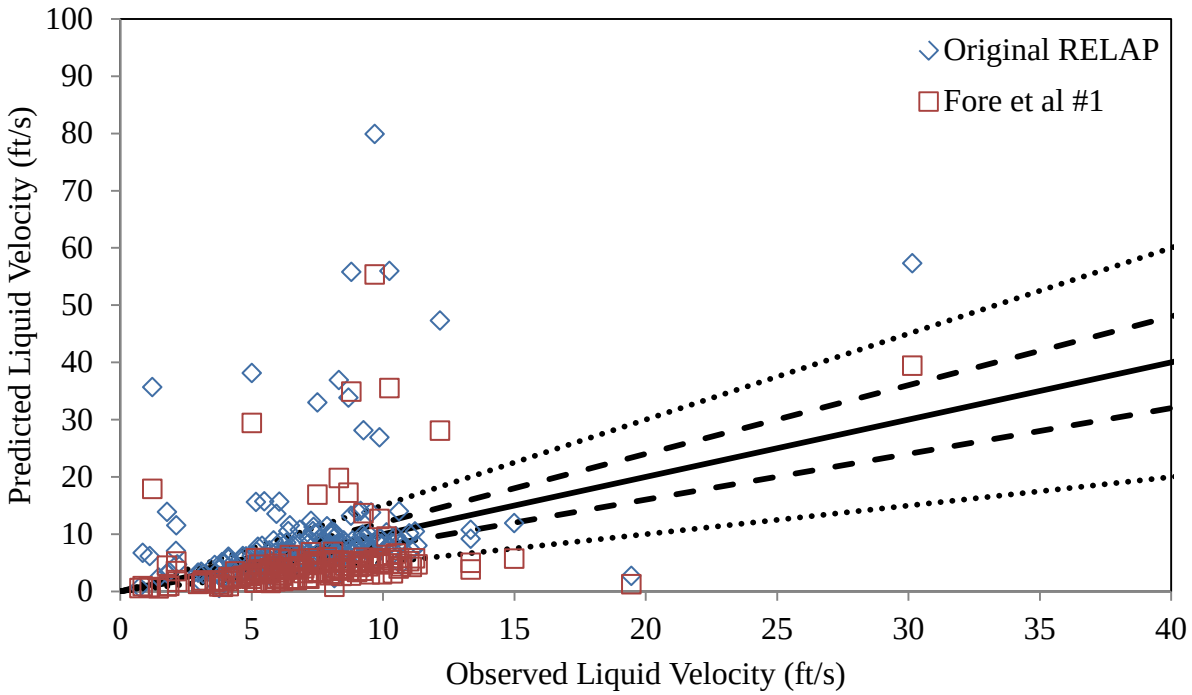

Figure 132: Comparison of the Liquid Velocity Prediction of the RELAP5/MOD3.3 [40] Interfacial Friction Factor Correlation to the First Fore et al [26] Interfacial Friction Factor Correlation

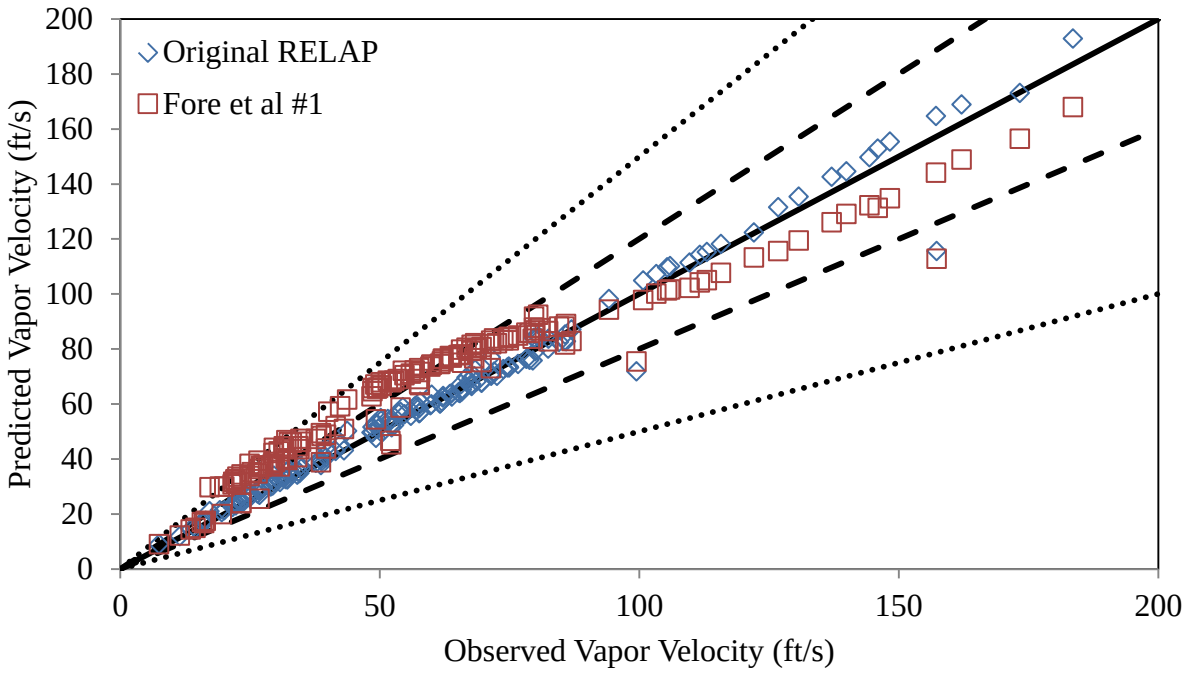

Figure 133: Comparison of the Vapor Velocity Prediction of RELAP5/MOD3.3 [40] Interfacial Friction Factor Correlation to the First Fore et al [26] Interfacial Friction Factor Correlation

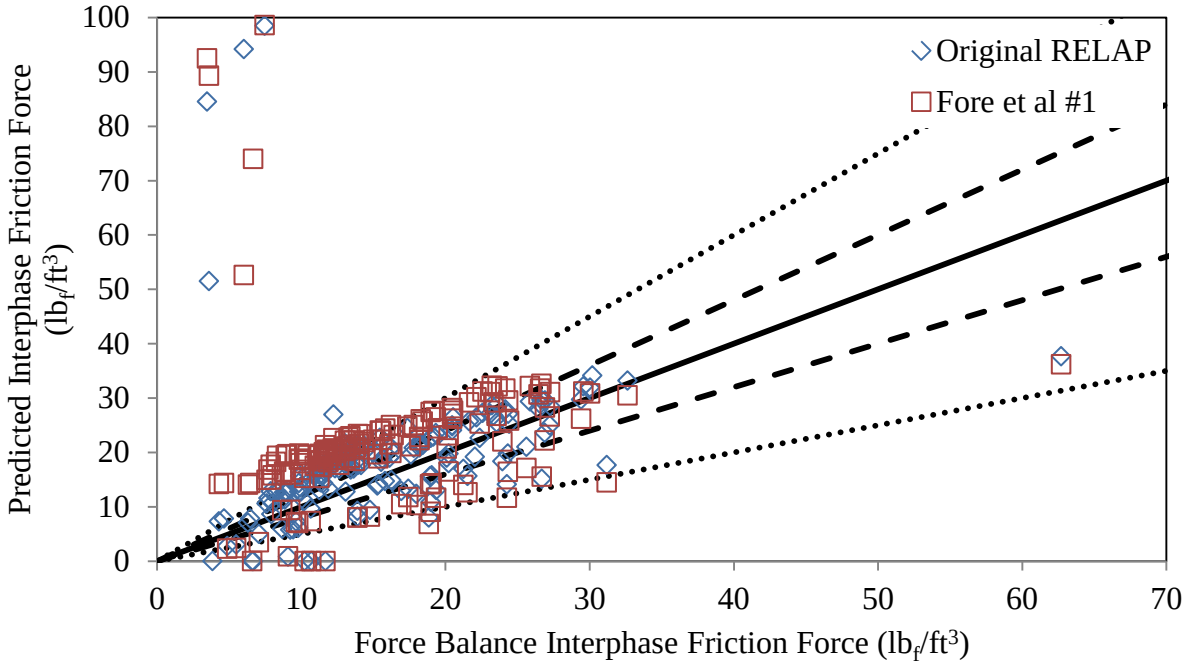

Figure 134: Comparison of the Interphase Friction Force of RELAP5/MOD3.3 [40] Interfacial Friction Factor Correlation to the First Fore et al [26] Interphase Friction Factor Correlation

Table 28 shows the errors that are produced by both the original RELAP f_i correlation compared to the first Fore et al [26] f_i correlation. Similar to the case with the Wallis [86] f_i correlation in Section 4.5.1.1, the first Fore et al correlation with a shift only improves the prediction of the liquid velocity for data points where the original RELAP model was experiencing very high errors.

Table 28: Comparison of Errors of the Original RELAP5/MOD3.3 [40] Interfacial Friction Factor Correlation to the First Fore et al [26] Interfacial Friction Factor Correlation

			Original RELAP					Fore et al f_i Correlation #1				
Total			dP/dz	α	v_f	v_g	F_{int}	dP/dz	α	v_f	v_g	F_{int}
All Annular	163	Mean Average	27.74%	4.54%	85.21%	4.53%	106.13%	77.19%	17.39%	66.62%	21.81%	903.78%
		Median Average	18.82%	3.70%	26.26%	3.55%	30.34%	69.25%	18.52%	48.79%	20.53%	51.89%
		± 20%	86	161	57	159	53	18	88	12	76	20
		- Percentage	52.76%	98.77%	34.97%	97.55%	32.52%	11.04%	53.99%	7.36%	46.63%	12.27%
		± 50%	131	163	123	163	128	60	163	84	160	77
		- Percentage	80.37%	100.00%	75.46%	100.00%	78.53%	36.81%	100.00%	51.53%	98.16%	47.24%
		Maximum	113.29%	42.36%	2816.63%	27.78%	2965.69%	303.62%	42.39%	1362.51%	72.41%	38573.39%
Air-Water	94	Mean Average	14.33%	3.35%	117.88%	2.89%	83.17%	53.06%	12.83%	67.83%	15.54%	1157.24%
		Median Average	12.17%	3.05%	31.24%	2.44%	19.58%	46.80%	13.59%	41.76%	13.21%	36.09%
		± 20%	77	94	31	94	48	11	70	11	63	19
		- Percentage	81.91%	100.00%	32.98%	100.00%	51.06%	11.70%	74.47%	11.70%	67.02%	20.21%
		± 50%	92	94	62	94	88	50	94	67	94	67
		- Percentage	97.87%	100.00%	65.96%	100.00%	93.62%	53.19%	100.00%	71.28%	100.00%	71.28%
		Maximum	113.29%	8.74%	2816.63%	9.97%	2965.69%	220.43%	31.16%	1362.51%	46.14%	38573.39%
Steam-Water	69	Mean Average	46.01%	6.17%	40.72%	6.77%	137.42%	110.06%	23.61%	64.98%	30.35%	558.50%
		Median Average	47.61%	4.77%	22.14%	6.14%	46.86%	108.88%	25.76%	56.65%	30.27%	72.95%
		± 20%	9	67	26	65	5	7	18	1	13	1
		- Percentage	13.04%	97.10%	37.68%	94.20%	7.25%	10.14%	26.09%	1.45%	18.84%	1.45%
		± 50%	39	69	61	69	40	10	69	17	66	10
		- Percentage	56.52%	100.00%	88.41%	100.00%	57.97%	14.49%	100.00%	24.64%	95.65%	14.49%
		Maximum	99.95%	42.36%	660.97%	27.78%	2335.38%	303.62%	42.39%	487.42%	72.41%	23308.11%

4.5.1.3: The Second Fore, Beus and Bauer f_i Correlation

The second f_i correlation that was produced by Fore et al [26], which is given in Equations 229 and 230, includes a multiplier for the film thickness that is inversely proportional to the Reynolds number of the vapor core, in addition to the shift that was proposed for their first

correlation. The additional Reynolds number multiplier made the second Fore et al correlation have a much closer fit to their data than their first correlation, and should produce more accurate results within RELAP than was seen with the first correlation.

In Figure 136, the pressure gradient prediction of the original RELAP f_i correlation and the second Fore et al f_i correlation are compared with respect to the observed pressure gradient. Generally, the pressure gradient prediction of the second Fore et al f_i correlation matches well with the observed data, with only a few points outside the ±50% range. The second Fore et al f_i correlation appears to have a slight underprediction bias for the pressure gradient, which correlates with the overprediction of the void fraction seen in Figure 137.

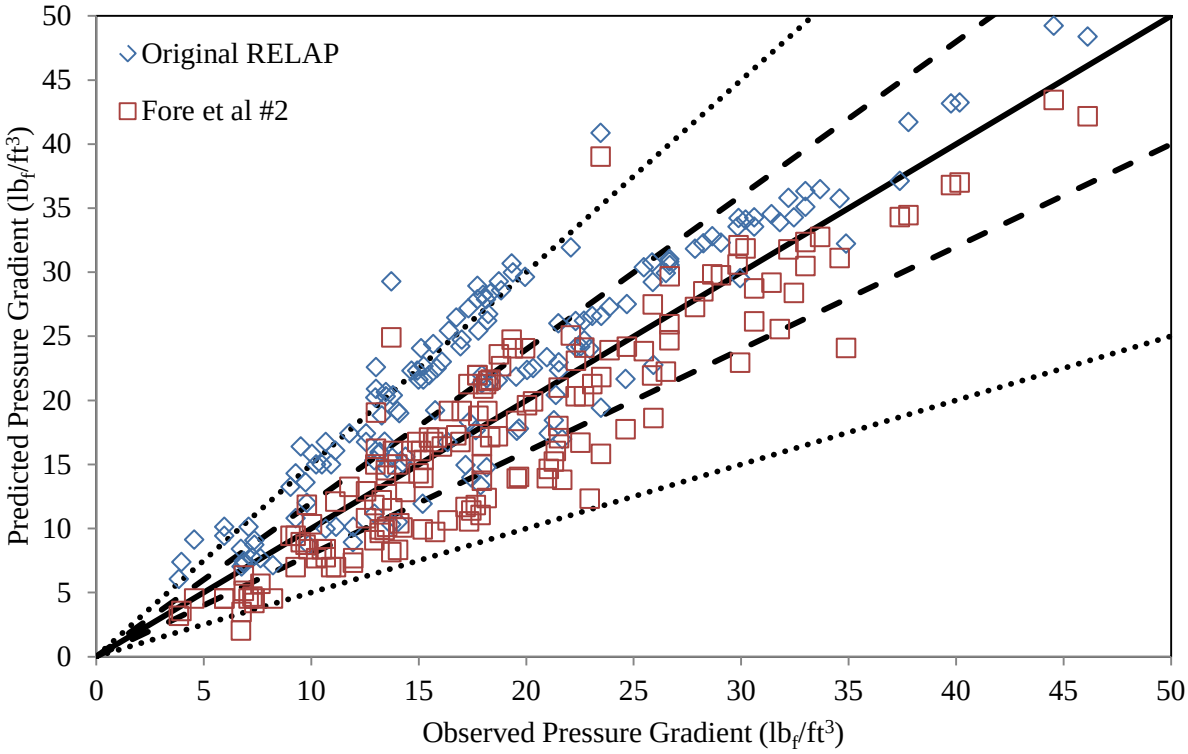

Figure 135: Comparison of the Pressure Gradient Prediction of the RELAP5/MOD3.3 [40429] Interfacial Friction Factor Correlation to the Second Fore et al [26] Interfacial Friction Factor Correlation

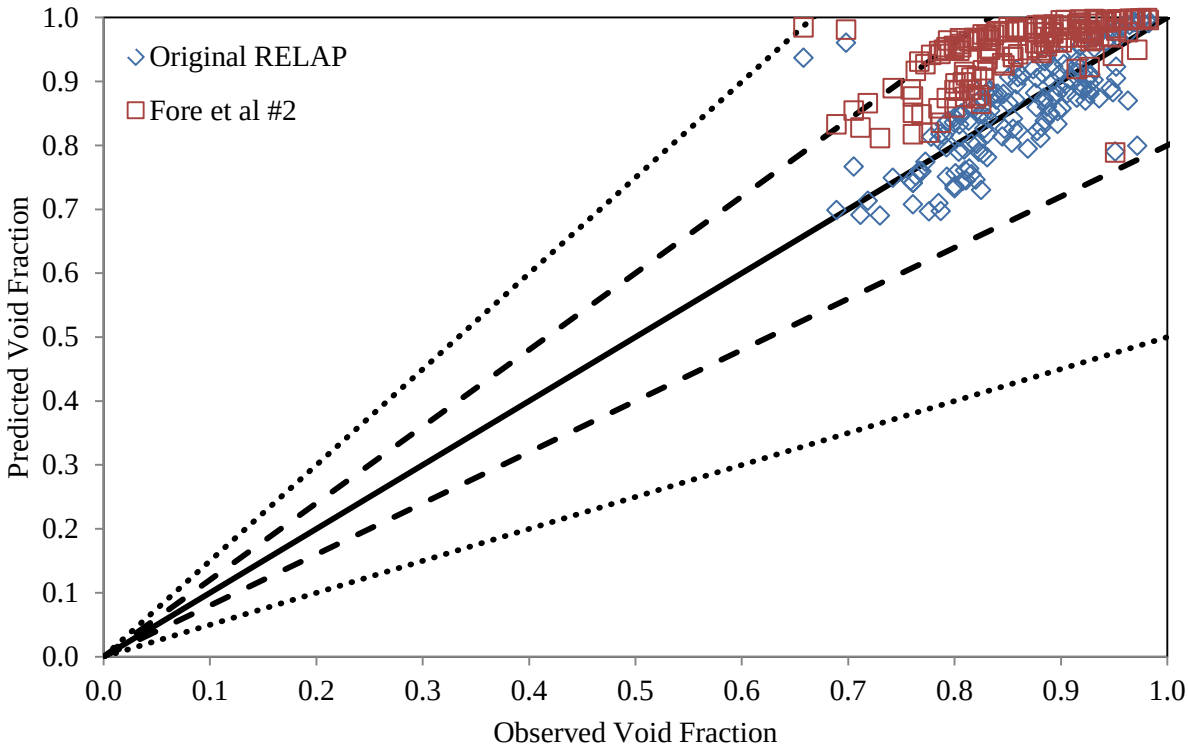

Figure 136: Comparison of the Void Fraction Prediction of the RELAP5/MOD3.3 [40] Interfacial Friction Factor Correlation to the Second Fore et al [26] Interfacial Friction Factor Correlation

The overprediction of the void fraction seen in Figure 136 indicates that there is a greater amount of vapor in the test section than had been observed in the various studies. Thus, it would be expected that in order to maintain continuity, the liquid velocity would need to be increased, as seen in Figure 138 while the vapor velocity would decrease, as seen in Figure 139. Ultimately, this results in a slightly smaller interphase friction force which is depicted in Figure 140.

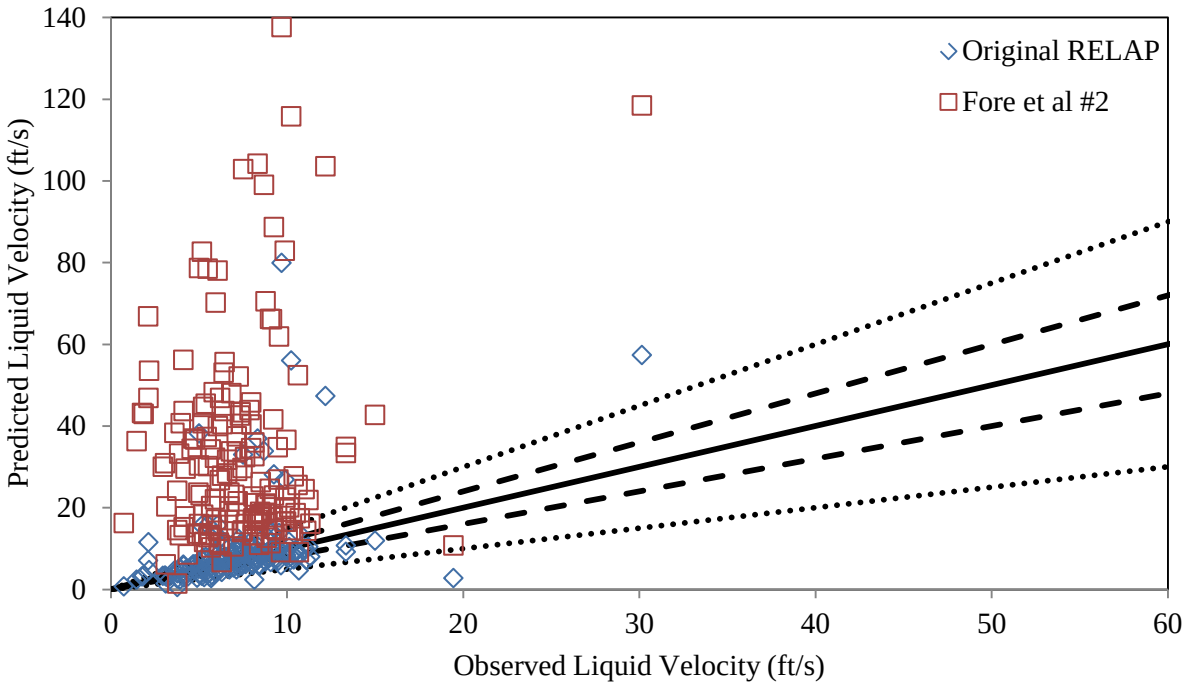

Figure 137: Comparison of the Liquid Velocity Prediction of the RELAP5/MOD3.3 [40] Interfacial Friction Factor Correlation to the Second Fore et al [26] Interfacial Friction Factor Correlation

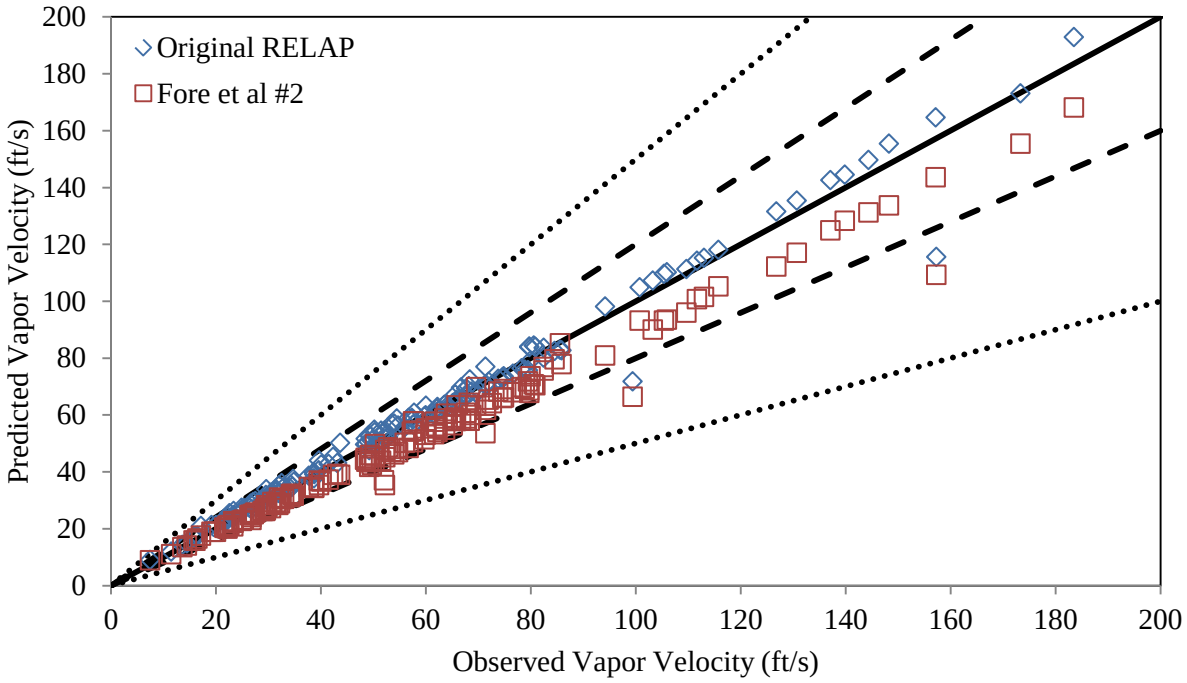

Figure 138: Comparison of the Vapor Velocity Prediction of the RELAP5/MOD3.3 [40] Interfacial Friction Factor Correlation to the Second Fore et al [26] Interfacial Friction Factor Correlation

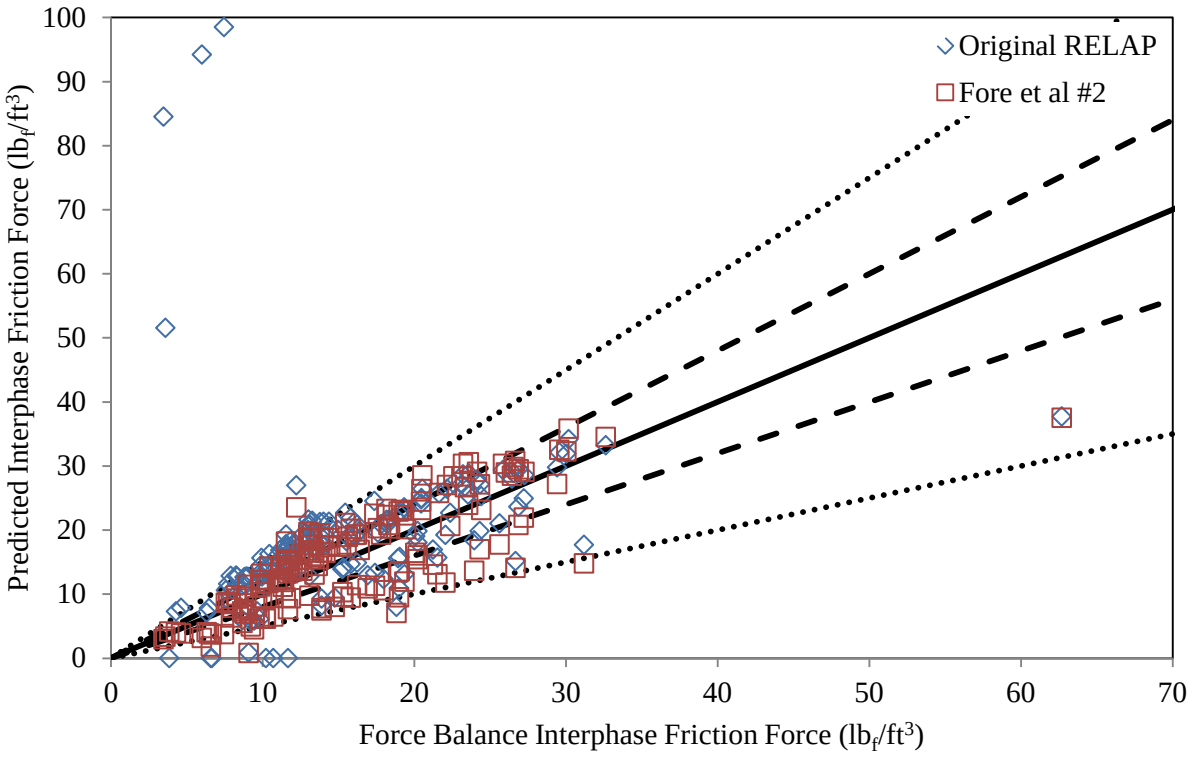

Figure 139: Comparison of the Interphase Friction Force Prediction of the RELAP5/MOD3.3 [40] Interfacial Friction Factor Correlation to the Second Fore et al [26] Interfacial Friction Factor Correlation

While the second Fore et al [26] f_i correlation appears to provide a more accurate depiction of the observed data than either the first Fore et al f_i correlation or the Wallis [86] f_i correlation, when the errors of the second Fore et al correlation are compared against the original RELAP f_i correlation, it does not appear to be a significant improvement over the existing RELAP model, as seen in Table 29. The pressure gradient and interphase friction force errors show significant improvement with the second Fore et al f_i correlation, although improvement appears limited to the steam-water data. However, the second Fore et al f_i correlation produces less accurate results for void fraction and phasic velocities, especially the liquid velocity.

Table 29: Comparison of Errors of the Original RELAP5/MOD3.3 [40] Interfacial Friction Factor to the Second Fore et al Interfacial Friction Factor

			Original RELAP					Fore et al f_i Correlation #2				
Total			dP/dz	α	v_f	v_g	F_{int}	dP/dz	α	v_f	v_g	F_{int}
All Annular	158	Mean Average	27.85%	4.60%	55.22%	4.61%	108.43%	18.41%	11.02%	467.76%	9.68%	25.19%
		Median Average	18.78%	3.81%	26.03%	3.58%	30.14%	15.72%	9.74%	289.24%	9.28%	21.46%
		± 20%	84	156	57	154	52	91	145	3	153	71
		- Percentage	53.16%	98.73%	36.08%	97.47%	32.91%	57.59%	91.77%	1.90%	96.84%	44.94%
		± 50%	127	158	123	158	123	155	158	11	158	148
		- Percentage	80.38%	100.00%	77.85%	100.00%	77.85%	98.10%	100.00%	6.96%	100.00%	93.67%
		Maximum	113.29%	42.36%	724.75%	27.78%	2965.69%	81.48%	49.61%	3050.73%	33.24%	92.20%
Air-Water	89	Mean Average	13.78%	3.39%	66.46%	2.94%	85.95%	18.42%	12.72%	697.57%	10.91%	24.37%
		Median Average	12.11%	3.13%	27.13%	2.45%	19.24%	14.59%	13.90%	548.39%	11.33%	20.46%
		± 20%	75	89	31	89	47	52	78	0	86	44
		- Percentage	84.27%	100.00%	34.83%	100.00%	52.81%	58.43%	87.64%	0.00%	96.63%	49.44%
		± 50%	88	89	62	89	83	87	89	0	89	83
		- Percentage	98.88%	100.00%	69.66%	100.00%	93.26%	97.75%	100.00%	0.00%	100.00%	93.26%
		Maximum	113.29%	8.74%	724.75%	9.97%	2965.69%	81.48%	21.35%	3050.73%	32.34%	92.20%
Steam-Water	69	Mean Average	46.01%	6.17%	40.72%	6.77%	137.42%	18.40%	8.82%	171.34%	8.10%	26.26%
		Median Average	47.61%	4.77%	22.14%	6.14%	46.86%	16.80%	7.99%	112.04%	7.83%	23.03%
		± 20%	9	67	26	65	5	39	67	3	67	27
		- Percentage	13.04%	97.10%	37.68%	94.20%	7.25%	56.52%	97.10%	4.35%	97.10%	39.13%
		± 50%	39	69	61	69	40	68	69	11	69	65
		- Percentage	56.52%	100.00%	88.41%	100.00%	57.97%	98.55%	100.00%	15.94%	100.00%	94.20%
		Maximum	99.95%	42.36%	660.97%	27.78%	2335.38%	66.27%	49.61%	2088.25%	33.24%	91.35%

4.5.1.4: The Wongwises and Kongkiatwanich f_i Correlation

The Wongwises and Kongkiatwanich [89] f_i correlation, shown in Equation 231, represents a different approach to calculating the interfacial friction factor, as it takes the form of multiplying together several dimensionless parameters raised to varying powers, rather than merely modifying the Wallis [86] correlation.

In Figure 141, we find that the pressure gradient predicted by the Wongwises and Kongkiatwanich [87] f_i correlation is very spread out in comparison to that using the original RELAP correlation. There does appear to be a bias towards overpredicting the pressure gradient,

which appears to occur at errors in excess of 100%. From the pressure gradient, it would be expected that the void fraction prediction would be underestimated for most points, which is the case in Figure 142. Likewise, this should result in a decreased liquid velocity and higher vapor velocity, which are seen in Figure 143 and Figure 144, respectively.

Based on earlier observations, it appears that with the Wongwises and Kongkiatwanich [87] f_i correlation, RELAP is underpredicting the interphase friction factor, which is resulting in more liquid flowing along the wall in the film, and less breaking off the film into entrained droplets. The lower liquid velocity and higher vapor velocity should result in a net increase in the interphase friction force, which is confirmed in Figure 145. However, it was not anticipated that the interphase friction force would increase as much as Figure 145 indicates.

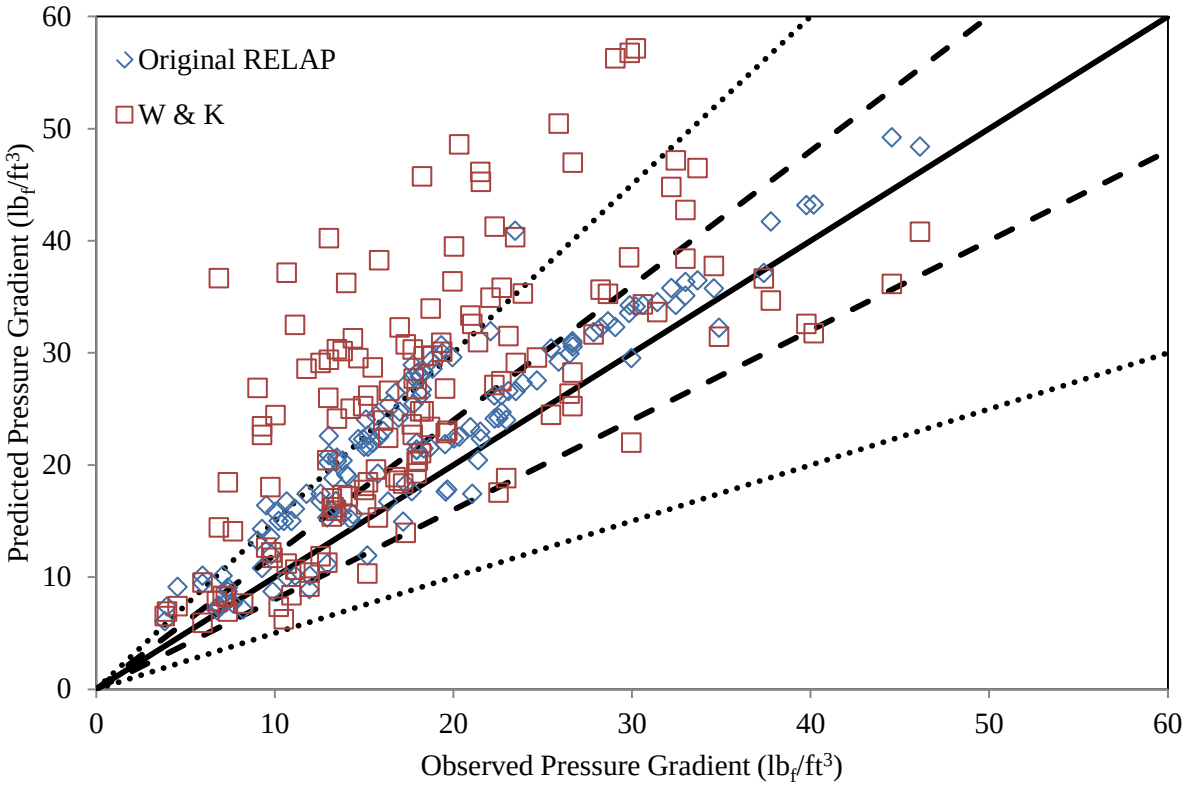

Figure 140: Comparison of the Pressure Gradient Predictions of the RELAP5/MOD3.3 [40] Interfacial Friction Factor Correlation to the Wongwises and Kongkiatwanich [87] Interfacial Friction Factor Correlation

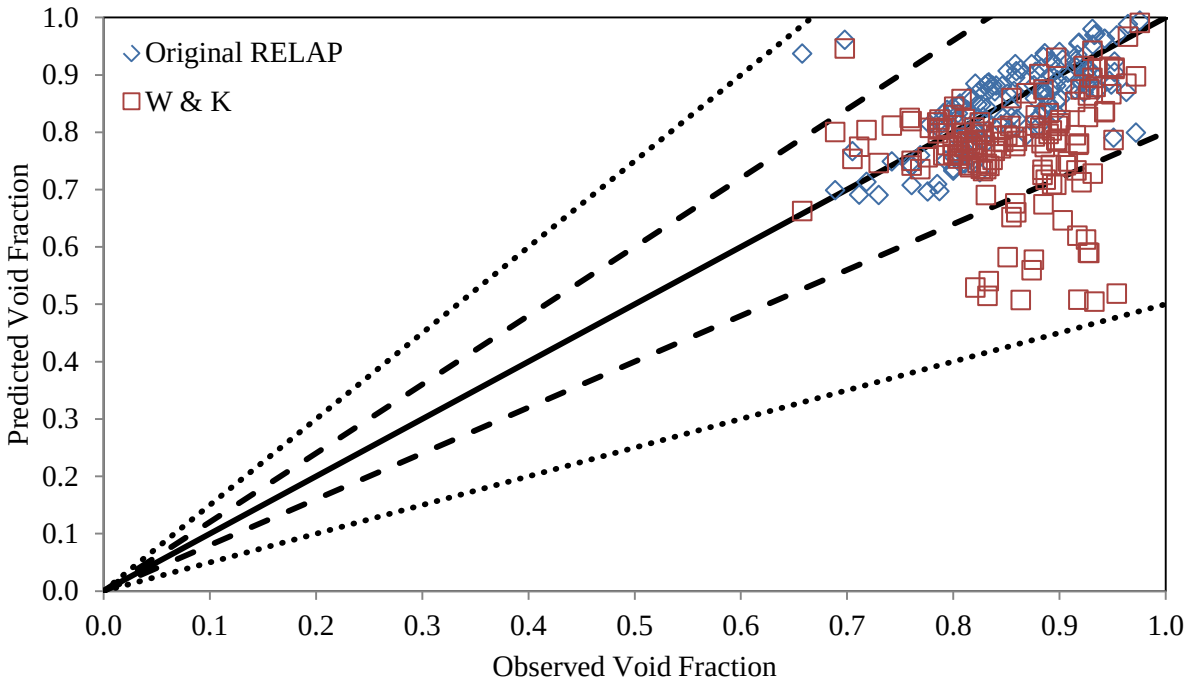

Figure 141: Comparison of the Void Fraction Prediction of the RELAP5/MOD3.3 [40] Interfacial Friction Factor Correlation to the Wongwises and Kongkiatwanich [87] Interfacial Friction Factor Correlation

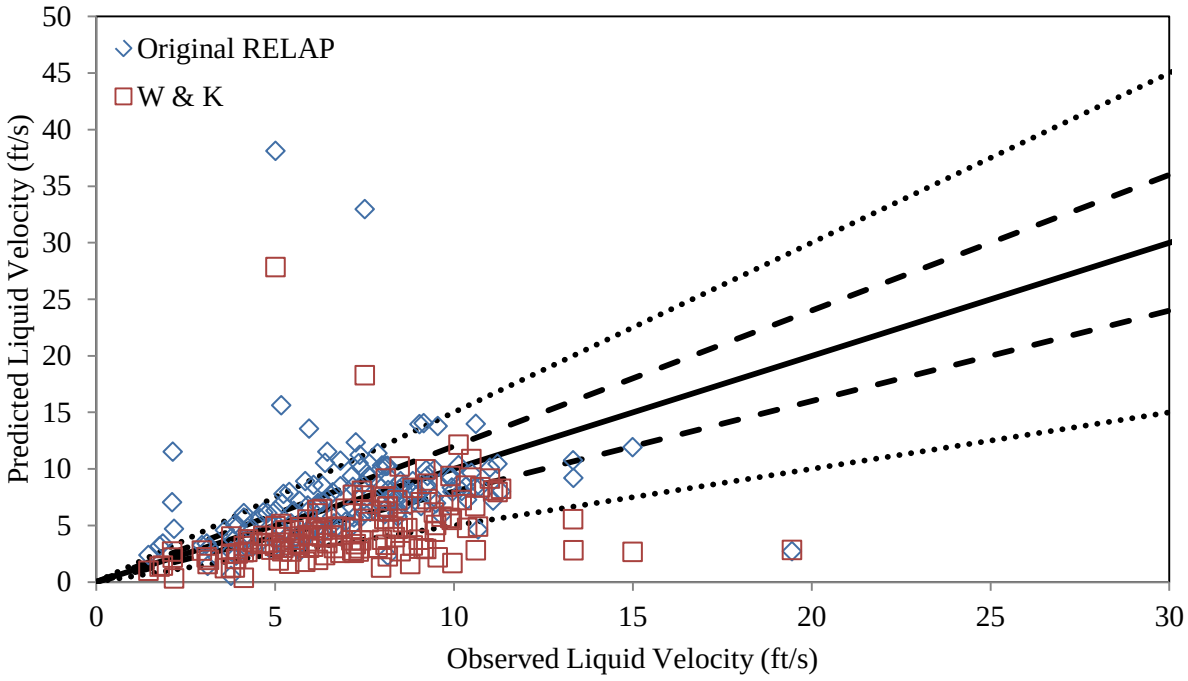

Figure 142: Comparison of the Liquid Velocity Prediction of the RELAP5/MOD3.3 [40] Interfacial Friction Factor Correlation to the Wongwises and Kongkiatwanich [87] Interfacial Friction Factor Correlation

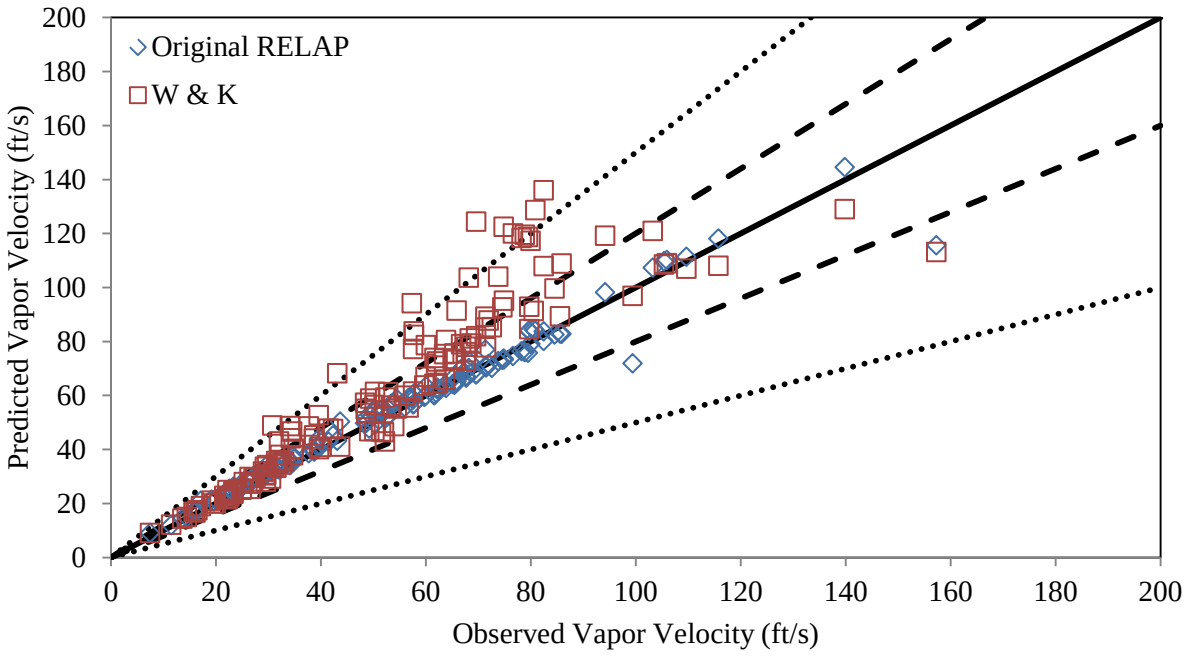

Figure 143: Comparison of the Vapor Velocity Prediction of RELAP5/MOD3.3 [40] Interfacial Friction Factor Correlation to the Wongwises and Kongkiatwanich [87] Interfacial Friction Factor Correlation

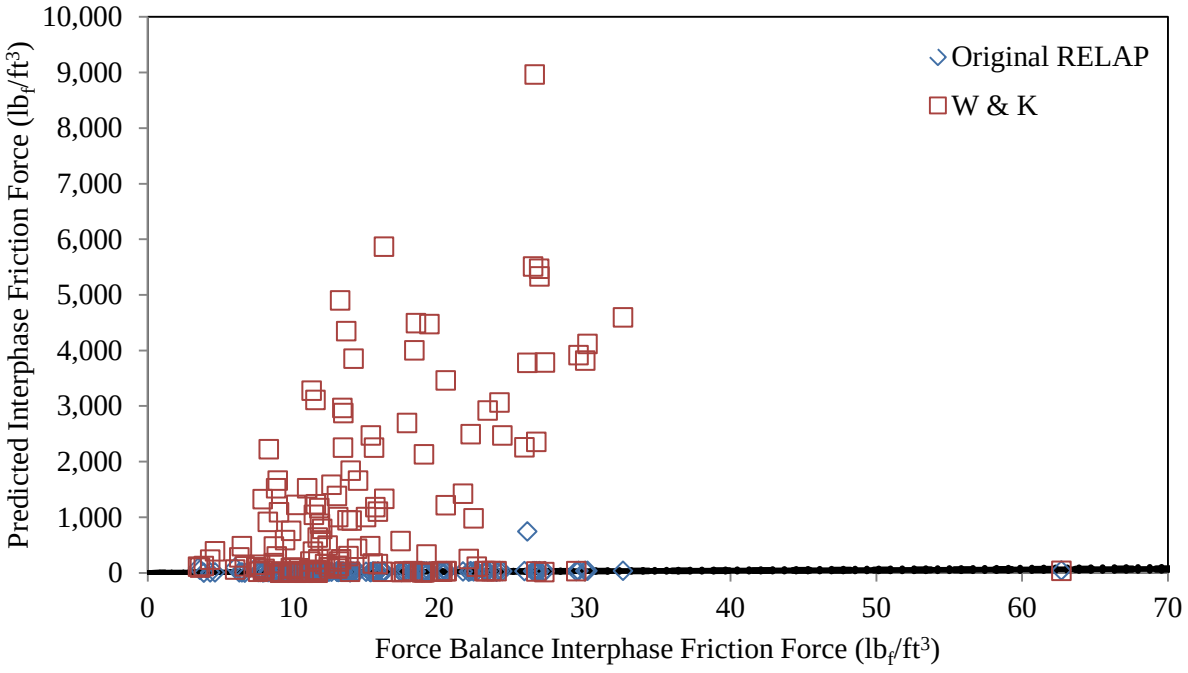

Figure 144: Comparison of the Interphase Friction Force Prediction of the RELAP5/MOD3.3 [40] Interfacial Friction Factor Correlation to the Wongwises and Kongkiatwanich [87] Interfacial Friction Factor Correlation

Table 30 compares the errors that have been calculated for the data points with which RELAP was able to obtain a result when the Wongwises and Kongkiatwanich [89] f_i correlation was implemented. As has been shown in Figure 140 through Figure 144, the RELAP results with the Wongwises and Kongkiatwanich f_i correlation do not appear to provide an improved prediction for any of the variables studied. Comparing the errors of the original RELAP f_i correlation to the Wongwises and Kongkiatwanich f_i correlation confirms that the modification does not improve upon the existing RELAP model.

Table 30: Comparison of Errors of the Original RELAP5/MOD3.3 [40] Interfacial Friction Factor Correlation to the Wongwises and Kongkiatwanich [87] Interfacial Friction Factor Correlation

			Original RELAP					W & K f_i Correlation				
Total			dP/dz	α	v_f	v_g	F_{int}	dP/dz	α	v_f	v_g	F_{int}
All Annular	141	Mean Average	28.42%	4.93%	40.77%	4.78%	96.53%	56.59%	11.41%	41.59%	16.99%	7292.96%
		Median Average	18.28%	4.29%	25.69%	3.60%	30.34%	36.40%	7.68%	36.34%	12.13%	3240.03%
		± 20%	74	139	51	137	47	44	117	34	105	6
		- Percentage	52.48%	98.58%	36.17%	97.16%	33.33%	31.21%	82.98%	24.11%	74.47%	4.26%
		± 50%	111	141	117	141	109	82	141	97	130	21
		- Percentage	78.72%	100.00%	82.98%	100.00%	77.30%	58.16%	100.00%	68.79%	92.20%	14.89%
		Maximum	99.95%	42.36%	660.97%	27.78%	2742.19%	434.10%	45.95%	456.01%	78.50%	36974.37%
Air-Water	72	Mean Average	11.56%	3.74%	40.82%	2.88%	57.33%	46.91%	13.64%	39.87%	20.44%	9539.88%
		Median Average	11.38%	3.91%	26.26%	2.35%	18.05%	25.76%	9.65%	36.25%	15.57%	7550.92%
		± 20%	65	72	25	72	42	26	56	18	49	5
		- Percentage	90.28%	100.00%	34.72%	100.00%	58.33%	36.11%	77.78%	25.00%	68.06%	6.94%
		± 50%	72	72	56	72	69	53	72	47	65	19
		- Percentage	100.00%	100.00%	77.78%	100.00%	95.83%	73.61%	100.00%	65.28%	90.28%	26.39%
		Maximum	34.70%	8.74%	339.08%	9.97%	2742.19%	434.10%	45.95%	143.30%	78.50%	36054.10%
Steam-Water	69	Mean Average	46.01%	6.17%	40.72%	6.77%	137.42%	66.69%	9.08%	43.39%	13.39%	4948.33%
		Median Average	47.61%	4.77%	22.14%	6.14%	46.86%	59.57%	5.73%	36.42%	8.37%	2074.12%
		± 20%	9	67	26	65	5	18	61	16	56	1
		- Percentage	13.04%	97.10%	37.68%	94.20%	7.25%	26.09%	88.41%	23.19%	81.16%	1.45%
		± 50%	39	69	61	69	40	29	69	50	65	2
		- Percentage	56.52%	100.00%	88.41%	100.00%	57.97%	42.03%	100.00%	72.46%	94.20%	2.90%
		Maximum	99.95%	42.36%	660.97%	27.78%	2335.38%	208.67%	36.51%	456.01%	64.17%	36974.37%

4.5.1.5 The Belt, Van't Westende and Portela f_i Correlation

The final f_i correlation that has been tested in RELAP is that of Belt et al [7], which is shown in Equation 233. The Belt et al f_i correlation represents a more simplified correlation than the Wallis [86] correlation, which may results in similar results.

Examining the pressure gradient prediction shown in Figure 146, we see a similar pattern to what was observed with the Wallis [86] f_i correlation, with the pressure gradient overpredicted for many data points, but underpredicted for a select few data points by the Belt et al [7] f_i correlation. Figure 147 shows that for most data points, the Belt et al f_i correlation underpredicts the void fraction, with some overprediction noticed for observed void fraction values greater than 0.95. Consequently, we find very similar liquid and vapor velocity patterns produced by the Belt et al f_i correlation as the Wallis f_i correlation in Figure 148 and Figure 149, respectively. Figure 150 shows the interphase friction force prediction of both the original RELAP f_i correlation and the Belt et al f_i correlation, which also compares very closely to the Wallis f_i correlation interphase friction force.

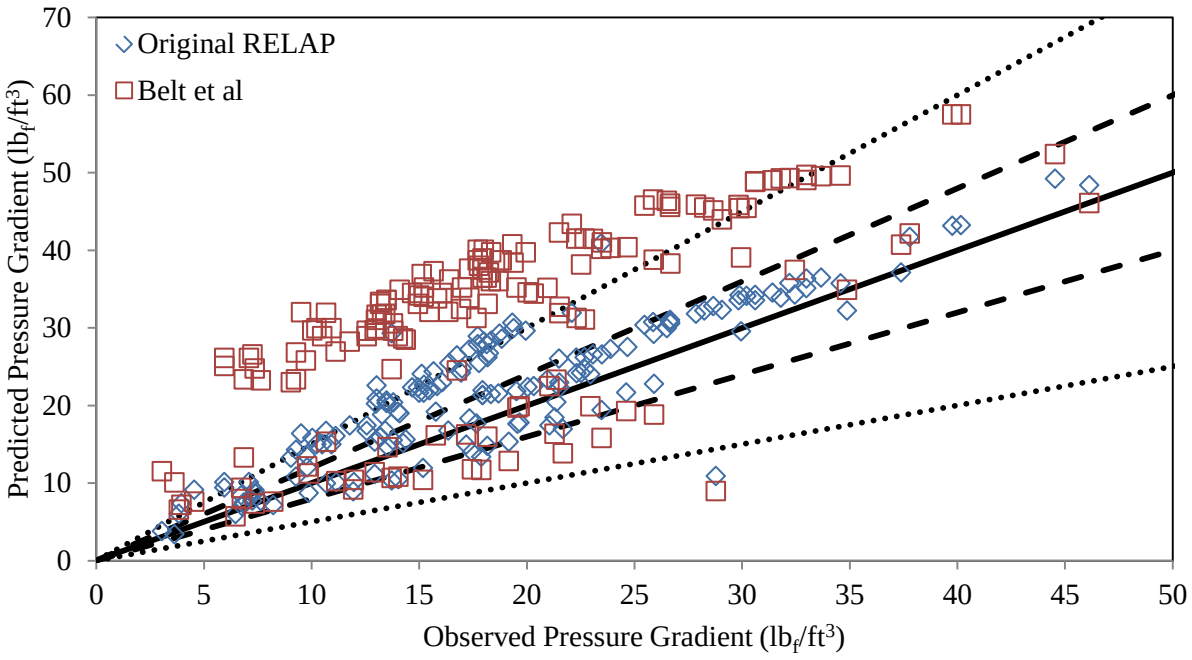

Figure 145: Comparison of the Pressure Gradient Prediction of the RELAP5/MOD3.3 [40] Interfacial Friction Factor Correlation to the Belt, Van't Westende and Portela [7] Interfacial Friction Factor Correlation

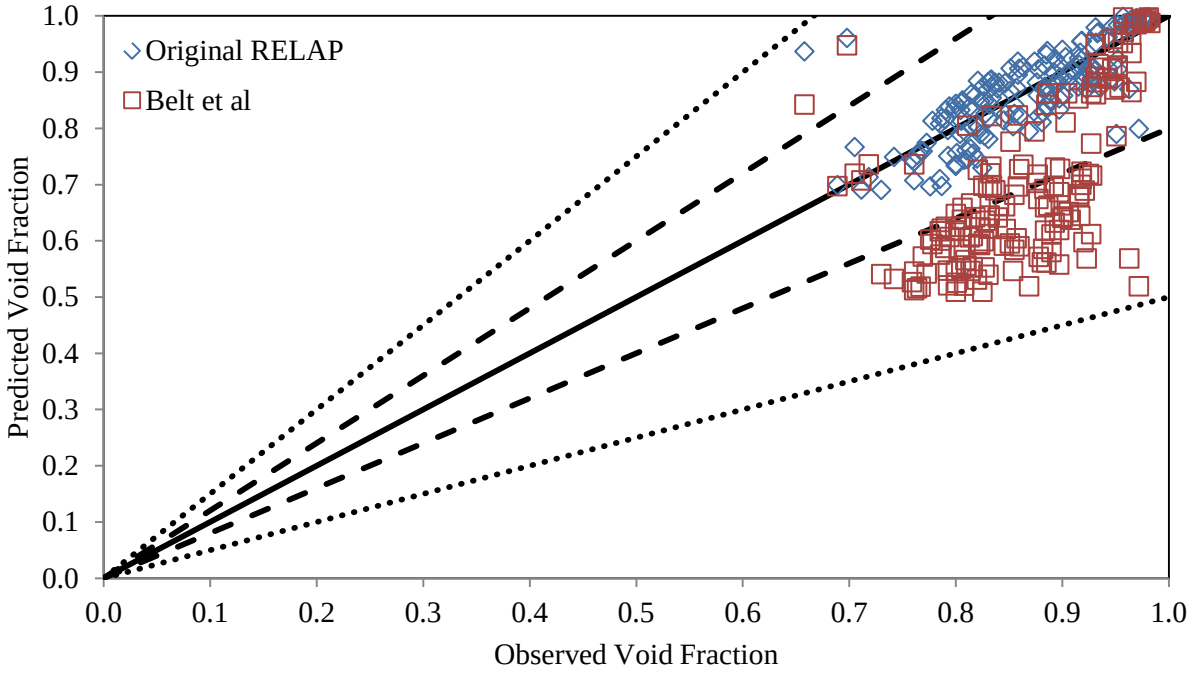

Figure 146: Comparison of the Void Fraction Prediction of the RELAP5/MOD3.3 [40] Interfacial Friction Factor Correlation to the Belt, Van't Westende and Portela [7] Interfacial Friction Factor Correlation

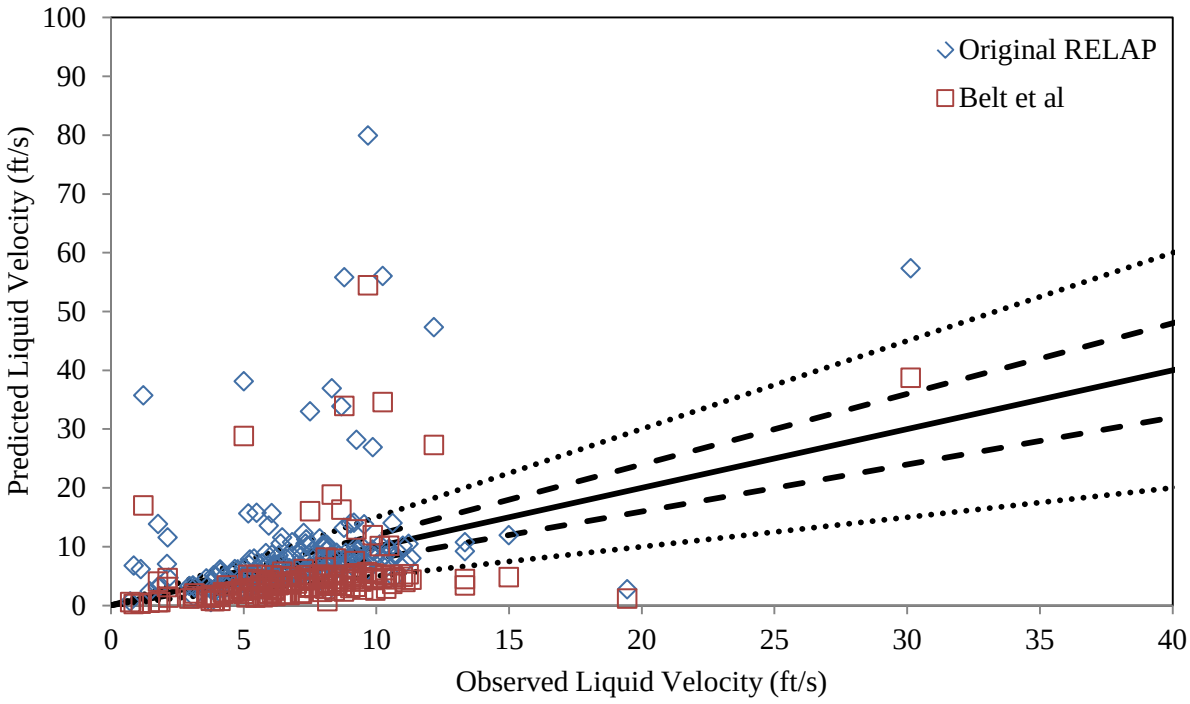

Figure 147: Comparison of the Liquid Velocity Prediction of the RELAP5/MOD3.3 [40] Interfacial Friction Factor Correlation to the Belt, Van't Westende and Portela [7] Interfacial Friction Factor Correlation

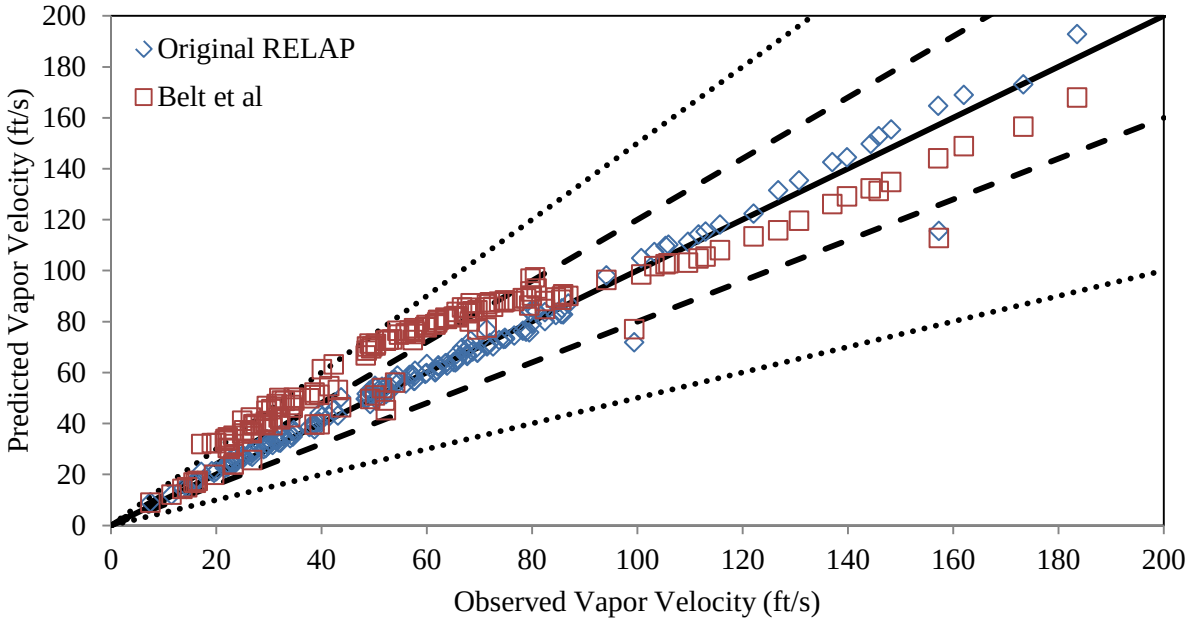

Figure 148: Comparison of the Vapor Velocity Prediction of the RELAP5/MOD3.3 [40] Interfacial Friction Factor Correlation to the Belt, Van't Westende and Portela [7] Interfacial Friction Factor Correlation

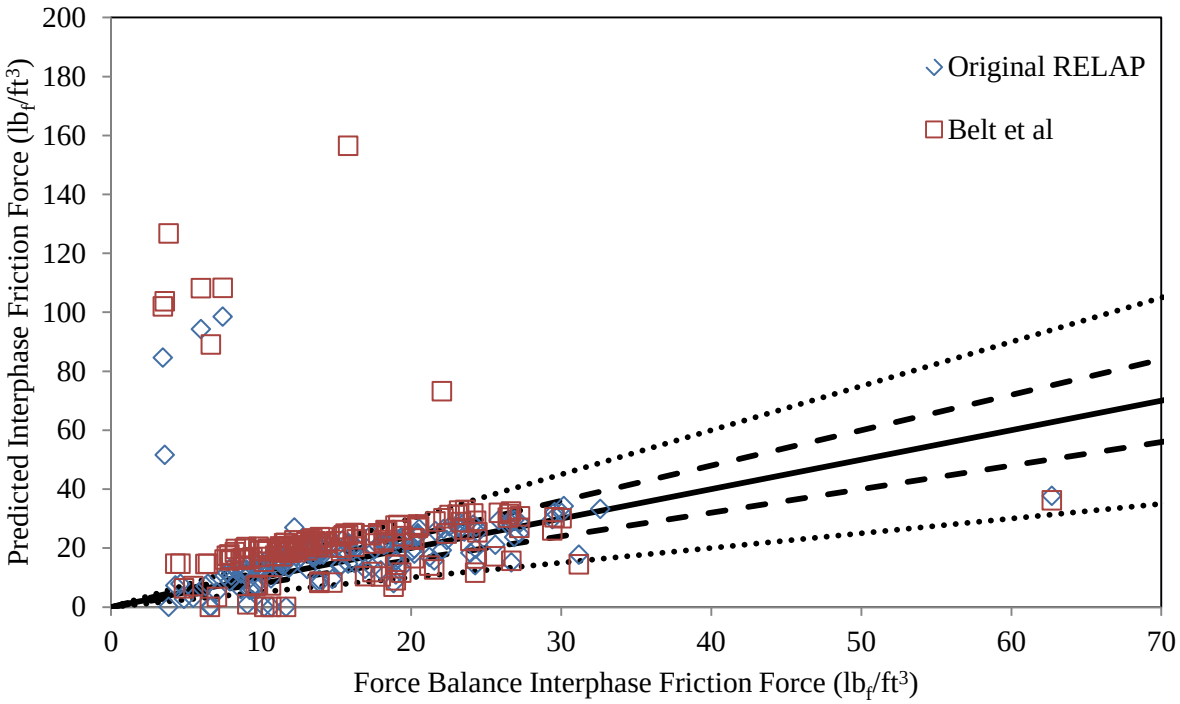

Figure 149: Comparison of the Interphase Friction Force Prediction of the RELAP5/MOD3.3 [40] Interfacial Friction Factor Correlation to the Belt, Van't Westende and Portela [7] Interfacial Friction Factor Correlation

In Table 31, we see the errors produced by both the original RELAP f_i correlation compared to that of Belt et al [7]. The Belt et al f_i correlation significantly increased the errors in RELAP for the pressure gradient, void fraction and vapor velocity. The mean average error of the liquid velocity improved. However, this is due to the reduction in error of an outlier data point with the original RELAP model. The median error for the liquid velocity for both air-water and steam-water increased significantly, and the number of data points within the ±20% and ±50% ranges decreased when the Belt et al f_i correlation was applied.

Table 31: Comparison of Errors of the Original RELAP5/MOD3.3 [40] Interfacial Friction Factor Correlation to the Belt, Van't Westende and Portela [7] Interfacial Friction Factor Correlation

			Original RELAP					Belt et al f_i Correlation				
Total			dP/dz	α	v_f	v_g	F_{int}	dP/dz	α	v_f	v_g	F_{int}
All Annular	163	Mean Average	27.74%	4.54%	85.21%	4.53%	106.13%	89.27%	20.02%	68.70%	25.93%	1667.77%
		Median Average	18.82%	3.70%	26.26%	3.55%	30.34%	79.81%	22.50%	53.56%	26.90%	55.32%
		± 20%	86	161	57	159	53	23	67	11	63	15
		- Percentage	52.76%	98.77%	34.97%	97.55%	32.52%	14.11%	41.10%	6.75%	38.65%	9.20%
		± 50%	131	163	123	163	128	50	163	70	147	69
		- Percentage	80.37%	100.00%	75.46%	100.00%	78.53%	30.67%	100.00%	42.94%	90.18%	42.33%
		Maximum	113.29%	42.36%	2816.63%	27.78%	2965.69%	338.71%	46.60%	1287.52%	85.85%	55756.48%
Air-Water	94	Mean Average	14.33%	3.35%	117.88%	2.89%	83.17%	65.82%	15.75%	70.93%	19.05%	1620.91%
		Median Average	12.17%	3.05%	31.24%	2.44%	19.58%	54.20%	18.17%	47.44%	17.63%	38.20%
		± 20%	77	94	31	94	48	15	53	9	51	15
		- Percentage	81.91%	100.00%	32.98%	100.00%	51.06%	15.96%	56.38%	9.57%	54.26%	15.96%
		± 50%	92	94	62	94	88	40	94	54	92	62
		- Percentage	97.87%	100.00%	65.96%	100.00%	93.62%	42.55%	100.00%	57.45%	97.87%	65.96%
		Maximum	113.29%	8.74%	2816.63%	9.97%	2965.69%	275.84%	36.03%	1287.52%	56.10%	50598.18%
Steam-Water	69	Mean Average	46.01%	6.17%	40.72%	6.77%	137.42%	121.22%	25.84%	65.67%	35.30%	1731.60%
		Median Average	47.61%	4.77%	22.14%	6.14%	46.86%	120.85%	28.05%	59.62%	36.69%	82.07%
		± 20%	9	67	26	65	5	8	14	2	12	0
		- Percentage	13.04%	97.10%	37.68%	94.20%	7.25%	11.59%	20.29%	2.90%	17.39%	0.00%
		± 50%	39	69	61	69	40	10	69	16	55	7
		- Percentage	56.52%	100.00%	88.41%	100.00%	57.97%	14.49%	100.00%	23.19%	79.71%	10.14%
		Maximum	99.95%	42.36%	660.97%	27.78%	2335.38%	338.71%	46.60%	474.42%	85.85%	55756.48%

4.5.2: Analyses of the Film Thickness Correlations

After comparing the different correlations for the interfacial friction factor, the next set of correlations to be examined predict the film thickness, δ, of the annular flow. In RELAP, the liquid film volume fraction, α_{ff}, is calculated instead of the film thickness, using Equations 115 through 117. The liquid film volume fraction is related to the film thickness by Equation 225.

4.5.2.1: The Hori, Nakasatomi, Nishikawa and Sekoguchi Film Thickness Correlation

The Hori et al [38] film thickness correlation resulted in transient errors for all data points when implemented properly. By accident, it was discovered that when the correlation did produce some very interesting results when the film thickness ratio, δ/D_H, that results from the Hori et al correlation is applied as shown in Equation 298.

$$\alpha_{ff} = \alpha_f \left[1 - \left(1 - 2\frac{\delta}{D_H}\right)^2\right] \tag{298}$$

The results of running RELAP with this errant modification are shown in Figures 151 through 155 and Table 32. Beginning with the pressure gradient prediction of RELAP, it is shown in Figure 151 that when RELAP is modified with the Hori et al [38] correlation, the pressure gradient appears to be slightly underpredicted, based on its comparison with the observed pressure gradient. As can be seen in Figure 152, the decreased pressure gradient correlates with an increased void fraction when the Hori et al correlation is used.

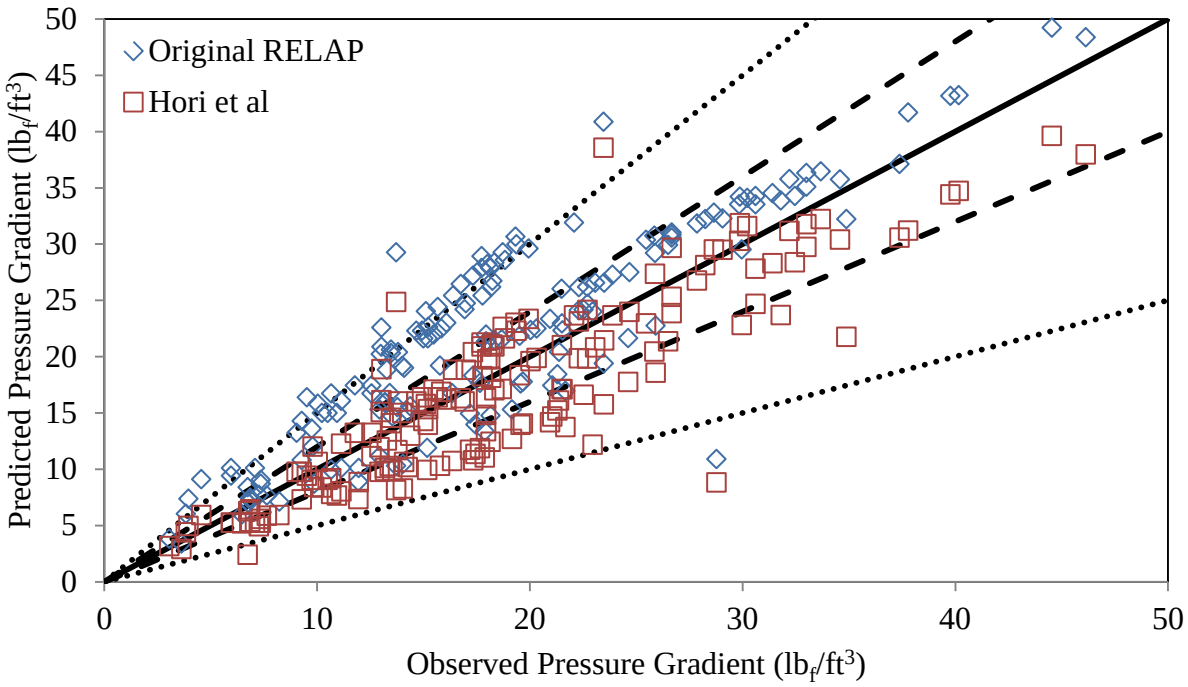

Figure 150: Comparison of the Pressure Gradient Prediction of the RELAP5/MOD3.3 [40] Liquid Film Volume Fraction Correlation to the Hori, Nishikawa and Sekoguchi [38] Film Thickness Correlation

Assuming that mass is conserved for both phases, an increased void fraction should result in a higher liquid velocity and a lower vapor velocity, which is found to be generally the case in Figure 153 for the liquid velocity and Figure 154 for the vapor velocity. The liquid velocity is consistently above the observed value for nearly all cases, and in many cases, the liquid velocity predicted by RELAP with the Hori et al correlation is several times that of the observed value. Combined with a void fraction that is consistently overpredicted, this would indicate that in many cases, the flow regime was approaching the mist flow pattern, and that the film thickness was being underpredicted. This is expected given the error made in determining the liquid film volume fraction in Equation 298.

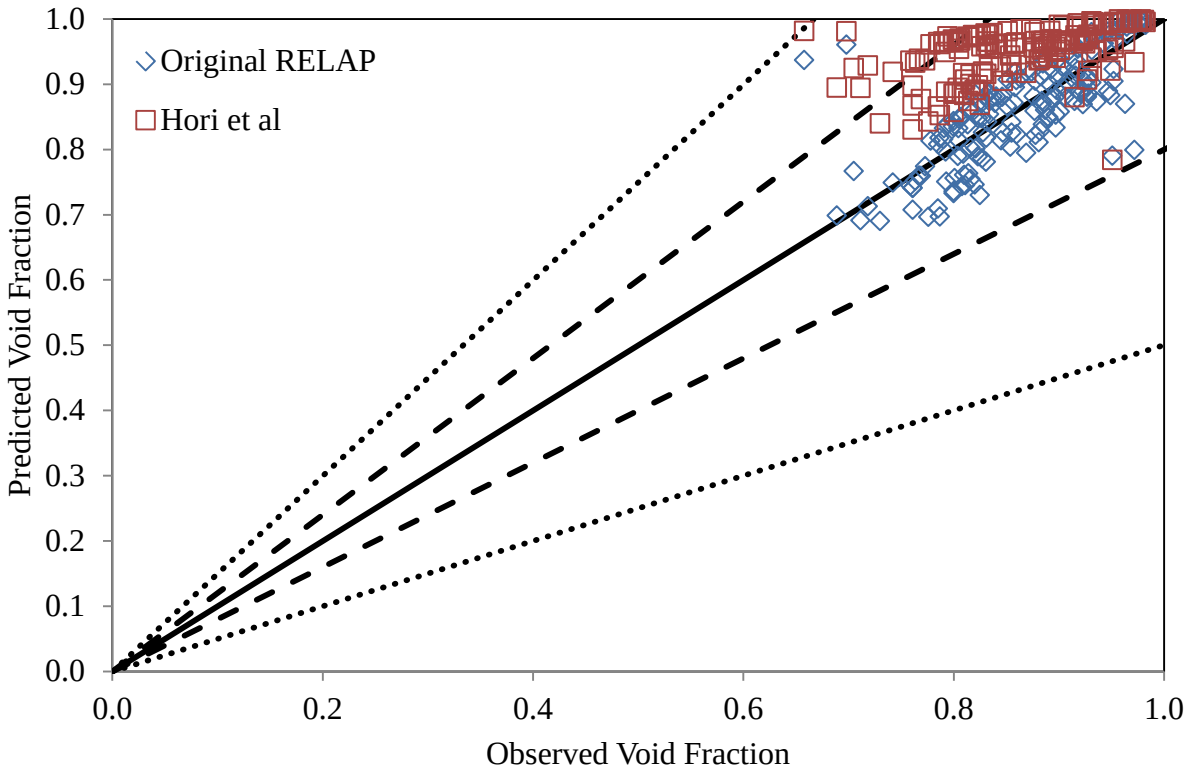

Figure 151: Comparison of the Void Fraction Prediction of the RELAP5/MOD3.3 [40] Liquid Film Volume Fraction Correlation to the Hori, Nishikawa and Sekoguchi [38] Film Thickness Correlation

With higher liquid velocities and lower vapor velocities, it would be expected that the interphase friction force that is predicted by RELAP would be lower with the Hori et al [38] film thickness correlation than RELAP in its unaltered form. As Figure 155 shows, the interphase friction force predicted with the Hori et al correlation is within ±50% of the force balance interphase friction force values for nearly all data points. The only significant improvement that can be noted over the original RELAP model is for the handful of outliers that are not shown, where the Hori et al correlation appears to have improved the interphase friction force prediction to be within ±50%.

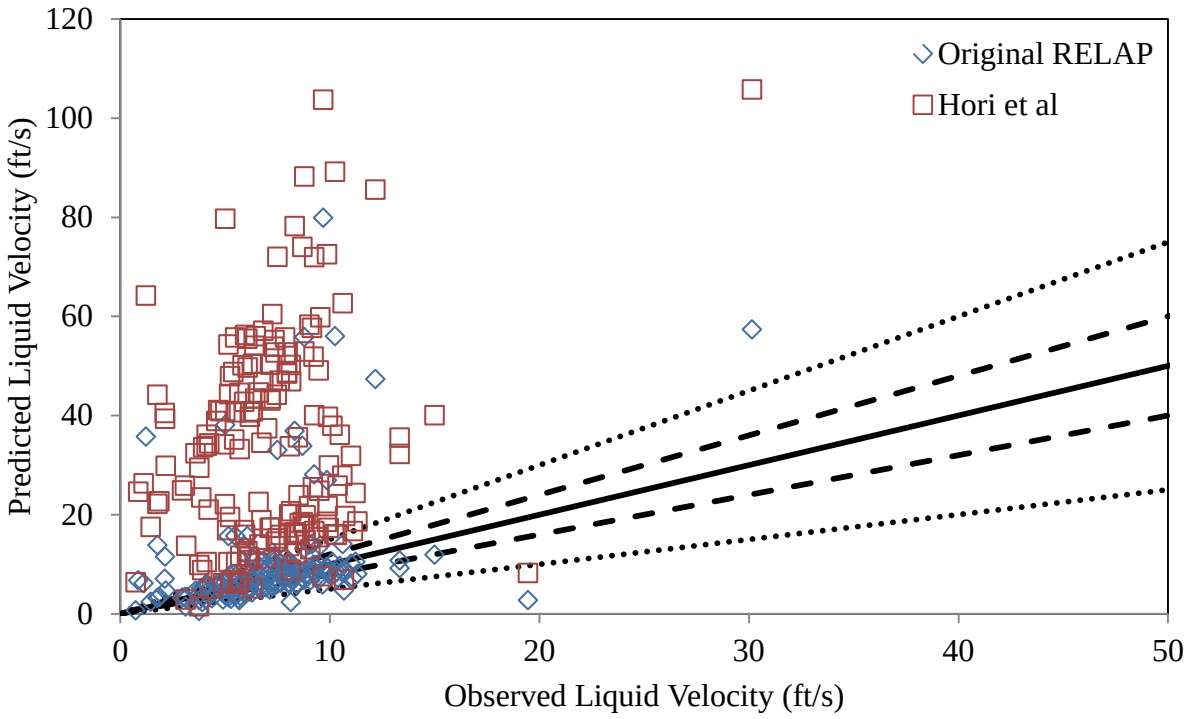

Figure 152: Comparison of the Liquid Velocity Prediction of the RELAP5/MOD3.3 [40] Liquid Film Volume Fraction Correlation to the Hori, Nishikawa and Sekoguchi [38] Film Thickness Correlation

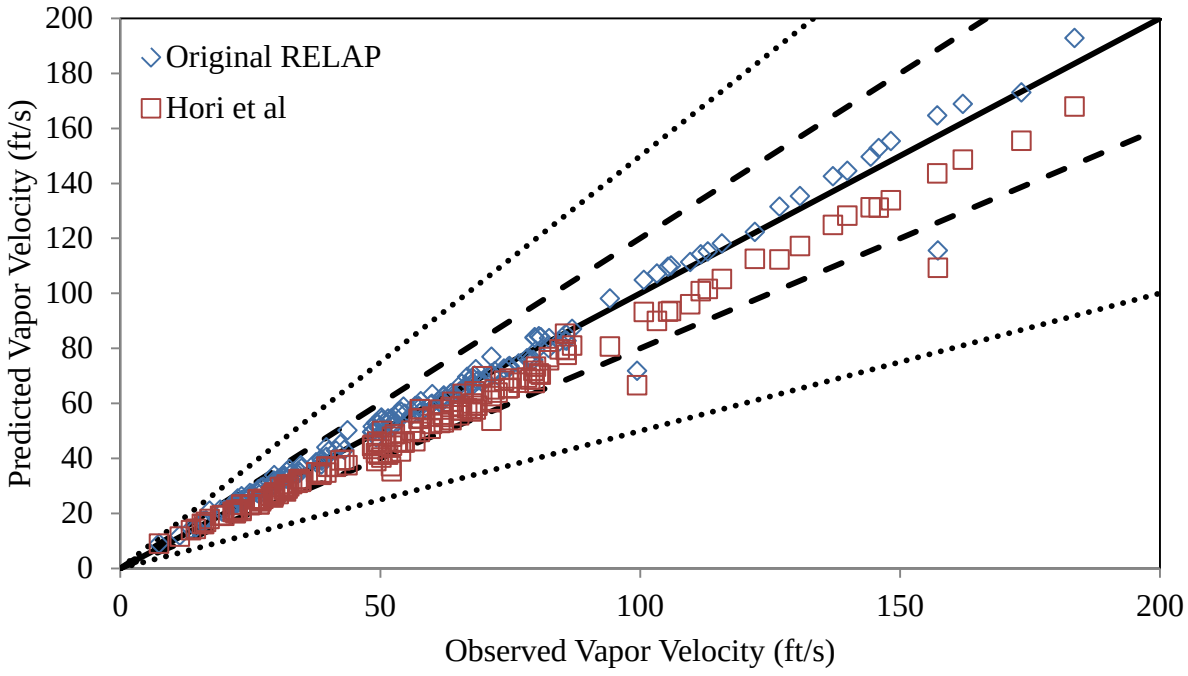

Figure 153: Comparison of the Vapor Velocity Prediction of the RELAP5/MOD3.3 [40] Liquid Film Volume Fraction Correlation to the Hori, Nishikawa and Sekoguchi [38] Film Thickness Correlation

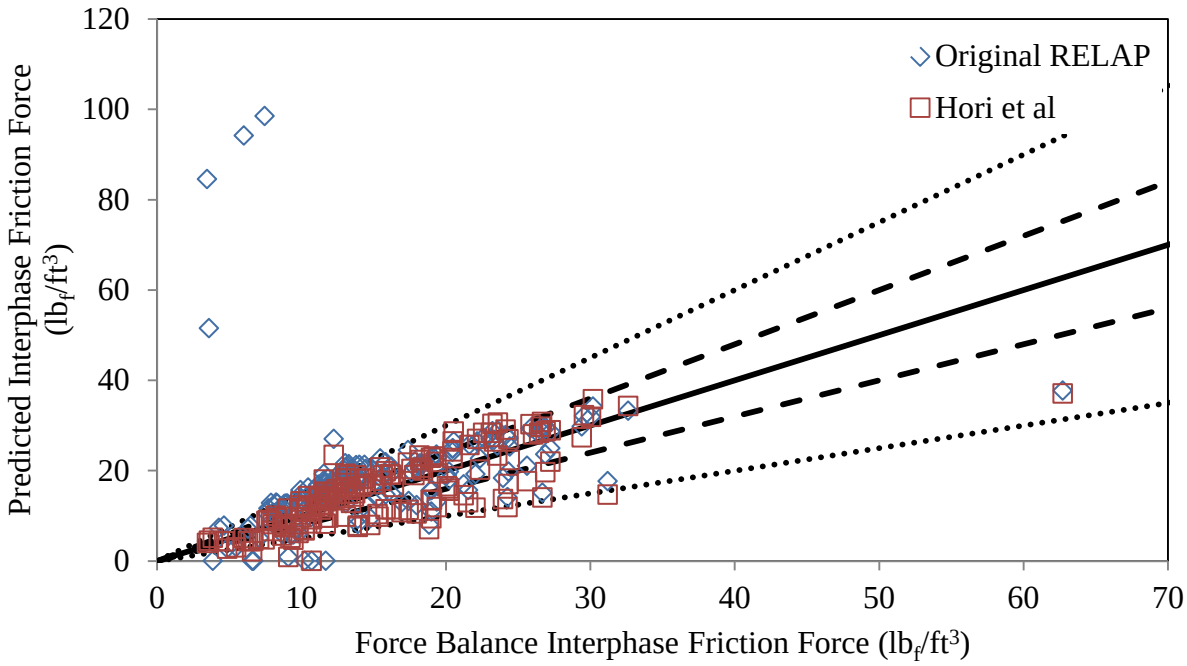

Figure 154: Comparison of the Interphase Friction Force Prediction of the RELAP5/MOD3.3 [40] Liquid Film Volume Fraction Correlation to the Hori, Nishikawa and Sekoguchi [38] Film Thickness Correlation

In Table 32, the errors of the original RELAP model are compared to the results from RELAP when the Hori et al [38] correlation is used. As seen in Figure 154, when the Hori et al correlation is substituted into RELAP, the Hori et al correlation provides significant improvement for data points where the original RELAP code significantly overpredicted the interphase friction force. However, based on the data presented in Table 32, it appears that the correlation provides improved interphase friction force prediction for most data points, as the median error with respect to the force balance values is improved for both air-water and steam-water data points. Also the number of data points for which the error percentage is within ±20% and ±50% has increased for the overall case.

Table 32 also indicates that the pressure gradient prediction has improved, particularly for the steam-water data. However, the improved pressure gradient prediction does not lead to

an improved void fraction prediction, while the liquid velocity has much higher errors with the Hori et al [38] film thickness correlation than the original RELAP model.

Table 32: Comparison of Errors of the Original RELAP5/MOD3.3 [40] Liquid Film Volume Fraction Correlation to the Hori, Nishikawa and Sekoguchi Film Thickness Correlation

			Original RELAP					Hori et al δ/D Correlation				
Total			dP/dz	α	v_f	v_g	F_{int}	dP/dz	α	v_f	v_g	F_{int}
All Annular	163	Mean Average	27.74%	4.54%	85.21%	4.53%	106.13%	17.85%	10.88%	490.30%	10.07%	24.87%
		Median Average	18.82%	3.70%	26.26%	3.55%	30.34%	14.67%	9.07%	418.53%	9.60%	21.74%
		± 20%	86	161	57	159	53	101	143	6	156	73
		- Percentage	52.76%	98.77%	34.97%	97.55%	32.52%	61.96%	87.73%	3.68%	95.71%	44.79%
		± 50%	131	163	123	163	128	159	163	13	163	153
		- Percentage	80.37%	100.00%	75.46%	100.00%	78.53%	97.55%	100.00%	7.98%	100.00%	93.87%
		Maximum	113.29%	42.36%	2816.63%	27.78%	2965.69%	81.15%	49.15%	5145.91%	33.05%	99.97%
Air-Water	94	Mean Average	18.63%	3.58%	117.86%	3.10%	86.14%	18.39%	12.70%	708.79%	10.54%	24.11%
		Median Average	13.08%	3.24%	28.08%	2.45%	21.45%	14.12%	12.23%	628.11%	10.35%	20.52%
		± 20%	69	94	30	94	42	57	76	0	92	45
		- Percentage	73.40%	100.00%	31.91%	100.00%	44.68%	60.64%	80.85%	0.00%	97.87%	47.87%
		± 50%	87	94	63	94	86	91	94	0	94	86
		- Percentage	92.55%	100.00%	67.02%	100.00%	91.49%	96.81%	100.00%	0.00%	100.00%	91.49%
		Maximum	113.29%	8.74%	2816.63%	14.89%	2965.69%	81.15%	31.11%	5145.91%	21.34%	91.91%
Steam-Water	69	Mean Average	40.15%	5.86%	40.74%	6.48%	133.37%	17.11%	8.41%	192.65%	9.43%	25.91%
		Median Average	44.01%	4.57%	22.39%	5.42%	43.43%	14.67%	7.40%	101.01%	8.28%	24.50%
		± 20%	17	67	27	65	11	44	67	6	64	28
		- Percentage	24.64%	97.10%	39.13%	94.20%	15.94%	63.77%	97.10%	8.70%	92.75%	40.58%
		± 50%	44	69	60	69	42	68	69	13	69	67
		- Percentage	63.77%	100.00%	86.96%	100.00%	60.87%	98.55%	100.00%	18.84%	100.00%	97.10%
		Maximum	99.95%	42.36%	660.97%	27.78%	2335.38%	64.34%	49.15%	1739.19%	33.05%	99.97%

4.5.2.2: The Fukano and Furukawa Film Thickness Correlation

The Fukano and Furukawa [28] correlation for film thickness is described in Equations 238, 239 and 241. As we compared the results between the original RELAP model and the Fukano and Furukawa [28] correlation, it is shown that the Fukano and Furukawa correlation provides very similar results to the unmodified RELAP model. In Figure 155, the pressure gradient prediction of both models is shown, with the Fukano and Furukawa film thickness correlation providing a small increase in the pressure gradient over the unmodified RELAP

model. This translates to an only slightly noticeable change in the void fraction prediction in Figure 156, with most data points showing an unchanged void fraction prediction. When the liquid velocity is examined in Figure 157, the liquid velocity for most data points is unchanged. The notable exception of several outliers by the unmodified RELAP model where the liquid velocity is significantly overpredicted compared to the observed liquid velocity, where the Fukano and Furukawa appears to offer some improvement over the original RELAP model. Many of these data points coincide with the observed vapor velocity exceeding 85 ft/s, which Figure 158 shows a disparity between the original RELAP model and the Fukano and Furukawa correlation that does not exist when the observed vapor velocity is less than 85 ft/s. In Figure 159, the interphase friction force prediction of both the unmodified RELAP model and the Fukano and Furukawa correlation match, with the exception of a few outliers.

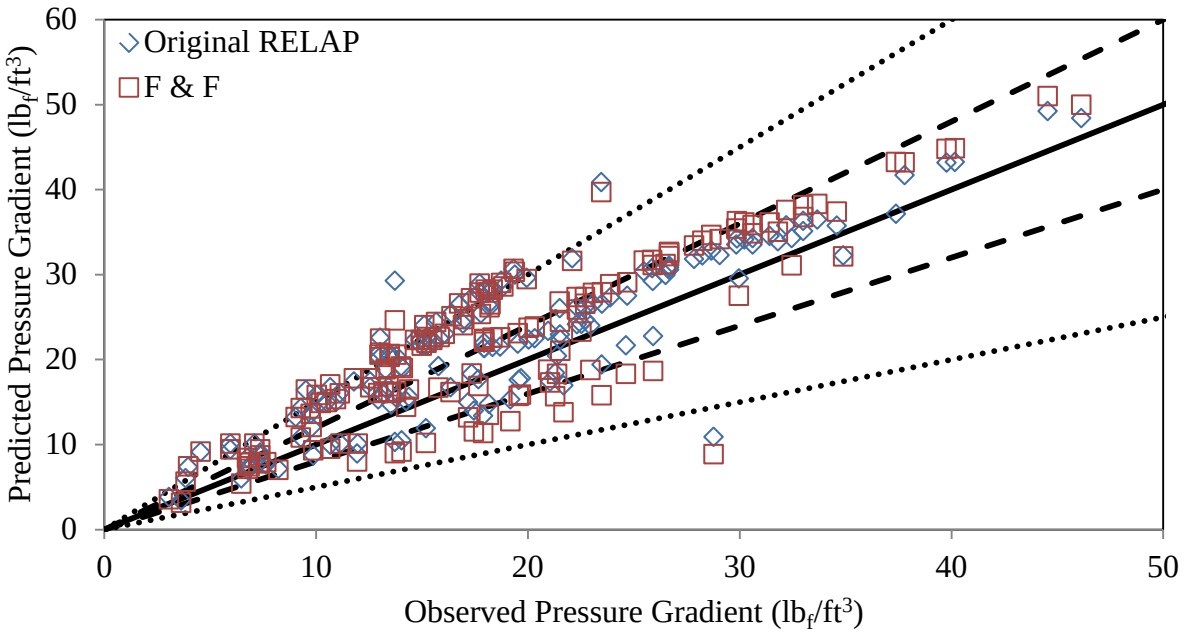

Figure 155: Comparison of the Pressure Gradient Prediction of the RELAP5/MOD3.3 [40] Liquid Film Volume Fraction Correlation to the Fukano and Furukawa [28] Film Thickness Correlation

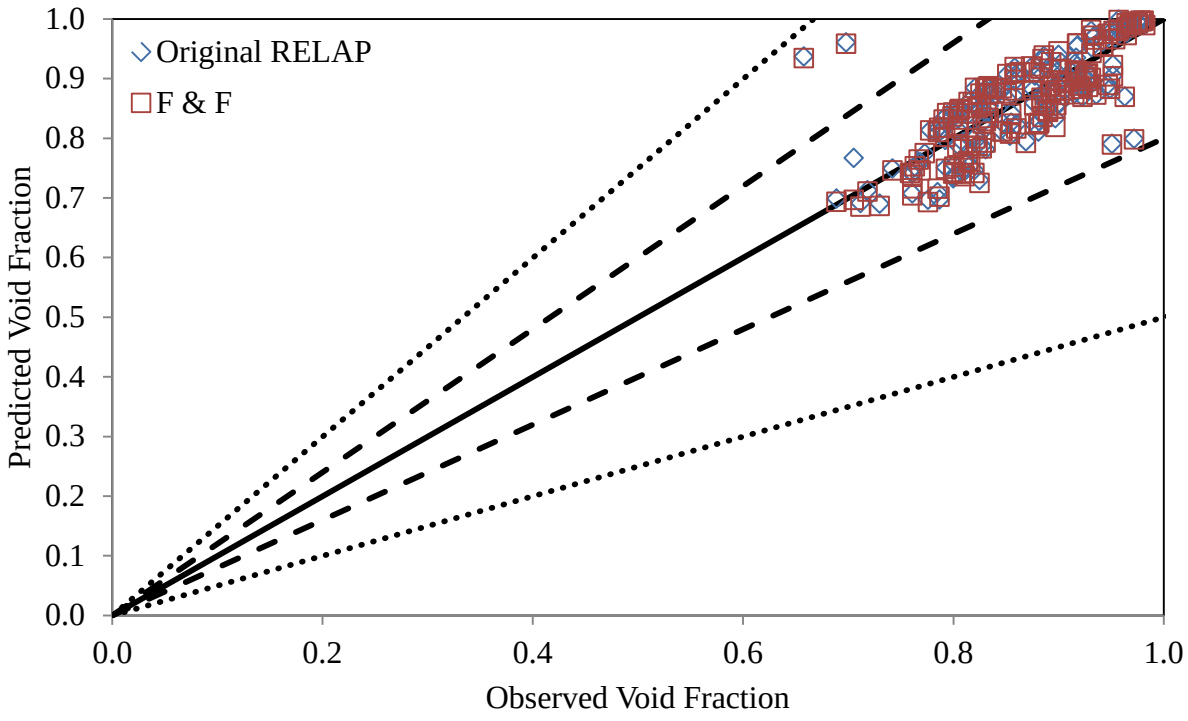

Figure 156: Comparison of the Void Fraction Prediction of the RELAP5/MOD3.3 [40] Liquid Film Volume Fraction Correlation to the Fukano and Furukawa [28] Film Thickness Correlation

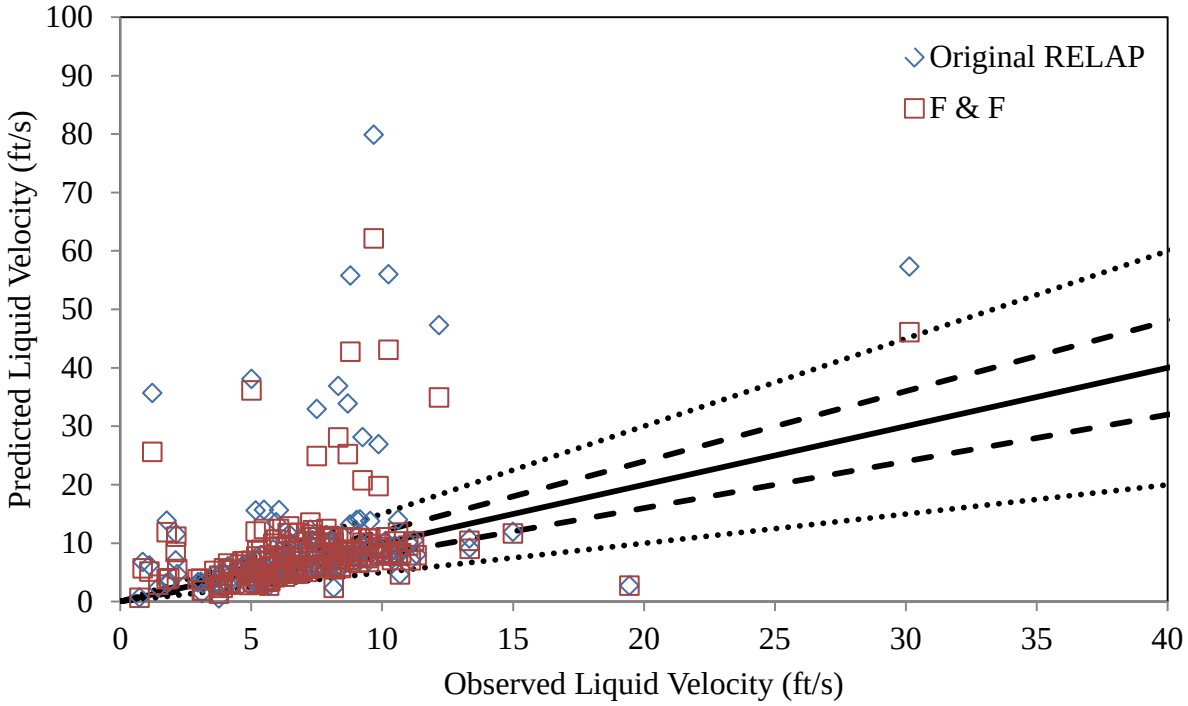

Figure 157: Comparison of the Liquid Velocity Prediction of the RELAP5/MOD3.3 [40] Liquid Film Volume Fraction Correlation to the Fukano and Furukawa [28] Film Thickness Correlation

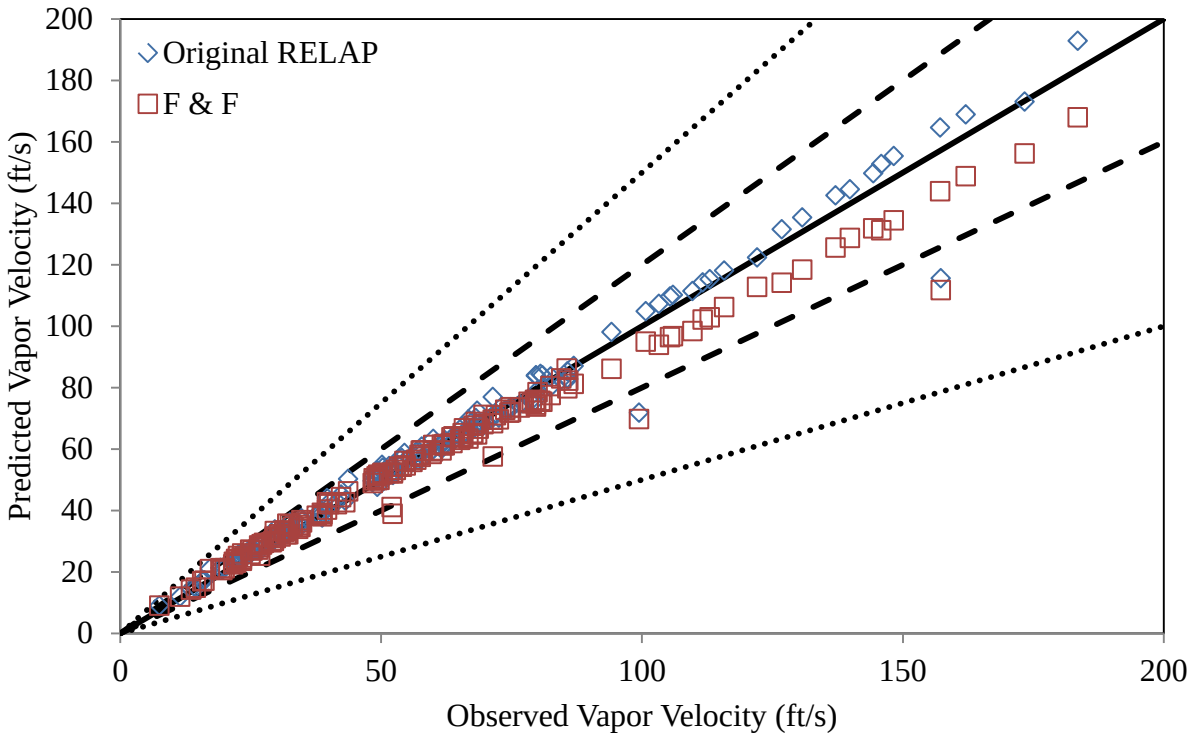

Figure 158: Comparison of the Vapor Velocity Prediction of the RELAP5/MOD3.3 [40] Liquid Film Volume Fraction Correlation to the Fukano and Furukawa [28] Film Thickness Correlation

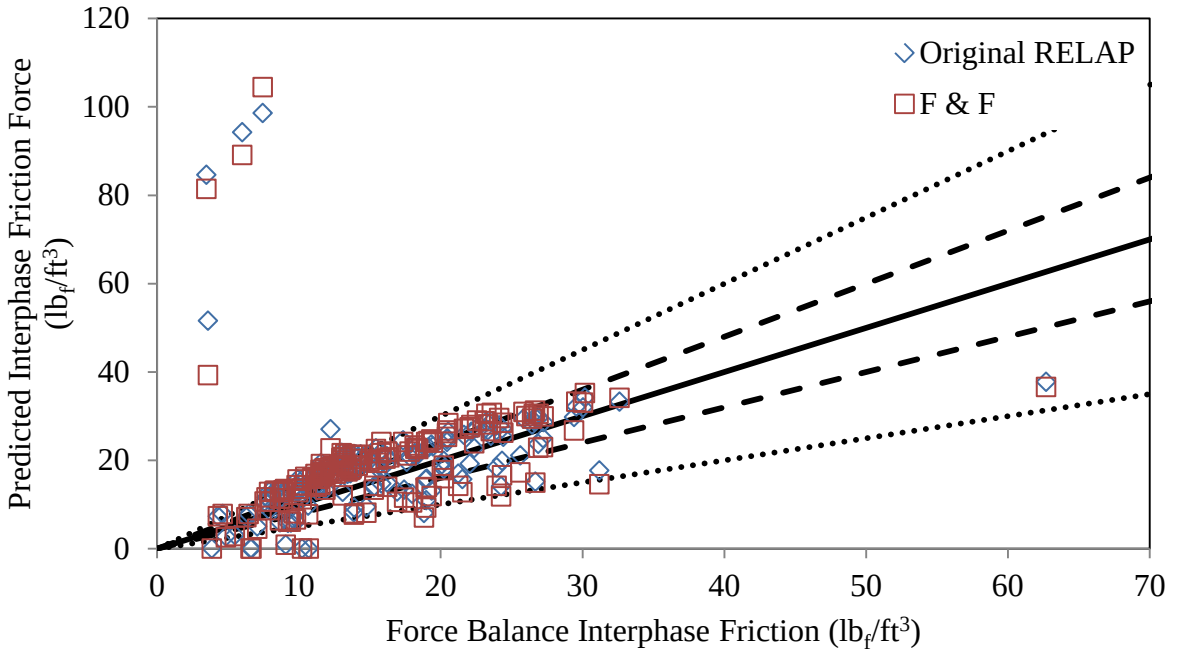

Figure 159: Comparison of the Interphase Friction Force Prediction of the RELAP5/MOD3.3 [40] Liquid Film Volume Fraction Correlation to the Fukano and Furukawa [28] Film Thickness Correlation

Comparing the errors of the unmodified RELAP model and the Fukano and Furukawa [28] film thickness correlation shows that the Fukano and Furukawa correlation provides less accurate predictions of pressure gradient, void fraction, phasic velocities and interphase friction force for most data points. Since the Fukano and Furukawa correlation provides some improvement for data points that are outliers for the unmodified RELAP model, the mean average error has shown some slight improvement in the case of liquid velocity and interphase friction, especially for steam-water.

Table 33: Comparison of Errors of the Original RELAP5/MOD3.3 [40] Liquid Film Volume Fraction Correlation to the Fukana and Furukawa [28] Film Thickness Correlation

			Original RELAP					F & F *δ/D* Correlation				
Total			dP/dz	α	v_f	v_g	F_{int}	dP/dz	α	v_f	v_g	F_{int}
All Annular	163	Mean Average	27.74%	4.54%	85.21%	4.53%	106.13%	30.75%	4.62%	73.96%	5.20%	90.09%
		Median Average	18.82%	3.70%	26.26%	3.55%	30.34%	23.28%	3.89%	28.55%	3.96%	35.11%
		± 20%	86	161	57	159	53	63	161	48	158	30
		- Percentage	52.76%	98.77%	34.97%	97.55%	32.52%	38.65%	98.77%	29.45%	96.93%	18.40%
		± 50%	131	163	123	163	128	131	163	121	163	125
		- Percentage	80.37%	100.00%	75.46%	100.00%	78.53%	80.37%	100.00%	74.23%	100.00%	76.69%
		Maximum	113.29%	42.36%	2816.63%	27.78%	2965.69%	100.86%	41.99%	1992.25%	29.87%	2934.21%
Air-Water	94	Mean Average	14.33%	3.35%	117.88%	2.89%	83.17%	19.46%	3.31%	98.75%	4.85%	60.17%
		Median Average	12.17%	3.05%	31.24%	2.44%	19.58%	18.44%	3.28%	38.39%	3.74%	27.18%
		± 20%	77	94	31	94	48	54	94	25	92	25
		- Percentage	81.91%	100.00%	32.98%	100.00%	51.06%	57.45%	100.00%	26.60%	97.87%	26.60%
		± 50%	92	94	62	94	88	92	94	59	94	85
		- Percentage	97.87%	100.00%	65.96%	100.00%	93.62%	97.87%	100.00%	62.77%	100.00%	90.43%
		Maximum	113.29%	8.74%	2816.63%	9.97%	2965.69%	79.14%	7.77%	1992.25%	25.52%	2934.21%
Steam-Water	69	Mean Average	46.01%	6.17%	40.72%	6.77%	137.42%	46.13%	6.40%	40.17%	5.68%	130.85%
		Median Average	47.61%	4.77%	22.14%	6.14%	46.86%	46.41%	5.07%	23.06%	4.32%	45.85%
		± 20%	9	67	26	65	5	9	67	23	66	5
		- Percentage	13.04%	97.10%	37.68%	94.20%	7.25%	13.04%	97.10%	33.33%	95.65%	7.25%
		± 50%	39	69	61	69	40	39	69	62	69	40
		- Percentage	56.52%	100.00%	88.41%	100.00%	57.97%	56.52%	100.00%	89.86%	100.00%	57.97%
		Maximum	99.95%	42.36%	660.97%	27.78%	2335.38%	100.86%	41.99%	621.05%	29.87%	2243.71%

4.5.2.3: The Berna, Escriva, Munoz-Cobo and Herranz Film Thickness Correlation

The Berna et al [8] film thickness correlation is defined by Equations 237, 238, 239, 240 and 242. There appears to be very similar results of the Berna et al [8] film thickness correlation to those with the Fukano and Furukawa [28] film thickness correlation. In Figure 160, we find that for most data points that Berna et al predict as slightly higher pressure gradient than the unmodified RELAP model, all when the unmodified RELAP model has overpredicted the pressure gradient with respect to the observed value. When the original RELAP model has underpredicted the pressure gradient, the trend has been for the Berna et al correlation to predict a lesser pressure gradient. Only upon close examination of the void fraction predictions in Figure 161 is it noticeable that there are small differences between the predicted void fractions of the unmodified RELAP model and the Berna et al correlation.

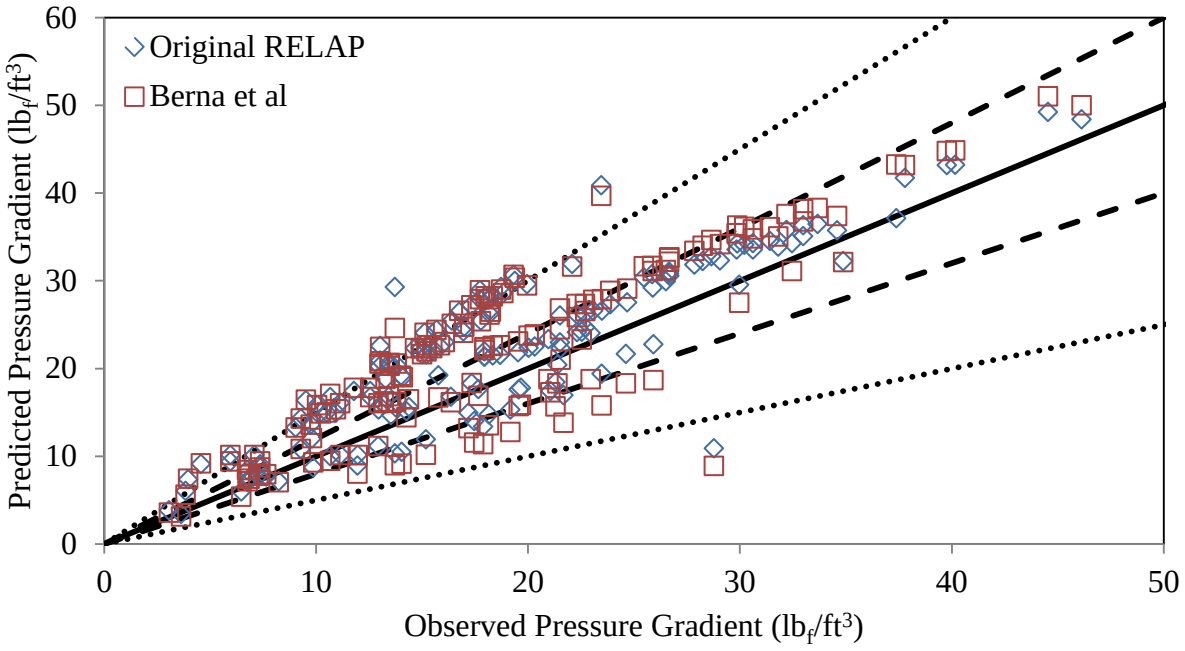

Figure 160: Comparison of the Pressure Gradient Prediction of the RELAP5/MOD3.3 [40] Liquid Film Volume Fraction Correlation to the Berna, Escriva, Munoz-Cobo and Herranz [8] Film Thickness Correlation

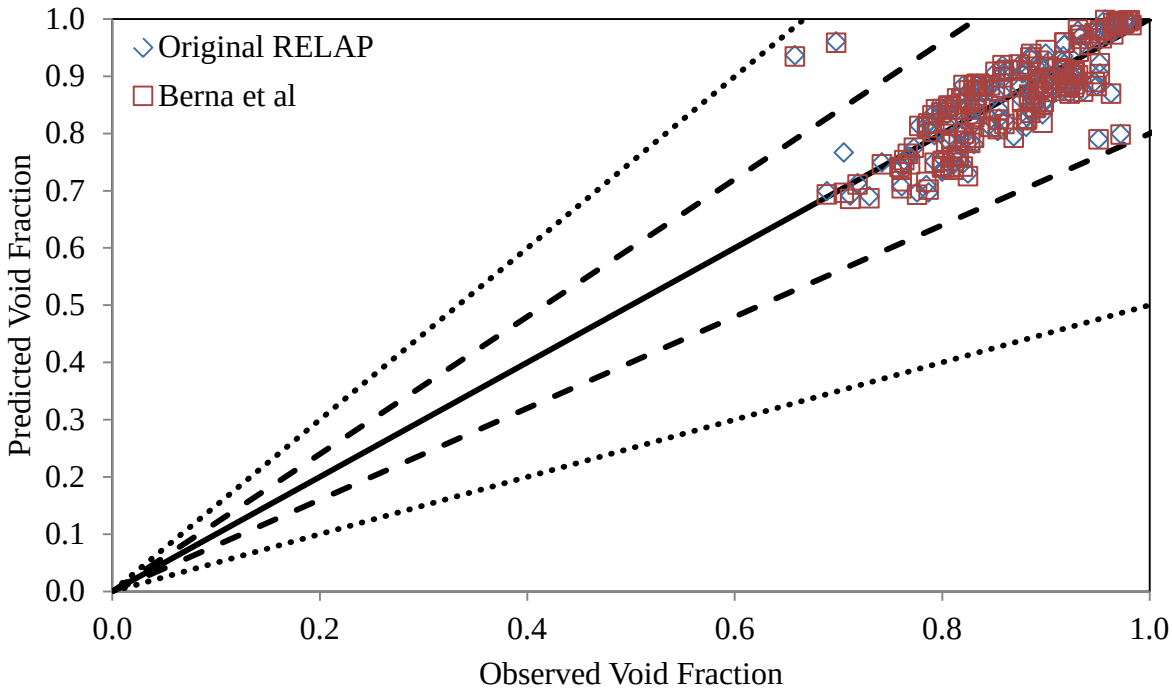

Figure 161: Comparison of the Void Fraction Prediction of the RELAP5/MOD3.3 [40] Liquid Film Volume Fraction Correlation to the Berna, Escriva, Munoz-Cobo and Herranz [8] Film Thickness Correlation

As was noticed in Figure 157 with the Fukano and Furukawa [28], the liquid velocity that is predicted by the unmodified RELAP model in Figure 162 has less outstanding outliers when the Berna et al [8] film thickness correlation is implemented. The similarities are also noticed with the vapor velocity predictions shown in Figure 163. Figure 164 shows the interphase friction force predictions of the unmodified RELAP model and the Berna et al film thickness correlation, which like the Fukano and Furukawa film thickness correlation shows that the interphase friction force predicted by the unmodified RELAP model matches the Berna et al correlation well, with the exception of a few outliers.

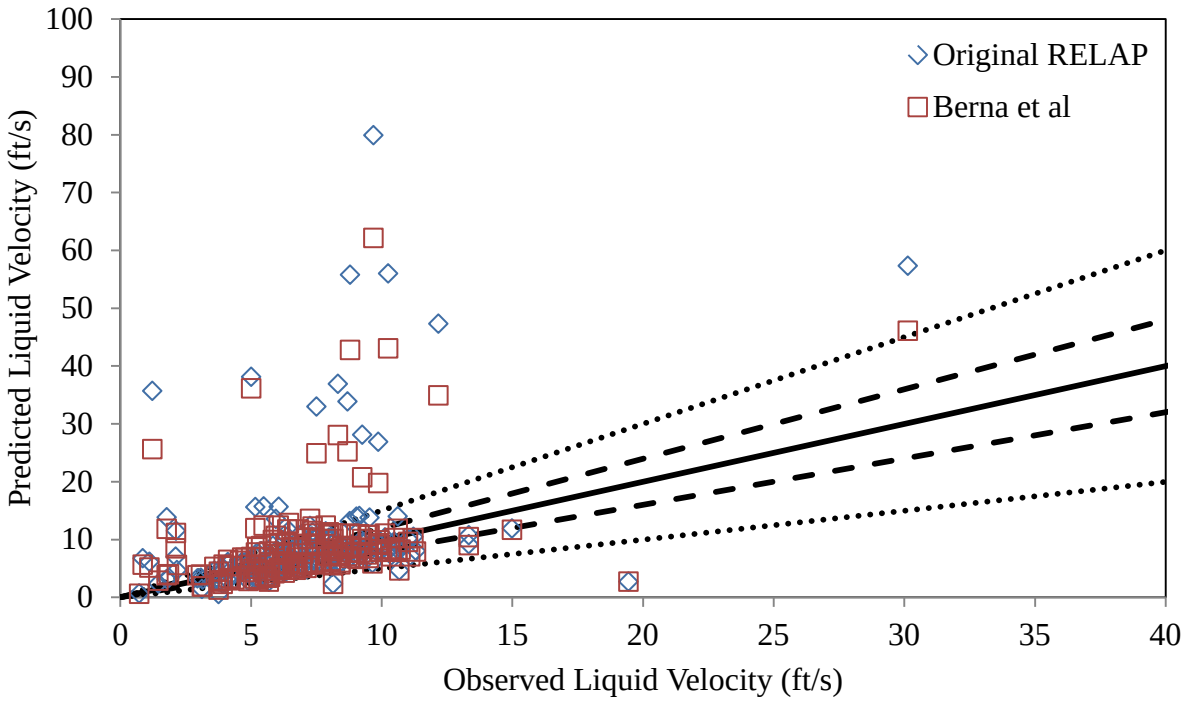

Figure 162: Comparison of the Liquid Velocity Prediction of the RELAP5/MOD3.3 [40] Liquid Film Volume Fraction Correlation to the Berna, Escriva, Munoz-Cobo and Herranz [8] Film Thickness Correlation

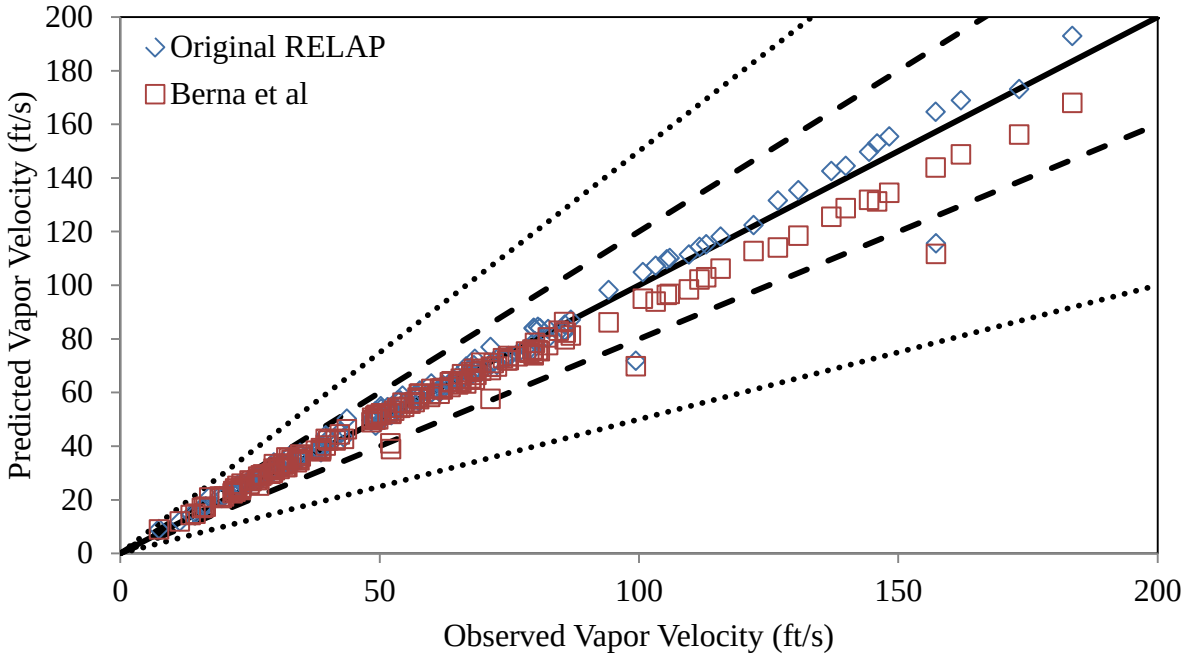

Figure 163: Comparison of the Vapor Velocity Prediction of the RELAP5/MOD3.3 [40] Liquid Film Volume Fraction Correlation to the Berna, Escriva, Munoz-Cobo and Herranz [8] Film Thickness Correlation

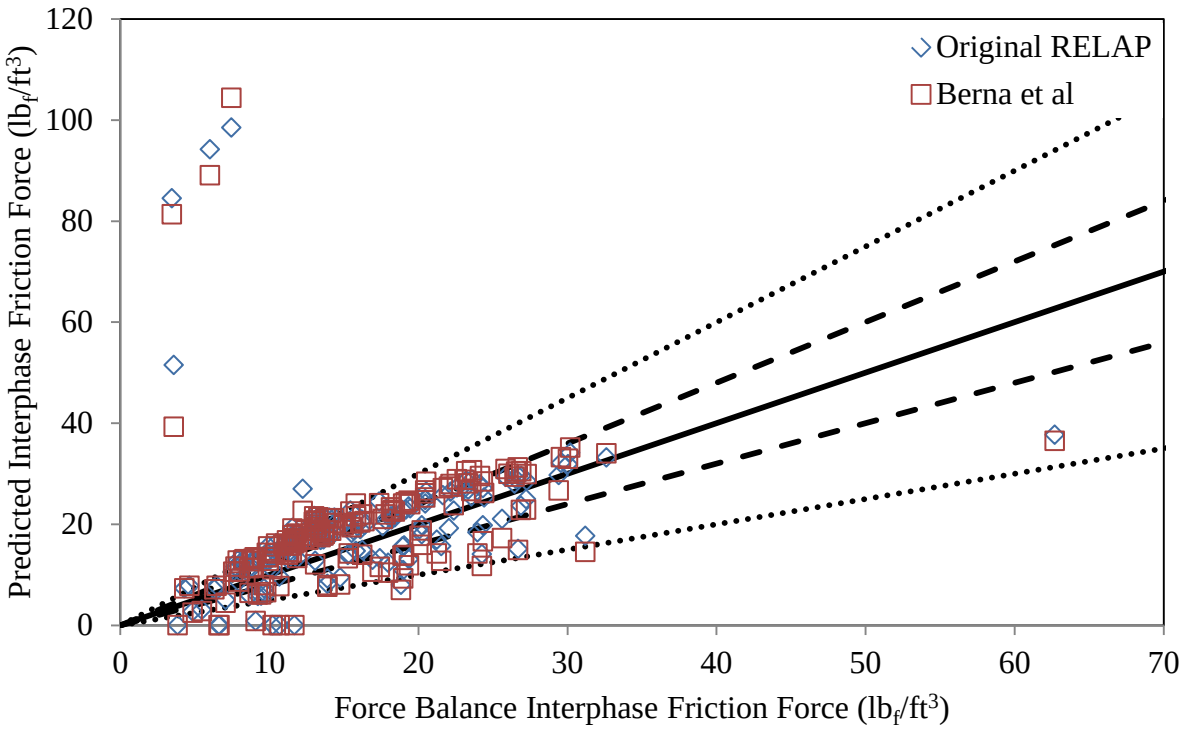

Figure 164: Comparison of the Interphase Friction Force Prediction of the RELAP5/MOD3.3 [40] Liquid Film Volume Fraction Correlation to the Berna, Escriva, Munoz-Cobo and Herranz [8] Film Thickness Correlation

Table 34 shows the errors of the original RELAP model and the Berna et al [8] film thickness correlation. The results show that the Berna et al correlation mainly improves upon data points where the maximum error for the unmodified RELAP model occurred for pressure gradient, void fraction, liquid velocity and interphase friction. However, for most data points, the Berna et al film thickness correlation provides a less accurate prediction of the interphase friction than the unmodified RELAP model.

Table 34: Comparison of Errors of the Original RELAP5/MOD3.3 [40] Liquid Film Volume Fraction Correlation to the Berna, Escriva, Munoz-Cobo and Herranz [8] Film Thickness Correlation

Total			Original RELAP					Berna et al δ/D Correlation				
			dP/dz	α	v_f	v_g	F_{int}	dP/dz	α	v_f	v_g	F_{int}
All Annular	163	Mean Average	27.74%	4.54%	85.21%	4.53%	106.13%	30.75%	4.62%	73.96%	5.20%	90.09%
		Median Average	18.82%	3.70%	26.26%	3.55%	30.34%	23.28%	3.89%	28.55%	3.96%	35.11%
		± 20%	86	161	57	159	53	63	161	48	158	30
		- Percentage	52.76%	98.77%	34.97%	97.55%	32.52%	38.65%	98.77%	29.45%	96.93%	18.40%
		± 50%	131	163	123	163	128	131	163	121	163	125
		- Percentage	80.37%	100.00%	75.46%	100.00%	78.53%	80.37%	100.00%	74.23%	100.00%	76.69%
		Maximum	113.29%	42.36%	2816.63%	27.78%	2965.69%	100.86%	41.99%	1992.25%	29.87%	2934.21%
Air-Water	94	Mean Average	14.33%	3.35%	117.88%	2.89%	83.17%	19.46%	3.31%	98.75%	4.85%	60.17%
		Median Average	12.17%	3.05%	31.24%	2.44%	19.58%	18.44%	3.28%	38.39%	3.74%	27.18%
		± 20%	77	94	31	94	48	54	94	25	92	25
		- Percentage	81.91%	100.00%	32.98%	100.00%	51.06%	57.45%	100.00%	26.60%	97.87%	26.60%
		± 50%	92	94	62	94	88	92	94	59	94	85
		- Percentage	97.87%	100.00%	65.96%	100.00%	93.62%	97.87%	100.00%	62.77%	100.00%	90.43%
		Maximum	113.29%	8.74%	2816.63%	9.97%	2965.69%	79.14%	7.77%	1992.25%	25.52%	2934.21%
Steam-Water	69	Mean Average	46.01%	6.17%	40.72%	6.77%	137.42%	46.13%	6.40%	40.17%	5.68%	130.85%
		Median Average	47.61%	4.77%	22.14%	6.14%	46.86%	46.41%	5.07%	23.06%	4.32%	45.85%
		± 20%	9	67	26	65	5	9	67	23	66	5
		- Percentage	13.04%	97.10%	37.68%	94.20%	7.25%	13.04%	97.10%	33.33%	95.65%	7.25%
		± 50%	39	69	61	69	40	39	69	62	69	40
		- Percentage	56.52%	100.00%	88.41%	100.00%	57.97%	56.52%	100.00%	89.86%	100.00%	57.97%
		Maximum	99.95%	42.36%	660.97%	27.78%	2335.38%	100.86%	41.99%	621.05%	29.87%	2243.71%

4.5.3: Analyses of the Entrainment Correlations

The next correlations to be studied are the entrainment correlations. RELAP does not directly use entrainment correlations to determine the amount of liquid that is within the vapor core. Instead, the liquid volume of the droplets within the core is calculated using Equation 118. In order to implement the entrainment correlations into the RELAP, Equation 234 was derived to relate the entrainment, E, to the liquid volume of the droplets, α_{fd}. Some assumptions had to be made in order for Equation 234 to derived from Equation 226 and be inserted into RELAP. The velocity of the liquid film, v_{ff}, was approximated as the liquid velocity, v_f, while the liquid droplet

velocity, v_{fd}, was approximated as the vapor velocity, v_g. Additionally, the liquid film volume fraction, α_{ff}, was approximated as the liquid volume fraction, α_f.

4.5.3.1: The Ishii and Mishima Entrainment Correlation

The Ishii and Mishima [47] entrainment correlation is used in RELAP to calculate the liquid film volume fraction, although the method is circuitously described within the RELAP manual. [70] In this case, the Ishii and Mishima entrainment correlation has been applied in a more direct manner with the hope of achieving a more desirable result. Unfortunately, it was discovered in running RELAP modified with the Ishii and Mishima entrainment correlation that most of the air-water data points resulted in RELAP experiencing transient errors. The steam-water data did not appear to be affected by the same errors.

In Figure 165, the pressure gradient prediction of the original RELAP model is compared to RELAP that has been modified with the Ishii and Mishima [47] correlation. For the data points which produced usable results, the Ishii and Mishima entrainment correlation appears to have matched the observed pressure gradient slightly better than the unmodified RELAP model runs. As with the unmodified RELAP model data, the Ishii and Mishima correlation appears to slightly overpredict the pressure gradient for most data points that have been analyzed.

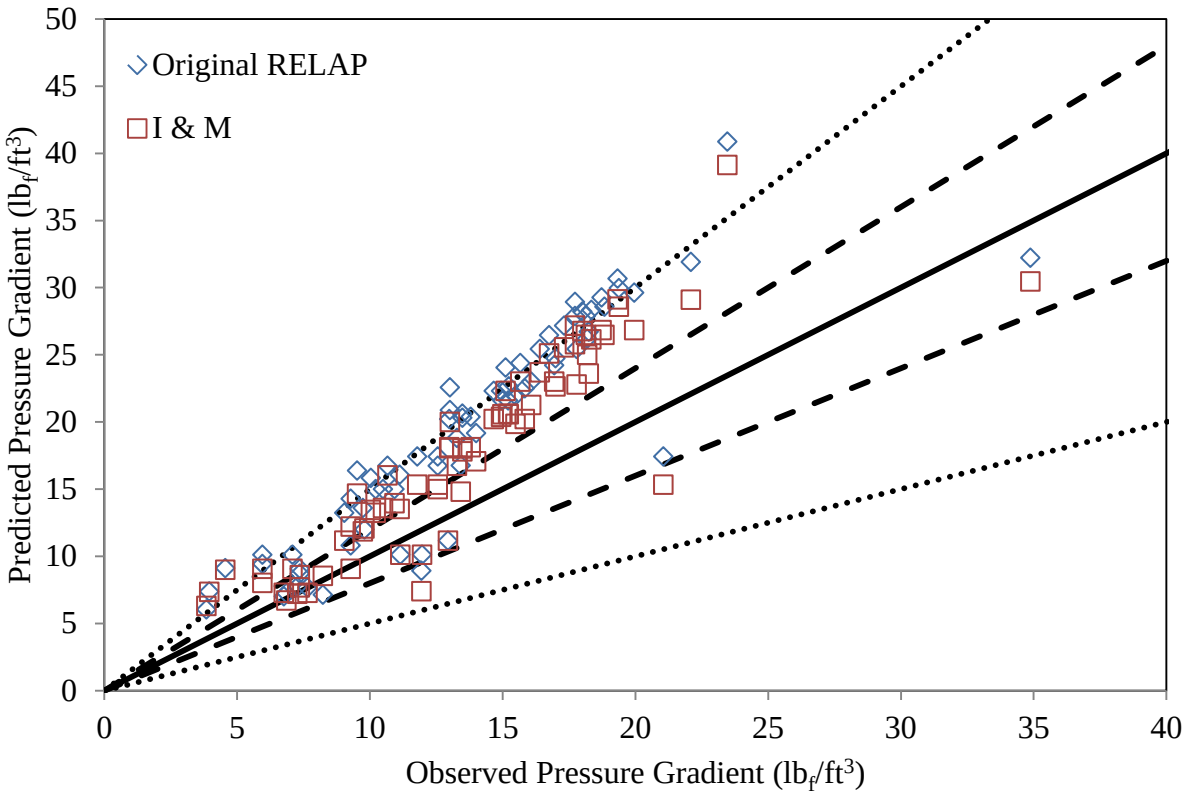

Figure 165: Comparison of the Pressure Gradient Prediction of the RELAP5/MOD3.3 [40] Droplet Volume Fraction Correlation to the Ishii and Mishima [47] Entrainment Correlation

The void fraction predictions of the unmodified RELAP model and the Ishii and Mishima [47] correlation are shown in Figure 166, with both models appearing to match the observed void fraction for most observable data points. The liquid velocity prediction shown in Figure 167 indicates that the Ishii and Mishima correlation appears to predict higher liquid velocities than the unmodified RELAP model, but that both models mostly predict liquid velocities that are within ±50% of the observed liquid velocity with only a few outliers. Figure 168 indicates for the observed data points that the vapor velocity is very well predicted by both the unmodified RELAP model and the Ishii and Mishima entrainment correlation.

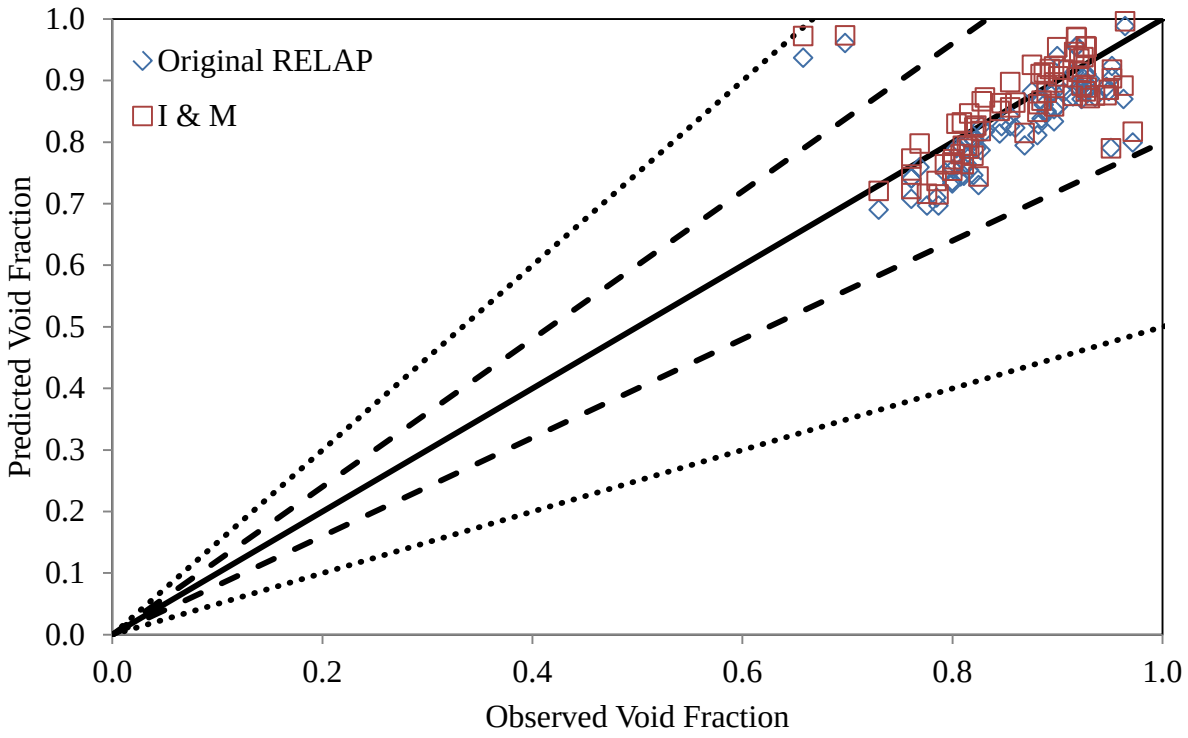

Figure 166: Comparison of the Void Fraction Prediction of the RELAP5/MOD3.3 [40] Droplet Volume Fraction Correlation to the Ishii and Mishima [47] Entrainment Correlation

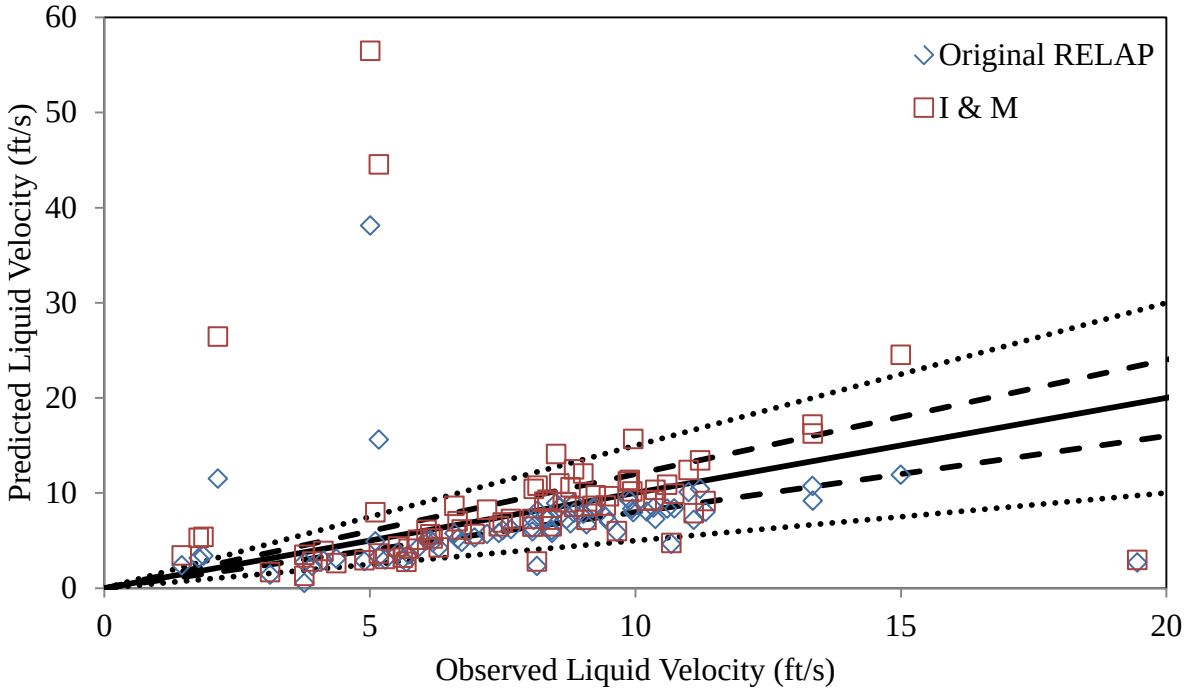

Figure 167: Comparison of the Liquid Velocity Prediction of the RELAP5/MOD3.3 [40] Droplet Volume Fraction Correlation to the Ishii and Mishima [47] Entrainment Correlation

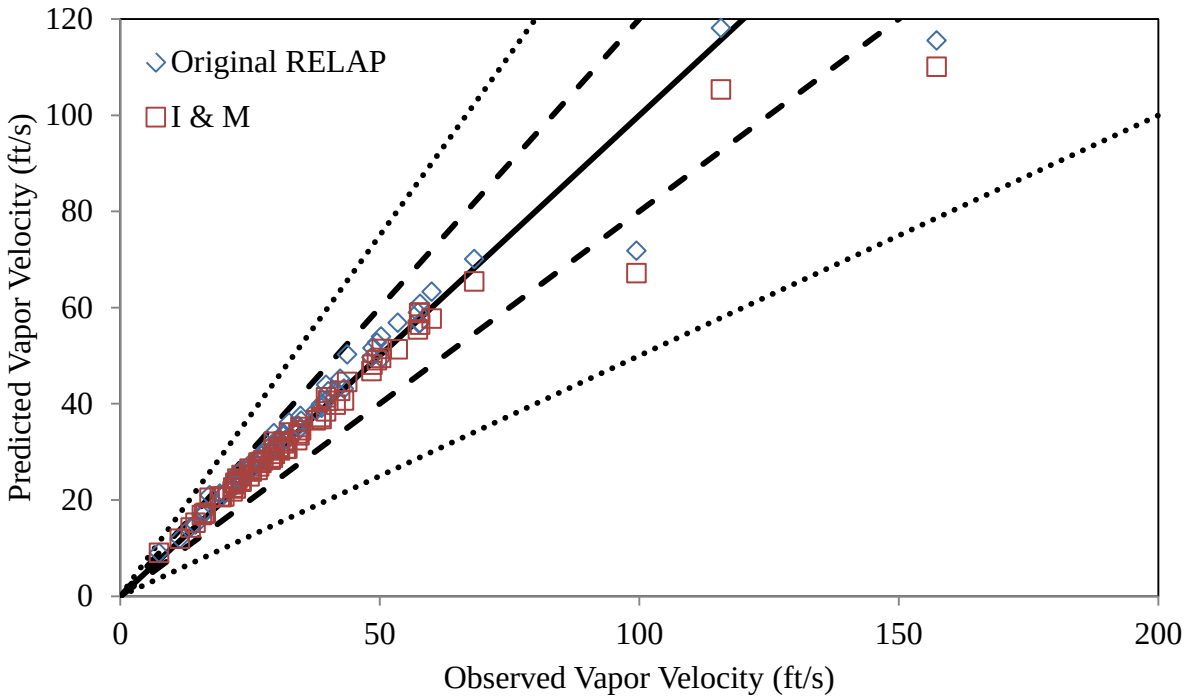

Figure 168: Comparison of Vapor Velocity Prediction of the RELAP5/MOD3.3 [40] Droplet Volume Fraction Correlation to the Ishii and Mishima [47] Entrainment Correlation

In Figure 169, the interphase friction force that is predicted by the unmodified RELAP model and RELAP with the Ishii and Mishima [47] correlation is shown. Both models produce similar results for the interphase friction force for most data points, and both appear to slightly overestimate the interphase friction force for most cases, when compared to the force balance value.

Table 35 provides a comparison of the error percentages of the unmodified RELAP model and the Ishii and Mishima [47] entrainment correlation. As only 4 air-water data points produced a solution with the Ishii and Mishima entrainment correlation, the only significant conclusion that can be drawn from the data is that the Ishii and Mishima entrainment correlation is too unstable to use for modeling air-water two-phase flow, as it appears to easily trigger transient errors. However, when looking at the steam-water data, it appears that the Ishii and Mishima correlation does provide some benefit to improving the modeling of two-phase flow.

The median average error improved for all variables that are examined for the steam-water data, and the mean average error improved for the pressure gradient, void fraction, vapor velocity and interphase friction force. The one drawback that is noticed with the Ishii and Mishima entrainment correlation is that the maximum errors increased for the void fraction, phasic velocities and interphase friction force. The most significant increase in maximum error appears to be with the liquid velocity.

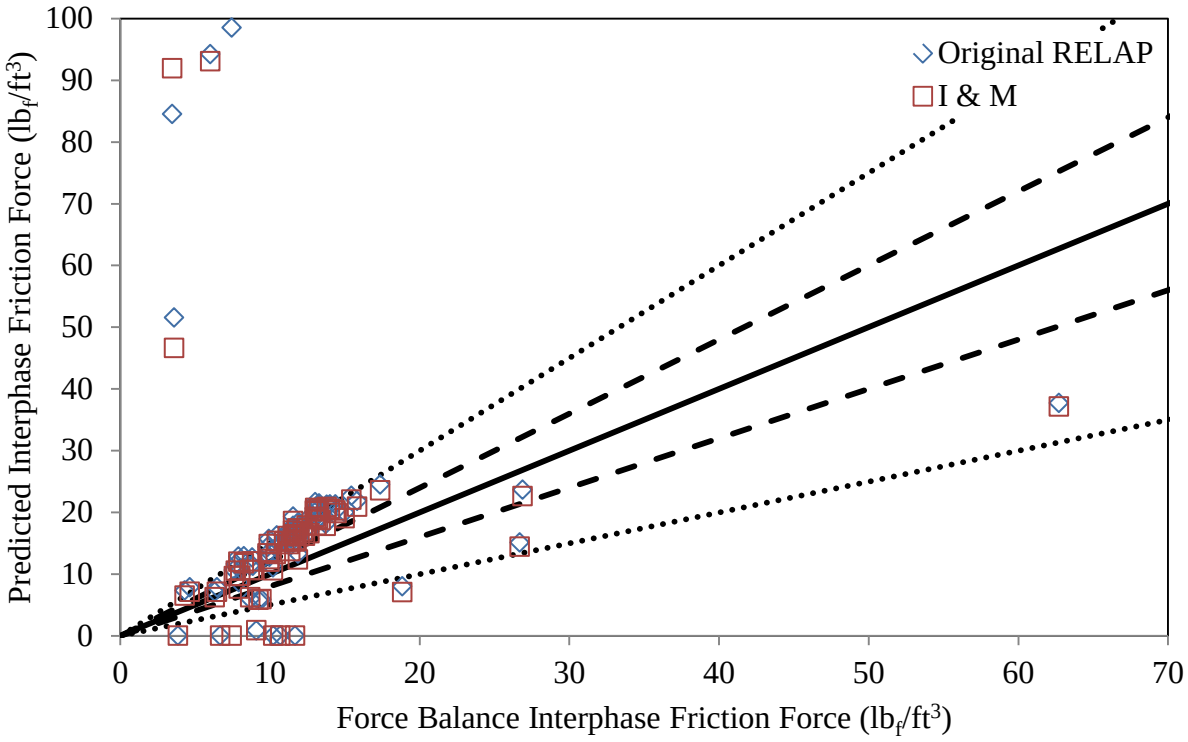

Figure 169: Comparison of the Interphase Friction Force Prediction of the RELAP5/MOD3.3 [40] Droplet Volume Fraction Correlation to the Ishii and Mishima [47] Entrainment Correlation

Table 35: Comparison of Errors of the Original RELAP5/MOD3.3 [40] Droplet Volume Fraction Correlation to the Ishii and Mishima [47] Entrainment Correlation

	Total		Original RELAP					Ishii and Mishima *E* Correlation				
			dP/dz	α	v_f	v_g	F_{int}	dP/dz	α	v_f	v_g	F_{int}
All Annular	73	Mean Average	44.00%	6.03%	44.31%	6.50%	132.15%	33.44%	5.04%	69.48%	4.53%	111.86%
		Median Average	46.45%	4.57%	22.63%	5.48%	45.97%	33.20%	3.59%	21.14%	3.29%	40.06%
		± 20%	12	71	26	69	5	14	71	35	71	6
		- Percentage	16.44%	97.26%	35.62%	94.52%	6.85%	19.18%	97.26%	47.95%	97.26%	8.22%
		± 50%	43	73	61	73	43	63	73	58	73	53
		- Percentage	58.90%	100.00%	83.56%	100.00%	58.90%	86.30%	100.00%	79.45%	100.00%	72.60%
		Maximum	99.95%	42.36%	660.97%	27.78%	2335.38%	97.04%	47.78%	1136.04%	32.47%	2548.13%
Air-Water	4	Mean Average	9.35%	3.72%	106.30%	1.80%	41.22%	11.61%	5.15%	321.01%	3.82%	41.26%
		Median Average	5.93%	4.01%	79.94%	1.76%	37.88%	3.77%	5.65%	193.52%	2.13%	37.24%
		± 20%	3	4	0	4	0	3	4	0	4	0
		- Percentage	75.00%	100.00%	0.00%	100.00%	0.00%	75.00%	100.00%	0.00%	100.00%	0.00%
		± 50%	4	4	0	4	3	4	4	0	4	3
		- Percentage	100.00%	100.00%	0.00%	100.00%	75.00%	100.00%	100.00%	0.00%	100.00%	75.00%
		Maximum	25.37%	4.40%	201.71%	2.02%	57.53%	38.06%	6.02%	761.46%	9.03%	62.54%
Steam-Water	69	Mean Average	46.01%	6.17%	40.72%	6.77%	137.42%	34.70%	5.04%	54.90%	4.57%	115.95%
		Median Average	47.61%	4.77%	22.14%	6.14%	46.86%	33.58%	3.43%	19.98%	3.31%	40.18%
		± 20%	9	67	26	65	5	11	67	35	67	6
		- Percentage	13.04%	97.10%	37.68%	94.20%	7.25%	15.94%	97.10%	50.72%	97.10%	8.70%
		± 50%	39	69	61	69	40	59	69	58	69	50
		- Percentage	56.52%	100.00%	88.41%	100.00%	57.97%	85.51%	100.00%	84.06%	100.00%	72.46%
		Maximum	99.95%	42.36%	660.97%	27.78%	2335.38%	97.04%	47.78%	1136.04%	32.47%	2548.13%

4.5.3.2: The First Sawant, Ishii and Mori Entrainment Correlation

As was the case with the Ishii and Mishima [47] entrainment correlation, most of the air-water RELAP simulations that had been modified with the first Sawant et al [71] entrainment correlation ended in transient errors. However, there were no transient errors with any steam-water data points, and so the bulk of the data analysis that is conducted for the first Sawant et al entrainment correlation will involve the steam-water data points.

In Figure 170, the pressure gradient predictions for the unmodified RELAP model and the first Sawant et al [71] entrainment correlation are shown, with very similar results for the data points at which the first Sawant et al entrainment model did not experience a transient error.

For the data points shown, both the unmodified RELAP model and the first Sawant et al entrainment model appear to overpredict the pressure gradient by about 50% in many cases, with only a few points showing underprediction. This correlates with the underprediction of void fraction for most data points that is noticed for both the first Sawant et al entrainment correlation and the unmodified RELAP model in Figure 171.

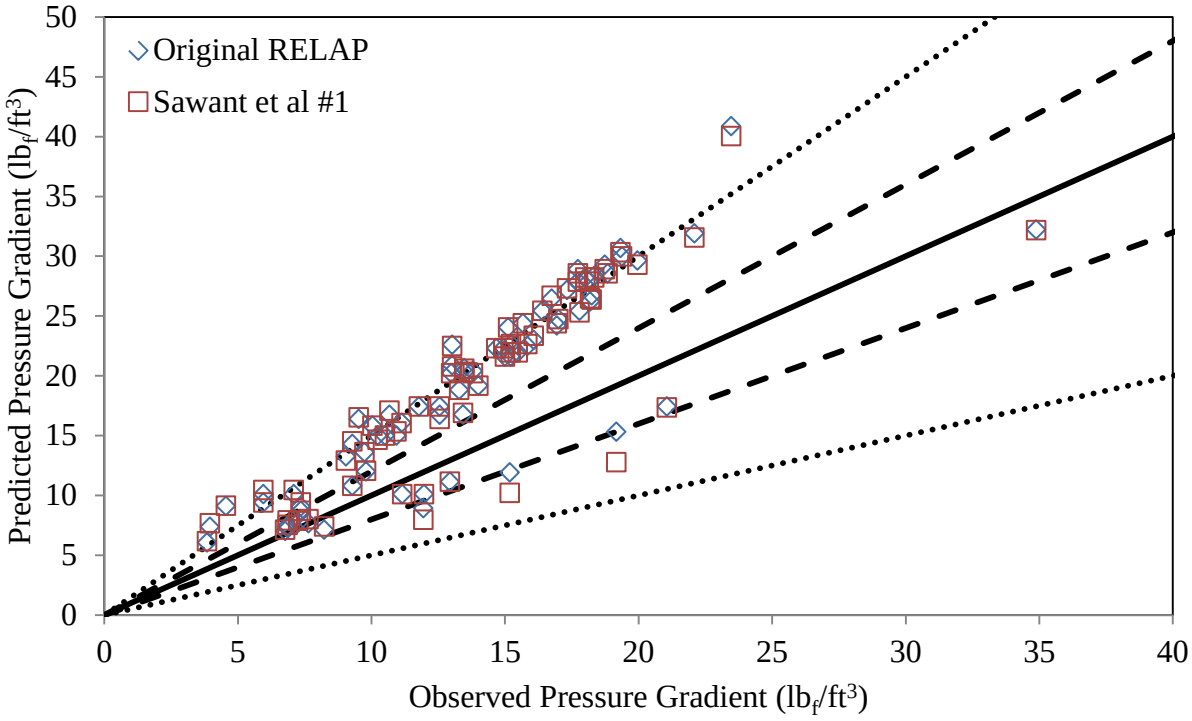

Figure 170: Comparison of the Pressure Gradient Prediction of the RELAP5/MOD3.3 [40] Droplet Volume Fraction Correlation to the First Sawant, Ishii and Mori [69] Entrainment Correlation

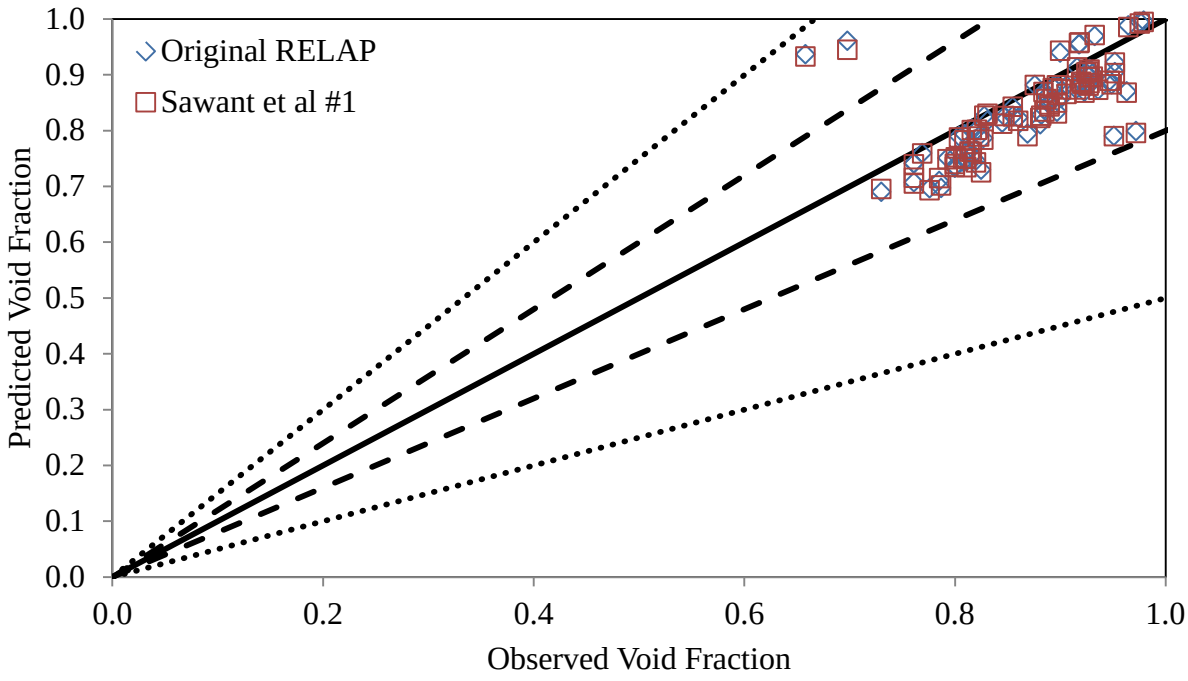

Figure 171: Comparison of the Void Fraction Prediction of the RELAP5/MOD3.3 [40] Droplet Volume Fraction Correlation to the First Sawant, Ishii and Mori [69] Entrainment Correlation

With an underprediction of void fraction, it is expected that for most data points, the liquid velocity is also underpredicted, while the vapor velocity is overpredicted, in order to maintain continuity. While the liquid velocity does appear to be underpredicted in Figure 172, the vapor velocity only appears to be a very close match to the observed vapor velocity for both the unmodified RELAP model and the first Sawant et al [71] entrainment correlation in Figure 174. Finally, as we look at the interphase friction force that is predicted by both the unmodified RELAP model and the first Sawant et al correlation in Figure 175, the general trend is that the interphase friction force is overpredicted.

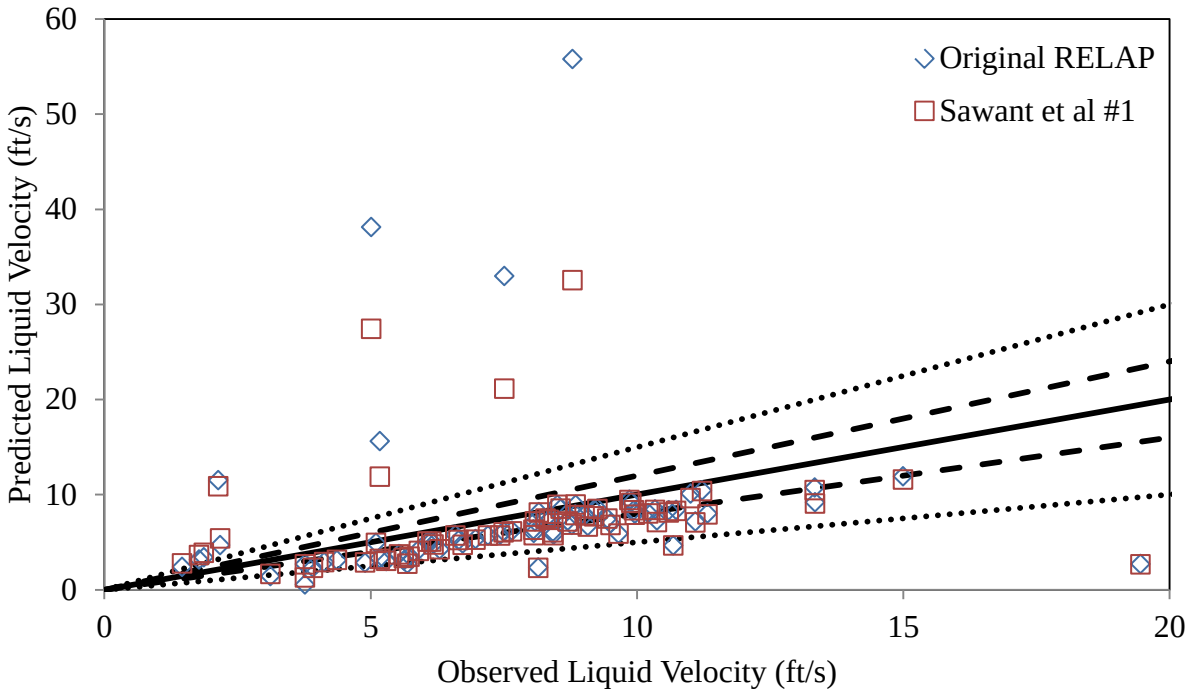

Figure 172: Comparison of the Liquid Velocity Prediction for the RELAP5/MOD3.3 [40] Droplet Volume Fraction Correlation to the First Sawant, Ishii and Mori [69] Entraiment Correlation

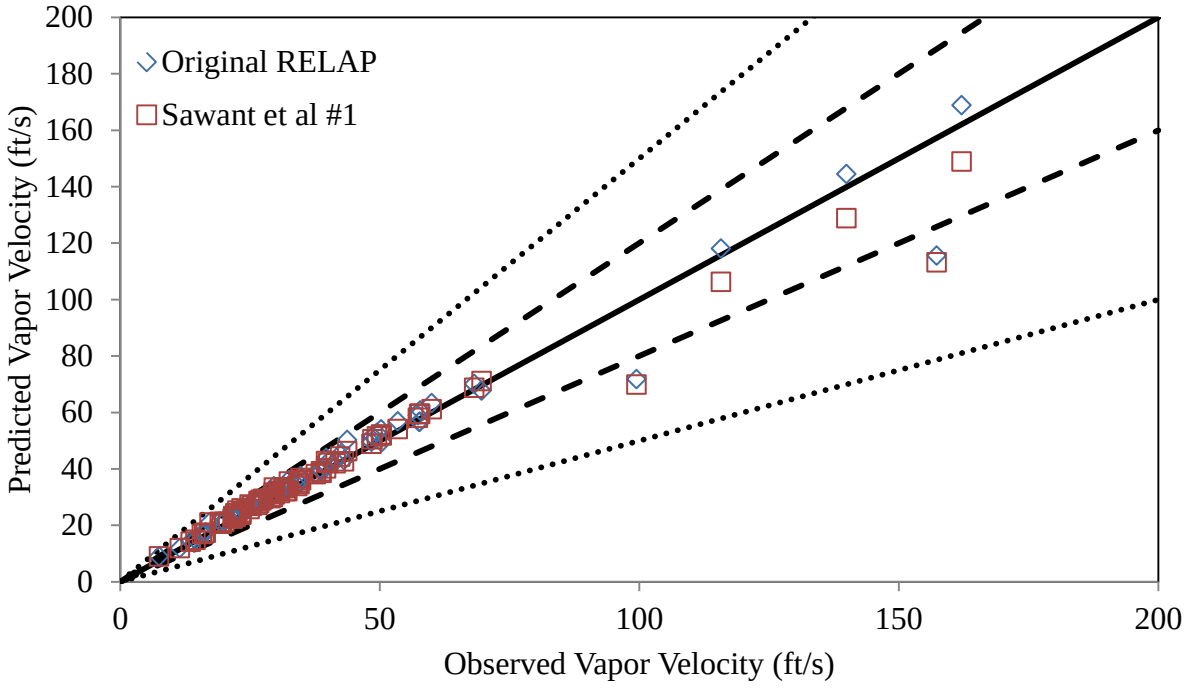

Figure 173: Comparison of the Vapor Velocity Prediction for the RELAP5/MOD3.3 [40] Droplet Volume Fraction Correlation to the First Sawant, Ishii and Mori [69] Entrainment Correlation

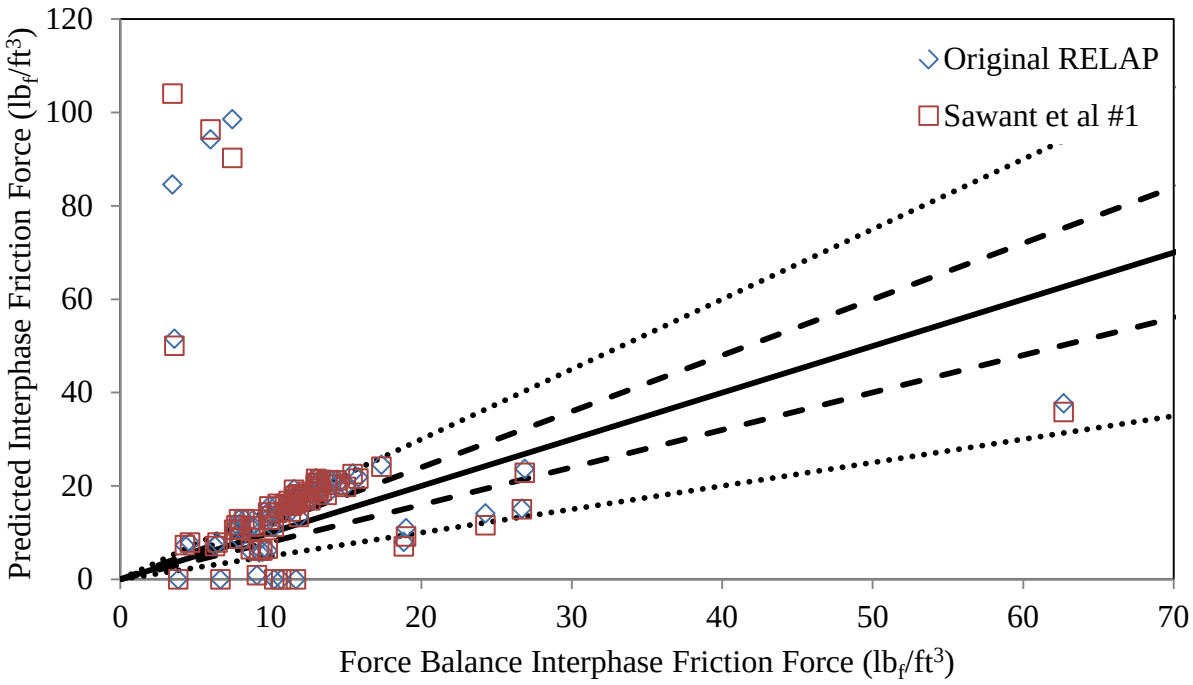

Figure 174: Comparison of the Interphase Friction Force Prediction of the RELAP5/MOD3.3 Droplet Volume Fraction Correlation to the First Sawant, Ishii and Mori [69] Entrainment Correlation

Table 36 shows the errors of both the original RELAP model and the first Sawant et al [71] entrainment model for the 76 data points for which a solution could be obtained. The first Sawant et al model only shows modest improvements over the original RELAP model for the steam-water data, and as has been stated, proved to be very unreliable in being able to model the air-water data.

Table 36: Comparison of Errors of the Original RELAP5/MOD3.3 [40] Droplet Volume Fraction Correlation to the First Sawant, Ishii and Mori [69] Entrainment Correlation

			Original RELAP					Sawant et al *E* Correlation #1				
Total			dP/dz	α	v_f	v_g	F_{int}	dP/dz	α	v_f	v_g	F_{int}
All Annular	76	Mean Average	42.93%	5.90%	55.58%	6.38%	128.54%	43.82%	6.01%	47.59%	5.63%	134.29%
		Median Average	45.95%	4.49%	24.93%	5.44%	45.76%	45.32%	4.80%	25.81%	4.21%	45.59%
		± 20%	13	74	26	72	5	13	74	23	73	5
		- Percentage	17.11%	97.37%	34.21%	94.74%	6.58%	17.11%	97.37%	30.26%	96.05%	6.58%
		± 50%	46	76	61	76	46	46	76	62	76	45
		- Percentage	60.53%	100.00%	80.26%	100.00%	60.53%	60.53%	100.00%	81.58%	100.00%	59.21%
		Maximum	99.95%	42.36%	660.97%	27.78%	2335.38%	100.41%	41.76%	447.15%	29.77%	2896.38%
Air-Water	7	Mean Average	12.55%	3.21%	202.06%	2.51%	40.98%	19.66%	3.26%	147.31%	5.10%	42.02%
		Median Average	8.64%	3.89%	115.52%	2.02%	38.12%	15.11%	4.08%	129.68%	3.26%	34.67%
		± 20%	4	7	0	7	0	4	7	0	7	0
		- Percentage	57.14%	100.00%	0.00%	100.00%	0.00%	57.14%	100.00%	0.00%	100.00%	0.00%
		± 50%	7	7	0	7	6	7	7	0	7	4
		- Percentage	100.00%	100.00%	0.00%	100.00%	85.71%	100.00%	100.00%	0.00%	100.00%	57.14%
		Maximum	25.37%	4.40%	534.59%	4.21%	57.53%	33.45%	4.80%	270.20%	8.24%	62.81%
Steam-Water	69	Mean Average	46.01%	6.17%	40.72%	6.77%	137.42%	46.28%	6.29%	37.47%	5.68%	143.65%
		Median Average	47.61%	4.77%	22.14%	6.14%	46.86%	46.65%	5.03%	23.16%	4.26%	45.61%
		± 20%	9	67	26	65	5	9	67	23	66	5
		- Percentage	13.04%	97.10%	37.68%	94.20%	7.25%	13.04%	97.10%	33.33%	95.65%	7.25%
		± 50%	39	69	61	69	40	39	69	62	69	41
		- Percentage	56.52%	100.00%	88.41%	100.00%	57.97%	56.52%	100.00%	89.86%	100.00%	59.42%
		Maximum	99.95%	42.36%	660.97%	27.78%	2335.38%	100.41%	41.76%	447.15%	29.77%	2896.38%

4.5.3.3: The Second Sawant, Ishii and Mori Entrainment Correlation

As has been the case with the two previous entrainment model correlations, the second Sawant et al [71] entrainment correlation, given in Equation 250, also produced transient errors for most of the air-water data, making comparisons of results from both data sets limited to mostly steam-water data.

As we look at the results that are available for comparing the second Sawant et al [71] correlation to the unmodified RELAP, we find that the results are very similar to those found with the first Sawant et al [69] entrainment correlation. In Figure 176, the pressure gradient is overpredicted for most data points with both the unmodified RELAP and the second Sawant et al

entrainment correlation. This results in the underprediction of the void fraction for most data points by both models in Figure 177. With the void fraction underpredicted, continuity dictates that the liquid velocity will also be underpredicted, as shown in Figure 178 and that the vapor velocity will be overpredicted, which can be seen in Figure 179. An increased velocity difference results in an overprediction of the interphase friction force, which is shown in Figure 180.

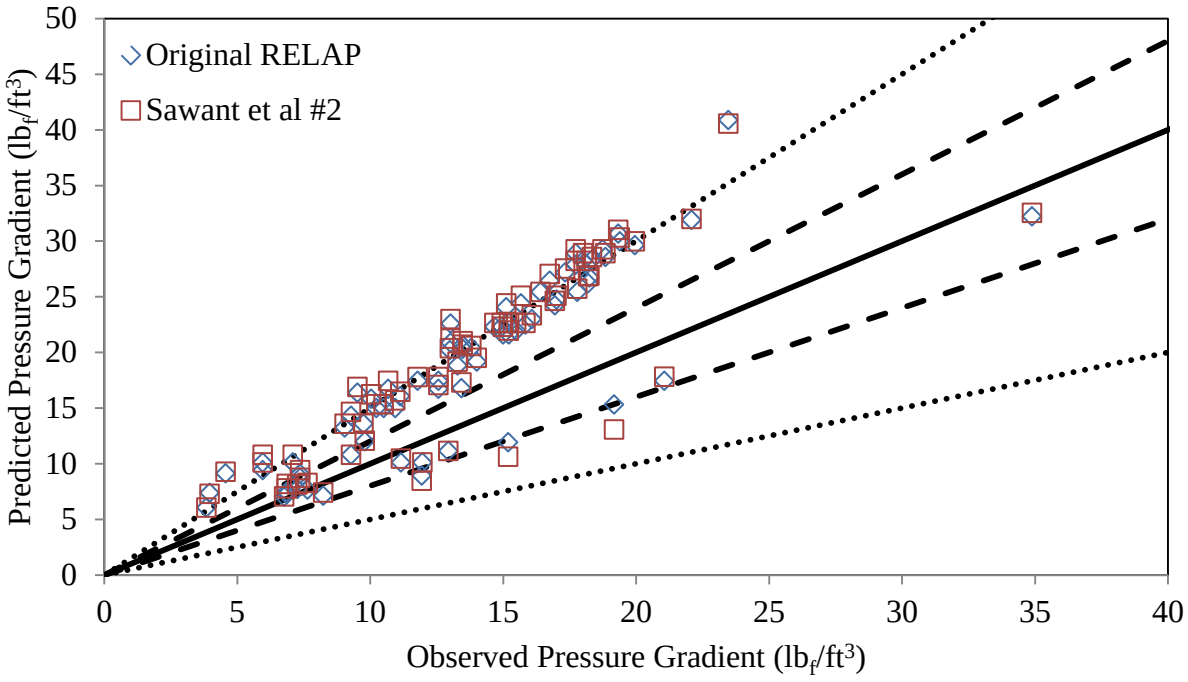

Figure 175: Comparison of the Pressure Gradient Prediction of the RELAP5/MOD3.3 [40] Droplet Volume Fraction Correlation to the Second Sawant, Ishii and Mori Entrainment Correlation

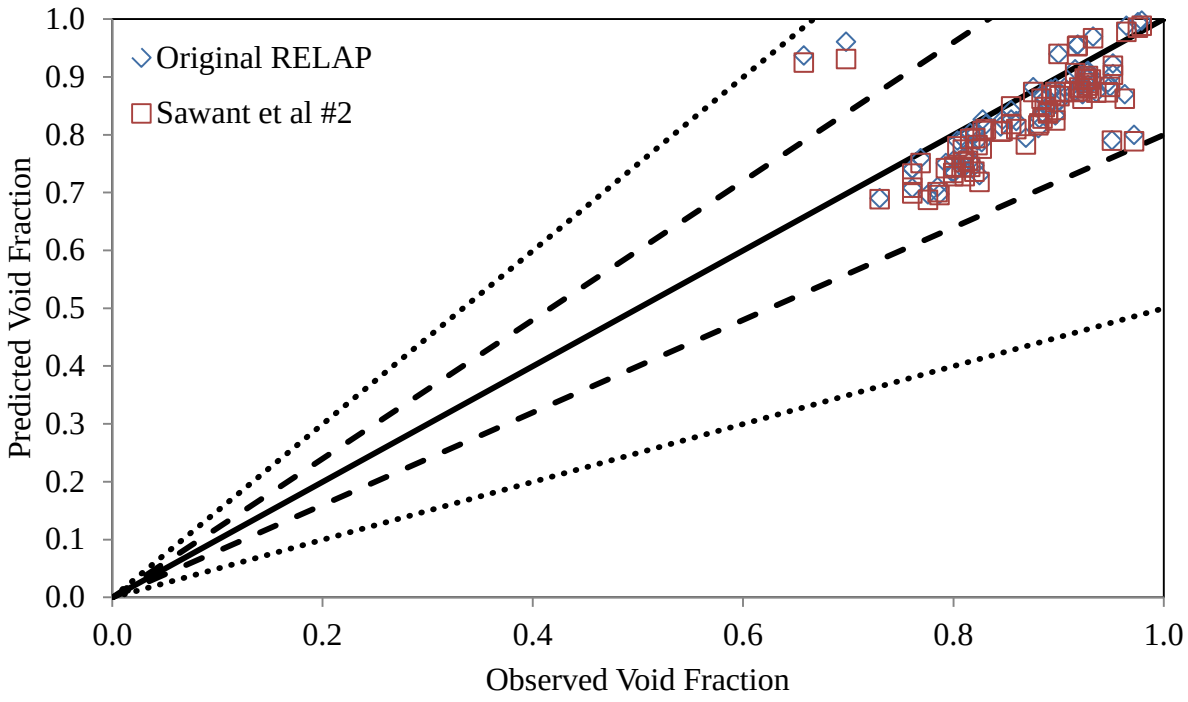

Figure 176: Comparison of the Void Fraction Prediction of the RELAP5/MOD3.3 [40] Droplet Volume Fraction Correlations to the Second Sawant, Ishii and Mori Entrainment Correlation

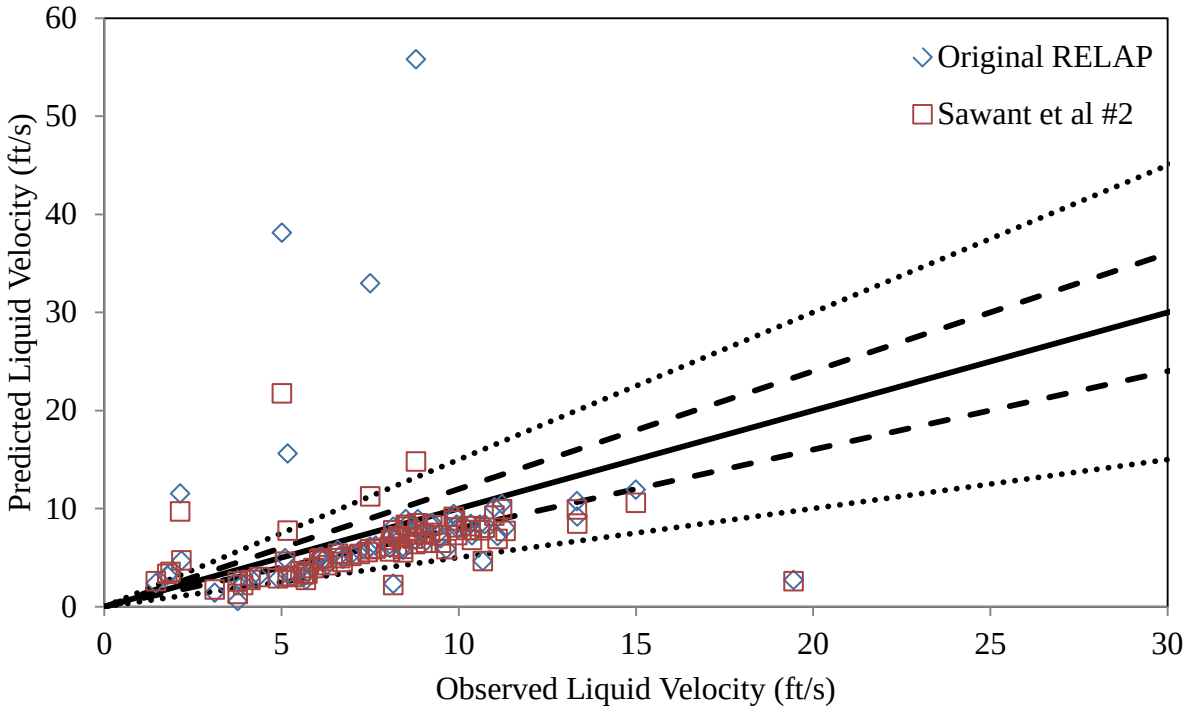

Figure 177: Comparison of the Liquid Velocity Prediction of the RELAP5/MOD3.3 [40] Droplet Volume Fraction Correlation to the Second Sawant, Ishii and Mori Entrainment Correlation

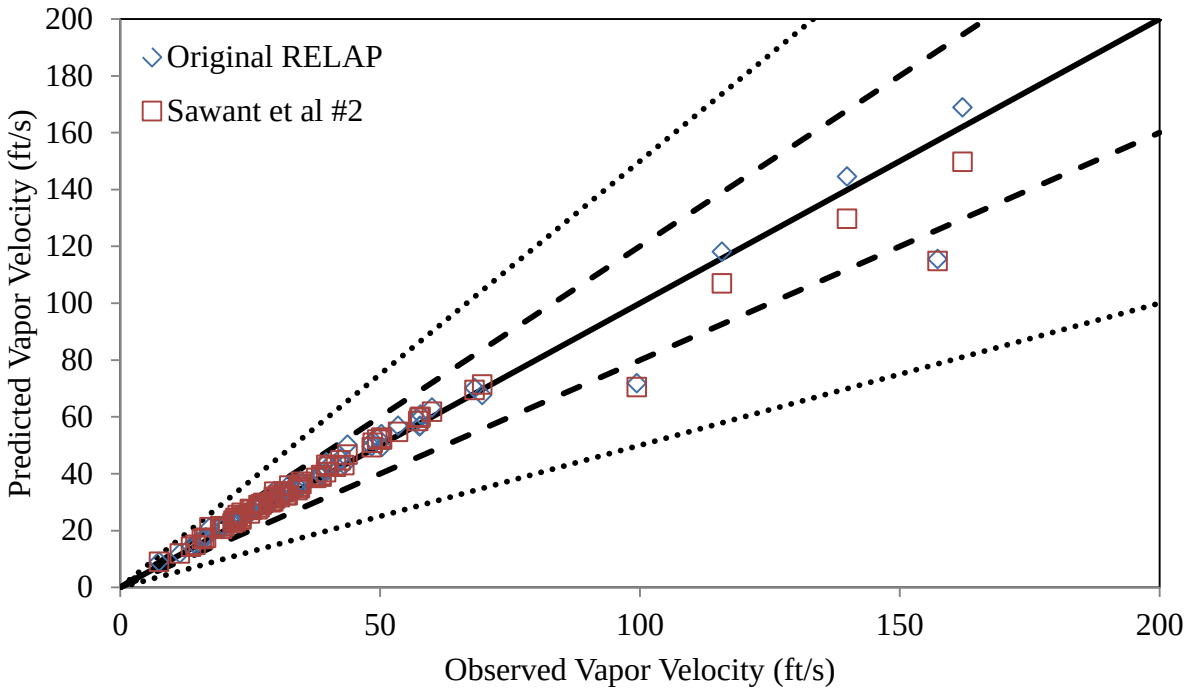

Figure 178: Comparison of the Vapor Velocity Prediction of the RELAP5/MOD3.3 [40] Droplet Volume Fraction Correlation to the Second Sawant, Ishii and Mori Entrainment Correlation

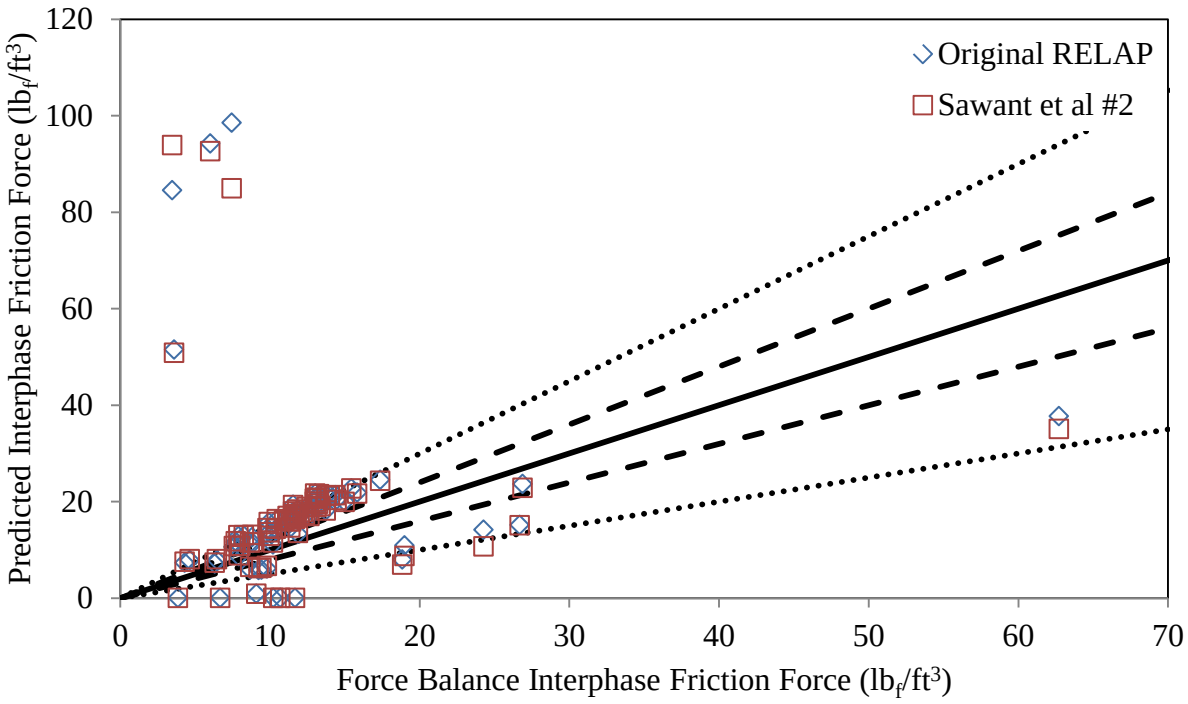

Figure 179: Comparison of the Interphase Friction Force Prediction of the RELAP5/MOD3.3 [40] Droplet Volume Fraction Correlation to the Second Sawant, Ishii and Mori Entrainment Correlation

Like the first Sawant et al [71] correlation, the second Sawant et al correlation [73] does not appear to provide any significant improvements to the modelling of the steam-water flow. While modest improvement can be seen in the errors of the phasic velocities in Table 37, these improvements are small at best.

Table 37: Comparison of Errors of the Original RELAP5/MOD3.3 [40] Droplet Volume Fraction Correlation to the Second Sawant, Ishii and Mori Entrainment Correlation

			Original RELAP					Sawant et al *E* Correlation #2				
Total			dP/dz	α	v_f	v_g	F_{int}	dP/dz	α	v_f	v_g	F_{int}
All Annular	76	Mean Average	42.93%	5.90%	55.58%	6.38%	128.54%	45.79%	6.59%	41.11%	6.22%	130.17%
		Median Average	45.95%	4.49%	24.93%	5.44%	45.76%	48.67%	5.06%	28.99%	4.97%	47.18%
		± 20%	13	74	26	72	5	13	74	19	73	5
		- Percentage	17.11%	97.37%	34.21%	94.74%	6.58%	17.11%	97.37%	25.00%	96.05%	6.58%
		± 50%	46	76	61	76	46	41	76	64	76	44
		- Percentage	60.53%	100.00%	80.26%	100.00%	60.53%	53.95%	100.00%	84.21%	100.00%	57.89%
		Maximum	99.95%	42.36%	660.97%	27.78%	2335.38%	103.00%	40.50%	352.53%	29.17%	2605.07%
Air-Water	7	Mean Average	12.55%	3.21%	202.06%	2.51%	40.98%	20.40%	2.69%	76.68%	5.05%	42.59%
		Median Average	8.64%	3.89%	115.52%	2.02%	38.12%	18.94%	3.61%	77.32%	3.61%	33.91%
		± 20%	4	7	0	7	0	4	7	0	7	0
		- Percentage	57.14%	100.00%	0.00%	100.00%	0.00%	57.14%	100.00%	0.00%	100.00%	0.00%
		± 50%	7	7	0	7	6	7	7	2	7	4
		- Percentage	100.00%	100.00%	0.00%	100.00%	85.71%	100.00%	100.00%	28.57%	100.00%	57.14%
		Maximum	25.37%	4.40%	534.59%	4.21%	57.53%	31.92%	4.38%	116.20%	7.62%	63.26%
Steam-Water	69	Mean Average	46.01%	6.17%	40.72%	6.77%	137.42%	48.37%	6.98%	37.51%	6.34%	139.05%
		Median Average	47.61%	4.77%	22.14%	6.14%	46.86%	50.14%	5.70%	26.57%	5.12%	47.35%
		± 20%	9	67	26	65	5	9	67	19	66	5
		- Percentage	13.04%	97.10%	37.68%	94.20%	7.25%	13.04%	97.10%	27.54%	95.65%	7.25%
		± 50%	39	69	61	69	40	34	69	62	69	40
		- Percentage	56.52%	100.00%	88.41%	100.00%	57.97%	49.28%	100.00%	89.86%	100.00%	57.97%
		Maximum	99.95%	42.36%	660.97%	27.78%	2335.38%	103.00%	40.50%	352.53%	29.17%	2605.07%

4.5.4: Analysis of the Critical Weber Number, We_{crit}

Lastly, the critical Weber number is explored as a parameter than may be adjusted to improve upon the existing interphase friction prediction, as well as the prediction of related parameters such as the pressure gradient, void fraction and phasic velocities. RELAP [40,69] uses a critical Weber number of 3.0, while many documented sources [9,64,74] state that the

critical Weber number should be 12. Thus, the first step was to run RELAP for the annular flow data points with a critical Weber number of 12.0. To gauge the sensitivity of RELAP to the critical Weber number, additional simulations were carried at for We_{crit} = 6.0 and We_{crit} = 24.0. It was discovered in the sensitivity analysis is that since RELAP places a limit on droplet sizes, which is met when $We_{crit} \geq 6.0$, the results of the three different sets of simulations were identical. Therefore, the results of the unmodified RELAP will be compared against only the We_{crit} = 12 scenario for all data points in this dissertation.

In Figure 181, the pressure gradient predicted by RELAP using both a droplet critical Weber number of 3 and a droplet critical Weber number of 12 are compared against the observed pressure gradient. There appears to be little difference between the two models, although when the critical Weber number is 12, it appears that the pressure gradient is slightly higher.

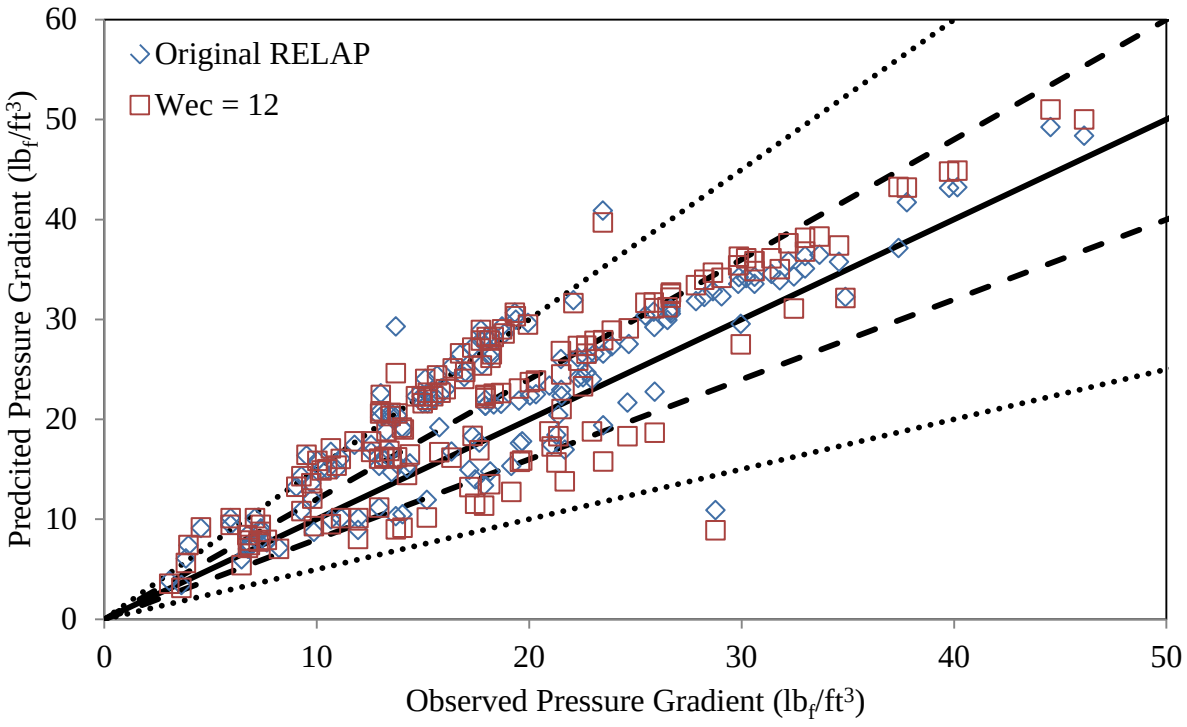

Figure 180: Comparison of the Pressure Gradient Prediction of RELAP5/MOD3.3 [40] with a Droplet Critical Weber Number of 3.0 to a Droplet Critical Weber Number of 12.0

For the void fraction prediction in Figure 182, there also appears to be little change in the model from We_{crit} =3.0 to We_{crit} = 12.0. However, the differences are more noticeable when examining the phasic velocities. First, with the liquid velocity in Figure 183, it appears that when We_{crit} = 12.0, that the liquid velocity is closer to the expected value than when We_{crit} = 3.0, particularly for data points where the unmodified RELAP liquid velocity was significantly different from the observed value. For vapor velocities, there appears to be very little difference when the observed value is less than 85 ft/s in Figure 184, but as the velocity increases above that point, the vapor velocity is underpredicted for We_{crit} = 12.0. The interphase friction force for both the unmodified RELAP model and for We_{crit} = 12.0 appear to match very closely to each other in Figure 185.

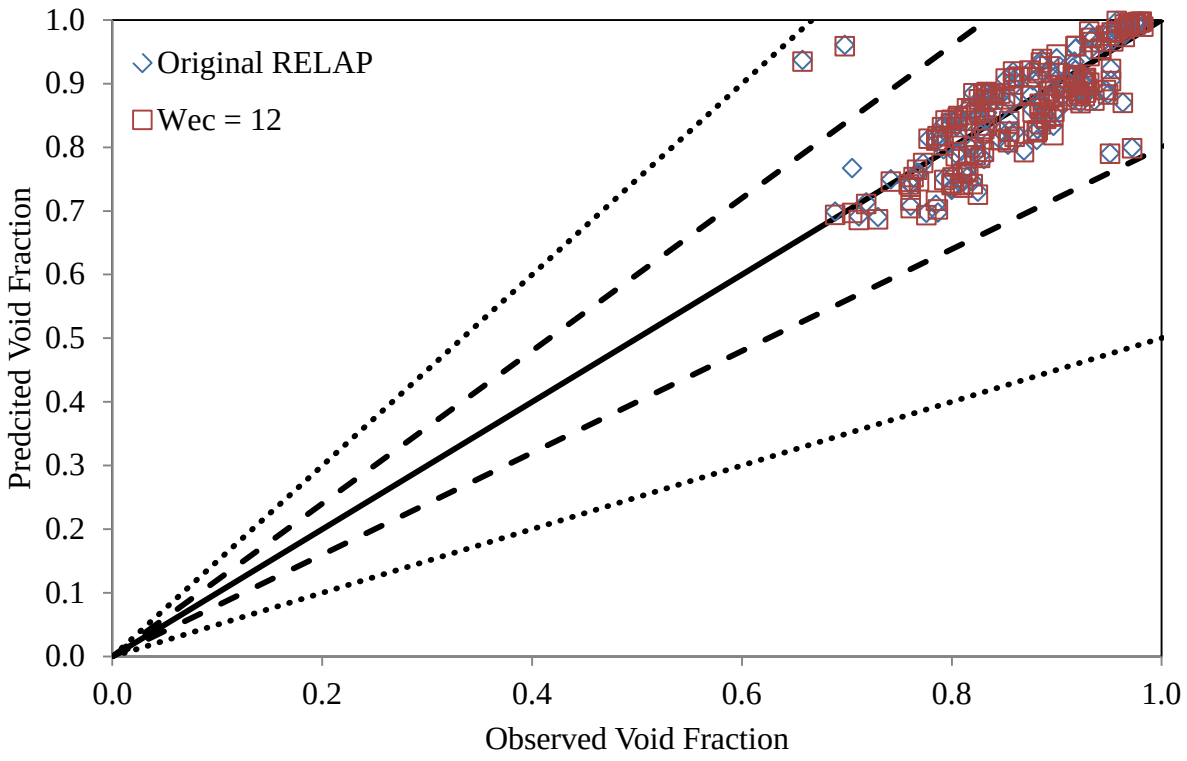

Figure 181: Comparison of the Void Fraction Prediction of RELAP5/MOD3.3 [40] with a Droplet Critical Weber Number of 3.0 to a Droplet Critical Weber Number of 12.0

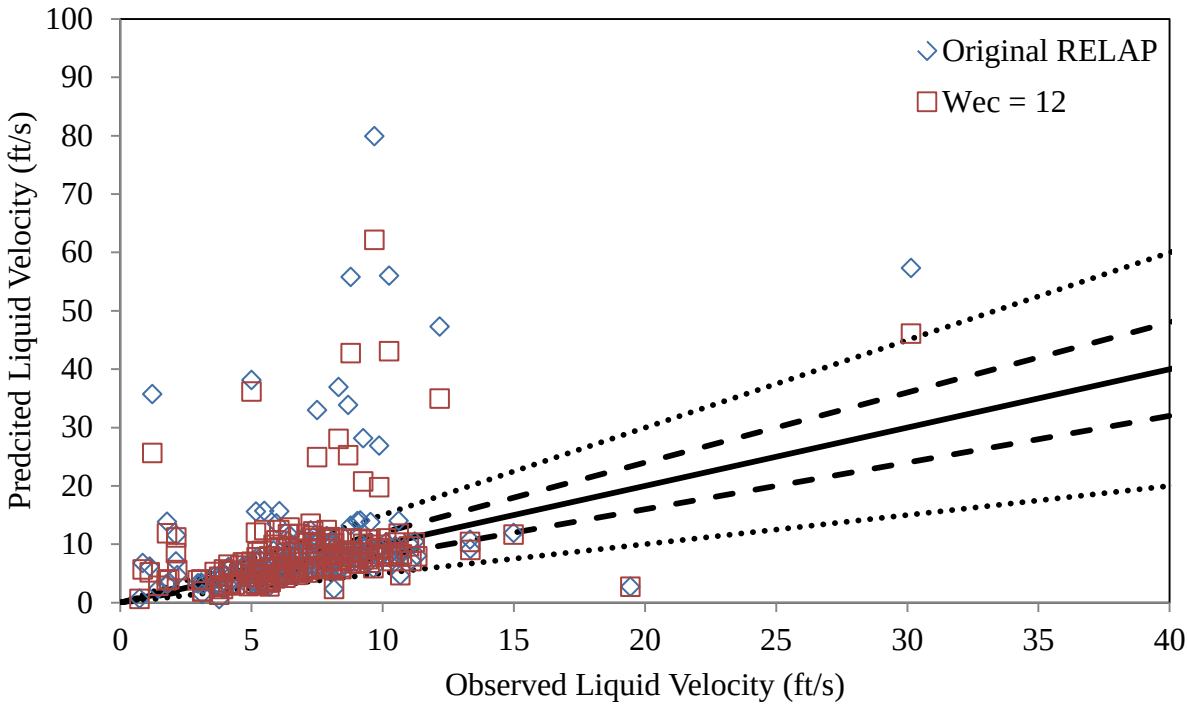

Figure 182: Comparison of the Liquid Velocity Prediction of RELAP5/MOD3.3 [40] with a Droplet Critical Weber Number of 3.0 to a Droplet Critical Weber Number of 12.0

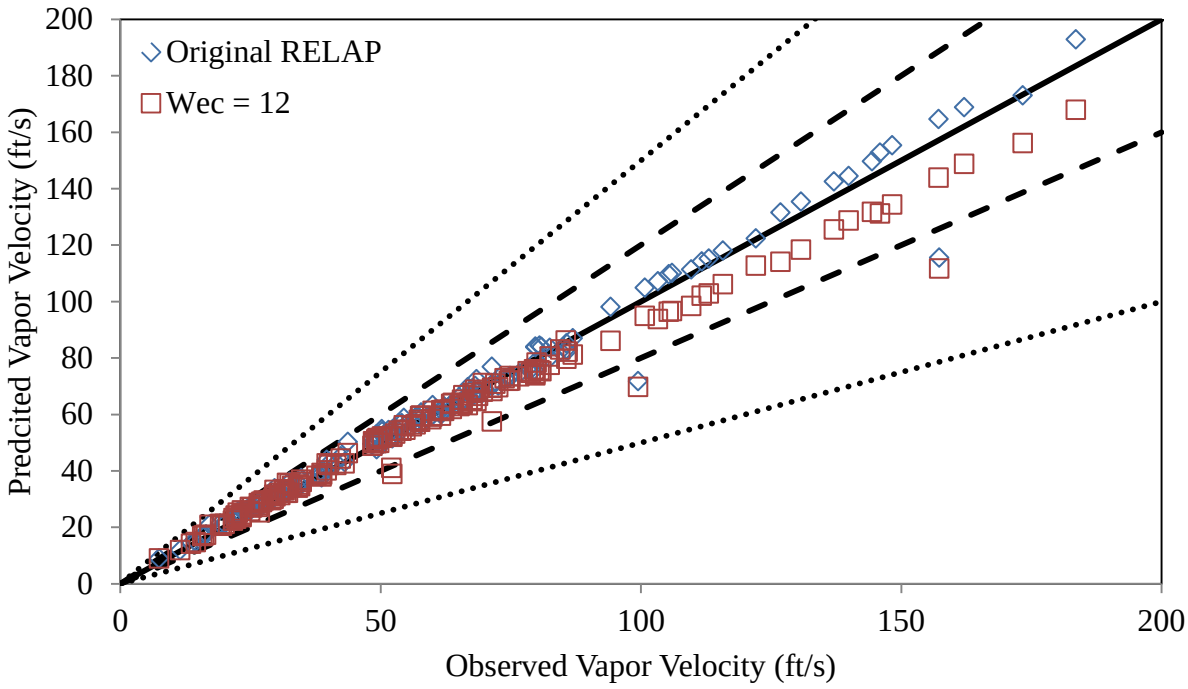

Figure 183: Comparison of the Vapor Velocity Prediction of RELAP5/MOD3.3 [40] with a Droplet Critical Weber Number of 3.0 to a Droplet Critical Weber Number of 12.0

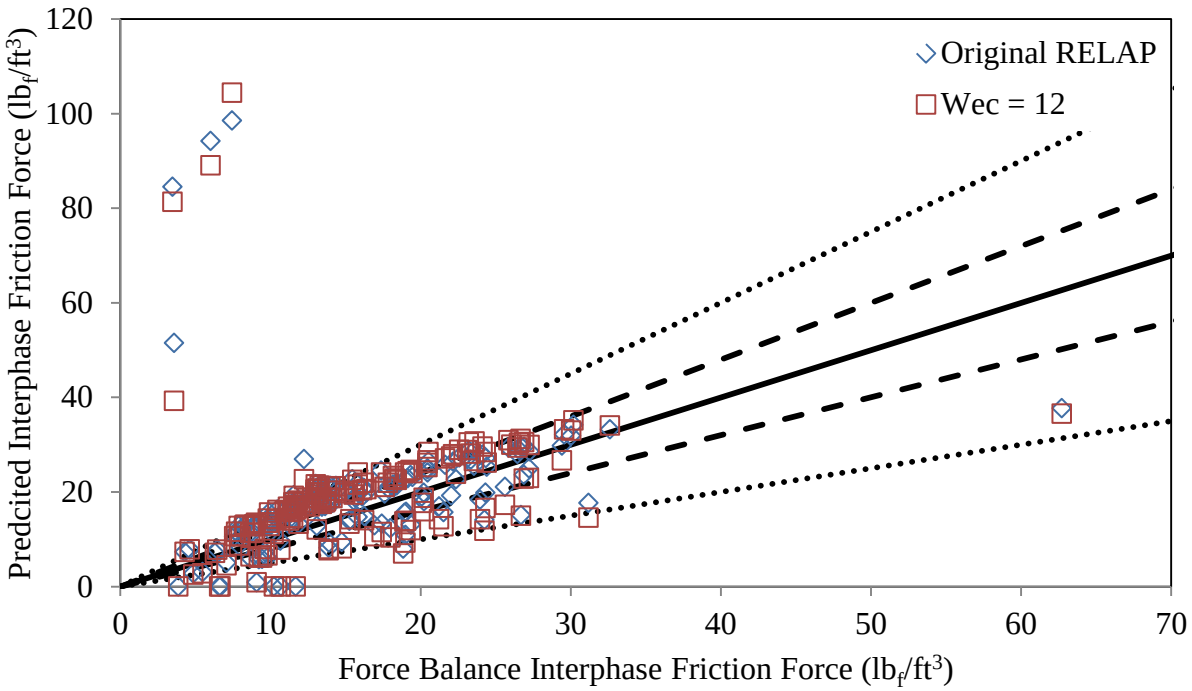

Figure 184: Comparison of the Interphase Friction Force Prediction of RELAP5/MOD3.3 [40] with a Droplet Critical Weber Number of 3.0 to a Droplet Critical Weber Number of 12.0

Comparing the errors for We_{crit} = 3.0 and We_{crit} = 12.0 in Table 38, it is shown that increasing to 12, does improve the maximum error a little, but does not appear to significantly improve upon the maximum error or the overall errors with in the RELAP model.

Table 38: Comparison of Errors of the Original RELAP5/MOD3.3 [40] Critical Weber Number to a Critical Weber Number of 12

Total			Original RELAP					We_{crit} = 12				
			dP/dz	α	v_f	v_g	F_{int}	dP/dz	α	v_f	v_g	F_{int}
All Annular	163	Mean Average	27.74%	4.54%	85.21%	4.53%	106.13%	30.75%	4.62%	73.96%	5.20%	90.09%
		Median Average	18.82%	3.70%	26.26%	3.55%	30.34%	23.28%	3.89%	28.55%	3.96%	35.11%
		± 20%	86	161	57	159	53	63	161	48	158	30
		- Percentage	52.76%	98.77%	34.97%	97.55%	32.52%	38.65%	98.77%	29.45%	96.93%	18.40%
		± 50%	131	163	123	163	128	131	163	121	163	125
		- Percentage	80.37%	100.00%	75.46%	100.00%	78.53%	80.37%	100.00%	74.23%	100.00%	76.69%
		Maximum	113.29%	42.36%	2816.63%	27.78%	2965.69%	100.86%	41.99%	1992.25%	29.87%	2934.21%
Air-Water	94	Mean Average	14.33%	3.35%	117.88%	2.89%	83.17%	19.46%	3.31%	98.75%	4.85%	60.17%
		Median Average	12.17%	3.05%	31.24%	2.44%	19.58%	18.44%	3.28%	38.39%	3.74%	27.18%
		± 20%	77	94	31	94	48	54	94	25	92	25
		- Percentage	81.91%	100.00%	32.98%	100.00%	51.06%	57.45%	100.00%	26.60%	97.87%	26.60%
		± 50%	92	94	62	94	88	92	94	59	94	85
		- Percentage	97.87%	100.00%	65.96%	100.00%	93.62%	97.87%	100.00%	62.77%	100.00%	90.43%
		Maximum	113.29%	8.74%	2816.63%	9.97%	2965.69%	79.14%	7.77%	1992.25%	25.52%	2934.21%
Steam-Water	69	Mean Average	46.01%	6.17%	40.72%	6.77%	137.42%	46.13%	6.40%	40.17%	5.68%	130.85%
		Median Average	47.61%	4.77%	22.14%	6.14%	46.86%	46.41%	5.07%	23.06%	4.32%	45.85%
		± 20%	9	67	26	65	5	9	67	23	66	5
		- Percentage	13.04%	97.10%	37.68%	94.20%	7.25%	13.04%	97.10%	33.33%	95.65%	7.25%
		± 50%	39	69	61	69	40	39	69	62	69	40
		- Percentage	56.52%	100.00%	88.41%	100.00%	57.97%	56.52%	100.00%	89.86%	100.00%	57.97%
		Maximum	99.95%	42.36%	660.97%	27.78%	2335.38%	100.86%	41.99%	621.05%	29.87%	2243.71%

V. Discussion

5.1: Conclusions

Interphase friction is one of the most important parameters to be modeled in one-dimensional, two-phase vertical flow, as it is the chief mechanism used to predict vapor distribution within such a system. This carries significance in the safety of a nuclear reactor, as well as applications in the petroleum industry, where air and crude oil mix within a well, or any industry where two-phase flow occurs. The ability to accurately predict the interphase friction enables those modeling two-phase flow to more accurately predict the vapor distribution within these flows and enhance the safety and/or performance of those systems.

Using a more detailed force balance than has been typically used for one-dimensional two-phase flow analysis, a more detailed interphase friction force calculation has been developed that accounts for changes in vapor density, void fraction and liquid and vapor velocity with respect to height. While these changes may be negligible in many cases, they also prove to be significant in others. This interphase friction force was non-dimensionalized, so that the data from several different studies could be used to develop a general correlation for predicting the interphase friction, resulting in Equation 299.

$$F_{INT} = \alpha(1-\alpha)\left(\rho_f - \rho_g\right)g \times \begin{cases} 1 \; if \; Fr_m \leq 12.73 \\ 0.660 {Fr_m}^{0.1631} \; if \; 12.73 < Fr_m < 1719 \\ 3.70 \times 10^{-5} {Fr_m}^{1.477} if \; Fr_m \geq 1719 \end{cases} \qquad 299$$

where Fr_m is the mixture Froude number and is given in Equation 54.

As part of the development of the correlation, it has been observed that the interphase friction that occurs with one-dimensional, two-phase vertical flow behaves in one of three ways, based on comparisons between the data with various flow regime maps. In the case where $Fr_m \leq$ 12.73, the interphase friction force is equal to the buoyancy of the vapor phase within the liquid

phase, and no additional mechanism appears to affect the interphase friction. Flow regime maps indicate that this is true for bubbly flow and for much of slug flow. When $12.73 < Fr_m < 1719$, the interphase friction enters a transitional region that flow regime maps indicate coincide with the breaking up of slug flow. In slug flow, when the amount of vapor flowing exceeds a certain threshold, the liquid slugs between the Taylor bubbles begin to break apart and waves in the liquid film along the wall have been observed to fall into the Taylor bubbles, creating a flow regime that has been called churn-turbulent [15,81], frothy [58,60] or emulsion [51]. This region includes both the slug flow regime as well as much of the annular flow regime, indicating that this region include cases where annular flow has set up with waves in the liquid film breaking up into the vapor core. Finally, there is a region where interphase friction is exceedingly sensitive to the velocity difference between the vapor and liquid phases, and appears to occur when the vapor volumetric flux significantly exceeds that of the liquid. This appears to be a subset of the annular flow regime, and accounts for the cases with the highest void fractions, suggesting that these cases may be when the film thickness is very thin, where the surface tension of the liquid is significantly contributing to the inertia of the liquid.

This correlation has been compared against the correlations that are used to predict interphase friction force in RELAP5/MOD2, RELAP5/MOD3.3, RELAP5-3D and TRACE, which represent the most widely used nuclear thermal hydraulic codes in the United States. The correlation has been shown to produce significantly more accurate results than RELAP5/MOD2 and TRACE. For bubbly flow, the correlation produces equally accurate results as RELAP5/MOD3.3 and RELAP5-3D, with a slight improvement for slug flow and significant improvements for annular flow.

5.2: Recommendations for Future Work

While the correlation that has been developed shows great promise in improving the interphase friction predictions of nuclear thermal hydraulic codes, along with other one-dimensional two-phase flow models, there is still a significant amount of work that can be done to improve upon the correlation and better understand the physical implications of the correlation.

First and foremost, the author recommends the development of a test apparatus that is designed to study one-dimensional two-phase flow, for which a multitude of tests can be carried out. Of the data used to develop the correlation, only one data set came from a study that was undertaken after the year 2000 (Schlegal) [72], with the rest taking place between the late 1950's and the early 1970's. [11,29,31,32,59,84] Based on observations within the data, there appear to be pros and cons to conducting experiments using modern technology versus the methods employed more than half a century ago. However, no direct comparison of accuracy between both methods appears to have been published or is readily available. Thus, the author suggests that an apparatus be built that employs the characteristics of several of these studies, that offers ways to compare different methods against each other. Among the older studies, the author is particular impressed with that of Govier et al, as it appears to offer the most useful data. However, the author would also suggest the implementation of modern instrumentation that was used by Schlegal and compare void fraction measurements from the impedance probes used by Schlegal with results from quick closing valves produced in studies like Govier et al, Turner and Oshinowo. The author would suggest that such an apparatus be able to accommodate pipes of a range of different diameters, and that pressure taps and impedance probes should also be used to determine the entrance length of two-phase flow. The author would also suggest that

apparatuses may be designed to adjust inclination, in order to test results vertically, horizontally and at various angles.

While the author would certainly like to see the correlation that has been developed tested within such an apparatus, there is another study that the author would like to suggest first. In the different studies that were examined, no calculation was provided that proved that the flow was fully developed within the test section, with most authors assuming that sufficient entrance length was added to the system to ensure that the two-phase flow was fully developed. Some studies used entrance lengths several times larger than the test section itself, while others used sections that were significantly shorter. The author suggests that a series of impedance probes and pressure taps be placed downstream of the mixing tee, and use changes in pressure drop and void fraction to determine the entrance length for pipes of several diameters, along with testing different liquids and vapors at various temperatures and pressures. A correlation that can accurately predict the entrance length of two-phase flow would benefit future research as it would allow investigators to better design test equipment and maximize the resources available.

To test the correlation, the author suggests a series of experiments in a test apparatus like the one suggested, but only after the entrance length has been determined to ensure that entrance effects do not affect the data. Ideally, the author would like to see comparisons of void fraction observations using both impedance probes and quick closing valves.

The author would also recommend further testing of the correlation in one-dimensional, two-phase flow models, including the nuclear thermal hydraulic codes RELAP5/MOD2, RELAP5-3D and TRACE, which were not available to the author for modification.

Appendix A: Derivation of Steady-State Two-Phase Cocurrent Upflow Interphase Friction Force

To derive the interphase friction force for a steady-state two-phase cocurrent upflow scenario, we begin with a diagram like that shown in Figure 186. In this case, we assume that the upflow is occurring within a control volume of a pipe of hydraulic diameter, D_H, over a small change in height of Δz. The system is assumed to be adiabatic and that there is no phase change between the two phases. For the sake of simplicity, the phases are considered separated, with the vapor to the left and the liquid to the right.

The change in height is small enough that changes in void fraction, α, pressure, P, vapor density, ρ_g, vapor velocity, v_g, and liquid velocity, v_f, can be assumed to change approximately linearly with respect to height. This assumption allows us to set our variables at the center of the control volume and consider values at the inlets and outlets to vary by +/- $\Delta/2$. The reason for setting up the control volume in such a way is due to the fact that the variables α, P, v_f and v_g are considered to be volume averaged values in the data to be analyzed with the equations that are derived.

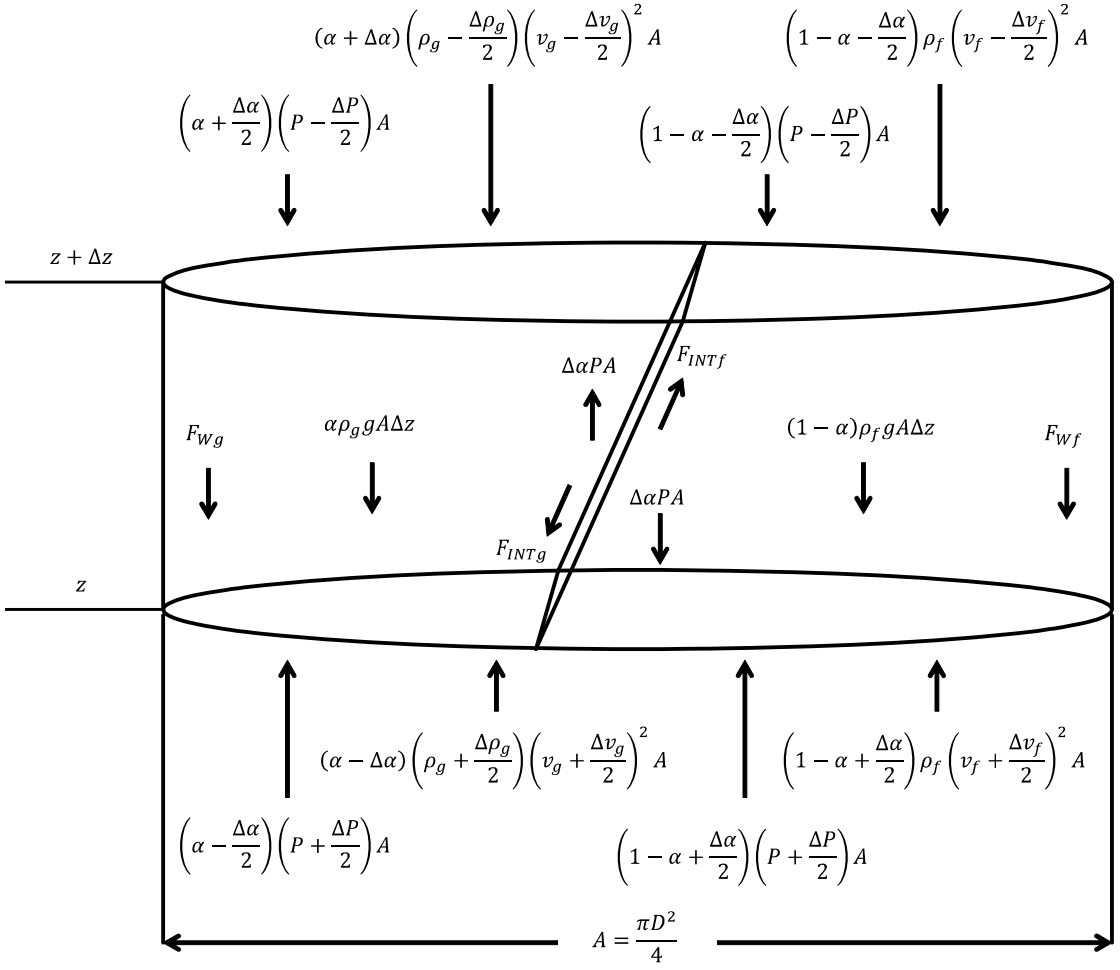

Figure 186: Not-to-Scale Control Volume Diagram with Momentum Fluxes and Forces

For the derivation, we begin by examining the relevant conservation equations. Namely, those are the continuity equations for the liquid and vapor phases, shown in Equations A1 and A2, respectively, and the conservation of linear momentum equations for the overall system , and the liquid and vapor phases, shown in Equations A3, A4 and A5, respectively.

$$\frac{d}{dt}m_f = W_{fi} - W_{fo} = 0 \tag{A1}$$

$$\frac{d}{dt}m_g = W_{gi} - W_{go} = 0 \tag{A2}$$

$$\frac{d}{dt}p = \frac{d}{dt}(m\cdot V) = V\cdot\left(\frac{d}{dt}m\right) + m\cdot\left(\frac{d}{dt}V\right) = \Sigma(W\cdot V) + \Sigma(m\cdot a) = \Sigma(W\cdot V) + \Sigma F = 0 \tag{A3}$$

$$\frac{d}{dt}p_f = \frac{d}{dt}\left(m_f\cdot V_f\right) = V_f\cdot\left(\frac{d}{dt}m_f\right) + m_f\cdot\left(\frac{d}{dt}V_f\right) = \Sigma\left(W_f\cdot V_f\right) + \Sigma\left(m_f\cdot a_f\right)$$

$$\frac{d}{dt}p_f = \Sigma\left(W_f\cdot V_f\right) + \Sigma\left(m_f\cdot a_f\right) = \Sigma\left(W_f\cdot V_f\right) + \Sigma F_f = 0 \tag{A4}$$

$$\frac{d}{dt}p_g = \frac{d}{dt}\left(m_g\cdot V_g\right) = V_g\cdot\left(\frac{d}{dt}m_g\right) + m_g\cdot\left(\frac{d}{dt}V_g\right) = \Sigma(W\cdot V) + \Sigma(m\cdot a)$$

$$\frac{d}{dt}p_g = \Sigma\left(W_f\cdot V_f\right) + \Sigma\left(m_f\cdot a_f\right) = \Sigma\left(W_g\cdot V_g\right) + \Sigma F_g = 0 \tag{A5}$$

where m is the mass, W is the mass flow rate, p is the momentum, V is the velocity, a is the acceleration and F is the force. The subscripts f and g pertain to liquid and vapor phases, respectively, while the subscripts i and o pertain to in and out, respectively.

Each of the five equations will be analyzed to produce the derivation of the equations needed to calculate the interphase friction force. We begin with the continuity of the liquid phase, Equation A1.

$$\frac{d}{dt}m_f = W_{fi} - W_{fo} = 0 \tag{A1}$$

We find that W_{fi} and W_{fo} can be substituted as:

$$W_{fi} = \left(1 - \alpha + \frac{\Delta\alpha}{2}\right)\cdot\rho_f\cdot\left(V_f + \frac{\Delta V_f}{2}\right)\cdot A \tag{A6}$$

$$W_{fo} = \left(1 - \alpha - \frac{\Delta\alpha}{2}\right)\cdot\rho_f\cdot\left(V_f - \frac{\Delta V_f}{2}\right)\cdot A \tag{A7}$$

Substituting Equations A6 and A7 into Equation A1, we find:

$$\left(1 - \alpha + \frac{\Delta\alpha}{2}\right)\cdot\rho_f\cdot\left(V_f + \frac{\Delta V_f}{2}\right)\cdot A - \left(1 - \alpha - \frac{\Delta\alpha}{2}\right)\cdot\rho_f\cdot\left(V_f - \frac{\Delta V_f}{2}\right)\cdot A = 0$$

Or more simply,

$$\left(1-\alpha+\frac{\Delta\alpha}{2}\right)\cdot\rho_f\cdot\left(V_f+\frac{\Delta V_f}{2}\right)\cdot A = \left(1-\alpha-\frac{\Delta\alpha}{2}\right)\cdot\rho_f\cdot\left(V_f-\frac{\Delta V_f}{2}\right)\cdot A$$

First, we can eliminate the common terms of ρ_f and A from the equation

$$\left(1-\alpha+\frac{\Delta\alpha}{2}\right)\cdot\left(V_f+\frac{\Delta V_f}{2}\right) = \left(1-\alpha-\frac{\Delta\alpha}{2}\right)\cdot\left(V_f-\frac{\Delta V_f}{2}\right)$$

Distributing the polynomials we find:

$$(1-\alpha)\cdot V_f + \frac{V_f\cdot\Delta\alpha}{2} \ldots + \frac{(1-\alpha)\cdot\Delta V_f}{2} + \frac{\Delta\alpha\cdot\Delta V_f}{4} = (1-\alpha)\cdot V_f - \frac{V_f\cdot\Delta\alpha}{2} - \frac{(1-\alpha)\cdot\Delta V_f}{2} + \frac{\Delta\alpha\cdot\Delta V_f}{4}$$

Next, we will eliminate the like terms on each side of the equation. Also, the products of two or more differences are considered to be of a significantly smaller order of magnitude than a single difference. Therefore, products of differences will also be eliminated.

$$\frac{V_f\cdot\Delta\alpha}{2} + \frac{(1-\alpha)\cdot\Delta V_f}{2} = -\frac{V_f\cdot\Delta\alpha}{2} - \frac{(1-\alpha)\cdot\Delta V_f}{2}$$

As we move like terms to each side, we get:

$$V_f\cdot\Delta\alpha = -(1-\alpha)\cdot\Delta V_f$$

Dividing each side by *-(1-α)*, we find that:

$$\Delta V_f = -\frac{V_f}{(1-\alpha)}\cdot\Delta\alpha \qquad \text{(A8)}$$

Next, we will look at Equation A2, the continuity of the vapor phase. The process for determining the differential equation is similar to that for the liquid phase. First we examine the mass flow rate into and out of the control volume, given in Equations A9 and A10, respectively.

$$\frac{d}{dt}m_g = W_{gi} - W_{go} = 0 \qquad \text{(A2)}$$

$$W_{gi} = \left(\alpha-\frac{\Delta\alpha}{2}\right)\left(\rho_g+\frac{\Delta\rho_g}{2}\right)\cdot\left(V_g+\frac{\Delta V_g}{2}\right)A \qquad \text{(A9)}$$

$$W_{go} = \left(\alpha+\frac{\Delta\alpha}{2}\right)\left(\rho_g-\frac{\Delta\rho_g}{2}\right)\cdot\left(V_g-\frac{\Delta V_g}{2}\right)A \qquad \text{(A10)}$$

Inserting Equations A9 and A10 into Equation A2, we find:

$$\left(\alpha-\frac{\Delta\alpha}{2}\right)\left(\rho_g+\frac{\Delta\rho_g}{2}\right)\cdot\left(V_g+\frac{\Delta V_g}{2}\right)A = \left(\alpha+\frac{\Delta\alpha}{2}\right)\left(\rho_g-\frac{\Delta\rho_g}{2}\right)\cdot\left(V_g-\frac{\Delta V_g}{2}\right)A$$

Next, we will divide each side of the equation by A and then distribute the polynomials:

$$\left(\alpha - \frac{\Delta\alpha}{2}\right)\left(\rho_g + \frac{\Delta\rho_g}{2}\right)\cdot\left(V_g + \frac{\Delta V_g}{2}\right) = \left(\alpha + \frac{\Delta\alpha}{2}\right)\left(\rho_g - \frac{\Delta\rho_g}{2}\right)\cdot\left(V_g - \frac{\Delta V_g}{2}\right)$$

$$\begin{pmatrix} \alpha\cdot\rho_g\cdot V_g \ldots \\ + \frac{\alpha\cdot\rho_g\cdot\Delta V_g}{2} \ldots \\ + \frac{\alpha\cdot V_g\cdot\Delta\rho_g}{2} \ldots \\ + \frac{\alpha\cdot\Delta\rho_g\cdot\Delta V_g}{4} \end{pmatrix} - \begin{pmatrix} \frac{\rho_g\cdot V_g\cdot\Delta\alpha}{2} \ldots \\ + \frac{\rho_g\cdot\Delta\alpha\cdot\Delta V_g}{4} \ldots \\ + \frac{V_g\cdot\Delta\alpha\cdot\Delta\rho_g}{4} \ldots \\ + \frac{\Delta\alpha\cdot\Delta\rho_g\cdot\Delta V_g}{8} \end{pmatrix} = \alpha\cdot\rho_g\cdot V_g - \frac{\alpha\cdot\rho_g\cdot\Delta V_g}{2} - \frac{\alpha\cdot V_g\cdot\Delta\rho_g}{2} \ldots + \frac{\alpha\cdot\Delta\rho_g\cdot\Delta V_g}{4} \ldots + \frac{\rho_g\cdot V_g\cdot\Delta\alpha}{2} - \frac{\rho_g\cdot\Delta\alpha\cdot\Delta V_g}{4} - \frac{V_g\cdot\Delta\alpha\cdot\Delta\rho_g}{4} \ldots + \frac{\Delta\alpha\cdot\Delta\rho_g\cdot\Delta V_g}{8}$$

At this point, we simplify the equation by subtracting $\alpha\rho_g V_g$ from both sides and approximating all products of differences to be equal to 0.

$$\frac{\alpha\cdot\rho_g\cdot\Delta V_g}{2} + \frac{\alpha\cdot V_g\cdot\Delta\rho_g}{2} - \frac{\rho_g\cdot V_g\cdot\Delta\alpha}{2} = -\frac{\alpha\cdot\rho_g\cdot\Delta V_g}{2} - \frac{\alpha\cdot V_g\cdot\Delta\rho_g}{2} + \frac{\rho_g\cdot V_g\cdot\Delta\alpha}{2}$$

Next, we will combine the like variables

$$\alpha\cdot\rho_g\cdot\Delta V_g + \alpha\cdot V_g\cdot\Delta\rho_g = \rho_g\cdot V_g\cdot\Delta\alpha$$

Dividing by $\alpha\rho_g$, we get:

$$\Delta V_g + \frac{V_g\cdot\Delta\rho_g}{\rho_g} = \frac{V_g\cdot\Delta\alpha}{\alpha}$$

Subtracting $V_g\Delta\rho_g/\rho_g$ from both sides of the equation, we find

$$\Delta V_g = V_g\cdot\left(\frac{\Delta\alpha}{\alpha} - \frac{\Delta\rho_g}{\rho_g}\right) \tag{A11}$$

For now, we will save Equations A8 and A11 in their current form until later in the derivation for further processing and incorporation into the derivation of the interphase friction force. At this time, we will begin working on the overall conservation of linear momentum equation, which is used to help check the validity of the solutions for the interphase friction force derived from each phases. This process starts with Equation A3.

$$\frac{d}{dt}p = \frac{d}{dt}(m\cdot V) = V\cdot\left(\frac{d}{dt}m\right) + m\cdot\left(\frac{d}{dt}V\right) = \Sigma(W\cdot V) + \Sigma(m\cdot a) = \Sigma(W\cdot V) + \Sigma F = 0 \tag{A3}$$

First, we will find the sum of the momentum:

$$\Sigma(W\cdot V) = W_{fi}\cdot V_{fi} + W_{gi}\cdot V_{gi} - \left(W_{fo}\cdot V_{fo} + W_{go}\cdot V_{go}\right)$$

Substituting Equations A6, A7, A9 and A10 for W_{fi}, W_{gi}, W_{fo} and W_{go}, as well as substituting the *+/- ΔV/2* for the velocities, we obtain:

$$W_{fi}\cdot V_{fi} = \left(1-\alpha+\frac{\Delta\alpha}{2}\right)\cdot\rho_f\cdot\left(V_f+\frac{\Delta V_f}{2}\right)\cdot A\cdot\left(V_f+\frac{\Delta V_f}{2}\right)$$

$$W_{gi}\cdot V_{gi} = \left(\alpha-\frac{\Delta\alpha}{2}\right)\left(\rho_g+\frac{\Delta\rho_g}{2}\right)\cdot\left(V_g+\frac{\Delta V_g}{2}\right)A\cdot\left(V_g+\frac{\Delta V_g}{2}\right)$$

$$W_{fo}\cdot V_{fo} = \left(1-\alpha-\frac{\Delta\alpha}{2}\right)\cdot\rho_f\cdot\left(V_f-\frac{\Delta V_f}{2}\right)\cdot A\cdot\left(V_f-\frac{\Delta V_f}{2}\right)$$

$$W_{go}\cdot V_{go} = \left(\alpha+\frac{\Delta\alpha}{2}\right)\left(\rho_g-\frac{\Delta\rho_g}{2}\right)\cdot\left(V_g-\frac{\Delta V_g}{2}\right)A\cdot\left(V_g-\frac{\Delta V_g}{2}\right)$$

With cross-multiplication, we expand the polynomials and assume that the products of differences are negligible to simplify the equation:

$$W_{fi}\cdot V_{fi} = \left(1-\alpha+\frac{\Delta\alpha}{2}\right)\cdot\rho_f\cdot\left(V_f+\frac{\Delta V_f}{2}\right)^2\cdot A$$

$$W_{fi}\cdot V_{fi} = \rho_f\cdot A\cdot\left(1-\alpha+\frac{\Delta\alpha}{2}\right)\cdot\left(V_f{}^2+V_f\cdot\Delta V_f+\frac{\Delta V_f{}^2}{4}\right)$$

$$W_{fi}\cdot V_{fi} = \rho_f\cdot A\cdot\left[\left(1-\alpha+\frac{\Delta\alpha}{2}\right)\cdot\left(V_f{}^2+V_f\cdot\Delta V_f\right)\right]$$

$$W_{fi}\cdot V_{fi} = \rho_f\cdot A\cdot\left[(1-\alpha)\cdot V_f{}^2+(1-\alpha)\cdot V_f\cdot\Delta V_f+\frac{V_f{}^2\cdot\Delta\alpha}{2}+\frac{V_f\cdot\Delta\alpha\cdot\Delta V_f}{4}\right]$$

$$W_{fi}\cdot V_{fi} = \rho_f\cdot A\cdot\left[(1-\alpha)\cdot V_f{}^2+(1-\alpha)\cdot V_f\cdot\Delta V_f+\frac{V_f{}^2\cdot\Delta\alpha}{2}\right] \qquad \text{(A12)}$$

$$W_{gi}\cdot V_{gi} = \left(\alpha-\frac{\Delta\alpha}{2}\right)\left(\rho_g+\frac{\Delta\rho_g}{2}\right)\left(V_g+\frac{\Delta V_g}{2}\right)^2 A$$

$$W_{gi}\cdot V_{gi} = \left(\alpha\cdot\rho_g+\frac{\alpha\cdot\Delta\rho_g}{2}-\frac{\rho_g\cdot\Delta\alpha}{2}-\frac{\Delta\alpha\cdot\Delta\rho_g}{4}\right)\cdot\left(V_g{}^2+V_g\cdot\Delta V_g+\frac{\Delta V_g{}^2}{4}\right)\cdot A$$

$$W_{gi}\cdot V_{gi} = \left(\alpha\cdot\rho_g+\frac{\alpha\cdot\Delta\rho_g}{2}-\frac{\rho_g\cdot\Delta\alpha}{2}\right)\cdot\left(V_g{}^2+V_g\cdot\Delta V_g\right)\cdot A$$

$$W_{gi}\cdot V_{gi} = \left(\begin{array}{l}\alpha\cdot\rho_g\cdot V_g{}^2+\dfrac{\alpha\cdot V_g{}^2\cdot\Delta\rho_g}{2}-\dfrac{\rho_g\cdot V_g{}^2\cdot\Delta\alpha}{2}\ \ldots\\ +\alpha\cdot\rho_g\cdot V_g\cdot\Delta V_g+\dfrac{\alpha\cdot V_g\cdot\Delta V_g\cdot\Delta\rho_g}{4}-\dfrac{\rho_g\cdot V_g\cdot\Delta V_g\cdot\Delta\alpha}{4}\end{array}\right)\cdot A$$

$$W_{gi}\cdot V_{gi} = \left(\alpha\cdot\rho_g\cdot V_g^{\,2} + \frac{\alpha\cdot V_g^{\,2}\cdot\Delta\rho_g}{2} - \frac{\rho_g\cdot V_g^{\,2}\cdot\Delta\alpha}{2} + \alpha\cdot\rho_g\cdot V_g\cdot\Delta V_g\right)\cdot A \tag{A13}$$

$$W_{fo}\cdot V_{fo} = \left(1-\alpha-\frac{\Delta\alpha}{2}\right)\cdot\rho_f\cdot\left(V_f-\frac{\Delta V_f}{2}\right)^2\cdot A$$

$$W_{fo}\cdot V_{fo} = \left(1-\alpha-\frac{\Delta\alpha}{2}\right)\cdot\rho_f\cdot\left(V_f^{\,2}-V_f\cdot\Delta V_f+\frac{\Delta V_f^{\,2}}{4}\right)\cdot A$$

$$W_{fo}\cdot V_{fo} = \rho_f\cdot A\cdot\left[\left(1-\alpha-\frac{\Delta\alpha}{2}\right)\cdot\left(V_f^{\,2}-V_f\cdot\Delta V_f\right)\right]$$

$$W_{fo}\cdot V_{fo} = \rho_f\cdot A\cdot\left[(1-\alpha)\cdot V_f^{\,2}-(1-\alpha)\cdot V_f\cdot\Delta V_f-\frac{V_f^{\,2}\cdot\Delta\alpha}{2}+\frac{V_f\cdot\Delta\alpha\cdot\Delta V_f}{4}\right]$$

$$W_{fo}\cdot V_{fo} = \rho_f\cdot A\cdot\left[(1-\alpha)\cdot V_f^{\,2}-(1-\alpha)\cdot V_f\cdot\Delta V_f-\frac{V_f^{\,2}\cdot\Delta\alpha}{2}\right] \tag{A14}$$

$$W_{go}\cdot V_{go} = \left(\alpha+\frac{\Delta\alpha}{2}\right)\left(\rho_g-\frac{\Delta\rho_g}{2}\right)\left(V_g-\frac{\Delta V_g}{2}\right)^2 A$$

$$W_{go}\cdot V_{go} = \left(\alpha\cdot\rho_g-\frac{\alpha\cdot\Delta\rho_g}{2}+\frac{\rho_g\cdot\Delta\alpha}{2}-\frac{\Delta\alpha\cdot\Delta\rho_g}{4}\right)\cdot\left(V_g^{\,2}-V_g\cdot\Delta V_g+\frac{\Delta V_g^{\,2}}{4}\right)\cdot A$$

$$W_{go}\cdot V_{go} = \left(\alpha\cdot\rho_g-\frac{\alpha\cdot\Delta\rho_g}{2}+\frac{\rho_g\cdot\Delta\alpha}{2}\right)\cdot\left(V_g^{\,2}-V_g\cdot\Delta V_g\right)\cdot A$$

$$W_{go}\cdot V_{go} = \left(\begin{array}{l}\alpha\cdot\rho_g\cdot V_g^{\,2}-\frac{\alpha\cdot V_g^{\,2}\cdot\Delta\rho_g}{2}+\frac{\rho_g\cdot V_g^{\,2}\cdot\Delta\alpha}{2}-\alpha\cdot\rho_g\cdot V_g\cdot\Delta V_g\ \ldots\\ +\frac{\alpha\cdot V_g\cdot\Delta V_g\cdot\Delta\rho_g}{2}-\frac{\rho_g\cdot V_g\cdot\Delta V_g\cdot\Delta\alpha}{2}\end{array}\right)\cdot A$$

$$W_{go}\cdot V_{go} = \left(\alpha\cdot\rho_g\cdot V_g^{\,2}-\frac{\alpha\cdot V_g^{\,2}\cdot\Delta\rho_g}{2}+\frac{\rho_g\cdot V_g^{\,2}\cdot\Delta\alpha}{2}-\alpha\cdot\rho_g\cdot V_g\cdot\Delta V_g\right)\cdot A \tag{A15}$$

When Equations A12, A13, A14 and A15 are summed, we find:

$$\Sigma(W\cdot V) = W_{fi}\cdot V_{fi} + W_{gi}\cdot V_{gi} - \left(W_{fo}\cdot V_{fo} + W_{go}\cdot V_{go}\right)$$

$$\Sigma(W\cdot V) = \left[\begin{array}{l} \rho_f\cdot A\cdot\left[(1-\alpha)\cdot V_f^{\,2} + (1-\alpha)\cdot V_f\cdot\Delta V_f + \frac{V_f^{\,2}\cdot\Delta\alpha}{2}\right] \ldots \\ +\left(\alpha\cdot\rho_g\cdot V_g^{\,2} + \frac{\alpha\cdot V_g^{\,2}\cdot\Delta\rho_g}{2} - \frac{\rho_g\cdot V_g^{\,2}\cdot\Delta\alpha}{2} + \alpha\cdot\rho_g\cdot V_g\cdot\Delta V_g\right)\cdot A \end{array}\right] \ldots$$
$$+ - \left[\begin{array}{l} \rho_f\cdot A\cdot\left[(1-\alpha)\cdot V_f^{\,2} - (1-\alpha)\cdot V_f\cdot\Delta V_f - \frac{V_f^{\,2}\cdot\Delta\alpha}{2}\right] \ldots \\ +\left(\alpha\cdot\rho_g\cdot V_g^{\,2} - \frac{\alpha\cdot V_g^{\,2}\cdot\Delta\rho_g}{2} + \frac{\rho_g\cdot V_g^{\,2}\cdot\Delta\alpha}{2} - \alpha\cdot\rho_g\cdot V_g\cdot\Delta V_g\right)\cdot A \end{array}\right]$$

When we combine like terms, we find that several terms cancel out or can be added together:

$$\Sigma(W\cdot V) = \left[\begin{array}{l} \rho_f\cdot A\cdot\left[\begin{array}{l}(1-\alpha)\cdot V_f^{\,2} + (1-\alpha)\cdot V_f\cdot\Delta V_f + \frac{V_f^{\,2}\cdot\Delta\alpha}{2} - (1-\alpha)\cdot V_f^{\,2} \ldots\end{array}\right] \ldots \\ \quad +(1-\alpha)\cdot V_f\cdot\Delta V_f + \frac{V_f^{\,2}\cdot\Delta\alpha}{2} \\ +\left(\begin{array}{l}\alpha\cdot\rho_g\cdot V_g^{\,2} + \frac{\alpha\cdot V_g^{\,2}\cdot\Delta\rho_g}{2} - \frac{\rho_g\cdot V_g^{\,2}\cdot\Delta\alpha}{2} + \alpha\cdot\rho_g\cdot V_g\cdot\Delta V_g - \alpha\cdot\rho_g\cdot V_g^{\,2} \ldots\end{array}\right)\cdot A \\ \quad +\frac{\alpha\cdot V_g^{\,2}\cdot\Delta\rho_g}{2} - \frac{\rho_g\cdot V_g^{\,2}\cdot\Delta\alpha}{2} + \alpha\cdot\rho_g\cdot V_g\cdot\Delta V_g \end{array}\right]$$

$$\Sigma(W\cdot V) = \rho_f\cdot A\cdot\left[2\cdot(1-\alpha)\cdot V_f\cdot\Delta V_f + V_f^{\,2}\cdot\Delta\alpha\right] \ldots$$
$$+\left(\alpha\cdot V_g^{\,2}\cdot\Delta\rho_g + 2\alpha\cdot\rho_g\cdot V_g\cdot\Delta V_g - \rho_g\cdot V_g^{\,2}\cdot\Delta\alpha\right)\cdot A$$

$$\Sigma(W\cdot V) = \rho_f\cdot V_f\cdot A\cdot\left[2\cdot(1-\alpha)\cdot\Delta V_f + V_f\cdot\Delta\alpha\right] \ldots \qquad \text{(A16)}$$
$$+ V_g\cdot A\cdot\left(\alpha\cdot V_g\cdot\Delta\rho_g - \rho_g\cdot V_g\cdot\Delta\alpha + 2\alpha\cdot\rho_g\cdot\Delta V_g\right)$$

Next, we will look at the sum of the forces on the control volume:

$$\Sigma F = \left(\alpha - \frac{\Delta\alpha}{2}\right)\cdot\left(P + \frac{\Delta P}{2}\right)\cdot A + \left(1 - \alpha + \frac{\Delta\alpha}{2}\right)\cdot\left(P + \frac{\Delta P}{2}\right)\cdot A - F_{Wg} - \alpha\cdot\rho_g\cdot g\cdot A\cdot\Delta z \ldots$$
$$+ F_{INTg} - \Delta\alpha\cdot P\cdot A + \Delta\alpha\cdot P\cdot A - F_{INTf} - (1-\alpha)\cdot\rho_f\cdot g\cdot A\cdot\Delta z - F_{Wf} \ldots$$
$$+ -\left(\alpha + \frac{\Delta\alpha}{2}\right)\cdot\left(P - \frac{\Delta P}{2}\right)\cdot A - \left(1 - \alpha - \frac{\Delta\alpha}{2}\right)\cdot\left(P - \frac{\Delta P}{2}\right)\cdot A$$

For this derivation, we will assume that wall friction with the vapor phase, F_{Wg}, is negligible. Also, we can cancel out the interface force ($\Delta\alpha PA$) that each phase acts on the other.

$$\Sigma F = \left(\alpha - \frac{\Delta\alpha}{2}\right)\cdot\left(P + \frac{\Delta P}{2}\right)\cdot A + \left(1 - \alpha + \frac{\Delta\alpha}{2}\right)\cdot\left(P + \frac{\Delta P}{2}\right)\cdot A - \alpha\cdot\rho_g\cdot g\cdot A\cdot\Delta z - F_{INTg} \ldots$$
$$+ F_{INTf} - (1-\alpha)\cdot\rho_f\cdot g\cdot A\cdot\Delta z - F_{Wf} - \left(\alpha + \frac{\Delta\alpha}{2}\right)\cdot\left(P - \frac{\Delta P}{2}\right)\cdot A \ldots$$
$$+ -\left(1 - \alpha - \frac{\Delta\alpha}{2}\right)\cdot\left(P - \frac{\Delta P}{2}\right)\cdot A$$

As F_{INTg} and F_{INTf} are equal in magnitude, we will substitute F_{INT} in place of each variable, effectively canceling out each force on the over all force balance. Also, we can cross-multiply each polynomial, and assume that the products of differences are negligible:

$$\Sigma F = \left(\alpha\cdot P - \frac{P\cdot\Delta\alpha}{2} + \frac{\alpha\cdot\Delta P}{2} - \frac{\Delta\alpha\cdot\Delta P}{4}\right)\cdot A \ldots$$
$$+\left[(1-\alpha)\cdot P + \frac{P\cdot\Delta\alpha}{2} + \frac{(1-\alpha)\cdot\Delta P}{2} + \frac{\Delta\alpha\cdot\Delta P}{4}\right]\cdot A - \alpha\cdot\rho_g\cdot g\cdot A\cdot\Delta z \ldots$$
$$+ -(1-\alpha)\cdot\rho_f\cdot g\cdot A\cdot\Delta z - F_{Wf} - \left(\alpha\cdot P + \frac{P\cdot\Delta\alpha}{2} - \frac{\alpha\cdot\Delta P}{2} - \frac{\Delta\alpha\cdot\Delta P}{4}\right)\cdot A \ldots$$
$$+ -\left[(1-\alpha)\cdot P - \frac{P\cdot\Delta\alpha}{2} - \frac{(1-\alpha)\cdot\Delta P}{2} + \frac{\Delta\alpha\cdot\Delta P}{4}\right]\cdot A$$

$$\Sigma F = \left(\alpha\cdot P - \frac{P\cdot\Delta\alpha}{2} + \frac{\alpha\cdot\Delta P}{2}\right)\cdot A \ldots$$
$$+\left[(1-\alpha)\cdot P + \frac{P\cdot\Delta\alpha}{2} + \frac{(1-\alpha)\cdot\Delta P}{2}\right]\cdot A - \alpha\cdot\rho_g\cdot g\cdot A\cdot\Delta z \ldots$$
$$+ -(1-\alpha)\cdot\rho_f\cdot g\cdot A\cdot\Delta z - F_{Wf} - \left(\alpha\cdot P + \frac{P\cdot\Delta\alpha}{2} - \frac{\alpha\cdot\Delta P}{2}\right)\cdot A \ldots$$
$$+ -\left[(1-\alpha)\cdot P - \frac{P\cdot\Delta\alpha}{2} - \frac{(1-\alpha)\cdot\Delta P}{2}\right]\cdot A$$

Combining like terms,we find:

$$\Sigma F = \left(\alpha\cdot P - \frac{P\cdot\Delta\alpha}{2} + \frac{\alpha\cdot\Delta P}{2}\right)\cdot A - \left(\alpha\cdot P + \frac{P\cdot\Delta\alpha}{2} - \frac{\alpha\cdot\Delta P}{2}\right)\cdot A \ldots$$
$$+\left[(1-\alpha)\cdot P + \frac{P\cdot\Delta\alpha}{2} + \frac{(1-\alpha)\cdot\Delta P}{2}\right]\cdot A - \left[(1-\alpha)\cdot P - \frac{P\cdot\Delta\alpha}{2} - \frac{(1-\alpha)\cdot\Delta P}{2}\right]\cdot A \ldots$$
$$+ -(1-\alpha)\cdot\rho_f\cdot g\cdot A\cdot\Delta z - \alpha\cdot\rho_g\cdot g\cdot A\cdot\Delta z - F_{Wf}$$

$$\Sigma F = \left(\alpha\cdot P - \frac{P\cdot\Delta\alpha}{2} + \frac{\alpha\cdot\Delta P}{2} - \alpha\cdot P - \frac{P\cdot\Delta\alpha}{2} + \frac{\alpha\cdot\Delta P}{2}\right)\cdot A \ldots$$
$$+\left[(1-\alpha)\cdot P + \frac{P\cdot\Delta\alpha}{2} + \frac{(1-\alpha)\cdot\Delta P}{2} - (1-\alpha)\cdot P + \frac{P\cdot\Delta\alpha}{2} + \frac{(1-\alpha)\cdot\Delta P}{2}\right]\cdot A \ldots$$
$$+ -\left[(1-\alpha)\cdot\rho_f + \alpha\cdot\rho_g\right]\cdot g\cdot A\cdot\Delta z - F_{Wf}$$

$$\Sigma F = (\alpha\cdot\Delta P - P\cdot\Delta\alpha)\cdot A + [P\cdot\Delta\alpha + (1-\alpha)\cdot\Delta P]\cdot A - \left[(1-\alpha)\cdot\rho_f + \alpha\cdot\rho_g\right]\cdot g\cdot A\cdot\Delta z - F_{Wf}$$

$$\Sigma F = [\alpha\cdot\Delta P - P\cdot\Delta\alpha + P\cdot\Delta\alpha + (1-\alpha)\cdot\Delta P]\cdot A - \left[(1-\alpha)\cdot\rho_f + \alpha\cdot\rho_g\right]\cdot g\cdot A\cdot\Delta z - F_{Wf}$$

$$\Sigma F = [\alpha\cdot\Delta P + (1-\alpha)\cdot\Delta P]\cdot A - \left[(1-\alpha)\cdot\rho_f + \alpha\cdot\rho_g\right]\cdot g\cdot A\cdot\Delta z - F_{Wf}$$

$$\Sigma F = \Delta P\cdot A - \left[(1-\alpha)\cdot\rho_f + \alpha\cdot\rho_g\right]\cdot g\cdot A\cdot\Delta z - F_{Wf} \tag{A17}$$

And so we can combine Equations A16 and A17 into Equation 3 to find:

$$\begin{aligned}\Sigma(W\cdot V) + \Sigma F = {} & \rho_f\cdot V_f\cdot A\cdot\left[2\cdot(1-\alpha)\cdot\Delta V_f + V_f\cdot\Delta\alpha\right] \ldots \\ & + V_g\cdot A\cdot\left(\alpha\cdot V_g\cdot\Delta\rho_g - \rho_g\cdot V_g\cdot\Delta\alpha + 2\cdot\alpha\rho_g\cdot\Delta V_g\right) \ldots \\ & + \Delta P\cdot A - \left[(1-\alpha)\cdot\rho_f + \alpha\cdot\rho_g\right]\cdot g\cdot A\cdot\Delta z - F_{Wf}\end{aligned} = 0 \tag{A18}$$

If we take Equation A18 and divide by $A\Delta z$, we develop the Conservation of Linear Momentum Equation on a per unit volume basis.

$$\frac{\begin{bmatrix}\rho_f\cdot V_f\cdot A\cdot\left[2\cdot(1-\alpha)\cdot\Delta V_f + V_f\cdot\Delta\alpha\right] \ldots \\ + V_g\cdot A\cdot\left(\alpha\cdot V_g\cdot\Delta\rho_g - \rho_g\cdot V_g\cdot\Delta\alpha + 2\cdot\alpha\rho_g\cdot\Delta V_g\right) \ldots \\ + \Delta P\cdot A - \left[(1-\alpha)\cdot\rho_f + \alpha\cdot\rho_g\right]\cdot g\cdot A\cdot\Delta z - F_{Wf}\end{bmatrix}}{A\cdot\Delta z} = 0$$

$$\begin{bmatrix}\dfrac{\rho_f\cdot V_f\cdot A\cdot\left[2\cdot(1-\alpha)\cdot\Delta V_f + V_f\cdot\Delta\alpha\right]}{A\cdot\Delta z} \ldots \\ + \dfrac{V_g\cdot A\cdot\left(\alpha\cdot V_g\cdot\Delta\rho_g - \rho_g\cdot V_g\cdot\Delta\alpha + 2\cdot\alpha\rho_g\cdot\Delta V_g\right)}{A\cdot\Delta z} \ldots \\ + \dfrac{\Delta P\cdot A}{A\Delta z} - \dfrac{\left[(1-\alpha)\cdot\rho_f + \alpha\cdot\rho_g\right]\cdot g\cdot A\cdot\Delta z}{A\cdot\Delta z} - \dfrac{F_{Wf}}{A\cdot\Delta z}\end{bmatrix} = 0$$

At this point, we will cancel out the like terms. Also, the friction force between the liquid and the wall, $F_{Wf}/A\Delta z$, will be simplified to F_{wf}, with the lower case *w* indicating that the force is per unit volume.

$$\begin{bmatrix}\dfrac{\rho_f\cdot V_f\cdot\left[2\cdot(1-\alpha)\cdot\Delta V_f + V_f\cdot\Delta\alpha\right]}{\Delta z} + \dfrac{V_g\cdot\left(\alpha\cdot V_g\cdot\Delta\rho_g - \rho_g\cdot V_g\cdot\Delta\alpha + 2\cdot\alpha\rho_g\cdot\Delta V_g\right)}{\Delta z} \ldots \\ + \dfrac{\Delta P}{\Delta z} - \left[(1-\alpha)\cdot\rho_f + \alpha\cdot\rho_g\right]\cdot g - F_{wf}\end{bmatrix} = 0$$

$$\begin{aligned}\frac{\Delta P}{\Delta z} - \left[(1-\alpha)\cdot\rho_f + \alpha\cdot\rho_g\right]\cdot g - F_{wf} \ldots & = 0 \\ + 2\cdot(1-\alpha)\cdot\rho_f\cdot V_f\cdot\frac{\Delta V_f}{\Delta z} + \rho_f\cdot V_f^{\,2}\cdot\frac{\Delta\alpha}{\Delta z} \ldots & \\ + \alpha\cdot V_g^{\,2}\cdot\frac{\Delta\rho_g}{\Delta z} - \rho_g\cdot V_g^{\,2}\cdot\frac{\Delta\alpha}{\Delta z} + 2\cdot\alpha\cdot\rho_g\cdot V_g\cdot\frac{\Delta V_g}{\Delta z} & \end{aligned} \tag{A19}$$

If we substitute Equations A8 and A11 into Equation A19, then we get:

$$\frac{\Delta P}{\Delta z} - \left[(1-\alpha)\cdot\rho_f + \alpha\cdot\rho_g\right]\cdot g - F_{wf} \ldots = 0$$

$$+ 2\cdot(1-\alpha)\cdot\rho_f\cdot V_f\cdot\frac{\frac{-V_f\cdot\Delta\alpha}{(1-\alpha)}}{\Delta z} + \rho_f\cdot V_f^{\,2}\cdot\frac{\Delta\alpha}{\Delta z} \ldots$$

$$+ \alpha\cdot V_g^{\,2}\cdot\frac{\Delta\rho_g}{\Delta z} - \rho_g\cdot V_g^{\,2}\cdot\frac{\Delta\alpha}{\Delta z} + 2\cdot\alpha\cdot\rho_g\cdot V_g\cdot\frac{V_g\cdot\left(\frac{\Delta\alpha}{\alpha} - \frac{\Delta\rho_g}{\rho_g}\right)}{\Delta z}$$

We distribute the substitutions in to the equation and cancel out terms:

$$\frac{\Delta P}{\Delta z} - \left[(1-\alpha)\cdot\rho_f + \alpha\cdot\rho_g\right]\cdot g - F_{wf} - 2\cdot\rho_f\cdot V_f^{\,2}\cdot\frac{\Delta\alpha}{\Delta z} \ldots = 0$$

$$+ \rho_f\cdot V_f^{\,2}\cdot\frac{\Delta\alpha}{\Delta z} + \alpha\cdot V_g^{\,2}\cdot\frac{\Delta\rho_g}{\Delta z} - \rho_g\cdot V_g^{\,2}\cdot\frac{\Delta\alpha}{\Delta z} + 2\cdot\rho_g\cdot V_g^{\,2}\cdot\frac{\Delta\alpha}{\Delta z} - 2\cdot\alpha\cdot V_g^{\,2}\cdot\frac{\Delta\rho_g}{\Delta z}$$

$$\frac{\Delta P}{\Delta z} - \left[(1-\alpha)\cdot\rho_f + \alpha\cdot\rho_g\right]\cdot g - F_{wf} - \rho_f\cdot V_f^{\,2}\cdot\frac{\Delta\alpha}{\Delta z} \ldots = 0$$

$$+ \rho_g\cdot V_g^{\,2}\cdot\frac{\Delta\alpha}{\Delta z} - \alpha\cdot V_g^{\,2}\cdot\frac{\Delta\rho_g}{\Delta z}$$

$$\frac{\Delta P}{\Delta z} = \left[(1-\alpha)\cdot\rho_f + \alpha\cdot\rho_g\right]\cdot g + F_{wf} + \left(\rho_f\cdot V_f^{\,2} - \rho_g\cdot V_g^{\,2}\right)\cdot\frac{\Delta\alpha}{\Delta z} + \alpha\cdot V_g^{\,2}\cdot\frac{\Delta\rho_g}{\Delta z} \qquad \text{(A20)}$$

According to Wallis [84], the pressure gradient in a two-phase flow can be divided into three components:

$$\frac{\Delta P}{\Delta z} = \frac{\Delta P_H}{\Delta z} + \frac{\Delta P_F}{\Delta z} + \frac{\Delta P_A}{\Delta z} \qquad \text{(A21)}$$

where ΔP_H is the change in hydrostatic pressure, ΔP_F is the change in pressure due to wall friction and ΔP_A is the change in pressure due to acceleration.

If we were to breakdown Equation A20 into the components of Equation A21, we would find that:

$$\frac{\Delta P_H}{\Delta z} = \left[(1-\alpha)\cdot\rho_f + \alpha\cdot\rho_g\right]\cdot g \qquad \text{(A22)}$$

$$\frac{\Delta P_F}{\Delta z} = F_{wf} \qquad \text{(A23)}$$

$$\frac{\Delta P_A}{\Delta z} = \left(\rho_f\cdot V_f^{\,2} - \rho_g\cdot V_g^{\,2}\right)\cdot\frac{\Delta\alpha}{\Delta z} + \alpha\cdot V_g^{\,2}\cdot\frac{\Delta\rho_g}{\Delta z} \qquad \text{(A24)}$$

Next, we will look at the Conservation of Linear Momentum for the liquid phase. We begin with Equation A4:

$$\frac{d}{dt}p_f = \Sigma\left(W_f \cdot V_f\right) + \Sigma\left(m_f \cdot a_f\right) = \Sigma\left(W_f \cdot V_f\right) + \Sigma F_f = W_{fi} \cdot V_{fi} - W_{fo} \cdot V_{fo} + \Sigma F_f = 0 \qquad \text{(A4)}$$

We substitute Equation A12 and A14 for the momentum terms and use Figure 1 to identify the forces on the liquid phase.

$$\begin{aligned} W_{fi} \cdot V_{fi} - W_{fo} \cdot V_{fo} + \Sigma F_f = {} & \rho_f \cdot A \cdot \left[(1-\alpha) \cdot {V_f}^2 + (1-\alpha) \cdot V_f \cdot \Delta V_f + \frac{{V_f}^2 \cdot \Delta\alpha}{2} \right] \ldots \\ & + -\rho_f \cdot A \cdot \left[(1-\alpha) \cdot {V_f}^2 - (1-\alpha) \cdot V_f \cdot \Delta V_f - \frac{{V_f}^2 \cdot \Delta\alpha}{2} \right] \ldots \\ & + \left(1 - \alpha + \frac{\Delta\alpha}{2}\right) \cdot \left(P + \frac{\Delta P}{2}\right) \cdot A + F_{INTf} - (1-\alpha) \cdot \rho_f \cdot g \cdot A \cdot \Delta z \ldots \\ & + -F_{Wf} - P \cdot A \cdot \Delta\alpha - \left(1 - \alpha - \frac{\Delta\alpha}{2}\right) \cdot \left(P - \frac{\Delta P}{2}\right) \cdot A \end{aligned}$$

Cross-multiplying the polynomials, we find:

$$\begin{aligned} & \rho_f \cdot A \cdot \left[(1-\alpha) \cdot {V_f}^2 + (1-\alpha) \cdot V_f \cdot \Delta V_f + \frac{{V_f}^2 \cdot \Delta\alpha}{2} - (1-\alpha) \cdot {V_f}^2 + (1-\alpha) \cdot V_f \cdot \Delta V_f + \frac{{V_f}^2 \cdot \Delta\alpha}{2} \right] \ldots = 0 \\ & + \left[(1-\alpha) \cdot P + \frac{(1-\alpha) \cdot \Delta P}{2} + \frac{P \cdot \Delta\alpha}{2} + \frac{\Delta\alpha \cdot \Delta P}{4} \right] \cdot A + F_{INTf} - (1-\alpha) \cdot \rho_f \cdot g \cdot A \cdot \Delta z \ldots \\ & + -F_{Wf} - P \cdot A \cdot \Delta\alpha - \left[(1-\alpha) \cdot P - \frac{(1-\alpha) \cdot \Delta P}{2} - \frac{P \cdot \Delta\alpha}{2} + \frac{\Delta\alpha \cdot \Delta P}{4} \right] \cdot A \end{aligned}$$

Cancelling terms out and assuming the products of differences are negligible, we find:

$$\begin{aligned} & \rho_f \cdot A \cdot \left[2 \cdot (1-\alpha) \cdot V_f \cdot \Delta V_f + {V_f}^2 \cdot \Delta\alpha \right] \ldots = 0 \\ & + \left[(1-\alpha) \cdot \Delta P + P \cdot \Delta\alpha \right] \cdot A + F_{INTf} - (1-\alpha) \cdot \rho_f \cdot g \cdot A \cdot \Delta z \ldots \\ & + -F_{Wf} - P \cdot A \cdot \Delta\alpha \end{aligned}$$

Finally, we cancel out the term $PA\Delta\alpha$:

$$\begin{aligned} & \rho_f \cdot A \cdot \left[2 \cdot (1-\alpha) \cdot V_f \cdot \Delta V_f + {V_f}^2 \cdot \Delta\alpha \right] \ldots = 0 \\ & + (1-\alpha) \cdot A \cdot \Delta P + F_{INTf} - (1-\alpha) \cdot \rho_f \cdot g \cdot A \cdot \Delta z - F_{Wf} \end{aligned} \qquad \text{(A25)}$$

Next, we will substitute Equation A8 into Equation A25:

$$\begin{aligned} & \rho_f \cdot A \cdot \left[2 \cdot (1-\alpha) \cdot V_f \cdot \frac{-V_f \cdot \Delta\alpha}{(1-\alpha)} + {V_f}^2 \cdot \Delta\alpha \right] \ldots = 0 \\ & + (1-\alpha) \cdot A \cdot \Delta P + F_{INTf} - (1-\alpha) \cdot \rho_f \cdot g \cdot A \cdot \Delta z - F_{Wf} \end{aligned}$$

$$\rho_f \cdot A \cdot \left(-2 \cdot {V_f}^2 \cdot \Delta\alpha + {V_f}^2 \cdot \Delta\alpha \right) + (1-\alpha) \cdot A \cdot \Delta P + F_{INTf} - (1-\alpha) \cdot \rho_f \cdot g \cdot A \cdot \Delta z - F_{Wf} = 0$$

$$-\rho_f \cdot {V_f}^2 \cdot A \cdot \Delta\alpha + (1-\alpha) \cdot A \cdot \Delta P + F_{INTf} - (1-\alpha) \cdot \rho_f \cdot g \cdot A \cdot \Delta z - F_{Wf} = 0$$

If we divide by $A\Delta z$, then we can solve for a per unit volume basis:

$$\frac{-\rho_f \cdot V_f^{\,2} \cdot A \cdot \Delta\alpha}{A \cdot \Delta z} + \frac{(1-\alpha) \cdot A \cdot \Delta P}{A \cdot \Delta z} + \frac{F_{INTf}}{A \cdot \Delta z} - \frac{(1-\alpha) \cdot \rho_f \cdot g \cdot A \cdot \Delta z}{A \cdot \Delta z} - \frac{F_{Wf}}{A \cdot \Delta z} = 0$$

If we substitute F_{int} for $F_{INTf}/A\Delta z$ and F_{wf} for $F_{Wf}/A\Delta z$, and cancel out like terms, then our equation becomes:

$$(1-\alpha) \cdot \frac{\Delta P}{\Delta z} - (1-\alpha) \cdot \rho_f \cdot g + F_{int} - F_{wf} - \rho_f \cdot V_f^{\,2} \cdot \frac{\Delta\alpha}{\Delta z} = 0 \tag{A26}$$

For the purposes of this study, the goal is to solve for the interphase friction force per unit volume, F_{int}, thus Equation A26 will be rewritten as:

$$F_{int} = (1-\alpha) \cdot \left(\rho_f \cdot g - \frac{\Delta P}{\Delta z} \right) + F_{wf} + \rho_f \cdot V_f^{\,2} \cdot \frac{\Delta\alpha}{\Delta z} \tag{A27}$$

Now, we will solve the Conservation of Linear Momentum Balance for the vapor phase, beginning with Equation A5

$$\frac{d}{dt} p_g = \Sigma\left(W_f \cdot V_f\right) + \Sigma\left(m_f \cdot a_f\right) = \Sigma\left(W_g \cdot V_g\right) + \Sigma F_g = 0 \tag{A5}$$

$$\Sigma\left(W_g \cdot V_g\right) + \Sigma F_g = W_{gi} \cdot V_{gi} - W_{go} \cdot V_{go} + \Sigma F_g = 0$$

We substitute in Equations A13 and A15 for the momentum and use Figure A1 to determine the forces acting on the vapor phase.

$$\begin{aligned} W_{gi} \cdot V_{gi} - W_{go} \cdot V_{go} \ldots = 0 = {} & \left(\alpha \cdot \rho_g \cdot V_g^{\,2} + \frac{\alpha \cdot V_g^{\,2} \cdot \Delta\rho_g}{2} - \frac{\rho_g \cdot V_g^{\,2} \cdot \Delta\alpha}{2} + \alpha \cdot \rho_g \cdot V_g \cdot \Delta V_g \right) \cdot A \ldots \\ & + \Sigma F_g \\ & + - \left[\left(\alpha \cdot \rho_g \cdot V_g^{\,2} - \frac{\alpha \cdot V_g^{\,2} \cdot \Delta\rho_g}{2} + \frac{\rho_g \cdot V_g^{\,2} \cdot \Delta\alpha}{2} - \alpha \cdot \rho_g \cdot V_g \cdot \Delta V_g \right) \cdot A \right] \ldots \\ & + \left(\alpha - \frac{\Delta\alpha}{2} \right) \cdot \left(P + \frac{\Delta P}{2} \right) \cdot A - F_{Wg} - \alpha \cdot \rho_g \cdot g \cdot A \cdot \Delta z + P \cdot A \cdot \Delta\alpha \ldots \\ & + - F_{INTg} - \left(\alpha + \frac{\Delta\alpha}{2} \right) \cdot \left(P - \frac{\Delta P}{2} \right) \cdot A \end{aligned}$$

We begin by combining the like terms and cross-multiplying the polynomials of the force balance

$$\begin{aligned} & \left(\begin{aligned} & \alpha \cdot \rho_g \cdot V_g^{\,2} + \frac{\alpha \cdot V_g^{\,2} \cdot \Delta\rho_g}{2} - \frac{\rho_g \cdot V_g^{\,2} \cdot \Delta\alpha}{2} + \alpha \cdot \rho_g \cdot V_g \cdot \Delta V_g - \alpha \cdot \rho_g \cdot V_g^{\,2} \ldots \\ & + \frac{\alpha \cdot V_g^{\,2} \cdot \Delta\rho_g}{2} - \frac{\rho_g \cdot V_g^{\,2} \cdot \Delta\alpha}{2} + \alpha \cdot \rho_g \cdot V_g \cdot \Delta V_g \end{aligned} \right) \cdot A \ldots = 0 \\ & + \left(\alpha \cdot P + \frac{\alpha \cdot \Delta P}{2} - \frac{P \cdot \Delta\alpha}{2} - \frac{\Delta\alpha \cdot \Delta P}{4} \right) \cdot A - F_{Wg} - \alpha \cdot \rho_g \cdot g \cdot A \cdot \Delta z + P \cdot A \cdot \Delta\alpha \ldots \\ & + - F_{INTg} - \left(\alpha \cdot P - \frac{\alpha \cdot \Delta P}{2} + \frac{P \cdot \Delta\alpha}{2} - \frac{\Delta\alpha \cdot \Delta P}{4} \right) \cdot A \end{aligned}$$

Now we will combine the like terms and cancel out the products of differences that are assumed to be negligible. Also, we assume that F_{Wg} is negligible.

$$\left(\alpha\cdot V_g^{\,2}\cdot\Delta\rho_g - \rho_g\cdot V_g^{\,2}\cdot\Delta\alpha + 2\cdot\alpha\cdot\rho_g\cdot V_g\cdot\Delta V_g\right)\cdot A \ldots = 0$$
$$+\left(\alpha\cdot P + \frac{\alpha\cdot\Delta P}{2} - \frac{P\cdot\Delta\alpha}{2} - \alpha\cdot P + \frac{\alpha\cdot\Delta P}{2} - \frac{P\cdot\Delta\alpha}{2}\right)\cdot A \ldots$$
$$+ -F_{INTg} - \alpha\cdot\rho_g\cdot g\cdot A\cdot\Delta z + P\cdot A\cdot\Delta\alpha$$

$$\left(\alpha\cdot V_g^{\,2}\cdot\Delta\rho_g - \rho_g\cdot V_g^{\,2}\cdot\Delta\alpha + 2\cdot\alpha\cdot\rho_g\cdot V_g\cdot\Delta V_g\right)\cdot A \ldots = 0$$
$$+(\alpha\cdot\Delta P - P\cdot\Delta\alpha)\cdot A - F_{INTg} - \alpha\cdot\rho_g\cdot g\cdot A\cdot\Delta z + P\cdot A\cdot\Delta\alpha$$

$$\left(\alpha\cdot V_g^{\,2}\cdot\Delta\rho_g - \rho_g\cdot V_g^{\,2}\cdot\Delta\alpha + 2\cdot\alpha\cdot\rho_g\cdot V_g\cdot\Delta V_g\right)\cdot A \ldots = 0$$
$$+\alpha\cdot A\cdot\Delta P - F_{INTg} - \alpha\cdot\rho_g\cdot g\cdot A\cdot\Delta z$$

At this point, we will substitute in Equation A11 and combine like terms:

$$\left[\alpha\cdot V_g^{\,2}\cdot\Delta\rho_g - \rho_g\cdot V_g^{\,2}\cdot\Delta\alpha + 2\cdot\alpha\cdot\rho_g\cdot V_g\cdot\left[V_g\cdot\left(\frac{\Delta\alpha}{\alpha} - \frac{\Delta\rho_g}{\rho_g}\right)\right]\right]\cdot A \ldots = 0$$
$$+\alpha\cdot A\cdot\Delta P - F_{INTg} - \alpha\cdot\rho_g\cdot g\cdot A\cdot\Delta z$$

$$\left(\alpha\cdot V_g^{\,2}\cdot\Delta\rho_g - \rho_g\cdot V_g^{\,2}\cdot\Delta\alpha + 2\cdot\alpha\cdot\rho_g\cdot V_g^{\,2}\cdot\frac{\Delta\alpha}{\alpha} - 2\cdot\alpha\cdot\rho_g\cdot V_g^{\,2}\cdot\frac{\Delta\rho_g}{\rho_g}\right)\cdot A \ldots = 0$$
$$+\alpha\cdot A\cdot\Delta P - F_{INTg} - \alpha\cdot\rho_g\cdot g\cdot A\cdot\Delta z$$

$$\left(\alpha\cdot V_g^{\,2}\cdot\Delta\rho_g - \rho_g\cdot V_g^{\,2}\cdot\Delta\alpha + 2\cdot\rho_g\cdot V_g^{\,2}\cdot\Delta\alpha - 2\cdot\alpha\cdot V_g^{\,2}\cdot\Delta\rho_g\right)\cdot A \ldots = 0$$
$$+\alpha\cdot A\cdot\Delta P - F_{INTg} - \alpha\cdot\rho_g\cdot g\cdot A\cdot\Delta z$$

$$\rho_g\cdot V_g^{\,2}\cdot A\cdot\Delta\alpha - \alpha\cdot V_g^{\,2}\cdot A\cdot\Delta\rho_g + \alpha\cdot A\cdot\Delta P - F_{INTg} - \alpha\cdot\rho_g\cdot g\cdot A\cdot\Delta z = 0$$

Now, we will divide our equation by $A\Delta z$:

$$\frac{\rho_g\cdot V_g^{\,2}\cdot A\cdot\Delta\alpha}{A\cdot\Delta z} - \frac{\alpha\cdot V_g^{\,2}\cdot A\cdot\Delta\rho_g}{A\cdot\Delta z} + \frac{\alpha\cdot A\cdot\Delta P}{A\cdot\Delta z} - \frac{F_{INTg}}{A\cdot\Delta z} - \frac{\alpha\cdot\rho_g\cdot g\cdot A\cdot\Delta z}{A\cdot\Delta z} = 0$$

We cancel out like terms and substitute F_{int} for $F_{INTg}/A\Delta z$:

$$\rho_g\cdot V_g^{\,2}\cdot\frac{\Delta\alpha}{\Delta z} - \alpha\cdot V_g^{\,2}\cdot\frac{\Delta\rho_g}{\Delta z} + \alpha\cdot\frac{\Delta P}{\Delta z} - F_{int} - \alpha\cdot\rho_g\cdot g = 0 \qquad \text{(A28)}$$

Solving for F_{int}, we find:

$$F_{int} = \alpha\cdot\left(\frac{\Delta P}{\Delta z} - \rho_g\cdot g\right) - \alpha\cdot V_g^{\,2}\cdot\frac{\Delta\rho_g}{\Delta z} + \rho_g\cdot V_g^{\,2}\cdot\frac{\Delta\alpha}{\Delta z} \qquad \text{(A29)}$$

To summarize the equations derived so far:

The Conservation of Liquid Mass

$$\Delta V_f = \frac{-V_f \cdot \Delta\alpha}{(1-\alpha)} \tag{A8}$$

The Conservation of Vapor Mass

$$\Delta V_g = V_g \cdot \left(\frac{\Delta\alpha}{\alpha} - \frac{\Delta\rho_g}{\rho_g} \right) \tag{A11}$$

The Overall Conservation of Linear Momentum

$$\frac{\Delta P}{\Delta z} = \left[(1-\alpha)\cdot\rho_f + \alpha\cdot\rho_g \right] \cdot g + F_{wf} + \left(\rho_f \cdot V_f^{\,2} - \rho_g \cdot V_g^{\,2} \right) \cdot \frac{\Delta\alpha}{\Delta z} + \alpha \cdot V_g^{\,2} \cdot \frac{\Delta\rho_g}{\Delta z} \tag{A20}$$

The Conservation of Linear Momentum for the Liquid Phase

$$F_{int} = (1-\alpha)\cdot\left(\rho_f \cdot g - \frac{\Delta P}{\Delta z} \right) + F_{wf} + \rho_f \cdot V_f^{\,2} \cdot \frac{\Delta\alpha}{\Delta z} \tag{A27}$$

The Conservation of Linear Momentum for the Vapor Phase

$$F_{int} = \alpha\cdot\left(\frac{\Delta P}{\Delta z} - \rho_g \cdot g \right) - \alpha \cdot V_g^{\,2} \cdot \frac{\Delta\rho_g}{\Delta z} + \rho_g \cdot V_g^{\,2} \cdot \frac{\Delta\alpha}{\Delta z} \tag{A29}$$

Equations A27 and A29 give us two different equations for F_{int}. However, we can combine the two equations by first solving for $\Delta\alpha/\Delta z$, and develop a single equation for F_{int}. First, from Equation A27, we find:

$$\frac{\Delta\alpha}{\Delta z} = \frac{F_{int} - (1-\alpha)\cdot\left(\rho_f \cdot g - \frac{\Delta P}{\Delta z} \right) - F_{wf}}{\rho_f \cdot V_f^{\,2}} \tag{A30}$$

From Equation A29, we find:

$$\frac{\Delta\alpha}{\Delta z} = \frac{F_{int} - \alpha\cdot\left(\frac{\Delta P}{\Delta z} - \rho_g \cdot g \right) + \alpha \cdot V_g^{\,2} \cdot \frac{\Delta\rho_g}{\Delta z}}{\rho_g \cdot V_g^{\,2}} \tag{A31}$$

If we combine Equations A30 and A31, we find:

$$\frac{\Delta\alpha}{\Delta z} = \frac{F_{int} - (1-\alpha)\cdot\left(\rho_f \cdot g - \frac{\Delta P}{\Delta z} \right) - F_{wf}}{\rho_f \cdot V_f^{\,2}} = \frac{F_{int} - \alpha\cdot\left(\frac{\Delta P}{\Delta z} - \rho_g \cdot g \right) + \alpha \cdot V_g^{\,2} \cdot \frac{\Delta\rho_g}{\Delta z}}{\rho_g \cdot V_g^{\,2}}$$

Our next step is to multiply each side by $\rho_f \rho_g V_f^2 V_g^2$, and then we will combine like terms:

$$\left[F_{int} - (1-\alpha)\cdot\left(\rho_f \cdot g - \frac{\Delta P}{\Delta z}\right) - F_{wf}\right]\cdot\left(\rho_g \cdot V_g^{\,2}\right) = \left[\begin{array}{l} F_{int} - \alpha\cdot\left(\dfrac{\Delta P}{\Delta z} - \rho_g \cdot g\right) \ldots \\ + \alpha \cdot V_g^{\,2} \cdot \dfrac{\Delta \rho_g}{\Delta z} \end{array}\right]\cdot\left(\rho_f \cdot V_f^{\,2}\right)$$

$$F_{int}\cdot\left(\rho_g \cdot V_g^{\,2} - \rho_f \cdot V_f^{\,2}\right) = \left(\rho_g \cdot V_g^{\,2}\right)\cdot\left[(1-\alpha)\cdot\left(\rho_f \cdot g - \frac{\Delta P}{\Delta z}\right) + F_{wf}\right] \ldots + \left(\rho_f \cdot V_f^{\,2}\right)\cdot\left[\alpha \cdot V_g^{\,2}\cdot\frac{\Delta \rho_g}{\Delta z} - \alpha\cdot\left(\frac{\Delta P}{\Delta z} - \rho_g \cdot g\right)\right]$$

$$F_{int} = \frac{\left[(1-\alpha)\cdot\left(\rho_f \cdot g - \dfrac{\Delta P}{\Delta z}\right) + F_{wf}\right]\cdot\left(\rho_g \cdot V_g^{\,2}\right) \ldots + \left[\alpha \cdot V_g^{\,2}\cdot\dfrac{\Delta \rho_g}{\Delta z} - \alpha\cdot\left(\dfrac{\Delta P}{\Delta z} - \rho_g \cdot g\right)\right]\cdot\left(\rho_f \cdot V_f^{\,2}\right)}{\rho_g \cdot V_g^{\,2} - \rho_f \cdot V_f^{\,2}} \qquad \text{(A32)}$$

From Equation A32, we can also derive an expression that can be used to predict the void fraction, α, for a given control volume.

$$F_{int} = \frac{\left[(1-\alpha)\cdot\left(\rho_f \cdot g - \dfrac{\Delta P}{\Delta z}\right) + F_{wf}\right]\cdot\left(\rho_g \cdot V_g^{\,2}\right) \ldots + \left[\alpha \cdot V_g^{\,2}\cdot\dfrac{\Delta \rho_g}{\Delta z} - \alpha\cdot\left(\dfrac{\Delta P}{\Delta z} - \rho_g \cdot g\right)\right]\cdot\left(\rho_f \cdot V_f^{\,2}\right)}{\rho_g \cdot V_g^{\,2} - \rho_f \cdot V_f^{\,2}} \qquad \text{(A32)}$$

Multiplying each side by $\rho_g V_g^{\,2} - \rho_f V_f^{\,2}$:

$$F_{int}\cdot\left(\rho_g \cdot V_g^{\,2} - \rho_f \cdot V_f^{\,2}\right) = \left[(1-\alpha)\cdot\left(\rho_f \cdot g - \frac{\Delta P}{\Delta z}\right) + F_{wf}\right]\cdot\left(\rho_g \cdot V_g^{\,2}\right) \ldots + \left[\alpha \cdot V_g^{\,2}\cdot\frac{\Delta \rho_g}{\Delta z} - \alpha\cdot\left(\frac{\Delta P}{\Delta z} - \rho_g \cdot g\right)\right]\cdot\left(\rho_f \cdot V_f^{\,2}\right)$$

Factoring out α:

$$F_{int}\cdot\left(\rho_g \cdot V_g^{\,2} - \rho_f \cdot V_f^{\,2}\right) = \left(\rho_f \cdot g - \frac{\Delta P}{\Delta z}\right)\cdot\left(\rho_g \cdot V_g^{\,2}\right) - \alpha\left(\rho_f \cdot g - \frac{\Delta P}{\Delta z}\right)\cdot\left(\rho_g \cdot V_g^{\,2}\right) \ldots + F_{wf}\cdot\left(\rho_g \cdot V_g^{\,2}\right) + \alpha\cdot\left(V_g^{\,2}\cdot\frac{\Delta \rho_g}{\Delta z} - \frac{\Delta P}{\Delta z} + \rho_g \cdot g\right)\cdot\left(\rho_f \cdot V_f^{\,2}\right)$$

Combining terms:

$$F_{int}\cdot\left(\rho_g\cdot V_g^{\,2}-\rho_f\cdot V_f^{\,2}\right)-\left(\begin{matrix}\rho_f\cdot g-\dfrac{\Delta P}{\Delta z}\ \ldots\\ +F_{wf}\end{matrix}\right)\cdot\left(\rho_g\cdot V_g^{\,2}\right)=\alpha\cdot\left[\begin{matrix}\left(\begin{matrix}V_g^{\,2}\cdot\dfrac{\Delta\rho_g}{\Delta z}-\dfrac{\Delta P}{\Delta z}\ \ldots\\ +\rho_g\cdot g\end{matrix}\right)\cdot\left(\rho_f\cdot V_f^{\,2}\right)\ \ldots\\ +\left(\dfrac{\Delta P}{\Delta z}-\rho_f\cdot g\right)\cdot\left(\rho_g\cdot V_g^{\,2}\right)\end{matrix}\right]$$

The final result for the expression to solve for the void fraction, α, is Equation A33:

$$\alpha=\frac{F_{int}\cdot\left(\rho_g\cdot V_g^{\,2}-\rho_f\cdot V_f^{\,2}\right)-\left(\rho_f\cdot g-\dfrac{\Delta P}{\Delta z}+F_{wf}\right)\cdot\left(\rho_g\cdot V_g^{\,2}\right)}{\left(V_g^{\,2}\cdot\dfrac{\Delta\rho_g}{\Delta z}-\dfrac{\Delta P}{\Delta z}+\rho_g\cdot g\right)\cdot\left(\rho_f\cdot V_f^{\,2}\right)-\left(\rho_f\cdot g-\dfrac{\Delta P}{\Delta z}\right)\cdot\left(\rho_g\cdot V_g^{\,2}\right)} \tag{A33}$$

Another term that is useful for performing calculations for interphase friction is the void fraction gradient $\Delta\alpha/\Delta z$. Once again, we begin with Equations A27 and A29:

$$F_{int}=(1-\alpha)\cdot\left(\rho_f\cdot g-\frac{\Delta P}{\Delta z}\right)\ \ldots=\alpha\cdot\left(\frac{\Delta P}{\Delta z}-\rho_g\cdot g\right)-\alpha\cdot V_g^{\,2}\cdot\frac{\Delta\rho_g}{\Delta z}+\rho_g\cdot V_g^{\,2}\cdot\frac{\Delta\alpha}{\Delta z}$$
$$+F_{wf}+\rho_f\cdot V_f^{\,2}\cdot\frac{\Delta\alpha}{\Delta z}$$

$$(1-\alpha)\cdot\left(\rho_f\cdot g-\frac{\Delta P}{\Delta z}\right)+F_{wf}+\rho_f\cdot V_f^{\,2}\cdot\frac{\Delta\alpha}{\Delta z}=\alpha\cdot\left(\frac{\Delta P}{\Delta z}-\rho_g\cdot g\right)-\alpha\cdot V_g^{\,2}\cdot\frac{\Delta\rho_g}{\Delta z}+\rho_g\cdot V_g^{\,2}\cdot\frac{\Delta\alpha}{\Delta z}$$

When solving for $\Delta\alpha/\Delta z$ this becomes:

$$\frac{\Delta\alpha}{\Delta z}=\frac{(1-\alpha)\cdot\left(\rho_f\cdot g-\dfrac{\Delta P}{\Delta z}\right)+F_{wf}-\left[\alpha\cdot\left(\dfrac{\Delta P}{\Delta z}-\rho_g\cdot g\right)-\alpha\cdot V_g^{\,2}\cdot\dfrac{\Delta\rho_g}{\Delta z}\right]}{\rho_g\cdot V_g^{\,2}-\rho_f\cdot V_f^{\,2}}$$

This equation can be simplified further to:

$$\frac{\Delta\alpha}{\Delta z}=\frac{-(1-\alpha)\cdot\dfrac{\Delta P}{\Delta z}+(1-\alpha)\cdot\rho_f\cdot g+F_{wf}+\alpha\cdot\rho_g\cdot g-\alpha\cdot\dfrac{\Delta P}{\Delta z}+\alpha\cdot V_g^{\,2}\cdot\dfrac{\Delta\rho_g}{\Delta z}}{-\left(\rho_f\cdot V_f^{\,2}-\rho_g\cdot V_g^{\,2}\right)}$$

$$\frac{\Delta\alpha}{\Delta z}=\frac{-\left[(1-\alpha)\cdot\dfrac{\Delta P}{\Delta z}+\alpha\cdot\dfrac{\Delta P}{\Delta z}\right]+\left[(1-\alpha)\cdot\rho_f\cdot g+\alpha\cdot\rho_g\cdot g\right]+F_{wf}+\alpha\cdot V_g^{\,2}\cdot\dfrac{\Delta\rho_g}{\Delta z}}{-\left(\rho_f\cdot V_f^{\,2}-\rho_g\cdot V_g^{\,2}\right)}$$

$$\frac{\Delta\alpha}{\Delta z}=\frac{\dfrac{\Delta P}{\Delta z}-\left[(1-\alpha)\cdot\rho_f+\alpha\cdot\rho_g\right]\cdot g-F_{wf}-\alpha\cdot V_g^{\,2}\cdot\dfrac{\Delta\rho_g}{\Delta z}}{\rho_f\cdot V_f^{\,2}-\rho_g\cdot V_g^{\,2}} \tag{A34}$$

Using the relationship identified in Equation A21, we can rewrite Equation A34 as:

$$\frac{\Delta\alpha}{\Delta z} = \frac{\frac{\Delta P_A}{\Delta z} - \alpha \cdot V_g^{\,2} \cdot \frac{\Delta \rho_g}{\Delta z}}{\rho_f \cdot V_f^{\,2} - \rho_g \cdot V_g^{\,2}} \tag{A35}$$

At this point, it should be mentioned that in most case studies, V_f and V_g are not measured and are based on the flow rate through the system. Therefore, we define V_f and V_g in terms of the liquid and vapor mass flow rates, respectively.

$$V_f = \frac{W_f}{(1-\alpha)\cdot\rho_f \cdot A} \tag{A36}$$

$$V_g = \frac{W_g}{\alpha \cdot \rho_g \cdot A} \tag{A37}$$

Thus, we can recalculate each of our derived equations in terms of parameters that are either fixed or directly measured in each experiment. We begin with the Conservation of Liquid Mass Equation.

$$\Delta V_f = \frac{-V_f \cdot \Delta\alpha}{(1-\alpha)} = \frac{-W_f \cdot \Delta\alpha}{(1-\alpha)^2 \cdot \rho_f \cdot A} \tag{A38}$$

The Conservation of Vapor Mass becomes:

$$\Delta V_g = V_g \cdot \left(\frac{\Delta\alpha}{\alpha} - \frac{\Delta\rho_g}{\rho_g}\right) = \frac{W_g}{\alpha\cdot\rho_g\cdot A}\cdot\left(\frac{\Delta\alpha}{\alpha} - \frac{\Delta\rho_g}{\rho_g}\right) \tag{A39}$$

As we have already substituted the continuity equations into the linear momentum equations, there is no need to implement Equations A38 and A39 into a new set of Conservation of Linear Momentum equations. Instead, we can directly substitute Equations A36 and A37 into Equations A20, A27, A29, A32 and A35 to derive the desired equations. We begin with the overall Conservation of Linear Momentum Equation:

$$\frac{\Delta P}{\Delta z} = \left[(1-\alpha)\cdot\rho_f + \alpha\cdot\rho_g\right]\cdot g + F_{wf} + \left(\rho_f\cdot V_f^{\,2} - \rho_g \cdot V_g^{\,2}\right)\cdot\frac{\Delta\alpha}{\Delta z} + \alpha\cdot V_g^{\,2}\cdot\frac{\Delta\rho_g}{\Delta z} = 0 \tag{A20}$$

$$\frac{\Delta P}{\Delta z} = \left[(1-\alpha)\cdot\rho_f + \alpha\cdot\rho_g\right]\cdot g + F_{wf} \ldots + \left[\rho_f\cdot\left[\frac{W_f}{(1-\alpha)\cdot\rho_f\cdot A}\right]^2 - \rho_g\cdot\left(\frac{W_g}{\alpha\cdot\rho_g\cdot A}\right)^2\right]\cdot\frac{\Delta\alpha}{\Delta z} + \alpha\cdot\left(\frac{W_g}{\alpha\cdot\rho_g\cdot A}\right)^2\cdot\frac{\Delta\rho_g}{\Delta z}$$

After some distrbuting of the squares and canceling out terms, the Conservation of Linear Momentum Equation becomes:

$$\frac{\Delta P}{\Delta z} = \left[(1-\alpha)\cdot\rho_f + \alpha\cdot\rho_g\right]\cdot g + F_{wf} \ldots + \left[\frac{W_f^{\,2}}{(1-\alpha)^2\cdot\rho_f\cdot A^2} - \frac{W_g^{\,2}}{\alpha^2\cdot\rho_g\cdot A^2}\right]\cdot\frac{\Delta\alpha}{\Delta z} + \frac{W_g^{\,2}}{\alpha\cdot\rho_g^{\,2}\cdot A^2}\cdot\frac{\Delta\rho_g}{\Delta z} \tag{A40}$$

Next, we look at the Conservation of Linear Momentum for the Liquid Phase, Equation A27:

$$F_{int} = (1-\alpha)\cdot\left(\rho_f\cdot g - \frac{\Delta P}{\Delta z}\right) + F_{wf} + \rho_f\cdot V_f^{\,2}\cdot\frac{\Delta\alpha}{\Delta z} \tag{A27}$$

$$F_{int} = (1-\alpha)\cdot\left(\rho_f\cdot g - \frac{\Delta P}{\Delta z}\right) + F_{wf} + \rho_f\cdot\left[\frac{W_f}{(1-\alpha)\cdot\rho_f\cdot A}\right]^2\cdot\frac{\Delta\alpha}{\Delta z}$$

$$F_{int} = (1-\alpha)\cdot\left(\rho_f\cdot g - \frac{\Delta P}{\Delta z}\right) + F_{wf} + \frac{W_f^{\,2}}{(1-\alpha)^2\cdot\rho_f\cdot A^2}\cdot\frac{\Delta\alpha}{\Delta z} \tag{A41}$$

Now, the Conservation of Linear Momentum for the Vapor Phase, Equation A29:

$$F_{int} = \alpha\cdot\left(\frac{\Delta P}{\Delta z} - \rho_g\cdot g\right) - \alpha\cdot V_g^{\,2}\cdot\frac{\Delta\rho_g}{\Delta z} + \rho_g\cdot V_g^{\,2}\cdot\frac{\Delta\alpha}{\Delta z} \tag{A29}$$

$$F_{int} = \alpha\cdot\left(\frac{\Delta P}{\Delta z} - \rho_g\cdot g\right) - \alpha\cdot\left(\frac{W_g}{\alpha\cdot\rho_g\cdot A}\right)^2\cdot\frac{\Delta\rho_g}{\Delta z} + \rho_g\cdot\left(\frac{W_g}{\alpha\cdot\rho_g\cdot A}\right)^2\cdot\frac{\Delta\alpha}{\Delta z}$$

$$F_{int} = \alpha\cdot\left(\frac{\Delta P}{\Delta z} - \rho_g\cdot g\right) - \frac{W_g^{\,2}}{\alpha\cdot\rho_g^{\,2}\cdot A^2}\cdot\frac{\Delta\rho_g}{\Delta z} + \frac{W_g^{\,2}}{\alpha^2\cdot\rho_g\cdot A^2}\cdot\frac{\Delta\alpha}{\Delta z} \tag{A42}$$

For the combined interphase friction force equation, Equation A32, we find:

$$F_{int} = \frac{\left[(1-\alpha)\cdot\left(\rho_f\cdot g - \frac{\Delta P}{\Delta z}\right) + F_{wf}\right]\cdot\left(\rho_g\cdot V_g^{\,2}\right) \ldots + \left[\alpha\cdot V_g^{\,2}\cdot\frac{\Delta\rho_g}{\Delta z} - \alpha\cdot\left(\frac{\Delta P}{\Delta z} - \rho_g\cdot g\right)\right]\cdot\left(\rho_f\cdot V_f^{\,2}\right)}{\rho_g\cdot V_g^{\,2} - \rho_f\cdot V_f^{\,2}} \tag{A32}$$

$$F_{int} = \frac{\left[(1-\alpha)\cdot\left(\rho_f\cdot g - \frac{\Delta P}{\Delta z}\right) + F_{wf}\right]\cdot\left[\rho_g\cdot\left(\frac{W_g}{\alpha\cdot\rho_g\cdot A}\right)^2\right] \ldots}{+\left[\alpha\cdot\left(\frac{W_g}{\alpha\cdot\rho_g\cdot A}\right)^2\cdot\frac{\Delta\rho_g}{\Delta z} - \alpha\cdot\left(\frac{\Delta P}{\Delta z} - \rho_g\cdot g\right)\right]\cdot\left[\rho_f\cdot\left[\frac{W_f}{(1-\alpha)\cdot\rho_f\cdot A}\right]^2\right]}$$
$$\rho_g\cdot\left(\frac{W_g}{\alpha\cdot\rho_g\cdot A}\right)^2 - \rho_f\cdot\left[\frac{W_f}{(1-\alpha)\cdot\rho_f\cdot A}\right]^2$$

The combined interphase friction force equation becomes:

$$F_{int} = \frac{\left[(1-\alpha)\cdot\left(\rho_f\cdot g - \frac{\Delta P}{\Delta z}\right) + F_{wf}\right]\cdot\left(\frac{W_g^{\,2}}{\alpha^2\cdot\rho_g\cdot A^2}\right) \ldots}{+\left[\frac{W_g^{\,2}}{\alpha\cdot\rho_g^{\,2}\cdot A^2}\cdot\frac{\Delta\rho_g}{\Delta z} - \alpha\cdot\left(\frac{\Delta P}{\Delta z} - \rho_g\cdot g\right)\right]\cdot\frac{W_f^{\,2}}{(1-\alpha)^2\cdot\rho_f\cdot A^2}}$$
$$\frac{W_g^{\,2}}{\alpha^2\cdot\rho_g\cdot A^2} - \frac{W_f^{\,2}}{(1-\alpha)^2\cdot\rho_f\cdot A^2} \qquad \text{(A43)}$$

Next, we will solve for the void fraction, α, starting with Equation A33:

$$\alpha = \frac{F_{int}\cdot\left(\rho_g\cdot V_g^{\,2} - \rho_f\cdot V_f^{\,2}\right) - \left(\rho_f\cdot g - \frac{\Delta P}{\Delta z} + F_{wf}\right)\cdot\left(\rho_g\cdot V_g^{\,2}\right)}{\left(V_g^{\,2}\cdot\frac{\Delta\rho_g}{\Delta z} - \frac{\Delta P}{\Delta z} + \rho_g\cdot g\right)\cdot\left(\rho_f\cdot V_f^{\,2}\right) - \left(\rho_f\cdot g - \frac{\Delta P}{\Delta z}\right)\cdot\left(\rho_g\cdot V_g^{\,2}\right)} \qquad \text{(A33)}$$

Substituting Equations A36 and A37 into Equation A33, we find:

$$\alpha = \frac{F_{int}\cdot\left[\rho_g\cdot\left(\frac{W_g}{\alpha\cdot\rho_g\cdot A}\right)^2 - \rho_f\cdot\left[\frac{W_f}{(1-\alpha)\cdot\rho_f\cdot A}\right]^2\right] - \left(\rho_f\cdot g - \frac{\Delta P}{\Delta z} + F_{wf}\right)\cdot\left[\rho_g\cdot\left(\frac{W_g}{\alpha\cdot\rho_g\cdot A}\right)^2\right]}{\left[\left(\frac{W_g}{\alpha\cdot\rho_g\cdot A}\right)^2\cdot\frac{\Delta\rho_g}{\Delta z} - \frac{\Delta P}{\Delta z} + \rho_g\cdot g\right]\cdot\left[\rho_f\cdot\left[\frac{W_f}{(1-\alpha)\cdot\rho_f\cdot A}\right]^2\right] - \left(\rho_f\cdot g - \frac{\Delta P}{\Delta z}\right)\cdot\left[\rho_g\cdot\left(\frac{W_g}{\alpha\cdot\rho_g\cdot A}\right)^2\right]}$$

If we distribute the square powers, we get:

$$\alpha = \frac{F_{int}\cdot\left[\rho_g\cdot\frac{W_g^{\,2}}{\alpha^2\cdot\rho_g^{\,2}\cdot A^2} - \rho_f\cdot\frac{W_f^{\,2}}{(1-\alpha)^2\cdot\rho_f^{\,2}\cdot A^2}\right] - \left(\rho_f\cdot g - \frac{\Delta P}{\Delta z} + F_{wf}\right)\cdot\left(\rho_g\cdot\frac{W_g^{\,2}}{\alpha^2\cdot\rho_g^{\,2}\cdot A^2}\right)}{\left(\frac{W_g^{\,2}}{\alpha^2\cdot\rho_g^{\,2}\cdot A^2}\cdot\frac{\Delta\rho_g}{\Delta z} - \frac{\Delta P}{\Delta z} + \rho_g\cdot g\right)\cdot\left[\rho_f\cdot\frac{W_f^{\,2}}{(1-\alpha)^2\cdot\rho_f^{\,2}\cdot A^2}\right] - \left(\rho_f\cdot g - \frac{\Delta P}{\Delta z}\right)\cdot\left(\rho_g\cdot\frac{W_g^{\,2}}{\alpha^2\cdot\rho_g^{\,2}\cdot A^2}\right)}$$

Cancelling out the densities, we get:

$$\alpha = \frac{F_{int}\cdot\left[\frac{W_g^{\,2}}{\alpha^2\cdot\rho_g\cdot A^2} - \frac{W_f^{\,2}}{(1-\alpha)^2\cdot\rho_f\cdot A^2}\right] - \left(\rho_f\cdot g - \frac{\Delta P}{\Delta z} + F_{wf}\right)\cdot\left(\frac{W_g^{\,2}}{\alpha^2\cdot\rho_g\cdot A^2}\right)}{\left(\frac{W_g^{\,2}}{\alpha^2\cdot\rho_g^{\,2}\cdot A^2}\cdot\frac{\Delta\rho_g}{\Delta z} - \frac{\Delta P}{\Delta z} + \rho_g\cdot g\right)\cdot\left[\frac{W_f^{\,2}}{(1-\alpha)^2\cdot\rho_f\cdot A^2}\right] - \left(\rho_f\cdot g - \frac{\Delta P}{\Delta z}\right)\cdot\left(\frac{W_g^{\,2}}{\alpha^2\cdot\rho_g\cdot A^2}\right)}$$

If we multiply the numerartor and denominator by $\alpha^2(1-\alpha)^2$, then we find that:

$$\alpha = \frac{F_{int}\cdot\left[\frac{W_g^{\,2}}{\alpha^2\cdot\rho_g\cdot A^2} - \frac{W_f^{\,2}}{(1-\alpha)^2\cdot\rho_f\cdot A^2}\right] - \left(\rho_f\cdot g - \frac{\Delta P}{\Delta z} + F_{wf}\right)\cdot\left(\frac{W_g^{\,2}}{\alpha^2\cdot\rho_g\cdot A^2}\right)}{\left(\frac{W_g^{\,2}}{\alpha^2\cdot\rho_g^{\,2}\cdot A^2}\cdot\frac{\Delta\rho_g}{\Delta z} - \frac{\Delta P}{\Delta z} + \rho_g\cdot g\right)\cdot\left[\frac{W_f^{\,2}}{(1-\alpha)^2\cdot\rho_f\cdot A^2}\right] - \left(\rho_f\cdot g - \frac{\Delta P}{\Delta z}\right)\cdot\left(\frac{W_g^{\,2}}{\alpha^2\cdot\rho_g\cdot A^2}\right)}\cdot\frac{\alpha^2\cdot(1-\alpha)^2}{\alpha^2\cdot(1-\alpha)^2}$$

$$\alpha = \frac{F_{int}\cdot\left[\frac{(1-\alpha)^2\cdot W_g^{\,2}}{\rho_g\cdot A^2} - \frac{\alpha^2\cdot W_f^{\,2}}{\rho_f\cdot A^2}\right] - \left(\rho_f\cdot g - \frac{\Delta P}{\Delta z} + F_{wf}\right)\cdot\left[\frac{(1-\alpha)^2\cdot W_g^{\,2}}{\rho_g\cdot A^2}\right]}{\left[\frac{(1-\alpha)^2\cdot W_g^{\,2}}{\rho_g^{\,2}\cdot A^2}\cdot\frac{\Delta\rho_g}{\Delta z} - \frac{\Delta P}{\Delta z} + \rho_g\cdot g\right]\cdot\left(\frac{\alpha^2\cdot W_f^{\,2}}{\rho_f\cdot A^2}\right) - \left(\rho_f\cdot g - \frac{\Delta P}{\Delta z}\right)\cdot\left[\frac{(1-\alpha)^2\cdot W_g^{\,2}}{\rho_g\cdot A^2}\right]}$$

Next, we begin the process for solving for the void fraction, α, by distributing the polynomials:

$$\alpha = \frac{F_{int}\cdot\left[\frac{\left(\alpha^2 - 2\cdot\alpha + 1\right)\cdot W_g^{\,2}}{\rho_g\cdot A^2} - \frac{\alpha^2\cdot W_f^{\,2}}{\rho_f\cdot A^2}\right] - \left(\rho_f\cdot g - \frac{\Delta P}{\Delta z} + F_{wf}\right)\cdot\left[\frac{\left(\alpha^2 - 2\cdot\alpha + 1\right)\cdot W_g^{\,2}}{\rho_g\cdot A^2}\right]}{\left[\frac{\left(\alpha^2 - 2\cdot\alpha + 1\right)\cdot W_g^{\,2}}{\rho_g^{\,2}\cdot A^2}\cdot\frac{\Delta\rho_g}{\Delta z} - \frac{\Delta P}{\Delta z} + \rho_g\cdot g\right]\cdot\left(\frac{\alpha^2\cdot W_f^{\,2}}{\rho_f\cdot A^2}\right) - \left(\rho_f\cdot g - \frac{\Delta P}{\Delta z}\right)\cdot\left[\frac{\left(\alpha^2 - 2\cdot\alpha + 1\right)\cdot W_g^{\,2}}{\rho_g\cdot A^2}\right]}$$

$$\alpha = \frac{\begin{aligned} &F_{int}\cdot\left[\alpha^2\cdot\left(\frac{W_g^{\,2}}{\rho_g\cdot A^2}-\frac{W_f^{\,2}}{\rho_f\cdot A^2}\right)-2\cdot\alpha\cdot\frac{W_g^{\,2}}{\rho_g\cdot A^2}+\frac{W_g^{\,2}}{\rho_g\cdot A^2}\right]-\left(\rho_f\cdot g-\frac{\Delta P}{\Delta z}+F_{wf}\right)\cdot\left(\frac{W_g^{\,2}}{\rho_g\cdot A^2}\right)\cdot\alpha^2 \ldots \\ &+2\cdot\alpha\cdot\left(\rho_f\cdot g-\frac{\Delta P}{\Delta z}+F_{wf}\right)\cdot\left(\frac{W_g^{\,2}}{\rho_g\cdot A^2}\right)-\left(\rho_f\cdot g-\frac{\Delta P}{\Delta z}+F_{wf}\right)\cdot\left(\frac{W_g^{\,2}}{\rho_g\cdot A^2}\right) \end{aligned}}{\begin{aligned} &\frac{W_g^{\,2}\cdot W_f^{\,2}}{\rho_g^{\,2}\cdot\rho_f\cdot A^4}\cdot\frac{\Delta\rho_g}{\Delta z}\cdot\alpha^4-2\cdot\frac{W_g^{\,2}\cdot W_f^{\,2}}{\rho_g^{\,2}\cdot\rho_f\cdot A^4}\cdot\frac{\Delta\rho_g}{\Delta z}\alpha^3+\frac{W_g^{\,2}\cdot W_f^{\,2}}{\rho_g^{\,2}\cdot\rho_f\cdot A^4}\cdot\frac{\Delta\rho_g}{\Delta z}\cdot\alpha^2 \ldots \\ &+\left(\rho_g\cdot g-\frac{\Delta P}{\Delta z}\right)\cdot\frac{W_f^{\,2}}{\rho_f\cdot A^2}\cdot\alpha^2-\left(\rho_f\cdot g-\frac{\Delta P}{\Delta z}\right)\cdot\frac{W_g^{\,2}}{\rho_g\cdot A^2}\cdot\alpha^2 \ldots \\ &+2\cdot\left(\rho_f\cdot g-\frac{\Delta P}{\Delta z}\right)\cdot\frac{W_g^{\,2}}{\rho_g\cdot A^2}\cdot\alpha-\left(\rho_f\cdot g-\frac{\Delta P}{\Delta z}\right)\cdot\frac{W_g^{\,2}}{\rho_g\cdot A^2} \end{aligned}}$$

Combining the like terms we find:

$$\alpha = \frac{\begin{aligned} &\left[F_{int}\cdot\left(\frac{W_g^{\,2}}{\rho_g\cdot A^2}-\frac{W_f^{\,2}}{\rho_f\cdot A^2}\right)-\left(\rho_f\cdot g-\frac{\Delta P}{\Delta z}+F_{wf}\right)\cdot\left(\frac{W_g^{\,2}}{\rho_g\cdot A^2}\right)\right]\cdot\alpha^2 \ldots \\ &+2\left[\left(\rho_f\cdot g-\frac{\Delta P}{\Delta z}+Fwf\right)\cdot\left(\frac{W_g^{\,2}}{\rho_g\cdot A^2}\right)-\frac{W_g^{\,2}}{\rho_g\cdot A^2}\right]\cdot\alpha \ldots \\ &+\frac{F_{int}\cdot W_g^{\,2}}{\rho_g\cdot A^2}-\left(\rho_f\cdot g-\frac{\Delta P}{\Delta z}+F_{wf}\right)\cdot\left(\frac{W_g^{\,2}}{\rho_g\cdot A^2}\right) \end{aligned}}{\begin{aligned} &\frac{W_g^{\,2}\cdot W_f^{\,2}}{\rho_g^{\,2}\cdot\rho_f\cdot A^4}\cdot\frac{\Delta\rho_g}{\Delta z}\cdot\alpha^4-2\cdot\frac{W_g^{\,2}\cdot W_f^{\,2}}{\rho_g^{\,2}\cdot\rho_f\cdot A^4}\cdot\frac{\Delta\rho_g}{\Delta z}\alpha^3 \ldots \\ &+\left[\frac{W_g^{\,2}\cdot W_f^{\,2}}{\rho_g^{\,2}\cdot\rho_f\cdot A^4}\cdot\frac{\Delta\rho_g}{\Delta z}+\left(\rho_g\cdot g-\frac{\Delta P}{\Delta z}\right)\cdot\frac{W_f^{\,2}}{\rho_f\cdot A^2}-\left(\rho_f\cdot g-\frac{\Delta P}{\Delta z}\right)\cdot\frac{W_g^{\,2}}{\rho_g\cdot A^2}\right]\cdot\alpha^2 \ldots \\ &+2\cdot\left(\rho_f\cdot g-\frac{\Delta P}{\Delta z}\right)\cdot\frac{W_g^{\,2}}{\rho_g\cdot A^2}\cdot\alpha-\left(\rho_f\cdot g-\frac{\Delta P}{\Delta z}\right)\cdot\frac{W_g^{\,2}}{\rho_g\cdot A^2} \end{aligned}}$$

Now, the denominator of the right side of the equation is multiplied to both sides of the equation:

$$\frac{W_g^{\,2}\cdot W_f^{\,2}}{\rho_g^{\,2}\cdot\rho_f\cdot A^4}\cdot\frac{\Delta\rho_g}{\Delta z}\cdot\alpha^5 - 2\cdot\frac{W_g^{\,2}\cdot W_f^{\,2}}{\rho_g^{\,2}\cdot\rho_f\cdot A^4}\cdot\frac{\Delta\rho_g}{\Delta z}\alpha^4 \ldots = \left[\begin{array}{l} F_{int}\cdot\left(\frac{W_g^{\,2}}{\rho_g\cdot A^2} - \frac{W_f^{\,2}}{\rho_f\cdot A^2}\right)\ldots \\ +\left(\frac{\Delta P}{\Delta z} - F_{wf} - \rho_f\cdot g\right)\cdot\left(\frac{W_g^{\,2}}{\rho_g\cdot A^2}\right) \end{array}\right]\cdot\alpha^2 \ldots$$

$$+\left[\begin{array}{l} \frac{W_g^{\,2}\cdot W_f^{\,2}}{\rho_g^{\,2}\cdot\rho_f\cdot A^4}\cdot\frac{\Delta\rho_g}{\Delta z}\ldots \\ +\left(\rho_g\cdot g - \frac{\Delta P}{\Delta z}\right)\cdot\frac{W_f^{\,2}}{\rho_f\cdot A^2}\ldots \\ +\left(\frac{\Delta P}{\Delta z} - \rho_f\cdot g\right)\cdot\frac{W_g^{\,2}}{\rho_g\cdot A^2} \end{array}\right]\cdot\alpha^3 \ldots + 2\left[\left(\rho_f\cdot g - \frac{\Delta P}{\Delta z} + Fwf\right)\cdot\left(\frac{W_g^{\,2}}{\rho_g\cdot A^2}\right) - \frac{W_g^{\,2}}{\rho_g\cdot A^2}\right]\cdot\alpha \ldots$$

$$+2\cdot\left(\rho_f\cdot g - \frac{\Delta P}{\Delta z}\right)\cdot\frac{W_g^{\,2}}{\rho_g\cdot A^2}\cdot\alpha^2 \ldots + \frac{F_{int}\cdot W_g^{\,2}}{\rho_g\cdot A^2} - \left(\rho_f\cdot g - \frac{\Delta P}{\Delta z} + F_{wf}\right)\cdot\left(\frac{W_g^{\,2}}{\rho_g\cdot A^2}\right)$$

$$+\left(\frac{\Delta P}{\Delta z} - \rho_f\cdot g\right)\cdot\frac{W_g^{\,2}}{\rho_g\cdot A^2}\cdot\alpha$$

Moving all terms to the left side of the equation, we get a quintic equation for the void fraction, α:

$$\frac{W_g^{\,2}\cdot W_f^{\,2}}{\rho_g^{\,2}\cdot\rho_f\cdot A^4}\cdot\frac{\Delta\rho_g}{\Delta z}\cdot\alpha^5 - 2\cdot\frac{W_g^{\,2}\cdot W_f^{\,2}}{\rho_g^{\,2}\cdot\rho_f\cdot A^4}\cdot\frac{\Delta\rho_g}{\Delta z}\alpha^4 \ldots = 0 \qquad \text{(A44)}$$

$$+\left[\frac{W_g^{\,2}\cdot W_f^{\,2}}{\rho_g^{\,2}\cdot\rho_f\cdot A^4}\cdot\frac{\Delta\rho_g}{\Delta z} + \left(\rho_g\cdot g - \frac{\Delta P}{\Delta z}\right)\cdot\frac{W_f^{\,2}}{\rho_f\cdot A^2} + \left(\frac{\Delta P}{\Delta z} - \rho_f\cdot g\right)\cdot\frac{W_g^{\,2}}{\rho_g\cdot A^2}\right]\cdot\alpha^3 \ldots$$

$$+\left[\begin{array}{l} 2\cdot\left(\rho_f\cdot g - \frac{\Delta P}{\Delta z}\right)\cdot\frac{W_g^{\,2}}{\rho_g\cdot A^2} - F_{int}\cdot\left(\frac{W_g^{\,2}}{\rho_g\cdot A^2} - \frac{W_f^{\,2}}{\rho_f\cdot A^2}\right)\ldots \\ +\left(F_{wf} + \rho_f\cdot g - \frac{\Delta P}{\Delta z}\right)\cdot\left(\frac{W_g^{\,2}}{\rho_g\cdot A^2}\right) \end{array}\right]\cdot\alpha^2 \ldots$$

$$+\left[\left(\frac{\Delta P}{\Delta z} - \rho_f\cdot g\right)\cdot\frac{W_g^{\,2}}{\rho_g\cdot A^2} - 2\left[\left(\rho_f\cdot g - \frac{\Delta P}{\Delta z} + Fwf\right)\cdot\left(\frac{W_g^{\,2}}{\rho_g\cdot A^2}\right) - \frac{W_g^{\,2}}{\rho_g\cdot A^2}\right]\right]\cdot\alpha \ldots$$

$$+\left(\rho_f\cdot g - \frac{\Delta P}{\Delta z} + F_{wf}\right)\cdot\left(\frac{W_g^{\,2}}{\rho_g\cdot A^2}\right) - \frac{F_{int}\cdot W_g^{\,2}}{\rho_g\cdot A^2}$$

The quintic equation for the void fraction that is given in Equation A44 can be also be described as:

$$A\cdot\alpha^5 + B\cdot\alpha^4 + C\cdot\alpha^3 + D\cdot\alpha^2 + E\cdot\alpha + F = 0 \tag{A45A}$$

where

$$A = \frac{W_g^{\,2}\cdot W_f^{\,2}}{\rho_g^{\,2}\cdot\rho_f\cdot A^4}\cdot\frac{\Delta\rho_g}{\Delta z} \tag{A45B}$$

$$B = -2\cdot\frac{W_g^{\,2}\cdot W_f^{\,2}}{\rho_g^{\,2}\cdot\rho_f\cdot A^4}\cdot\frac{\Delta\rho_g}{\Delta z} \tag{A45C}$$

$$C = \frac{W_g^{\,2}\cdot W_f^{\,2}}{\rho_g^{\,2}\cdot\rho_f\cdot A^4}\cdot\frac{\Delta\rho_g}{\Delta z} + \left(\rho_g\cdot g - \frac{\Delta P}{\Delta z}\right)\cdot\frac{W_f^{\,2}}{\rho_f\cdot A^2} + \left(\frac{\Delta P}{\Delta z} - \rho_f\cdot g\right)\cdot\frac{W_g^{\,2}}{\rho_g\cdot A^2} \tag{A45D}$$

$$D = 2\cdot\left(\rho_f\cdot g - \frac{\Delta P}{\Delta z}\right)\cdot\frac{W_g^{\,2}}{\rho_g\cdot A^2} - F_{int}\cdot\left(\frac{W_g^{\,2}}{\rho_g\cdot A^2} - \frac{W_f^{\,2}}{\rho_f\cdot A^2}\right) + \left(F_{wf} + \rho_f\cdot g - \frac{\Delta P}{\Delta z}\right)\cdot\left(\frac{W_g^{\,2}}{\rho_g\cdot A^2}\right) \tag{A45E}$$

$$E = \left(\frac{\Delta P}{\Delta z} - \rho_f\cdot g\right)\cdot\frac{W_g^{\,2}}{\rho_g\cdot A^2} - 2\left[\left(\rho_f\cdot g - \frac{\Delta P}{\Delta z} + Fwf\right)\cdot\left(\frac{W_g^{\,2}}{\rho_g\cdot A^2}\right) - \frac{W_g^{\,2}}{\rho_g\cdot A^2}\right] \tag{A45F}$$

$$F = \left(\rho_f\cdot g - \frac{\Delta P}{\Delta z} + F_{wf}\right)\cdot\left(\frac{W_g^{\,2}}{\rho_g\cdot A^2}\right) - \frac{F_{int}\cdot W_g^{\,2}}{\rho_g\cdot A^2} \tag{A45G}$$

There is no explicit solution for a general quintic equation, like there is for quadratic, cubic and quartic equations. Instead, in order to determine the void fraction, a solution scheme such as Newton-Raphson will need to be employed to discover for which void fraction does Equation A45A-G reach 0.

Finally, we take a look at the void fraction gradient equation:

$$\frac{\Delta\alpha}{\Delta z} = \frac{\frac{\Delta P_A}{\Delta z} - \alpha\cdot V_g^{\,2}\cdot\frac{\Delta\rho_g}{\Delta z}}{\rho_f\cdot V_f^{\,2} - \rho_g\cdot V_g^{\,2}} \tag{A35}$$

$$\frac{\Delta\alpha}{\Delta z} = \frac{\frac{\Delta P_A}{\Delta z} - \alpha\cdot\left(\frac{W_g}{\alpha\cdot\rho_g\cdot A}\right)^2\cdot\frac{\Delta\rho_g}{\Delta z}}{\rho_f\cdot\left[\frac{W_f}{(1-\alpha)\cdot\rho_f\cdot A}\right]^2 - \rho_g\cdot\left(\frac{W_g}{\alpha\cdot\rho_g\cdot A}\right)^2}$$

The void fraction gradient equation becomes:

$$\frac{\Delta\alpha}{\Delta z} = \frac{\frac{\Delta P_A}{\Delta z} - \frac{W_g^{\,2}}{\alpha\cdot\rho_g^{\,2}\cdot A^2}\cdot\frac{\Delta\rho_g}{\Delta z}}{\frac{W_f^{\,2}}{(1-\alpha)^2\cdot\rho_f\cdot A^2} - \frac{W_g^{\,2}}{\alpha^2\cdot\rho_g\cdot A^2}} \tag{A46}$$

One final approximation that can be made to further breakdown the momentum, interphase friction and void fraction gradient equations is the application of the ideal gas law. Specifically, we start with:

$$\rho_g = \frac{P}{R_g\cdot T} \tag{A47}$$

where R_g is the ideal gas constant for a particular gas.

Since R_g and T are considered constants for the control volume, we can derive that:

$$\Delta\rho_g = \frac{\Delta P}{R_g\cdot T} \tag{A48}$$

Now we can substitute Equations A47 and A48 into Equations A41, A42, A43 and A46. The Conservation of Linear Momentum for the Liquid Phase remains unchanged because it does not include a term for the density or change in density of the vapor. Beginning with the Overall Conservation of Linear Momentum Equation, we find:

$$\frac{\Delta P}{\Delta z} = \left[(1-\alpha)\cdot\rho_f + \alpha\cdot\rho_g\right]\cdot g + F_{wf}\ \ldots + \left[\frac{W_f^{\,2}}{(1-\alpha)^2\cdot\rho_f\cdot A^2} - \frac{W_g^{\,2}}{\alpha^2\cdot\rho_g\cdot A^2}\right]\cdot\frac{\Delta\alpha}{\Delta z} + \frac{W_g^{\,2}}{\alpha\cdot\rho_g^{\,2}\cdot A^2}\cdot\frac{\Delta\rho_g}{\Delta z} \tag{A40}$$

$$\frac{\Delta P}{\Delta z} = \left[(1-\alpha)\cdot\rho_f + \alpha\cdot\frac{P}{R_g\cdot T}\right]\cdot g + F_{wf}\ \ldots + \left[\frac{W_f^{\,2}}{(1-\alpha)^2\cdot\rho_f\cdot A^2} - \frac{W_g^{\,2}}{\alpha^2\cdot\frac{P}{R_g\cdot T}\cdot A^2}\right]\cdot\frac{\Delta\alpha}{\Delta z} + \frac{W_g^{\,2}}{\alpha\cdot\left(\frac{P}{R_g\cdot T}\right)^2\cdot A^2}\cdot\frac{\frac{\Delta P}{R_g\cdot T}}{\Delta z}$$

$$\frac{\Delta P}{\Delta z} = \left[(1-\alpha)\cdot\rho_f + \frac{\alpha\cdot P}{R_g\cdot T}\right]\cdot g + F_{wf}\ \ldots + \left[\frac{W_f^{\,2}}{(1-\alpha)^2\cdot\rho_f\cdot A^2} - \frac{W_g^{\,2}\cdot R_g\cdot T}{\alpha^2\cdot P\cdot A^2}\right]\cdot\frac{\Delta\alpha}{\Delta z} + \frac{W_g^{\,2}\cdot R_g^{\,2}\cdot T^2}{\alpha\cdot P^2\cdot A^2\cdot R_g\cdot T}\cdot\frac{\Delta P}{\Delta z}$$

$$\left(1 - \frac{W_g^{\,2}\cdot R_g\cdot T}{\alpha\cdot P^2\cdot A^2}\right)\cdot\frac{\Delta P}{\Delta z} = \left[(1-\alpha)\cdot\rho_f + \frac{\alpha\cdot P}{R_g\cdot T}\right]\cdot g + F_{wf} \ldots + \left[\frac{W_f^{\,2}}{(1-\alpha)^2\cdot\rho_f\cdot A^2} - \frac{W_g^{\,2}\cdot R_g\cdot T}{\alpha^2\cdot P\cdot A^2}\right]\cdot\frac{\Delta\alpha}{\Delta z}$$

Thus, for an ideal gas, the Overall Conservation of Linear Momentum Equation is:

$$\frac{\Delta P}{\Delta z} = \frac{\left[(1-\alpha)\cdot\rho_f + \frac{\alpha\cdot P}{R_g\cdot T}\right]\cdot g + F_{wf} + \left[\frac{W_f^{\,2}}{(1-\alpha)^2\cdot\rho_f\cdot A^2} - \frac{W_g^{\,2}\cdot R_g\cdot T}{\alpha^2\cdot P\cdot A^2}\right]\cdot\frac{\Delta\alpha}{\Delta z}}{\left(1 - \frac{W_g^{\,2}\cdot R_g\cdot T}{\alpha\cdot P^2\cdot A^2}\right)} \tag{A49}$$

Next, we will substitute Equations A47 and A48 into the Conservation of Linear Momentum Equation for the Vapor Phase, Equation A42:

$$F_{int} = \alpha\cdot\left(\frac{\Delta P}{\Delta z} - \rho_g\cdot g\right) - \frac{W_g^{\,2}}{\alpha\cdot\rho_g^{\,2}\cdot A^2}\cdot\frac{\Delta\rho_g}{\Delta z} + \frac{W_g^{\,2}}{\alpha^2\cdot\rho_g\cdot A^2}\cdot\frac{\Delta\alpha}{\Delta z} \tag{A42}$$

$$F_{int} = \alpha\cdot\left(\frac{\Delta P}{\Delta z} - \frac{P}{R_g\cdot T}\cdot g\right) - \frac{W_g^{\,2}}{\alpha\cdot\left(\frac{P}{R_g\cdot T}\right)^2\cdot A^2}\cdot\frac{\frac{\Delta P}{R_g\cdot T}}{\Delta z} + \frac{W_g^{\,2}}{\alpha^2\cdot\frac{P}{R_g\cdot T}\cdot A^2}\cdot\frac{\Delta\alpha}{\Delta z}$$

Now, we cancel out the like terms:

$$F_{int} = \alpha\cdot\left(\frac{\Delta P}{\Delta z} - \frac{P\cdot g}{R_g\cdot T}\right) - \frac{W_g^{\,2}\cdot R_g^{\,2}\cdot T^2}{\alpha\cdot P^2\cdot A^2\cdot R_g\cdot T}\cdot\frac{\Delta P}{\Delta z} + \frac{W_g^{\,2}\cdot R_g\cdot T}{\alpha^2\cdot P\cdot A^2}\cdot\frac{\Delta\alpha}{\Delta z}$$

This results in the Conservation of Linear Momentum for the Vapor Phase Approximated as an Ideal Gas:

$$F_{int} = \alpha\cdot\left(\frac{\Delta P}{\Delta z} + \frac{P\cdot g}{R_g\cdot T}\right) - \frac{W_g^{\,2}\cdot R_g\cdot T}{\alpha\cdot P^2\cdot A^2}\cdot\frac{\Delta P}{\Delta z} + \frac{W_g^{\,2}\cdot R_g\cdot T}{\alpha^2\cdot P\cdot A^2}\cdot\frac{\Delta\alpha}{\Delta z} \tag{A50}$$

Next, we will substitute Equations A47 and A48 into the Interphase Friction Force Equation, Equation A43:

$$F_{int} = \frac{\left[(1-\alpha)\cdot\left(\rho_f\cdot g - \frac{\Delta P}{\Delta z}\right) + F_{wf}\right]\cdot\left(\frac{W_g{}^2}{\alpha^2\cdot\rho_g\cdot A^2}\right) \ldots + -\left[\frac{W_g{}^2}{\alpha\cdot\rho_g{}^2\cdot A^2}\cdot\frac{\Delta\rho_g}{\Delta z} - \alpha\cdot\left(\frac{\Delta P}{\Delta z} - \rho_g\cdot g\right)\right]\cdot\frac{W_f{}^2}{(1-\alpha)^2\cdot\rho_f\cdot A^2}}{\frac{W_g{}^2}{\alpha^2\cdot\rho_g\cdot A^2} - \frac{W_f{}^2}{(1-\alpha)^2\cdot\rho_f\cdot A^2}} \qquad \text{(A43)}$$

$$F_{int} = \frac{\left[(1-\alpha)\cdot\left(\rho_f\cdot g - \frac{\Delta P}{\Delta z}\right) + F_{wf}\right]\cdot\left(\frac{W_g{}^2}{\alpha^2\cdot\frac{P}{R_g\cdot T}\cdot A^2}\right) \ldots + -\left[\frac{W_g{}^2}{\alpha\cdot\left(\frac{P}{R_g\cdot T}\right)^2\cdot A^2}\cdot\frac{\frac{\Delta P}{R_g\cdot T}}{\Delta z} - \alpha\cdot\left(\frac{\Delta P}{\Delta z} - \frac{P}{R_g\cdot T}\cdot g\right)\right]\cdot\frac{W_f{}^2}{(1-\alpha)^2\cdot\rho_f\cdot A^2}}{\frac{W_g{}^2}{\alpha^2\cdot\frac{P}{R_g\cdot T}\cdot A^2} - \frac{W_f{}^2}{(1-\alpha)^2\cdot\rho_f\cdot A^2}}$$

Cancelling out like terms, we find:

$$F_{int} = \frac{\left[(1-\alpha)\cdot\left(\rho_f\cdot g - \frac{\Delta P}{\Delta z}\right) + F_{wf}\right]\cdot\left(\frac{W_g{}^2\cdot R_g\cdot T}{\alpha^2\cdot P\cdot A^2}\right) \ldots + -\left[\frac{W_g{}^2\cdot R_g{}^2\cdot T^2}{\alpha\cdot P^2\cdot A^2\cdot R_g\cdot T}\cdot\frac{\Delta P}{\Delta z} - \alpha\cdot\left(\frac{\Delta P}{\Delta z} - \frac{P}{R_g\cdot T}\cdot g\right)\right]\cdot\frac{W_f{}^2}{(1-\alpha)^2\cdot\rho_f\cdot A^2}}{\frac{W_g{}^2\cdot R_g\cdot T}{\alpha^2\cdot P\cdot A^2} - \frac{W_f{}^2}{(1-\alpha)^2\cdot\rho_f\cdot A^2}}$$

$$F_{int} = \frac{\left[(1-\alpha)\cdot\left(\rho_f\cdot g - \frac{\Delta P}{\Delta z}\right) + F_{wf}\right]\cdot\left(\frac{W_g{}^2\cdot R_g\cdot T}{\alpha^2\cdot P\cdot A^2}\right) \ldots + -\left[\frac{W_g{}^2\cdot R_g\cdot T}{\alpha\cdot P^2\cdot A^2}\cdot\frac{\Delta P}{\Delta z} - \alpha\cdot\left(\frac{\Delta P}{\Delta z} - \frac{P}{R_g\cdot T}\cdot g\right)\right]\cdot\frac{W_f{}^2}{(1-\alpha)^2\cdot\rho_f\cdot A^2}}{\frac{W_g{}^2\cdot R_g\cdot T}{\alpha^2\cdot P\cdot A^2} - \frac{W_f{}^2}{(1-\alpha)^2\cdot\rho_f\cdot A^2}} \tag{A51}$$

Finally, we will substitute Equations A47 and A48 into The Void Fraction Gradient Equation, Equation A46:

$$\frac{\Delta\alpha}{\Delta z} = \frac{\frac{\Delta P_A}{\Delta z} - \frac{W_g{}^2}{\alpha\cdot\rho_g{}^2\cdot A^2}\cdot\frac{\Delta\rho_g}{\Delta z}}{\frac{W_f{}^2}{(1-\alpha)^2\cdot\rho_f\cdot A^2} - \frac{W_g{}^2}{\alpha^2\cdot\rho_g\cdot A^2}} \tag{A46}$$

$$\frac{\Delta\alpha}{\Delta z} = \frac{\frac{\Delta P_A}{\Delta z} - \frac{W_g{}^2}{\alpha\cdot\left(\frac{P}{R_g\cdot T}\right)^2\cdot A^2}\cdot\frac{\frac{\Delta P}{R_g\cdot T}}{\Delta z}}{\frac{W_f{}^2}{(1-\alpha)^2\cdot\rho_f\cdot A^2} - \frac{W_g{}^2}{\alpha^2\cdot\frac{P}{R_g\cdot T}\cdot A^2}}$$

Cancelling out like terms, we find:

$$\frac{\Delta\alpha}{\Delta z} = \frac{\frac{\Delta P_A}{\Delta z} - \frac{W_g{}^2\cdot R_g{}^2\cdot T^2}{\alpha\cdot P^2\cdot A^2\cdot R_g\cdot T}\cdot\frac{\Delta P}{\Delta z}}{\frac{W_f{}^2}{(1-\alpha)^2\cdot\rho_f\cdot A^2} - \frac{W_g{}^2\cdot R_g\cdot T}{\alpha^2\cdot P\cdot A^2}}$$

$$\frac{\Delta\alpha}{\Delta z} = \frac{\frac{\Delta P_A}{\Delta z} - \frac{W_g{}^2\cdot R_g\cdot T}{\alpha\cdot P^2\cdot A^2}\cdot\frac{\Delta P}{\Delta z}}{\frac{W_f{}^2}{(1-\alpha)^2\cdot\rho_f\cdot A^2} - \frac{W_g{}^2\cdot R_g\cdot T}{\alpha^2\cdot P\cdot A^2}} \tag{A52}$$

As part of this study, it is important to determine the sensitivities of the derived equations to the variables that make up these equations. This is done to understand the uncertainty that comes with these equations. We are especially concerned with how each variable impacts the interphase friction. We begin with Equation A32:

$$F_{int} = \frac{\left[(1-\alpha)\cdot\left(\rho_f\cdot g - \frac{\Delta P}{\Delta z}\right) + F_{wf}\right]\cdot\left(\rho_g\cdot V_g^{\,2}\right) \ldots + \left[\alpha\cdot V_g^{\,2}\cdot\frac{\Delta\rho_g}{\Delta z} - \alpha\cdot\left(\frac{\Delta P}{\Delta z} - \rho_g\cdot g\right)\right]\cdot\left(\rho_f\cdot V_f^{\,2}\right)}{\rho_g\cdot V_g^{\,2} - \rho_f\cdot V_f^{\,2}} \tag{A32}$$

If we rewrite the pressure gradient, $\Delta P/\Delta z$, as PG and the vapor density gradient, $\Delta\rho_g/\Delta z$ as ρgG, then we can write the interphase friction equation as a function of several variables.

$$f_{int}(\alpha, \rho_f, PG, F_{wf}, \rho_g, V_g, \rho gG, V_f) := \frac{\left[(1-\alpha)\cdot\left(\rho_f\cdot g - PG\right) + F_{wf}\right]\cdot\left(\rho_g\cdot V_g^{\,2}\right) \ldots + \left[\alpha\cdot V_g^{\,2}\cdot\rho gG - \alpha\cdot\left(PG - \rho_g\cdot g\right)\right]\cdot\left(\rho_f\cdot V_f^{\,2}\right)}{\rho_g\cdot V_g^{\,2} - \rho_f\cdot V_f^{\,2}} \tag{A53}$$

And so we can find the sensitivity of each variable of the function f_{int} by taking the derivative of the function with respect to each variable.

The Sensitivity of the Interphase Friction Force to the Void Fraction

$$\frac{\Delta F_{int}}{\Delta\alpha} = -\frac{V_g^{\,2}\cdot\rho_g\cdot\left(\frac{\Delta P}{\Delta z} - g\cdot\rho_f\right) - V_f^{\,2}\cdot\rho_f\cdot\left(\frac{\Delta\rho_g}{\Delta z}\cdot V_g^{\,2} - \frac{\Delta P}{\Delta z} + g\cdot\rho_g\right)}{V_f^{\,2}\cdot\rho_f - V_g^{\,2}\cdot\rho_g} \tag{A54}$$

The Sensitivity of the Interphase Friction Force to the Liquid Density

$$\frac{\Delta F_{int}}{\Delta\rho_f} = \frac{V_f^{\,2}\cdot\left[V_g^{\,2}\cdot\rho_g\cdot\left[F_{wf} + (\alpha-1)\cdot\left(\frac{\Delta P}{\Delta z} - g\cdot\rho_f\right)\right] \ldots + V_f^{\,2}\cdot\rho_f\cdot\left[\alpha\cdot\left(\frac{\Delta P}{\Delta z} - g\cdot\rho_g\right) - V_g^{\,2}\cdot\alpha\cdot\frac{\Delta\rho_g}{\Delta z}\right]\right]}{\left(V_f^{\,2}\cdot\rho_f - V_g^{\,2}\cdot\rho_g\right)^2} \ldots + -\frac{V_f^{\,2}\cdot\left[\alpha\cdot\left(\frac{\Delta P}{\Delta z} - g\cdot\rho_g\right) - V_g^{\,2}\cdot\alpha\cdot\frac{\Delta\rho_g}{\Delta z}\right] - V_g^{\,2}\cdot g\cdot\rho_g\cdot(\alpha-1)}{V_f^{\,2}\cdot\rho_f - V_g^{\,2}\cdot\rho_g} \tag{A55}$$

The Sensitivity of the Interphase Friction Force to the Pressure Gradient

$$\frac{\Delta F_{int}}{\Delta\left(\frac{\Delta P}{\Delta z}\right)} = -\frac{\alpha\cdot\rho_f\cdot V_f^{\,2} + \rho_g\cdot(\alpha-1)\cdot V_g^{\,2}}{V_f^{\,2}\cdot\rho_f - V_g^{\,2}\cdot\rho_g} \tag{A56}$$

The Sensitivity of the Interphase Friction Force to the Wall Friction

$$\frac{\Delta F_{int}}{\Delta F_{wf}} = -\frac{V_g^{\,2}\cdot\rho_g}{V_f^{\,2}\cdot\rho_f - V_g^{\,2}\cdot\rho_g} \tag{A57}$$

The Sensitivity of the Interphase Friction Force to the Vapor Density

$$\frac{\Delta F_{int}}{\Delta\rho_g} = -\frac{V_g^{\,2}\cdot\left[F_{wf} + (\alpha-1)\cdot\left(\frac{\Delta P}{\Delta z} - g\cdot\rho_f\right)\right] - V_f^{\,2}\cdot\alpha\cdot g\cdot\rho_f}{V_f^{\,2}\cdot\rho_f - V_g^{\,2}\cdot\rho_g} \ldots + -\frac{V_g^{\,2}\cdot\left[\begin{array}{l} V_g^{\,2}\cdot\rho_g\cdot\left[F_{wf} + (\alpha-1)\cdot\left(\frac{\Delta P}{\Delta z} - g\cdot\rho_f\right)\right] \ldots \\ + V_f^{\,2}\cdot\rho_f\cdot\left[\alpha\cdot\left(\frac{\Delta P}{\Delta z} - g\cdot\rho_g\right) - V_g^{\,2}\cdot\alpha\cdot\frac{\Delta\rho_g}{\Delta z}\right] \end{array}\right]}{\left(V_f^{\,2}\cdot\rho_f - V_g^{\,2}\cdot\rho_g\right)^2} \tag{A58}$$

The Sensitivity of the Interphase Friction Force to the Vapor Velocity

$$\frac{\Delta F_{int}}{\Delta V_g} = -\frac{2\cdot V_g\cdot\rho_g\cdot\left[F_{wf} + (\alpha-1)\cdot\left(\frac{\Delta P}{\Delta z} - g\cdot\rho_f\right)\right] - 2\cdot V_f^{\,2}\cdot V_g\cdot\alpha\cdot\frac{\Delta\rho_g}{\Delta z}\cdot\rho_f}{V_f^{\,2}\cdot\rho_f - V_g^{\,2}\cdot\rho_g} \ldots + -\frac{2\cdot V_g\cdot\rho_g\cdot\left[\begin{array}{l} V_g^{\,2}\cdot\rho_g\cdot\left[F_{wf} + (\alpha-1)\cdot\left(\frac{\Delta P}{\Delta z} - g\cdot\rho_f\right)\right] \ldots \\ + V_f^{\,2}\cdot\rho_f\cdot\left[\alpha\cdot\left(\frac{\Delta P}{\Delta z} - g\cdot\rho_g\right) - V_g^{\,2}\cdot\alpha\cdot\frac{\Delta\rho_g}{\Delta z}\right] \end{array}\right]}{\left(V_f^{\,2}\cdot\rho_f - V_g^{\,2}\cdot\rho_g\right)^2} \tag{A59}$$

The Sensitivity of the Interphase Friction Force to the Vapor Density Gradient

$$\frac{\Delta F_{int}}{\Delta\left(\frac{\Delta\rho_g}{\Delta z}\right)} = \frac{V_f^{\,2}\cdot V_g^{\,2}\cdot\alpha\cdot\rho_f}{V_f^{\,2}\cdot\rho_f - V_g^{\,2}\cdot\rho_g} \tag{A60}$$

The Sensitivity of the Interphase Friction Force to the Liquid Velocity

$$\frac{\Delta F_{int}}{\Delta V_f} = \frac{2\cdot V_f\cdot\rho_f\cdot\left[\begin{array}{l} V_g{}^2\cdot\rho_g\cdot\left[F_{wf} + (\alpha - 1)\cdot\left(\frac{\Delta P}{\Delta z} - g\cdot\rho_f\right)\right] \ldots \\ + V_f{}^2\cdot\rho_f\cdot\left[\alpha\cdot\left(\frac{\Delta P}{\Delta z} - g\cdot\rho_g\right) - V_g{}^2\cdot\alpha\cdot\frac{\Delta\rho_g}{\Delta z}\right]\end{array}\right]}{\left(V_f{}^2\cdot\rho_f - V_g{}^2\cdot\rho_g\right)^2} \ldots + -\frac{2\cdot V_f\cdot\rho_f\cdot\left[\alpha\cdot\left(\frac{\Delta P}{\Delta z} - g\cdot\rho_g\right) - V_g{}^2\cdot\alpha\cdot\frac{\Delta\rho_g}{\Delta z}\right]}{V_f{}^2\cdot\rho_f - V_g{}^2\cdot\rho_g} \quad \text{(A61)}$$

These equations help tell us how sensitive the interphase friction equation is to the parameter against which the derivative is taken. For this study, there is particular importance placed on the sensitivity to wall friction (Equation A57) because it is a value that cannot be measured, but must be derived from a correlation. All other variables are either measured or directly calculated from measured qualities.

However, it may be more useful to derive the sensitivities of interphase friction to from variables that can just be measured. In that event, we should look at Equation A50, and derive the sensitivities for each variable.

$$F_{int} = \frac{\left[(1-\alpha)\cdot\left(\rho_f\cdot g - \frac{\Delta P}{\Delta z}\right) + F_{wf}\right]\cdot\left(\frac{W_g{}^2\cdot R_g\cdot T}{\alpha^2\cdot P\cdot A^2}\right) \ldots + -\left[\frac{W_g{}^2\cdot R_g\cdot T}{\alpha\cdot P^2\cdot A^2}\cdot\frac{\Delta P}{\Delta z} - \alpha\cdot\left(\frac{\Delta P}{\Delta z} - \frac{P}{R_g\cdot T}\cdot g\right)\right]\cdot\frac{W_f{}^2}{(1-\alpha)^2\cdot\rho_f\cdot A^2}}{\frac{W_g{}^2\cdot R_g\cdot T}{\alpha^2\cdot P\cdot A^2} - \frac{W_f{}^2}{(1-\alpha)^2\cdot\rho_f\cdot A^2}} \quad \text{(A51)}$$

Let us substitute $A = \pi D^2/4$ into Equation A51, so that we may solve for the sensitivity to the pipe diameter, which is more logical to measure and use to calculate the area.

$$F_{int} = \frac{\left[(1-\alpha)\cdot\left(\rho_f\cdot g - \frac{\Delta P}{\Delta z}\right) + F_{wf}\right]\cdot\left(\frac{16W_g{}^2\cdot R_g\cdot T}{\alpha^2\cdot P\cdot\pi^2\cdot D^4}\right) \ldots + -\left[\frac{16\cdot W_g{}^2\cdot R_g\cdot T}{\alpha\cdot P^2\cdot\pi^2\cdot D^4}\cdot\frac{\Delta P}{\Delta z} - \alpha\cdot\left(\frac{\Delta P}{\Delta z} - \frac{P}{R_g\cdot T}\cdot g\right)\right]\cdot\frac{16\cdot W_f{}^2}{(1-\alpha)^2\cdot\rho_f\cdot\pi^2\cdot}}{\frac{16\cdot W_g{}^2\cdot R_g\cdot T}{\alpha^2\cdot P\cdot\pi^2\cdot D^4} - \frac{16\cdot W_f{}^2}{(1-\alpha)^2\cdot\rho_f\cdot\pi^2\cdot D^4}} \quad \text{(A62)}$$

The Sensitivity of the Interphase Friction Force to the Void Fraction

$$\frac{\Delta F_{int}}{\Delta\alpha} = -\frac{\dfrac{16\cdot W_f^{\,2}\cdot\left(\dfrac{\Delta P}{\Delta z} - \dfrac{P\cdot g}{R_g\cdot T_g} + \dfrac{16\cdot\dfrac{\Delta P}{\Delta z}\cdot R_g\cdot T_g\cdot W_g^{\,2}}{\pi^2\cdot D^4\cdot P^2\cdot\alpha^2}\right)}{\pi^2\cdot D^4\cdot\rho_f\cdot(\alpha-1)^2} \ldots + \dfrac{32\cdot W_f^{\,2}\cdot\left[\alpha\cdot\left(\dfrac{\Delta P}{\Delta z} - \dfrac{P\cdot g}{R_g\cdot T_g}\right) - \dfrac{16\cdot\dfrac{\Delta P}{\Delta z}\cdot R_g\cdot T_g\cdot W_g^{\,2}}{\pi^2\cdot D^4\cdot P^2\cdot\alpha}\right]}{\pi^2\cdot D^4\cdot\rho_f\cdot(\alpha-1)^3} \ldots + \dfrac{32\cdot R_g\cdot T_g\cdot W_g^{\,2}\cdot\left[F_{wf} + (\alpha-1)\cdot\left(\dfrac{\Delta P}{\Delta z} - g\cdot\rho_f\right)\right]}{\pi^2\cdot D^4\cdot P\cdot\alpha^3} \ldots + \dfrac{16\cdot R_g\cdot T_g\cdot W_g^{\,2}\cdot\left(\dfrac{\Delta P}{\Delta z} - g\cdot\rho_f\right)}{\pi^2\cdot D^4\cdot P\cdot\alpha^2}}{\dfrac{16\cdot W_f^{\,2}}{\pi^2\cdot D^4\cdot\rho_f\cdot(\alpha-1)^2} - \dfrac{16\cdot R_g\cdot T_g\cdot W_g^{\,2}}{\pi^2\cdot D^4\cdot P\cdot\alpha^2}} \ldots$$

$$+ -\frac{\left[\dfrac{16\cdot W_f^{\,2}\cdot\left[\alpha\cdot\left(\dfrac{\Delta P}{\Delta z} - \dfrac{P\cdot g}{R_g\cdot T_g}\right) \ldots + \left[+ -\dfrac{16\cdot\dfrac{\Delta P}{\Delta z}\cdot R_g\cdot T_g\cdot W_g^{\,2}}{\pi^2\cdot D^4\cdot P^2\cdot\alpha}\right]\right]}{\pi^2\cdot D^4\cdot\rho_f\cdot(\alpha-1)^2} \ldots + \dfrac{16\cdot R_g\cdot T_g\cdot W_g^{\,2}\cdot\left[F_{wf} + (\alpha-1)\cdot\left(\dfrac{\Delta P}{\Delta z} - g\cdot\rho_f\right)\right]}{\pi^2\cdot D^4\cdot P\cdot\alpha^2}\right]\cdot\left[\dfrac{32\cdot W_f^{\,2}}{\pi^2\cdot D^4\cdot\rho_f\cdot(\alpha-1)^3} + -\dfrac{32\cdot R_g\cdot T_g\cdot W_g^{\,2}}{\pi^2\cdot D^4\cdot P\cdot\alpha^3}\right]}{\left[\dfrac{16\cdot W_f^{\,2}}{\pi^2\cdot D^4\cdot\rho_f\cdot(\alpha-1)^2} - \dfrac{16\cdot R_g\cdot T_g\cdot W_g^{\,2}}{\pi^2\cdot D^4\cdot P\cdot\alpha^2}\right]^2} \qquad \text{(A63)}$$

The Sensitivity of the Interphase Friction Force to the Liquid Density

$$\frac{16\cdot W_f{}^2\cdot\left[\alpha\cdot\left(\frac{\Delta P}{\Delta z}-\frac{P\cdot g}{R_g\cdot T_g}\right)-\frac{16\cdot\frac{\Delta P}{\Delta z}\cdot R_g\cdot T_g\cdot W_g{}^2}{\pi^2\cdot D^4\cdot P^2\cdot\alpha}\right]}{\pi^2\cdot D^4\cdot\rho_f{}^2\cdot(\alpha-1)^2}\ \ldots$$

$$\frac{\Delta F_{int}}{\Delta\rho_f}=\frac{+\frac{16\cdot R_g\cdot T_g\cdot W_g{}^2\cdot g\cdot(\alpha-1)}{\pi^2\cdot D^4\cdot P\cdot\alpha^2}}{\frac{16\cdot W_f{}^2}{\pi^2\cdot D^4\cdot\rho_f\cdot(\alpha-1)^2}-\frac{16\cdot R_g\cdot T_g\cdot W_g{}^2}{\pi^2\cdot D^4\cdot P\cdot\alpha^2}}\ \ldots \tag{A64}$$

$$+\frac{16\cdot W_f{}^2\cdot\left[\frac{16\cdot W_f{}^2\cdot\left[\alpha\cdot\left(\frac{\Delta P}{\Delta z}-\frac{P\cdot g}{R_g\cdot T_g}\right)-\frac{16\cdot\frac{\Delta P}{\Delta z}\cdot R_g\cdot T_g\cdot W_g{}^2}{\pi^2\cdot D^4\cdot P^2\cdot\alpha}\right]}{\pi^2\cdot D^4\cdot\rho_f\cdot(\alpha-1)^2}+\frac{16\cdot R_g\cdot T_g\cdot W_g{}^2\cdot\left[F_{wf}+(\alpha-1)\cdot\left(\frac{\Delta P}{\Delta z}-g\cdot\rho_f\right)\right]}{\pi^2\cdot D^4\cdot P\cdot\alpha^2}\right]}{\pi^2\cdot D^4\cdot\rho_f{}^2\cdot(\alpha-1)^2\cdot\left[\frac{16\cdot W_f{}^2}{\pi^2\cdot D^4\cdot\rho_f\cdot(\alpha-1)^2}-\frac{16\cdot R_g\cdot T_g\cdot W_g{}^2}{\pi^2\cdot D^4\cdot P\cdot\alpha^2}\right]}$$

The Sensitivity of the Interphase Friction Force to the Pressure Gradient

$$\frac{\Delta F_{int}}{\Delta\left(\frac{\Delta P}{\Delta z}\right)}=-\frac{\frac{16\cdot W_f{}^2\cdot\left(\alpha-\frac{16\cdot R_g\cdot T_g\cdot W_g{}^2}{\pi^2\cdot D^4\cdot P^2\cdot\alpha}\right)}{\pi^2\cdot D^4\cdot\rho_f\cdot(\alpha-1)^2}+\frac{16\cdot R_g\cdot T_g\cdot W_g{}^2\cdot(\alpha}{\pi^2\cdot D^4\cdot P\cdot\alpha^2}}{\frac{16\cdot W_f{}^2}{\pi^2\cdot D^4\cdot\rho_f\cdot(\alpha-1)^2}-\frac{16\cdot R_g\cdot T_g\cdot W_g{}^2}{\pi^2\cdot D^4\cdot P\cdot\alpha^2}} \tag{A65}$$

The Sensitivity of the Interphase Friction Force to the Wall Friction

$$\frac{\Delta F_{int}}{\Delta F_{wf}}=-\frac{16\cdot R_g\cdot T_g\cdot W_g{}^2}{\pi^2\cdot D^4\cdot P\cdot\alpha^2\cdot\left[\frac{16\cdot W_f{}^2}{\pi^2\cdot D^4\cdot\rho_f\cdot(\alpha-1)^2}-\frac{16\cdot R_g\cdot T_g\cdot V}{\pi^2\cdot D^4\cdot P\cdot(}\right.} \tag{A66}$$

The Sensitivity of the Interphase Friction Force to the Vapor Mass Flow Rate

$$\frac{\Delta f_{intp}}{\Delta W_g} = -\frac{\dfrac{32\cdot R_g\cdot T_g\cdot W_g\cdot\left[F_{wf}+(\alpha-1)\cdot\left(\dfrac{\Delta P}{\Delta z}-g\cdot\rho_f\right)\right]}{\pi^2\cdot D^4\cdot P\cdot\alpha^2}\ \ldots}{\begin{aligned}&+\frac{512\cdot\dfrac{\Delta P}{\Delta z}\cdot R_g\cdot T_g\cdot W_f{}^2\cdot W_g}{\pi^4\cdot D^8\cdot P^2\cdot\alpha\cdot\rho_f\cdot(\alpha-1)^2}\\ &\frac{16\cdot W_f{}^2}{\pi^2\cdot D^4\cdot\rho_f\cdot(\alpha-1)^2}-\frac{16\cdot R_g\cdot T_g\cdot W_g{}^2}{\pi^2\cdot D^4\cdot P\cdot\alpha^2}\end{aligned}\ \ldots} \tag{A67}$$

$$+\frac{32\cdot R_g\cdot T_g\cdot W_g\cdot\left[\dfrac{16\cdot W_f{}^2\cdot\left[\alpha\cdot\left(\dfrac{\Delta P}{\Delta z}-\dfrac{P\cdot g}{R_g\cdot T_g}\right)-\dfrac{16\cdot\dfrac{\Delta P}{\Delta z}\cdot R_g\cdot T_g\cdot W_g{}^2}{\pi^2\cdot D^4\cdot P^2\cdot\alpha}\right]}{\pi^2\cdot D^4\cdot\rho_f\cdot(\alpha-1)^2}+\dfrac{16\cdot R_g\cdot T_g\cdot W_g{}^2\cdot\left[F_{wf}+(\alpha-1)\cdot\left(\dfrac{\Delta P}{\Delta z}-g\cdot\rho_f\right)\right]}{\pi^2\cdot D^4\cdot P\cdot\alpha^2}\right]}{\pi^2\cdot D^4\cdot P\cdot\alpha^2\cdot\left[\dfrac{16\cdot W_f{}^2}{\pi^2\cdot D^4\cdot\rho_f\cdot(\alpha-1)^2}-\dfrac{16\cdot R_g\cdot T_g\cdot W_g{}^2}{\pi^2\cdot D^4\cdot P\cdot\alpha^2}\right]^2}$$

The Sensitivity of the Interphase Friction Force to the Vapor Temperature

$$\frac{\Delta F_{int}}{\Delta T_g} = -\frac{\dfrac{16\cdot W_f{}^2\cdot\left(\dfrac{P\cdot\alpha\cdot g}{R_g\cdot T_g{}^2}-\dfrac{16\cdot\dfrac{\Delta P}{\Delta z}\cdot R_g\cdot W_g{}^2}{\pi^2\cdot D^4\cdot P^2\cdot\alpha}\right)}{\pi^2\cdot D^4\cdot\rho_f\cdot(\alpha-1)^2}+\dots}{\dfrac{16\cdot W_f{}^2}{\pi^2\cdot D^4\cdot\rho_f\cdot(\alpha-1)^2}-\dfrac{16\cdot R_g\cdot T_g\cdot W_g{}^2}{\pi^2\cdot D^4\cdot P\cdot\alpha^2}}+\dots \qquad \text{(A68)}$$

$$+\frac{16\cdot R_g\cdot W_g{}^2\cdot\left[F_{wf}+(\alpha-1)\cdot\left(\dfrac{\Delta P}{\Delta z}-g\cdot\rho_f\right)\right]}{\pi^2\cdot D^4\cdot P\cdot\alpha^2}$$

$$+-\frac{16\cdot R_g\cdot W_g{}^2\cdot\left[\dfrac{16\cdot W_f{}^2\cdot\left[\alpha\cdot\left(\dfrac{\Delta P}{\Delta z}-\dfrac{P\cdot g}{R_g\cdot T_g}\right)-\dfrac{16\cdot\dfrac{\Delta P}{\Delta z}\cdot R_g\cdot T_g\cdot W_g{}^2}{\pi^2\cdot D^4\cdot P^2\cdot\alpha}\right]}{\pi^2\cdot D^4\cdot\rho_f\cdot(\alpha-1)^2}+\dfrac{16\cdot R_g\cdot T_g\cdot W_g{}^2\cdot\left[F_{wf}+(\alpha-1)\cdot\left(\dfrac{\Delta P}{\Delta z}-g\cdot\rho_f\right)\right]}{\pi^2\cdot D^4\cdot P\cdot\alpha^2}\right]}{\pi^2\cdot D^4\cdot P\cdot\alpha^2\cdot\left[\dfrac{16\cdot W_f{}^2}{\pi^2\cdot D^4\cdot\rho_f\cdot(\alpha-1)^2}-\dfrac{16\cdot R_g\cdot T_g\cdot W_g{}^2}{\pi^2\cdot D^4\cdot P\cdot\alpha^2}\right]^2}$$

The Sensitivity of the Interphase Friction Force to the Pressure

$$\frac{\Delta F_{int}}{\Delta P} = \frac{\dfrac{16 \cdot W_f^{\,2} \cdot \left(\dfrac{\alpha \cdot g}{R_g \cdot T_g} - \dfrac{32 \cdot \dfrac{\Delta P}{\Delta z} \cdot R_g \cdot T_g \cdot W_g^{\,2}}{\pi^2 \cdot D^4 \cdot P^3 \cdot \alpha} \right)}{\pi^2 \cdot D^4 \cdot \rho_f \cdot (\alpha - 1)^2} \ldots + \dfrac{16 \cdot R_g \cdot T_g \cdot W_g^{\,2} \cdot \left[F_{wf} + (\alpha - 1) \cdot \left(\dfrac{\Delta P}{\Delta z} - g \cdot \rho_f \right) \right]}{\pi^2 \cdot D^4 \cdot P^2 \cdot \alpha^2}}{\dfrac{16 \cdot W_f^{\,2}}{\pi^2 \cdot D^4 \cdot \rho_f \cdot (\alpha - 1)^2} - \dfrac{16 \cdot R_g \cdot T_g \cdot W_g^{\,2}}{\pi^2 \cdot D^4 \cdot P \cdot \alpha^2}} \ldots + \frac{16 \cdot R_g \cdot T_g \cdot W_g^{\,2} \cdot \left[\dfrac{16 \cdot W_f^{\,2} \cdot \left[\alpha \cdot \left(\dfrac{\Delta P}{\Delta z} - \dfrac{P \cdot g}{R_g \cdot T_g} \right) - \dfrac{16 \cdot \dfrac{\Delta P}{\Delta z} \cdot R_g \cdot T_g \cdot W_g^{\,2}}{\pi^2 \cdot D^4 \cdot P^2 \cdot \alpha} \right]}{\pi^2 \cdot D^4 \cdot \rho_f \cdot (\alpha - 1)^2} + \dfrac{16 \cdot R_g \cdot T_g \cdot W_g^{\,2} \cdot \left[F_{wf} + (\alpha - 1) \cdot \left(\dfrac{\Delta P}{\Delta z} - g \cdot \rho_f \right) \right]}{\pi^2 \cdot D^4 \cdot P \cdot \alpha^2} \right]}{\pi^2 \cdot D^4 \cdot P^2 \cdot \alpha^2 \cdot \left[\dfrac{16 \cdot W_f^{\,2}}{\pi^2 \cdot D^4 \cdot \rho_f \cdot (\alpha - 1)^2} - \dfrac{16 \cdot R_g \cdot T_g \cdot W_g^{\,2}}{\pi^2 \cdot D^4 \cdot P \cdot \alpha^2} \right]^2} \qquad \text{(A69)}$$

The Sensitivity of the Interphase Friction Force to the Pipe Diameter

$$\frac{\Delta F_{int}}{\Delta D} = \frac{\dfrac{64\cdot W_f^{\,2}\cdot\left[\alpha\cdot\left(\dfrac{\Delta P}{\Delta z}-\dfrac{P\cdot g}{R_g\cdot T_g}\right)-\dfrac{16\cdot\dfrac{\Delta P}{\Delta z}\cdot R_g\cdot T_g\cdot W_g^{\,2}}{\pi^2\cdot D^4\cdot P^2\cdot\alpha}\right]}{\pi^2\cdot D^5\cdot\rho_f\cdot(\alpha-1)^2}\ \ldots}{\begin{array}{l}+\dfrac{64\cdot R_g\cdot T_g\cdot W_g^{\,2}\cdot\left[F_{wf}+(\alpha-1)\cdot\left(\dfrac{\Delta P}{\Delta z}-g\cdot\rho_f\right)\right]}{\pi^2\cdot D^5\cdot P\cdot\alpha^2}\ \ldots\\ +-\dfrac{1024\cdot\dfrac{\Delta P}{\Delta z}\cdot R_g\cdot T_g\cdot W_f^{\,2}\cdot W_g^{\,2}}{\pi^4\cdot D^9\cdot P^2\cdot\alpha\cdot\rho_f\cdot(\alpha-1)^2}\end{array}\ \ldots} \qquad \text{(A70)}$$

$$\frac{\dfrac{16\cdot W_f^{\,2}}{\pi^2\cdot D^4\cdot\rho_f\cdot(\alpha-1)^2}-\dfrac{16\cdot R_g\cdot T_g\cdot W_g^{\,2}}{\pi^2\cdot D^4\cdot P\cdot\alpha^2}}{+-\dfrac{\left[\begin{array}{l}16\cdot W_f^{\,2}\cdot\left[\alpha\cdot\left(\dfrac{\Delta P}{\Delta z}-\dfrac{P\cdot g}{R_g\cdot T_g}\right)\ldots\right.\\ \left.+-\dfrac{16\cdot\dfrac{\Delta P}{\Delta z}\cdot R_g\cdot T_g\cdot W_g^{\,2}}{\pi^2\cdot D^4\cdot P^2\cdot\alpha}\right]\end{array}}{\pi^2\cdot D^4\cdot\rho_f\cdot(\alpha-1)^2}\ \ldots}{+-\dfrac{\left[\begin{array}{l}\dfrac{16\cdot W_f^{\,2}\cdot\left[\alpha\cdot\left(\dfrac{\Delta P}{\Delta z}-\dfrac{P\cdot g}{R_g\cdot T_g}\right)\ldots\right.}{\pi^2\cdot D^4\cdot\rho_f\cdot(\alpha-1)^2}\ldots\\ \left.+-\dfrac{16\cdot\dfrac{\Delta P}{\Delta z}\cdot R_g\cdot T_g\cdot W_g^{\,2}}{\pi^2\cdot D^4\cdot P^2\cdot\alpha}\right]\\ +\dfrac{16\cdot R_g\cdot T_g\cdot W_g^{\,2}\cdot\left[F_{wf}+(\alpha-1)\cdot\left(\dfrac{\Delta P}{\Delta z}-g\cdot\rho_f\right)\right]}{\pi^2\cdot D^4\cdot P\cdot\alpha^2}\end{array}}{\left[\dfrac{16\cdot W_f^{\,2}}{\pi^2\cdot D^4\cdot\rho_f\cdot(\alpha-1)^2}-\dfrac{16\cdot R_g\cdot T_g\cdot W_g^{\,2}}{\pi^2\cdot D^4\cdot P\cdot\alpha^2}\right]^2}\cdot\left[\dfrac{64\cdot W_f^{\,2}}{\pi^2\cdot D^5\cdot\rho_f\cdot(\alpha-1)^2}+-\dfrac{64\cdot R_g\cdot T_g\cdot W_g^{\,2}}{\pi^2\cdot D^5\cdot P\cdot\alpha^2}\right]$$

The Sensitivity of the Interphase Friction Force to the Liquid Mass Flow Rate

$$\frac{\Delta F_{int}}{\Delta W_f} = \frac{32\cdot W_f\cdot\left[\frac{16\cdot W_f^{\,2}\cdot\left[\alpha\cdot\left(\frac{\Delta P}{\Delta z}-\frac{P\cdot g}{R_g\cdot T_g}\right)-\frac{16\cdot\frac{\Delta P}{\Delta z}\cdot R_g\cdot T_g\cdot W_g^{\,2}}{\pi^2\cdot D^4\cdot P^2\cdot\alpha}\right]}{\pi^2\cdot D^4\cdot\rho_f\cdot(\alpha-1)^2}+\frac{16\cdot R_g\cdot T_g\cdot W_g^{\,2}\cdot\left[F_{wf}+(\alpha-1)\cdot\left(\frac{\Delta P}{\Delta z}-g\cdot\rho_f\right)\right]}{\pi^2\cdot D^4\cdot P\cdot\alpha^2}\right]}{\pi^2\cdot D^4\cdot\rho_f\cdot(\alpha-1)^2\cdot\left[\frac{16\cdot W_f^{\,2}}{\pi^2\cdot D^4\cdot\rho_f\cdot(\alpha-1)^2}-\frac{16\cdot R_g\cdot T_g\cdot W_g^{\,2}}{\pi^2\cdot D^4\cdot P\cdot\alpha^2}\right]^2}+\frac{32\cdot W_f\cdot\left[\alpha\cdot\left(\frac{\Delta P}{\Delta z}-\frac{P\cdot g}{R_g\cdot T_g}\right)-\frac{16\cdot\frac{\Delta P}{\Delta z}\cdot R_g\cdot T_g\cdot W_g^{\,2}}{\pi^2\cdot D^4\cdot P^2\cdot\alpha}\right]}{\pi^2\cdot D^4\cdot\rho_f\cdot(\alpha-1)^2\cdot\left[\frac{16\cdot W_f^{\,2}}{\pi^2\cdot D^4\cdot\rho_f\cdot(\alpha-1)^2}-\frac{16\cdot R_g\cdot T_g\cdot W_g^{\,2}}{\pi^2\cdot D^4\cdot P\cdot\alpha^2}\right]} \qquad \text{(A71)}$$

Summary

The Conservation of Liquid Mass

$$\Delta V_f = \frac{-V_f \cdot \Delta\alpha}{(1-\alpha)} \tag{A8}$$

The Conservation of Vapor Mass

$$\Delta V_g = V_g \cdot \left(\frac{\Delta\alpha}{\alpha} - \frac{\Delta\rho_g}{\rho_g} \right) \tag{A11}$$

The Overall Conservation of Linear Momentum Equation

$$\frac{\Delta P}{\Delta z} = \left[(1-\alpha)\cdot\rho_f + \alpha\cdot\rho_g \right]\cdot g + F_{wf} + \left(\rho_f \cdot V_f^{\,2} - \rho_g \cdot V_g^{\,2} \right)\cdot\frac{\Delta\alpha}{\Delta z} + \alpha\cdot V_g^{\,2}\cdot\frac{\Delta\rho_g}{\Delta z} \tag{A20}$$

The Conservation of Linear Momentum for the Liquid Phase

$$F_{int} = (1-\alpha)\cdot\left(\rho_f \cdot g - \frac{\Delta P}{\Delta z} \right) + F_{wf} + \rho_f \cdot V_f^{\,2}\cdot\frac{\Delta\alpha}{\Delta z} \tag{A27}$$

The Conservation of Linear Momentum for the Vapor Phase

$$F_{int} = \alpha\cdot\left(\frac{\Delta P}{\Delta z} - \rho_g \cdot g \right) - \alpha\cdot V_g^{\,2}\cdot\frac{\Delta\rho_g}{\Delta z} + \rho_g \cdot V_g^{\,2}\cdot\frac{\Delta\alpha}{\Delta z} \tag{A29}$$

The Interphase Friction Force Equation

$$F_{int} = \frac{\begin{aligned}&\left[(1-\alpha)\cdot\left(\rho_f \cdot g - \frac{\Delta P}{\Delta z} \right) + F_{wf} \right]\cdot\left(\rho_g \cdot V_g^{\,2} \right) \ldots \\ &+ \left[\alpha\cdot V_g^{\,2}\cdot\frac{\Delta\rho_g}{\Delta z} - \alpha\cdot\left(\frac{\Delta P}{\Delta z} - \rho_g \cdot g \right) \right]\cdot\left(\rho_f \cdot V_f^{\,2} \right)\end{aligned}}{\rho_g \cdot V_g^{\,2} - \rho_f \cdot V_f^{\,2}} \tag{A32}$$

The Void Fraction Equation

$$\alpha = \frac{F_{int}\cdot\left(\rho_g \cdot V_g^{\,2} - \rho_f \cdot V_f^{\,2} \right) - \left(\rho_f \cdot g - \frac{\Delta P}{\Delta z} + F_{wf} \right)\cdot\left(\rho_g \cdot V_g^{\,2} \right)}{\left(V_g^{\,2}\cdot\frac{\Delta\rho_g}{\Delta z} - \frac{\Delta P}{\Delta z} + \rho_g \cdot g \right)\cdot\left(\rho_f \cdot V_f^{\,2} \right) + \left(\rho_f \cdot g - \frac{\Delta P}{\Delta z} \right)\cdot\left(\rho_g \cdot V_g^{\,2} \right)} \tag{A33}$$

The Void Fraction Gradient Equation

$$\frac{\Delta\alpha}{\Delta z} = \frac{\frac{\Delta P_A}{\Delta z} - \alpha\cdot V_g^{\,2}\cdot\frac{\Delta\rho_g}{\Delta z}}{\rho_f \cdot V_f^{\,2} - \rho_g \cdot V_g^{\,2}} \tag{A35}$$

The Overall Conservation of Linear Momentum Equation as a Function of Mass Flow Rate

$$\frac{\Delta P}{\Delta z} = \left[(1-\alpha)\cdot\rho_f + \alpha\cdot\rho_g\right]\cdot g + F_{wf} \ldots + \left[\frac{W_f^{\,2}}{(1-\alpha)^2\cdot\rho_f\cdot A^2} - \frac{W_g^{\,2}}{\alpha^2\cdot\rho_g\cdot A^2}\right]\cdot\frac{\Delta\alpha}{\Delta z} + \frac{W_g^{\,2}}{\alpha\cdot\rho_g^{\,2}\cdot A^2}\cdot\frac{\Delta\rho_g}{\Delta z} \tag{A40}$$

The Conservation of Linear Momentum for the Liquid Phase as a Function of Mass Flow Rate

$$F_{int} = (1-\alpha)\cdot\left(\rho_f\cdot g - \frac{\Delta P}{\Delta z}\right) + F_{wf} + \frac{W_f^{\,2}}{(1-\alpha)^2\cdot\rho_f\cdot A^2}\cdot\frac{\Delta\alpha}{\Delta z} \tag{A41}$$

The Conservation of Linear Momentum for the Vapor Phase as Function of Mass Flow Rate

$$F_{int} = \alpha\cdot\left(\frac{\Delta P}{\Delta z} - \rho_g\cdot g\right) - \frac{W_g^{\,2}}{\alpha\cdot\rho_g^{\,2}\cdot A^2}\cdot\frac{\Delta\rho_g}{\Delta z} + \frac{W_g^{\,2}}{\alpha^2\cdot\rho_g\cdot A^2}\cdot\frac{\Delta\alpha}{\Delta z} \tag{A42}$$

The Interphase Friction Force Equation as a Function of Mass Flow Rate

$$F_{int} = \frac{\left[(1-\alpha)\cdot\left(\rho_f\cdot g - \frac{\Delta P}{\Delta z}\right) + F_{wf}\right]\cdot\left(\frac{W_g^{\,2}}{\alpha^2\cdot\rho_g\cdot A^2}\right) \ldots + -\left[\frac{W_g^{\,2}}{\alpha\cdot\rho_g^{\,2}\cdot A^2}\cdot\frac{\Delta\rho_g}{\Delta z} - \alpha\cdot\left(\frac{\Delta P}{\Delta z} - \rho_g\cdot g\right)\right]\cdot\frac{W_f^{\,2}}{(1-\alpha)^2\cdot\rho_f\cdot A^2}}{\frac{W_g^{\,2}}{\alpha^2\cdot\rho_g\cdot A^2} - \frac{W_f^{\,2}}{(1-\alpha)^2\cdot\rho_f\cdot A^2}} \tag{A43}$$

The Void Fraction Equation

$$A\cdot\alpha^5 + B\cdot\alpha^4 + C\cdot\alpha^3 + D\cdot\alpha^2 + E\cdot\alpha + F = 0 \tag{A45A}$$

where

$$A = \frac{W_g^{\,2}\cdot W_f^{\,2}}{\rho_g^{\,2}\cdot\rho_f\cdot A^4}\cdot\frac{\Delta\rho_g}{\Delta z} \tag{A45B}$$

$$B = -2\cdot\frac{W_g^{\,2}\cdot W_f^{\,2}}{\rho_g^{\,2}\cdot\rho_f\cdot A^4}\cdot\frac{\Delta\rho_g}{\Delta z} \tag{A45C}$$

$$C = \frac{W_g^{\,2}\cdot W_f^{\,2}}{\rho_g^{\,2}\cdot\rho_f\cdot A^4}\cdot\frac{\Delta\rho_g}{\Delta z} + \left(\rho_g\cdot g - \frac{\Delta P}{\Delta z}\right)\cdot\frac{W_f^{\,2}}{\rho_f\cdot A^2} + \left(\frac{\Delta P}{\Delta z} - \rho_f\cdot g\right)\cdot\frac{W_g^{\,2}}{\rho_g\cdot A^2} \tag{A45D}$$

$$D = 2\cdot\left(\rho_f\cdot g - \frac{\Delta P}{\Delta z}\right)\cdot\frac{W_g^{\,2}}{\rho_g\cdot A^2} - F_{int}\cdot\left(\frac{W_g^{\,2}}{\rho_g\cdot A^2} - \frac{W_f^{\,2}}{\rho_f\cdot A^2}\right) + \left(F_{wf} + \rho_f\cdot g - \frac{\Delta P}{\Delta z}\right)\cdot\left(\frac{W_g^{\,2}}{\rho_g\cdot A^2}\right) \tag{A45E}$$

$$E = \left(\frac{\Delta P}{\Delta z} - \rho_f\cdot g\right)\cdot\frac{W_g^{\,2}}{\rho_g\cdot A^2} - 2\left[\left(\rho_f\cdot g - \frac{\Delta P}{\Delta z} + Fwf\right)\cdot\left(\frac{W_g^{\,2}}{\rho_g\cdot A^2}\right) - \frac{W_g^{\,2}}{\rho_g\cdot A^2}\right] \tag{A45F}$$

$$F = \left(\rho_f\cdot g - \frac{\Delta P}{\Delta z} + F_{wf}\right)\cdot\left(\frac{W_g^{\,2}}{\rho_g\cdot A^2}\right) - \frac{F_{int}\cdot W_g^{\,2}}{\rho_g\cdot A^2} \tag{A45G}$$

The Void Fraction Gradient Equation as a Function of Mass Flow Rate

$$\frac{\Delta\alpha}{\Delta z} = \frac{\dfrac{\Delta P_A}{\Delta z} - \dfrac{W_g^{\,2}}{\alpha\cdot\rho_g^{\,2}\cdot A^2}\cdot\dfrac{\Delta\rho_g}{\Delta z}}{\dfrac{W_f^{\,2}}{(1-\alpha)^2\cdot\rho_f\cdot A^2} - \dfrac{W_g^{\,2}}{\alpha^2\cdot\rho_g\cdot A^2}} \tag{A46}$$

The Conservation of Linear Momentum for the Liquid Phase as a Function of Mass Flow Rate with the Vapor Phase Approximated as an Ideal Gas

$$\frac{\Delta P}{\Delta z} = \frac{\left[(1-\alpha)\cdot\rho_f + \frac{\alpha\cdot P}{R_g\cdot T}\right]\cdot g + F_{wf} + \left[\frac{W_f{}^2}{(1-\alpha)^2\cdot\rho_f\cdot A^2} - \frac{W_g{}^2\cdot R_g\cdot T}{\alpha^2\cdot P\cdot A^2}\right]\cdot\frac{\Delta\alpha}{\Delta z}}{\left(1 - \frac{W_g{}^2\cdot R_g\cdot T}{\alpha\cdot P^2\cdot A^2}\right)} \tag{A48}$$

The Conservation of Linear Momentum for the Vapor Phase as Function of Mass Flow Rate with the Vapor Phase Approximated as an Ideal Gas

$$F_{int} = \alpha\cdot\left(\frac{\Delta P}{\Delta z} + \frac{P\cdot g}{R_g\cdot T}\right) - \frac{W_g{}^2\cdot R_g\cdot T}{\alpha\cdot P^2\cdot A^2}\cdot\frac{\Delta P}{\Delta z} + \frac{W_g{}^2\cdot R_g\cdot T}{\alpha^2\cdot P\cdot A^2}\cdot\frac{\Delta\alpha}{\Delta z} \tag{A50}$$

The Interphase Friction Force Equation as a Function of Mass Flow Rate with the Vapor Phase Approximated as an Ideal Gas

$$F_{int} = \frac{\left[(1-\alpha)\cdot\left(\rho_f\cdot g - \frac{\Delta P}{\Delta z}\right) + F_{wf}\right]\cdot\left(\frac{W_g{}^2\cdot R_g\cdot T}{\alpha^2\cdot P\cdot A^2}\right) \ldots + -\left[\frac{W_g{}^2\cdot R_g\cdot T}{\alpha\cdot P^2\cdot A^2}\cdot\frac{\Delta P}{\Delta z} - \alpha\cdot\left(\frac{\Delta P}{\Delta z} - \frac{P}{R_g\cdot T}\cdot g\right)\right]\cdot\frac{W_f{}^2}{(1-\alpha)^2\cdot\rho_f\cdot A^2}}{\frac{W_g{}^2\cdot R_g\cdot T}{\alpha^2\cdot P\cdot A^2} - \frac{W_f{}^2}{(1-\alpha)^2\cdot\rho_f\cdot A^2}} \tag{A51}$$

The Void Fraction Gradient Equation as a Function of Mass Flow Rate with the Vapor Phase Approximated as an Ideal Gas

$$\frac{\Delta\alpha}{\Delta z} = \frac{\frac{\Delta P_A}{\Delta z} - \frac{W_g{}^2\cdot R_g\cdot T}{\alpha\cdot P^2\cdot A^2}\cdot\frac{\Delta P}{\Delta z}}{\frac{W_f{}^2}{(1-\alpha)^2\cdot\rho_f\cdot A^2} - \frac{W_g{}^2\cdot R_g\cdot T}{\alpha^2\cdot P\cdot A^2}} \tag{A52}$$

Sensitivity of Interphase Friction to the Void Fraction

$$\frac{\Delta f_{int}}{\Delta\alpha} = -\frac{V_g{}^2\cdot\rho_g\cdot\left(\frac{\Delta P}{\Delta z} - g\cdot\rho_f\right) - V_f{}^2\cdot\rho_f\cdot\left(\frac{\Delta\rho_g}{\Delta z}\cdot V_g{}^2 - \frac{\Delta P}{\Delta z} + g\cdot\rho_g\right)}{V_f{}^2\cdot\rho_f - V_g{}^2\cdot\rho_g} \tag{A54}$$

Sensitivity of Interphase Friction to Liquid Density

$$\frac{\Delta f_{int}}{\Delta \rho_f} = \frac{V_f^2 \cdot \left[\begin{array}{l} V_g^2 \cdot \rho_g \cdot \left[F_{wf} + (\alpha - 1) \cdot \left(\frac{\Delta P}{\Delta z} - g \cdot \rho_f \right) \right] \ldots \\ + V_f^2 \cdot \rho_f \cdot \left[\alpha \cdot \left(\frac{\Delta P}{\Delta z} - g \cdot \rho_g \right) - V_g^2 \cdot \alpha \cdot \frac{\Delta \rho_g}{\Delta z} \right] \end{array} \right]}{\left(V_f^2 \cdot \rho_f - V_g^2 \cdot \rho_g \right)^2} \ldots + - \frac{V_f^2 \cdot \left[\alpha \cdot \left(\frac{\Delta P}{\Delta z} - g \cdot \rho_g \right) - V_g^2 \cdot \alpha \cdot \frac{\Delta \rho_g}{\Delta z} \right] - V_g^2 \cdot g \cdot \rho_g \cdot (\alpha - 1)}{V_f^2 \cdot \rho_f - V_g^2 \cdot \rho_g} \tag{A55}$$

Sensitivity of Interphase Friction to Pressure Gradient

$$\frac{\Delta f_{int}}{\Delta PGF} = - \frac{\alpha \cdot \rho_f \cdot V_f^2 + \rho_g \cdot (\alpha - 1) \cdot V_g^2}{V_f^2 \cdot \rho_f - V_g^2 \cdot \rho_g} \tag{A56}$$

Sensitivity of Interphase Friction to Wall Friction

$$\frac{\Delta f_{int}}{\Delta F_{wf}} = - \frac{V_g^2 \cdot \rho_g}{V_f^2 \cdot \rho_f - V_g^2 \cdot \rho_g} \tag{A57}$$

Sensitivity of Interphase Friction to Vapor Density

$$\frac{\Delta f_{int}}{\Delta \rho_g} = - \frac{V_g^2 \cdot \left[F_{wf} + (\alpha - 1) \cdot \left(\frac{\Delta P}{\Delta z} - g \cdot \rho_f \right) \right] - V_f^2 \cdot \alpha \cdot g \cdot \rho_f}{V_f^2 \cdot \rho_f - V_g^2 \cdot \rho_g} \ldots + - \frac{V_g^2 \cdot \left[\begin{array}{l} V_g^2 \cdot \rho_g \cdot \left[F_{wf} + (\alpha - 1) \cdot \left(\frac{\Delta P}{\Delta z} - g \cdot \rho_f \right) \right] \ldots \\ + V_f^2 \cdot \rho_f \cdot \left[\alpha \cdot \left(\frac{\Delta P}{\Delta z} - g \cdot \rho_g \right) - V_g^2 \cdot \alpha \cdot \frac{\Delta \rho_g}{\Delta z} \right] \end{array} \right]}{\left(V_f^2 \cdot \rho_f - V_g^2 \cdot \rho_g \right)^2} \tag{A58}$$

Sensitivity of Interphase Friction to Vapor Velocity

$$\frac{\Delta f_{int}}{\Delta V_g} = - \frac{2 \cdot V_g \cdot \rho_g \cdot \left[F_{wf} + (\alpha - 1) \cdot \left(\frac{\Delta P}{\Delta z} - g \cdot \rho_f \right) \right] - 2 \cdot V_f^2 \cdot V_g \cdot \alpha \cdot \frac{\Delta \rho_g}{\Delta z} \cdot \rho_f}{V_f^2 \cdot \rho_f - V_g^2 \cdot \rho_g} \ldots + - \frac{2 \cdot V_g \cdot \rho_g \cdot \left[\begin{array}{l} V_g^2 \cdot \rho_g \cdot \left[F_{wf} + (\alpha - 1) \cdot \left(\frac{\Delta P}{\Delta z} - g \cdot \rho_f \right) \right] \ldots \\ + V_f^2 \cdot \rho_f \cdot \left[\alpha \cdot \left(\frac{\Delta P}{\Delta z} - g \cdot \rho_g \right) - V_g^2 \cdot \alpha \cdot \frac{\Delta \rho_g}{\Delta z} \right] \end{array} \right]}{\left(V_f^2 \cdot \rho_f - V_g^2 \cdot \rho_g \right)^2} \tag{A59}$$

Sensitivity of Interphase Friction to Vapor Density Gradient

$$\frac{\Delta f_{int}}{\Delta\left(\frac{\Delta\rho_g}{\Delta z}\right)} = \frac{V_f^{\,2}\cdot V_g^{\,2}\cdot\alpha\cdot\rho_f}{V_f^{\,2}\cdot\rho_f - V_g^{\,2}\cdot\rho_g} \tag{A60}$$

Sensitivity of Interphase Friction to Liquid Velocity

$$\frac{\Delta f_{int}}{\Delta V_f} = \frac{\begin{matrix}2\cdot V_f\cdot\rho_f\cdot\left[V_g^{\,2}\cdot\rho_g\cdot\left[F_{wf} + (\alpha-1)\cdot\left(\frac{\Delta P}{\Delta z} - g\cdot\rho_f\right)\right]\ldots\right.\\ \left.+ V_f^{\,2}\cdot\rho_f\cdot\left[\alpha\cdot\left(\frac{\Delta P}{\Delta z} - g\cdot\rho_g\right) - V_g^{\,2}\cdot\alpha\cdot\frac{\Delta\rho_g}{\Delta z}\right]\right]}{\left(V_f^{\,2}\cdot\rho_f - V_g^{\,2}\cdot\rho_g\right)^2}\ldots \\ +-\frac{2\cdot V_f\cdot\rho_f\cdot\left[\alpha\cdot\left(\frac{\Delta P}{\Delta z} - g\cdot\rho_g\right) - V_g^{\,2}\cdot\alpha\cdot\frac{\Delta\rho_g}{\Delta z}\right]}{V_f^{\,2}\cdot\rho_f - V_g^{\,2}\cdot\rho_g} \end{matrix} \tag{A61}$$

Sensitivity of Interphase Friction to Void Fraction Expanded

$$\frac{\Delta f_{intp}}{\Delta \alpha} = -\frac{\dfrac{16\cdot W_f{}^2\cdot\left(\dfrac{\Delta P}{\Delta z} - \dfrac{P\cdot g}{R_g\cdot T_g} + \dfrac{16\cdot\dfrac{\Delta P}{\Delta z}\cdot R_g\cdot T_g\cdot W_g{}^2}{\pi^2\cdot D^4\cdot P^2\cdot\alpha^2}\right)}{\pi^2\cdot D^4\cdot\rho_f\cdot(\alpha-1)^2} \ldots + \dfrac{32\cdot W_f{}^2\cdot\left[\alpha\cdot\left(\dfrac{\Delta P}{\Delta z} - \dfrac{P\cdot g}{R_g\cdot T_g}\right) - \dfrac{16\cdot\dfrac{\Delta P}{\Delta z}\cdot R_g\cdot T_g\cdot W_g{}^2}{\pi^2\cdot D^4\cdot P^2\cdot\alpha}\right]}{\pi^2\cdot D^4\cdot\rho_f\cdot(\alpha-1)^3} \ldots + \dfrac{32\cdot R_g\cdot T_g\cdot W_g{}^2\cdot\left[F_{wf} + (\alpha-1)\cdot\left(\dfrac{\Delta P}{\Delta z} - g\cdot\rho_f\right)\right]}{\pi^2\cdot D^4\cdot P\cdot\alpha^3} \ldots + \dfrac{16\cdot R_g\cdot T_g\cdot W_g{}^2\cdot\left(\dfrac{\Delta P}{\Delta z} - g\cdot\rho_f\right)}{\pi^2\cdot D^4\cdot P\cdot\alpha^2}}{\dfrac{16\cdot W_f{}^2}{\pi^2\cdot D^4\cdot\rho_f\cdot(\alpha-1)^2} - \dfrac{16\cdot R_g\cdot T_g\cdot W_g{}^2}{\pi^2\cdot D^4\cdot P\cdot\alpha^2}} \ldots + \dfrac{\left[\dfrac{16\cdot W_f{}^2\cdot\left[\alpha\cdot\left(\dfrac{\Delta P}{\Delta z} - \dfrac{P\cdot g}{R_g\cdot T_g}\right) \ldots + \dfrac{16\cdot\dfrac{\Delta P}{\Delta z}\cdot R_g\cdot T_g\cdot W_g{}^2}{\pi^2\cdot D^4\cdot P^2\cdot\alpha}\right]}{\pi^2\cdot D^4\cdot\rho_f\cdot(\alpha-1)^2} \ldots + \dfrac{16\cdot R_g\cdot T_g\cdot W_g{}^2\cdot\left[F_{wf} + (\alpha-1)\cdot\left(\dfrac{\Delta P}{\Delta z} - g\cdot\rho_f\right)\right]}{\pi^2\cdot D^4\cdot P\cdot\alpha^2}\right]\cdot\left[\dfrac{32\cdot W_f{}^2}{\pi^2\cdot D^4\cdot\rho_f\cdot(\alpha-1)^3} \ldots + \dfrac{32\cdot R_g\cdot T_g\cdot W_g{}^2}{\pi^2\cdot D^4\cdot P\cdot\alpha^3}\right]}{\left[\dfrac{16\cdot W_f{}^2}{\pi^2\cdot D^4\cdot\rho_f\cdot(\alpha-1)^2} - \dfrac{16\cdot R_g\cdot T_g\cdot W_g{}^2}{\pi^2\cdot D^4\cdot P\cdot\alpha^2}\right]^2} \qquad \text{(A63)}$$

Sensitivity of Interphase Friction to Liquid Density Expanded

$$\frac{\Delta f_{intp}}{\Delta \rho_f} = \frac{\dfrac{16 \cdot W_f^{\,2} \cdot \left[\alpha \cdot \left(\dfrac{\Delta P}{\Delta z} - \dfrac{P \cdot g}{R_g \cdot T_g} \right) - \dfrac{16 \cdot \dfrac{\Delta P}{\Delta z} \cdot R_g \cdot T_g \cdot W_g^{\,2}}{\pi^2 \cdot D^4 \cdot P^2 \cdot \alpha} \right]}{\pi^2 \cdot D^4 \cdot \rho_f^{\,2} \cdot (\alpha - 1)^2} \ldots + \dfrac{16 \cdot R_g \cdot T_g \cdot W_g^{\,2} \cdot g \cdot (\alpha - 1)}{\pi^2 \cdot D^4 \cdot P \cdot \alpha^2}}{\dfrac{16 \cdot W_f^{\,2}}{\pi^2 \cdot D^4 \cdot \rho_f \cdot (\alpha - 1)^2} - \dfrac{16 \cdot R_g \cdot T_g \cdot W_g^{\,2}}{\pi^2 \cdot D^4 \cdot P \cdot \alpha^2}} \ldots + \frac{16 \cdot W_f^{\,2} \cdot \left[\dfrac{16 \cdot W_f^{\,2} \cdot \left[\alpha \cdot \left(\dfrac{\Delta P}{\Delta z} - \dfrac{P \cdot g}{R_g \cdot T_g} \right) - \dfrac{16 \cdot \dfrac{\Delta P}{\Delta z} \cdot R_g \cdot T_g \cdot W_g^{\,2}}{\pi^2 \cdot D^4 \cdot P^2 \cdot \alpha} \right]}{\pi^2 \cdot D^4 \cdot \rho_f \cdot (\alpha - 1)^2} \ldots + \dfrac{16 \cdot R_g \cdot T_g \cdot W_g^{\,2} \cdot \left[F_{wf} + (\alpha - 1) \cdot \left(\dfrac{\Delta P}{\Delta z} - g \cdot \rho_f \right) \right]}{\pi^2 \cdot D^4 \cdot P \cdot \alpha^2} \right]}{\pi^2 \cdot D^4 \cdot \rho_f^{\,2} \cdot (\alpha - 1)^2 \cdot \left[\dfrac{16 \cdot W_f^{\,2}}{\pi^2 \cdot D^4 \cdot \rho_f \cdot (\alpha - 1)^2} - \dfrac{16 \cdot R_g \cdot T_g \cdot W_g^{\,2}}{\pi^2 \cdot D^4 \cdot P \cdot \alpha^2} \right]^2} \tag{A64}$$

Sensitivity of Interphase Friction to Pressure Gradient Expanded

$$\frac{\Delta f_{intp}}{\Delta PGF} = -\frac{\dfrac{16 \cdot W_f^{\,2} \cdot \left(\alpha - \dfrac{16 \cdot R_g \cdot T_g \cdot W_g^{\,2}}{\pi^2 \cdot D^4 \cdot P^2 \cdot \alpha} \right)}{\pi^2 \cdot D^4 \cdot \rho_f \cdot (\alpha - 1)^2} + \dfrac{16 \cdot R_g \cdot T_g \cdot W_g^{\,2} \cdot (\alpha - 1)}{\pi^2 \cdot D^4 \cdot P \cdot \alpha^2}}{\dfrac{16 \cdot W_f^{\,2}}{\pi^2 \cdot D^4 \cdot \rho_f \cdot (\alpha - 1)^2} - \dfrac{16 \cdot R_g \cdot T_g \cdot W_g^{\,2}}{\pi^2 \cdot D^4 \cdot P \cdot \alpha^2}} \tag{A65}$$

Sensitivity of Interphase Friction to Wall Friction Expanded

$$\frac{\Delta f_{intp}}{\Delta F_{wf}} = -\frac{16 \cdot R_g \cdot T_g \cdot W_g^{\,2}}{\pi^2 \cdot D^4 \cdot P \cdot \alpha^2 \cdot \left[\dfrac{16 \cdot W_f^{\,2}}{\pi^2 \cdot D^4 \cdot \rho_f \cdot (\alpha - 1)^2} - \dfrac{16 \cdot R_g \cdot T_g \cdot W_g^{\,2}}{\pi^2 \cdot D^4 \cdot P \cdot \alpha^2} \right]} \tag{A66}$$

Sensitivity of Interphase Friction to Vapor Mass Flow Rate Expanded

$$\frac{\Delta f_{intp}}{\Delta W_g} = -\frac{\frac{32 \cdot R_g \cdot T_g \cdot W_g \cdot \left[F_{wf} + (\alpha - 1) \cdot \left(\frac{\Delta P}{\Delta z} - g \cdot \rho_f \right) \right]}{\pi^2 \cdot D^4 \cdot P \cdot \alpha^2} \ldots + -\frac{512 \cdot \frac{\Delta P}{\Delta z} \cdot R_g \cdot T_g \cdot W_f^{\,2} \cdot W_g}{\pi^4 \cdot D^8 \cdot P^2 \cdot \alpha \cdot \rho_f \cdot (\alpha - 1)^2}}{\frac{16 \cdot W_f^{\,2}}{\pi^2 \cdot D^4 \cdot \rho_f \cdot (\alpha - 1)^2} - \frac{16 \cdot R_g \cdot T_g \cdot W_g^{\,2}}{\pi^2 \cdot D^4 \cdot P \cdot \alpha^2}} \ldots + -\frac{32 \cdot R_g \cdot T_g \cdot W_g \cdot \left[\frac{16 \cdot W_f^{\,2} \cdot \left[\alpha \cdot \left(\frac{\Delta P}{\Delta z} - \frac{P \cdot g}{R_g \cdot T_g} \right) - \frac{16 \cdot \frac{\Delta P}{\Delta z} \cdot R_g \cdot T_g \cdot W_g^{\,2}}{\pi^2 \cdot D^4 \cdot P^2 \cdot \alpha} \right]}{\pi^2 \cdot D^4 \cdot \rho_f \cdot (\alpha - 1)^2} \ldots + \frac{16 \cdot R_g \cdot T_g \cdot W_g^{\,2} \cdot \left[F_{wf} + (\alpha - 1) \cdot \left(\frac{\Delta P}{\Delta z} - g \cdot \rho_f \right) \right]}{\pi^2 \cdot D^4 \cdot P \cdot \alpha^2} \right]}{\pi^2 \cdot D^4 \cdot P \cdot \alpha^2 \cdot \left[\frac{16 \cdot W_f^{\,2}}{\pi^2 \cdot D^4 \cdot \rho_f \cdot (\alpha - 1)^2} - \frac{16 \cdot R_g \cdot T_g \cdot W_g^{\,2}}{\pi^2 \cdot D^4 \cdot P \cdot \alpha^2} \right]^2} \quad \text{(A67)}$$

Sensitivity of Interphase Friction to Temperature Expanded

$$\frac{\Delta f_{intp}}{\Delta T_g} = -\frac{\dfrac{16\cdot W_f^{\,2}\cdot\left(\dfrac{P\cdot\alpha\cdot g}{R_g\cdot T_g^{\,2}} - \dfrac{16\cdot\dfrac{\Delta P}{\Delta z}\cdot R_g\cdot W_g^{\,2}}{\pi^2\cdot D^4\cdot P^2\cdot\alpha}\right)}{\pi^2\cdot D^4\cdot\rho_f\cdot(\alpha-1)^2} \ldots + \dfrac{16\cdot R_g\cdot W_g^{\,2}\cdot\left[F_{wf} + (\alpha-1)\cdot\left(\dfrac{\Delta P}{\Delta z} - g\cdot\rho_f\right)\right]}{\pi^2\cdot D^4\cdot P\cdot\alpha^2}}{\dfrac{16\cdot W_f^{\,2}}{\pi^2\cdot D^4\cdot\rho_f\cdot(\alpha-1)^2} - \dfrac{16\cdot R_g\cdot T_g\cdot W_g^{\,2}}{\pi^2\cdot D^4\cdot P\cdot\alpha^2}} \ldots + -\dfrac{16\cdot R_g\cdot W_g^{\,2}\cdot\left[\dfrac{16\cdot W_f^{\,2}\cdot\left[\alpha\cdot\left(\dfrac{\Delta P}{\Delta z} - \dfrac{P\cdot g}{R_g\cdot T_g}\right) - \dfrac{16\cdot\dfrac{\Delta P}{\Delta z}\cdot R_g\cdot T_g\cdot W_g^{\,2}}{\pi^2\cdot D^4\cdot P^2\cdot\alpha}\right]}{\pi^2\cdot D^4\cdot\rho_f\cdot(\alpha-1)^2} \ldots + \dfrac{16\cdot R_g\cdot T_g\cdot W_g^{\,2}\cdot\left[F_{wf} + (\alpha-1)\cdot\left(\dfrac{\Delta P}{\Delta z} - g\cdot\rho_f\right)\right]}{\pi^2\cdot D^4\cdot P\cdot\alpha^2}\right]}{\pi^2\cdot D^4\cdot P\cdot\alpha^2\cdot\left[\dfrac{16\cdot W_f^{\,2}}{\pi^2\cdot D^4\cdot\rho_f\cdot(\alpha-1)^2} - \dfrac{16\cdot R_g\cdot T_g\cdot W_g^{\,2}}{\pi^2\cdot D^4\cdot P\cdot\alpha^2}\right]^2} \quad \text{(A68)}$$

Sensitivity to Interphase Friction to Pressure Expanded

$$\frac{\Delta f_{intp}}{\Delta P} = \frac{\dfrac{16\cdot W_f{}^2\cdot\left(\dfrac{\alpha\cdot g}{R_g\cdot T_g} - \dfrac{32\cdot\dfrac{\Delta P}{\Delta z}\cdot R_g\cdot T_g\cdot W_g{}^2}{\pi^2\cdot D^4\cdot P^3\cdot\alpha}\right)}{\pi^2\cdot D^4\cdot\rho_f\cdot(\alpha-1)^2} \ldots + \dfrac{16\cdot R_g\cdot T_g\cdot W_g{}^2\cdot\left[F_{wf} + (\alpha-1)\cdot\left(\dfrac{\Delta P}{\Delta z} - g\cdot\rho_f\right)\right]}{\pi^2\cdot D^4\cdot P^2\cdot\alpha^2}}{\dfrac{16\cdot W_f{}^2}{\pi^2\cdot D^4\cdot\rho_f\cdot(\alpha-1)^2} - \dfrac{16\cdot R_g\cdot T_g\cdot W_g{}^2}{\pi^2\cdot D^4\cdot P\cdot\alpha^2}} \ldots + \dfrac{16\cdot R_g\cdot T_g\cdot W_g{}^2\cdot\left[\dfrac{16\cdot W_f{}^2\cdot\left[\alpha\cdot\left(\dfrac{\Delta P}{\Delta z} - \dfrac{P\cdot g}{R_g\cdot T_g}\right) - \dfrac{16\cdot\dfrac{\Delta P}{\Delta z}\cdot R_g\cdot T_g\cdot W_g{}^2}{\pi^2\cdot D^4\cdot P^2\cdot\alpha}\right]}{\pi^2\cdot D^4\cdot\rho_f\cdot(\alpha-1)^2} \ldots + \dfrac{16\cdot R_g\cdot T_g\cdot W_g{}^2\cdot\left[F_{wf} + (\alpha-1)\cdot\left(\dfrac{\Delta P}{\Delta z} - g\cdot\rho_f\right)\right]}{\pi^2\cdot D^4\cdot P\cdot\alpha^2}\right]}{\pi^2\cdot D^4\cdot P^2\cdot\alpha^2\cdot\left[\dfrac{16\cdot W_f{}^2}{\pi^2\cdot D^4\cdot\rho_f\cdot(\alpha-1)^2} - \dfrac{16\cdot R_g\cdot T_g\cdot W_g{}^2}{\pi^2\cdot D^4\cdot P\cdot\alpha^2}\right]^2} \quad \text{(A69)}$$

Sensitivity of Interphase Friction to Pipe Diameter Expanded

$$\frac{\Delta f_{intp}}{\Delta D} = \frac{\dfrac{64\cdot W_f^{\,2}\cdot\left[\alpha\cdot\left(\dfrac{\Delta P}{\Delta z}-\dfrac{P\cdot g}{R_g\cdot T_g}\right)-\dfrac{16\cdot\dfrac{\Delta P}{\Delta z}\cdot R_g\cdot T_g\cdot W_g^{\,2}}{\pi^2\cdot D^4\cdot P^2\cdot\alpha}\right]}{\pi^2\cdot D^5\cdot\rho_f\cdot(\alpha-1)^2}\ \ldots}{\dfrac{16\cdot W_f^{\,2}}{\pi^2\cdot D^4\cdot\rho_f\cdot(\alpha-1)^2}-\dfrac{16\cdot R_g\cdot T_g\cdot W_g^{\,2}}{\pi^2\cdot D^4\cdot P\cdot\alpha^2}}\ \ldots \tag{A70}$$

$$+\frac{64\cdot R_g\cdot T_g\cdot W_g^{\,2}\cdot\left[F_{wf}+(\alpha-1)\cdot\left(\dfrac{\Delta P}{\Delta z}-g\cdot\rho_f\right)\right]}{\pi^2\cdot D^5\cdot P\cdot\alpha^2}\ \ldots$$

$$+\frac{-\dfrac{1024\cdot\dfrac{\Delta P}{\Delta z}\cdot R_g\cdot T_g\cdot W_f^{\,2}\cdot W_g^{\,2}}{\pi^4\cdot D^9\cdot P^2\cdot\alpha\cdot\rho_f\cdot(\alpha-1)^2}}{\dfrac{16\cdot W_f^{\,2}}{\pi^2\cdot D^4\cdot\rho_f\cdot(\alpha-1)^2}-\dfrac{16\cdot R_g\cdot T_g\cdot W_g^{\,2}}{\pi^2\cdot D^4\cdot P\cdot\alpha^2}}\ \ldots$$

$$+\frac{\left[\dfrac{16\cdot W_f^{\,2}\cdot\left[\alpha\cdot\left(\dfrac{\Delta P}{\Delta z}-\dfrac{P\cdot g}{R_g\cdot T_g}\right)\ldots+\left[-\dfrac{16\cdot\dfrac{\Delta P}{\Delta z}\cdot R_g\cdot T_g\cdot W_g^{\,2}}{\pi^2\cdot D^4\cdot P^2\cdot\alpha}\right]\right]}{\pi^2\cdot D^4\cdot\rho_f\cdot(\alpha-1)^2}\ \ldots+\dfrac{16\cdot R_g\cdot T_g\cdot W_g^{\,2}\cdot\left[F_{wf}+(\alpha-1)\cdot\left(\dfrac{\Delta P}{\Delta z}-g\cdot\rho_f\right)\right]}{\pi^2\cdot D^4\cdot P\cdot\alpha^2}\right]\cdot\left[\dfrac{64\cdot W_f^{\,2}}{\pi^2\cdot D^5\cdot\rho_f\cdot(\alpha-1)^2}\ \ldots+\left[-\dfrac{64\cdot R_g\cdot T_g\cdot W_g^{\,2}}{\pi^2\cdot D^5\cdot P\cdot\alpha^2}\right]\right]}{\left[\dfrac{16\cdot W_f^{\,2}}{\pi^2\cdot D^4\cdot\rho_f\cdot(\alpha-1)^2}-\dfrac{16\cdot R_g\cdot T_g\cdot W_g^{\,2}}{\pi^2\cdot D^4\cdot P\cdot\alpha^2}\right]^2}$$

Sensitivity of Interphase Friction to Liquid Mass Flow Rate Expanded

$$\frac{\Delta f_{intp}}{\Delta W_f} = \frac{32 \cdot W_f \cdot \left[\frac{16 \cdot W_f^{\,2} \cdot \left[\alpha \cdot \left(\frac{\Delta P}{\Delta z} - \frac{P \cdot g}{R_g \cdot T_g} \right) - \frac{16 \cdot \frac{\Delta P}{\Delta z} \cdot R_g \cdot T_g \cdot W_g^{\,2}}{\pi^2 \cdot D^4 \cdot P^2 \cdot \alpha} \right]}{\pi^2 \cdot D^4 \cdot \rho_f \cdot (\alpha - 1)^2} \ldots + \frac{16 \cdot R_g \cdot T_g \cdot W_g^{\,2} \cdot \left[F_{wf} + (\alpha - 1) \cdot \left(\frac{\Delta P}{\Delta z} - g \cdot \rho_f \right) \right]}{\pi^2 \cdot D^4 \cdot P \cdot \alpha^2} \right]}{\pi^2 \cdot D^4 \cdot \rho_f \cdot (\alpha - 1)^2 \cdot \left[\frac{16 \cdot W_f^{\,2}}{\pi^2 \cdot D^4 \cdot \rho_f \cdot (\alpha - 1)^2} - \frac{16 \cdot R_g \cdot T_g \cdot W_g^{\,2}}{\pi^2 \cdot D^4 \cdot P \cdot \alpha^2} \right]^2} \ldots$$

$$+ \frac{32 \cdot W_f \cdot \left[\alpha \cdot \left(\frac{\Delta P}{\Delta z} - \frac{P \cdot g}{R_g \cdot T_g} \right) - \frac{16 \cdot \frac{\Delta P}{\Delta z} \cdot R_g \cdot T_g \cdot W_g^{\,2}}{\pi^2 \cdot D^4 \cdot P^2 \cdot \alpha} \right]}{\pi^2 \cdot D^4 \cdot \rho_f \cdot (\alpha - 1)^2 \cdot \left[\frac{16 \cdot W_f^{\,2}}{\pi^2 \cdot D^4 \cdot \rho_f \cdot (\alpha - 1)^2} - \frac{16 \cdot R_g \cdot T_g \cdot W_g^{\,2}}{\pi^2 \cdot D^4 \cdot P \cdot \alpha^2} \right]} \quad \text{(A71)}$$

Variables

a	Acceleration, Coefficient when a Subscript is Included
A	Area
D	Diameter
F	Force
m	Mass
M	Molar Mass
p	Linear Momentum
P	Pressure
R	Ideal Gas Constant for a Particular Gas
t	Time
T	Temperature
V	Velocity
W	Mass Flow Rate
x	Variable
z	Height
α	Vapor Volume Fraction
ρ	Density

Subscripts

b	Bar (or Universal)
f	Liquid
g	Vapor
h	Hydraulic
i	In
int	Interphase (Per Unit Volume)
INTf	Interphase-Liquid
INTg	Interphase-Vapor
o	Out
wf	Wall-Liquid (Per Unit Volume)
Wf	Wall-Liquid
Wg	Wall-Vapor

Appendix B: Collected Data

Gill, Hewitt and Lacey [29]

Vapor	Liquid	P (psia)	T (°F)	D (ft)	H (ft)	$\Delta P/\Delta L$ (lb_f/ft^3)	Vapor Fraction, α_g	Liquid Fraction, α_f	W_L (lb_m/s)	W_G (lb_m/s)
Air	Water	15.2381	72.0000	0.1042	3.9167	3.6330	0.9695	0.0305	0.0139	0.0556
Air	Water	15.3541	66.2000	0.1042	3.9167	3.0570	0.9650	0.0350	0.0208	0.0556
Air	Water	17.4232	72.5000	0.1042	3.9167	14.2570	0.9156	0.0844	0.2778	0.0556
Air	Water	17.6553	64.0000	0.1042	3.9167	17.6660	0.8986	0.1014	0.3472	0.0556
Air	Water	15.9922	67.5000	0.1042	3.9167	6.4690	0.9780	0.0220	0.0208	0.0833
Air	Water	17.0558	66.1000	0.1042	3.9167	11.9460	0.9646	0.0354	0.0972	0.0833
Air	Water	17.7520	64.0000	0.1042	3.9167	13.7250	0.9569	0.0431	0.1389	0.0833
Air	Water	19.2023	67.1000	0.1042	3.9167	19.5700	0.9429	0.0571	0.2778	0.0833
Air	Water	19.4924	58.0000	0.1042	3.9167	21.3850	0.9316	0.0684	0.3472	0.0833
Air	Water	18.6028	66.0000	0.1042	3.9167	15.1860	0.9756	0.0244	0.0972	0.1111
Air	Water	18.1000	64.4000	0.1042	3.9167	17.4570	0.9686	0.0314	0.1389	0.1111
Air	Water	20.2465	65.2000	0.1042	3.9167	21.2960	0.9576	0.0424	0.2083	0.1111
Air	Water	21.1167	65.4000	0.1042	3.9167	24.6290	0.9470	0.0530	0.2778	0.1111
Air	Water	18.7189	68.5000	0.1042	3.9167	13.7250	0.9826	0.0174	0.2778	0.1389
Air	Water	19.9951	66.0000	0.1042	3.9167	19.1710	0.9792	0.0208	0.0972	0.1389
Air	Water	20.6720	64.9000	0.1042	3.9167	21.6810	0.9745	0.0255	0.1389	0.1389
Air	Water	21.9869	63.0000	0.1042	3.9167	25.9190	0.9678	0.0322	0.2083	0.1389
Air	Water	22.5864	63.0000	0.1042	3.9167	28.7790	0.9573	0.0427	0.0278	0.1389
Air	Water	21.0394	63.4000	0.1042	3.9167	23.4830	0.9811	0.0189	0.0972	0.1667
Air	Water	22.3737	62.0000	0.1042	3.9167	26.3440	0.9756	0.0244	0.1389	0.1667
Air	Water	17.6940	66.1000	0.1042	3.9167	14.0430	0.9524	0.0476	0.1389	0.0833
Air	Water	18.1581	54.0000	0.1042	3.9167	17.1910	0.9342	0.0658	0.2083	0.0833
Air	Water	18.8929	61.0000	0.1042	3.9167	19.6720	0.9422	0.0578	0.2778	0.0833
Air	Water	18.8736	60.0000	0.1042	3.9167	17.8870	0.9699	0.0301	0.1389	0.1111

Govier et al [11,31,32]

Run Number	Vapor	Liquid	P (psia)	T (°F)	D (ft)	H (ft)	$\Delta P/\Delta L$ (lb_f/ft^3)	Vapor Fraction, α_g	Liquid Fraction, α_f	W_L (lb_m/s)	W_G (lb_m/s)
122A	Air	Water	72.0000	85.0000	0.1250	22.8800	22.9570	0.5984	0.4016	0.6675	0.0118
123A	Air	Water	72.0000	85.0000	0.1250	22.8800	17.7168	0.6825	0.3175	0.6675	0.0152
124A	Air	Water	72.0000	84.0000	0.1250	22.8800	15.9077	0.6732	0.3268	0.6675	0.0194
125A	Air	Water	72.0000	80.0000	0.1250	22.8800	16.5315	0.7059	0.2941	0.6675	0.0208
126A	Air	Water	72.0000	80.0000	0.1250	22.8800	20.4616	0.6825	0.3175	0.6675	0.0301
127A	Air	Water	72.0000	80.0000	0.1250	22.8800	19.2764	0.7167	0.2833	0.6675	0.0400
128A	Air	Water	72.0000	81.0000	0.1250	22.8800	16.5315	0.7602	0.2398	0.6675	0.0558
129A	Air	Water	72.0000	86.0000	0.1250	22.8800	14.6600	0.8172	0.1828	0.6675	0.0860
130A	Air	Water	72.0000	86.0000	0.1250	22.8800	14.0986	0.8538	0.1462	0.6675	0.1158
131A	Air	Water	72.0000	89.0000	0.1250	22.8800	17.3425	0.8778	0.1222	0.6675	0.1228
186A	Air	Water	110.0000	77.0000	0.1250	22.8800	33.0630	0.5169	0.4831	0.6675	0.0119
187A	Air	Water	110.0000	76.0000	0.1250	22.8800	24.4541	0.5951	0.4049	0.6675	0.0177
188A	Air	Water	110.0000	80.0000	0.1250	22.8800	19.8378	0.6124	0.3876	0.6675	0.0224
189A	Air	Water	110.0000	83.0000	0.1250	22.8800	17.7168	0.6894	0.3106	0.6675	0.0292
190A	Air	Water	110.0000	82.0000	0.1250	22.8800	19.2140	0.6805	0.3195	0.6675	0.0342
191A	Air	Water	110.0000	90.0000	0.1250	22.8800	21.9588	0.6491	0.3509	0.6675	0.0436
192A	Air	Water	110.0000	95.0000	0.1250	22.8800	21.3974	0.6689	0.3311	0.6675	0.0521
193A	Air	Water	110.0000	87.0000	0.1250	22.8800	18.5901	0.7396	0.2604	0.6675	0.0792
194A	Air	Water	110.0000	83.0000	0.1250	22.8800	16.5315	0.7845	0.2155	0.6675	0.1011
257S	Air	Water	36.0000	79.0000	0.1250	22.8800	18.2782	0.6441	0.3559	0.6675	0.0089
258S	Air	Water	36.0000	80.0000	0.1250	22.8800	20.8983	0.7297	0.2703	0.6675	0.0160
259S	Air	Water	36.0000	81.0000	0.1250	22.8800	15.0343	0.8316	0.1684	0.6675	0.0607
27A	Air	Water	18.0000	82.0000	0.1250	22.8800	18.4654	0.6942	0.3058	0.6675	0.0068
280D	Air	Water	36.0000	62.0000	0.0525	22.8800	25.7642	0.5633	0.4367	0.1142	0.0008
281D	Air	Water	36.0000	62.0000	0.0525	22.8800	21.7093	0.6337	0.3663	0.1142	0.0011
282D	Air	Water	36.0000	62.0000	0.0525	22.8800	18.7149	0.6795	0.3205	0.1142	0.0015
283D	Air	Water	36.0000	63.0000	0.0525	22.8800	18.7149	0.7305	0.2695	0.1142	0.0029
284D	Air	Water	36.0000	63.0000	0.0525	22.8800	20.5864	0.7361	0.2639	0.1142	0.0043
285D	Air	Water	36.0000	64.0000	0.0525	22.8800	22.4579	0.7305	0.2695	0.1142	0.0052
286D	Air	Water	36.0000	64.0000	0.0525	22.8800	23.2065	0.7512	0.2488	0.1142	0.0062
286S	Air	Water	36.0000	78.0000	0.2083	22.8800	20.5864	0.6047	0.3953	1.8465	0.0359
287D	Air	Water	36.0000	64.0000	0.0525	22.8800	23.4560	0.7691	0.2309	0.1142	0.0076
288D	Air	Water	36.0000	64.0000	0.0525	22.8800	23.2065	0.7305	0.2695	0.1142	0.0057
289D	Air	Water	36.0000	64.0000	0.0525	22.8800	24.2046	0.8179	0.1821	0.1142	0.0084
28A	Air	Water	18.0000	80.0000	0.1250	22.8800	19.9626	0.7608	0.2392	0.6675	0.0154
290D	Air	Water	36.0000	64.0000	0.0525	22.8800	26.5128	0.8308	0.1692	0.1142	0.0107
29A	Air	Water	18.0000	79.0000	0.1250	22.8800	17.2177	0.7409	0.2591	0.6675	0.0138
308S	Air	Water	36.0000	69.0000	0.0854	22.8800	64.8784	0.5146	0.4854	2.6263	0.0132
309S	Air	Water	36.0000	67.0000	0.0854	22.8800	62.3830	0.3857	0.6143	2.6263	0.0066
30A	Air	Water	18.0000	80.0000	0.1250	22.8800	34.6226	0.6377	0.3623	0.6675	0.0019
310S	Air	Water	36.0000	67.0000	0.0854	22.8800	63.6307	0.4678	0.5322	2.6263	0.0110
311S	Air	Water	36.0000	67.0000	0.0854	22.8800	65.5022	0.5370	0.4630	2.6263	0.0146

Run Number	Vapor	Liquid	P (psia)	T (°F)	D (ft)	H (ft)	ΔP/ΔL (lbf/ft3)	Vapor Fraction, αg	Liquid Fraction, αf	WL (lbm/s)	WG (lbm/s)
312S	Air	Water	36.0000	72.0000	0.0854	22.8800	65.5022	0.2413	0.7587	2.6263	0.0035
31A	Air	Water	18.0000	79.0000	0.1250	22.8800	27.1366	0.5763	0.4237	0.6675	0.0033
32A	Air	Water	18.0000	77.0000	0.1250	22.8800	23.0817	0.6587	0.3413	0.6675	0.0046
33A	Air	Water	18.0000	76.0000	0.1250	22.8800	18.0911	0.7297	0.2703	0.6675	0.0103
345S	Air	Water	36.0000	79.0000	0.1250	22.8800	13.5371	0.8339	0.1661	0.6675	0.0714
346S	Air	Water	36.0000	66.0000	0.1250	22.8800	17.5296	0.7788	0.2212	0.6675	0.0396
350S	Air	Water	36.0000	67.0000	0.1250	22.8800	15.2215	0.7988	0.2012	0.6675	0.0520
351S	Air	Water	36.0000	67.0000	0.1250	22.8800	19.9626	0.7297	0.2703	0.6675	0.0314
352S	Air	Water	36.0000	67.0000	0.1250	22.8800	21.8341	0.7033	0.2967	0.6675	0.0236
353S	Air	Water	36.0000	67.0000	0.1250	22.8800	21.0231	0.7110	0.2890	0.6675	0.0166
354S	Air	Water	36.0000	67.0000	0.1250	22.8800	23.5184	0.5951	0.4049	0.6675	0.0059
355S	Air	Water	36.0000	67.0000	0.1250	22.8800	19.9626	0.6711	0.3289	0.6675	0.0108
356S	Air	Water	36.0000	79.0000	0.1250	22.8800	33.6868	0.4775	0.5225	0.6675	0.0035
360S	Air	Water	36.0000	80.0000	0.1250	22.8800	14.4729	0.8374	0.1626	0.6675	0.0700
380D	Air	Water	36.0000	70.0000	0.0854	22.8800	19.4635	0.6988	0.3012	0.3119	0.0114
381D	Air	Water	36.0000	70.0000	0.0854	22.8800	17.9663	0.7849	0.2151	0.3119	0.0215
382D	Air	Water	36.0000	70.0000	0.0854	22.8800	18.2782	0.8127	0.1873	0.3119	0.0289
383D	Air	Water	36.0000	70.0000	0.0854	22.8800	18.4030	0.8051	0.1949	0.3119	0.0248
386D	Air	Water	36.0000	70.0000	0.0854	22.8800	15.9701	0.7118	0.2882	0.3119	0.0055
387D	Air	Water	36.0000	70.0000	0.0854	22.8800	20.5864	0.6933	0.3067	0.3119	0.0103
388D	Air	Water	36.0000	70.0000	0.0854	22.8800	20.0250	0.7375	0.2625	0.3119	0.0141
389D	Air	Water	36.0000	70.0000	0.0854	22.8800	21.5845	0.6466	0.3534	0.3119	0.0029
390D	Air	Water	36.0000	70.0000	0.0854	22.8800	16.9682	0.6951	0.3049	0.3119	0.0052
391D	Air	Water	36.0000	70.0000	0.0854	22.8800	15.7205	0.7326	0.2674	0.3119	0.0070
392D	Air	Water	36.0000	70.0000	0.0854	22.8800	31.0667	0.4819	0.5181	0.3119	0.0014
395D	Air	Water	36.0000	70.0000	0.0854	22.8800	18.2782	0.6337	0.3663	0.0250	0.0012
396D	Air	Water	36.0000	72.0000	0.0854	22.8800	12.5390	0.7567	0.2433	0.0250	0.0027
397D	Air	Water	36.0000	72.0000	0.0854	22.8800	12.1647	0.7674	0.2326	0.0250	0.0052
398D	Air	Water	36.0000	72.0000	0.0854	22.8800	12.1023	0.7753	0.2247	0.0250	0.0072
399D	Air	Water	36.0000	72.0000	0.0854	22.8800	11.2289	0.7732	0.2268	0.0250	0.0060
400D	Air	Water	36.0000	72.0000	0.0854	22.8800	12.3518	0.7921	0.2079	0.0250	0.0107
401D	Air	Water	36.0000	72.0000	0.0854	22.8800	10.7923	0.8258	0.1742	0.0250	0.0139
402D	Air	Water	36.0000	71.0000	0.0854	22.8800	6.7374	0.9045	0.0955	0.0250	0.0254
405D	Air	Water	36.0000	70.0000	0.0854	22.8800	12.5390	0.7942	0.2058	0.0250	0.0119
406D	Air	Water	36.0000	70.0000	0.0854	22.8800	8.6089	0.8765	0.1235	0.0250	0.0207
481S	Air	Water	36.0000	78.0000	0.2083	22.8800	27.0119	0.4737	0.5263	1.8465	0.0106
482S	Air	Water	36.0000	79.0000	0.2083	22.8800	30.0062	0.4980	0.5020	1.8465	0.0132
483S	Air	Water	36.0000	79.0000	0.2083	22.8800	26.9495	0.5283	0.4717	1.8465	0.0169
484S	Air	Water	36.0000	79.0000	0.2083	22.8800	23.5184	0.5556	0.4444	1.8465	0.0227
487S	Air	Water	36.0000	78.0000	0.2083	22.8800	21.2102	0.6350	0.3650	1.8465	0.0451
488S	Air	Water	36.0000	78.0000	0.2083	22.8800	18.5278	0.6644	0.3356	1.8465	0.0606
489S	Air	Water	36.0000	79.0000	0.2083	22.8800	20.4616	0.6540	0.3460	1.8465	0.0532
490S	Air	Water	36.0000	79.0000	0.2083	22.8800	17.2801	0.6894	0.3106	1.8465	0.0762
491S	Air	Water	36.0000	78.0000	0.2083	22.8800	17.7168	0.7118	0.2882	1.8465	0.0921
85S	Air	Water	36.0000	78.0000	0.2083	22.8800	21.2102	0.5851	0.4149	1.8465	0.0294

Oshinowo [59]

Run Number	Vapor	% Glycerol	P (psia)	T (°F)	D (ft)	H (ft)	$\Delta P/\Delta L$ (lb_f/ft^3)	Vapor Fraction, α_g	Liquid Fraction, α_f	W_L (lb_m/s)	W_G (lb_m/s)
1002	Air	0.0	25.9000	62.0000	0.0827	12.9900	71.3398	0.0723	0.9277	2.2933	0.0003
1003	Air	0.0	29.2000	54.0000	0.0827	12.9900	49.6753	0.6023	0.3977	1.4400	0.0160
1004	Air	0.0	24.4000	62.0000	0.0827	12.9900	68.8647	0.1746	0.8254	2.0533	0.0004
1005	Air	0.0	25.5000	52.0000	0.0827	12.9900	68.5589	0.0919	0.9081	2.0800	0.0005
1006	Air	0.0	25.9000	55.5000	0.0827	12.9900	65.9755	0.1717	0.8283	2.0800	0.0011
1007	Air	0.0	26.7000	71.0000	0.0827	12.9900	63.5918	0.1844	0.8156	2.0800	0.0015
1008	Air	0.0	27.6000	73.0000	0.0827	12.9900	61.2082	0.2532	0.7468	2.0800	0.0025
1009	Air	0.0	28.0000	74.0000	0.0827	12.9900	59.2238	0.2948	0.7052	2.0800	0.0032
1010	Air	0.0	28.2000	75.0000	0.0827	12.9900	58.4314	0.2936	0.7064	2.0800	0.0035
1011	Air	0.0	24.9000	76.0000	0.0827	12.9900	68.3592	0.0746	0.9254	2.0800	0.0004
1012	Air	0.0	24.6000	77.0000	0.0827	12.9900	73.6320	0.0630	0.9370	2.0800	0.0003
1013	Air	0.0	26.9000	56.5000	0.0827	12.9900	61.5986	0.2543	0.7457	2.0267	0.0022
1014	Air	0.0	27.3000	59.5000	0.0827	12.9900	58.2365	0.3104	0.6896	1.9200	0.0033
1015	Air	0.0	27.4000	60.0000	0.0827	12.9900	57.6458	0.3260	0.6740	1.9733	0.0036
1016	Air	0.0	28.4000	63.0000	0.0827	12.9900	55.2536	0.4116	0.5884	1.9200	0.0058
1017	Air	0.0	24.2000	61.0000	0.0827	12.9900	67.5557	0.0731	0.9269	1.8667	0.0003
1018	Air	0.0	24.5000	64.0000	0.0827	12.9900	66.3639	0.1012	0.8988	1.8667	0.0005
1019	Air	0.0	24.7000	65.0000	0.0827	12.9900	65.9708	0.1116	0.8884	1.8667	0.0006
1020	Air	0.0	25.2000	66.5000	0.0827	12.9900	63.9866	0.1457	0.8543	1.8667	0.0009
1021	Air	0.0	21.4000	68.5000	0.0827	12.9900	60.0120	0.2358	0.7642	1.8667	0.0020
1022	Air	0.0	27.2000	70.0000	0.0827	12.9900	57.6285	0.2954	0.7046	1.8667	0.0030
1023	Air	0.0	27.7000	72.0000	0.0827	12.9900	54.4526	0.3636	0.6364	1.8667	0.0044
1024	Air	0.0	28.4000	49.5000	0.0827	12.9900	54.8629	0.4069	0.5931	1.8400	0.0058
1025	Air	0.0	28.7000	73.0000	0.0827	12.9900	53.2608	0.4474	0.5526	1.8667	0.0074
1026	Air	0.0	23.2000	66.0000	0.0827	12.9900	66.1950	0.0624	0.9376	1.6000	0.0002
1027	Air	0.0	23.2000	51.0000	0.0827	12.9900	66.3592	0.0734	0.9266	1.6960	0.0003
1028	Air	0.0	24.4000	49.5000	0.0827	12.9900	63.9726	0.1029	0.8971	1.5627	0.0005
1029	Air	0.0	24.7000	68.0000	0.0827	12.9900	63.2114	0.1202	0.8798	1.6000	0.0006
1030	Air	0.0	26.0000	70.0000	0.0827	12.9900	59.2416	0.1636	0.8364	1.6000	0.0010
1031	Air	0.0	26.3000	52.5000	0.0827	12.9900	60.0243	0.2231	0.7769	1.5893	0.0016
1032	Air	0.0	27.1000	72.0000	0.0827	12.9900	54.0733	0.3075	0.6925	1.6000	0.0028
1033	Air	0.0	27.2000	54.0000	0.0827	12.9900	51.2654	0.4133	0.5867	1.5627	0.0050
1034	Air	0.0	27.5000	72.5000	0.0827	12.9900	48.9113	0.4624	0.5376	1.6000	0.0068
1035	Air	0.0	28.1000	54.0000	0.0827	12.9900	48.9113	0.4855	0.5145	1.6000	0.0082
1036	Air	0.0	28.9000	74.5000	0.0827	12.9900	48.5118	0.5711	0.4289	1.6000	0.0125
1037	Air	0.0	24.3000	55.5000	0.0827	12.9900	63.8123	0.0607	0.9393	1.3067	0.0002
1038	Air	0.0	26.1000	58.5000	0.0827	12.9900	61.5930	0.1405	0.8595	1.3600	0.0006
1039	Air	0.0	25.8000	63.0000	0.0827	12.9900	55.2566	0.2676	0.7324	1.3387	0.0017
1040	Air	0.0	26.2000	63.5000	0.0827	12.9900	49.3120	0.3671	0.6329	1.3067	0.0031
1041	Air	0.0	26.7000	52.0000	0.0827	12.9900	46.5148	0.4387	0.5613	1.3333	0.0046
1042	Air	0.0	26.7000	55.0000	0.0827	12.9900	44.1310	0.4879	0.5121	1.3333	0.0067

Run Number	Vapor	% Glycerol	P (psia)	T (°F)	D (ft)	H (ft)	$\Delta P/\Delta L$ (lb_f/ft^3)	Vapor Fraction, α_g	Liquid Fraction, α_f	W_L (lb_m/s)	W_G (lb_m/s)
1043	Air	0.0	27.0000	55.5000	0.0827	12.9900	42.9392	0.5202	0.4798	1.3333	0.0087
1044	Air	0.0	27.8000	63.0000	0.0827	12.9900	43.7379	0.5890	0.4110	1.3333	0.0124
1045	Air	0.0	28.3000	57.5000	0.0827	12.9900	46.1154	0.6162	0.3838	1.3333	0.0157
1046	Air	0.0	28.9000	75.5000	0.0827	12.9900	44.5304	0.6584	0.3416	1.3333	0.0180
1047	Air	0.0	29.9000	64.5000	0.0827	12.9900	42.5582	0.6821	0.3179	1.3067	0.0212
1048	Air	0.0	29.4000	65.5000	0.0827	12.9900	46.5042	0.6717	0.3283	1.2800	0.0223
1049	Air	0.0	29.2000	59.0000	0.0827	12.9900	46.1306	0.7116	0.2884	1.0133	0.0292
1050	Air	0.0	25.7000	53.5000	0.0827	12.9900	41.3380	0.4613	0.5387	1.0667	0.0045
1051	Air	0.0	25.4000	50.0000	0.0827	12.9900	59.5961	0.1271	0.8729	1.0667	0.0005
1052	Air	0.0	25.6000	54.0000	0.0827	12.9900	53.2460	0.2399	0.7601	1.0667	0.0013
1053	Air	0.0	25.4000	59.5000	0.0827	12.9900	52.6238	0.2590	0.7410	1.0083	0.0014
1054	Air	0.0	25.9000	56.0000	0.0827	12.9900	46.0975	0.3607	0.6393	1.0667	0.0026
1057	Air	0.0	25.9000	62.0000	0.0827	12.9900	37.3645	0.5832	0.4168	1.0667	0.0079
1058	Air	0.0	26.7000	71.0000	0.0827	12.9900	38.9552	0.6353	0.3647	1.0667	0.0127
1059	Air	0.0	27.0000	62.5000	0.0827	12.9900	40.5396	0.6572	0.3428	1.0667	0.0161
1060	Air	0.0	28.2000	73.0000	0.0827	12.9900	42.5294	0.6636	0.3364	1.0667	0.0223
1061	Air	0.0	28.5000	64.0000	0.0827	12.9900	43.7472	0.7104	0.2896	1.0507	0.0249
1062	Air	0.0	29.4000	75.0000	0.0827	12.9900	44.5454	0.6890	0.3110	1.0560	0.0297
1064	Air	0.0	24.4000	46.0000	0.0827	12.9900	39.3737	0.4416	0.5584	0.8000	0.0031
1065	Air	0.0	24.8000	46.0000	0.0827	12.9900	33.0195	0.5728	0.4272	0.8000	0.0057
1066	Air	0.0	24.9000	60.5000	0.0827	12.9900	32.2268	0.6289	0.3711	0.8000	0.0081
1067	Air	0.0	25.7000	74.5000	0.0827	12.9900	33.0195	0.6549	0.3451	0.8000	0.0124
1068	Air	0.0	25.5000	62.5000	0.0827	12.9900	33.4190	0.6647	0.3353	0.8000	0.0138
1069	Air	0.0	26.7000	75.5000	0.0827	12.9900	35.8034	0.7214	0.2786	0.8000	0.0221
1070	Air	0.0	27.2000	77.5000	0.0827	12.9900	37.7883	0.7185	0.2815	0.8000	0.0272
1071	Air	0.0	27.9000	64.5000	0.0827	12.9900	39.7732	0.7590	0.2410	0.8000	0.0320
1072	Air	0.0	24.7000	57.5000	0.0827	12.9900	31.4136	0.5225	0.4775	0.5333	0.0032
1073	Air	0.0	23.9000	57.5000	0.0827	12.9900	25.8495	0.6439	0.3561	0.5333	0.0054
1074	Air	0.0	24.2000	59.5000	0.0827	12.9900	25.8495	0.6208	0.3792	0.5333	0.0080
1075	Air	0.0	24.2000	68.5000	0.0827	12.9900	27.8394	0.6728	0.3272	0.5333	0.0122
1076	Air	0.0	24.4000	61.0000	0.0827	12.9900	27.8394	0.6884	0.3116	0.5333	0.0147
1077	Air	0.0	24.4000	71.0000	0.0827	12.9900	29.8230	0.7133	0.2867	0.5333	0.0187
1078	Air	0.0	24.9000	72.5000	0.0827	12.9900	27.8394	0.7422	0.2578	0.5333	0.0236
1079	Air	0.0	25.6000	61.0000	0.0827	12.9900	31.8066	0.7636	0.2364	0.5333	0.0268
1080	Air	0.0	26.4000	76.5000	0.0827	12.9900	30.6152	0.7780	0.2220	0.5333	0.0347
1081	Air	0.0	27.2000	78.5000	0.0827	12.9900	32.9981	0.8046	0.1954	0.5333	0.0388
1082	Air	0.0	27.2000	63.5000	0.0827	12.9900	34.5887	0.7908	0.2092	0.5333	0.0403
1083	Air	0.0	28.7000	64.0000	0.0827	12.9900	32.9981	0.8000	0.2000	0.5333	0.0437
1084	Air	0.0	28.4000	64.0000	0.0827	12.9900	33.6750	0.8064	0.1936	0.5263	0.0454
1085	Air	0.0	23.7000	51.5000	0.0827	12.9900	28.6090	0.5509	0.4491	0.4467	0.0027
1086	Air	0.0	23.4000	80.0000	0.0827	12.9900	24.6810	0.6266	0.3734	0.4442	0.0037
1087	Air	0.0	23.1000	54.5000	0.0827	12.9900	21.8971	0.6214	0.3786	0.4442	0.0055
1088	Air	0.0	23.1000	62.5000	0.0827	12.9900	23.0893	0.6867	0.3133	0.4442	0.0069
1089	Air	0.0	23.2000	57.5000	0.0827	12.9900	21.8971	0.7052	0.2948	0.4442	0.0081

Run Number	Vapor	% Glycerol	P (psia)	T (°F)	D (ft)	H (ft)	$\Delta P/\Delta L$ (lb_f/ft^3)	Vapor Fraction, α_g	Liquid Fraction, α_f	W_L (lb_m/s)	W_G (lb_m/s)
1090	Air	0.0	23.4000	64.5000	0.0827	12.9900	24.6810	0.6809	0.3191	0.4442	0.0110
1091	Air	0.0	23.6000	62.5000	0.0827	12.9900	25.4586	0.6873	0.3127	0.4492	0.0138
1092	Air	0.0	23.9000	68.5000	0.0827	12.9900	25.0743	0.7301	0.2699	0.4442	0.0204
1093	Air	0.0	24.2000	63.0000	0.0827	12.9900	25.8826	0.7671	0.2329	0.4393	0.0242
1094	Air	0.0	24.7000	69.5000	0.0827	12.9900	25.4738	0.7855	0.2145	0.4442	0.0307
1095	Air	0.0	27.4000	65.5000	0.0827	12.9900	28.6605	0.8260	0.1740	0.4319	0.0469
1096	Air	0.0	25.4000	71.0000	0.0827	12.9900	26.6660	0.7994	0.2006	0.4442	0.0363
1097	Air	0.0	26.2000	73.0000	0.0827	12.9900	28.2515	0.8145	0.1855	0.4442	0.0415
1098	Air	0.0	28.4000	66.0000	0.0827	12.9900	29.0622	0.8324	0.1676	0.4121	0.0501
1099	Air	0.0	29.1000	68.5000	0.0827	12.9900	30.2162	0.8208	0.1792	0.4418	0.0518
1100	Air	0.0	29.3000	67.5000	0.0827	12.9900	29.8816	0.8335	0.1665	0.4396	0.0527
1101	Air	0.0	23.2000	68.5000	0.0827	12.9900	26.6749	0.5416	0.4584	0.3455	0.0022
1102	Air	0.0	23.2000	74.5000	0.0827	12.9900	24.6893	0.6012	0.3988	0.3455	0.0025
1103	Air	0.0	22.4000	72.5000	0.0827	12.9900	19.8813	0.7139	0.2861	0.3480	0.0047
1104	Air	0.0	22.8000	74.5000	0.0827	12.9900	19.8813	0.6717	0.3283	0.3480	0.0065
1105	Air	0.0	22.9000	66.5000	0.0827	12.9900	21.8949	0.7000	0.3000	0.3578	0.0084
1107	Air	0.0	23.1000	75.0000	0.0827	12.9900	20.7118	0.7220	0.2780	0.3455	0.0107
1110	Air	0.0	32.2000	68.5000	0.0827	12.9900	23.8451	0.7301	0.2699	0.3480	0.0154
1111	Air	0.0	23.3000	76.5000	0.0827	12.9900	18.7261	0.7728	0.2272	0.3455	0.0204
1112	Air	0.0	23.7000	78.0000	0.0827	12.9900	21.5048	0.7925	0.2075	0.3455	0.0265
1113	Air	0.0	24.0000	69.5000	0.0827	12.9900	22.6974	0.8133	0.1867	0.3455	0.0322
1114	Air	0.0	24.3000	71.0000	0.0827	12.9900	23.0793	0.8231	0.1769	0.3504	0.0341
1115	Air	0.0	24.9000	78.5000	0.0827	12.9900	23.8900	0.8370	0.1630	0.3455	0.0406
1116	Air	0.0	27.3000	70.5000	0.0827	12.9900	25.8959	0.8514	0.1486	0.3406	0.0516
1117	Air	0.0	23.0000	70.5000	0.0827	12.9900	23.4525	0.6301	0.3699	0.3480	0.0031
1118	Air	0.0	29.2000	71.5000	0.0827	12.9900	26.6790	0.8584	0.1416	0.3445	0.0588
1119	Air	0.0	29.2000	72.0000	0.0827	12.9900	22.7111	0.8861	0.1139	0.2468	0.0597
1120	Air	0.0	26.2000	74.5000	0.0827	12.9900	21.5177	0.8740	0.1260	0.2468	0.0478
1121	Air	0.0	24.1000	73.0000	0.0827	12.9900	20.0384	0.8595	0.1405	0.2481	0.0416
1122	Air	0.0	23.4000	72.5000	0.0827	12.9900	18.6883	0.8405	0.1595	0.2493	0.0352
1123	Air	0.0	23.4000	70.0000	0.0827	12.9900	18.3376	0.8462	0.1538	0.2468	0.0345
1124	Air	0.0	23.0000	70.5000	0.0827	12.9900	17.9439	0.8266	0.1734	0.2468	0.0292
1126	Air	0.0	22.7000	66.5000	0.0827	12.9900	17.9439	0.7786	0.2214	0.2468	0.0206
1127	Air	0.0	22.7000	58.5000	0.0827	12.9900	19.1310	0.7457	0.2543	0.2468	0.0149
1128	Air	0.0	22.7000	64.5000	0.0827	12.9900	18.7374	0.7081	0.2919	0.2468	0.0110
1129	Air	0.0	22.7000	60.5000	0.0827	12.9900	19.9308	0.7127	0.2873	0.2468	0.0081
1130	Air	0.0	22.2000	63.5000	0.0827	12.9900	17.8932	0.7289	0.2711	0.2502	0.0062
1131	Air	0.0	22.4000	66.0000	0.0827	12.9900	29.0463	0.6526	0.3474	0.2517	0.0045
1132	Air	0.0	22.6000	68.5000	0.0827	12.9900	20.7243	0.6185	0.3815	0.2468	0.0028
1133	Air	0.0	23.2000	70.5000	0.0827	12.9900	29.2097	0.5150	0.4850	0.2369	0.0016
1135	Air	0.0	19.5000	79.5000	0.0827	12.9900	12.7887	0.7520	0.2480	0.1481	0.0048
1137	Air	0.0	24.2000	71.5000	0.0827	12.9900	14.3841	0.8931	0.1069	0.1481	0.0389
1138	Air	0.0	22.5000	78.5000	0.0827	12.9900	12.9451	0.8832	0.1168	0.1481	0.0342
1139	Air	0.0	22.1000	71.5000	0.0827	12.9900	13.1891	0.8572	0.1428	0.1481	0.0273

Run Number	Vapor	% Glycerol	P (psia)	T (°F)	D (ft)	H (ft)	$\Delta P/\Delta L$ (lb_f/ft^3)	Vapor Fraction, α_g	Liquid Fraction, α_f	W_L (lb_m/s)	W_G (lb_m/s)
1140	Air	0.0	22.0000	77.5000	0.0827	12.9900	13.1891	0.8509	0.1491	0.1481	0.0265
1141	Air	0.0	22.1000	77.5000	0.0827	12.9900	13.9837	0.8133	0.1867	0.1481	0.0186
1142	Air	0.0	22.0000	72.5000	0.0827	12.9900	15.5792	0.7694	0.2306	0.1481	0.0141
1143	Air	0.0	22.2000	76.5000	0.0827	12.9900	16.3738	0.7543	0.2457	0.1481	0.0116
1144	Air	0.0	22.2000	53.5000	0.0827	12.9900	17.9692	0.7220	0.2780	0.1481	0.0081
1145	Air	0.0	21.9000	54.0000	0.0827	12.9900	14.7396	0.6919	0.3081	0.1456	0.0060
1150	Air	0.0	21.5000	62.0000	0.0827	12.9900	7.6497	0.9185	0.0815	0.0513	0.0318
1151	Air	0.0	21.4000	67.5000	0.0827	12.9900	7.2651	0.9000	0.1000	0.0494	0.0268
1152	Air	0.0	21.5000	65.5000	0.0827	12.9900	8.7446	0.8613	0.1387	0.0497	0.0199
1153	Air	0.0	21.1000	65.5000	0.0827	12.9900	10.7242	0.8116	0.1884	0.0528	0.0157
1154	Air	0.0	21.7000	64.0000	0.0827	12.9900	13.2826	0.7711	0.2289	0.0494	0.0108
2001	Air	0.0	25.0000	62.0000	0.0827	12.9900	69.7445	0.0578	0.9422	2.0800	0.0003
2002	Air	0.0	25.3000	63.0000	0.0827	12.9900	68.5589	0.0908	0.9092	2.0800	0.0005
2003	Air	0.0	25.6000	65.0000	0.0827	12.9900	67.5605	0.1075	0.8925	2.0800	0.0007
2004	Air	0.0	24.6000	60.0000	0.0827	12.9900	69.9442	0.0618	0.9382	2.0800	0.0003
2005	Air	0.0	26.6000	61.0000	0.0827	12.9900	65.3765	0.1717	0.8283	2.0800	0.0012
2006	Air	0.0	27.2000	62.0000	0.0827	12.9900	63.5918	0.2064	0.7936	2.0800	0.0018
2007	Air	0.0	27.6000	63.0000	0.0827	12.9900	63.1925	0.2353	0.7647	2.0800	0.0022
2008	Air	0.0	27.7000	64.0000	0.0827	12.9900	61.2082	0.2659	0.7341	2.0800	0.0028
2009	Air	0.0	28.1000	64.5000	0.0827	12.9900	59.6170	0.2977	0.7023	2.0800	0.0034
2010	Air	0.0	28.1000	56.5000	0.0827	12.9900	60.8088	0.2873	0.7127	2.0800	0.0032
2011	Air	0.0	24.1000	58.5000	0.0827	12.9900	68.3543	0.0671	0.9329	1.8667	0.0003
2012	Air	0.0	24.1000	61.0000	0.0827	12.9900	67.1688	0.1887	0.8113	1.8667	0.0004
2013	Air	0.0	24.3000	62.5000	0.0827	12.9900	65.9708	0.1068	0.8932	1.8667	0.0006
2014	Air	0.0	26.1000	64.0000	0.0827	12.9900	63.5873	0.1676	0.8324	1.8667	0.0011
2015	Air	0.0	25.2000	65.0000	0.0827	12.9900	61.6031	0.2035	0.7965	1.8667	0.0016
2016	Air	0.0	26.5000	66.5000	0.0827	12.9900	60.0120	0.2358	0.7642	1.8667	0.0020
2017	Air	0.0	26.8000	69.0000	0.0827	12.9900	58.0279	0.2775	0.7225	1.8667	0.0025
2018	Air	0.0	27.2000	69.5000	0.0827	12.9900	56.8361	0.2983	0.7017	1.8667	0.0031
2019	Air	0.0	27.3000	80.0000	0.0827	12.9900	56.0437	0.3335	0.6665	1.8667	0.0035
2020	Air	0.0	27.8000	70.5000	0.0827	12.9900	55.2450	0.3566	0.6434	1.8667	0.0040
2021	Air	0.0	27.9000	71.0000	0.0827	12.9900	54.4526	0.3717	0.6283	1.8667	0.0046
2022	Air	0.0	23.1000	58.0000	0.0827	12.9900	66.3885	0.0509	0.9491	1.6000	0.0002
2023	Air	0.0	23.9000	59.0000	0.0827	12.9900	65.5958	0.0751	0.9249	1.6000	0.0003
2024	Air	0.0	24.4000	60.0000	0.0827	12.9900	65.7955	0.1040	0.8960	1.6000	0.0005
2025	Air	0.0	24.7000	62.0000	0.0827	12.9900	62.8181	0.1301	0.8699	1.6000	0.0006
2026	Air	0.0	25.6000	62.3000	0.0827	12.9900	62.4187	0.1561	0.8439	1.6000	0.0009
2027	Air	0.0	26.1000	54.5000	0.0827	12.9900	59.6348	0.2032	0.7968	1.6000	0.0015
2028	Air	0.0	26.0000	57.0000	0.0827	12.9900	58.0488	0.2306	0.7694	1.6000	0.0017
2029	Air	0.0	26.4000	57.5000	0.0827	12.9900	55.5152	0.3032	0.6968	1.6000	0.0027
2030	Air	0.0	26.9000	58.5000	0.0827	12.9900	52.4879	0.3647	0.6353	1.6000	0.0036
2031	Air	0.0	27.2000	59.0000	0.0827	12.9900	50.8962	0.4104	0.5896	1.6000	0.0046
2032	Air	0.0	27.5000	59.5000	0.0827	12.9900	49.7040	0.4306	0.5694	1.6000	0.0055
2033	Air	0.0	27.5000	61.0000	0.0827	12.9900	48.9113	0.4595	0.5405	1.6000	0.0065

Run Number	Vapor	% Glycerol	P (psia)	T (°F)	D (ft)	H (ft)	$\Delta P/\Delta L$ (lb_f/ft^3)	Vapor Fraction, α_g	Liquid Fraction, α_f	W_L (lb_m/s)	W_G (lb_m/s)
2034	Air	0.0	27.9000	62.0000	0.0827	12.9900	48.5118	0.5173	0.4827	1.6000	0.0086
2036	Air	0.0	25.8000	58.5000	0.0827	12.9900	62.0031	0.1029	0.8971	1.3333	0.0005
2037	Air	0.0	25.8000	60.5000	0.0827	12.9900	61.2106	0.1543	0.8457	1.3333	0.0007
2038	Air	0.0	26.0000	62.0000	0.0827	12.9900	58.4337	0.1879	0.8121	1.3333	0.0011
2039	Air	0.0	26.0000	63.0000	0.0827	12.9900	53.2668	0.2092	0.7908	1.3333	0.0019
2040	Air	0.0	25.8000	64.0000	0.0827	12.9900	49.6911	0.3422	0.6578	1.3333	0.0027
2041	Air	0.0	26.2000	52.0000	0.0827	12.9900	47.7067	0.3013	0.6987	1.3333	0.0038
2042	Air	0.0	26.3000	64.5000	0.0827	12.9900	45.7223	0.4451	0.5549	1.3333	0.0047
2043	Air	0.0	26.4000	52.8000	0.0827	12.9900	45.3229	0.3607	0.6393	1.3333	0.0056
2044	Air	0.0	26.5000	55.0000	0.0827	12.9900	44.1310	0.4994	0.5006	1.3333	0.0068
2045	Air	0.0	27.0000	55.5000	0.0827	12.9900	28.9860	0.5461	0.4539	1.3333	0.0084
2046	Air	0.0	27.4000	58.5000	0.0827	12.9900	44.1310	0.5711	0.4289	1.3333	0.0098
2047	Air	0.0	28.6000	60.0000	0.0827	12.9900	46.1154	0.6225	0.3775	1.3333	0.0173
2048	Air	0.0	28.2000	60.5000	0.0827	12.9900	45.3229	0.6173	0.3827	1.3333	0.0142
2051	Air	0.0	25.0000	62.0000	0.0827	12.9900	51.7739	0.2044	0.7956	1.0667	0.0006
2052	Air	0.0	25.2000	66.5000	0.0827	12.9900	54.0382	0.2141	0.7859	1.0667	0.0011
2053	Air	0.0	25.5000	58.5000	0.0827	12.9900	50.4702	0.2896	0.7104	1.0667	0.0017
2054	Air	0.0	25.6000	60.0000	0.0827	12.9900	46.0975	0.3717	0.6283	1.0667	0.0027
2055	Air	0.0	25.5000	61.0000	0.0827	12.9900	42.1302	0.3150	0.6850	1.0667	0.0036
2056	Air	0.0	25.5000	62.5000	0.0827	12.9900	40.5396	0.4613	0.5387	1.0667	0.0044
2057	Air	0.0	25.6000	62.5000	0.0827	12.9900	38.9552	0.5185	0.4815	1.0667	0.0053
2058	Air	0.0	25.6000	64.5000	0.0827	12.9900	42.7540	0.5405	0.4595	1.0667	0.0062
2059	Air	0.0	25.8000	66.0000	0.0827	12.9900	36.9715	0.5832	0.4168	1.0667	0.0076
2060	Air	0.0	26.3000	66.5000	0.0827	12.9900	38.1630	0.5994	0.4006	1.0667	0.0107
2061	Air	0.0	27.1000	68.0000	0.0827	12.9900	40.1466	0.6642	0.3358	1.0667	0.0165
2062	Air	0.0	28.2000	69.5000	0.0827	12.9900	42.5294	0.6705	0.3295	1.0667	0.0220
2063	Air	0.0	28.2000	68.5000	0.0827	12.9900	49.1041	0.7081	0.2919	1.0667	0.0261
2064	Air	0.0	24.8000	58.5000	0.0827	12.9900	38.1878	0.4775	0.5225	0.8000	0.0033
2064	Air	0.0	24.9000	64.0000	0.0827	12.9900	48.1186	0.2728	0.7272	0.8000	0.0014
2065	Air	0.0	24.9000	56.0000	0.0827	12.9900	42.5571	0.3867	0.6133	0.8000	0.0022
2066	Air	0.0	24.9000	57.0000	0.0827	12.9900	38.1878	0.4468	0.5532	0.8000	0.0031
2068	Air	0.0	24.7000	58.5000	0.0827	12.9900	35.0044	0.5225	0.4775	0.8000	0.0044
2069	Air	0.0	24.6000	60.0000	0.0827	12.9900	32.6200	0.5595	0.4405	0.8000	0.0059
2070	Air	0.0	24.8000	60.5000	0.0827	12.9900	31.4341	0.5983	0.4017	0.8000	0.0076
2071	Air	0.0	25.1000	58.5000	0.0827	12.9900	32.6200	0.6347	0.3653	0.8000	0.0098
2072	Air	0.0	25.8000	62.5000	0.0827	12.9900	34.2117	0.6815	0.3185	0.8000	0.0157
2073	Air	0.0	26.9000	64.5000	0.0827	12.9900	34.6112	0.6977	0.3023	0.8000	0.0203
2074	Air	0.0	27.3000	66.5000	0.0827	12.9900	37.3888	0.7052	0.2948	0.8000	0.0262
2075	Air	0.0	28.6000	66.5000	0.0827	12.9900	40.1727	0.7421	0.2579	0.8000	0.0332
2076	Air	0.0	24.8000	66.5000	0.0827	12.9900	31.4341	0.5630	0.4370	0.8000	0.0068
2077	Air	0.0	24.9000	67.5000	0.0827	12.9900	32.2268	0.6975	0.3025	0.8000	0.0084
2078	Air	0.0	25.0000	58.0000	0.0827	12.9900	44.9123	0.3324	0.6676	0.5333	0.0018
2079	Air	0.0	24.4000	60.5000	0.0827	12.9900	27.2809	0.4769	0.5231	0.5333	0.0027
2080	Air	0.0	23.7000	68.5000	0.0827	12.9900	29.4238	0.5728	0.4272	0.5333	0.0034

Run Number	Vapor	% Glycerol	P (psia)	T (°F)	D (ft)	H (ft)	$\Delta P/\Delta L$ (lb_f/ft^3)	Vapor Fraction, α_g	Liquid Fraction, α_f	W_L (lb_m/s)	W_G (lb_m/s)
2081	Air	0.0	23.5000	59.5000	0.0827	12.9900	27.4402	0.6018	0.3982	0.5333	0.0045
2082	Air	0.0	23.5000	68.5000	0.0827	12.9900	25.4565	0.6827	0.3173	0.5333	0.0060
2083	Air	0.0	23.6000	70.5000	0.0827	12.9900	25.4565	0.6861	0.3139	0.5333	0.0084
2084	Air	0.0	24.1000	72.5000	0.0827	12.9900	26.6480	0.7075	0.2925	0.5333	0.0112
2085	Air	0.0	24.6000	72.5000	0.0827	12.9900	27.4402	0.7121	0.2879	0.5333	0.0176
2086	Air	0.0	25.2000	74.0000	0.0827	12.9900	28.2324	0.7428	0.2572	0.5333	0.0235
2087	Air	0.0	25.7000	74.5000	0.0827	12.9900	30.6152	0.7728	0.2272	0.5333	0.0295
2088	Air	0.0	26.6000	74.5000	0.0827	12.9900	31.4136	0.7867	0.2133	0.5333	0.0363
2089	Air	0.0	27.7000	76.5000	0.0827	12.9900	32.2058	0.8318	0.1682	0.5333	0.0422
2090	Air	0.0	23.9000	58.8000	0.0827	12.9900	31.4349	0.5116	0.4884	0.4442	0.0022
2091	Air	0.0	23.2000	60.5000	0.0827	12.9900	25.4738	0.6214	0.3786	0.4442	0.0035
2092	Air	0.0	23.2000	62.5000	0.0827	12.9900	23.4888	0.6491	0.3509	0.4442	0.0047
2093	Air	0.0	23.0000	63.5000	0.0827	12.9900	21.4976	0.6786	0.3214	0.4442	0.0061
2094	Air	0.0	23.0000	66.5000	0.0827	12.9900	22.2966	0.6775	0.3225	0.4442	0.0073
2095	Air	0.0	23.2000	67.5000	0.0827	12.9900	23.4888	0.7046	0.2954	0.4442	0.0084
2096	Air	0.0	26.0000	70.0000	0.0827	12.9900	61.2106	0.1462	0.8538	1.3333	0.0007
2097	Air	0.0	23.6000	72.0000	0.0827	12.9900	24.6810	0.7533	0.2467	0.4442	0.0157
2098	Air	0.0	24.1000	58.5000	0.0827	12.9900	25.0743	0.7439	0.2561	0.4442	0.0213
2099	Air	0.0	24.7000	58.5000	0.0827	12.9900	25.8670	0.7671	0.2329	0.4442	0.0264
2100	Air	0.0	25.2000	60.5000	0.0827	12.9900	26.6660	0.7902	0.2098	0.4442	0.0332
2101	Air	0.0	25.8000	62.3000	0.0827	12.9900	27.8582	0.8058	0.1942	0.4442	0.0391
2102	Air	0.0	28.0000	63.5000	0.0827	12.9900	29.8432	0.8341	0.1659	0.4442	0.0483
2103	Air	0.0	23.6000	66.0000	0.0827	12.9900	26.6749	0.5601	0.4399	0.3455	0.0022
2104	Air	0.0	22.9000	66.0000	0.0827	12.9900	21.4486	0.5965	0.4035	0.3455	0.0035
2105	Air	0.0	22.8000	66.5000	0.0827	12.9900	19.9188	0.6786	0.3214	0.3455	0.0049
2106	Air	0.0	22.8000	67.5000	0.0827	12.9900	19.5191	0.7173	0.2827	0.3455	0.0064
2107	Air	0.0	22.3000	68.0000	0.0827	12.9900	20.7118	0.7106	0.2894	0.3455	0.0080
2108	Air	0.0	23.1000	68.5000	0.0827	12.9900	22.3040	0.6983	0.3017	0.3455	0.0108
2109	Air	0.0	23.2000	70.0000	0.0827	12.9900	21.5048	0.7486	0.2514	0.3455	0.0174
2110	Air	0.0	23.6000	70.5000	0.0827	12.9900	21.1114	0.7694	0.2306	0.3455	0.0224
2111	Air	0.0	23.9000	70.5000	0.0827	12.9900	22.3040	0.7942	0.2058	0.3455	0.0320
2112	Air	0.0	24.6000	71.0000	0.0827	12.9900	23.4966	0.8185	0.1815	0.3455	0.0362
2113	Air	0.0	26.3000	72.0000	0.0827	12.9900	24.6893	0.8303	0.1697	0.3455	0.0433
2114	Air	0.0	23.3000	62.5000	0.0827	12.9900	21.9176	0.5936	0.4064	0.2468	0.0024
2115	Air	0.0	22.4000	64.5000	0.0827	12.9900	17.1442	0.6983	0.3017	0.2468	0.0041
2116	Air	0.0	22.5000	64.5000	0.0827	12.9900	15.5572	0.6850	0.3150	0.2468	0.0061
2117	Air	0.0	22.5000	66.0000	0.0827	12.9900	18.7374	0.7301	0.2699	0.2468	0.0086
2118	Air	0.0	22.7000	67.0000	0.0827	12.9900	19.5309	0.7387	0.2613	0.2468	0.0128
2119	Air	0.0	22.6000	69.5000	0.0827	12.9900	17.9439	0.7676	0.2324	0.2468	0.0189
2120	Air	0.0	23.0000	68.5000	0.0827	12.9900	17.9439	0.8051	0.1949	0.2468	0.0248
2121	Air	0.0	23.2000	69.5000	0.0827	12.9900	17.9439	0.8393	0.1607	0.2468	0.0332
2122	Air	0.0	24.2000	70.5000	0.0827	12.9900	20.3244	0.8636	0.1364	0.2468	0.0429
2123	Air	0.0	28.2000	70.5000	0.0827	12.9900	22.3175	0.8850	0.1150	0.2468	0.0563
2124	Air	0.0	24.1000	70.5000	0.0827	12.9900	19.5309	0.8584	0.1416	0.2468	0.0394

Run Number	Vapor	% Glycerol	P (psia)	T (°F)	D (ft)	H (ft)	$\Delta P/\Delta L$ (lb_f/ft^3)	Vapor Fraction, α_g	Liquid Fraction, α_f	W_L (lb_m/s)	W_G (lb_m/s)
2125	Air	0.0	21.9000	70.5000	0.0827	12.9900	14.7783	0.7202	0.2798	0.1481	0.0031
2126	Air	0.0	21.7000	72.5000	0.0827	12.9900	13.1891	0.7162	0.2838	0.1481	0.0047
2127	Air	0.0	21.9000	71.5000	0.0827	12.9900	15.5792	0.7405	0.2595	0.1481	0.0065
2128	Air	0.0	22.1000	72.5000	0.0827	12.9900	17.5688	0.7416	0.2584	0.1481	0.0086
2129	Air	0.0	22.0000	73.5000	0.0827	12.9900	15.5792	0.7613	0.2387	0.1481	0.0136
2130	Air	0.0	21.9000	65.0000	0.0827	12.9900	13.9837	0.8191	0.1809	0.1481	0.0209
2132	Air	0.0	22.4000	66.5000	0.0827	12.9900	13.7835	0.8775	0.1225	0.1481	0.0334
2137	Air	0.0	22.1000	71.0000	0.0827	12.9900	9.8738	0.9312	0.0688	0.0494	0.0482
2138	Air	0.0	21.1000	76.0000	0.0827	12.9900	6.8619	0.9329	0.0671	0.0494	0.0372
2139	Air	0.0	20.8000	76.0000	0.0827	12.9900	6.8619	0.9179	0.0821	0.0494	0.0298
2140	Air	0.0	20.8000	76.0000	0.0827	12.9900	8.4686	0.8688	0.1312	0.0494	0.0202
2141	Air	0.0	20.9000	77.5000	0.0827	12.9900	10.0754	0.8439	0.1561	0.0494	0.0171
2142	Air	0.0	21.5000	71.0000	0.0827	12.9900	12.8794	0.7792	0.2208	0.0494	0.0104
2143	Air	0.0	21.9000	72.0000	0.0827	12.9900	14.4861	0.7578	0.2422	0.0494	0.0079
2145	Air	0.0	21.4000	71.0000	0.0827	12.9900	10.0754	0.7676	0.2324	0.0494	0.0035
2146	Air	0.0	28.5000	49.0000	0.0827	12.9900	55.2450	0.3757	0.6243	1.8667	0.0056
2147	Air	0.0	28.7000	51.0000	0.0827	12.9900	49.2314	0.5358	0.4642	1.6000	0.0096
2148	Air	0.0	28.1000	52.0000	0.0827	12.9900	44.9298	0.6052	0.3948	1.3333	0.0132
2149	Air	0.0	29.2000	54.5000	0.0827	12.9900	46.9142	0.6156	0.3844	1.3333	0.0180
3001	Air	16.0	25.3000	65.0000	0.0827	12.9900	77.1516	0.0549	0.9451	2.1720	0.0003
3002	Air	16.0	25.0000	68.0000	0.0827	12.9900	72.8245	0.0532	0.9468	1.6290	0.0002
3003	Air	16.0	25.9000	69.5000	0.0827	12.9900	71.5678	0.0451	0.9549	1.3575	0.0002
3004	Air	16.0	24.9000	70.5000	0.0827	12.9900	76.9348	0.0503	0.9497	2.1177	0.0003
3005	Air	16.0	25.9000	71.0000	0.0827	12.9900	75.0015	0.0861	0.9139	2.1177	0.0005
3006	Air	16.0	26.1000	71.5000	0.0827	12.9900	72.4133	0.1497	0.8503	2.0091	0.0010
3007	Air	16.0	25.1000	73.5000	0.0827	12.9900	76.9348	0.0428	0.9572	2.1177	0.0003
3008	Air	16.0	23.9000	73.5000	0.0827	12.9900	74.5894	0.0555	0.9445	1.9014	0.0003
3009	Air	16.0	24.2000	73.5000	0.0827	12.9900	73.5150	0.0705	0.9295	1.9014	0.0004
3010	Air	16.0	24.5000	73.5000	0.0827	12.9900	71.7894	0.1110	0.8890	1.9014	0.0006
3011	Air	16.0	23.7000	74.0000	0.0827	12.9900	73.0392	0.0468	0.9532	1.6290	0.0002
3012	Air	16.0	24.7000	75.0000	0.0827	12.9900	70.8853	0.0867	0.9133	1.6290	0.0004
3014	Air	16.0	23.2000	76.0000	0.0827	12.9900	8.7375	0.9012	0.0988	0.0503	0.0481
3015	Air	16.0	21.9000	76.0000	0.0827	12.9900	8.3049	0.9254	0.0746	0.0503	0.0419
3016	Air	16.0	25.2000	76.0000	0.0827	12.9900	67.0357	0.0861	0.9139	1.0860	0.0003
3017	Air	16.0	25.4000	71.5000	0.0827	12.9900	60.5716	0.1960	0.8040	1.0860	0.0006
3018	Air	16.0	25.4000	71.5000	0.0827	12.9900	57.1281	0.2410	0.7590	1.0860	0.0011
3019	Air	16.0	25.8000	73.0000	0.0827	12.9900	48.0863	0.3913	0.6087	1.0860	0.0028
3020	Air	16.0	25.5000	73.0000	0.0827	12.9900	39.9037	0.5601	0.4399	1.0860	0.0063
3021	Air	16.0	26.6000	73.5000	0.0827	12.9900	39.4741	0.6069	0.3931	1.0860	0.0086
3022	Air	16.0	28.2000	73.5000	0.0827	12.9900	42.0584	0.6994	0.3006	1.0860	0.0174
3023	Air	16.0	23.2000	74.0000	0.0827	12.9900	25.7121	0.5746	0.4254	0.3518	0.0021
3024	Air	16.0	23.0000	75.0000	0.0827	12.9900	18.3835	0.6994	0.3006	0.3518	0.0071
3025	Air	16.0	22.9000	75.5000	0.0827	12.9900	20.5398	0.7358	0.2642	0.3518	0.0138
3026	Air	16.0	24.1000	75.5000	0.0827	12.9900	21.3996	0.7850	0.2150	0.3518	0.0249

Run Number	Vapor	% Glycerol	P (psia)	T (°F)	D (ft)	H (ft)	$\Delta P/\Delta L$ (lb_f/ft^3)	Vapor Fraction, α_g	Liquid Fraction, α_f	W_L (lb_m/s)	W_G (lb_m/s)
3027	Air	16.0	24.7000	76.5000	0.0827	12.9900	23.5559	0.8191	0.1809	0.3518	0.0345
3028	Air	16.0	26.6000	76.5000	0.0827	12.9900	25.7121	0.8399	0.1601	0.3518	0.0443
3029	Air	16.0	21.7000	75.5000	0.0827	12.9900	14.0566	0.7012	0.2988	0.1508	0.0024
3030	Air	16.0	21.8000	76.0000	0.0827	12.9900	12.7681	0.7301	0.2699	0.1508	0.0052
3031	Air	16.0	22.1000	76.0000	0.0827	12.9900	15.7812	0.7512	0.2488	0.1508	0.0080
3032	Air	16.0	21.8000	76.5000	0.0827	12.9900	12.7681	0.8249	0.1751	0.1508	0.0198
3035	Air	16.0	26.2000	77.0000	0.0827	12.9900	15.5664	0.9445	0.0555	0.1508	0.0535
3036	Air	16.0	21.2000	77.0000	0.0827	12.9900	8.9538	0.7306	0.2694	0.0503	0.0022
3037	Air	16.0	21.4000	78.0000	0.0827	12.9900	12.4279	0.7514	0.2486	0.0503	0.0075
3038	Air	16.0	21.1000	78.0000	0.0827	12.9900	8.9538	0.8283	0.1717	0.0503	0.0149
3039	Air	16.0	21.9000	87.5000	0.0827	12.9900	5.0537	0.9058	0.0942	0.0503	0.0281
3040	Air	16.0	22.1000	78.5000	0.0827	12.9900	8.5212	0.9249	0.0751	0.0503	0.0414
3041	Air	16.0	25.4000	78.8000	0.0827	12.9900	9.8256	0.9387	0.0613	0.0503	0.0565
3042	Air	16.0	25.5000	78.0000	0.0827	12.9900	8.9455	0.9428	0.0572	0.0164	0.0574
3043	Air	16.0	21.9000	78.5000	0.0827	12.9900	2.4011	0.9520	0.0480	0.0182	0.0425
3044	Air	16.0	21.7000	80.0000	0.0827	12.9900	19.8732	0.9347	0.0653	0.0183	0.0312
3045	Air	16.0	20.4000	78.0000	0.0827	12.9900	5.1281	0.8682	0.1318	0.0177	0.0179
3046	Air	16.0	21.1000	80.0000	0.0827	12.9900	10.8482	0.7665	0.2335	0.0177	0.0073
3047	Air	16.0	25.1000	68.0000	0.0827	12.9900	3.2215	0.9642	0.0358	0.0127	0.0614
3048	Air	16.0	25.8000	69.5000	0.0827	12.9900	3.4058	0.9618	0.0382	0.0135	0.0617
3049	Air	16.0	25.5000	69.5000	0.0827	12.9900	50.6768	0.3353	0.6647	1.0861	0.0020
3050	Air	16.0	25.8000	70.8000	0.0827	12.9900	3.2147	0.9636	0.0364	0.0125	0.0512
3051	Air	16.0	25.8000	72.5000	0.0827	12.9900	45.5020	0.4468	0.5532	1.0860	0.0034
4001	Air	35.0	25.0000	75.0000	0.0827	12.9900	81.8218	0.0659	0.9341	1.9363	0.0003
4002	Air	35.0	26.2000	75.0000	0.0827	12.9900	69.3009	0.1676	0.8324	1.2171	0.0006
4003	Air	35.0	26.8000	76.0000	0.0827	12.9900	78.8291	0.0763	0.9237	1.6597	0.0003
4004	Air	35.0	25.6000	73.0000	0.0827	12.9900	85.6335	0.0434	0.9566	2.1576	0.0002
4005	Air	35.0	26.8000	73.5000	0.0827	12.9900	82.5858	0.0879	0.9121	2.1576	0.0006
4006	Air	35.0	27.3000	73.5000	0.0827	12.9900	82.5858	0.1191	0.8809	2.1576	0.0009
4007	Air	35.0	26.0000	73.5000	0.0827	12.9900	73.2039	0.1035	0.8965	1.1065	0.0003
4008	Air	35.0	25.8000	74.0000	0.0827	12.9900	67.1160	0.1260	0.8740	1.1065	0.0006
4009	Air	35.0	25.4000	74.0000	0.0827	12.9900	61.0214	0.2543	0.7457	1.1065	0.0013
4010	Air	35.0	26.4000	74.8000	0.0827	12.9900	50.2469	0.4087	0.5913	1.1065	0.0030
4011	Air	35.0	26.2000	75.0000	0.0827	12.9900	43.2204	0.5399	0.4601	1.1065	0.0058
4012	Air	35.0	26.6000	75.0000	0.0827	12.9900	41.3430	0.5948	0.4052	1.1065	0.0084
4013	Air	35.0	28.0000	76.8000	0.0827	12.9900	43.6897	0.6908	0.3092	1.1065	0.0154
4014	Air	35.0	27.2000	76.0000	0.0827	12.9900	24.9610	0.8387	0.1613	0.3584	0.0453
4015	Air	35.0	25.0000	76.5000	0.0827	12.9900	23.5523	0.8428	0.1572	0.3584	0.0377
4016	Air	35.0	24.0000	76.5000	0.0827	12.9900	20.7418	0.7861	0.2139	0.3584	0.0242
4017	Air	35.0	23.4000	76.5000	0.0827	12.9900	20.2723	0.7520	0.2480	0.3584	0.0149
4018	Air	35.0	23.2000	76.5000	0.0827	12.9900	18.8636	0.7324	0.2676	0.3584	0.0086
4019	Air	35.0	23.1000	76.0000	0.0827	12.9900	18.8636	0.6844	0.3156	0.3584	0.0057
4020	Air	35.0	23.3000	75.5000	0.0827	12.9900	22.6132	0.6329	0.3671	0.3584	0.0028
4024	Air	35.0	22.0000	78.0000	0.0827	12.9900	12.8137	0.7769	0.2231	0.1536	0.0132

Run Number	Vapor	% Glycerol	P (psia)	T (°F)	D (ft)	H (ft)	$\Delta P/\Delta L$ (lb_f/ft^3)	Vapor Fraction, α_g	Liquid Fraction, α_f	W_L (lb_m/s)	W_G (lb_m/s)
4025	Air	35.0	22.1000	78.0000	0.0827	12.9900	14.2199	0.7422	0.2578	0.1536	0.0074
4026	Air	35.0	22.0000	75.5000	0.0827	12.9900	12.8137	0.7353	0.2647	0.1536	0.0052
4027	Air	35.0	21.9000	75.5000	0.0827	12.9900	14.2199	0.7064	0.2936	0.1536	0.0021
4028	Air	35.0	21.9000	75.5000	0.0827	12.9900	11.8716	0.6925	0.3075	0.0512	0.0014
4030	Air	35.0	21.8000	79.8000	0.0827	12.9900	10.4585	0.7618	0.2382	0.0512	0.0078
4031	Air	35.0	21.8000	79.5000	0.0827	12.9900	6.4649	0.8179	0.1821	0.0512	0.0152
4032	Air	35.0	22.2000	77.5000	0.0827	12.9900	2.7921	0.9017	0.0983	0.0512	0.0301
4033	Air	35.0	22.1000	77.0000	0.0827	12.9900	3.6454	0.9237	0.0763	0.0512	0.0413
4034	Air	35.0	26.0000	79.0000	0.0827	12.9900	5.5228	0.9410	0.0590	0.0512	0.0587
4035	Air	35.0	25.1000	76.5000	0.0827	12.9900	0.5977	0.9514	0.0486	0.0185	0.0573
4036	Air	35.0	20.6000	81.0000	0.0827	12.9900	0.3545	0.9358	0.0642	0.0185	0.0404
4037	Air	35.0	20.4000	75.5000	0.0827	12.9900	0.1182	0.9208	0.0792	0.0185	0.0314
4038	Air	35.0	20.8000	76.0000	0.0827	12.9900	5.3863	0.8214	0.1786	0.0185	0.0140
4039	Air	35.0	21.7000	76.5000	0.0827	12.9900	9.6953	0.7590	0.2410	0.0185	0.0075
4040	Air	35.0	20.7000	82.0000	0.0827	12.9900	6.8180	0.7445	0.2555	0.0185	0.0030
5001	Air	56.0	25.1000	73.5000	0.0827	12.9900	93.5995	0.0474	0.9526	1.9583	0.0002
5002	Air	56.0	25.4000	74.0000	0.0827	12.9900	90.8768	0.0827	0.9173	1.9420	0.0004
5003	Air	56.0	26.0000	75.0000	0.0827	12.9900	87.9442	0.1145	0.8855	1.9188	0.0007
5004	Air	56.0	27.5000	76.5000	0.0827	12.9900	81.0465	0.1757	0.8243	1.9188	0.0013
5005	Air	56.0	27.9000	75.5000	0.0827	12.9900	72.7873	0.2676	0.7324	1.7495	0.0025
5006	Air	56.0	22.8000	75.5000	0.0827	12.9900	79.9411	0.1145	0.8855	1.1513	0.0003
5007	Air	56.0	22.5000	77.0000	0.0827	12.9900	76.3554	0.1503	0.8497	1.1287	0.0006
5008	Air	56.0	24.2000	77.0000	0.0827	12.9900	67.1238	0.2416	0.7584	1.1287	0.0011
5009	Air	56.0	26.9000	77.5000	0.0827	12.9900	53.7931	0.4179	0.5821	1.1287	0.0032
5010	Air	56.0	26.7000	78.0000	0.0827	12.9900	44.5686	0.5428	0.4572	1.1287	0.0066
5011	Air	56.0	26.9000	77.8000	0.0827	12.9900	44.0553	0.6353	0.3647	1.1287	0.0084
5012	Air	56.0	27.8000	76.5000	0.0827	12.9900	45.5880	0.6243	0.3757	1.1287	0.0124
5013	Air	56.0	28.7000	76.0000	0.0827	12.9900	47.1278	0.6746	0.3254	1.1287	0.0189
5014	Air	56.0	22.3000	76.3000	0.0827	12.9900	24.0373	0.8318	0.1682	0.3656	0.0461
5015	Air	56.0	24.9000	77.0000	0.0827	12.9900	22.4990	0.8046	0.1954	0.3656	0.0366
5016	Air	56.0	23.9000	77.8000	0.0827	12.9900	20.1914	0.7769	0.2231	0.3656	0.0258
5017	Air	56.0	23.5000	77.8000	0.0827	12.9900	19.9350	0.7364	0.2636	0.3656	0.0150
5018	Air	56.0	23.1000	77.8000	0.0827	12.9900	18.4037	0.6815	0.3185	0.3656	0.0077
5019	Air	56.0	23.1000	80.0000	0.0827	12.9900	17.8909	0.6676	0.3324	0.3656	0.0056
5020	Air	56.0	23.3000	78.5000	0.0827	12.9900	21.9862	0.6046	0.3954	0.3656	0.0032
5021	Air	56.0	24.1000	78.5000	0.0827	12.9900	29.4462	0.5231	0.4769	0.3541	0.0019
5024	Air	56.0	22.3000	79.3000	0.0827	12.9900	9.1805	0.7775	0.2225	0.1567	0.0301
5026	Air	56.0	22.2000	78.8000	0.0827	12.9900	11.7445	0.7439	0.2561	0.1567	0.0082
5027	Air	56.0	22.2000	78.5000	0.0827	12.9900	10.7189	0.7964	0.2036	0.1567	0.0055
5028	Air	56.0	22.3000	78.8000	0.0827	12.9900	13.2829	0.6121	0.3879	0.1567	0.0027
5029	Air	56.0	26.7000	79.0000	0.0827	12.9900	3.8033	0.9173	0.0827	0.0522	0.0597
5031	Air	56.0	21.2000	79.5000	0.0827	12.9900	0.4701	0.8757	0.1243	0.0522	0.0316
5032	Air	56.0	21.2000	79.0000	0.0827	12.9900	4.0597	0.7844	0.2156	0.0522	0.0149
5033	Air	56.0	21.6000	79.0000	0.0827	12.9900	7.1294	0.7306	0.2694	0.0522	0.0080

Run Number	Vapor	% Glycerol	P (psia)	T (°F)	D (ft)	H (ft)	$\Delta P/\Delta L$ (lb_f/ft^3)	Vapor Fraction, α_g	Liquid Fraction, α_f	W_L (lb_m/s)	W_G (lb_m/s)
5034	Air	56.0	21.7000	79.5000	0.0827	12.9900	6.6166	0.7116	0.2884	0.0522	0.0053
5036	Air	56.0	27.6000	78.0000	0.0827	12.9900	3.3381	0.9335	0.0665	0.0277	0.0642
5037	Air	56.0	22.1000	78.0000	0.0827	12.9900	0.2106	0.9139	0.0861	0.0281	0.0438
5039	Air	56.0	21.2000	78.3000	0.0827	12.9900	5.4488	0.7803	0.2197	0.0279	0.0128
5040	Air	56.0	21.3000	78.0000	0.0827	12.9900	6.3310	0.7474	0.2526	0.0284	0.0079
5041	Air	56.0	21.4000	79.3000	0.0827	12.9900	5.1060	0.7283	0.2717	0.0274	0.0045
5042	Air	56.0	25.4000	74.8000	0.0827	12.9900	93.0432	0.0543	0.9457	1.9752	0.0002
5043	Air	56.0	23.7000	76.0000	0.0827	12.9900	82.0470	0.0994	0.9006	1.3827	0.0004
5044	Air	56.0	24.6000	77.0000	0.0827	12.9900	86.6380	0.1081	0.8919	1.6366	0.0004
5045	Air	56.0	25.4000	77.0000	0.0827	12.9900	92.7865	0.0561	0.9439	1.9752	0.0002
5046	Air	56.0	23.6000	77.0000	0.0827	12.9900	81.5164	0.1225	0.8775	1.3657	0.0004
6001	Air	60.5	25.6000	75.5000	0.0827	12.9900	95.2537	0.0566	0.9434	1.9839	0.0003
6002	Air	60.5	26.0000	77.0000	0.0827	12.9900	92.9292	0.0884	0.9116	1.9725	0.0005
6003	Air	60.5	24.5000	77.5000	0.0827	12.9900	80.6054	0.1607	0.8393	1.4170	0.0007
6005	Air	60.5	26.7000	75.0000	0.0827	12.9900	100.5285	0.0393	0.9607	2.2106	0.0002
6006	Air	60.5	26.4000	75.5000	0.0827	12.9900	92.4249	0.0948	0.9052	1.9272	0.0005
6008	Air	60.5	27.9000	76.5000	0.0827	12.9900	89.5271	0.1514	0.8486	1.9725	0.0011
6009	Air	60.5	28.5000	77.5000	0.0827	12.9900	88.7331	0.2075	0.7925	1.9555	0.0018
6010	Air	60.5	23.2000	77.5000	0.0827	12.9900	82.6949	0.0231	0.9769	1.1336	0.0002
6011	Air	60.5	24.7000	77.5000	0.0827	12.9900	68.8320	0.2358	0.7642	1.1336	0.0011
6012	Air	60.5	27.1000	77.5000	0.0827	12.9900	56.8086	0.3896	0.6104	1.1506	0.0030
6013	Air	60.5	27.0000	77.0000	0.0827	12.9900	49.2202	0.4942	0.5058	1.1506	0.0062
6014	Air	60.5	27.4000	77.3000	0.0827	12.9900	47.1225	0.5526	0.4474	1.1336	0.0087
6015	Air	60.5	28.8000	77.5000	0.0827	12.9900	49.2120	0.6572	0.3428	1.1336	0.0179
6016	Air	60.5	24.2000	76.5000	0.0827	12.9900	34.6200	0.4860	0.5140	0.3777	0.0020
6017	Air	60.5	23.6000	77.5000	0.0827	12.9900	22.5505	0.5694	0.4306	0.3714	0.0037
6018	Air	60.5	23.3000	78.0000	0.0827	12.9900	20.9519	0.6145	0.3855	0.3672	0.0055
6019	Air	60.5	23.3000	77.8000	0.0827	12.9900	19.9007	0.6532	0.3468	0.3672	0.0082
6020	Air	60.5	23.5000	78.5000	0.0827	12.9900	20.4263	0.7243	0.2757	0.3672	0.0155
6021	Air	60.5	25.2000	76.0000	0.0827	12.9900	23.0589	0.7913	0.2087	0.3651	0.0363
6022	Air	60.5	26.9000	76.0000	0.0827	12.9900	24.0740	0.8040	0.1960	0.3682	0.0439
6023	Air	60.5	22.6000	76.0000	0.0827	12.9900	23.8401	0.5884	0.4116	0.1537	0.0023
6024	Air	60.5	22.0000	78.8000	0.0827	12.9900	12.1133	0.6902	0.3098	0.1579	0.0057
6025	Air	60.5	22.3000	75.0000	0.0827	12.9900	12.0730	0.7040	0.2960	0.1574	0.0078
6027	Air	60.5	22.7000	77.0000	0.0827	12.9900	10.2325	0.8312	0.1688	0.1584	0.0354
6028	Air	60.5	25.0000	78.8000	0.0827	12.9900	11.0279	0.8613	0.1387	0.1574	0.0467
6029	Air	60.5	27.2000	77.0000	0.0827	12.9900	11.8136	0.8728	0.1272	0.1574	0.0553
6030	Air	60.5	26.7000	76.0000	0.0827	12.9900	3.9343	0.9087	0.0913	0.0525	0.0581
6031	Air	60.5	23.3000	76.3000	0.0827	12.9900	5.0212	0.8960	0.1040	0.0530	0.0459
6032	Air	60.5	22.1000	77.0000	0.0827	12.9900	1.0848	0.8653	0.1347	0.0551	0.0324
6033	Air	60.5	21.1000	76.5000	0.0827	12.9900	3.9343	0.7786	0.2214	0.0525	0.0154
6034	Air	60.5	22.0000	74.0000	0.0827	12.9900	7.8256	0.7434	0.2566	0.0525	0.0084
6035	Air	60.5	22.0000	75.8000	0.0827	12.9900	7.3106	0.7092	0.2908	0.0525	0.0056
6037	Air	60.5	26.8000	75.8000	0.0827	12.9900	0.7996	0.9491	0.0509	0.0187	0.0605

Run Number	Vapor	% Glycerol	P (psia)	T (°F)	D (ft)	H (ft)	$\Delta P/\Delta L$ (lb_f/ft^3)	Vapor Fraction, α_g	Liquid Fraction, α_f	W_L (lb_m/s)	W_G (lb_m/s)
6041	Air	60.5	21.6000	76.0000	0.0827	12.9900	4.6925	0.7457	0.2543	0.0190	0.0082
6042	Air	60.5	21.8000	76.3000	0.0827	12.9900	4.3395	0.7110	0.2890	0.0185	0.0054

Runge [84]

Run Number	Vapor	Liquid	P (psia)	T (°F)	D (ft)	H (ft)	$\Delta P/\Delta L$ (lb_f/ft^3)	Vapor Fraction, α_g	Liquid Fraction, α_f	W_L (lb_m/s)	W_G (lb_m/s)
1	Steam	Water	65.0000	297.9541	0.0874	5.1667	13.4837	0.8970	0.1030	0.3680	0.0400
3	Steam	Water	65.0000	297.9541	0.0874	5.1667	13.0247	0.9210	0.0790	0.3630	0.0480
4	Steam	Water	65.0000	297.9541	0.0874	5.1667	13.0247	0.9270	0.0730	0.3770	0.0570
5	Steam	Water	65.0000	297.9541	0.0874	5.1667	10.0410	0.8930	0.1070	0.2430	0.0390
6	Steam	Water	65.0000	297.9541	0.0874	5.1667	11.1312	0.9280	0.0720	0.2470	0.0480
8	Steam	Water	65.0000	297.9541	0.0874	5.1667	16.7542	0.8110	0.1890	0.5250	0.0290
10	Steam	Water	65.0000	297.9541	0.0874	5.1667	17.7870	0.8600	0.1400	0.5110	0.0390
11	Steam	Water	65.0000	297.9541	0.0874	5.1667	18.2460	0.8870	0.1130	0.5190	0.0480
13	Steam	Water	65.0000	297.9541	0.0874	5.1667	25.6477	0.6490	0.3510	0.7300	0.0130
14	Steam	Water	65.0000	297.9541	0.0874	5.1667	23.4673	0.7290	0.2710	0.7390	0.0210
15	Steam	Water	65.0000	297.9541	0.0874	5.1667	34.8854	0.7610	0.2390	0.7570	0.0300
16	Steam	Water	65.0000	297.9541	0.0874	5.1667	22.0903	0.8090	0.1910	0.7240	0.0390
17	Steam	Water	65.0000	297.9541	0.0874	5.1667	15.3197	0.8210	0.1790	0.3600	0.0240
18	Steam	Water	65.0000	297.9541	0.0874	5.1667	18.2460	0.7850	0.2150	0.3600	0.0140
19	Steam	Water	65.0000	297.9541	0.0874	5.1667	25.9346	0.6020	0.3980	0.3750	0.0070
20	Steam	Water	65.0000	297.9541	0.0874	5.1667	13.4263	0.8900	0.1100	0.2550	0.0340
21	Steam	Water	65.0000	297.9541	0.0874	5.1667	13.4837	0.8900	0.1100	0.3600	0.0390
22	Steam	Water	65.0000	297.9541	0.0874	5.1667	9.5246	0.8850	0.1150	0.2340	0.0320
23	Steam	Water	65.0000	297.9541	0.0874	5.1667	11.8771	0.8190	0.1810	0.2340	0.0220
24	Steam	Water	65.0000	297.9541	0.0874	5.1667	16.8689	0.7820	0.2180	0.2520	0.0110
25	Steam	Water	65.0000	297.9541	0.0874	5.1667	21.0575	0.6580	0.3420	0.2520	0.0590
27	Steam	Water	65.0000	297.9541	0.0874	5.1667	3.9590	0.9520	0.0480	0.0930	0.0200
28	Steam	Water	65.0000	297.9541	0.0874	5.1667	8.8935	0.8600	0.1400	0.0880	0.0120
30	Steam	Water	65.0000	297.9541	0.0874	5.1667	3.8443	0.9520	0.0480	0.0810	0.0200
31	Steam	Water	65.0000	297.9541	0.0874	5.1667	18.1312	0.7570	0.2430	0.5160	0.0230
32	Steam	Water	65.0000	297.9541	0.0874	5.1667	20.7706	0.7180	0.2820	0.5270	0.0170
33	Steam	Water	65.0000	297.9541	0.0874	5.1667	21.0001	0.7300	0.2700	0.5190	0.0160
34	Steam	Water	65.0000	297.9541	0.0874	5.1667	23.4673	0.6980	0.3020	0.5210	0.0990
35	Steam	Water	65.0000	297.9541	0.0874	5.1667	25.0165	0.6660	0.3340	0.7190	0.0230
36	Steam	Water	135.0000	350.2133	0.0874	5.1667	13.6743	0.7900	0.2100	0.1190	0.0160
37	Steam	Water	135.0000	350.2133	0.0874	5.1667	13.0628	0.7610	0.2390	0.1050	0.0160
38	Steam	Water	135.0000	350.2133	0.0874	5.1667	12.5625	0.7970	0.2030	0.1050	0.0160
39	Steam	Water	135.0000	350.2133	0.0874	5.1667	11.7287	0.8100	0.1900	0.1450	0.0190
40	Steam	Water	135.0000	350.2133	0.0874	5.1667	13.4519	0.7300	0.2700	0.1780	0.0160
41	Steam	Water	135.0000	350.2133	0.0874	5.1667	14.5637	0.7340	0.2660	0.1870	0.0170
42	Steam	Water	135.0000	350.2133	0.0874	5.1667	16.3424	0.6900	0.3100	0.3050	0.0170
43	Steam	Water	135.0000	350.2133	0.0874	5.1667	19.0662	0.6340	0.3660	0.4300	0.0150
44	Steam	Water	135.0000	350.2133	0.0874	5.1667	20.6226	0.6580	0.3420	0.5040	0.0250
45	Steam	Water	135.0000	350.2133	0.0874	5.1667	18.5659	0.7170	0.2830	0.3670	0.0250
46	Steam	Water	135.0000	350.2133	0.0874	5.1667	15.5086	0.7850	0.2150	0.2410	0.0240
47	Steam	Water	135.0000	350.2133	0.0874	5.1667	11.7843	0.8370	0.1630	0.2180	0.0270
48	Steam	Water	135.0000	350.2133	0.0874	5.1667	10.0612	0.8210	0.1790	0.1450	0.0240

Run Number	Vapor	Liquid	P (psia)	T (°F)	D (ft)	H (ft)	$\Delta P/\Delta L$ (lb_f/ft^3)	Vapor Fraction, α_g	Liquid Fraction, α_f	W_L (lb_m/s)	W_G (lb_m/s)
49	Steam	Water	135.0000	350.2133	0.0874	5.1667	10.5614	0.8130	0.1870	0.1630	0.0270
50	Steam	Water	135.0000	350.2133	0.0874	5.1667	8.8382	0.8690	0.1310	0.3200	0.0260
51	Steam	Water	135.0000	350.2133	0.0874	5.1667	7.3374	0.8530	0.1470	0.3200	0.0240
52	Steam	Water	135.0000	350.2133	0.0874	5.1667	8.0600	0.8610	0.1390	0.3200	0.0260
53	Steam	Water	135.0000	350.2133	0.0874	5.1667	6.3369	0.8810	0.1190	0.1050	0.0300
55	Steam	Water	135.0000	350.2133	0.0874	5.1667	6.8927	0.8630	0.1370	0.1450	0.0280
56	Steam	Water	135.0000	350.2133	0.0874	5.1667	8.7271	0.8400	0.1600	0.1050	0.0059
57	Steam	Water	135.0000	350.2133	0.0874	5.1667	8.0600	0.8570	0.1430	0.0740	0.0170
58	Steam	Water	135.0000	350.2133	0.0874	5.1667	14.5637	0.7460	0.2540	0.2280	0.0180
59	Steam	Water	135.0000	350.2133	0.0874	5.1667	13.5075	0.8090	0.1910	0.2030	0.0200
60	Steam	Water	135.0000	350.2133	0.0874	5.1667	15.3975	0.7380	0.2620	0.2820	0.0190
61	Steam	Water	135.0000	350.2133	0.0874	5.1667	17.0650	0.7780	0.2220	0.3980	0.0200
62	Steam	Water	135.0000	350.2133	0.0874	5.1667	16.7871	0.7460	0.2540	0.3920	0.0190
63	Steam	Water	135.0000	350.2133	0.0874	5.1667	20.0111	0.7060	0.2940	0.5340	0.0190
64	Steam	Water	135.0000	350.2133	0.0874	5.1667	19.6220	0.6590	0.3410	0.5340	0.0190
65	Steam	Water	135.0000	350.2133	0.0874	5.1667	22.7905	0.6900	0.3100	0.5120	0.0180
66	Steam	Water	135.0000	350.2133	0.0874	5.1667	26.1812	0.6420	0.3580	0.5940	0.0180
67	Steam	Water	135.0000	350.2133	0.0874	5.1667	42.3013	0.6580	0.3420	0.7580	0.0190
68	Steam	Water	135.0000	350.2133	0.0874	5.1667	15.2307	0.7840	0.2160	0.1970	0.0190
70	Steam	Water	135.0000	350.2133	0.0874	5.1667	12.0067	0.8290	0.1710	0.1970	0.0280
71	Steam	Water	135.0000	350.2133	0.0874	5.1667	10.2279	0.8970	0.1030	0.1970	0.0430
73	Steam	Water	135.0000	350.2133	0.0874	5.1667	15.2307	0.8270	0.1730	0.4420	0.0470
74	Steam	Water	135.0000	350.2133	0.0874	5.1667	14.6748	0.8450	0.1550	0.4500	0.0530
75	Steam	Water	135.0000	350.2133	0.0874	5.1667	12.5625	0.8840	0.1160	0.3130	0.0600
76	Steam	Water	135.0000	350.2133	0.0874	5.1667	11.7843	0.8970	0.1030	0.3100	0.0640
77	Steam	Water	135.0000	350.2133	0.0874	5.1667	13.2852	0.8820	0.1180	0.3320	0.0500
78	Steam	Water	135.0000	350.2133	0.0874	5.1667	15.1195	0.8080	0.1920	0.4760	0.0430
79	Steam	Water	135.0000	350.2133	0.0874	5.1667	25.8477	0.6020	0.3980	0.6500	0.0140
80	Steam	Water	135.0000	350.2133	0.0874	5.1667	18.0100	0.8250	0.1750	0.6480	0.0440
81	Steam	Water	135.0000	350.2133	0.0874	5.1667	17.7321	0.8040	0.1960	0.6470	0.0560
82	Steam	Water	135.0000	350.2133	0.0874	5.1667	18.3435	0.8160	0.1840	0.6590	0.0510
83	Steam	Water	135.0000	350.2133	0.0874	5.1667	14.0078	0.8760	0.1240	0.3520	0.0680
84	Steam	Water	135.0000	350.2133	0.0874	5.1667	17.7321	0.8200	0.1800	0.6800	0.0480
85	Steam	Water	135.0000	350.2133	0.0874	5.1667	13.6187	0.7780	0.2220	0.2350	0.0230
86	Steam	Water	135.0000	350.2133	0.0874	5.1667	29.5720	0.5000	0.5000	0.2310	0.0040
87	Steam	Water	135.0000	350.2133	0.0874	5.1667	10.6726	0.8690	0.1310	0.2260	0.0390
88	Steam	Water	135.0000	350.2133	0.0874	5.1667	9.2829	0.9060	0.0940	0.2260	0.0560
90	Steam	Water	135.0000	350.2133	0.0874	5.1667	9.2829	0.9160	0.0840	0.1430	0.0570
92	Steam	Water	135.0000	350.2133	0.0874	5.1667	8.6715	0.8490	0.1510	0.1130	0.0220
93	Steam	Water	135.0000	350.2133	0.0874	5.1667	12.1734	0.8030	0.1970	0.1030	0.0130
94	Steam	Water	135.0000	350.2133	0.0874	5.1667	21.4008	0.6410	0.3590	0.1130	0.0040
96	Steam	Water	135.0000	350.2133	0.0874	5.1667	4.5581	0.9360	0.0640	0.1130	0.0330
97	Steam	Water	135.0000	350.2133	0.0874	5.1667	22.4013	0.6660	0.3340	0.5120	0.0180
98	Steam	Water	135.0000	350.2133	0.0874	5.1667	19.6220	0.7850	0.2150	0.5090	0.0310

Run Number	Vapor	Liquid	P (psia)	T (°F)	D (ft)	H (ft)	$\Delta P/\Delta L$ (lb_f/ft^3)	Vapor Fraction, α_g	Liquid Fraction, α_f	W_L (lb_m/s)	W_G (lb_m/s)
99	Steam	Water	135.0000	350.2133	0.0874	5.1667	15.6754	0.8010	0.1990	0.4980	0.0440
100	Steam	Water	135.0000	350.2133	0.0874	5.1667	15.8421	0.8310	0.1690	0.4600	0.0580
101	Steam	Water	135.0000	350.2133	0.0874	5.1667	19.9555	0.8160	0.1840	0.6890	0.0610
107	Steam	Water	215.0000	387.9092	0.0874	5.1667	19.2751	0.7480	0.2520	0.5830	0.0440
108	Steam	Water	215.0000	387.9092	0.0874	5.1667	22.0906	0.6960	0.3040	0.5820	0.0320
109	Steam	Water	215.0000	387.9092	0.0874	5.1667	25.7724	0.6010	0.3990	0.5860	0.0160
110	Steam	Water	215.0000	387.9092	0.0874	5.1667	20.9536	0.7500	0.2500	0.5840	0.0360
111	Steam	Water	215.0000	387.9092	0.0874	5.1667	18.1923	0.7870	0.2130	0.5830	0.0500
112	Steam	Water	215.0000	387.9092	0.0874	5.1667	16.4055	0.8100	0.1900	0.5830	0.0620
113	Steam	Water	215.0000	387.9092	0.0874	5.1667	17.0011	0.8230	0.1770	0.5720	0.0690
114	Steam	Water	215.0000	387.9092	0.0874	5.1667	22.0365	0.7220	0.2780	0.6520	0.0350
115	Steam	Water	215.0000	387.9092	0.0874	5.1667	27.3967	0.6360	0.3640	0.6590	0.0140
116	Steam	Water	215.0000	387.9092	0.0874	5.1667	18.1381	0.7760	0.2240	0.6610	0.0510
117	Steam	Water	215.0000	387.9092	0.0874	5.1667	17.3260	0.8000	0.2000	0.6640	0.0620
118	Steam	Water	215.0000	387.9092	0.0874	5.1667	23.4442	0.6950	0.3050	0.8150	0.0410
119	Steam	Water	215.0000	387.9092	0.0874	5.1667	19.3293	0.7610	0.2390	0.8030	0.0580
120	Steam	Water	215.0000	387.9092	0.0874	5.1667	18.7337	0.7690	0.2310	0.7400	0.0690
121	Steam	Water	215.0000	387.9092	0.0874	5.1667	15.4851	0.8280	0.1720	0.4790	0.0750
122	Steam	Water	215.0000	387.9092	0.0874	5.1667	14.9436	0.8210	0.1790	0.4820	0.0670
123	Steam	Water	215.0000	387.9092	0.0874	5.1667	16.0807	0.8140	0.1860	0.4870	0.0580
124	Steam	Water	215.0000	387.9092	0.0874	5.1667	11.8575	0.8090	0.1910	0.2190	0.0350
125	Steam	Water	215.0000	387.9092	0.0874	5.1667	18.8420	0.6980	0.3020	0.2190	0.0180
126	Steam	Water	215.0000	387.9092	0.0874	5.1667	23.4442	0.6500	0.3500	0.2160	0.0120
127	Steam	Water	215.0000	387.9092	0.0874	5.1667	10.5039	0.8810	0.1190	0.2140	0.0540
128	Steam	Water	215.0000	387.9092	0.0874	5.1667	9.7459	0.9010	0.0990	0.2140	0.0670
129	Steam	Water	215.0000	387.9092	0.0874	5.1667	9.0420	0.9250	0.0750	0.2140	0.0800
133	Steam	Water	215.0000	387.9092	0.0874	5.1667	10.2873	0.8210	0.1790	0.1020	0.0170
134	Steam	Water	215.0000	387.9092	0.0874	5.1667	12.9403	0.7780	0.2220	0.1020	0.0130
135	Steam	Water	215.0000	387.9092	0.0874	5.1667	24.2022	0.5400	0.4600	0.3980	0.0110
136	Steam	Water	215.0000	387.9092	0.0874	5.1667	17.3260	0.7730	0.2270	0.4150	0.0370
137	Steam	Water	215.0000	387.9092	0.0874	5.1667	14.9978	0.7930	0.2070	0.4130	0.0520
138	Steam	Water	215.0000	387.9092	0.0874	5.1667	12.9945	0.8470	0.1530	0.4150	0.0700
139	Steam	Water	215.0000	387.9092	0.0874	5.1667	13.8066	0.8550	0.1450	0.4170	0.0820
140	Steam	Water	215.0000	387.9092	0.0874	5.1667	16.9470	0.7850	0.2150	0.4870	0.0490
141	Steam	Water	215.0000	387.9092	0.0874	5.1667	34.0563	0.4990	0.5010	0.7320	0.0140
142	Steam	Water	215.0000	387.9092	0.0874	5.1667	26.9635	0.6510	0.3490	0.7260	0.0310
143	Steam	Water	215.0000	387.9092	0.0874	5.1667	23.1735	0.6980	0.3020	0.7920	0.0410
144	Steam	Water	215.0000	387.9092	0.0874	5.1667	19.3834	0.7300	0.2700	0.7760	0.0550
145	Steam	Water	215.0000	387.9092	0.0874	5.1667	18.8420	0.7610	0.2390	0.7190	0.0630
146	Steam	Water	215.0000	387.9092	0.0874	5.1667	24.0939	0.6580	0.3420	0.5910	0.0200
147	Steam	Water	215.0000	387.9092	0.0874	5.1667	16.0807	0.7530	0.2470	0.3280	0.0360
148	Steam	Water	215.0000	387.9092	0.0874	5.1667	12.5613	0.8550	0.1450	0.2860	0.0600
149	Steam	Water	215.0000	387.9092	0.0874	5.1667	15.2144	0.8000	0.2000	0.4020	0.0500
153	Steam	Water	215.0000	387.9092	0.0874	5.1667	9.8000	0.9510	0.0490	0.0600	0.0200

Run Number	Vapor	Liquid	P (psia)	T (°F)	D (ft)	H (ft)	$\Delta P/\Delta L$ (lb_f/ft^3)	Vapor Fraction, α_g	Liquid Fraction, α_f	W_L (lb_m/s)	W_G (lb_m/s)
154	Steam	Water	215.0000	387.9092	0.0874	5.1667	6.7680	0.9280	0.0720	0.0730	0.0300
157	Steam	Water	215.0000	387.9092	0.0874	5.1667	15.3768	0.8420	0.1580	0.0980	0.0180
158	Steam	Water	215.0000	387.9092	0.0874	5.1667	10.5039	0.9000	0.1000	0.0980	0.0300
159	Steam	Water	215.0000	387.9092	0.0874	5.1667	8.2298	0.9310	0.0690	0.0980	0.0380
160	Steam	Water	215.0000	387.9092	0.0874	5.1667	7.3635	0.9470	0.0530	0.0980	0.0430
161	Steam	Water	215.0000	387.9092	0.0874	5.1667	7.0928	0.9630	0.0370	0.0980	0.0520
162	Steam	Water	215.0000	387.9092	0.0874	5.1667	7.3635	0.9270	0.0730	0.0980	0.0580
163	Steam	Water	215.0000	387.9092	0.0874	5.1667	16.7845	0.7540	0.2460	0.1510	0.0200
164	Steam	Water	215.0000	387.9092	0.0874	5.1667	12.6155	0.8160	0.1840	0.1510	0.0310
165	Steam	Water	215.0000	387.9092	0.0874	5.1667	11.3160	0.8790	0.1210	0.1510	0.0380
166	Steam	Water	215.0000	387.9092	0.0874	5.1667	10.6122	0.8890	0.1110	0.1510	0.0420
167	Steam	Water	215.0000	387.9092	0.0874	5.1667	16.4597	0.7750	0.2250	0.1640	0.0200
168	Steam	Water	215.0000	387.9092	0.0874	5.1667	13.3735	0.8610	0.1390	0.1640	0.0300
169	Steam	Water	215.0000	387.9092	0.0874	5.1667	11.3160	0.8930	0.1070	0.1640	0.0380
170	Steam	Water	215.0000	387.9092	0.0874	5.1667	10.9370	0.8210	0.1790	0.1640	0.0440
171	Steam	Water	215.0000	387.9092	0.0874	5.1667	19.5459	0.6770	0.3230	0.2070	0.0180
172	Steam	Water	215.0000	387.9092	0.0874	5.1667	14.6729	0.7360	0.2640	0.2130	0.0290
173	Steam	Water	215.0000	387.9092	0.0874	5.1667	16.8387	0.6610	0.3390	0.2310	0.0250
174	Steam	Water	215.0000	387.9092	0.0874	5.1667	14.6729	0.7080	0.2920	0.0980	0.0170
179	Steam	Water	215.0000	387.9092	0.0874	5.1667	5.9558	0.9230	0.0770	0.0980	0.0520
180	Steam	Water	215.0000	387.9092	0.0874	5.1667	5.9558	0.9200	0.0800	0.0980	0.0560
181	Steam	Water	215.0000	387.9092	0.0874	5.1667	16.8928	0.7810	0.2190	0.1800	0.0190
182	Steam	Water	215.0000	387.9092	0.0874	5.1667	14.1856	0.8840	0.1160	0.1770	0.0270
183	Steam	Water	215.0000	387.9092	0.0874	5.1667	11.9657	0.9150	0.0850	0.1740	0.0350
184	Steam	Water	215.0000	387.9092	0.0874	5.1667	11.1536	0.9490	0.0510	0.1770	0.0420
185	Steam	Water	215.0000	387.9092	0.0874	5.1667	10.9370	0.9720	0.0280	0.1770	0.0470
186	Steam	Water	215.0000	387.9092	0.0874	5.1667	19.3834	0.7760	0.2240	0.2410	0.0180
187	Steam	Water	215.0000	387.9092	0.0874	5.1667	16.2431	0.8600	0.1400	0.2360	0.0280
188	Steam	Water	215.0000	387.9092	0.0874	5.1667	14.0773	0.8970	0.1030	0.2360	0.0350
189	Steam	Water	215.0000	387.9092	0.0874	5.1667	12.9403	0.9270	0.0730	0.2290	0.0430
190	Steam	Water	215.0000	387.9092	0.0874	5.1667	20.4663	0.7530	0.2470	0.2730	0.0170
191	Steam	Water	215.0000	387.9092	0.0874	5.1667	17.7050	0.8110	0.1890	0.2750	0.0270
192	Steam	Water	215.0000	387.9092	0.0874	5.1667	16.7304	0.8210	0.1790	0.2710	0.0290

Schlegal [75]

Run Number	Vapor	Liquid	P (psia)	T (°F)	D (ft)	H (ft)	$\Delta P/\Delta L$ (lb_f/ft^3)	Vapor Fraction, α_g	Liquid Fraction, α_f	W_L (lb_m/s)	W_G (lb_m/s)
D6-0005-0015-P1-1	Air	Water	26.5985	77.0000	0.4987	3.6304	38.6593	0.3685	0.6315	2.0761	0.0127
D6-0005-0015-P1-2	Air	Water	27.7689	77.0000	0.4987	4.0992	41.9319	0.3335	0.6665	2.0761	0.0127
D6-0005-0015-P1-3	Air	Water	28.9483	77.0000	0.4987	3.6903	44.5409	0.2985	0.7015	2.0761	0.0127
D6-0005-0015-P1-4	Air	Water	29.9600	77.0000	0.4987	2.9921	45.1616	0.2810	0.7190	2.0761	0.0127
D6-0005-0015-P2-1	Air	Water	39.3932	75.2000	0.4987	3.6304	41.2481	0.3330	0.6670	1.6425	0.0209
D6-0005-0015-P2-2	Air	Water	40.5837	75.2000	0.4987	4.0992	43.0018	0.3160	0.6840	1.6425	0.0209
D6-0005-0015-P2-3	Air	Water	41.7835	75.2000	0.4987	3.6903	44.2014	0.2985	0.7015	1.6425	0.0209
D6-0005-0015-P2-4	Air	Water	42.8127	75.2000	0.4987	2.9921	44.7428	0.2870	0.7130	1.6425	0.0209
D6-0005-0030-P1-1	Air	Water	27.4103	71.6000	0.4987	3.6304	38.1991	0.3835	0.6165	2.0887	0.0291
D6-0005-0030-P1-2	Air	Water	28.5056	71.6000	0.4987	4.0992	40.4034	0.3740	0.6260	2.0887	0.0291
D6-0005-0030-P1-3	Air	Water	29.6093	71.6000	0.4987	3.6903	40.5226	0.3735	0.6265	2.0887	0.0291
D6-0005-0030-P1-4	Air	Water	30.5562	71.6000	0.4987	2.9921	47.3953	0.3760	0.6240	2.0887	0.0291
D6-0005-0030-P2-1	Air	Water	38.7260	75.2000	0.4987	3.6304	37.3937	0.4010	0.5990	1.7563	0.0434
D6-0005-0030-P2-2	Air	Water	39.7621	75.2000	0.4987	4.0992	37.7540	0.3915	0.6085	1.7563	0.0434
D6-0005-0030-P2-3	Air	Water	40.8063	75.2000	0.4987	3.6903	37.5797	0.3850	0.6150	1.7563	0.0434
D6-0005-0030-P2-4	Air	Water	41.7021	75.2000	0.4987	2.9921	37.6230	0.3860	0.6140	1.7563	0.0434
D6-0005-0050-P1-1	Air	Water	26.1141	71.6000	0.4987	3.6304	34.0570	0.4445	0.5555	2.2386	0.0520
D6-0005-0050-P1-2	Air	Water	27.0650	71.6000	0.4987	4.0992	34.9517	0.4465	0.5535	2.2386	0.0520
D6-0005-0050-P1-3	Air	Water	28.0234	71.6000	0.4987	3.6903	34.3537	0.4550	0.5450	2.2386	0.0520
D6-0005-0050-P1-4	Air	Water	28.8455	71.6000	0.4987	2.9921	34.6216	0.4645	0.5355	2.2386	0.0520
D6-0005-0050-P2-1	Air	Water	38.7758	75.2000	0.4987	3.6304	33.9995	0.4610	0.5390	2.0073	0.0697
D6-0005-0050-P2-2	Air	Water	39.7050	75.2000	0.4987	4.0992	33.1685	0.4715	0.5285	2.0074	0.0697
D6-0005-0050-P2-3	Air	Water	40.6414	75.2000	0.4987	3.6903	32.9954	0.4690	0.5310	2.0074	0.0697
D6-0005-0050-P2-4	Air	Water	41.4447	75.2000	0.4987	2.9921	32.9463	0.4550	0.5450	2.0074	0.0697
D6-0005-0090-P1-1	Air	Water	26.3007	71.6000	0.4987	3.6304	27.7289	0.5630	0.4370	2.2886	0.0904
D6-0005-0090-P1-2	Air	Water	27.0316	71.6000	0.4987	4.0992	26.3412	0.5765	0.4235	2.2886	0.0904
D6-0005-0090-P1-3	Air	Water	27.7681	71.6000	0.4987	3.6903	25.2984	0.5950	0.4050	2.2886	0.0904
D6-0005-0090-P1-4	Air	Water	28.3999	71.6000	0.4987	2.9921	25.6870	0.6045	0.3955	2.2886	0.0904
D6-0005-0090-P2-1	Air	Water	38.6756	73.4000	0.4987	3.6304	30.8354	0.5130	0.4870	2.0717	0.1140
D6-0005-0090-P2-2	Air	Water	39.5056	73.4000	0.4987	4.0992	29.2963	0.5305	0.4695	2.0717	0.1140
D6-0005-0090-P2-3	Air	Water	40.3420	73.4000	0.4987	3.6903	29.2601	0.5310	0.4690	2.0717	0.1140
D6-0005-0090-P2-4	Air	Water	41.0596	73.4000	0.4987	2.9921	29.1771	0.5210	0.4790	2.0717	0.1140
D6-0005-0150-P1-1	Air	Water	26.0662	71.6000	0.4987	3.6304	24.1621	0.6095	0.3905	2.3594	0.1444
D6-0005-0150-P1-2	Air	Water	26.6990	71.6000	0.4987	4.0992	22.6218	0.6320	0.3680	2.3594	0.1444
D6-0005-0150-P1-3	Air	Water	27.3367	71.6000	0.4987	3.6903	21.3366	0.6510	0.3490	2.3594	0.1444
D6-0005-0150-P1-4	Air	Water	27.8838	71.6000	0.4987	2.9921	21.0103	0.6670	0.3330	2.3594	0.1444
D6-0005-0150-P2-1	Air	Water	38.4911	73.4000	0.4987	3.6304	23.1266	0.6360	0.3640	1.8330	0.1969
D6-0005-0150-P2-2	Air	Water	39.0920	73.4000	0.4987	4.0992	20.5329	0.6700	0.3300	1.8330	0.1969
D6-0005-0150-P2-3	Air	Water	39.6976	73.4000	0.4987	3.6903	19.9783	0.6840	0.3160	1.8330	0.1969
D6-0005-0150-P2-4	Air	Water	40.2171	73.4000	0.4987	2.9921	19.8934	0.6745	0.3255	1.8330	0.1969
D6-0005-0300-P1-1	Air	Water	24.3655	73.4000	0.4987	3.6304	16.5683	0.7280	0.2720	2.2561	0.2911

Run Number	Vapor	Liquid	P (psia)	T (°F)	D (ft)	H (ft)	$\Delta P/\Delta L$ (lb_f/ft^3)	Vapor Fraction, α_g	Liquid Fraction, α_f	W_L (lb_m/s)	W_G (lb_m/s)
D6-0005-0300-P1-2	Air	Water	24.7805	73.4000	0.4987	4.0992	13.6037	0.7705	0.2295	2.2561	0.2911
D6-0005-0300-P1-3	Air	Water	25.1988	73.4000	0.4987	3.6903	12.9039	0.7825	0.2175	2.2561	0.2911
D6-0005-0300-P1-4	Air	Water	25.5575	73.4000	0.4987	2.9921	13.2623	0.7840	0.2160	2.2561	0.2911
D6-0005-0300-P2-1	Air	Water	38.2739	73.4000	0.4987	3.6304	17.2586	0.7215	0.2785	1.9246	0.3682
D6-0005-0300-P2-2	Air	Water	38.7056	73.4000	0.4987	4.0992	14.5208	0.7780	0.2220	1.9246	0.3682
D6-0005-0300-P2-3	Air	Water	39.1407	73.4000	0.4987	3.6903	13.6396	0.7905	0.2095	1.9246	0.3682
D6-0005-0300-P2-4	Air	Water	39.5139	73.4000	0.4987	2.9921	13.8207	0.7745	0.2255	1.9246	0.3682
D6-0005-0500-P1-1	Air	Water	23.5500	73.4000	0.4987	3.6304	13.1741	0.8190	0.1810	2.3199	0.4344
D6-0005-0500-P1-2	Air	Water	23.8899	73.4000	0.4987	4.0992	10.9033	0.8055	0.1945	2.3199	0.4344
D6-0005-0500-P1-3	Air	Water	24.2325	73.4000	0.4987	3.6903	10.2439	0.8235	0.1765	2.3199	0.4344
D6-0005-0500-P1-4	Air	Water	24.5264	73.4000	0.4987	2.9921	11.0286	0.8385	0.1615	2.3199	0.4344
D6-0010-0015-P1-1	Air	Water	25.9717	73.4000	0.4987	3.6304	40.6728	0.3405	0.6595	3.6645	0.0142
D6-0010-0015-P1-2	Air	Water	27.1630	73.4000	0.4987	4.0992	43.0018	0.3185	0.6815	3.6645	0.0142
D6-0010-0015-P1-3	Air	Water	28.3636	73.4000	0.4987	3.6903	43.9184	0.2965	0.7035	3.6645	0.0142
D6-0010-0015-P1-4	Air	Water	29.3935	73.4000	0.4987	2.9921	45.7200	0.2775	0.7225	3.6645	0.0142
D6-0010-0015-P2-1	Air	Water	38.8238	68.0000	0.4987	3.6304	46.5983	0.2645	0.7355	4.1461	0.0234
D6-0010-0015-P2-2	Air	Water	40.0836	68.0000	0.4987	4.0992	45.3455	0.2765	0.7235	4.1461	0.0234
D6-0010-0015-P2-3	Air	Water	41.3531	68.0000	0.4987	3.6903	45.2201	0.2890	0.7110	4.1461	0.0234
D6-0010-0015-P2-4	Air	Water	42.4422	68.0000	0.4987	2.9921	44.8126	0.2910	0.7090	4.1461	0.0234
D6-0010-0030-P1-1	Air	Water	25.7626	75.2000	0.4987	3.6304	43.8369	0.3040	0.6960	4.0631	0.0278
D6-0010-0030-P1-2	Air	Water	26.9411	75.2000	0.4987	4.0992	42.7980	0.3155	0.6845	4.0631	0.0278
D6-0010-0030-P1-3	Air	Water	28.1287	75.2000	0.4987	3.6903	42.3903	0.3250	0.6750	4.0631	0.0278
D6-0010-0030-P1-4	Air	Water	29.1476	75.2000	0.4987	2.9921	41.8111	0.3295	0.6705	4.0631	0.0278
D6-0010-0030-P2-1	Air	Water	38.6666	69.8000	0.4987	3.6304	41.6508	0.3460	0.6540	4.2119	0.0401
D6-0010-0030-P2-2	Air	Water	39.7864	69.8000	0.4987	4.0992	40.1996	0.3825	0.6175	4.2119	0.0401
D6-0010-0030-P2-3	Air	Water	40.9148	69.8000	0.4987	3.6903	39.9001	0.3935	0.6065	4.2119	0.0401
D6-0010-0030-P2-4	Air	Water	41.8829	69.8000	0.4987	2.9921	39.6473	0.3680	0.6320	4.2119	0.0401
D6-0010-0050-P1-1	Air	Water	25.9094	75.2000	0.4987	3.6304	38.0840	0.3855	0.6145	4.0187	0.0485
D6-0010-0050-P1-2	Air	Water	26.9281	75.2000	0.4987	4.0992	37.9068	0.3885	0.6115	4.0187	0.0485
D6-0010-0050-P1-3	Air	Water	27.9546	75.2000	0.4987	3.6903	42.5601	0.4065	0.5935	4.0187	0.0485
D6-0010-0050-P1-4	Air	Water	28.8352	75.2000	0.4987	2.9921	33.2255	0.4145	0.5855	4.0187	0.0485
D6-0010-0050-P2-1	Air	Water	40.4629	69.8000	0.4987	3.6304	36.1856	0.4350	0.5650	4.0606	0.0712
D6-0010-0050-P2-2	Air	Water	41.4330	69.8000	0.4987	4.0992	34.4932	0.4740	0.5260	4.0606	0.0712
D6-0010-0050-P2-3	Air	Water	42.4105	69.8000	0.4987	3.6903	34.1273	0.4745	0.5255	4.0606	0.0712
D6-0010-0050-P2-4	Air	Water	43.2491	69.8000	0.4987	2.9921	34.1330	0.4490	0.5510	4.0606	0.0712
D6-0010-0090-P1-1	Air	Water	26.3801	75.2000	0.4987	3.6304	32.7914	0.4830	0.5170	3.9632	0.0904
D6-0010-0090-P1-2	Air	Water	27.2521	75.2000	0.4987	4.0992	30.8757	0.4880	0.5120	3.9632	0.0904
D6-0010-0090-P1-3	Air	Water	28.1309	75.2000	0.4987	3.6903	32.4294	0.4910	0.5090	3.9632	0.0904
D6-0010-0090-P1-4	Air	Water	28.8848	75.2000	0.4987	2.9921	27.7112	0.5040	0.4960	3.9632	0.0904
D6-0010-0090-P2-1	Air	Water	38.9876	69.8000	0.4987	3.6304	31.1806	0.5105	0.4895	4.3229	0.1270
D6-0010-0090-P2-2	Air	Water	39.8211	69.8000	0.4987	4.0992	29.3472	0.5535	0.4465	4.3229	0.1270
D6-0010-0090-P2-3	Air	Water	40.6611	69.8000	0.4987	3.6903	29.0903	0.5635	0.4365	4.3229	0.1270
D6-0010-0090-P2-4	Air	Water	41.3816	69.8000	0.4987	2.9921	29.1771	0.5375	0.4625	4.3229	0.1270
D6-0010-0150-P1-1	Air	Water	25.7268	75.2000	0.4987	3.6304	23.8744	0.6200	0.3800	4.0770	0.1572

Run Number	Vapor	Liquid	P (psia)	T (°F)	D (ft)	H (ft)	$\Delta P/\Delta L$ (lb_f/ft^3)	Vapor Fraction, α_g	Liquid Fraction, α_f	W_L (lb_m/s)	W_G (lb_m/s)
D6-0010-0150-P1-2	Air	Water	26.3565	75.2000	0.4987	4.0992	34.4422	0.6240	0.3760	4.0770	0.1572
D6-0010-0150-P1-3	Air	Water	26.9910	75.2000	0.4987	3.6903	37.5797	0.6440	0.3560	4.0770	0.1572
D6-0010-0150-P2-1	Air	Water	39.4250	69.8000	0.4987	3.6304	24.0470	0.6035	0.3965	4.3521	0.2196
D6-0010-0150-P2-2	Air	Water	40.0442	69.8000	0.4987	4.0992	21.4500	0.6865	0.3135	4.3521	0.2196
D6-0010-0150-P2-3	Air	Water	40.6682	69.8000	0.4987	3.6903	20.7707	0.7055	0.2945	4.3521	0.2196
D6-0010-0150-P2-4	Air	Water	41.2035	69.8000	0.4987	2.9921	20.6613	0.6765	0.3235	4.3521	0.2196
D6-0010-0300-P1-1	Air	Water	25.2982	73.4000	0.4987	3.6304	18.4667	0.6805	0.3195	4.3652	0.3043
D6-0010-0300-P1-2	Air	Water	25.7906	73.4000	0.4987	4.0992	23.0294	0.7210	0.2790	4.3652	0.3043
D6-0010-0300-P1-3	Air	Water	26.2868	73.4000	0.4987	3.6903	13.4132	0.7645	0.2355	4.3652	0.3043
D6-0010-0300-P1-4	Air	Water	26.7125	73.4000	0.4987	2.9921	15.1469	0.7565	0.2435	4.3652	0.3043
D6-0010-0300-P2-1	Air	Water	39.4767	71.6000	0.4987	3.6304	18.6968	0.7100	0.2900	4.4163	0.3925
D6-0010-0300-P2-2	Air	Water	39.9372	71.6000	0.4987	4.0992	15.4888	0.7815	0.2185	4.4163	0.3925
D6-0010-0300-P2-3	Air	Water	40.4013	71.6000	0.4987	3.6903	14.1490	0.8050	0.1950	4.4164	0.3925
D6-0010-0300-P2-4	Air	Water	40.7994	71.6000	0.4987	2.9921	13.8905	0.7675	0.2325	4.4164	0.3925
D6-0010-0500-P1-1	Air	Water	25.6231	73.4000	0.4987	3.6304	15.6478	0.7880	0.2120	5.1658	0.4631
D6-0010-0500-P1-2	Air	Water	26.0042	73.4000	0.4987	4.0992	12.5337	0.8065	0.1935	5.1658	0.4631
D6-0010-0500-P1-3	Air	Water	26.3884	73.4000	0.4987	3.6903	11.5456	0.8215	0.1785	5.1658	0.4631
D6-0010-0500-P1-4	Air	Water	26.7179	73.4000	0.4987	2.9921	11.3777	0.8130	0.1870	5.1658	0.4631
D6-0030-0015-P1-1	Air	Water	27.9476	73.4000	0.4987	3.6304	49.4172	0.2090	0.7910	12.1215	0.0148
D6-0030-0015-P1-2	Air	Water	29.3159	73.4000	0.4987	4.0992	49.9820	0.2055	0.7945	12.1216	0.0148
D6-0030-0015-P1-3	Air	Water	30.6948	73.4000	0.4987	3.6903	50.1439	0.2040	0.7960	12.1216	0.0148
D6-0030-0015-P1-4	Air	Water	31.8777	73.4000	0.4987	2.9921	49.6987	0.2045	0.7955	12.1217	0.0148
D6-0030-0015-P2-1	Air	Water	40.5190	71.6000	0.4987	3.6304	49.3021	0.2140	0.7860	11.9944	0.0229
D6-0030-0015-P2-2	Air	Water	41.8679	71.6000	0.4987	4.0992	49.1158	0.2170	0.7830	11.9944	0.0229
D6-0030-0015-P2-3	Air	Water	43.2272	71.6000	0.4987	3.6903	49.0686	0.2205	0.7795	11.9945	0.0229
D6-0030-0015-P2-4	Air	Water	44.3933	71.6000	0.4987	2.9921	48.5819	0.2225	0.7775	11.9945	0.0229
D6-0030-0030-P1-1	Air	Water	28.6226	75.2000	0.4987	3.6304	45.3902	0.2800	0.7200	12.0673	0.0324
D6-0030-0030-P1-2	Air	Water	29.8438	75.2000	0.4987	4.0992	44.3775	0.2915	0.7085	12.0673	0.0324
D6-0030-0030-P1-3	Air	Water	31.0746	75.2000	0.4987	3.6903	43.9184	0.2510	0.7490	12.0674	0.0324
D6-0030-0030-P1-4	Air	Water	32.1304	75.2000	0.4987	2.9921	43.4864	0.2545	0.7455	12.0674	0.0324
D6-0030-0030-P2-1	Air	Water	38.9879	71.6000	0.4987	3.6304	45.5052	0.2790	0.7210	12.8590	0.0404
D6-0030-0030-P2-2	Air	Water	40.2174	71.6000	0.4987	4.0992	44.4284	0.2900	0.7100	12.8590	0.0404
D6-0030-0030-P2-3	Air	Water	41.4563	71.6000	0.4987	3.6903	44.1448	0.2980	0.7020	12.8591	0.0404
D6-0030-0030-P2-4	Air	Water	42.5192	71.6000	0.4987	2.9921	43.7656	0.3000	0.7000	12.8591	0.0404
D6-0030-0050-P1-1	Air	Water	27.3708	75.2000	0.4987	3.6304	41.7659	0.3660	0.6340	12.8677	0.0503
D6-0030-0050-P1-2	Air	Water	28.4809	75.2000	0.4987	4.0992	39.9958	0.3535	0.6465	12.8677	0.0503
D6-0030-0050-P1-3	Air	Water	29.5995	75.2000	0.4987	3.6903	39.5605	0.3615	0.6385	12.8678	0.0503
D6-0030-0050-P1-4	Air	Water	30.5592	75.2000	0.4987	2.9921	39.2983	0.3645	0.6355	12.8678	0.0503
D6-0030-0050-P2-1	Air	Water	39.0278	71.6000	0.4987	3.6304	40.8454	0.3550	0.6450	12.2622	0.0706
D6-0030-0050-P2-2	Air	Water	40.1075	71.6000	0.4987	4.0992	38.6711	0.4065	0.5935	12.2622	0.0706
D6-0030-0050-P2-3	Air	Water	41.1956	71.6000	0.4987	3.6903	38.2588	0.4240	0.5760	12.2623	0.0706
D6-0030-0050-P2-4	Air	Water	42.1290	71.6000	0.4987	2.9921	37.9721	0.3900	0.6100	12.2623	0.0706
D6-0030-0090-P1-1	Air	Water	27.5028	75.2000	0.4987	3.6304	38.0265	0.4065	0.5935	12.9495	0.0851
D6-0030-0090-P1-2	Air	Water	28.4954	75.2000	0.4987	4.0992	35.5122	0.4205	0.5795	12.9496	0.0851

Run Number	Vapor	Liquid	P (psia)	T (°F)	D (ft)	H (ft)	$\Delta P/\Delta L$ (lb_f/ft^3)	Vapor Fraction, α_g	Liquid Fraction, α_f	W_L (lb_m/s)	W_G (lb_m/s)
D6-0030-0090-P1-3	Air	Water	29.4956	75.2000	0.4987	3.6903	34.8631	0.4295	0.5705	12.9496	0.0851
D6-0030-0090-P1-4	Air	Water	30.3537	75.2000	0.4987	2.9921	34.8310	0.4335	0.5665	12.9496	0.0851
D6-0030-0090-P2-1	Air	Water	38.9479	73.4000	0.4987	3.6304	36.0705	0.4350	0.5650	12.4536	0.1233
D6-0030-0090-P2-2	Air	Water	39.8946	73.4000	0.4987	4.0992	33.5251	0.4865	0.5135	12.4536	0.1233
D6-0030-0090-P2-3	Air	Water	40.8486	73.4000	0.4987	3.6903	33.1086	0.5010	0.4990	12.4537	0.1233
D6-0030-0090-P2-4	Air	Water	41.6671	73.4000	0.4987	2.9921	32.8765	0.4700	0.5300	12.4537	0.1233
D6-0030-0150-P1-1	Air	Water	26.6860	73.4000	0.4987	3.6304	30.4327	0.5336	0.4665	12.4240	0.1383
D6-0030-0150-P1-2	Air	Water	27.4650	73.4000	0.4987	4.0992	27.3092	0.5575	0.4425	12.4240	0.1383
D6-0030-0150-P1-3	Air	Water	28.2501	73.4000	0.4987	3.6903	26.8264	0.5730	0.4270	12.4240	0.1383
D6-0030-0150-P1-4	Air	Water	28.9236	73.4000	0.4987	2.9921	26.8736	0.5825	0.4175	12.4241	0.1383
D6-0030-0150-P2-1	Air	Water	38.5697	73.4000	0.4987	3.6304	28.0740	0.4840	0.5160	12.2205	0.2088
D6-0030-0150-P2-2	Air	Water	39.2947	73.4000	0.4987	4.0992	25.0165	0.6220	0.3780	12.2205	0.2088
D6-0030-0150-P2-3	Air	Water	40.0253	73.4000	0.4987	3.6903	24.8456	0.6400	0.3600	12.2205	0.2088
D6-0030-0150-P2-4	Air	Water	40.6521	73.4000	0.4987	2.9921	24.3607	0.6105	0.3895	12.2205	0.2088
D6-0030-0300-P1-1	Air	Water	26.3855	73.4000	0.4987	3.6304	22.1486	0.6910	0.3090	11.4277	0.2999
D6-0030-0300-P1-2	Air	Water	26.9261	73.4000	0.4987	4.0992	18.6477	0.7040	0.2960	11.4277	0.2999
D6-0030-0300-P1-3	Air	Water	27.4709	73.4000	0.4987	3.6903	17.9975	0.7245	0.2755	11.4278	0.2999
D6-0030-0300-P1-4	Air	Water	27.9383	73.4000	0.4987	2.9921	17.1014	0.7260	0.2740	11.4278	0.2999
D6-0030-0300-P2-1	Air	Water	39.3714	71.6000	0.4987	3.6304	22.7814	0.6790	0.3210	12.1706	0.3660
D6-0030-0300-P2-2	Air	Water	39.9349	71.6000	0.4987	4.0992	19.4120	0.7345	0.2655	12.1706	0.3660
D6-0030-0300-P2-3	Air	Water	40.5029	71.6000	0.4987	3.6903	18.2805	0.7530	0.2470	12.1706	0.3660
D6-0030-0300-P2-4	Air	Water	40.9901	71.6000	0.4987	2.9921	18.0088	0.7125	0.2875	12.1707	0.3660
D6-0030-0500-P1-1	Air	Water	25.7512	73.4000	0.4987	3.6304	18.3517	0.7505	0.2495	12.7667	0.5027
D6-0030-0500-P1-2	Air	Water	26.2105	73.4000	0.4987	4.0992	16.1512	0.7685	0.2315	12.7667	0.5027
D6-0030-0500-P1-3	Air	Water	26.6734	73.4000	0.4987	3.6903	14.4885	0.7895	0.2105	12.7667	0.5027
D6-0030-0500-P1-4	Air	Water	27.0705	73.4000	0.4987	2.9921	14.0999	0.7805	0.2195	12.7667	0.5027
D6-0050-0015-P1-1	Air	Water	26.5355	75.2000	0.4987	3.6304	52.8689	0.1590	0.8410	20.5874	0.0150
D6-0050-0015-P1-2	Air	Water	27.9699	75.2000	0.4987	4.0992	52.4785	0.1650	0.8350	20.5875	0.0150
D6-0050-0015-P1-3	Air	Water	29.4154	75.2000	0.4987	3.6903	52.1814	0.1715	0.8285	20.5876	0.0150
D6-0050-0015-P1-4	Air	Water	30.6555	75.2000	0.4987	2.9921	51.6532	0.1745	0.8255	20.5876	0.0150
D6-0050-0015-P2-1	Air	Water	39.8249	69.8000	0.4987	3.6304	49.8199	0.2060	0.7940	19.5962	0.0240
D6-0050-0015-P2-2	Air	Water	41.1967	69.8000	0.4987	4.0992	49.7782	0.2075	0.7925	19.5962	0.0240
D6-0050-0015-P2-3	Air	Water	42.5792	69.8000	0.4987	3.6903	49.9741	0.2080	0.7920	19.5963	0.0240
D6-0050-0015-P2-4	Air	Water	43.7651	69.8000	0.4987	2.9921	49.6289	0.2075	0.7925	19.5964	0.0240
D6-0050-0030-P1-1	Air	Water	26.7101	75.2000	0.4987	3.6304	48.0940	0.2380	0.7620	20.5305	0.0313
D6-0050-0030-P1-2	Air	Water	28.0006	75.2000	0.4987	4.0992	47.1288	0.2500	0.7500	20.5306	0.0313
D6-0050-0030-P1-3	Air	Water	29.3011	75.2000	0.4987	3.6903	46.4652	0.2615	0.7385	20.5307	0.0313
D6-0050-0030-P1-4	Air	Water	30.4168	75.2000	0.4987	2.9921	45.9294	0.2665	0.7335	20.5308	0.0313
D6-0050-0030-P2-1	Air	Water	42.3480	71.6000	0.4987	3.6304	45.7929	0.2730	0.7270	18.3012	0.0476
D6-0050-0030-P2-2	Air	Water	43.5949	71.6000	0.4987	4.0992	45.2436	0.2805	0.7195	18.3012	0.0476
D6-0050-0030-P2-3	Air	Water	44.8515	71.6000	0.4987	3.6903	44.8239	0.2870	0.7130	18.3013	0.0476
D6-0050-0030-P2-4	Air	Water	45.9295	71.6000	0.4987	2.9921	44.6032	0.2885	0.7115	18.3014	0.0476
D6-0050-0050-P1-1	Air	Water	26.1749	75.2000	0.4987	3.6304	47.1736	0.2690	0.7310	20.2087	0.0507
D6-0050-0050-P1-2	Air	Water	27.3635	75.2000	0.4987	4.0992	42.4923	0.3105	0.6895	20.2087	0.0507

Run Number	Vapor	Liquid	P (psia)	T (°F)	D (ft)	H (ft)	$\Delta P/\Delta L$ (lb_f/ft^3)	Vapor Fraction, α_g	Liquid Fraction, α_f	W_L (lb_m/s)	W_G (lb_m/s)
D6-0050-0050-P1-3	Air	Water	28.5613	75.2000	0.4987	3.6903	41.7677	0.3365	0.6635	20.2088	0.0507
D6-0050-0050-P1-4	Air	Water	29.5889	75.2000	0.4987	2.9921	41.2527	0.3420	0.6580	20.2089	0.0507
D6-0050-0050-P2-1	Air	Water	42.0962	73.4000	0.4987	3.6304	41.7659	0.3435	0.6565	18.8297	0.0807
D6-0050-0050-P2-2	Air	Water	43.2055	73.4000	0.4987	4.0992	39.8939	0.3625	0.6375	18.8298	0.0807
D6-0050-0050-P2-3	Air	Water	44.3233	73.4000	0.4987	3.6903	39.1643	0.3705	0.6295	18.8299	0.0807
D6-0050-0050-P2-4	Air	Water	45.2823	73.4000	0.4987	2.9921	38.8795	0.3585	0.6415	18.8299	0.0807
D6-0050-0090-P1-1	Air	Water	26.1693	73.4000	0.4987	3.6304	39.9825	0.3985	0.6015	20.5799	0.0889
D6-0050-0090-P1-2	Air	Water	27.2133	73.4000	0.4987	4.0992	37.6011	0.3955	0.6045	20.5799	0.0889
D6-0050-0090-P1-3	Air	Water	28.2653	73.4000	0.4987	3.6903	36.7873	0.4105	0.5895	20.5800	0.0889
D6-0050-0090-P1-4	Air	Water	29.1677	73.4000	0.4987	2.9921	36.4364	0.4110	0.5890	20.5801	0.0889
D6-0050-0090-P2-1	Air	Water	42.8846	73.4000	0.4987	3.6304	37.8539	0.3980	0.6020	18.5259	0.1394
D6-0050-0090-P2-2	Air	Water	43.8784	73.4000	0.4987	4.0992	35.3593	0.4460	0.5540	18.5260	0.1394
D6-0050-0090-P2-3	Air	Water	44.8798	73.4000	0.4987	3.6903	34.7499	0.4645	0.5355	18.5260	0.1394
D6-0050-0090-P2-4	Air	Water	45.7389	73.4000	0.4987	2.9921	34.4820	0.4295	0.5705	18.5261	0.1394
D6-0050-0150-P1-1	Air	Water	25.7170	73.4000	0.4987	3.6304	33.3092	0.5155	0.4845	21.2528	0.1383
D6-0050-0150-P1-2	Air	Water	26.5669	73.4000	0.4987	4.0992	30.0096	0.5120	0.4880	21.2528	0.1383
D6-0050-0150-P1-3	Air	Water	27.4233	73.4000	0.4987	3.6903	29.2601	0.5325	0.4675	21.2529	0.1383
D6-0050-0150-P1-4	Air	Water	28.1580	73.4000	0.4987	2.9921	29.1073	0.5395	0.4605	21.2530	0.1383
D6-0050-0150-P2-1	Air	Water	41.7875	73.4000	0.4987	3.6304	31.6408	0.5040	0.4960	19.7497	0.2086
D6-0050-0150-P2-2	Air	Water	42.6008	73.4000	0.4987	4.0992	33.6780	0.5545	0.4455	19.7498	0.2086
D6-0050-0150-P2-3	Air	Water	43.4204	73.4000	0.4987	3.6903	34.4103	0.5760	0.4240	19.7498	0.2086
D6-0050-0150-P2-4	Air	Water	44.1234	73.4000	0.4987	2.9921	15.3563	0.5480	0.4520	19.7498	0.2086
D6-0050-0300-P1-1	Air	Water	27.4877	73.4000	0.4987	3.6304	25.0250	0.6645	0.3355	20.1332	0.2844
D6-0050-0300-P1-2	Air	Water	28.1178	73.4000	0.4987	4.0992	22.4180	0.6655	0.3345	20.1332	0.2844
D6-0050-0300-P1-3	Air	Water	28.7528	73.4000	0.4987	3.6903	21.1669	0.6880	0.3120	20.1332	0.2844
D6-0050-0300-P1-4	Air	Water	29.2975	73.4000	0.4987	2.9921	20.6613	0.6780	0.3220	20.1333	0.2844
D6-0050-0500-P1-1	Air	Water	26.9536	73.4000	0.4987	3.6304	19.2721	0.7335	0.2665	20.3093	0.4564
D6-0050-0500-P1-2	Air	Water	27.4716	73.4000	0.4987	4.0992	19.0553	0.7445	0.2555	20.3094	0.4564
D6-0050-0500-P1-3	Air	Water	27.9937	73.4000	0.4987	3.6903	16.8090	0.7655	0.2345	20.3094	0.4564
D6-0050-0500-P1-4	Air	Water	28.4416	73.4000	0.4987	2.9921	16.4732	0.7545	0.2455	20.3094	0.4564
D6-0100-0015-P1-1	Air	Water	26.6537	73.4000	0.4987	3.6304	55.7454	0.1145	0.8855	41.5330	0.0149
D6-0100-0015-P1-2	Air	Water	28.1791	73.4000	0.4987	4.0992	55.9432	0.1160	0.8840	41.5332	0.0149
D6-0100-0015-P1-3	Air	Water	29.7163	73.4000	0.4987	3.6903	55.6337	0.1200	0.8800	41.5334	0.0149
D6-0100-0015-P1-4	Air	Water	31.0351	73.4000	0.4987	2.9921	55.2828	0.1215	0.8785	41.5336	0.0149
D6-0100-0015-P2-1	Air	Water	38.3172	75.2000	0.4987	3.6304	54.8824	0.1290	0.8710	41.2581	0.0236
D6-0100-0015-P2-2	Air	Water	39.8232	75.2000	0.4987	4.0992	55.0260	0.1305	0.8695	41.2583	0.0236
D6-0100-0015-P2-3	Air	Water	41.3408	75.2000	0.4987	3.6903	54.8414	0.1330	0.8670	41.2585	0.0236
D6-0100-0015-P2-4	Air	Water	42.6428	75.2000	0.4987	2.9921	54.6546	0.1325	0.8675	41.2587	0.0236
D6-0100-0030-P1-1	Air	Water	27.3498	73.4000	0.4987	3.6304	52.2361	0.1720	0.8280	41.1377	0.0295
D6-0100-0030-P1-2	Air	Water	28.7734	73.4000	0.4987	4.0992	52.2747	0.1760	0.8240	41.1379	0.0295
D6-0100-0030-P1-3	Air	Water	30.2079	73.4000	0.4987	3.6903	51.6154	0.1835	0.8165	41.1381	0.0295
D6-0100-0030-P1-4	Air	Water	31.4386	73.4000	0.4987	2.9921	51.2343	0.1870	0.8130	41.1382	0.0295
D6-0100-0030-P2-1	Air	Water	36.8745	75.2000	0.4987	3.6304	51.6033	0.1835	0.8165	43.8160	0.0430
D6-0100-0030-P2-2	Air	Water	38.2855	75.2000	0.4987	4.0992	51.6124	0.1865	0.8135	43.8162	0.0430

Run Number	Vapor	Liquid	P (psia)	T (°F)	D (ft)	H (ft)	$\Delta P/\Delta L$ (lb_f/ft^3)	Vapor Fraction, α_g	Liquid Fraction, α_f	W_L (lb_m/s)	W_G (lb_m/s)
D6-0100-0030-P2-3	Air	Water	39.7076	75.2000	0.4987	3.6903	51.2193	0.1915	0.8085	43.8164	0.0430
D6-0100-0030-P2-4	Air	Water	40.9275	75.2000	0.4987	2.9921	50.9551	0.1935	0.8065	43.8166	0.0430
D6-0100-0050-P1-1	Air	Water	27.3226	75.2000	0.4987	3.6304	48.3817	0.2370	0.7630	41.5119	0.0536
D6-0100-0050-P1-2	Air	Water	28.6326	75.2000	0.4987	4.0992	48.0459	0.2450	0.7550	41.5121	0.0536
D6-0100-0050-P1-3	Air	Water	29.9527	75.2000	0.4987	3.6903	47.0878	0.2555	0.7445	41.5123	0.0536
D6-0100-0050-P1-4	Air	Water	31.0851	75.2000	0.4987	2.9921	46.8368	0.2595	0.7405	41.5124	0.0536
D6-0100-0050-P2-1	Air	Water	38.3806	75.2000	0.4987	3.6304	47.8064	0.2470	0.7530	42.2403	0.0785
D6-0100-0050-P2-2	Air	Water	39.6789	75.2000	0.4987	4.0992	47.4345	0.2545	0.7455	42.2405	0.0785
D6-0100-0050-P2-3	Air	Water	40.9873	75.2000	0.4987	3.6903	46.7482	0.2635	0.7365	42.2406	0.0785
D6-0100-0050-P2-4	Air	Water	42.1097	75.2000	0.4987	2.9921	46.3482	0.2675	0.7325	42.2408	0.0785
D6-0100-0090-P1-1	Air	Water	27.3780	75.2000	0.4987	3.6304	45.6203	0.2845	0.7155	40.3966	0.0820
D6-0100-0090-P1-2	Air	Water	28.6051	75.2000	0.4987	4.0992	44.8870	0.2960	0.7040	40.3968	0.0820
D6-0100-0090-P1-3	Air	Water	29.8417	75.2000	0.4987	3.6903	43.8052	0.3095	0.6905	40.3970	0.0820
D6-0100-0090-P1-4	Air	Water	30.9026	75.2000	0.4987	2.9921	43.4864	0.3150	0.6850	40.3971	0.0820
D6-0100-0090-P2-1	Air	Water	39.6066	75.2000	0.4987	3.6304	44.7574	0.3015	0.6985	40.9670	0.1224
D6-0100-0090-P2-2	Air	Water	40.8069	75.2000	0.4987	4.0992	43.7151	0.3150	0.6850	40.9671	0.1224
D6-0100-0090-P2-3	Air	Water	42.0164	75.2000	0.4987	3.6903	42.7865	0.3285	0.6715	40.9673	0.1224
D6-0100-0090-P2-4	Air	Water	43.0541	75.2000	0.4987	2.9921	42.4394	0.3335	0.6665	40.9674	0.1224
D6-0100-0150-P1-1	Air	Water	27.1841	75.2000	0.4987	3.6304	38.7744	0.4010	0.5990	41.0930	0.1360
D6-0100-0150-P1-2	Air	Water	28.2024	75.2000	0.4987	4.0992	36.9388	0.4120	0.5880	41.0931	0.1360
D6-0100-0150-P1-3	Air	Water	29.2285	75.2000	0.4987	3.6903	35.6554	0.4300	0.5700	41.0933	0.1360
D6-0100-0150-P1-4	Air	Water	30.1088	75.2000	0.4987	2.9921	35.3894	0.4405	0.5595	41.0934	0.1360
D6-0100-0150-P2-1	Air	Water	40.5413	75.2000	0.4987	3.6304	37.1061	0.4275	0.5725	40.5467	0.1993
D6-0100-0150-P2-2	Air	Water	41.5269	75.2000	0.4987	4.0992	35.6141	0.4340	0.5660	40.5469	0.1993
D6-0100-0150-P2-3	Air	Water	42.5201	75.2000	0.4987	3.6903	34.2405	0.4465	0.5535	40.5470	0.1993
D6-0100-0150-P2-4	Air	Water	43.3722	75.2000	0.4987	2.9921	34.3424	0.4550	0.5450	40.5471	0.1993
D6-0100-0300-P1-1	Air	Water	27.4083	73.4000	0.4987	3.6304	28.8794	0.5550	0.4450	41.2723	0.2822
D6-0100-0300-P1-2	Air	Water	28.1842	73.4000	0.4987	4.0992	44.1737	0.5795	0.4205	41.2724	0.2822
D6-0100-0300-P1-3	Air	Water	28.9662	73.4000	0.4987	3.6903	41.9375	0.6105	0.3895	41.2725	0.2822
D6-0100-0300-P2-1	Air	Water	39.4412	77.0000	0.4987	3.6304	26.8659	0.5840	0.4160	42.3227	0.4388
D6-0100-0300-P2-2	Air	Water	40.1783	77.0000	0.4987	4.0992	27.7168	0.5795	0.4205	42.3228	0.4388
D6-0100-0300-P2-3	Air	Water	40.9210	77.0000	0.4987	3.6903	27.4490	0.6120	0.3880	42.3229	0.4388
D6-0100-0300-P2-4	Air	Water	41.5582	77.0000	0.4987	2.9921	16.6826	0.6300	0.3700	42.3230	0.4388
D6-0100-0500-P1-1	Air	Water	26.1627	75.2000	0.4987	3.6304	20.7679	0.7105	0.2895	42.5758	0.4851
D6-0100-0500-P1-2	Air	Water	26.8064	75.2000	0.4987	4.0992	24.4051	0.6875	0.3125	42.5759	0.4851
D6-0100-0500-P1-3	Air	Water	27.4550	75.2000	0.4987	3.6903	32.5992	0.7145	0.2855	42.5759	0.4851
D6-0100-0500-P1-4	Air	Water	28.0115	75.2000	0.4987	2.9921	6.4915	0.7105	0.2895	42.5760	0.4851
D8-0005-0001-P1-1	Air	Water	26.5662	77.0000	0.6660	3.4300	59.2474	0.0930	0.9070	3.4394	0.0044
D8-0005-0001-P1-2	Air	Water	28.0529	77.0000	0.6660	3.6631	58.7841	0.0685	0.9315	3.4394	0.0044
D8-0005-0001-P1-3	Air	Water	29.7420	77.0000	0.6660	4.3957	59.6299	0.0575	0.9425	3.4394	0.0044
D8-0005-0001-P1-4	Air	Water	31.2496	77.0000	0.6660	2.7972	58.4624	0.0580	0.9420	3.4394	0.0044
D8-0005-0001-P2-1	Air	Water	38.9026	73.4000	0.6660	3.4300	57.1162	0.0855	0.9145	3.3496	0.0066
D8-0005-0001-P2-2	Air	Water	40.3792	73.4000	0.6660	3.6631	56.6175	0.0860	0.9140	3.3496	0.0066

Run Number	Vapor	Liquid	P (psia)	T (°F)	D (ft)	H (ft)	$\Delta P/\Delta L$ (lb_f/ft^3)	Vapor Fraction, α_g	Liquid Fraction, α_f	W_L (lb_m/s)	W_G (lb_m/s)
D8-0005-0001-P2-3	Air	Water	42.0569	73.4000	0.6660	4.3957	57.4917	0.0875	0.9125	3.3497	0.0066
D8-0005-0001-P2-4	Air	Water	43.5543	73.4000	0.6660	2.7972	56.2224	0.1005	0.8995	3.3497	0.0066
D8-0005-0002-P1-1	Air	Water	26.4712	77.0000	0.6660	3.4300	56.3855	0.1335	0.8665	3.5101	0.0044
D8-0005-0002-P1-2	Air	Water	27.9565	77.0000	0.6660	3.6631	55.8192	0.1075	0.8925	3.5101	0.0044
D8-0005-0002-P1-3	Air	Water	29.6439	77.0000	0.6660	4.3957	56.4464	0.1110	0.8890	3.5101	0.0044
D8-0005-0002-P1-4	Air	Water	31.1501	77.0000	0.6660	2.7972	55.2518	0.1155	0.8845	3.5102	0.0044
D8-0005-0002-P2-1	Air	Water	38.6852	75.2000	0.6660	3.4300	45.6686	0.2660	0.7340	3.4778	0.0198
D8-0005-0002-P2-2	Air	Water	40.1622	75.2000	0.6660	3.6631	45.8413	0.4370	0.5630	3.4778	0.0198
D8-0005-0002-P2-3	Air	Water	41.8402	75.2000	0.6660	4.3957	46.4685	0.4375	0.5625	3.4779	0.0198
D8-0005-0002-P2-4	Air	Water	43.3380	75.2000	0.6660	2.7972	45.2467	0.2750	0.7250	3.4779	0.0198
D8-0005-0003-P1-1	Air	Water	25.8250	78.8000	0.6660	3.4300	54.3152	0.1505	0.8495	3.4939	0.0066
D8-0005-0003-P1-2	Air	Water	27.3117	78.8000	0.6660	3.6631	53.4816	0.1375	0.8625	3.4939	0.0066
D8-0005-0003-P1-3	Air	Water	29.0008	78.8000	0.6660	4.3957	53.8332	0.1555	0.8445	3.4940	0.0066
D8-0005-0003-P1-4	Air	Water	30.5084	78.8000	0.6660	2.7972	51.9666	0.1660	0.8340	3.4940	0.0066
D8-0005-0004-P1-1	Air	Water	26.0165	78.8000	0.6660	3.4300	51.0271	0.1665	0.8335	3.4939	0.0154
D8-0005-0004-P1-2	Air	Water	27.5032	78.8000	0.6660	3.6631	50.1176	0.1780	0.8220	3.4939	0.0154
D8-0005-0004-P1-3	Air	Water	29.1923	78.8000	0.6660	4.3957	50.6497	0.1955	0.8045	3.4940	0.0154
D8-0005-0004-P1-4	Air	Water	30.6999	78.8000	0.6660	2.7972	49.2786	0.1890	0.8110	3.4940	0.0154
D8-0005-0005-P1-1	Air	Water	25.5304	80.6000	0.6660	3.4300	47.9825	0.2220	0.7780	3.5055	0.0243
D8-0005-0005-P1-2	Air	Water	27.0168	80.6000	0.6660	3.6631	47.0387	0.2250	0.7750	3.5055	0.0243
D8-0005-0005-P1-3	Air	Water	28.7055	80.6000	0.6660	4.3957	47.8464	0.2295	0.7705	3.5055	0.0243
D8-0005-0005-P1-4	Air	Water	30.2127	80.6000	0.6660	2.7972	46.1427	0.2275	0.7725	3.5055	0.0243
D8-0005-0015-P1-1	Air	Water	26.0613	80.6000	0.6660	3.4300	46.3993	0.2485	0.7515	3.4722	0.0287
D8-0005-0015-P1-2	Air	Water	27.5476	80.6000	0.6660	3.6631	45.7273	0.2385	0.7615	3.4722	0.0287
D8-0005-0015-P1-3	Air	Water	29.2363	80.6000	0.6660	4.3957	45.9934	0.2480	0.7520	3.4722	0.0287
D8-0005-0015-P1-4	Air	Water	30.7436	80.6000	0.6660	2.7972	45.4707	0.2565	0.7435	3.4722	0.0287
D8-0005-0015-P2-1	Air	Water	38.7644	77.0000	0.6660	3.4300	42.2587	0.3270	0.6730	3.4936	0.0397
D8-0005-0015-P2-2	Air	Water	40.2432	77.0000	0.6660	3.6631	42.9905	0.3070	0.6930	3.4936	0.0397
D8-0005-0015-P2-3	Air	Water	41.9233	77.0000	0.6660	4.3957	44.2354	0.2980	0.7020	3.4936	0.0397
D8-0005-0015-P2-4	Air	Water	43.4229	77.0000	0.6660	2.7972	42.7081	0.2960	0.7040	3.4936	0.0397
D8-0005-0020-P2-1	Air	Water	39.2692	80.6000	0.6660	3.4300	43.2939	0.3215	0.6785	4.7767	0.0529
D8-0005-0020-P2-2	Air	Water	40.7569	80.6000	0.6660	3.6631	42.0782	0.3250	0.6750	4.7767	0.0529
D8-0005-0020-P2-3	Air	Water	42.4472	80.6000	0.6660	4.3957	42.5249	0.3115	0.6885	4.7768	0.0529
D8-0005-0020-P2-4	Air	Water	43.9560	80.6000	0.6660	2.7972	40.7669	0.3325	0.6675	4.7768	0.0529
D8-0005-0025-P2-1	Air	Water	38.6152	80.6000	0.6660	3.4300	40.9191	0.3355	0.6645	4.8779	0.0662
D8-0005-0025-P2-2	Air	Water	40.1033	80.6000	0.6660	3.6631	39.9116	0.3375	0.6625	4.8779	0.0662
D8-0005-0025-P2-3	Air	Water	41.7941	80.6000	0.6660	4.3957	40.4343	0.3500	0.6500	4.8779	0.0662
D8-0005-0025-P2-4	Air	Water	43.3032	80.6000	0.6660	2.7972	38.3776	0.3725	0.6275	4.8780	0.0662
D8-0005-0030-P1-1	Air	Water	25.9523	80.6000	0.6660	3.4300	41.0409	0.3500	0.6500	3.4930	0.0529
D8-0005-0030-P1-2	Air	Water	27.4383	80.6000	0.6660	3.6631	39.8546	0.3490	0.6510	3.4930	0.0529
D8-0005-0030-P1-3	Air	Water	29.1266	80.6000	0.6660	4.3957	40.7669	0.3585	0.6415	3.4930	0.0529
D8-0005-0030-P1-4	Air	Water	30.6335	80.6000	0.6660	2.7972	38.5269	0.3590	0.6410	3.4930	0.0529
D8-0005-0030-P2-1	Air	Water	39.0106	77.0000	0.6660	3.4300	38.1790	0.3885	0.6115	3.5227	0.0816
D8-0005-0030-P2-2	Air	Water	40.4887	77.0000	0.6660	3.6631	37.5739	0.4025	0.5975	3.5227	0.0816

Run Number	Vapor	Liquid	P (psia)	T (°F)	D (ft)	H (ft)	$\Delta P/\Delta L$ (lb_f/ft^3)	Vapor Fraction, α_g	Liquid Fraction, α_f	W_L (lb_m/s)	W_G (lb_m/s)
D8-0005-0030-P2-3	Air	Water	42.1680	77.0000	0.6660	4.3957	38.2486	0.4080	0.5920	3.5228	0.0816
D8-0005-0030-P2-4	Air	Water	43.6668	77.0000	0.6660	2.7972	36.1377	0.4035	0.5965	3.5228	0.0816
D8-0005-0040-P2-1	Air	Water	39.0664	82.4000	0.6660	3.4300	37.9354	0.4105	0.5895	4.8516	0.1036
D8-0005-0040-P2-2	Air	Water	40.5549	82.4000	0.6660	3.6631	36.6047	0.4155	0.5845	4.8516	0.1036
D8-0005-0040-P2-3	Air	Water	42.2461	82.4000	0.6660	4.3957	37.2508	0.4095	0.5905	4.8516	0.1036
D8-0005-0040-P2-4	Air	Water	43.7555	82.4000	0.6660	2.7972	34.9430	0.4325	0.5675	4.8517	0.1036
D8-0005-0050-P1-1	Air	Water	26.4451	82.4000	0.6660	3.4300	35.9869	0.4425	0.5575	3.4948	0.9482
D8-0005-0050-P1-2	Air	Water	27.9303	82.4000	0.6660	3.6631	35.0082	0.4450	0.5550	3.4948	0.9482
D8-0005-0050-P1-3	Air	Water	29.6178	82.4000	0.6660	4.3957	35.8254	0.4560	0.5440	3.4948	0.9482
D8-0005-0050-P1-4	Air	Water	31.1240	82.4000	0.6660	2.7972	33.0017	0.4560	0.5440	3.4948	0.9482
D8-0005-0050-P2-1	Air	Water	38.8908	82.4000	0.6660	3.4300	32.5770	0.4840	0.5160	4.9084	0.1389
D8-0005-0050-P2-1	Air	Water	39.2026	78.8000	0.6660	3.4300	32.8814	0.5050	0.4950	3.5606	0.1301
D8-0005-0050-P2-2	Air	Water	40.3789	82.4000	0.6660	3.6631	31.9863	0.4860	0.5140	4.9084	0.1389
D8-0005-0050-P2-2	Air	Water	40.6817	78.8000	0.6660	3.6631	32.1003	0.5070	0.4930	3.5606	0.1301
D8-0005-0050-P2-3	Air	Water	42.0696	82.4000	0.6660	4.3957	31.9768	0.4925	0.5075	4.9084	0.1389
D8-0005-0050-P2-3	Air	Water	42.3622	78.8000	0.6660	4.3957	32.6895	0.4995	0.5005	3.5607	0.1301
D8-0005-0050-P2-4	Air	Water	43.5787	82.4000	0.6660	2.7972	29.8658	0.5155	0.4845	4.9085	0.1389
D8-0005-0050-P2-4	Air	Water	43.8622	78.8000	0.6660	2.7972	30.2392	0.4970	0.5030	3.5607	0.1301
D8-0005-0060-P2-1	Air	Water	39.1297	82.4000	0.6660	3.4300	30.6893	0.5035	0.4965	4.9153	0.1610
D8-0005-0060-P2-2	Air	Water	40.6171	82.4000	0.6660	3.6631	29.8767	0.5015	0.4985	4.9154	0.1610
D8-0005-0060-P2-3	Air	Water	42.3071	82.4000	0.6660	4.3957	30.2663	0.5195	0.4805	4.9154	0.1610
D8-0005-0060-P2-4	Air	Water	43.8154	82.4000	0.6660	2.7972	27.5512	0.5495	0.4505	4.9154	0.1610
D8-0005-0090-P1-1	Air	Water	24.9135	82.4000	0.6660	3.4300	26.7314	0.5970	0.4030	3.5710	0.1698
D8-0005-0090-P1-2	Air	Water	26.3987	82.4000	0.6660	3.6631	25.9425	0.5915	0.4085	3.5710	0.1698
D8-0005-0090-P1-3	Air	Water	28.0862	82.4000	0.6660	4.3957	26.8453	0.5970	0.4030	3.5710	0.1698
D8-0005-0090-P1-4	Air	Water	29.5924	82.4000	0.6660	2.7972	23.2207	0.6015	0.3985	3.5710	0.1698
D8-0005-0090-P2-1	Air	Water	38.6037	78.8000	0.6660	3.4300	25.8789	0.6240	0.3760	3.6854	0.2293
D8-0005-0090-P2-2	Air	Water	40.0799	78.8000	0.6660	3.6631	24.6882	0.6305	0.3695	3.6854	0.2293
D8-0005-0090-P2-3	Air	Water	41.7571	78.8000	0.6660	4.3957	25.0398	0.6145	0.3855	3.6854	0.2293
D8-0005-0090-P2-4	Air	Water	43.2542	78.8000	0.6660	2.7972	22.1007	0.6105	0.3895	3.6855	0.2293
D8-0005-0150-P1-1	Air	Water	25.7238	84.2000	0.6660	3.4300	21.3729	0.6220	0.3780	3.5284	0.2822
D8-0005-0150-P1-3	Air	Water	28.8880	84.2000	0.6660	4.3957	19.4332	0.6590	0.3410	3.5284	0.2822
D8-0005-0150-P1-4	Air	Water	30.3902	84.2000	0.6660	2.7972	15.3809	0.6680	0.3320	3.5284	0.2822
D8-0010-0015-P1-1	Air	Water	26.3316	77.0000	0.6660	3.4300	47.3127	0.1625	0.8375	7.0909	0.0287
D8-0010-0015-P1-2	Air	Water	27.8190	77.0000	0.6660	3.6631	46.6396	0.2140	0.7860	7.0910	0.0287
D8-0010-0015-P1-3	Air	Water	29.5089	77.0000	0.6660	4.3957	47.3713	0.2300	0.7700	7.0910	0.0287
D8-0010-0015-P1-4	Air	Water	31.0172	77.0000	0.6660	2.7972	45.6201	0.2380	0.7620	7.0910	0.0287
D8-0010-0015-P2-1	Air	Water	38.8049	84.2000	0.6660	3.4300	47.5563	0.2410	0.7590	7.2856	0.0353
D8-0010-0015-P2-1	Air	Water	38.3958	80.6000	0.6660	3.4300	38.8488	0.3735	0.6265	7.8637	0.0397
D8-0010-0015-P2-2	Air	Water	40.2923	84.2000	0.6660	3.6631	46.6966	0.2340	0.7660	7.2857	0.0353
D8-0010-0015-P2-2	Air	Water	39.8771	80.6000	0.6660	3.6631	39.6265	0.3700	0.6300	7.8637	0.0397
D8-0010-0015-P2-3	Air	Water	41.9822	84.2000	0.6660	4.3957	47.2763	0.2295	0.7705	7.2857	0.0353
D8-0010-0015-P2-3	Air	Water	41.5600	80.6000	0.6660	4.3957	40.4343	0.3675	0.6325	7.8637	0.0397
D8-0010-0015-P2-4	Air	Water	43.0622	80.6000	0.6660	2.7972	38.7509	0.3650	0.6350	7.8638	0.0397

Run Number	Vapor	Liquid	P (psia)	T (°F)	D (ft)	H (ft)	$\Delta P/\Delta L$ (lb_f/ft^3)	Vapor Fraction, α_g	Liquid Fraction, α_f	W_L (lb_m/s)	W_G (lb_m/s)
D8-0010-0015-P2-4	Air	Water	43.4905	84.2000	0.6660	2.7972	45.5454	0.2575	0.7425	7.2858	0.0353
D8-0010-0020-P2-1	Air	Water	38.7182	84.2000	0.6660	3.4300	44.6335	0.2775	0.7225	7.4297	0.0485
D8-0010-0020-P2-2	Air	Water	40.2063	84.2000	0.6660	3.6631	43.5607	0.2735	0.7265	7.4298	0.0485
D8-0010-0020-P2-3	Air	Water	41.8970	84.2000	0.6660	4.3957	43.9978	0.2855	0.7145	7.4298	0.0485
D8-0010-0020-P2-4	Air	Water	43.4061	84.2000	0.6660	2.7972	42.3348	0.3125	0.6875	7.4298	0.0485
D8-0010-0025-P2-1	Air	Water	39.0298	84.2000	0.6660	3.4300	41.8325	0.3415	0.6585	7.3840	0.0662
D8-0010-0025-P2-2	Air	Water	40.5176	84.2000	0.6660	3.6631	40.7669	0.3430	0.6570	7.3840	0.0662
D8-0010-0025-P2-3	Air	Water	42.2079	84.2000	0.6660	4.3957	41.2895	0.3380	0.6620	7.3841	0.0662
D8-0010-0025-P2-4	Air	Water	43.7167	84.2000	0.6660	2.7972	39.3482	0.3605	0.6395	7.3841	0.0662
D8-0010-0030-P1-1	Air	Water	26.6008	77.0000	0.6660	3.4300	41.8325	0.2700	0.7300	7.0798	0.0529
D8-0010-0030-P1-2	Air	Water	28.0871	77.0000	0.6660	3.6631	41.2800	0.3180	0.6820	7.0799	0.0529
D8-0010-0030-P1-3	Air	Water	29.7758	77.0000	0.6660	4.3957	41.8597	0.3280	0.6720	7.0799	0.0529
D8-0010-0030-P1-4	Air	Water	31.2831	77.0000	0.6660	2.7972	39.6469	0.3340	0.6660	7.0800	0.0529
D8-0010-0030-P2-1	Air	Water	38.8835	80.6000	0.6660	3.4300	36.1087	0.4430	0.5570	7.7403	0.0816
D8-0010-0030-P2-2	Air	Water	40.3655	80.6000	0.6660	3.6631	37.9731	0.4170	0.5830	7.7403	0.0816
D8-0010-0030-P2-3	Air	Water	42.0493	80.6000	0.6660	4.3957	39.3414	0.3840	0.6160	7.7404	0.0816
D8-0010-0030-P2-4	Air	Water	43.5521	80.6000	0.6660	2.7972	37.7056	0.3725	0.6275	7.7404	0.0816
D8-0010-0040-P2-1	Air	Water	38.4383	84.2000	0.6660	3.4300	38.6052	0.3920	0.6080	7.5447	0.1036
D8-0010-0040-P2-2	Air	Water	39.9264	84.2000	0.6660	3.6631	37.4029	0.4005	0.5995	7.5447	0.1036
D8-0010-0040-P2-3	Air	Water	41.6171	84.2000	0.6660	4.3957	38.0111	0.3975	0.6025	7.5448	0.1036
D8-0010-0040-P2-4	Air	Water	43.1262	84.2000	0.6660	2.7972	35.9137	0.4145	0.5855	7.5448	0.1036
D8-0010-0050-P1-1	Air	Water	25.8189	78.8000	0.6660	3.4300	36.9003	0.4140	0.5860	7.3414	0.0926
D8-0010-0050-P1-2	Air	Water	27.3049	78.8000	0.6660	3.6631	36.3196	0.4275	0.5725	7.3414	0.0926
D8-0010-0050-P1-3	Air	Water	28.9931	78.8000	0.6660	4.3957	36.8232	0.4260	0.5740	7.3415	0.0926
D8-0010-0050-P1-4	Air	Water	30.5000	78.8000	0.6660	2.7972	34.4204	0.4295	0.5705	7.3415	0.0926
D8-0010-0050-P2-1	Air	Water	39.0083	84.2000	0.6660	3.4300	33.6730	0.4650	0.5350	7.5087	0.1389
D8-0010-0050-P2-1	Air	Water	39.5735	80.6000	0.6660	3.4300	33.5512	0.4760	0.5240	7.6516	0.1279
D8-0010-0050-P2-2	Air	Water	40.4964	84.2000	0.6660	3.6631	32.4995	0.4645	0.5355	7.5087	0.1389
D8-0010-0050-P2-2	Air	Water	41.0548	80.6000	0.6660	3.6631	33.6968	0.4805	0.5195	7.6516	0.1279
D8-0010-0050-P2-3	Air	Water	42.1871	84.2000	0.6660	4.3957	32.7845	0.4685	0.5315	7.5088	0.1389
D8-0010-0050-P2-3	Air	Water	42.7377	80.6000	0.6660	4.3957	34.2100	0.4725	0.5275	7.6517	0.1279
D8-0010-0050-P2-4	Air	Water	43.6962	84.2000	0.6660	2.7972	30.6125	0.4970	0.5030	7.5088	0.1389
D8-0010-0050-P2-4	Air	Water	44.2399	80.6000	0.6660	2.7972	31.5831	0.4765	0.5235	7.6517	0.1279
D8-0010-0060-P2-1	Air	Water	40.1495	86.0000	0.6660	3.4300	31.4809	0.4990	0.5010	7.3514	0.1654
D8-0010-0060-P2-2	Air	Water	41.6373	86.0000	0.6660	3.6631	30.3328	0.4975	0.5025	7.3514	0.1654
D8-0010-0060-P2-3	Air	Water	43.3276	86.0000	0.6660	4.3957	30.7890	0.5085	0.4915	7.3514	0.1654
D8-0010-0060-P2-4	Air	Water	44.8364	86.0000	0.6660	2.7972	28.3725	0.5380	0.4620	7.3515	0.1654
D8-0010-0090-P1-1	Air	Water	25.6562	80.6000	0.6660	3.4300	27.7056	0.5875	0.4125	7.5362	0.1720
D8-0010-0090-P1-2	Air	Water	27.1385	80.6000	0.6660	3.6631	26.7408	0.5870	0.4130	7.5363	0.1720
D8-0010-0090-P1-3	Air	Water	28.8227	80.6000	0.6660	4.3957	27.1304	0.5915	0.4085	7.5363	0.1720
D8-0010-0090-P1-4	Air	Water	30.3260	80.6000	0.6660	2.7972	24.2660	0.5995	0.4005	7.5363	0.1720
D8-0010-0090-P2-1	Air	Water	39.0463	82.4000	0.6660	3.4300	27.0358	0.5715	0.4285	7.9613	0.2271
D8-0010-0090-P2-2	Air	Water	40.5262	82.4000	0.6660	3.6631	26.2846	0.5710	0.4290	7.9613	0.2271
D8-0010-0090-P2-3	Air	Water	42.2075	82.4000	0.6660	4.3957	26.7978	0.5800	0.4200	7.9613	0.2271

Run Number	Vapor	Liquid	P (psia)	T (°F)	D (ft)	H (ft)	$\Delta P/\Delta L$ (lb_f/ft^3)	Vapor Fraction, α_g	Liquid Fraction, α_f	W_L (lb_m/s)	W_G (lb_m/s)
D8-0010-0090-P2-4	Air	Water	43.7082	82.4000	0.6660	2.7972	24.1167	0.5900	0.4100	7.9614	0.2271
D8-0010-0120-P1-1	Air	Water	27.1106	87.8000	0.6660	3.4300	25.2700	0.5620	0.4380	8.3166	0.2227
D8-0010-0120-P1-2	Air	Water	28.5984	87.8000	0.6660	3.6631	24.1750	0.5680	0.4320	8.3166	0.2227
D8-0010-0120-P1-3	Air	Water	30.2887	87.8000	0.6660	4.3957	24.3746	0.5895	0.4105	8.3166	0.2227
D8-0010-0120-P1-4	Air	Water	31.7974	87.8000	0.6660	2.7972	21.4287	0.5940	0.4060	8.3167	0.2227
D8-0010-0150-P1-1	Air	Water	26.2585	134.6000	0.6660	3.4300	21.8601	0.6645	0.3355	7.4922	0.2911
D8-0010-0150-P1-2	Air	Water	27.7358	134.6000	0.6660	3.6631	21.0961	0.6770	0.3230	7.4922	0.2911
D8-0010-0150-P1-3	Air	Water	29.4143	134.6000	0.6660	4.3957	20.5735	0.6985	0.3015	7.4923	0.2911
D8-0010-0150-P1-4	Air	Water	30.9124	134.6000	0.6660	2.7972	18.6661	0.6990	0.3010	7.4923	0.2911
D8-0030-0015-P1-1	Air	Water	26.5696	82.4000	0.6660	3.4300	48.1652	0.2220	0.7780	21.6297	0.0287
D8-0030-0015-P1-2	Air	Water	28.0574	82.4000	0.6660	3.6631	48.4071	0.2060	0.7940	21.6298	0.0287
D8-0030-0015-P1-3	Air	Water	29.7477	82.4000	0.6660	4.3957	49.2243	0.2130	0.7870	21.6299	0.0287
D8-0030-0015-P1-4	Air	Water	31.2564	82.4000	0.6660	2.7972	47.6360	0.2280	0.7720	21.6300	0.0287
D8-0030-0015-P2-1	Air	Water	38.4052	82.4000	0.6660	3.4300	48.8959	0.2180	0.7820	21.5404	0.0397
D8-0030-0015-P2-2	Air	Water	39.8879	82.4000	0.6660	3.6631	48.4071	0.2200	0.7800	21.5405	0.0397
D8-0030-0015-P2-3	Air	Water	41.5725	82.4000	0.6660	4.3957	48.9868	0.2245	0.7755	21.5406	0.0397
D8-0030-0015-P2-4	Air	Water	43.0761	82.4000	0.6660	2.7972	47.4120	0.2400	0.7600	21.5407	0.0397
D8-0030-0030-P1-1	Air	Water	26.1608	82.4000	0.6660	3.4300	44.8770	0.2775	0.7225	22.1465	0.0529
D8-0030-0030-P1-2	Air	Water	27.6489	82.4000	0.6660	3.6631	44.3019	0.2675	0.7325	22.1466	0.0529
D8-0030-0030-P1-3	Air	Water	29.3396	82.4000	0.6660	4.3957	44.9956	0.2750	0.7250	22.1467	0.0529
D8-0030-0030-P1-4	Air	Water	30.8487	82.4000	0.6660	2.7972	42.9321	0.2900	0.7100	22.1468	0.0529
D8-0030-0030-P2-1	Air	Water	38.4915	82.4000	0.6660	3.4300	43.8419	0.3010	0.6990	21.8799	0.0794
D8-0030-0030-P2-2	Air	Water	39.9756	82.4000	0.6660	3.6631	42.9905	0.3070	0.6930	21.8800	0.0794
D8-0030-0030-P2-3	Air	Water	41.6619	82.4000	0.6660	4.3957	43.4752	0.3155	0.6845	21.8801	0.0794
D8-0030-0030-P2-4	Air	Water	43.1669	82.4000	0.6660	2.7972	41.2895	0.3355	0.6645	21.8802	0.0794
D8-0030-0050-P1-1	Air	Water	25.8138	84.2000	0.6660	3.4300	40.8582	0.3655	0.6345	22.6817	0.0926
D8-0030-0050-P1-2	Air	Water	27.3012	84.2000	0.6660	3.6631	39.6835	0.3505	0.6495	22.6818	0.0926
D8-0030-0050-P1-3	Air	Water	28.9911	84.2000	0.6660	4.3957	39.9591	0.3710	0.6290	22.6819	0.0926
D8-0030-0050-P1-4	Air	Water	30.4995	84.2000	0.6660	2.7972	38.0789	0.3820	0.6180	22.6820	0.0926
D8-0030-0050-P2-1	Air	Water	38.8207	82.4000	0.6660	3.4300	39.3359	0.3865	0.6135	22.0448	0.1235
D8-0030-0050-P2-2	Air	Water	40.3049	82.4000	0.6660	3.6631	37.9160	0.3910	0.6090	22.0449	0.1235
D8-0030-0050-P2-3	Air	Water	41.9911	82.4000	0.6660	4.3957	38.1536	0.3620	0.6380	22.0450	0.1235
D8-0030-0050-P2-4	Air	Water	43.4962	82.4000	0.6660	2.7972	35.9137	0.3635	0.6365	22.0451	0.1235
D8-0030-0090-P1-1	Air	Water	25.6800	84.2000	0.6660	3.4300	31.6636	0.5260	0.4740	23.5558	0.1654
D8-0030-0090-P1-2	Air	Water	27.1667	84.2000	0.6660	3.6631	30.5609	0.5270	0.4730	23.5559	0.1654
D8-0030-0090-P1-3	Air	Water	28.8558	84.2000	0.6660	4.3957	30.5989	0.5335	0.4665	23.5561	0.1654
D8-0030-0090-P1-4	Air	Water	30.3634	84.2000	0.6660	2.7972	28.3725	0.5360	0.4640	23.5562	0.1654
D8-0030-0090-P2-1	Air	Water	39.4986	84.2000	0.6660	3.4300	30.3849	0.5035	0.4965	22.3086	0.2448
D8-0030-0090-P2-2	Air	Water	40.9810	84.2000	0.6660	3.6631	28.9074	0.5220	0.4780	22.3087	0.2448
D8-0030-0090-P2-3	Air	Water	42.6652	84.2000	0.6660	4.3957	29.0309	0.5310	0.4690	22.3088	0.2448
D8-0030-0090-P2-4	Air	Water	44.1684	84.2000	0.6660	2.7972	26.8046	0.5385	0.4615	22.3089	0.2448
D8-0030-0120-P1-1	Air	Water	26.9135	87.8000	0.6660	3.4300	28.8017	0.5100	0.4900	23.8559	0.2227
D8-0030-0120-P1-2	Air	Water	28.4016	87.8000	0.6660	3.6631	27.0259	0.5270	0.4730	23.8560	0.2227
D8-0030-0120-P1-3	Air	Water	30.0924	87.8000	0.6660	4.3957	27.0829	0.5510	0.4490	23.8561	0.2227

Run Number	Vapor	Liquid	P (psia)	T (°F)	D (ft)	H (ft)	$\Delta P/\Delta L$ (lb_f/ft^3)	Vapor Fraction, α_g	Liquid Fraction, α_f	W_L (lb_m/s)	W_G (lb_m/s)
D8-0030-0120-P1-4	Air	Water	31.6015	87.8000	0.6660	2.7972	24.9380	0.5535	0.4465	23.8562	0.2227
D8-0030-0150-P1-1	Air	Water	26.0037	84.2000	0.6660	3.4300	25.7571	0.6070	0.3930	23.8786	0.2800
D8-0030-0150-P1-2	Air	Water	27.4878	84.2000	0.6660	3.6631	24.0610	0.6100	0.3900	23.8787	0.2800
D8-0030-0150-P1-3	Air	Water	29.1741	84.2000	0.6660	4.3957	24.3746	0.6170	0.3830	23.8789	0.2800
D8-0030-0150-P1-4	Air	Water	30.6791	84.2000	0.6660	2.7972	21.7274	0.6235	0.3765	23.8790	0.2800
D8-0050-0015-P1-1	Air	Water	25.8805	84.2000	0.6660	3.4300	50.0528	0.2205	0.7795	35.6302	0.0265
D8-0050-0015-P1-2	Air	Water	27.3679	84.2000	0.6660	3.6631	49.6615	0.2395	0.7605	35.6304	0.0265
D8-0050-0015-P1-3	Air	Water	29.0578	84.2000	0.6660	4.3957	50.1271	0.2560	0.7440	35.6306	0.0265
D8-0050-0015-P1-4	Air	Water	30.5662	84.2000	0.6660	2.7972	48.5320	0.2655	0.7345	35.6307	0.0265
D8-0050-0015-P2-1	Air	Water	38.9853	80.6000	0.6660	3.4300	50.9662	0.1860	0.8140	37.6315	0.0375
D8-0050-0015-P2-2	Air	Water	40.4709	80.6000	0.6660	3.6631	50.4597	0.1885	0.8115	37.6316	0.0375
D8-0050-0015-P2-3	Air	Water	42.1588	80.6000	0.6660	4.3957	51.0299	0.1930	0.8070	37.6318	0.0375
D8-0050-0015-P2-4	Air	Water	43.6653	80.6000	0.6660	2.7972	49.6519	0.2070	0.7930	37.6320	0.0375
D8-0050-0030-P1-1	Air	Water	25.9545	84.2000	0.6660	3.4300	46.3384	0.2570	0.7430	36.0638	0.0551
D8-0050-0030-P1-2	Air	Water	27.4419	84.2000	0.6660	3.6631	46.0124	0.2170	0.7830	36.0640	0.0551
D8-0050-0030-P1-3	Air	Water	29.1318	84.2000	0.6660	4.3957	46.7061	0.2005	0.7995	36.0642	0.0551
D8-0050-0030-P1-4	Air	Water	30.6402	84.2000	0.6660	2.7972	44.8734	0.2310	0.7690	36.0644	0.0551
D8-0050-0030-P2-1	Air	Water	39.1358	80.6000	0.6660	3.4300	46.5211	0.2580	0.7420	38.2137	0.0794
D8-0050-0030-P2-2	Air	Water	40.6207	80.6000	0.6660	3.6631	46.0124	0.2615	0.7385	38.2138	0.0794
D8-0050-0030-P2-3	Air	Water	42.3077	80.6000	0.6660	4.3957	46.5160	0.2670	0.7330	38.2140	0.0794
D8-0050-0030-P2-4	Air	Water	43.8135	80.6000	0.6660	2.7972	44.9481	0.2825	0.7175	38.2142	0.0794
D8-0050-0050-P1-1	Air	Water	26.0283	86.0000	0.6660	3.4300	43.7201	0.2935	0.7065	36.3564	0.0904
D8-0050-0050-P1-2	Air	Water	27.5153	86.0000	0.6660	3.6631	42.9905	0.3095	0.6905	36.3565	0.0904
D8-0050-0050-P1-3	Air	Water	29.2048	86.0000	0.6660	4.3957	43.1901	0.3040	0.6960	36.3567	0.0904
D8-0050-0050-P1-4	Air	Water	30.7128	86.0000	0.6660	2.7972	41.1402	0.2940	0.7060	36.3569	0.0904
D8-0050-0050-P2-1	Air	Water	38.4878	80.6000	0.6660	3.4300	41.8934	0.3785	0.6215	39.9865	0.1367
D8-0050-0050-P2-2	Air	Water	39.9734	80.6000	0.6660	3.6631	40.5388	0.3370	0.6630	39.9867	0.1367
D8-0050-0050-P2-3	Air	Water	41.6613	80.6000	0.6660	4.3957	40.8144	0.3625	0.6375	39.9869	0.1367
D8-0050-0050-P2-4	Air	Water	43.1678	80.6000	0.6660	2.7972	38.6763	0.3765	0.6235	39.9871	0.1367
D8-0050-0090-P1-1	Air	Water	25.7367	86.0000	0.6660	3.4300	35.4389	0.3720	0.6280	37.8797	0.1654
D8-0050-0090-P1-2	Air	Water	27.2238	86.0000	0.6660	3.6631	33.1837	0.4650	0.5350	37.8799	0.1654
D8-0050-0090-P1-3	Air	Water	28.9133	86.0000	0.6660	4.3957	33.2597	0.5225	0.4775	37.8801	0.1654
D8-0050-0090-P1-4	Air	Water	30.4213	86.0000	0.6660	2.7972	30.9858	0.4775	0.5225	37.8803	0.1654
D8-0050-0090-P2-1	Air	Water	39.1417	80.6000	0.6660	3.4300	35.6824	0.4880	0.5120	40.1460	0.2381
D8-0050-0090-P2-2	Air	Water	40.6270	80.6000	0.6660	3.6631	33.2977	0.4985	0.5015	40.1462	0.2381
D8-0050-0090-P2-3	Air	Water	42.3145	80.6000	0.6660	4.3957	33.3547	0.5035	0.4965	40.1464	0.2381
D8-0050-0090-P2-4	Air	Water	43.8206	80.6000	0.6660	2.7972	31.0605	0.5020	0.4980	40.1466	0.2381
D8-0050-0120-P1-1	Air	Water	27.4208	86.0000	0.6660	3.4300	32.9423	0.4590	0.5410	37.6445	0.2161
D8-0050-0120-P1-2	Air	Water	28.9082	86.0000	0.6660	3.6631	30.5609	0.4885	0.5115	37.6446	0.2161
D8-0050-0120-P1-3	Air	Water	30.5981	86.0000	0.6660	4.3957	30.4088	0.5045	0.4955	37.6448	0.2161
D8-0050-0120-P1-4	Air	Water	32.1065	86.0000	0.6660	2.7972	27.8499	0.5055	0.4945	37.6450	0.2161
D8-0050-0150-P1-1	Air	Water	25.6001	86.0000	0.6660	3.4300	28.8017	0.5540	0.4460	38.7536	0.2778
D8-0050-0150-P1-2	Air	Water	27.0864	86.0000	0.6660	3.6631	26.5697	0.5975	0.4025	38.7537	0.2778
D8-0050-0150-P1-3	Air	Water	28.7751	86.0000	0.6660	4.3957	26.7028	0.6090	0.3910	38.7539	0.2778

Run Number	Vapor	Liquid	P (psia)	T (°F)	D (ft)	H (ft)	$\Delta P/\Delta L$ (lb_f/ft^3)	Vapor Fraction, α_g	Liquid Fraction, α_f	W_L (lb_m/s)	W_G (lb_m/s)
D8-0050-0150-P1-4	Air	Water	30.2823	86.0000	0.6660	2.7972	24.2660	0.5870	0.4130	38.7541	0.2778
D8-0100-0015-P1-1	Air	Water	26.2783	86.0000	0.6660	3.4300	54.7415	0.1635	0.8365	68.5581	0.0287
D8-0100-0015-P1-2	Air	Water	27.7636	86.0000	0.6660	3.6631	53.9377	0.1355	0.8645	68.5584	0.0287
D8-0100-0015-P1-3	Air	Water	29.4510	86.0000	0.6660	4.3957	54.2608	0.1500	0.8500	68.5587	0.0287
D8-0100-0015-P1-4	Air	Water	30.9572	86.0000	0.6660	2.7972	53.1612	0.1675	0.8325	68.5591	0.0287
D8-0100-0015-P2-1	Air	Water	39.7085	82.4000	0.6660	3.4300	54.6197	0.1305	0.8695	65.4320	0.0397
D8-0100-0015-P2-2	Air	Water	41.1930	82.4000	0.6660	3.6631	54.1658	0.1335	0.8665	65.4323	0.0397
D8-0100-0015-P2-3	Air	Water	42.8797	82.4000	0.6660	4.3957	54.6409	0.1375	0.8625	65.4327	0.0397
D8-0100-0015-P2-4	Air	Water	44.3851	82.4000	0.6660	2.7972	53.6092	0.1500	0.8500	65.4330	0.0397
D8-0100-0030-P1-1	Air	Water	25.8543	86.0000	0.6660	3.4300	50.2964	0.2115	0.7885	69.7559	0.0551
D8-0100-0030-P1-2	Air	Water	27.3384	86.0000	0.6660	3.6631	49.8325	0.2040	0.7960	69.7562	0.0551
D8-0100-0030-P1-3	Air	Water	29.0247	86.0000	0.6660	4.3957	50.0321	0.2305	0.7695	69.7566	0.0551
D8-0100-0030-P1-4	Air	Water	30.5297	86.0000	0.6660	2.7972	48.7560	0.2450	0.7550	69.7569	0.0551
D8-0100-0030-P2-1	Air	Water	38.2335	82.4000	0.6660	3.4300	51.2098	0.1870	0.8130	69.3715	0.0750
D8-0100-0030-P2-2	Air	Water	39.7180	82.4000	0.6660	3.6631	50.7448	0.1925	0.8075	69.3718	0.0750
D8-0100-0030-P2-3	Air	Water	41.4046	82.4000	0.6660	4.3957	51.0299	0.1990	0.8010	69.3722	0.0750
D8-0100-0030-P2-4	Air	Water	42.9101	82.4000	0.6660	2.7972	49.5773	0.2150	0.7850	69.3725	0.0750
D8-0100-0050-P1-1	Air	Water	26.0285	86.0000	0.6660	3.4300	47.5563	0.2215	0.7785	69.9388	0.0926
D8-0100-0050-P1-2	Air	Water	27.5130	86.0000	0.6660	3.6631	47.0957	0.2505	0.7495	69.9391	0.0926
D8-0100-0050-P1-3	Air	Water	29.1997	86.0000	0.6660	4.3957	47.1337	0.2595	0.7405	69.9394	0.0926
D8-0100-0050-P1-4	Air	Water	30.7051	86.0000	0.6660	2.7972	45.6201	0.2765	0.7235	69.9398	0.0926
D8-0100-0050-P2-1	Air	Water	38.4512	84.2000	0.6660	3.4300	48.2870	0.2375	0.7625	74.3803	0.1235
D8-0100-0050-P2-2	Air	Water	39.9361	84.2000	0.6660	3.6631	47.4378	0.2575	0.7425	74.3806	0.1235
D8-0100-0050-P2-3	Air	Water	41.6231	84.2000	0.6660	4.3957	47.4188	0.2775	0.7225	74.3810	0.1235
D8-0100-0050-P2-4	Air	Water	43.1289	84.2000	0.6660	2.7972	45.8441	0.2790	0.7210	74.3814	0.1235
D8-0100-0090-P1-1	Air	Water	25.7250	87.8000	0.6660	3.4300	41.4671	0.3705	0.6295	69.3924	0.1632
D8-0100-0090-P1-2	Air	Water	27.2116	87.8000	0.6660	3.6631	38.9423	0.3570	0.6430	69.3928	0.1632
D8-0100-0090-P1-3	Air	Water	28.9007	87.8000	0.6660	4.3957	38.6287	0.3605	0.6395	69.3931	0.1632
D8-0100-0090-P1-4	Air	Water	30.4084	87.8000	0.6660	2.7972	36.6603	0.3650	0.6350	69.3934	0.1632
D8-0100-0090-P2-1	Air	Water	39.3881	84.2000	0.6660	3.4300	41.3453	0.3590	0.6410	74.1907	0.2403
D8-0100-0090-P2-2	Air	Water	40.8730	84.2000	0.6660	3.6631	39.0564	0.3925	0.6075	74.1910	0.2403
D8-0100-0090-P2-3	Air	Water	42.5601	84.2000	0.6660	4.3957	38.3912	0.4145	0.5855	74.1914	0.2403
D8-0100-0090-P2-4	Air	Water	44.0659	84.2000	0.6660	2.7972	36.5856	0.4140	0.5860	74.1918	0.2403
D8-0100-0120-P1-1	Air	Water	27.1681	86.0000	0.6660	3.4300	38.3616	0.3885	0.6115	69.5166	0.2227
D8-0100-0120-P1-2	Air	Water	28.6548	86.0000	0.6660	3.6631	35.6354	0.3995	0.6005	69.5169	0.2227
D8-0100-0120-P1-3	Air	Water	30.3439	86.0000	0.6660	4.3957	34.9702	0.4180	0.5820	69.5173	0.2227
D8-0100-0120-P1-4	Air	Water	31.8515	86.0000	0.6660	2.7972	33.0017	0.4165	0.5835	69.5176	0.2227
D8-0100-0150-P1-1	Air	Water	26.3504	87.8000	0.6660	3.4300	34.1601	0.5065	0.4935	69.7401	0.2955
D8-0100-0150-P1-2	Air	Water	27.8378	87.8000	0.6660	3.6631	31.3021	0.4905	0.5095	69.7404	0.2955
D8-0100-0150-P1-3	Air	Water	29.5277	87.8000	0.6660	4.3957	30.3138	0.5205	0.4795	69.7408	0.2955
D8-0100-0150-P1-4	Air	Water	31.0361	87.8000	0.6660	2.7972	28.3725	0.5200	0.4800	69.7411	0.2955

Turner [84]

Run Number	Vapor	Liquid	P (psia)	T (°F)	D (ft)	H (ft)	$\Delta P/\Delta L$ (lb_f/ft^3)	Vapor Fraction, α_g	Liquid Fraction, α_f	W_L (lb_m/s)	W_G (lb_m/s)
635	Air	Water	15.7000	50.0000	0.0858	3.0000	10.9217	0.8260	0.1740	0.0595	0.0104
639	Air	Water	18.1000	46.0000	0.0858	3.0000	10.6739	0.9540	0.0460	0.0685	0.0440
640	Air	Water	20.5000	44.0000	0.0858	3.0000	18.1654	0.9650	0.0350	0.1110	0.0618
641	Air	Water	15.7000	43.0000	0.0858	3.0000	14.4825	0.8000	0.2000	0.1490	0.0103
642	Air	Water	16.5000	45.0000	0.0858	3.0000	12.8589	0.8810	0.1190	0.1600	0.0218
643	Air	Water	18.2000	44.0000	0.0858	3.0000	16.3550	0.9080	0.0920	0.1810	0.0342
644	Air	Water	20.5000	42.0000	0.0858	3.0000	21.5371	0.9180	0.0820	0.2360	0.0474
645	Air	Water	24.1000	42.0000	0.0858	3.0000	32.4621	0.9030	0.0970	0.3720	0.0638
646	Air	Water	15.6000	45.0000	0.0858	3.0000	17.1659	0.7830	0.2170	0.2500	0.0111
647	Air	Water	17.1000	45.0000	0.0858	3.0000	18.8514	0.8540	0.1460	0.2710	0.0224
648	Air	Water	19.4000	45.0000	0.0858	3.0000	22.5345	0.8840	0.1160	0.3000	0.0363
649	Air	Water	22.9000	45.0000	0.0858	3.0000	29.9631	0.8920	0.1080	0.3600	0.0504
650	Air	Water	15.5000	57.0000	0.0458	3.0000	13.7864	0.8540	0.1460	0.0331	0.0042
651	Air	Water	15.9000	52.0000	0.0458	3.0000	19.7194	0.8390	0.1610	0.0563	0.0042
652	Air	Water	15.0000	65.0000	0.0458	3.0000	7.9791	0.8940	0.1060	0.0113	0.0041
654	Air	Water	15.7000	60.0000	0.0458	3.0000	15.7788	0.8980	0.1020	0.0331	0.0063
655	Air	Water	16.4000	55.0000	0.0458	3.0000	22.9600	0.8770	0.1230	0.0535	0.0065
656	Air	Water	15.9000	56.0000	0.0458	3.0000	20.9620	0.9170	0.0830	0.0331	0.0090
666	Air	Heptane	15.7000	66.0000	0.0858	3.0000	8.1623	0.8250	0.1750	0.1270	0.0083
667	Air	Heptane	16.0000	66.0000	0.0858	3.0000	7.9914	0.8790	0.1210	0.1270	0.0154
668	Air	Heptane	16.4000	55.0000	0.0858	3.0000	7.1046	0.9160	0.0840	0.1270	0.0226
669	Air	Heptane	18.4000	60.0000	0.0858	3.0000	8.1102	0.9400	0.0600	0.1270	0.0296
670	Air	Heptane	19.0000	59.0000	0.0858	3.0000	9.6616	0.9450	0.0550	0.1270	0.0364
671	Air	Heptane	15.3000	70.0000	0.0858	3.0000	7.8415	0.7620	0.2380	0.0428	0.0035
672	Air	Heptane	15.3000	66.0000	0.0858	3.0000	7.6495	0.7980	0.2020	0.0428	0.0056
672	Air	Heptane	15.3000	60.0000	0.0858	3.0000	6.8228	0.8520	0.1480	0.0428	0.0083
674	Air	Heptane	15.6000	58.0000	0.0858	3.0000	4.7267	0.9230	0.0770	0.0428	0.0155
675	Air	Heptane	16.2000	53.0000	0.0858	3.0000	4.4410	0.9500	0.0500	0.0428	0.0227

Appendix C: Shell Program for Running RELAP5/MOD3.3 Annular Flow Simulations

Annular.f

```
c     Randy Clark
c     This program is designed run RELAP for each of the Runge cases,
c     analyze the data and write its analysis to an output file.

      PROGRAM ANNULAR
      IMPLICIT NONE

      INTEGER I,J,K,L,M,N,Q,R,ST,RES(194),SSN,SYSTEM,TRIP1,TRIP2
      INTEGER TIMDIFF,FIN,STA
      DOUBLE PRECISION PRS(194),TEM(194),DIAM(194),EL(194),TL(194)
      DOUBLE PRECISION PGF(194),QUALS(194),MFF(194),MFG(194)
      DOUBLE PRECISION PRES,TMP,MFV,MFL,TOPP,XST,DPDZ,ENTL,TESTL,DI
      DOUBLE PRECISION TIM(101),P(5,101),FR(5,101),FWF(5,101)
      DOUBLE PRECISION FWG(5,101),RF(5,101),RG(5,101),MF(5,101)
      DOUBLE PRECISION MG(5,101),SIG(5,101),ALP(5,101),VFJ(6,101)
      DOUBLE PRECISION VGJ(6,101),VJJ(6,101),FIJ(6,101),TF(5,101)
      DOUBLE PRECISION TG(5,101),OUTP(107),FOUT(50),BETA(194)
      DOUBLE PRECISION JR(6,901)
      CHARACTER(4) RUNNO(194)
      CHARACTER(8) STUDY

      CALL READER(RES,RUNNO,PRS,TEM,DIAM,PGF,EL,TL,QUALS,MFF,MFG)
c     This subroutine reads the Runge Input file for all data
c     necessary to write the input file

c      PRINT *, "Reading the Runge Data"

      OPEN(UNIT=6, NAME="output.txt", STATUS="UNKNOWN")
      OPEN(UNIT=7, NAME="data.txt", STATUS="UNKNOWN")
      OPEN(UNIT=8, NAME="fricdata.txt", STATUS="UNKNOWN")
      N=SYSTEM("chmod 777 output.txt")
      Q=SYSTEM("chmod 777 data.txt")
      R=SYSTEM("chmod 777 fricdata.txt")

      WRITE(6,250) "Researcher","Run #","P (psia)","D (ft)","VFlow",
     1 "BSInt","JFlow","dP/dz","Vapor","Liquid","rhof","rhog","velf",
     2 "velg","vgj","muf","mug","sigma","fwallf","fwallg","drhog/dz",
     3 "da/dz","fij","FINT","Time"
250   FORMAT(A10,2X,A5,2X,A8,2X,A6,2X,A5,3X,A5,3X,A5,4X,A5,6X,A5,4X,A6,
     1 6X,A4,7X,A4,7X,A4,6X,A4,8X,A3,9X,A3,9X,A3,7X,A5,8X,A6,7X,A6,5X,
     2 A8,5X,A5,9X,A3,14X,A4,12X,A4)
      WRITE(6,251) "Regime","Regime","Regime","(lbf/ft3)","Fraction",
     1 "Fraction","(lbm/ft3)","(lbm/ft3)","(ft/s)","(ft/s)","(ft/s)",
     2 "(lbm/ft-s)","(lbm/ft-s)","(lbm/s2)","(lbm/ft3-s)",
     3 "(lbm/ft3-s)","(lbm/ft4)","(ft-1)","(lbf-s2/ft5)",
     4 "(lbf/ft3)","(s)"
251   FORMAT(37X,A6,2X,A6,2X,A6,2X,A9,2X,A8,2X,A8,2X,A9,2X,A9,3X,A6,
     1 4X,A6,5X,A6,4X,A10,2X,A10,3X,A8,3X,A11,2X,A11,2X,A9,4X,A6,4X,
     2 A12,7X,A9,12X,A3)
      WRITE(7,253) "Researcher","Run #","TRIP1","TRIP2","Runs",
```

```
     1 "Time (s)","Pressure (psia)","Void Fraction",
     2 "Liquid Temperature (deg F)","Vapor Temperature (deg F)"
253   FORMAT(A10,2X,A5,3X,A5,2X,A5,2X,A4,2X,A8,26X,A15,41X,A13,36X,A26,
     1 35X,A25)
      WRITE (7,254) ("#1","#2","#3","#4","#5",J=1,4)
254   FORMAT(50X,20(5X,A2,5X))
      WRITE (8,256) "Researcher","Run #","vgj","vg-vf","fij","FINT",
     1 "CO","DFVEL","C1","RELV","Ci","FIAnn","FI","Fi","JFIN","FIF",
     2 "FIG","Fintf","Fintg","Agf","Agf,lf","Agf,ld","alpff","alpfd"
256   FORMAT(A10,2X,A5,8X,A3,8X,A5,8X,A3,11X,A4,14X,A2,11X,A5,12X,A2,
     1 11X,A4,12X,A2,8X,A5,8X,A2,12X,A2,15X,A4,12X,A3,12X,A3,10X,A5,10X,
     2 A5,12X,A3,6X,A6,9X,A6,10X,A5,10X,A5)
      WRITE (8,257) "ft/s","ft/s","lbfs2/ft5","lbf/ft3","ft/s","ft/s",
     1 "lbfs2/ft5","lbf/ft3","lbf/ft3","lbf/ft3","ft-1","ft-1","ft-1"
257   FORMAT(25X,A4,7X,A4,7X,A9,6X,A7,25X,A4,26X,A4,9X,A9,28X,A7,55X,A7,
     1 8X,A7,10X,A4,7X,A4,11X,A4)

      DO I=1,166
           STA = TIME()
           L=6
           ST=RES(I)
           PRES=PRS(I)+PGF(I)*(0.25d0+EL(I)+TL(I)/2.0d0)/144.0d0
           TMP=TEM(I)
           MFV=MFG(I)
           MFL=MFF(I)
           DPDZ=PGF(I)
           XST=QUALS(I)
           ENTL=EL(I)
           TESTL=TL(I)
           DI=DIAM(I)
           TOPP=PRS(I)-(PGF(I)*(TL(I)/2.0d0)+12.50d0)/144.0d0
           TRIP1=0
           TRIP2=0
           K=1

301   CALL INWRITE(ST,PRES,TMP,MFV,MFL,XST,TOPP,DPDZ,ENTL,TESTL,DI)
c     This subroutine writes the input file that is to be run in RELAP

      CALL RERUN
c     This subroutine runs RELAP using the input file written in the
c     INWRITE subroutine

      CALL RELAPREAD(TRIP2,SSN)
c     This subroutine reads the RELAP output file

      IF(TRIP2.EQ.1)THEN
           GO TO 352
      END IF

      CALL SSCHECK(SSN,TRIP1)
c     This subroutine checks if the RELAP run achieved steady state, if
c     not, that data points will be averaged over the last 10 seconds
c     of the RELAP run

352   CALL VARSET(SSN,TRIP1,TRIP2,DI,OUTP,JR)
c     This subroutine sets the variables to be analyzed into a single
c     array OUTP
```

```
      CALL CALC(OUTP,SSN,JR,DI,TESTL,FOUT)
c     This subroutine will perform data analysis calculations to show
c     how well RELAP modeled the set up

      XST=(OUTP(51)*OUTP(31))/(OUTP(51)*OUTP(31)+(1-OUTP(51))*OUTP(26))
c     This determines the static quality at the last volume of the test
c     section.

c      IF((ABS(FOUT(1)-PGF(I))/PGF(I).GE.2.0d-1).AND.(TRIP2.NE.1))THEN
c           PRINT *, FOUT(1),PGF(I)
c           PRINT *, TOPP,QUALS,STMP
c           TOPP=TOPP+(FOUT(1)+PGF(I))*10.416667d0/144.0d0
c           QUALS=XST
c           PRES2=TOPP-PGF(I)*10.416667d0/144.0d0
c           IF(TOPP.GT.PRS(I))THEN
c                STMP=(PRES2-PRES*(1.0d0-OUTP(47)))/OUTP(47)
c                STMP=MAX(STMP,PRES+100.0d0)
c                STMP=MIN(STMP,PRES+150.0d0)
c           END IF
c           PRINT *, K
c           PRINT *, OUTP(51),OUTP(31),OUTP(26)
c           PRINT *, TOPP,QUALS,STMP
c           PAUSE
c           K=K+1
c           IF(K.LT.200)THEN
c                GO TO 301
c           END IF
c      END IF

      IF(RES(I).EQ.1)THEN
           STUDY="Gill    "
      ELSE IF(RES(I).EQ.2)THEN
           STUDY="Govier  "
      ELSE IF(RES(I).EQ.3)THEN
           STUDY="Oshinowo"
      ELSE IF(RES(I).EQ.4)THEN
           STUDY="Runge   "
      ELSE IF(RES(I).EQ.5)THEN
           STUDY="Turner  "
      ELSE
           STUDY="Other   "
      END IF

      FIN=TIME()
      TIMDIFF=FIN-STA

      WRITE(6,252) STUDY,RUNNO(I),PRS(I),DIAM(I),FOUT(5),FOUT(46),
     1 FOUT(20),FOUT(1),FOUT(13),1.0d0-FOUT(13),FOUT(8),FOUT(9),
     2 FOUT(16),FOUT(17),FOUT(18),FOUT(10),FOUT(11),FOUT(12),FOUT(6),
     3 FOUT(7),FOUT(2),FOUT(3),FOUT(19),FOUT(21),TIMDIFF
252   FORMAT(A8,4X,A4,3X,F8.4,2X,F6.4,2X,F5.3,2X,F6.3,3X,F5.3,2X,F9.4,
     1 3X,F8.6,2X,F8.6,2X,F9.6,2X,F9.6,2X,F8.4,2X,F8.4,2X,E10.5E1,2X,
     2 E10.5E1,2X,E10.5E1,2X,E10.5E1,2X,E11.6E1,2X,E11.6E1,2X,E9.4E1,
     3 2X,E10.4E1,2X,E13.8E1,5X,F10.5,5X,I10)
      WRITE(7,255) STUDY,RUNNO(I),TRIP1,TRIP2,K,(OUTP(J),J=1,6),
     1 (OUTP(J),J=47,51),(OUTP(J),J=52,61)
```

```
255    FORMAT(A8,4X,A4,3X,I5,2X,I5,3X,I3,2X,F9.4,2X,20(1X,F10.4,1X))
       WRITE(8,258) STUDY,RUNNO(I),FOUT(18),FOUT(17)-FOUT(16),FOUT(19),
      1 FOUT(29),FOUT(22),FOUT(23),FOUT(24),FOUT(25),FOUT(26),FOUT(27),
      2 FOUT(28),FOUT(32),FOUT(33),FOUT(34),FOUT(35),FOUT(36),FOUT(37),
      3 FOUT(38),FOUT(39),FOUT(40),FOUT(41),FOUT(42)
258    FORMAT(A8,4X,A4,5X,F10.5,2X,F10.5,2X,F10.5,2X,E13.6E2,2X,E13.5E2,
      1 2X,E13.6E2,2X,E13.5E2,2X,E13.5E2,2X,E13.5E2,2X,F10.5,2X,E11.5E2,
      2 2X,E13.5E2,2X,E13.5E2,9(2X,E13.5E2))

       END DO

       CLOSE(6)
       CLOSE(7)
       CLOSE(8)

       END
```

Reader.f

```
c     Randy Clark
c     This subroutine reads the input data to be used to write the
c     input files

c      PROGRAM READER
      SUBROUTINE READER(RES,RUNNO,PRS,TEM,DIAM,PGF,EL,TL,QUALS,MFF,MFG)

      IMPLICIT NONE

      INTEGER I,RES(194)
      DOUBLE PRECISION PRS(194),TEM(194),DIAM(194),EL(194),TL(194)
      DOUBLE PRECISION PGF(194),QUALS(194),MFF(194),MFG(194)
      CHARACTER(4) RUNNO(194)
      CHARACTER(8) STUDY

      OPEN(UNIT=5, NAME="annular.prn", STATUS="UNKNOWN")

      DO I=1,194
           READ (5,301) STUDY,RUNNO(I),PRS(I),TEM(I),DIAM(I),EL(I),
     1      TL(I),PGF(I),QUALS(I),MFF(I),MFG(I)
           IF(STUDY.EQ."Gill    ")THEN
                RES(I)=1
           ELSE IF(STUDY.EQ."Govier  ")THEN
                RES(I)=2
           ELSE IF(STUDY.EQ."Oshinowo")THEN
                RES(I)=3
           ELSE IF(STUDY.EQ."Runge   ")THEN
                RES(I)=4
           ELSE IF(STUDY.EQ."Turner  ")THEN
                RES(I)=5
           ELSE
                RES(I)=6
           END IF
      END DO
301   FORMAT(A8,8X,A4,4X,F6.2,5X,F5.1,4X,F6.4,3X,F7.4,3X,F7.4,3X,F7.4,
     1 4X,F6.4,4X,F6.4,4X,F6.4)

      CLOSE(5)

      END SUBROUTINE
```

```
c     Randy Clark
c     This subroutine is designed to write the RELAP input file

c      PROGRAM INWRITE
      SUBROUTINE INWRITE(ST,PRES,TMP,MFV,MFL,XST,TOPP,DPDZ,ENTL,TESTL,
     1 DI)

      IMPLICIT NONE

      INTEGER I,J,N,SYSTEM,MINCD,ST
      DOUBLE PRECISION PRES,TMP,MFV,MFL,XST,TOPP,DPDZ,ENTL,TESTL,DI,AR
      DOUBLE PRECISION RGH1,RGH2,EPP,TPP,XPP,PI
      CHARACTER(6) MINVAR

      OPEN(UNIT=3, NAME = "input.i", STATUS = "UNKNOWN")
      N=SYSTEM("chmod 777 input.i")

      WRITE (3,99) "*",ST,PRES,DPDZ
99    FORMAT(A1,2X,I1,2X,F7.3,2X,F7.4)
c     Card#     Prob.Typ.   Opt.
      WRITE (3,100) 100,"new","transnt"
100   FORMAT(I3,2X,A3,2X,A7)
c     Card#     RunOpt.
      WRITE (3,101) 101,"run"
101   FORMAT(I3,2X,A3)
c     Card# InUnits OutUnits
      WRITE(3,102) 102,"british","british"
102   FORMAT(I3,2X,A7,2X,A7)
c     Card#     CPUTimeLim1   CPUTimeLim2
      WRITE (3,103) 105,5.0,10.0
103   FORMAT(I3,2X,F3.1,2X,F4.1)
c     Card# Non-Condensible Gas
      IF(ST.NE.4)THEN
           WRITE(3,129) 110,"air"
      END IF
129   FORMAT(I3,2X,A3)
c     Card#     InitTimeVal
      WRITE (3,104) 200,0.0
104   FORMAT(I3,2X,F3.1)
c     Card# EndT MinDT MaxDT ssdtt MinEdFreq MajEdFreq RstFreq
      WRITE (3,105) 201,200.0,"1.0d-9",0.10,"00000",10,100,100
105   FORMAT(I3,2X,F5.1,2X,A6,2X,F4.2,2X,A5,2X,I3,2X,I4,2X,I4)

c     Minor Edits
c     Card#  Variable  Volume/Junction
      MINCD=300
      DO I=1,12
           IF(I.EQ.1)THEN
                MINVAR="p"
           ELSEIF(I.EQ.2)THEN
                MINVAR="floreg"
           ELSEIF(I.EQ.3)THEN
                MINVAR="fwalf"
           ELSEIF(I.EQ.4)THEN
```

```
                MINVAR="fwalg"
           ELSEIF(I.EQ.5)THEN
                MINVAR="rhof"
           ELSEIF(I.EQ.6)THEN
                MINVAR="rhog"
           ELSEIF(I.EQ.7)THEN
                MINVAR="viscf"
           ELSEIF(I.EQ.8)THEN
                MINVAR="viscg"
           ELSEIF(I.EQ.9)THEN
                MINVAR="sigma"
           ELSEIF(I.EQ.10)THEN
                MINVAR="voidf"
           ELSEIF(I.EQ.11)THEN
                MINVAR="tempf"
           ELSEIF(I.EQ.12)THEN
                MINVAR="tempg"
           ENDIF
           DO J=1,5
                MINCD=MINCD+1
                WRITE(3,106) MINCD,MINVAR,200000000+J*10000
106             FORMAT(I3,2X,A6,2X,I9)
           END DO
      END DO

      MINCD=MINCD+1

      WRITE(3,106) MINCD,"velfj ",150000000

      DO I=1,4
           MINCD=MINCD+1
           WRITE(3,106) MINCD,"velfj ",200000000+I*10000
      END DO

      MINCD=MINCD+1

      WRITE(3,106) MINCD,"velfj ",205000000

      MINCD=MINCD+1

      WRITE(3,106) MINCD,"velgj ",150000000

      DO I=1,4
           MINCD=MINCD+1
           WRITE(3,106) MINCD,"velgj ",200000000+I*10000
      END DO

      MINCD=MINCD+1

      WRITE(3,106) MINCD,"velgj ",205000000

      MINCD=MINCD+1

      WRITE(3,106) MINCD,"vgjj  ",150000000

      DO I=1,4
           MINCD=MINCD+1
```

```
     WRITE(3,106) MINCD,"vgjj  ",200000000+I*10000
END DO

MINCD=MINCD+1

WRITE(3,106) MINCD,"vgjj  ",205000000

MINCD=MINCD+1

WRITE(3,106) MINCD,"fij   ",150000000

DO I=1,4
     MINCD=MINCD+1
     WRITE(3,106) MINCD,"fij   ",200000000+I*10000
END DO

MINCD=MINCD+1

WRITE(3,106) MINCD,"fij   ",205000000

MINCD=MINCD+1

WRITE(3,106) MINCD,"iregj ",150000000

DO I=1,4
     MINCD=MINCD+1
     WRITE(3,106) MINCD,"iregj ",200000000+I*10000
END DO

MINCD=MINCD+1

WRITE(3,106) MINCD,"iregj ",205000000

MINCD=MINCD+1

WRITE(3,106) MINCD,"florgj",150000000

DO I=1,4
     MINCD=MINCD+1
     WRITE(3,106) MINCD,"florgj",200000000+I*10000
END DO

MINCD=MINCD+1

WRITE(3,106) MINCD,"florgj",205000000

PI=3.141592654d0
AR=PI*(DI/2.0d0)**2

IF(ST.EQ.1)THEN
     RGH1=4.92d-6
     RGH2=4.92d-6
ELSE IF(ST.EQ.2)THEN
     IF(DI.EQ.0.1250d0)THEN
          RGH1=3.28d-5
          RGH2=3.28d-5
     ELSE
```

```
                RGH1=4.92d-6
                RGH2=4.92d-6
           END IF
      ELSE IF(ST.EQ.3)THEN
           RGH1=4.92d-6
           RGH2=4.92d-6
      ELSE IF(ST.EQ.4)THEN
           RGH1=4.92d-6
           RGH2=4.92d-6
      ELSE IF(ST.EQ.5)THEN
           RGH1=4.92d-6
           RGH2=4.92d-6
      ELSE
           RGH1=4.92d-6
           RGH2=4.92d-6
      END IF

c     Components
c     Vapor Inlet Time Dependent Volume
c     Card#  Name  Comp.Typ.
      WRITE(3,107) 1000000,"vinvol","tmdpvol"
107   FORMAT(I7,2X,A8,2X,A8)
c     Card# Area Length Volume AzAng. Inc.Ang. dz Rough DH tlpvbfe
      WRITE(3,108) 1000101,AR,5.0,0.0,0.0,0.0,0.0,RGH1,DI,"0000000"
108   FORMAT(I7,2X,F5.3,2X,5(F5.1,2X),F10.8,2X,F6.4,2X,A7)
c     Card# ebt
c     e specifies the fluid (0=default or H20)
c     b specifies presence of boron (0=no boron,1=boron)
c     t specifies thermodynamic state quantities to be used
c     (t=0->Pressure,uf,ug,void fraction)
c     (t=1->Temperature,StaticQual.)
c     (t=2->Pressure,StaticQual.)
c     (t=3->Pressure,Temperature)
c     (t=4->Pressure,Temperature,StaticQual.)
c     (t=5->Temperature,StaticQual.,NonCondQual.)
c     (t=6->Pressure,uf,ug,Void.Frac.,NonCondQual.)
      IF(ST.NE.4)THEN
           WRITE(3,109) 1000200,"004"
           WRITE(3,130) 1000201,0.0,PRES,TMP,1.0
      ELSE
           WRITE(3,109) 1000200,"002"
           WRITE(3,110) 1000201,0.0,PRES,1.0
      END IF
109   FORMAT(I7,2X,A3)
110   FORMAT(I7,2X,F3.1,2X,F7.3,2X,F6.4)
130   FORMAT(I7,2X,F3.1,2X,F7.3,2X,F7.3,2X,F10.8)

c     Vapor Inlet Junction
c     Card# Name Comp.Typ.
      WRITE(3,107) 1050000,"vinjun","tmdpjun"
c     Card# FromVol ToVol Area
      WRITE(3,111) 1050101,100010000,106000000,0.0
111   FORMAT(I7,2X,I9,2X,I9,2X,F3.1)
c     Card# Control(0->Velocities,1->Mass Flow rates)
      WRITE(3,112) 1050200,1
112   FORMAT(I7,2X,I1)
c     Card# Time Liq.MassFlow Vap.MassFlow InterfaceVel.
```

```
      WRITE(3,113) 1050201,0.0,0.0,MFV,0
113   FORMAT(I7,2X,F5.1,2X,F5.3,2X,F5.3,2X,I1)
      WRITE(3,113) 1050202,200.0,0.0,MFV,0

c     Vapor Inlet Pipe
c     Card# Name Comp.Typ.
      WRITE(3,107) 1060000,"vinpip","pipe"
c     Card# Volumes
      WRITE(3,114) 1060001,1
114   FORMAT(I7,2X,I1)
c     Card# Area Volume#
      WRITE(3,115) 1060101,AR,1
115   FORMAT(I7,2X,F5.3,2X,I1)
c     Card# Length Volume#
      WRITE(3,116) 1060301,0.5,1
116   FORMAT(I7,2X,F8.5,2X,I1)
c     Card# Volume Volume#
      WRITE(3,116) 1060401,0.0,1
c     Card# Vert.Angle Volume#
      WRITE(3,116) 1060601,0.0,1
c     Card# dz Volume#
      WRITE(3,116) 1060701,0.0,1
c     Card# Rough. DH Volume#
      WRITE(3,117) 1060801,RGH1,DI,1
117   FORMAT(I7,2X,F10.8,2X,F6.4,2X,I1)
c     Card# tlpvbfe Vol.#
c     t->thermal front tracking model 0=off,1=on
c     l->mixture level tracking model 0=off,1=on
c     p->water packing scheme 0=on,1=off
c     v->vertical stratification model 0=on,1=off
c     b->interphase friction model 0=pipe,1=rod bundle,2=ORNL ANS
c     f->wall friction model 0=wall friction,1=no wall friction
c     e->(non)equilibrium 0=non-equilibrium model,1=equilibrium model
      WRITE(3,118) 1061001,"0011000",1
118   FORMAT(I7,2X,A7,2X,I1)
c     Card# ebt Var1 Var2 Var3 Var4 Var5 Vol#
c     e specifies the fluid (0=default or H20)
c     b specifies presence of boron (0=no boron,1=boron)
c     t specifies thermodynamic state quantities to be used
c     (t=0->Pressure,uf,ug,void fraction)
c     (t=1->Temperature,StaticQual.)
c     (t=2->Pressure,StaticQual.)
c     (t=3->Pressure,Temperature)
c     (t=4->Pressure,Temperature,StaticQual.)
c     (t=5->Temperature,StaticQual.,NonCondQual.)
c     (t=6->Pressure,uf,ug,Void.Frac.,NonCondQual.)
      IF(ST.NE.4)THEN
           WRITE(3,131) 1061201,"004",PRES,TMP,1.0,0.0,0.0,1
      ELSE
           WRITE(3,119) 1061201,"002",PRES,1.0,0.0,0.0,0.0,1
      END IF
119   FORMAT(I7,2X,A3,2X,F7.3,2X,4(F7.4,2X),I1)
131   FORMAT(I7,2X,A3,2X,F7.3,2X,F7.3,2X,3(F7.4,2X),I1)

c     Liquid Inlet Time Dependent Volume
c     Card# Name Comp.Typ.
      WRITE(3,107) 1100000,"linvol","tmdpvol"
```

```
c     Card# Area Length Volume AzAng. Inc.Ang. dz Rough DH tlpvbfe
c     t->thermal front tracking model 0=off,1=on
c     l->mixture level tracking model 0=off,1=on
c     p->water packing scheme 0=on,1=off
c     v->vertical stratification model 0=on,1=off
c     b->interphase friction model 0=pipe,1=rod bundle,2=ORNL ANS
c     f->wall friction model 0=wall friction,1=no wall friction
c     e->(non)equilibrium 0=non-equilibrium model,1=equilibrium model
      WRITE(3,108) 1100101,AR,5.0,0.0,0.0,0.0,0.0,RGH1,DI,"0000000"
c     Card# ebt
c     e specifies the fluid (0=default or H20)
c     b specifies presence of boron (0=no boron,1=boron)
c     t specifies thermodynamic state quantities to be used
c     (t=0->Pressure,uf,ug,void fraction)
c     (t=1->Temperature,StaticQual.)
c     (t=2->Pressure,StaticQual.)
c     (t=3->Pressure,Temperature)
c     (t=4->Pressure,Temperature,StaticQual.)
c     (t=5->Temperature,StaticQual.,NonCondQual.)
c     (t=6->Pressure,uf,ug,Void.Frac.,NonCondQual.)
      IF(ST.EQ.4)THEN
           WRITE(3,109) 1100200,"002"
           WRITE(3,110) 1100201,0.0,PRES,0.0
      ELSE
           WRITE(3,109) 1100200,"004"
           WRITE(3,130) 1100201,0.0,PRES,TMP,0.00000001
      END IF

c     Liquid Inlet Junction
c     Card# Name Comp.Typ.
      WRITE(3,107) 1150000,"linjun","tmdpjun"
c     Card# FromVol ToVol Area
      WRITE(3,111) 1150101,110010000,116000000,0.0
c     Card# Control(0->Velocities,1->Mass Flow rates)
      WRITE(3,112) 1150200,1
c     Card# Time Liq.MassFlow Vap.MassFlow InterfaceVel.
      WRITE(3,113) 1150201,0.0,MFL,0.0,0
      WRITE(3,113) 1150202,200.0,MFL,0.0,0

c     Liquid Inlet Pipe
c     Card# Name Comp.Typ.
      WRITE(3,107) 1160000,"linpip","pipe"
c     Card# Volumes
      WRITE(3,114) 1160001,1
c     Card# Area Volume#
      WRITE(3,115) 1160101,AR,1
c     Card# Length Volume#
      WRITE(3,116) 1160301,0.5,1
c     Card# Volume Volume#
      WRITE(3,116) 1160401,0.0,1
c     Card# Vert.Angle Volume#
      WRITE(3,116) 1160601,0.0,1
c     Card# dz Volume#
      WRITE(3,116) 1160701,0.0,1
c     Card# Rough. DH Volume#
      WRITE(3,117) 1160801,RGH1,DI,1
c     Card# tlpvbfe Vol.#
```

```
c     t->thermal front tracking model 0=off,1=on
c     l->mixture level tracking model 0=off,1=on
c     p->water packing scheme 0=on,1=off
c     v->vertical stratification model 0=on,1=off
c     b->interphase friction model 0=pipe,1=rod bundle,2=ORNL ANS
c     f->wall friction model 0=wall friction,1=no wall friction
c     e->(non)equilibrium 0=non-equilibrium model,1=equilibrium model
      WRITE(3,118) 1161001,"0011000",1
c     Card# ebt Var1 Var2 Var3 Var4 Var5 Vol#
      IF(ST.EQ.4)THEN
           WRITE(3,119) 1161201,"002",PRES,0.0,0.0,0.0,0.0,1
      ELSE
           WRITE(3,131) 1161201,"004",PRES,TMP,0.0,0.0,0.0,1
      END IF

c     Branch Mixer
c     Card# Name Comp.Typ.
      WRITE(3,107) 1200000,"lvmixer","branch"
c     Card# Junctions Init.Cond.Control (0->Velocities,=/0->Mass Flow)
      WRITE(3,120) 1200001,3,1
120   FORMAT(I7,2X,I1,2X,I1)
c     Card# Area Length Volume AzAng. Inc.Ang. dz Rough DH tlpvbfe
c     t->thermal front tracking model 0=off,1=on
c     l->mixture level tracking model 0=off,1=on
c     p->water packing scheme 0=on,1=off
c     v->vertical stratification model 0=on,1=off
c     b->interphase friction model 0=pipe,1=rod bundle,2=ORNL ANS
c     f->wall friction model 0=wall friction,1=no wall friction
c     e->(non)equilibrium 0=non-equilibrium model,1=equilibrium model
      WRITE(3,108) 1200101,AR,0.5,0.0,0.0,90.0,0.5,RGH1,DI,"0011000"
c     Card# ebt Var1 Var2 Var3 Var4 Var5 (only give necessary variables)
      IF(ST.EQ.4)THEN
           WRITE(3,121) 1200200,"002",PRES,XST
      ELSE
           WRITE(3,132) 1200200,"004",PRES,TMP,XST
      END IF
121   FORMAT(I7,2X,A3,2X,F7.3,2X,F6.4)
132   FORMAT(I7,2X,A3,2X,F7.3,2X,F7.3,2X,F6.4)
c     Card# FromVol. ToVol. Area FLoss RLoss jefvcahs
c     j=0 for branch connection
c     e->modified PV term in energy equation (0=no,1=yes)
c     f->CCFL model (0=off,1=on)
c     v->horizontal stratification entrainment/pullthrough (0=not applied,
c     1=upward oriented junction,2=downward oriented junction,3=centrally
c     located junction)
c     c->Choking model (0=on,1=off)
c     a->Area Change (0=smooth (user K only),1=full abrupt (AAC K+user K),
c     2=partial abrupt (K=1))
c     h->(non)homogeneous velocities (0=nonhomogeneous,1=homogeneous)
c     s->momentum flux (0=both to and from,1=from volume, but not to,
c     2=to volume but not from, 3=no momentum flux)
      WRITE(3,122) 1201101,106010000,120000000,AR,0.0,100.0,
     1 "00001000"
122   FORMAT(I7,2X,I9,2X,I9,2X,F5.3,2X,F3.1,2X,F7.3,2X,A8)
      WRITE(3,122) 1202101,116010000,120000000,AR,0.0,100.0,
     1 "00001000"
      WRITE(3,122) 1203101,120010000,125000000,AR,0.0,0.0,"00001000"
```

```
c     Card# Liq.MassFlow Vap.MassFlow InterfaceVel.
      WRITE(3,123) 1201201,0.0,MFV,0
123   FORMAT(I7,2X,F5.3,2X,F5.3,2X,I1)
      WRITE(3,123) 1202201,MFL,0.0,0
      WRITE(3,123) 1203201,MFL,MFV,0

c     Entrance Length Pipe
c     Card# Name Comp.Typ.
      WRITE(3,107) 1250000,"entpipe","pipe"
c     Card# Volumes
      WRITE(3,114) 1250001,2
c     Card# Area Volume#
      WRITE(3,115) 1250101,AR,2
c     Card# Area Junction#
      WRITE(3,115) 1250201,AR,1
c     Card# Length Volume#
      WRITE(3,116) 1250301,ENTL/2.0d0,2
c     Card# Volume Volume#
      WRITE(3,116) 1250401,0.0,2
c     Card# Vert.Angle Volume#
      WRITE(3,116) 1250601,90.0,2
c     Card# dz Volume#
      WRITE(3,116) 1250701,ENTL/2.0d0,2
c     Card# Rough. DH Volume#
      WRITE(3,117) 1250801,RGH1,DI,2
c     Card# tlpvbfe Vol.#
c     t->thermal front tracking model 0=off,1=on
c     l->mixture level tracking model 0=off,1=on
c     p->water packing scheme 0=on,1=off
c     v->vertical stratification model 0=on,1=off
c     b->interphase friction model 0=pipe,1=rod bundle,2=ORNL ANS
c     f->wall friction model 0=wall friction,1=no wall friction
c     e->(non)equilibrium 0=non-equilibrium model,1=equilibrium model
      WRITE(3,118) 1251001,"0011000",2
c     Card# jefvcahs Junction#
c     j=0 for branch connection
c     e->modified PV term in energy equation (0=no,1=yes)
c     f->CCFL model (0=off,1=on)
c     v->horizontal stratification entrainment/pullthrough (0=not applied,
c     1=upward oriented junction,2=downward oriented junction,3=centrally
c     located junction)
c     c->Choking model (0=on,1=off)
c     a->Area Change (0=smooth (user K only),1=full abrupt (AAC K+user K),
c     2=partial abrupt (K=1))
c     h->(non)homogeneous velocities (0=nonhomogeneous,1=homogeneous)
c     s->momentum flux (0=both to and from,1=from volume, but not to,
c     2=to volume but not from, 3=no momentum flux)
      WRITE(3,124) 1251101,"00001000",1
124   FORMAT(I7,2X,A8,2X,I1)
c     Card# ebt Var1 Var2 Var3 Var4 Var5 Vol#
c     e specifies the fluid (0=default or H20)
c     b specifies presence of boron (0=no boron,1=boron)
c     t specifies thermodynamic state quantities to be used
c     (t=0->Pressure,uf,ug,void fraction)
c     (t=1->Temperature,StaticQual.)
c     (t=2->Pressure,StaticQual.)
c     (t=3->Pressure,Temperature)
```

```
c     (t=4->Pressure,Temperature,StaticQual.)
c     (t=5->Temperature,StaticQual.,NonCondQual.)
c     (t=6->Pressure,uf,ug,Void.Frac.,NonCondQual.)
      EPP=PRES-(DPDZ*(ENTL+0.5d0)/2.0d0)/144.0d0
      IF(ST.EQ.4)THEN
           WRITE(3,119) 1251201,"002",EPP,XST,0.0,0.0,0.0,2
      ELSE
           WRITE(3,131) 1251201,"004",EPP,TMP,XST,0.0,0.0,2
      END IF
c     Card# Control(0=velocities in next card,1=mass flows)
      WRITE(3,125) 1251300,1
125   FORMAT(I7,2X,I1)
c     Card# Liq.MassFlow Vap.MassFlow IntfaceVel(=0) Junction#
      WRITE(3,126) 1251301,MFL,MFV,0,1
126   FORMAT(I7,2X,F5.3,2X,F5.3,2X,I1,2X,I1)

c     Entrance Length Connector to Test Section
c     Card# Name Comp.Typ.
      WRITE(3,107) 1500000,"entjun","sngljun"
c     Card# FromVol. ToVol. Area FLoss RLoss jefvcahs
c     j=0 for branch connection
c     e->modified PV term in energy equation (0=no,1=yes)
c     f->CCFL model (0=off,1=on)
c     v->horizontal stratification entrainment/pullthrough (0=not applied,
c     1=upward oriented junction,2=downward oriented junction,3=centrally
c     located junction)
c     c->Choking model (0=on,1=off)
c     a->Area Change (0=smooth (user K only),1=full abrupt (AAC K+user K),
c     2=partial abrupt (K=1))
c     h->(non)homogeneous velocities (0=nonhomogeneous,1=homogeneous)
c     s->momentum flux (0=both to and from,1=from volume, but not to,
c     2=to volume but not from, 3=no momentum flux)
      WRITE(3,122) 1500101,125010000,200000000,AR,0.0,0.0,"00001000"
c     Card# Cntrl.Word Liq.MassFlow Vap.MassFlow IfVel
      WRITE(3,127) 1500201,1,MFL,MFV,0
127   FORMAT(I7,2X,I1,2X,F5.3,2X,F5.3,2X,I1)

c     Test Section
c     Card# Name Comp.Typ.
      WRITE(3,107) 2000000,"testpipe","pipe"
c     Card# Volumes
      WRITE(3,114) 2000001,5
c     Card# Area Volume#
      WRITE(3,115) 2000101,AR,5
c     Card# Area Junction#
      WRITE(3,115) 2000201,AR,4
c     Card# Length Volume#
      WRITE(3,116) 2000301,TESTL/5.0d0,5
c     Card# Volume Volume#
      WRITE(3,116) 2000401,0.0,5
c     Card# Vert.Angle Volume#
      WRITE(3,116) 2000601,90.0,5
c     Card# dz Volume#
      WRITE(3,116) 2000701,TESTL/5.0d0,5
c     Card# Rough. DH Volume#
      WRITE(3,117) 2000801,RGH2,DI,5
c     Card# tlpvbfe Vol.#
```

```
c     t->thermal front tracking model 0=off,1=on
c     l->mixture level tracking model 0=off,1=on
c     p->water packing scheme 0=on,1=off
c     v->vertical stratification model 0=on,1=off
c     b->interphase friction model 0=pipe,1=rod bundle,2=ORNL ANS
c     f->wall friction model 0=wall friction,1=no wall friction
c     e->(non)equilibrium 0=non-equilibrium model,1=equilibrium model
      WRITE(3,118) 2001001,"0011000",5
c     Card# jefvcahs Junction#
c     j=0 for branch connection
c     e->modified PV term in energy equation (0=no,1=yes)
c     f->CCFL model (0=off,1=on)
c     v->horizontal stratification entrainment/pullthrough (0=not applied,
c     1=upward oriented junction,2=downward oriented junction,3=centrally
c     located junction)
c     c->Choking model (0=on,1=off)
c     a->Area Change (0=smooth (user K only),1=full abrupt (AAC K+user K),
c     2=partial abrupt (K=1))
c     h->(non)homogeneous velocities (0=nonhomogeneous,1=homogeneous)
c     s->momentum flux (0=both to and from,1=from volume, but not to,
c     2=to volume but not from, 3=no momentum flux)
      WRITE(3,124) 2001101,"00001000",4
c     Card# ebt Var1 Var2 Var3 Var4 Var5 Vol#
c     e specifies the fluid (0=default or H20)
c     b specifies presence of boron (0=no boron,1=boron)
c     t specifies thermodynamic state quantities to be used
c     (t=0->Pressure,uf,ug,void fraction)
c     (t=1->Temperature,StaticQual.)
c     (t=2->Pressure,StaticQual.)
c     (t=3->Pressure,Temperature)
c     (t=4->Pressure,Temperature,StaticQual.)
c     (t=5->Temperature,StaticQual.,NonCondQual.)
c     (t=6->Pressure,uf,ug,Void.Frac.,NonCondQual.)
      TPP=PRES-(DPDZ*(0.25d0+ENTL+TESTL/2.0d0))/144.0d0
      IF(ST.EQ.4)THEN
           WRITE(3,119) 2001201,"002",TPP,XST,0.0,0.0,0.0,5
      ELSE
           WRITE(3,131) 2001201,"004",TPP,TMP,XST,0.0,0.0,5
      END IF
c     Card# Control(0=velocities in next card,1=mass flows)
      WRITE(3,125) 2001300,1
c     Card# Liq.MassFlow Vap.MassFlow IntfaceVel(=0) Junction#
      WRITE(3,126) 2001301,MFL,MFV,0,4

c     Test Section Connector to Exit Section
c     Card# Name Comp.Typ.
      WRITE(3,107) 2050000,"extjun","sngljun"
c     Card# FromVol. ToVol. Area FLoss RLoss jefvcahs
c     j=0 for branch connection
c     e->modified PV term in energy equation (0=no,1=yes)
c     f->CCFL model (0=off,1=on)
c     v->horizontal stratification entrainment/pullthrough (0=not applied,
c     1=upward oriented junction,2=downward oriented junction,3=centrally
c     located junction)
c     c->Choking model (0=on,1=off)
c     a->Area Change (0=smooth (user K only),1=full abrupt (AAC K+user K),
c     2=partial abrupt (K=1))
```

```
c     h->(non)homogeneous velocities (0=nonhomogeneous,1=homogeneous)
c     s->momentum flux (0=both to and from,1=from volume, but not to,
c     2=to volume but not from, 3=no momentum flux)
      WRITE(3,122) 2050101,200010000,210000000,AR,0.0,0.0,"00001000"
c     Card# Cntrl.Word Liq.MassFlow Vap.MassFlow IfVel
      WRITE(3,127) 2050201,1,MFL,MFV,0

c     Outpipe Section
c     Card# Name Comp.Typ.
      WRITE(3,107) 2100000,"extpipe","pipe"
c     Card# Volumes
      WRITE(3,114) 2100001,2
c     Card# Area Volume#
      WRITE(3,115) 2100101,AR,2
c     Card# Area Junction#
      WRITE(3,115) 2100201,AR,1
c     Card# Length Volume#
      WRITE(3,116) 2100301,2.5,2
c     Card# Volume Volume#
      WRITE(3,116) 2100401,0.0,2
c     Card# Vert.Angle Volume#
      WRITE(3,116) 2100601,90.0,2
c     Card# dz Volume#
      WRITE(3,116) 2100701,2.5,2
c     Card# Rough. DH Volume#
      WRITE(3,117) 2100801,RGH2,DI,2
c     Card# tlpvbfe Vol.#
c     t->thermal front tracking model 0=off,1=on
c     l->mixture level tracking model 0=off,1=on
c     p->water packing scheme 0=on,1=off
c     v->vertical stratification model 0=on,1=off
c     b->interphase friction model 0=pipe,1=rod bundle,2=ORNL ANS
c     f->wall friction model 0=wall friction,1=no wall friction
c     e->(non)equilibrium 0=non-equilibrium model,1=equilibrium model
      WRITE(3,118) 2101001,"0011000",2
c     Card# jefvcahs Junction#
c     j=0 for branch connection
c     e->modified PV term in energy equation (0=no,1=yes)
c     f->CCFL model (0=off,1=on)
c     v->horizontal stratification entrainment/pullthrough (0=not applied,
c     1=upward oriented junction,2=downward oriented junction,3=centrally
c     located junction)
c     c->Choking model (0=on,1=off)
c     a->Area Change (0=smooth (user K only),1=full abrupt (AAC K+user K),
c     2=partial abrupt (K=1))
c     h->(non)homogeneous velocities (0=nonhomogeneous,1=homogeneous)
c     s->momentum flux (0=both to and from,1=from volume, but not to,
c     2=to volume but not from, 3=no momentum flux)
      WRITE(3,124) 2101101,"00001000",1
c     Card# ebt Var1 Var2 Var3 Var4 Var5 Vol#
c     e specifies the fluid (0=default or H20)
c     b specifies presence of boron (0=no boron,1=boron)
c     t specifies thermodynamic state quantities to be used
c     (t=0->Pressure,uf,ug,void fraction)
c     (t=1->Temperature,StaticQual.)
c     (t=2->Pressure,StaticQual.)
c     (t=3->Pressure,Temperature)
```

```
c     (t=4->Pressure,Temperature,StaticQual.)
c     (t=5->Temperature,StaticQual.,NonCondQual.)
c     (t=6->Pressure,uf,ug,Void.Frac.,NonCondQual.)
      XPP=PRES-(DPDZ*(ENTL+TESTL+0.25d0+2.5d0))/144.0d0
      IF(ST.EQ.4)THEN
           WRITE(3,119) 2101201,"002",XPP,XST,0.0,0.0,0.0,2
      ELSE
           WRITE(3,131) 2101201,"004",XPP,TMP,XST,0.0,0.0,2
      END IF
c     Card# Control(0=velocities in next card,1=mass flows)
      WRITE(3,125) 2101300,1
c     Card# Liq.MassFlow Vap.MassFlow IntfaceVel(=0) Junction#
      WRITE(3,126) 2101301,MFL,MFV,0,1

c     Test Section Outlet Junction
c     Card# Name Comp.Typ.
      WRITE(3,107) 2500000,"outjun","sngljun"
c     Card# FromVol. ToVol. Area FLoss RLoss jefvcahs
c     j=0 for branch connection
c     e->modified PV term in energy equation (0=no,1=yes)
c     f->CCFL model (0=off,1=on)
c     v->horizontal stratification entrainment/pullthrough (0=not applied,
c     1=upward oriented junction,2=downward oriented junction,3=centrally
c     located junction)
c     c->Choking model (0=on,1=off)
c     a->Area Change (0=smooth (user K only),1=full abrupt (AAC K+user K),
c     2=partial abrupt (K=1))
c     h->(non)homogeneous velocities (0=nonhomogeneous,1=homogeneous)
c     s->momentum flux (0=both to and from,1=from volume, but not to,
c     2=to volume but not from, 3=no momentum flux)
c      WRITE(3,122) 2500101,200010000,300000000,AR,0.0,0.0,"00001000"
      WRITE(3,122) 2500101,210010000,300000000,AR,0.0,0.0,"00001000"
c     Card# Cntrl.Word Liq.MassFlow Vap.MassFlow IfVel
      WRITE(3,127) 2500201,1,MFL,MFV,0

c     Outlet Time Dependent Volume
c     Card# Name Comp.Typ.
      WRITE(3,107) 3000000,"outvol","tmdpvol"
c     Liquid Inlet Time Dependent Volume
c     Card# Area Length Volume AzAng. Inc.Ang. dz Rough DH tlpvbfe
c     t->thermal front tracking model 0=off,1=on
c     l->mixture level tracking model 0=off,1=on
c     p->water packing scheme 0=on,1=off
c     v->vertical stratification model 0=on,1=off
c     b->interphase friction model 0=pipe,1=rod bundle,2=ORNL ANS
c     f->wall friction model 0=wall friction,1=no wall friction
c     e->(non)equilibrium 0=non-equilibrium model,1=equilibrium model
      WRITE(3,108) 3000101,AR,15.0,0.0,0.0,0.0,0.0,RGH2,DI,"0000000"
c     Card# ebt
c     e specifies the fluid (0=default or H20)
c     b specifies presence of boron (0=no boron,1=boron)
c     t specifies thermodynamic state quantities to be used
c     (t=0->Pressure,uf,ug,void fraction)
c     (t=1->Temperature,StaticQual.)
c     (t=2->Pressure,StaticQual.)
c     (t=3->Pressure,Temperature)
c     (t=4->Pressure,Temperature,StaticQual.)
```

```
c     (t=5->Temperature,StaticQual.,NonCondQual.)
c     (t=6->Pressure,uf,ug,Void.Frac.,NonCondQual.)
      IF(ST.EQ.4)THEN
           WRITE(3,109) 3000200,"002"
c     Card# Time Pressure Stat.Qual.
           WRITE(3,110) 3000201,0.0,TOPP,XST
      ELSE
           WRITE(3,109) 3000200,"004"
           WRITE(3,130) 3000201,0.0,TOPP,TMP,XST
      END IF

      WRITE(3,128) "."
128   FORMAT(A1)

      CLOSE(3)

      END SUBROUTINE
```

Rerun.f

```
c     Randy Clark
c     This subroutine runs RELAP using the input file written in the
c     INWRITE subroutine

c      PROGRAM RERUN
      SUBROUTINE RERUN

      IMPLICIT NONE

      INTEGER I,J,K,SYSTEM

      I=SYSTEM("rm input.o")
      J=SYSTEM("rm rstplt")
      K=SYSTEM("./relap5.x -i input.i -o input.o -Z tpfh2onew")

      END SUBROUTINE
```

```
c     Randy Clark
c     This subroutine is designed to read the RELAP output file

c      PROGRAM RELAPREAD
      SUBROUTINE RELAPREAD(TRIP2,SSN)

      IMPLICIT NONE

      INTEGER I,J,K,L,M,N,Q,R,S,T,U,V,TRIP2,SSN,SYSTEM
      DOUBLE PRECISION TM,TIM(901),P(5,901),FR(5,901),FWF(5,901)
      DOUBLE PRECISION FWG(5,901),RF(5,901),RG(5,901),MF(5,901)
      DOUBLE PRECISION MG(5,901),SIG(5,901),ALP(5,901),TF(5,901)
      DOUBLE PRECISION TG(5,901),VFJ(6,901),VGJ(6,901),VJJ(6,901)
      DOUBLE PRECISION FIJ(6,901),JR(6,901),FJR(6,901)
      CHARACTER(6) DTEXT1,DTEXT2

      OPEN(UNIT=4, NAME = "input.o", STATUS = "UNKNOWN")
      OPEN(UNIT=10, NAME = "properties1.txt", STATUS = "UNKNOWN")
      OPEN(UNIT=11, NAME = "properties2.txt", STATUS = "UNKNOWN")
      OPEN(UNIT=12, NAME = "properties3.txt", STATUS = "UNKNOWN")
      OPEN(UNIT=13, NAME = "velocities.txt", STATUS = "UNKNOWN")
      OPEN(UNIT=14, NAME = "frictions.txt", STATUS = "UNKNOWN")

      N=SYSTEM("chmod 777 properties1.txt")
      Q=SYSTEM("chmod 777 properties2.txt")
      R=SYSTEM("chmod 777 properties3.txt")
      S=SYSTEM("chmod 777 velocities.txt")
      T=SYSTEM("chmod 777 frictions.txt")


      TRIP2=0

      U=4

      DO K=1,U

      DTEXT1="Blanks"

      DO 40 WHILE(DTEXT1.NE."1 time")
           READ(4,212) DTEXT1
           IF(DTEXT1.EQ."0*****")THEN
                TRIP2=1
                SSN=(K-1)*50
                GO TO 350
           END IF
40    END DO
212   FORMAT(A6)

      DO J=1,3
           READ(4,*)
      END DO

c      PRINT *, "Big Skip # ",K
c      PRINT *, ((K-1)*50+1),((K-1)*50+50)
```

```
      DO I=1,50
           READ(4,201) TIM(I),P(1,I),P(2,I),P(3,I),P(4,I),P(5,I),
     1      FR(1,I),FR(2,I),FR(3,I),FR(4,I)
      END DO
201   FORMAT(2X,F8.5,5(6X,F7.3),4(7X,F6.4))

c      PRINT *, "Data Read Part 1 of Run ",K

      DO J=1,4
           READ(4,*)
      END DO

      DO I=1,50
           READ(4,202) TM,FR(5,I),FWF(1,I),FWF(2,I),FWF(3,I),FWF(4,I),
     1      FWF(5,I),FWG(1,I),FWG(2,I),FWG(3,I)
      END DO
202   FORMAT(2X,F8.5,7X,F6.4,5(7X,F6.3),4X,3(2X,E11.9E2))

c      PRINT *, "Data read Part 2 of Run ",K

      DO J=1,4
           READ(4,*)
      END DO

      DO I=1,50
           READ(4,203) TM,FWG(4,I),FWG(5,I),RF(1,I),RF(2,I),RF(3,I),
     1      RF(4,I),RF(5,I),RG(1,I),RG(2,I)
      END DO
203   FORMAT(2X,F8.5,4X,2(2X,E11.9E2),2X,5(F7.3,6X),2(E11.9E2,2X))

c      PRINT *, "Data read Part 3 of Run ",K

      DO J=1,4
           READ(4,*)
      END DO

      DO I=1,50
           READ(4,204) TM,RG(3,I),RG(4,I),RG(5,I),MF(1,I),MF(2,I),
     1      MF(3,I),MF(4,I),MF(5,I),MG(1,I)
      END DO
204   FORMAT(2X,F8.5,4X,3(2X,E11.9E2),6(2X,E11.9E2))

c      PRINT *, "Data read Part 4 or Run ",K

      DO J=1,4
           READ(4,*)
      END DO

      DO I=1,50
           READ(4,205) TM,MG(2,I),MG(3,I),MG(4,I),MG(5,I),SIG(1,I),
     1      SIG(2,I),SIG(3,I),SIG(4,I),SIG(5,I)
      END DO
205   FORMAT(2X,F8.5,4X,9(2X,E11.9E2))

c      PRINT *, "Data read Part 5 of Run ",K
```

```
      DO J=1,4
           READ(4,*)
      END DO

      DO I=1,50
           READ(4,206) TM,ALP(1,I),ALP(2,I),ALP(3,I),ALP(4,I),ALP(5,I),
     1      TF(1,I),TF(2,I),TF(3,I),TF(4,I)
           DO J=1,5
                ALP(J,I)=1.0d0-ALP(J,I)
           END DO
      END DO
206   FORMAT(2X,F8.5,6X,5(E11.9E2,2X),1X,4(F6.2,7X))



c      PRINT *, "Data read Part 6 of Run ",K

      DO J=1,4
           READ(4,*)
      END DO

      DO I=1,50
           READ(4,207) TM,TF(5,I),TG(1,I),TG(2,I),TG(3,I),TG(4,I),
     1      TG(5,I),VFJ(1,I),VFJ(2,I),VFJ(3,I)
      END DO
207   FORMAT(2X,F8.5,6(7X,F6.2),3(7X,F6.4))

c      PRINT *, "Data read of Part 7 of Run ",K

      DO J=1,4
           READ(4,*)
      END DO

      DO I=1,50
           READ(4,208) TM,VFJ(4,I),VFJ(5,I),VFJ(6,I),VGJ(1,I),VGJ(2,I),
     1      VGJ(3,I),VGJ(4,I),VGJ(5,I),VGJ(6,I)
      END DO
208   FORMAT(2X,F8.5,3(6X,F7.4),6(6X,F7.3))

c      PRINT *, "Data read of Part 8 of Run ",K

      DO J=1,4
           READ(4,*)
      END DO

      DO I=1,50
           READ(4,209) TM,VJJ(1,I),VJJ(2,I),VJJ(3,I),VJJ(4,I),VJJ(5,I),
     1      VJJ(6,I),FIJ(1,I),FIJ(2,I),FIJ(3,I)
      END DO
209   FORMAT(2X,F8.5,6(6X,F7.4),4X,3(2X,E11.9e2))

c      PRINT *, "Data Read Part 9 of Run ",K

      DO J=1,4
           READ(4,*)
      END DO
```

```
      DO I=1,50
           READ(4,210) TM,FIJ(4,I),FIJ(5,I),FIJ(6,I),JR(1,I),JR(2,I),
     1      JR(3,I),JR(4,I),JR(5,I),JR(6,I)
      END DO
210   FORMAT(2X,F8.5,4X,3(2X,E11.9e2),2X,6(F7.4,6X))

      DO J=1,4
           READ(4,*)
      END DO

      DO I=1,50
           READ(4,211) TM,FJR(1,I),FJR(2,I),FJR(3,I),FJR(4,I),FJR(5,I),
     1      FJR(6,I)
      END DO
211   FORMAT(2X,F8.5,6(7X,F6.4))

c      PRINT *, "Data Read of Part 10 of Run ",K

      DO I=1,50
           WRITE(10,213) TIM(I),(P(L,I),L=1,5),(TF(L,I),L=1,5),
     1      (TG(L,I),L=1,5),(RF(L,I),L=1,5),(RG(L,I),L=1,5)
213   FORMAT(2X,F9.5,5(2X,F8.3),10(2X,F6.2),5(2X,F6.3),5(2X,F7.5))
           WRITE(11,214) TIM(I),(MF(L,I),L=1,5),(MG(L,I),L=1,5),
     1      (SIG(L,I),L=1,5)
214   FORMAT(2X,F9.5,15(2X,E12.6E1))
           WRITE(12,215) TIM(I),(ALP(L,I),L=1,5),(FR(L,I),L=1,5),
     1      (JR(M,I),M=1,6),(FJR(M,I),M=1,6)
215   FORMAT(2X,F9.5,5(2X,F10.8),17(2X,F6.3))
           WRITE(13,216) TIM(I),(VFJ(M,I),M=1,6),(VGJ(M,I),M=1,6),
     1      (VJJ(M,I),M=1,6)
216   FORMAT(2X,F9.5,6(2X,F8.4),6(2X,F8.4),6(2X,F8.4))
           WRITE(14,217) TIM(I),(FWF(L,I),L=1,5),(FWG(L,I),L=1,5),
     1       (FIJ(M,I),M=1,6)
217   FORMAT(2X,F9.5,5(2X,E12.6E1),5(2X,E12.6E1),6(2X,E12.6E1))
      END DO

      END DO

      DTEXT2="Blanks"

      DO 42 WHILE(DTEXT2.NE."1 time")
           READ(4,212) DTEXT2
           IF(DTEXT2.EQ."0*****")THEN
                TRIP2=1
                SSN=U*50
                GO TO 350
           END IF
42    END DO

      DO J=1,3
           READ(4,*)
      END DO

c      PRINT *, "Final Big Skip"

      V=U*50+1
```

```
      READ(4,201) TIM(V),P(1,V),P(2,V),P(3,V),P(4,V),
     1 P(5,V),FR(1,V),FR(2,V),FR(3,V),FR(4,V)

c      PRINT *, "First part of Final set of data read"

      DO J=1,4
           READ(4,*)
      END DO

      READ(4,202) TM,FR(5,V),FWF(1,V),FWF(2,V),FWF(3,V),
     1 FWF(4,V),FWF(5,V),FWG(1,V),FWG(2,V),FWG(3,V)

c      PRINT *, "Second part of Final set of data read"

      DO J=1,4
           READ(4,*)
      END DO

      READ(4,203) TM,FWG(4,V),FWG(5,V),RF(1,V),RF(2,V),
     1 RF(3,V),RF(4,V),RF(5,V),RG(1,V),RG(2,V)

c      PRINT *, "Third part of Final set of data read"

      DO J=1,4
           READ(4,*)
      END DO

      READ(4,204) TM,RG(3,V),RG(4,V),RG(5,V),MF(1,V),
     1 MF(2,V),MF(3,V),MF(4,V),MF(5,V),MG(1,V)

c      PRINT *, "Fourth part of Final set of data read"

      DO J=1,4
           READ(4,*)
      END DO

      READ(4,205) TM,MG(2,V),MG(3,V),MG(4,V),MG(5,V),
     1 ALP(1,V),ALP(2,V),ALP(3,V),ALP(4,V),ALP(5,V)

c      PRINT *, "Fifth part of Final set of data read"

      DO J=1,4
           READ(4,*)
      END DO

      READ(4,206) TM,ALP(1,V),ALP(2,V),ALP(3,V),ALP(4,V),
     1 ALP(5,V),TF(1,V),TF(2,V),TF(3,V),TF(4,V)

c      PRINT *, "Sixth part of Final set of data read"

      DO J=1,4
           READ(4,*)
      END DO

      READ(4,207) TM,TF(5,V),TG(1,V),TG(2,V),TG(3,V),
     1 TG(4,V),TG(5,V),VFJ(1,V),VFJ(2,V),VFJ(3,V)
```

```
c      PRINT *, "Seventh part of Final set of data read"

       DO J=1,4
            READ(4,*)
       END DO

       READ(4,208) TM,VFJ(4,V),VFJ(5,V),VFJ(6,V),VGJ(1,V),
      1 VGJ(2,V),VGJ(3,V),VGJ(4,V),VGJ(5,V),VGJ(6,V)

c      PRINT *, "Eighth part of Final set of data read"

       DO J=1,4
            READ(4,*)
       END DO

       READ(4,209) TM,VJJ(1,V),VJJ(2,V),VJJ(3,V),VJJ(4,V),
      1 VJJ(5,V),VJJ(6,V),FIJ(1,V),FIJ(2,V),FIJ(3,V)
c      PRINT *, "Ninth part of Final set of data read"

       DO J=1,4
            READ(4,*)
       END DO

       READ(4,210) TM,FIJ(4,V),FIJ(5,V),FIJ(6,V),JR(1,V),
      1 JR(2,V),JR(3,V),JR(4,V),JR(5,V),JR(6,V)

       DO J=1,4
            READ(4,*)
       END DO

       READ(4,211) TM,FJR(1,V),FJR(2,V),FJR(3,V),FJR(4,V),FJR(5,V),
      1 FJR(6,V)


c      PRINT *, "Tenth part of Final set of data read"
c      PAUSE

       WRITE(10,213) TIM(V),(P(L,V),L=1,5),(TF(L,V),L=1,5),
      1 (TG(L,V),L=1,5),(RF(L,V),L=1,5),(RG(L,V),L=1,5)
       WRITE(11,214) TIM(V),(MF(L,V),L=1,5),
      1 (MG(L,V),L=1,5),(SIG(L,V),L=1,5)
       WRITE(12,215) TIM(V),(ALP(L,V),L=1,5),(FR(L,V),L=1,5),
      1 (JR(M,V),M=1,6),(FJR(M,V),M=1,6)
       WRITE(13,216) TIM(V),(VFJ(M,V),M=1,6),(VGJ(M,V),M=1,6),
      1 (VJJ(M,V),M=1,6)
       WRITE(14,217) TIM(V),(FWF(L,V),L=1,5),(FWG(L,V),L=1,5),
      1 (FIJ(M,V),M=1,6)

350    CLOSE(4)

       CLOSE(10)
       CLOSE(11)
       CLOSE(12)
       CLOSE(13)
       CLOSE(14)

       END SUBROUTINE
```

```
c     Randy Clark
c     This subroutine checks the pressure data to see if steady state
c     was achieved

      SUBROUTINE SSCHECK(SSN,TRIP1)

      IMPLICIT NONE

      INTEGER I,J,K,L,M,U,V,TRIP1,SSN
      DOUBLE PRECISION TIM(901),P(5,901),DIFF

      OPEN(UNIT=10, NAME="properties1.txt", STATUS="UNKNOWN")

      U=4
      V=50*U+1

      DO I=1,V
           READ(10,501) TIM(I),(P(K,I),K=1,5)
      END DO
501   FORMAT(2X,F9.5,5(2X,F8.3))

      L=10
      TRIP1=0

      DO 51 WHILE(M.NE.5)
         L=L+1
         M=0
         DO J=1,5
              DIFF=ABS(P(J,L)-P(J,L-1))
              DIFF=DIFF+ABS(P(J,L-1)-P(J,L-2))
              DIFF=DIFF+ABS(P(J,L-2)-P(J,L-3))
              DIFF=DIFF+ABS(P(J,L-3)-P(J,L-4))
              DIFF=DIFF+ABS(P(J,L-4)-P(J,L-5))
              DIFF=DIFF+ABS(P(J,L-5)-P(J,L-6))
              DIFF=DIFF+ABS(P(J,L-6)-P(J,L-7))
              DIFF=DIFF+ABS(P(J,L-7)-P(J,L-8))
              DIFF=DIFF+ABS(P(J,L-8)-P(J,L-9))
              DIFF=DIFF+ABS(P(J,L-9)-P(J,L-10))

              IF(DIFF.LT.0.01)THEN
                   M=M+1
              END IF

         END DO

         IF(L.EQ.V)THEN
              TRIP1=1
              M=5
         END IF

51    END DO

      SSN=L
```

```
CLOSE(10)

END SUBROUTINE
```

```
c     Randy Clark
c     This subroutine sets the variables to be analyzed into a single
c     array OUTP

      SUBROUTINE VARSET(SSN,TRIP1,TRIP2,DI,OUTP,JR)

      IMPLICIT NONE

      INTEGER I,J,L,M,U,V,W,TRIP1,TRIP2,TRIP3,SSN
      DOUBLE PRECISION TIM(901),P(5,901),FR(5,901),FWF(5,901)
      DOUBLE PRECISION FWG(5,901),RF(5,901),RG(5,901),MF(5,901)
      DOUBLE PRECISION MG(5,901),SIG(5,901),ALP(5,901),VFJ(6,901)
      DOUBLE PRECISION VGJ(6,901),VJJ(6,901),FIJ(6,901),TF(5,901)
      DOUBLE PRECISION TG(5,901),JR(6,901),FJR(6,901),OUTP(107),PI
      DOUBLE PRECISION PAREA,DI

      U=4
      V=50*U+1
      W=50*(U-1)+1

      PI=3.141592654d0
      PAREA=PI*(DI/2.0d0)**2

      OPEN(UNIT=10, NAME = "properties1.txt", STATUS = "UNKNOWN")
      OPEN(UNIT=11, NAME = "properties2.txt", STATUS = "UNKNOWN")
      OPEN(UNIT=12, NAME = "properties3.txt", STATUS = "UNKNOWN")
      OPEN(UNIT=13, NAME = "velocities.txt", STATUS = "UNKNOWN")
      OPEN(UNIT=14, NAME = "frictions.txt", STATUS = "UNKNOWN")


c      PRINT *, "Files Opened"
c      PRINT *, "TRIP2 = ",TRIP2

      IF((TRIP2.EQ.1).AND.(SSN.NE.0))THEN
           I=0
           DO 43 WHILE(I.NE.SSN)
                I=I+1
                READ(10,551) TIM(I),(P(L,I),L=1,5),(TF(L,I),L=1,5),
     1           (TG(L,I),L=1,5),(RF(L,I),L=1,5),(RG(L,I),L=1,5)
                READ(11,552) TIM(I),(MF(L,I),L=1,5),(MG(L,I),L=1,5),
     1           (SIG(L,I),L=1,5)
                READ(12,553) TIM(I),(ALP(L,I),L=1,5),(FR(L,I),L=1,5),
     1           (JR(M,I),M=1,6),(FJR(M,I),M=1,6)
                READ(13,554) TIM(I),(VFJ(M,I),M=1,6),(VGJ(M,I),M=1,6),
     1           (VJJ(M,I),M=1,6)
                READ(14,555) TIM(I),(FWF(L,I),L=1,5),(FWG(L,I),L=1,5),
     1           (FIJ(M,I),M=1,6)
43         END DO

c           PRINT *, "TRIP2=1, Files Read"
      ELSE IF(SSN.EQ.0)THEN
           GO TO 601
      ELSE
         DO I=1,V
```

```
      READ(10,551) TIM(I),(P(L,I),L=1,5),(TF(L,I),L=1,5),
     1  (TG(L,I),L=1,5),(RF(L,I),L=1,5),(RG(L,I),L=1,5)
      READ(11,552) TIM(I),(MF(L,I),L=1,5),(MG(L,I),L=1,5),
     2  (SIG(L,I),L=1,5)
      READ(12,553) TIM(I),(ALP(L,I),L=1,5),(FR(L,I),L=1,5),
     1  (JR(M,I),M=1,6),(FJR(M,I),M=1,6)
      READ(13,554) TIM(I),(VFJ(M,I),M=1,6),(VGJ(M,I),M=1,6),
     1  (VJJ(M,I),M=1,6)
      READ(14,555) TIM(I),(FWF(L,I),L=1,5),(FWG(L,I),L=1,5),
     1   (FIJ(M,I),M=1,6)
    END DO
551  FORMAT(2X,F9.5,5(2X,F8.3),10(2X,F6.2),5(2X,F6.3),5(2X,F7.5))
552  FORMAT(2X,F9.5,15(2X,E12.6E1))
553  FORMAT(2X,F9.5,5(2X,F10.8),17(2X,F6.3))
554  FORMAT(2X,F9.5,6(2X,F8.4),6(2X,F8.4),6(2X,F8.4))
555  FORMAT(2X,F9.5,5(2X,E12.6E1),5(2X,E12.6E1),6(2X,E12.6E1))
c     PRINT *, "Files Read"

     END IF

     TRIP3=2
601  IF(TRIP2.EQ.0)THEN
          IF(TRIP1.EQ.0)THEN
               TRIP3=0
          ELSE IF(TRIP1.EQ.1)THEN
               TRIP3=2
          END IF
     ELSE IF(TRIP2.EQ.1)THEN
          IF(SSN.EQ.0)THEN
               TRIP3=1
          ELSE
               TRIP3=2
          END IF
     END IF

     IF(TRIP3.EQ.0)THEN
          OUTP(1)=TIM(SSN)
          DO I=1,5
               OUTP(I+1)=P(I,SSN)
               OUTP(I+6)=FR(I,SSN)
               OUTP(I+11)=FWF(I,SSN)
               OUTP(I+16)=FWG(I,SSN)
               OUTP(I+21)=RF(I,SSN)
               OUTP(I+26)=RG(I,SSN)
               OUTP(I+31)=MF(I,SSN)
               OUTP(I+36)=MG(I,SSN)
               OUTP(I+41)=SIG(I,SSN)
               OUTP(I+46)=ALP(I,SSN)
               OUTP(I+51)=TF(I,SSN)
               OUTP(I+56)=TG(I,SSN)
          END DO
          DO I=1,6
               OUTP(I+61)=VFJ(I,SSN)
               OUTP(I+67)=VGJ(I,SSN)
               OUTP(I+73)=VJJ(I,SSN)
               OUTP(I+79)=FIJ(I,SSN)
               OUTP(I+85)=FJR(I,SSN)
```

```
          OUTP(I+91)=JR(I,SSN)
     END DO
ELSE IF(TRIP3.EQ.1)THEN
     OUTP(1)=TIM(1)
     DO I=2,97
          OUTP(I)=-99999999999999999999999999.0d0
     END DO

ELSE IF(TRIP3.EQ.2)THEN
     OUTP(1)=TIM(SSN)
     DO I=2,97
          OUTP(I)=0.0d0
     END DO
     DO J=1,50
          DO I=1,5
               OUTP(I+1)=OUTP(I+1)+P(I,J+SSN-50)
               OUTP(I+6)=OUTP(I+6)+FR(I,J+SSN-50)
               OUTP(I+11)=OUTP(I+11)+FWF(I,J+SSN-50)
               OUTP(I+16)=OUTP(I+16)+FWG(I,J+SSN-50)
               OUTP(I+21)=OUTP(I+21)+RF(I,J+SSN-50)
               OUTP(I+26)=OUTP(I+26)+RG(I,J+SSN-50)
               OUTP(I+31)=OUTP(I+31)+MF(I,J+SSN-50)
               OUTP(I+36)=OUTP(I+36)+MG(I,J+SSN-50)
               OUTP(I+41)=OUTP(I+41)+SIG(I,J+SSN-50)
               OUTP(I+46)=OUTP(I+46)+ALP(I,J+SSN-50)
               OUTP(I+51)=OUTP(I+51)+TF(I,J+SSN-50)
               OUTP(I+56)=OUTP(I+56)+TG(I,J+SSN-50)
          END DO
          DO I=1,6
               OUTP(I+61)=OUTP(I+61)+VFJ(I,J+SSN-50)
               OUTP(I+67)=OUTP(I+67)+VGJ(I,J+SSN-50)
               OUTP(I+73)=OUTP(I+73)+VJJ(I,J+SSN-50)
               OUTP(I+79)=OUTP(I+79)+FIJ(I,J+SSN-50)
               OUTP(I+85)=OUTP(I+85)+FJR(I,J+SSN-50)
               OUTP(I+91)=OUTP(I+91)+JR(I,J+SSN-50)
          END DO
     END DO

     DO I=2,97
          OUTP(I)=OUTP(I)/(50.0d0)
     END DO

END IF

DO I=1,6
     IF(OUTP(I+85).LE.5.5)THEN
          OUTP(I+97)=OUTP(I+79)*(OUTP(I+73)**2)
     ELSE
          OUTP(I+97)=OUTP(I+79)*(OUTP(I+67)-OUTP(I+61))**2
     END IF
END DO

CLOSE(10)
CLOSE(11)
CLOSE(12)
CLOSE(13)
CLOSE(14)
```

```
END SUBROUTINE
```

```
c     Randy Clark
c     This subroutine sets the variables to be analyzed into a single
c     array OUTP

      SUBROUTINE CALC(OUTP,SSN,JR,DI,TESTL,FOUT)

      IMPLICIT NONE

      INTEGER I,SSN
      DOUBLE PRECISION OUTP(107),DZ,RPGF,RRGG,RAGG,RVGG,PRES,FLOREG
      DOUBLE PRECISION FWALLF,RHOF,RHOG,MUF,MUG,SIGMA,ALPHAG,JVL,JVG
      DOUBLE PRECISION JVGJ,JFI,VDZ,JDZ,FWALLG,TEMPF,TEMPG,JFLRG,IFLRG
      DOUBLE PRECISION JR(6,901),FOUT(50),VVF(5),VVG(5),WF(5),WG(5)
      DOUBLE PRECISION WT(5),JALP(4),SIGJ(4),RFJ(4),RGJ(4),JGJ(4)
      DOUBLE PRECISION JFJ(4),JGJP(4),JFINT,PI,PAREA,PCRIT,JGJPA,JFIN
      DOUBLE PRECISION C1CL,REG,REF,A1,B1CL,KNOT,LFUNC,C0CL,C5CL,C6CL
      DOUBLE PRECISION C7CL,C8CL,C2CL,C3CL,C4CL,C9CL,VGJCL,GKI,CINFKI
      DOUBLE PRECISION C0KI,DSTAR,MUFN,VGJKI,C0CT,VGJCT,CNOT,DFVEL,CONE
      DOUBLE PRECISION RELV,CEYE,UC,CF,ALPFF,ALPFD,AGF,DNOT,REGA,FIA
      DOUBLE PRECISION CINGKI,CGJCT,FEYE,FI,VELF,VELG,RHOM,FINT,FIF,FIG
      DOUBLE PRECISION FINTF,FINTG,AGF1,AGF2,RED,CDD,DI,TESTL

c     OUTP(1) is the steady-state time
c     OUTP(2-6) are the pressures in the five test section volumes
c     OUTP(7-11) are the volume flow regimes
c     OUTP(12-16) are the liquid wall friction values
c     OUTP(17-21) are the vapor wall frition values
c     OUTP(22-26) are the liquid density values
c     OUTP(27-31) are the vapor density values
c     OUTP(32-36) are the liquid viscosity values
c     OUTP(37-41) are the vapor viscosity values
c     OUTP(42-46) are the liquid surface tension values
c     OUTP(47-51) are the void fraction values
c     OUTP(52-56) are the liquid temperatures
c     OUTP(57-61) are the vapor temperatures
c     OUTP(62-67) are the junction liquid velocities
c     OUTP(68-73) are the junction vapor velocities
c     OUTP(74-79) are the junction drift flux velocities
c     OUTP(80-85) are the interphase friction factor values
c     OUTP(86-91) are the junction flow regimes
c     OUTP(92-97) are the Bubbly/Slug interphase drag flow regimes
c     OUTP(98-103) are the interphase friction force values

c     Change in height between the center of the bottom volume and the
c     center of the top volume
      VDZ=4.0d0*(TESTL/5.0d0)
      JDZ=3.0d0*(TESTL/5.0d0)

c     Gradients in the test Section
      RPGF=144.0d0*(OUTP(2)-OUTP(6))/VDZ
      RRGG=(OUTP(27)-OUTP(31))/VDZ
      RAGG=(OUTP(51)-OUTP(47))/VDZ
      RVGG=(OUTP(72)-OUTP(69))/JDZ
```

```
      PI=3.141592654d0
      PAREA=PI*(DI/2.0d0)**2

      DO I=1,5
           VVF(I)=(OUTP(I+61)+OUTP(I+62))/2.0d0
           VVG(I)=(OUTP(I+67)+OUTP(I+68))/2.0d0
           WF(I)=(1-OUTP(I+46))*OUTP(I+21)*VVF(I)*PAREA
           WG(I)=OUTP(I+46)*OUTP(I+21)*VVG(I)*PAREA
           WT(I)=WF(I)+WG(I)
      END DO

      DO I=1,4
           JALP(I)=(OUTP(I+46)+OUTP(I+47))/2.0d0
           SIGJ(I)=(OUTP(I+41)+OUTP(I+42))/2.0d0
           RFJ(I)=(OUTP(I+21)+OUTP(I+22))/2.0d0
           RGJ(I)=(OUTP(I+26)+OUTP(I+27))/2.0d0
           JGJ(I)=JALP(I)*OUTP(I+68)
           JFJ(I)=(1-JALP(I))*OUTP(I+61)
           JGJP(I)=(SIGJ(I)*(RFJ(I)-RGJ(I))*32.174d0)/(RFJ(I)**2)
           JGJP(I)=JGJ(I)/(JGJP(I)**0.25d0)
      END DO

c     Average Values in the the Test Section
      PRES=0.0d0
      FLOREG=0.0d0
      IFLRG=0.0d0
      JFLRG=0.0d0
      FWALLF=0.0d0
      FWALLG=0.0d0
      RHOF=0.0d0
      RHOG=0.0d0
      MUF=0.0d0
      MUG=0.0d0
      SIGMA=0.0d0
      ALPHAG=0.0d0
      TEMPF=0.0d0
      TEMPG=0.0d0
      JVL=0.0d0
      JVG=0.0d0
      JVGJ=0.0d0
      JFI=0.0d0
      JFINT=0.0d0
      JFIN=0.0d0
      DO I=1,5
           PRES=PRES+OUTP(I+1)
           FLOREG=FLOREG+OUTP(I+6)
           FWALLF=FWALLF+OUTP(I+11)
           FWALLG=FWALLG+OUTP(I+16)
           RHOF=RHOF+OUTP(I+21)
           RHOG=RHOG+OUTP(I+26)
           MUF=MUF+OUTP(I+31)
           MUG=MUG+OUTP(I+36)
           SIGMA=SIGMA+OUTP(I+41)
           ALPHAG=ALPHAG+OUTP(I+46)
           TEMPF=TEMPF+OUTP(I+51)
           TEMPG=TEMPG+OUTP(I+56)
      END DO
```

```
      DO I=1,4
           JVL=JVL+OUTP(I+62)
           JVG=JVG+OUTP(I+68)
           JVGJ=JVGJ+OUTP(I+74)
           JFI=JFI+OUTP(I+80)
           JFLRG=JFLRG+OUTP(I+86)
           IFLRG=IFLRG+OUTP(I+92)
           JFINT=JFINT+OUTP(I+98)
           JFIN=JFIN+OUTP(I+103)
      END DO

      PRES=PRES/5.0d0
      FLOREG=FLOREG/5.0d0
      FWALLF=FWALLF/5.0d0
      FWALLG=FWALLG/5.0d0
      RHOF=RHOF/5.0d0
      RHOG=RHOG/5.0d0
      MUF=MUF/5.0d0
      MUG=MUG/5.0d0
      SIGMA=SIGMA/5.0d0
      ALPHAG=ALPHAG/5.0d0
      TEMPF=TEMPF/5.0d0
      TEMPG=TEMPG/5.0d0
      JVL=JVL/4.0d0
      JVG=JVG/4.0d0
      JVGJ=JVGJ/4.0d0
      JFI=JFI/4.0d0
      JFLRG=JFLRG/4.0d0
      IFLRG=IFLRG/4.0d0
      JFINT=JFINT/4.0d0
      JFIN=JFIN/4.0d0

      VELG=JVG
      VELF=JVL

c     Chexal-Lellouche Calculations
      PCRIT=3200.1123d0
      C1CL=ABS((4.0d0*PCRIT**2)/(PRES*(PCRIT-PRES)))
      REG=RHOG*ALPHAG*JVG*0.0874d0/MUF
      REF=RHOF*(1-ALPHAG)*JVL*0.0874d0/MUG
      IF((REG.GT.REF).OR.(REG.LT.0.0d0))THEN
           A1=1.0d0/(1.0d0+EXP(-REG/60000.0d0))
      ELSE
           A1=1.0d0/(1.0d0+EXP(-REF/60000.0d0))
      END IF
      B1CL=MIN(0.80d0,A1)
      KNOT=B1CL+(1.0d0-B1CL)*SQRT(SQRT(RHOG/RHOF))
      LFUNC=(1-EXP(-C1CL*ALPHAG))/(1-EXP(-C1CL))
      C0CL=ALPHAG**((1.0d0+1.57d0*(RHOG/RHOF))/(1-B1CL))
      C0CL=KNOT+(1.0d0-KNOT)*C0CL
      C0CL=LFUNC/C0CL
      C5CL=SQRT(150.0d0*(RHOG/RHOF))
      C6CL=C5CL/(1.0d0-C5CL)
      C7CL=((9.144d0/(2.54d0*12.0d0))/0.0874d0)**0.60d0
      C8CL=C7CL/(1-C7CL)
      IF(C5CL.GE.1.0d0)THEN
           C2CL=1.0d0
```

```
      ELSE
           C2CL=1.0d0/(1.0d0-EXP(-C6CL))
      END IF
      C3CL=MAX(0.50,2.0d0*EXP(-ABS(REF)/60000))
      IF(C7CL.GE.1.0d0)THEN
           C4CL=1.0d0
      ELSE
           C4CL=1.0d0/(1.0d0-EXP(-C8CL))
      END IF
      IF(REG.GE.0.0d0)THEN
           C9CL=(1.0d0-ALPHAG)*B1CL
      ELSE
           C9CL=MIN(0.7d0,(1-ALPHAG)**0.65d0)
      END IF
      VGJCL=SQRT(SQRT((RHOF-RHOG)*SIGMA*32.174d0/(RHOF**2)))
      VGJCL=1.41*VGJCL*C2CL*C3CL*C4CL*C9CL

c     Kataoka-Ishii
      GKI=(ALPHAG*RHOG*JVG+(1-ALPHAG)*RHOF*JVL)
      GKI=GKI*(1.0d4/(2.2d0*144.0d0*(2.54d0**2)))
      CINFKI=RHOF*SQRT(32.174d0*0.0874d0)
      CINFKI=CINFKI*(1.0d4/(2.2d0*144.0d0*2.54d0**2))
      CINFKI=1.0d0+0.2d0*SQRT(CINGKI/(ABS(GKI)+0.001d0))
      C0KI=CINFKI-(CINFKI-1.0d0)*SQRT(RHOG/RHOF)
      DSTAR=0.0874d0*SQRT((RHOF-RHOG)*32.174d0/SIGMA)
      MUFN=MUF/SQRT(SQRT(SIGMA/((RHOF-RHOG)*32.174d0))*RHOF*SIGMA)
      IF(DSTAR.LE.30.0d0)THEN
           VGJKI=SQRT(SQRT(SIGMA*(RHOF-RHOG)*32.174d0/(RHOF**2)))
           VGJKI=((RHOG/RHOF)**-0.157d0)*(MUFN**-0.562d0)*VGJKI
           VGJKI=0.0019*(DSTAR**0.809d0)*VGJKI
      ELSE
           VGJKI=SQRT(SQRT(SIGMA*(RHOF-RHOG)*32.174d0/(RHOF**2)))
           VGJKI=0.03d0*((RHOG/RHOF)**-0.157d0)*(MUFN**-0.562d0)*VGJKI
      END IF

c     Churn-Turbulent Bubbly Flow
      C0CT=C0KI
      VGJCT=1.41d0*SQRT(SQRT(SIGMA*(RHOF-RHOG)*32.174d0/(RHOF**2)))

      JGJPA=SQRT(SQRT(SIGMA*(32.174d0**2)*(RHOF-RHOG)/(RHOF**2)))
      JGJPA=ALPHAG*JVG/JGJPA

      IF(GKI.GE.100.0d0)THEN
           CNOT=C0CL
           DFVEL=VGJCL
      ELSE IF(GKI.LE.50.0)THEN
           IF(JGJPA.LE.0.5d0)THEN
                CNOT=C0CT
                DFVEL=VGJCT
           ELSE IF(JGJPA.GE.1.768d0)THEN
                CNOT=C0KI
                DFVEL=VGJKI
           ELSE
                CNOT=(JGJPA-0.50d0)*(C0KI-C0CT)/1.268d0+C0CT
                DFVEL=(JGJPA-0.50d0)*(VGJKI-CGJCT)/1.268d0+C0CT
           END IF
      ELSE
```

```
            IF(JGJPA.LE.0.5d0)THEN
                 CNOT=C0CT+(C0CL-C0CT)*(GKI-50.0d0)/50.0d0
                 DFVEL=VGJCT+(VGJCL-VGJCT)*(GKI-50.0d0)/50.0d0
            ELSE IF(JGJPA.GE.1.768d0)THEN
                 CNOT=C0KI+(C0CL-C0KI)*(GKI-50.0d0)/50.0d0
                 DFVEL=VGJKI+(VGJCL-VGJKI)*(GKI-50.0d0)/50.0d0
            ELSE
                 CNOT=(JGJPA-0.50d0)*(C0KI-C0CT)/1.268d0+C0CT
                 CNOT=CNOT+(C0CL-CNOT)*(GKI-50.0d0)/50.0d0
                 DFVEL=(JGJPA-0.50d0)*(VGJKI-CGJCT)/1.268d0+C0CT
                 DFVEL=DFVEL+(VGJCL-DFVEL)*(GKI-50.0d0)/50.0d0
            END IF
       END IF

       CONE=(1-ALPHAG*CNOT)/(1-ALPHAG)
       RELV=DFVEL/(1-ALPHAG)

c      Annular Flow
       UC=3.2d0*SQRT(SQRT(SIGMA*(RHOF-RHOG)*32.174d0/(RHOG**2)))
       CF=SQRT(SQRT((1-ALPHAG)*RHOF*ABS(VELF)*0.0874d0/MUF))
       CF=1.0d0-(1.0d-4)*CF
       ALPFF=(1.0d0-ALPHAG)*CF
       ALPFF=ALPFF*EXP((-7.5d-5)*((ALPHAG*VELG/UC)**6))
       ALPFD=((1-ALPHAG)-ALPFF)/(1-ALPFF)
       DNOT=1.50d0*SIGMA*32.174d0/(RHOG*(VELG-VELF)**2)
       AGF1=(4.0d0/0.0874d0)*((30*ALPFF)**(0.125d0))*SQRT(1-ALPFF)
       AGF2=(3.6*ALPFD/DNOT)*(1-ALPFF)
       AGF=AGF1+AGF2
       REGA=RHOG*ABS(VELG-VELF)*SQRT(ALPHAG)*0.0874d0/MUG
       IF(REGA.LE.500.0d0)THEN
            FIA=64.0d0/REGA
       ELSE IF(REGA.GE.1500.0d0)THEN
            FIA=0.02d0*(1.0d0+150.0d0*(1.0d0-SQRT(1.0d0-ALPFF)))
       ELSE
            FIA=0.02d0*(1.0d0+150.0d0*(1.0d0-SQRT(1.0d0-ALPFF)))
            FIA=FIA*(REGA-500.0d0)/1000.0d0
            FIA=((1500.0d0-REGA)/1000.0d0)*(64.0d0/REGA)+FIA
       END IF
       RED=RHOG*ABS(VELG-VELF)*DNOT*(ALPHAG**2.5d0)/MUG
       CDD=24.0d0*(1.0d0+0.1d0*(RED**0.75d0))/RED

c      Interphase Friction Force Calculations
       RHOM=ALPHAG*RHOG+(1.0d0-ALPHAG)*RHOF

       IF(JFLRG.LT.5.5d0)THEN
            CEYE=ALPHAG*((1.0d0-ALPHAG)**3)*(RHOF-RHOG)/(DFVEL**2.0d0)
            FEYE=CEYE*ABS(CONE*VELG-CNOT*VELF)*(CONE*VELG-CNOT*VELF)
            FI=(FEYE/(ALPHAG*RHOG))+(FEYE/((1-ALPHAG)*RHOF))
            FI=FI/(RHOM*(CONE*VELG-CNOT*VELF))
            FIF=ALPHAG*RHOG*FI
            FIG=(1.0d0-ALPHAG)*RHOF*FI
            FINTF=(1.0d0-ALPHAG)*RHOF*FIF*(CONE*VELG-CNOT*VELF)
            FINTG=ALPHAG*RHOG*FIG*(CONE*VELG-CNOT*VELF)
            FINT=JFI*ABS(CONE*VELG-CNOT*VELF)*(CONE*VELG-CNOT*VELF)
       ELSE
            CEYE=RHOG*(FIA*AGF1+CDD*AGF2)/(8.0d0*32.174d0)
            FEYE=CEYE*ABS(VELG-VELF)*(VELG-VELF)
```

```
      FI=(FEYE/(ALPHAG*RHOG))+(FEYE/((1-ALPHAG)*RHOF))
      FI=FI/(RHOM*(VELG-VELF))
      FIF=ALPHAG*RHOG*FI
      FIG=(1.0d0-ALPHAG)*RHOF*FI
      FINTF=(1.0d0-ALPHAG)*RHOF*FIF*(CONE*VELG-CNOT*VELF)
      FINTG=ALPHAG*RHOG*FIG*(CONE*VELG-CNOT*VELF)
      FINT=JFI*ABS(VELG-VELF)*(VELG-VELF)
END IF

FOUT(1)=RPGF
FOUT(2)=RRGG
FOUT(3)=RAGG
FOUT(4)=RVGG
FOUT(5)=FLOREG
FOUT(6)=FWALLF
FOUT(7)=FWALLG
FOUT(8)=RHOF
FOUT(9)=RHOG
FOUT(10)=MUF
FOUT(11)=MUG
FOUT(12)=SIGMA*32.174d0
FOUT(13)=ALPHAG
FOUT(14)=TEMPF
FOUT(15)=TEMPG
FOUT(16)=JVL
FOUT(17)=JVG
FOUT(18)=JVGJ
FOUT(19)=JFI
FOUT(20)=JFLRG
FOUT(21)=JFINT
FOUT(22)=CNOT
FOUT(23)=DFVEL
FOUT(24)=CONE
FOUT(25)=RELV
FOUT(26)=CEYE
FOUT(27)=FIA
FOUT(28)=FI
FOUT(29)=FINT
FOUT(30)=GKI
FOUT(31)=JGJPA
FOUT(32)=FEYE
FOUT(33)=JFIN
FOUT(34)=FIF
FOUT(35)=FIG
FOUT(36)=FINTF
FOUT(37)=FINTG
FOUT(38)=AGF
FOUT(39)=AGF1
FOUT(40)=AGF2
FOUT(41)=ALPFF
FOUT(42)=ALPFD
FOUT(43)=DNOT
FOUT(44)=RED
FOUT(45)=CDD
FOUT(46)=IFLRG

END SUBROUTINE
```

References

1. Akagawa, K., and Sakaguchi, T. 1966. “Fluctuation of Void Ratio in Two-Phase Flow (3rd Report, Absolute Velocities of Slugs and Small Bubbles, and Distribution of Small Bubbles in Liquid Slugs).” Bulletin of JSME. Vol. 9. p. 111-120.
2. Alamu, M.B. “Investigation of Periodic Structures in Gas-Liquid Flow.” 2010. Ph.D. Thesis. U. of Nottingham.
3. Asali, J.C., 1984. “Entrainment in Vertical Gas-Liquid Annular Flows.” Ph.D. Dissertation. U. of Illinois.
4. Asali, J.C., Hanratty,T.J., and Andreussi, P., 1985. “Interfacial Drag and Film Height for Vertical Annular Flow.” AIChE J. Vol. 31. pp. 895-902.
5. Azzopardi, B.J., 1997. “Drops in Annular Two-Phase Flow.” Int. J. Multiphase Flow. Vol. 23. pp. 1-53.
6. Balasubramaniam, R., Rame, E., Kizito, J., and Kassemi, M. 2006. “Two Phase Flow Modeling: Summary of Flow Regimes and Pressure Drop Correlations in Reduced and Partial Gravity.” NASA/CR-2006-214085. National Center for Space Exploration Research. Cleveland, OH.
7. Belt, R.J., Van’t Westende, J.M.C., and Portela, L.M., 2009. “Prediction of the Interfacial Shear-Stress in Vertical Annular Flow.” Int. J. Multiphase Flow. Vol. 35. pp. 689-697.
8. Berna, C., Escriva, A., Munoz-Cobo, J.L., and Herranz, L.E. 2015. “Development of New Correlations for Annular Flow.” Computational Methods in Multiphase Flow VIII. WIT Press. Southampton, UK. pp. 451-462.
9. Brodkey, R.S., 2012. The Phenomena of Fluid Motions. Addison-Wesley. Reading, MA.
10. Brooks, C., Hibiki, T., and Ishii, M. 2012. “Interfacial Drag Force in One-Dimensional Two-Fluid Model.” Prog. Nuc. Energy. Vol. 61. pp. 57-68.
11. Brown, R.A.S., Sullivan, G.A., and G.W. Govier. 1960. “The Upward Vertical Flow of Air-Water Mixtures III: Effect of Gas Phase Density on Flow Pattern, Holdup and Pressure Drop.” Can. J. Chem. Eng., pp. 62-66.
12. Chexal, B., and Lellouche, G. 1986. "A Full-Range Drift-Flux Correlation for Vertical Flows." EPRI NP-3989-SR.
13. Chexal, B., Lellouche, G., Horowitz, J., and Heazer, J. 1992. “A Void Fraction Correlation for Generalized Applications.” Prog. In Nuc. Ener., Vol. 27. pp. 255-295.
14. Chexal, B., Merilo, M., Maulbetsch, J., Horowitz, J., Harrison, J., Westacott, J., Peterson, C., Kastner, W., and Schmidt, H. 1997. “Void Fraction Technology for Design and Analysis.” EPRI TR-106326.
15. Chisholm, D. 1983. “Two-Phase Flow in Pipelines and Heat Exchangers.” 1st Edition. Longman.
16. Clark, R., and Kornhauser, A. 2012. “Modeling Two-Phase Flow in the Downcomer of a Once-Through Steam Generator using RELAP5/MOD2.” CAER-2009-15-1.
17. Cousins, L.B., Denton, W.H., and Hewitt, G.F., 1965. “Liquid Mass Transfer in Annular Two-Phase Flow.” Sump. On Two-Phase Flow. Exeter, UK. Vol. 1. Paper C4.
18. Cousins, L.B. and Hewitt, G.F., 1968. Liquid Phase Mass Transfer in Annular Two-Phase Flow: Droplet Deposition and Liquid Entrainment. UKAEA Report AERE-R5657.
19. Crawford, T.J., 1983. “Analysis of Steady State and Transient Two-Phase Flow in Downwardly Inclined Lines.” Ph.D. Thesis. Drexel University.

20. Davies, R.M., and Taylor, G.I. 1950. “The Mechanics of Large Bubbles Rising through Liquids in Tubes.” Proc. Of Roy. Soc. Vol. 200. Ser. A. pp. 375-390.
21. Drew, D., Cheng, L., and Lahey, R.T. 1979. “The Analysis of Virtual Mass Effects in Two-Phase Flow.” Int. J. Multiphase Flow. Vol. 5. pp. 233-242.
22. Duan, R., Koshizuka, S., and Oka, Y., 2003. “Two-Dimensional Simulation of Drop Deformation and Breakup at Around the Critical Weber Number.” Nuc. Eng. Des., Vol. 225. pp. 37-48.
23. Dumitrescu, D.T. 1943. “Stromung and Einer Luftbase in Senkrechten Rohr.” ZAMM. Vol. 23. pp. 139- 149.
24. Ellison, A.H., Klemm, R.B., Schwartz, A.M., Grubb, L.S. and Petrash, D.A., 1967. “Contact Angles of Mercury on Various Surfaces and the Effect of Temperature.” J. Chem. Eng. Data. Vol. 12. pp. 607-609.
25. Faeth, G.M., Hsiang, L.P., and Wu, P.K., 1996. “Structure and Breakup Properties of Sprays.” Int. J. Multiphase Flow. Vol. 21. pp. 99-127.
26. Fore, L.B., Beus, S.G., and Bauer, R.C., 2000. “Interfacial Friction in Gas-Liquid Annular Flow: Analogies to Full and Transition Roughness.” Int. J. Multiphase Flow. Vol. 26. pp. 1755-1769.
27. Fore, L.B., and Dukler, A.E., 1995. “Droplet Deposition and Momentum Transfer in Annular Flow.” A. I. Ch. E. J. Vol. 41. pp. 2040-2046.
28. Fukano, T., and Furukawa, T., 1998. “Prediction of the Effects of Liquid Viscosity on Interfacial Shear Stress and Frictional Pressure Drop in Vertical Upward Gas-Liquid Annular Flow.” Int. J. Multiphase Flow. Vol. 24. pp. 587-603.
29. Gill, L.E., Hewitt, G.F., and Lacey, P.M.C. 1963. “Sampling Probe Studies of the Gas Core in Annular Two-Phase Flow Part II. Studies of the Effect of Phase Flow Rates on Phase and Velocity Distribution.” United Kingdom Atomic Energy Authority. AERE-R 3955.
30. Govier, G.W., and Aziz, K., 1972. “The Flow of Complex Mixtures in Pipes.” Van Nostrand Reinhold Co.
31. Govier, G.W., Radford, B.A., and Dunn, J.S.C. 1957. “The Upwards Vertical Flow of Air-Water Mixtures I. Effect of Air and Water-Rates on Flow Pattern, Holdup and Pressure Drop.” Can. J. Chem. Eng., pp. 58-70.
32. Govier, G.W. and Short, W.L. 1958. “The Upward Vertical Flow of Air-Water Mixtures II. Effect of Tubing Diameter on Flow Pattern, Holdup and Pressure Drop.” Can. J. Chem. Eng., pp. 195-201.
33. Griffith, P., and Wallis, G. 1961. “Two-Phase Slug Flow.” J. Heat Transfer. pp. 307-318.
34. Harmathy, T.Z. 1960. “Velocity of Large Drops and Bubbles in Media of Infinite or Restricted Extent.” A.I.Ch.E., Vol 6. pp. 281-288.
35. Hazuku, T., Takamasa, T., and Matsumoro, Y. 2008. “Experimental Study on Axial Development of Liquid Film in Vertical Upward Annular Two-Phase Flow.” Int. J. Multiphase Flow. Vol. 34. pp. 111-127.
36. Hewitt, G.F. and Hall Taylor, N.S. 1970. “Annular Two-Phase Flow.” Pergamon. Oxford.
37. Hooker, H.H., and Popper, G.F. 1958. “A Gamma-Ray Attenuation Method for Void Fraction Determination in Experimental Boiling Heat Transfer Test Facilities.” Argonne National Laboratory. ANL-5766.

38. Hori, K., Nakasatomi, M., Nishikawa, K., and Sekoguchi, K. 1978. “Study of Ripple Region in Annular Two-Phase Flow (3rd Report, Effect of Liquid Viscosity on Gas-Liquid Interfacial Character and Friction Factor).” Trans. Jap. Soc. Mech. Eng. Vol. 44. pp. 3847-3856.
39. Hsiang, L.P., and Faeth, G.M. 1995. “Drop Deformation and Breakup due to Shock Wave and Steady Disturbances.” Int. J. Multiphase Flow. Vol. 21. pp. 545-560.
40. Information Systems Laboratories, Inc., 2003, RELAP5/MOD3.3.
41. Ishii, M. 1977. “One-Dimensional Drift-Flux Model and Constitutive Equations for Relative Motion between Phases in Various Two-Phase Flow Regimes.” ANL-77-47. Argonne National Laboratory.
42. Ishii, M. and Chawla, T.C. 1979. “Local Drag Laws in Dispersed Two-Phase Flow.” NUREG/CR-1230. Argonne National Laboratory.
43. Ishii, M., and Grolmes, M.A. 1975. “Inception Criteria for Droplet Entrainment in Two-Phase Concurrent Film Flow.” AIChE J. Vol. 21. pp. 308-318.
44. Ishii, M. and Hibiki, T. 2006. “Thermo-Fluid Dynamics of Two-Phase Flow.” Springer.
45. Ishii, M., Kim, S., and Kelly, J. 2005. “Development of Interfacial Area Transport Equation.” Nuc. Eng. And Tech., Vol. 37. pp. 525-536.
46. Ishii, M and Mishima, K. 1984. “Two-Fluid Model and Hydrodynamic Constitutive Relations.” Nuc. Eng. And Des. Vol. 82. pp. 107-126.
47. Ishii, M., and Mishima, K. 1989. “Droplet Entrainment Correlation in Annular Two-Phase Flow.” Int. J Heat Mass Transfer. Vol. 32. pp. 1835-1846.
48. Kataoka, I., and Ishii, M. 1987. "Drift Flux Model for Large Diameter Pipe and New Correlation for Pool Void Fraction." Int. J. Heat Mass Transfer. Vol. 30. pp. 1927-1939.
49. Kataoka, I., Ishii, M., and Mishima, K. 1983. “Generation and Size Distribution of Droplets in Annular Two-Phase Flow.” Trans. ASME. Vol. 105. pp. 230-238.
50. Kosky, P. G. 1971. “Thin Liquid Film under Simultaneous Shear and Gravity Forces.” Int. J. Heat Mass Transfer. Vol. 14. pp. 1220-1224.
51. Kozloff, B. 1954. “Forms of Flow of Gas-Liquid Mixtures and Their Stability Limits in Vertical Tubes.” Zhur. Tekh. Fiz. Vol. 24. pp. 2285-2288.
52. Lockhart, R.W., and Martinelli, R.C. 1949. “Proposed Correlation of Data for Isothermal Two-Phase, Two-Component Flow in Pipes.” Chem. Eng. Prog. Vol. 45. pp. 39-48.
53. Moeck, E.O. 1970. “Annular-Dispersed Two-Phase Flow and Critical Heat Flux.” Ph.D. Dissertation. McGill University.
54. Munson, B.R., Okiishi, T.H., Huebsch, W.W., and Rothmayer, A. P. 2013. "Fundamentals of Fluid Mechanics." 7th Edition. Wiley.
55. Neal, L.G. 1963. “Local Parameters in Cocurrent Mercury-Nitrogen Flow.” ANL-6625. Argonne National Laboratory.
56. Nicklin, D.J., and Davidson, J.F. 1962. “The Onset of Instability on Two-Phase Slug Flow.” Inst. Mech. Engr. Proc. Of Symp. On Two-Phase Flow., Paper 4.
57. Okawa, T., Goto, T., and Tamagoe, Y. 2010. “Liquid Film Behavior in Annular Two-Phase Flow under Flow Oscillation Conditions.” Int. J. Heat Mass Transfer. Vol. 53. pp. 962-971.
58. Optimized Thermal Systems. 2009. XProps. Version 2.0. Retrieved from http://www.optimizedthermalsystems.com/

59. Oshinowo, O. 1971. “Two-Phase Flow in a Vertical Tube Coil.” Ph.D. Thesis. University of Toronto. Toronto, Ontario, Canada.
60. Oshinowo, T. and Charles, M. E. 1974. "Vertical Two-Phase Flow Part I. Flow Pattern Correlations." Can. J. Chem. Engr. Vol. 52. pp. 25-35.
61. Oshinowo, T. and Charles, M. E. 1974. “Vertical Two-Phase Flow Part II. Holdup and Pressure Drop.” Can. J. Chem. Engr. Vol. 52. pp. 438-448.
62. Paras, S.V., and Karabelas, A.J. 1991. “Properties of the Liquid Layer in Horizontal Annular Flow.” Int. J. Multiphase Flow. Vol. 17. pp. 439-454.
63. Petrick, M. 1962. “A Study of Vapor Carryunder and Associated Problems.” ANL-6581. Argonne National Laboratory.
64. Pilch, M., and Erdman, C.A. 1987. “Use of Breakup time Data and Velocity History Data to Predict the Maximum Size of Stable Fragments for Acceleration-Induced Breakup of a Liquid Drop.” Int. J. Multiphase Flow. Vol. 13. pp. 741-757.
65. Ransom, V.H., Wagner, R.J., Trapp, J.A., Carlson, K.E., Kiser, D.M. Kuo, H., Chow, H., Nelson, R.A., and James, S.W. 1982. “RELAP5/MOD1 Code Manual Volume 1: Systems Models and Numerical Methods.” EG&G Idaho, Inc. NUREG/CR-1826.
66. Ransom, V.H., Wagner, R.J., Trapp, L.R., Johnsen, G.W., Kiser, D.M., and Riemke, R.A. 1985. “RELAP5/MOD2 Code Manual Volume 1: Code Structure, Systems Models and Solution Methods.” NUREG/CR-4312. EG&G Idaho, Inc.
67. RELAP5-3D Code Manual Volume I: Code Structure, System Models, and Solution Methods. 2005. INEEL-EXT-0083. Revision 2.4. Idaho National Laboratory.
68. RELAP5/MOD3.2 Code Manual Volume 1: Code Structure, System Models, and Solution Methods. 1995. NUREG/CR-5535. Idaho National Engineering Laboratory.
69. RELAP5/MOD3.3 Code Manual Volume I: Code Structure, System Models, and Solution Methods. 2001. NUREG/CR-5535. Information Systems Laboratories.
70. RELAP5/MOD3.3 Code Manual Volume IV: Models and Correlations. 2001. NUREG/CR-5335. Information Systems Laboratories.
71. Sawant, P., Ishii, M., and Mori, M. 2008. “Droplet Entrainment Correlation in Vertical Upward Co-Current Annular Two-Phase Flow.” Nuc. Eng. Des. Vol. 238. pp. 1342-1352.
72. Sawant, P., Ishii, M., Hazuku, T., Takamasa, T. and Mori, M. 2008. “Properties of Disturbance Waves in Vertical Annular Two-Phase Flow.” Nuc. Eng. Des., Vol. 238., pp. 3528-3541.
73. Sawant, P., Ishii, M., and Mori, M. 2014. “Prediction of Amount of Entrained Droplets in Vertical Annular Two-Phase Flow.” Int. J. Heat Fluid Flow. Vol. 30. pp. 715-728. 2009.
74. Sazhin, S. Droplets and Sprays. Springer. London.
75. Schlegal, J.P. 2009. “Experimental Study of Relative Velocity and Drag Force in Large Diameter Pipes.” Masters’ Thesis. Purdue University.
76. Schubring, D. 2009. “Behavior Interrelationships in Annular Flow.” Ph.D. Dissertation. U. of Wisconsin-Madison.
77. Schubring, D. and Shedd, T.A. 2011. “A Model for Pressure Loss, Film Thickness and Entrained Fraction for Gas-Liquid Annular Flow.” Int. J. Heat Fluid Flow. pp. 730-739.
78. Smissaert, G.E. 1963. “Two-Component Two-Phase Flow Parameters for Low Circulation Rates.” Argonne National Laboratory. ANL-6755.
79. Srivastava, R.P.S. 1973. “Liquid Film Thickness in Annular Flow.” Chem. Eng. Sci. Vol. 28. pp. 819-824.

80. Steen, D.A., and Wallis, G.B. 1964. The Transition from Annular to Annular-Mist Concurrent Two-Phase Down Flow. AEC Report NYO-3114-2.
81. Taitel, Y., Bornea, D., and Dukler, A.E. 1980. "Modeling Flow Pattern Transitions for Steady Upward Gas-Liquid Flow in Vertical Tubes." AIChE Journal. Vol. 26. pp. 345-354.
82. Tatterson, D.F., Dallman, J.C, and Hanratty, T.J. 1977. “Drop Sizes in Annular Gas-Liquid Flows.” AIChE. J. Vol. 23. pp. 68-76.
83. TRACE V5.0 Theory Manual: Field Equations, Solution Methods, and Physical Models. 2010. US Nuclear Regulatory Commission.
84. Turner, J.M. 1965. “Annular Two-Phase Flow.” Ph.D. Thesis. Dartmouth College. Hannover, New Hampshire.
85. Vince, M. A. and Lahey, R.T. 1982. "On the Development of an Objective Flow Regime Indicator." Int. J. Multiphase Flow. Vol. 8. pp 93-124.
86. Wallis, G.B. 1969. "One-Dimensional Two-Phase Flow." 1st Edition. McGraw-Hill.
87. Wicks, M. and Dukler, A.E. 1966. “In Situ Measurements of Drop Size Distribution in Two-Phase Flow: A New Method for Electrically Conducting Liquids.” Int. Heat Trans. Conf. Chicago.
88. Wilson, J.F, Grenda, R.J. and Patterson, J.F. 1962. “The Velocity of Rising Steam in a Bubbling Two-Phase Mixture.”, Trans. ANS, Vol. 5, pp. 151-2.
89. Wongwises, S., and Kongkiatwanich, W. 2001. “Interfacial Friction Factor in Vertical Upward Gas-Liquid Annular Two-Phase Flow.” Int. Comm. Heat Mass Transfer. Vol. 28. pp. 323-336.
90. Zuber, N. 1964. “On the Dispersed Two-Phase Flow in the Laminar Flow Regime.”, Chem. Eng. Sci., Vol. 19, pp. 897-917.
91. Zuber, N., and Findlay, J.A. 1965. "Average Volumetric Concentration in Two-Phase Flow Systems." J. Heat Transfer. Vol. 87. pp. 453-468.